

VOLUME 76

MARCH 2, 1972

NUMBER 5

JPCA X

THE JOURNAL OF

PHYSICAL
CHEMISTRY

PUBLISHED BIWEEKLY BY THE AMERICAN CHEMICAL SOCIETY

THE JOURNAL OF PHYSICAL CHEMISTRY

BRYCE CRAWFORD, Jr., *Editor*

STEPHEN PRAGER, *Associate Editor*

ROBERT W. CARR, Jr., FREDERIC A. VAN-CATLEDGE, *Assistant Editors*

EDITORIAL BOARD: A. O. ALLEN (1970-1974), J. R. BOLTON (1971-1975),
F. S. DAINTON (1972-1976), M. FIXMAN (1970-1974),
H. S. FRANK (1970-1974), R. R. HENTZ (1972-1976), J. R. HUIZENGA (1969-1973),
W. J. KAUFMANN (1969-1973), R. L. KAY (1972-1976), W. R. KRIGBAUM (1969-1973),
R. A. MARCUS (1968-1972), W. J. MOORE (1969-1973), J. A. POPLER (1971-1975),
B. S. RABINOVITCH (1971-1975), H. REISS (1970-1974), S. A. RICE (1969-1975),
F. S. ROWLAND (1968-1972), R. L. SCOTT (1968-1972),
R. SEIFERT (1968-1972), W. A. ZISMAN (1972-1976)

CHARLES R. BERTSCH, *Manager, Editorial Production*

AMERICAN CHEMICAL SOCIETY, 1155 Sixteenth St., N.W., Washington, D. C. 20036

FREDERICK T. WALL, *Executive Director*

Books and Journals Division

JOHN K. CRUM, *Director*

JOSEPH H. KUNEY, *Head, Business Operations Department*

RUTH REYNARD, *Assistant to the Director*

©Copyright, 1972, by the American Chemical Society. Published biweekly by the American Chemical Society at 20th and Northampton Sts., Easton, Pa. 18042. Second-class postage paid at Washington, D. C., and at additional mailing offices.

All manuscripts should be sent to *The Journal of Physical Chemistry*, Department of Chemistry, University of Minnesota, Minneapolis, Minn. 55455.

Additions and Corrections are published once yearly in the final issue. See Volume 75, Number 26 for the proper form.

Extensive or unusual alterations in an article after it has been set in type are made at the author's expense, and it is understood that by requesting such alterations the author agrees to defray the cost thereof.

The American Chemical Society and the Editor of *The Journal of Physical Chemistry* assume no responsibility for the statements and opinions advanced by contributors.

Correspondence regarding accepted copy, proofs, and reprints should be directed to Editorial Production Office, American Chemical Society, 20th and Northampton Sts., Easton, Pa. 18042. Manager: CHARLES R. BERTSCH. Assistant Editor: EDWARD A. BORGER.

Advertising Office: Century Communications Corporation, 142 East Avenue, Norwalk, Conn. 06851.

Business and Subscription Information

Remittances and orders for subscriptions and for single copies,

notices of changes of address and new professional connections, and claims for missing numbers should be sent to the Subscription Service Department, American Chemical Society, 1155 Sixteenth St., N.W., Washington, D. C. 20036. Allow 4 weeks for changes of address. Please include an old address label with the notification.

Claims for missing numbers will not be allowed (1) if received more than sixty days from date of issue, (2) if loss was due to failure of notice of change of address to be received before the date specified in the preceding paragraph, or (3) if the reason for the claim is "missing from files."

Subscription rates (1972): members of the American Chemical Society, \$20.00 for 1 year; to nonmembers, \$60.00 for 1 year. Those interested in becoming members should write to the Admissions Department, American Chemical Society, 1155 Sixteenth St., N.W., Washington, D. C. 20036. Postage to Canada and countries in the Pan-American Union, \$5.00; all other countries, \$6.00. Single copies for current year: \$3.00. Rates for back issues from Volume 56 to date are available from the Special Issues Sales Department, 1155 Sixteenth St., N.W., Washington, D. C. 20036.

This publication and the other ACS periodical publications are now available on microfilm. For information write to: MICROFILM, Special Issues Sales Department, 1155 Sixteenth St., N.W., Washington, D. C. 20036.

THE JOURNAL OF PHYSICAL CHEMISTRY

Volume 76, Number 5 March 2, 1972

JPCHAx 76(5) 615-804 (1972)

The Vacuum Ultraviolet Photolysis of Cyclohexanone	Alfred A. Scala* and Daniel G. Ballan	615
Exchange Mechanism and Arrhenius Parameters of Elementary Steps in the Reactions of Hydrogen Atoms with Water Vapor in Irradiated Mixtures of Hydrogen and Water Vapor	N. E. Bibler and R. F. Firestone*	621
The Effect of Ionic Dissociation of Organic Compounds on Their Rate of Reaction with Hydrated Electrons	Francis A. Peter and P. Neta*	630
Optical Bleaching Effects on the Paramagnetic Relaxation of Trapped Electrons in Methyltetrahydrofuran at 77°K	D. P. Lin and Larry Kevan*	636
Visible-Light Effects on Electronic Absorption Bands of Some Cation Radicals Produced by Photoionization at 77°K	Katsumi Kimura,* Shunji Katsumata, and Kazutoshi Sawada	639
Barriers to Rotation around the Amide Bond and the Central Carbon-Carbon Bond in Tetrabenzoyloxamide and Its Monothio and Dithio Analogs	Robert E. Carter* and Jan Sandström	642
The Infrared Spectrum of Matrix Isolated UO ₂ (g) and Its Thermodynamic Properties	S. Abramowitz* and N. Acquista	648
Location of Univalent Cations in Synthetic Zeolites of the Y and X Type with Varying Silicon to Aluminum Ratio. II. Dehydrated Potassium Exchanged Forms	W. J. Mortier,* H. J. Bosmans, and J. B. Uytterhoeven	650
A Potential Energy Surface for the Addition of Benzynes to Ethylene	David M. Hayes and Roald Hoffmann*	656
Potential Surfaces for the Addition of CH ₂ and CF ₂ to Ethylene and Isobutene	Roald Hoffmann,* David M. Hayes, and Philip S. Skell	664
A CNDO/2 Calculation on the Helical Conformations of a Tetrapeptide of Glycine. III. The ϕ - ψ Energy Surface	Robert Schor,* Hans Stymne, Gunnar Wettermark, and Carl W. David	670
A Model for the Simulation of the Electron Spin Resonance Spectra of Nitroxide-Type Probe Molecules in a Nematic Mesophase	Theodore Pietrzak	672
Adsorption on Flat Surfaces. III. Adsorption of Branched-Chain Alcohols	T. D. Blake* and W. H. Wade	675
Thermochemistry of Halide Exchange in an Anion-Exchange Resin	G. R. Choppin,* G. Y. Markovits, and M. E. Clark	680
Thermodynamic Properties of Hydrated and Ammoniated Electrons.	Gerard Lepoutre and Joshua Jortner*	683
Polyanions and Their Complexes. VIII. Interaction of Methylene Blue with Cellulosic Polyanions in Heterogeneous Systems	P. J. Baugh, J. B. Lawton, and G. O. Phillips*	688
Reactivities of Ion Pairs and Free Ions in Proton Abstraction Reactions. The Reaction between Polystyryl Carbanion Salts and Triphenylmethane.	L. L. Chan and J. Smid*	695
Comproportionation Kinetics of Stable Violene Radical Ions	Bruce C. Bennion, James J. Auburn, and Edward M. Eyring*	701
A General Solution for the Sequence of Two Competitive-Consecutive Second-Order Reactions.	Walter Y. Wen	704
The Adsorption Behavior of Tetraphenylborate Anions at a Mercury Electrode	Claudio Giomini* and Liliana Rampazzo	707
Transference Numbers of Potassium Chloride and Ionic Conductances in Ethylene Glycol at 25°	M. Carmo Santos and M. Spiro*	712

A Further Description of Complete Equilibrium Constants	William L. Marshall	720
Application of Significant Structures Theory to Some Hydrocarbon Liquids	G. L. Faerber, S. M. Breitling, A. MacKnight, and H. Eyring*	731
The Relationship of Crystalline Forms I, III, IV, and V of Anhydrous Sodium Sulfate as Determined by the Third Law of Thermodynamics	G. E. Brodale and W. F. Giauque*	737
The Vapor Pressure Isotope Effect in Aqueous Systems. I. H ₂ O-D ₂ O (-64° to 100°) and H ₂ ¹⁶ O-H ₂ ¹⁸ O (-17° to 16°); Ice and Liquid. II. Alkali Metal Chloride Solution in H ₂ O and D ₂ O (-5° to 100°)	Jovan Pupezin, Gyorgy Jakli, Gabor Jancso, and W. Alexander Van Hook*	743
Aggregation Equilibria of Xanthene Dyes	Judith E. Selwyn and Jeffrey I. Steinfeld*	762
The Association of Formic Acid in Carbon Tetrachloride Solution	Claybourne C. Snead	774
The Effects of Pressure and Thermodynamic Nonideality on the Sedimentation Equilibrium of Chemically Reacting Systems: Results with Lysozyme at pH 6.7 and 8.0	G. J. Howlett, P. D. Jeffrey, and L. W. Nichol*	777
Formation of Dynamic Patterns in a Fluid Layer	F. Gambale and A. Gliozzi*	783
X-Ray Study of the Conformation of the Molecule of 1,2-trans-Cyclopentanedicarboxylic Acid	E. Benedetti,* P. Corradini, and C. Pedone	790
Thermal Decomposition of 3-Halo-3-phenyldiazirine in Solution	Michael T. H. Liu* and K. Toriyama	797
Electron Spin Resonance Study of Transient Radicals in γ -Irradiated Organic Inclusion Compounds. II. The Palmitic Acid Urea Clathrate.	A. Faucitano, A. Perotti,* G. Allara, and F. Faucitano Martinotti	801

AUTHOR INDEX

Abramowitz, S., 648	Corradini, P., 790	Howlett, G. J., 777	Martinotti, F. F., 801	Schor, R., 670
Acquista, N., 648	David, C. W., 670	Jakli, G., 743	Mortier, W. J., 650	Selwyn, J. E., 762
Allara, G., 801	Eyring, E. M., 701	Jancso, G., 743	Neta, P., 630	Skell, P. S., 664
Auborn, J. J., 701	Eyring, H., 731	Jeffrey, P. D., 777	Nichol, L. W., 777	Smid, J., 695
Ballan, D. G., 615	Faerber, G. L., 731	Jortner, J., 683	Pedone, C., 790	Snead, C. C., 774
Baugh, P. J., 688	Faucitano, A., 801	Katsumata, S., 639	Perotti, A., 801	Spiro, M., 712
Benedetti, E., 790	Firestone, R. F., 621	Kevan, L., 636	Peter, F. A., 630	Steinfeld, J. I., 762
Bennion, B. C., 701	Gambale, F., 783	Kimura, K., 639	Phillips, G. O., 688	Stymne, H., 670
Bibler, N. E., 621	Giauque, W. F., 737	Lawton, J. B., 688	Pietrzak, T., 672	Toriyama, K., 797
Blake, T. D., 675	Giomini, C., 707	Lepoutre, G., 683	Pupezin, J., 743	Uytterhoeven, J. B., 650
Bosmans, H. J., 650	Gliozzi, A., 783	Lin, D. P., 636	Rampazzo, L., 707	Van Hook, W. A., 743
Breitling, S. M., 731	Hayes, D. M., 656, 664	Liu, M. T. H., 797	Sandström, J., 642	Wade, W. H., 675
Brodale, G. E., 737	Hoffmann, R., 656, 664	MacKnight, A., 731	Santos, M. C., 712	Wen, W. Y., 704
Carter, R. E., 642		Markovits, G. Y., 680	Sawada, K., 639	Wettermark, G., 670
Chan, L. L., 695		Marshall, W. L., 720	Scala, A. A., 615	
Choppin, G. R., 680				
Clark, M. E., 680				

In papers with more than one author the name of the author to whom inquiries about the paper should be addressed is marked with an asterisk in the by-line.

THE JOURNAL OF PHYSICAL CHEMISTRY

Registered in U. S. Patent Office © Copyright, 1972, by the American Chemical Society

VOLUME 76, NUMBER 5 MARCH 2, 1972

The Vacuum Ultraviolet Photolysis of Cyclohexanone¹

by Alfred A. Scala* and Daniel G. Ballan

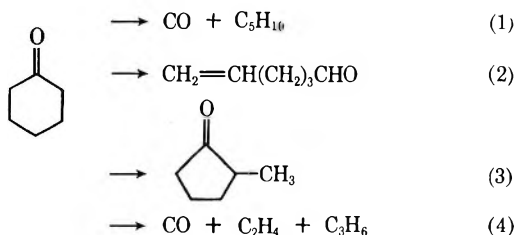
Department of Chemistry, Worcester Polytechnic Institute, Worcester, Massachusetts 01609 (Received April 22, 1971)

Publication costs assisted by the U. S. Atomic Energy Commission

In the vacuum ultraviolet photolysis of cyclohexanone, the major modes of decomposition of the electronically excited ketone are as follows: $\text{CO} + \text{C}_5\text{H}_{10}$, A; $\text{CH}_2 + \text{CO} + 2\text{C}_2\text{H}_4$, B; $\text{CH}_2 + \text{CO} + (\text{CH}_2)_4$, C; $\text{CO} + \text{C}_2\text{H}_4 + \text{C}_3\text{H}_6$, D; $\text{H} + \text{C}_6\text{H}_9\text{O}$, E; $\text{H}_2 + \text{C}_6\text{H}_9\text{O}$, F. The quantum yield for reaction A is 0.68 at 147.0 nm and it becomes less important as the energy of the incident light is increased. Ethylene is the most abundant hydrocarbon product at each wavelength, being produced primarily from reaction B and/or reaction C followed by decomposition of the tetramethylene diradical of two molecules of ethylene ($\phi \simeq 0.2$). Reaction D is unimportant and occurs with a maximum quantum yield of 0.03. Experiments with cyclohexanone- α - d_4 have shown that the C_5H_{10} produced in reaction A undergoes secondary decomposition to C_2H_4 and C_3H_6 . The remainder of the decomposition of cyclohexanone is accounted for by reactions E and F which become more significant as the energy of the incident light is increased. The mechanisms for reactions A–D are best interpreted in terms of diradicals $(\text{CH}_2)_n$ where $n = 1, 3, 4$, and 5. That nonacyl σ cleavage is unimportant at 147.0 nm indicates that energy absorption occurs primarily at the carbonyl group. Intramolecular hydrogen atom transfer to yield 5-hexenal was not observed.

Introduction

The near-ultraviolet photochemistry of cyclohexanone has been thoroughly investigated and is characterized by reactions 1–4.² The quantum yield for reaction 1 is close to 0.8 while the quantum yield



for reactions 3 and 4 combined is about 0.04. The formation of 5-hexenal occurs with a quantum yield of about 0.2. Reaction 2 is an intramolecular hydrogen atom transfer and is less important in cyclohexanone photolysis than the formation of 4-pentalenal is in cyclopentanone photolysis. Shortridge and Lee³ have shown that in the benzene sensitization of cyclohexanone reaction 1 occurs through singlet sensitization while

reaction 2 occurs through triplet sensitization. Freeman⁴ has also demonstrated that the occurrence of reaction 2 in the liquid phase γ -radiolysis of cyclohexanone involves the lowest triplet excited state of cyclohexanone.

In view of the scarcity of information concerning the interaction of complex organic molecules with vacuum ultraviolet radiation and our continuing interest in this subject, we have photolyzed cyclohexanone in the vacuum ultraviolet. The object of this study was to determine the primary processes which occur and to compare the photolytic mechanism in the vacuum ultraviolet with the near-ultraviolet photochemistry of cyclohexanone.

(1) This research was supported by the U. S. Atomic Energy Commission [AT (30-1)-3945].

(2) For a review see (a) R. Srinivasan, *Advan. Photochem.*, **1**, 83 (1963). (b) J. Calvert and J. N. Pitts, Jr., "Photochemistry," Wiley, New York, N. Y., 1966, p 406.

(3) R. G. Shortridge, Jr., and E. K. C. Lee, *J. Amer. Chem. Soc.*, **92**, 2228 (1970).

(4) A. Singh and G. R. Freeman, *J. Phys. Chem.*, **69**, 666 (1965).

Experimental Section

Photolyses. Microwave powered xenon, krypton, and argon resonance lamps were attached to a 1-l. reaction vessel through a ground glass joint. The lamps which had LiF windows contained 0.5 Torr of gas and were gettered with titanium. No cooling was required in order to maintain a constant output. The outputs of the lamps used in this study as measured on a McPherson 1m vacuum monochromator were: Xe, 147.0 nm 99%, 129.5 nm 1%; Kr, 123.6 nm 89%, 116.5 nm 11%; Ar, 106.7 nm 78%, 104.8 nm 11%, 121.5 nm (Lyman α) 11%. The intensity of the lamps was approximately: Xe, 2×10^{15} quanta/sec; Kr, 5×10^{14} quanta/sec; Ar, 5×10^{13} quanta/sec. Conversions were usually kept below 0.1%.

Since photolysis of cyclohexanone, I.P. 9.14 eV, at 123.6 nm (10.0 eV) and 106.7–104.8 nm (~ 11.7 eV) causes ionization of cyclohexanone, saturation current measurements were made using a 500 cm³ cylindrical cell containing two parallel plate stainless steel electrodes (5-cm diameter) separated by a distance of 5 cm. A potential difference was applied using a John Fluke Model 415 B regulated high voltage power supply and the current was measured on a Victoreen Model 1001 micromicroammeter. The current in the empty cell was always less than 1% of that observed during the photolysis of cyclohexanone. Saturation current measurements were usually determined with 2 Torr of cyclohexanone in the cell. At this pressure and at intensities of *ca.* 5×10^{11} quanta/sec, good saturation currents were obtained which were independent of small changes in pressure.

Analyses. After irradiation, noncondensables were distilled off at liquid or solid nitrogen temperature and measured in a gas burette. The relative analysis of the noncondensable gases was performed on A.E.I. MS-10 mass spectrometer. The condensables were then injected into an F and M Model 810 gas chromatograph equipped with a flame ionization detector and containing a 30 ft squalane on 60–80 mesh Chromosorb P column operated at 25° and a helium flow of 60 cm³/min. The CO:C₂H₄ ratios for the argon photolysis experiments, where the conversions were too low for accurate analysis using the MS-10, were determined by distilling everything noncondensable at 195°K and obtaining the analysis on a Bell & Howell 21-491 high resolution mass spectrometer. Calculation of the contribution of products other than ethylene to the *m/e* 28 attributed to ethylene indicate that their contribution would be less than 5%.

In special high conversion, high pressure experiments which were performed to determine if 5-hexenal was a product, the photolysis mixture was immediately injected onto either a 9 ft, 10% diisodecyl phthalate column operated at 50° and a helium flow of 30 cm³/min, or a 3 ft, Poropak Q-S column operated at 160° and a helium flow of 40 cm³/min. Each of these col-

umns has the capability of separating 5-hexenal from cyclohexanone. The isotopic composition of the ethylene was determined by injecting the entire photolysis mixture onto a 6-ft silica gel column operated at 45° and a helium flow of 20 cm³/min and condensing the ethylene at the exit of the chromatograph. The composition of the ethylene was then determined using the MS10 mass spectrometer. The cracking patterns used to calculate these results were obtained by running authentic samples of the various deuterated ethylenes on the MS-10.

The quantum yield measurements at 123.6 and 106.7–104.8 nm are based upon the determination of the ionization efficiency of cyclohexanone, the saturation current during photolysis and the ethylene yield.⁵ Nitric oxide was used as a standard in these experiments. Quantum yields at 147.0 nm are based upon CO₂ actinometry.⁶

Materials. Matheson, chromatography-quality, cyclohexanone was purified by distillation on a thirty theoretical plate, spinning band column. Only a middle fraction which contained no detectable impurities, as determined by analyses on both a 12 ft, 15% (wt/wt) squalane on Chromosorb P column, operated at ambient temperature and a helium flow of 60 cm³/min and on a 10 ft, 10% (wt/wt) diisodecyl phthalate on Chromosorb P column operated at 60° and a helium flow of 30 cm³/min, was used. This sample was thoroughly degassed by several trap-to-trap distillations and stored in a darkened vessel on the vacuum line. Cyclohexanone- α -d₄ was prepared by the method of Seibl and Gauman,⁷ by six exchanges of the α -hydrogens in a well stirred mixture of 10% DCl-D₃PO₄ in D₂O and cyclohexanone. After several trap-to-trap distillations, the nuclear magnetic resonance spectrum of the ketone showed no absorption due to α -hydrogens. The isotopic purity of the cyclohexanone- α -d₄ as determined by mass spectrometry indicated that 97–98% exchange had occurred in the α -positions and the composition of the ketone was 91% d₄, 7% d₃, and 2% d₂.

Nitric oxide (Matheson), hydrogen sulfide (Matheson) and ethylene (Thomas A. Edison) were all used without further purification other than trap-to-trap distillation. The small amount of ethane, propane and propylene contained in the ethylene was insignificant in our experiments.

Results

The product distributions obtained in the photolysis of cyclohexanone at 147.0, 123.6 and 106.7–104.8 nm both in the presence and absence of nitric oxide are presented in Table I. The conversion in most experi-

(5) P. Ausloos and S. G. Lias, *Radiat. Res. Rev.*, **1**, 75 (1998).

(6) J. Y. Yang and F. M. Servedio, *Can. J. Chem.*, **46**, 338 (1968).

(7) J. Seibl and T. Gauman, *Helv. Chim. Acta*, **46**, 2857 (1963).

Table I: Photolysis of Cyclohexanone^a

	147.0 nm		123.6 nm		106.7 nm	
	None	Additive	None	Additive	None	Additive
	None	10% NO	None	10% NO	None	10% NO
CO	100 (0.91) ^b	100 (0.89) ^b	100 (0.60) ^b	100 (0.61) ^b	100 (0.42) ^b	100 (0.41) ^b
H ₂	29.9	22.9	62.0	31.5	91.0	nd
CH ₄	2.3	1.5	13.8	4.7	16.3	5.2
C ₂ H ₂	1.2	1.1	2.91	1.90	4.2	nd
C ₂ H ₄	52.6 (0.48) ^b	47.4 (0.42) ^b	97.1 (0.58) ^b	83.6 (0.51) ^b	100 (0.42) ^b	90.5 (0.37) ^b
C ₃ H ₆	2.9	0.1	4.24	<0.1	2.16	<0.5
C ₃ H ₈	9.65	6.6	17.2	10.0	9.16	6.57
C ₄ H ₈	2.9	0.25	3.25	<0.1	0.81	0.65
C ₄ H ₁₀	0.25	0.26	3.32	3.19	6.32	5.81
<i>c</i> -C ₃ H ₆	5.2	5.2	4.08	1.42	2.42	0.45
1-C ₄ H ₈	5.5	1.2	9.15	2.10	10.3	4.11
<i>n</i> -C ₄ H ₁₀	5.4	<0.1	1.16	<0.1	0.27	<0.1
<i>c</i> -C ₄ H ₈	0.64	<0.1	0.9	nd	0.85	0.52
1-C ₅ H ₁₀	21.7	9.1	4.31	0.23	2.45	0.43
<i>c</i> -C ₅ H ₁₀	32.4	22.8	2.14	0.74	0.85	0.70

^a Pressure, 2.0 Torr. ^b Quantum yield.

Table II: Photolyses of Cyclohexanone- α -d₄^a Isotopic Composition of Ethylene and Hydrogen

	Additive	% Distribution ^b						
		C ₂ H ₄	C ₂ H ₂ D ₂	C ₂ D ₄	Other	H ₂	HD	D ₂
147.0 nm	none	40.0	43.8	3.8	12.8	55.2	36.6	8.2
147.0 nm	10% NO	41.1	44.8	3.5	10.6	69.6	22.4	8.0
123.6 nm	none	38.8	46.7	3.0	12.5	55.3	37.2	7.5
123.6 nm	10% NO	39.4	49.6	3.2	7.8	71.5	24.0	4.5

^a Total pressure, 2 Torr. ^b The ethylene yields have been corrected for the insufficient deuteration of cyclohexanone- α -d₄. The hydrogen yields have not been corrected.

ments was 0.1%. In order to facilitate comparison, the product yields are all given relative to carbon monoxide. The quantum yields for the 123.6 and 106.7–104.8-nm photolyses were obtained from the measured ionization efficiencies of cyclohexanone, 0.24 ± 0.02 at both wavelengths, and from saturation currents measured during the course of the photolyses.⁵ The isotopic compositions of the ethylene and hydrogen formed when cyclohexanone- α -d₄ is photolyzed at 147.0 and 123.6 nm are reported in Table II. The isotopic compositions from the 106.7–104.8 nm photolyses were not determined because the low intensity of the argon lamp made accumulation of sufficient products for these analyses difficult.

In addition to the results reported in Tables I and II, the following observations were made. In high conversion, high pressure experiments, with as much as 1.5 atm N₂ added to 2.0 Torr of cyclohexanone, designed to determine whether 5-hexenal was a product, no 5-hexenal was ever detected even though the Poropak Q-S column used for this analysis is capable of detecting small amounts ($\phi = 0.03$) of 5-hexenal in the presence of large amounts of cyclohexanone. There was no attempt to measure other oxygen containing compounds.

When cyclohexanone was photolyzed at 147.0 nm in the presence of 2% ethylene, the yields of ethane, propane, and butane increased factors of 2.4, 1.9, and 3.5, respectively. The changes observed in the ratios total-C₃H₆:C₂H₄ and total-C₅H₁₀:C₂H₄ upon the addition of varying amounts of nitrogen to the 147.0-nm photolysis of 2 Torr of cyclohexanone are presented in Figure 1. The dependence of the ratios 1-C₃H₆:*c*-C₃H₆ and 1-C₅H₁₀:*c*-C₅H₁₀ upon the nitrogen pressure are presented in Figure 2. When 25% H₂S was added to cyclohexanone prior to photolysis, increases in the methane yields (CO = 100) to 20, 30, and 37 were observed at 147.0, 126.0, and 106.7–104.8 nm, respectively. When cyclohexanone- α -d₄ was photolyzed at 147.0 and 123.6 nm in the presence of 25% H₂S, at least 79 and 82% of the methane, respectively, contained at least two D atoms. When a mass spectrum was run of the entire reaction mixture from a high conversion (1%) 147.0-nm photolysis, a small peak was observed at *m/e* 112.

Discussion

The absence of 5-hexenal among the products even at high pressure suggests that although intramolecular

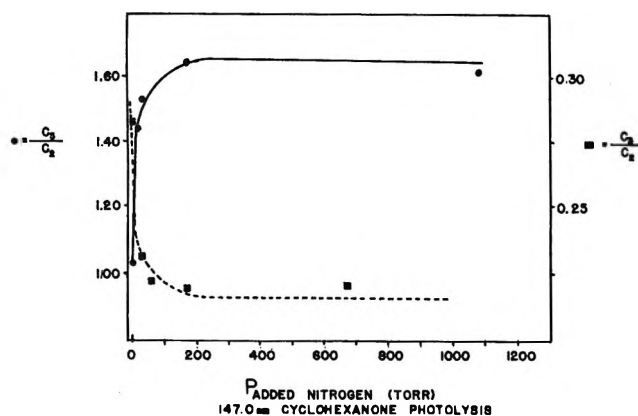


Figure 1. The dependence of the ratios total- $C_3H_6:C_2H_4$ and total- $C_5H_{10}:C_2H_4$ upon the pressure of added nitrogen at 147.0 nm.

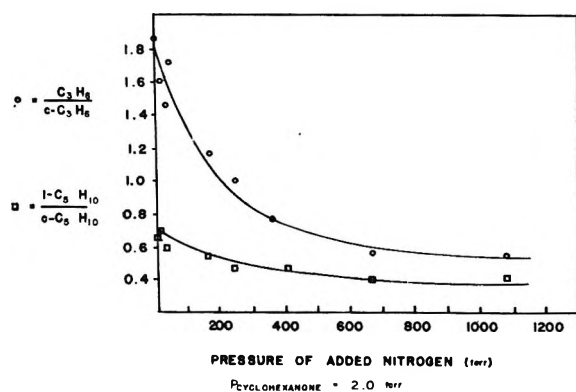
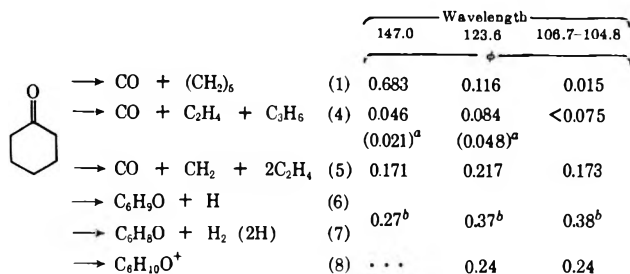


Figure 2. The dependence of the ratios 1- $C_3H_6:c-C_3H_6$ and 1- $C_5H_{10}:c-C_5H_{10}$ upon the pressure of added nitrogen at 147.0 nm.

hydrogen transfer, reaction 2, is an important process in the near-ultraviolet photolysis and liquid phase radiolysis of cyclohexanone, this reaction is characteristic of the low lying states which are formed in those systems. This is corroborated by Freeman's⁴ demonstration that the $n-\pi^*$ triplet is the state responsible for reaction 2 in the liquid phase radiolysis. The absence of 5-hexenal among the products may be taken as evidence that the $n-\pi^*$ triplet state is not populated in the vacuum ultraviolet photolysis of cyclohexanone.

Although the product yields reported in Table I make it immediately obvious that the vacuum ultraviolet photolysis of cyclohexanone is quite complex, it is possible to arrive at a reasonable mechanism for the photodecomposition of cyclohexanone on the bases of material balance, the effects of scavengers and inert gas upon product yields, and the isotopic composition of the ethylene and hydrogen produced in the photolyses of cyclohexanone- $\alpha-d_4$. The individual reactions along with the quantum yield assigned to each are given in Scheme I. Each reaction will be discussed in turn and the evidence for it cited. The mechanism for the 147.0-nm photolysis is considerably simpler and as a

Scheme I

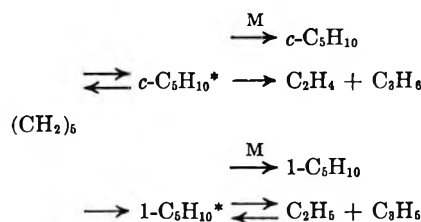


^a See text. ^b Hydrogen yield. Not quantum yield for reactions 6 and 7.

consequence better understood than the shorter wavelength photolyses.

At 147.0 nm reaction 1 is the major process occurring. The pentamethylene diradical which is produced undergoes a number of subsequent reactions which result in the observed products. These reactions are shown in Scheme II.

Scheme II



At 2 Torr the quantum yield of reaction 1 may be assigned according to equation I, which is based upon Scheme II, where $\phi_{C_2D_4}$ is the quantum yield for the production of C_2D_4 from the photolysis of

$$\phi_1 = \phi_{c-C_5H_{10}} + 5\phi_{C_2D_4} + \phi_{1-C_5H_{10}} + \phi_{\text{allyl}} \quad (I)$$

cyclohexanone- $\alpha-d_4$ and the coefficient 5 assumes that only one decomposition in five of cyclopentane-1,1,2,2- d_4 produces C_2D_4 , and ϕ_{allyl} is the estimated quantum yield of allyl radicals which do not re-form 1-pentene. The effect of nitric oxide on the product yields is quite revealing. Both the yields of cyclopentane and 1-pentene are reduced by the presence of nitric oxide. This suggests that the lifetime of the pentamethylene diradical is sufficiently long for it to undergo a few collisions at 2 Torr and be partially scavenged by nitric oxide. The observation of McKnight, Lee, and Rowland⁸ that oxygen scavenges the triplet trimethylene diradical produced by the addition of methylene to ethylene is consistent with this interpretation. The effect of nitric oxide on the 1-pentene yield is more pronounced than it is on the cyclopentane yield because although the secondary decomposition of cyclopentane is irreversible, the secondary decomposition

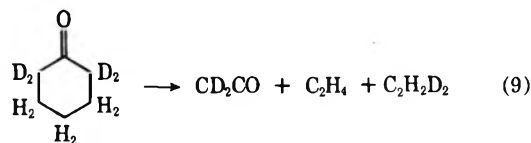
(8) C. McKnight, E. K. C. Lee, and F. S. Rowland, *J. Amer. Chem. Soc.*, **89**, 469 (1967).

of 1-pentene is reversible by virtue of the fact that the great majority of the 1-pentene undergoing secondary decomposition will produce ethyl and allyl radicals. A portion of these radicals in the absence of free radical scavengers will recombine to produce 1-pentene. It has been shown that 85% of the reactions of ethyl radicals with allyl radicals produce 1-pentene.⁹ Since the allyl radicals arise from 1-pentene decomposition, it is possible to assign the entire 1-pentene yield to reaction 1 despite the fact that it is quite sensitive to nitric oxide. In order to complete the assessment of ϕ_1 , it is only necessary to estimate the yield of allyl radicals (ϕ_{allyl}) which do not re-form 1-pentene.¹⁰

Figure 1 demonstrates that at 147.0 nm as little as 100 Torr of nitrogen is sufficient to quench all of the secondary decomposition of both *c*-C₅H₁₀ and 1-C₅H₁₀ to smaller molecules. The high pressure limits of both the C₅H₁₀:C₂H₄ and C₃H₆:C₂H₄ ratios are consistent with the quantum yields given in Scheme I. The values required for these ratios by Scheme I are 1.75 and 0.19, respectively. Figure 2 demonstrates that although 100 Torr of nitrogen is sufficient to quench the secondary decomposition of C₆H₁₀ to smaller molecules a considerably higher pressure (500 Torr) is required to quench the ring opening of excited cyclopentane back to the pentamethylene diradical. This is consistent with the expected higher energy of activation of the former fragmentation reaction. Although this effect might be the result of an energy dependence of the partitioning of the pentamethylene between the two alternate paths available, it seems that the difference in the energies of activation for cyclization and isomerization would be too small to account for the trend observed in Figure 2.¹¹ The dependence of the ratio 1-C₃H₆:*c*-C₃H₆ upon pressure indicates that at least one and probably both reaction 4 and the secondary decomposition of cyclopentane produce a trimethylene diradical which may either cyclize to cyclopropane or isomerize to propylene.

The maximum quantum yield for reaction 4 is estimated by taking the difference between the total C₃H₆ and C₃H₄ yields and the C₃H₆ yield which has been attributed to the secondary decomposition of cyclopentane. The quantum yields given in Scheme I for reaction 4 are maxima because some of the C₃H₆ is formed in free radical reactions. The values given in parentheses for ϕ_4 in Scheme I are the values calculated from the mechanism and the observed C₂H₂D₂:C₂H₄ from the photolysis of cyclohexanone- α -d₄ at 147.0 and 123.6 nm. The absolute values assigned to ϕ_4 are not as important as the conclusion that this reaction is quite unimportant at all wavelengths.

The ethylene yield which has not been accounted for by reactions 1 and 4 may be attributed to reaction 5. The mechanism presented thus far and the observed C₂H₂D₂:C₂H₄ ratios require that reaction 5 occurs as indicated in reaction 9 for cyclohexanone- α -d₄.



Although reaction 9 indicates the production of ketene, any ketene produced will certainly decompose to carbon monoxide and CD₂. When 25% H₂S was used as a trap for the methylene produced during photolysis, the yield of methane, which is the product of the reaction of methylene with large amounts of H₂S, was exactly that predicted by Scheme I at 147.0 nm, *i.e.*, $\phi_{\text{CH}_4} = 0.17$, while at 123.6 nm the yield of methane was only 64% of that predicted, *i.e.*, $\phi_{\text{CH}_4} = 0.14$. More important than the quantum yield of methane in these experiments however is the isotopic composition of the methane. The reaction of CD₂ with H₂S will produce CH₂D₂ while the corresponding reaction of CH₂ produces CH₄.^{12,13} In the photolysis of cyclohexanone- α -d₄ in the presence of H₂S the ratio CD₂H₂/CH₄ is 16 and 19 at 147.0 and 123.6 nm, respectively, indicating that the overwhelming majority of the methylene produced originates from the α -carbon atom. It is not possible for this effect to be the result of CD₂H radicals produced directly from the ketone because the methyl radical yield in the absence of H₂S is an order of magnitude too low to account for the CD₂H₂ yield.

In the absence of hydrogen sulfide the majority of the methylene produced probably inserts into the ketone which is the predominant species present. The decomposition of the vibrationally excited methylcyclohexanone is a potential source of the small number of methyl radicals present. Methyl radicals may also be produced by the abstraction of hydrogen by methylene. The observation of a peak at $m/e = M + 14$ in the mass spectrum of the entire reaction mixture after photolysis at 147.0 nm is an indication that some of the methylcyclohexanone produced in reaction 10

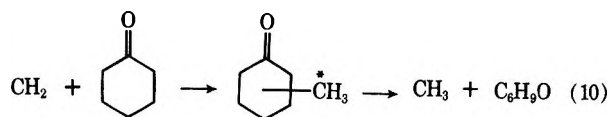
(9) D. G. L. James and D. E. Troughton, *Trans. Faraday Soc.*, **62**, 145 (1966).

(10) The calculation of ϕ_{allyl} is based upon an estimation of the ratio [C₂H₆]:[C₃H₆]. This ratio is obtained from the ratio [*n*-C₄H₁₀]:[1-C₅H₁₀] where [1-C₅H₁₀] is the yield of 1-pentene which can be attributed to recombination of ethyl and allyl radicals. It is assumed that the allyl radicals which do not react with ethyl radicals will mainly combine with each other to form 1,5-hexadiene (not measured). The yield of 1,5-hexadiene is estimated from the ratio [C₂H₆]:[C₃H₆] and the butane yield. The ratios [C₂H₆]:[C₃H₆] calculated in this way are 0.9, 0.9, and 0.17 at 147.0, 123.6, and 106.7-104.8, respectively. The value at 106.7-104.8 is obviously in error due to the large effect of small absolute errors on the ratio of two small numbers. The quantum yield of allyl radicals which do not form 1-pentene was then calculated from $\phi_{\text{allyl}} = 2 \times 1 \times \phi_{\text{butane}}$. Although this calculation is approximate, it provides a reasonable estimate of ϕ_{allyl} . The values for ϕ_{allyl} at 147.0, 123.6, and 106.7-104.8 are 0.10, 0.014, and 0.002, respectively.

(11) O'Neal and Benson have estimated the difference in the energies of activation for cyclization and isomerization of the trimethylene diradical to be only 1 kcal/mol: (a) H. E. O'Neal and S. W. Benson, *J. Phys. Chem.*, **72**, 1866 (1968).

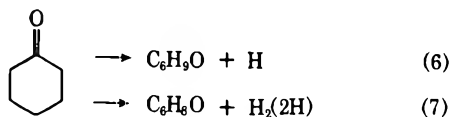
(12) P. Ausloos and S. G. Lias, *J. Chem. Phys.*, **44**, 521 (1966).

(13) A. A. Scala and P. Ausloos, *ibid.*, **47**, 5129 (1967).



does not decompose.

The probable source of hydrogen is the direct detachment of either a hydrogen atom or molecule as shown in reactions 6 and 7.



The effect of nitric oxide on the hydrogen yield and the isotopic composition of the hydrogen produced in the photolysis of cyclohexanone- α - d_4 indicates that a substantial part of the hydrogen is produced from hydrogen atoms. Based upon the assumption that the quantum yield for the disappearance of cyclohexanone is approximately one and upon material balance considerations as well as the measured quantum yields of carbon monoxide it can be seen that the divergence of the carbon monoxide yield from unity is paralleled by an increase in the hydrogen yield. Consequently it can be concluded that reactions 6 and 7 are the principal reactions which do not produce carbon monoxide and that these reactions become more important as the incident energy increases. Similar observations have been made in the vacuum ultraviolet photolyses of 2- and 3-pentanone¹⁴ and 3-methyl-2-butanone.¹⁵

The mechanism for the 147.0-nm photolysis is quite simple as shown in Scheme I and consequently allows some further conclusions to be drawn. Since reaction 5 produces methylene almost exclusively from the α -carbon atom, it probably results from acyl cleavage followed by α - β carbon-carbon cleavage to produce ketene and a tetramethylene diradical most of which subsequently decomposes to two molecules of ethylene. This net reaction probably does not occur by the same reactions in the reversed sequence because of the expected indiscriminate nature of σ -cleavage and the small quantum yield attributed to reaction 4, which may arise from initial β - γ σ -cleavage. The mechanism indicates that the predominant reaction path for cyclohexanone irradiated at 147.0 nm is acyl cleavage.¹⁶ This observation confirms the assignment of the 150 nm absorption band of ketones to the π - π^* transition.¹⁷

At 123.6 and 106.7–104.8 the mechanism is quite complex and not as easily interpreted. The increase in the hydrogen yields and the lesser importance of acyl cleavage at these energies may be due to the pop-

ulation of a C-H σ - σ^* states. Ionic reactions may also contribute to the production of hydrogen. Even at 106.7–104.8 nm the parent ion produced with a quantum yield of 0.24 will not contain enough energy to undergo a fragmentation reaction. Therefore the ionized ketone will either undergo neutralization or perhaps a proton transfer to a neutral ketone molecule.¹⁸ If neutralization of either the parent ion or the protonated ketone is homogenous, then it is possible that hydrogen will be produced. If on the other hand the neutralization occurs at the wall, it is conceivable that no observable products would be formed.

The acetylene and allene produced in the photolysis of cyclohexanone probably result from the secondary decomposition of vibrationally excited C_2H_4 and C_3H_6 . The origins of the remaining products are clearly free radicals. Ethyl radicals probably result from hydrogen atom addition to ethylene, while methyl radicals result from reaction 10.

Diradicals of structure $(\text{CH}_2)_n$ ($n = 1, 3, 4, 5$) have been found to be significant intermediates in the interpretation of the gas phase vacuum ultraviolet photolysis of cyclohexanone. The versatility of these polymethylene diradicals has been pointed out by Benson¹⁹ who has interpreted the thermal isomerization of cyclopropane in terms of a trimethylene diradical intermediate. Indeed, Benson has interpreted a large number of reactions of cyclic molecules, both qualitatively and quantitatively in terms of diradical intermediates.²⁰ The recent literature makes it abundantly clear that polymethylene diradicals are intermediates in a large number of reactions.²¹ The preponderance of acyl cleavage at 147.0 nm indicates that energy deposition in cyclohexanone occurs mainly at the carbonyl group.

(14) A. A. Scala and P. Ausloos, *J. Phys. Chem.*, **70**, 260 (1966).

(15) A. A. Scala, *ibid.*, **74**, 2639 (1970).

(16) We have made a similar observation in the 147.0-nm photolysis of cyclopentanone.

(17) H. L. McMurry, *J. Chem. Phys.*, **9**, 231 (1941).

(18) Two other conceivable ionic reactions of the parent ion are H_2 and H_2^- transfer. It is impossible to evaluate the importance of these reactions at this time.

(19) S. W. Benson, *J. Chem. Phys.*, **34**, 521 (1961).

(20) H. E. O'Neal and S. W. Benson, *J. Phys. Chem.*, **72**, 1866 (1968).

(21) (a) O. P. Strausz, P. J. Kozak, G. N. C. Woodall, A. G. Sherwood, and H. E. Gunning, *Can. J. Chem.*, **46**, 1317 (1968); (b) G. R. DeMare, L. G. Walker, O. P. Strausz, and H. E. Gunning, *ibid.*, **44**, 457 (1966); (c) E. G. Spittler and G. W. Klein, *J. Phys. Chem.*, **72**, 1432 (1968); (d) P. Ausloos, R. E. Rebert, and S. G. Lias, *ibid.*, **72**, 3904 (1968); (e) A. A. Scala and P. Ausloos, *J. Chem. Phys.*, **49**, 2282 (1968); (f) R. J. Cvetanovic, H. E. Avery, and R. S. Irvin, *ibid.*, **46**, 1993 (1967); (g) P. Dowd and K. Sachder, *J. Amer. Chem. Soc.*, **89**, 715 (1967).

Exchange Mechanism and Arrhenius Parameters of Elementary Steps in the Reactions of Hydrogen Atoms with Water Vapor in Irradiated Mixtures of Hydrogen and Water Vapor

by N. E. Bibler and R. F. Firestone*

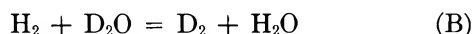
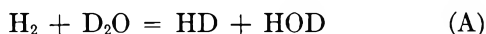
Department of Chemistry, The Ohio State University, Columbus, Ohio 43210 (Received September 7, 1971)

Publication costs assisted by The Ohio State University

Efficiencies of the ionizing radiation induced exchange reactions, $H_2 + D_2O = HD + HOD$ and $H_2 + D_2O = D_2 + H_2O$, have been measured at 84–381°. $G(HD)$ is equal to 13.1 ± 0.3 molecules/100 eV and is independent of temperature, under conditions employed, in the range 114–150°. At higher temperatures HD is formed by a chain reaction propagated by $H + D_2O \rightarrow HD + OD$ and $H + D_2O \rightarrow HOD + D$ at comparable rates, and D_2 is formed by $H + D_2O \rightarrow D_2 + OH$ at a much slower rate at 213–381°. Activation energies and relative frequency factors for these elementary steps and for $D + D_2O \rightarrow D_2 + OD$ have been evaluated.

Introduction

Previous investigations of the ionizing radiation induced exchange between hydrogen and water vapor have shown that the rate of exchange is directly proportional to radiation intensity (dose rate) and is generally dependent upon (D_2O-H_2) or (H_2O-D_2) and upon temperature,^{1,2} but that the efficiency of exchange, $G(HD)$ molecules/100 eV, is independent of dose rate, temperature and the mole fraction of hydrogen over an appreciable range of values of these parameters in reaction vessels of ordinary size (0.1–5.1).^{1,2} It has also been shown that $G(HD)$ increases rapidly in H_2O-D_2 mixtures as the reaction temperature is increased beyond this region of constancy, because of the onset and acceleration of a chain reaction propagated by reactions of D atoms with H_2O .² This article is a report of results of an extension of the previous investigation² to D_2O-H_2 mixtures over a wider range of temperatures and with special emphasis on effects of $(D_2O)-(H_2)$, vapor density and temperature on the efficiencies of overall exchange reactions, A and B



in the chain reaction region established by these parameters.

In the region of constancy $G(HD)$ is a measure of the yield of hydrogen atoms from the direct radiolysis of water vapor, G_D or G_H , and its value is, accordingly, a matter of great interest and some significance in radiation chemistry, *per se*. The observation that alternative methods used to measure G_D or G_H from heavy and light water vapor, respectively, provide estimated values which differ substantially from the exchange yield in the region of constancy is, accordingly, also a matter

of great interest, which has been discussed at some length in a recent review article.³ We have chosen to restrict our attention in this article to interpretation of the behavior of the exchange systems, D_2O-H_2 and H_2O-D_2 , without further direct reference to this question, because we have no new data which bear directly on it and have nothing original to say about it at this time. We present, instead, a rationale for our conclusion that hydrogen atoms are the only immediate precursors of HD. In addition, and at least as significantly, values of the Arrhenius parameters of several competing and parallel elementary steps which are shown to be responsible for exchange reactions, A and B, in the temperature range 218–381° are estimated.

Experimental Section

Reagents. Tritiated water (TOD), deuterium oxide mixtures were prepared by quantitative oxidation of gaseous mixtures of carrier-free tritium (O.R.N.L.) and 98.5 D atom % hydrogen (Matheson Co.) over CuO at 400°, following passage of the T_2 , D_2 mixtures through a heated palladium thimble. The high specific activity water so obtained was diluted for use with carefully purified⁴ deuterium oxide generously provided by Dr. E. J. Hart of The Argonne National Laboratory. High purity protium (H_2) (0.03 mol % N_2 , 0.005 mol % CO_2) and carbon monoxide (0.02 mol % H_2 , 0.1 mol % CO_2 , 0.0004 mol % O_2) were purchased from The Matheson Co. in break-seal Pyrex vessels and were used without further purification. Hydrogen deuteride purchased

(1) J. H. Baxendale and G. P. Gilbert, *J. Amer. Chem. Soc.*, **86**, 516 (1964).

(2) R. F. Firestone, *ibid.*, **79**, 5593 (1957).

(3) R. S. Dixon, *Radiat. Res. Rev.*, **2**, 237 (1970).

(4) E. J. Hart, S. Gordon, and D. A. Hutchison, *J. Amer. Chem. Soc.*, **75**, 6165 (1953).

from Merck, Sharpe, and Dohme of Montreal (98 atom % D) was employed for preparation of calibration mixtures for the mass spectrometer.

Dosimetry. The specific activity of TOD, DOD reactant mixtures was determined by (a) quantitative conversion of carefully measured liquid aliquots to gaseous hydrogen over hot metallic zinc employing the method of Graff and Rittenberg,⁵ (b) introduction of the gaseous hydrogen so obtained into a 300 cm³ cylindrical (7.7 cm length) ionization chamber, (c) addition of high purity N₂ to bring the contents of the chamber to atmospheric pressure, and (d) measurement of the voltage drop produced by passage of the saturation ionization current through a calibrated ($\pm 1\%$) resistance. The specific activity of reactant water was found to be 19.9 ± 0.4 C/mol, assuming an average β -particle energy equal to 5.69×10^3 eV⁶ and that 34.9 eV are required on the average to form an ion pair in dry N₂.⁷ At all vapor densities and in all reaction vessels employed in this work it is apparent that in excess of 99% of the energy of the tritium β -particles is absorbed by water vapor molecules.⁸ Thus, allowing for an uncertainty of 0.2% in measurement of the quantities of reactant water introduced to each reaction vessel, the energy absorbed by the reaction system is determined with a precision essentially equal to that obtainable in the specific activity measurements. The most likely source of systematic error in the latter is inadvertent dilution by traces of light water in the zinc reactor tube which are not removable by exhaustive baking and pumping prior to admission of TOD-DOD aliquots. Mass spectrometric analysis of hydrogen produced by reduction of TOD-DOD aliquots in the zinc reactor permits us to set an upper limit of 5 atom % protium, corresponding to a possible maximum absolute negative error of 5% in dosimetry.

Preparation of Reaction Vessels and Reaction Mixtures. The procedure employed for preparation of reaction vessels and of reaction mixtures was identical with that described previously.² Reaction vessels were spherical Pyrex flasks equipped with a breakseal tube for removal of products and unconsumed reactants and with a biaxially centered thermocouple well and of an average internal volume of 270 cm³. Reaction temperatures were maintained within $\pm 1\%$ on the centigrade scale by immersing the reaction vessels in a constant temperature fluidized sand bath.

Analysis of Samples. Relative quantities of HD, D₂, and H₂ produced by reactions of TOD-DOD-H₂ mixtures were determined with the aid of a Consolidated 21-620 mass spectrometer equipped with an isotope ratio accessory. The mass spectrometer was calibrated with each use by means of synthetic mixtures of appropriate composition. Absolute yields of HD and D₂ are based upon measured ratios of the several isotopic forms and the total quantities of hydrogen recovered from reaction mixtures by previously described meth-

ods.² HD:H₂ ratios were reproducible within an average extreme deviation among successive aliquots of $\pm 2\%$ at ratios in the range 0.02-0.30, and D₂-HD ratios were determined within an average extreme deviation of $\pm 7\%$ at ratios in the range 0.02-0.05. D₂:H₂ ratios employed in computing $G(D_2)$ values were obtained from the product of the HD:H₂ and D₂:HD ratios for each sample. Measured D₂:H₂ values lay in the range 10^{-4} to 10^{-2} and were equal from sample to sample to computed values within $\pm 7\%$ on the average, but with a markedly higher relative frequency of occurrence of greater than average deviations than among D₂:HD values. Gaseous products of TOD-DOD-CO mixtures which are noncondensable at -196° (D₂-CO-CH₄) were determined quantitatively by gas-solid chromatography on $1/4$ in, 8 ft silica gel columns. CO₂:CO ratios of the gaseous fraction noncondensable at -78° were measured mass spectrometrically. The specific activity of tritium in gaseous products was determined by ionization chamber measurements as described above in the section concerning dosimetry.

Results

Exchange Yields in TOD-DOD-H₂ Mixtures. Table I presents 100-eV yields of HD and of D₂ formed by irradiating gaseous mixtures of TOD, DOD and H₂ with H³ β -particles at temperatures from 84 to 381 $^\circ$, at water vapor densities from 0.239 mg/cm³ to 1.07 mg/cm³, and at protium concentrations in the range 0.121 mol % to 1.05 mol %. Data indicating radiation dose, fraction of protium converted, and dose rate are also included in Table I. Previous work demonstrated a lack of sensitivity of exchange yields in TOH-HOH-D₂ mixtures to modest variations in dose rate under all conditions employed.² Similarly, we find no evidence suggesting that either $G(\text{HD})$ or $G(D_2)$ are dependent upon dose rate in the narrow range investigated (3×10^{17} to 1×10^{18} eV/l. min).

Figure 1 demonstrates that $G(\text{HD})$ is independent of temperature within experimental uncertainty at lower temperatures in the range explored, but that this plateau region extends to higher temperatures in heavy-water vapor than in light-water at similar water:hydrogen ratios and that its extent is greater at lesser water vapor densities and is independent of the water:hydrogen ratio. The plateau value of $G(\text{HD})$ from heavy water vapor, 13.1 ± 0.3 molecules/100 eV, is equal within experimental errors to that obtained with light water vapor. This conclusion is a consequence of a recent and more reliable measurement of W_{CH} (27.0 eV/ion pair)⁷ than that previously used to calculate dose rates in H₂O-D₂ experiments based upon ion cur-

(5) J. Graff and D. Rittenberg, *Anal. Chem.*, **24**, 878 (1952).

(6) W. L. Pillinger, J. J. Hentges, and J. A. Blair, *Phys. Rev.*, **121**, 232 (1961).

(7) W. P. Jesse and J. Sadauskis, *ibid.*, **97**, 1668 (1955).

(8) L. M. Dorfman, *Phys. Rev.*, **95**, 393 (1954).

Table I: 100-eV Yields of HD and of D₂ from TOD-DOD-H Mixtures

Expt no.	T, °C	10 ⁻¹⁸ Dose, eV/g	Vapor density, mg/ml	Mol % H ₂	% Convn of H ₂	Molecules/100 eV	
						G(HD)	G(D ₂)
14	84	10.3	0.308	0.121	3.59	10.8	1.0
17	85	5.92	0.239	0.159	1.94	10.2	0.7
11	95	6.48	0.455	0.827	1.99	9.6	0.7
19	99	8.04	0.544	0.684	3.03	11.7	0.6
7	105	7.94	0.632	0.585	2.77	10.7	...
12	110	18.9	0.649	0.573	7.52	12.2	0.7
6	114	10.3	0.717	0.521	4.42	13.3	...
8	125	11.9	0.617	0.610	5.17	13.5	1.2
5	126	18.4	0.677	0.566	7.68	13.2	0.6
9	134	13.2	1.07	0.350	5.54	13.0	0.6
20	137	8.33	0.629	0.599	3.60	13.5	0.9
22	143	11.4	0.582	0.640	5.40	14.6	...
21	150	15.8	0.629	0.602	6.49	12.9	0.7
25	168	9.56	0.709	0.535	4.66	15.1	0.5
27	184	9.09	0.379	0.978	4.54	15.4	0.5
35	184	28.4	0.620	0.738	11.9	15.1	0.7
29	224	8.93	0.603	0.364	8.18	16.5	0.8
30	245	5.07	0.575	0.368	5.40	19.2	0.5
33	266	2.02	0.593	0.736	1.76	31.6	1.6
32	281	2.55	0.590	0.737	3.85	54.4	1.4
34	296	1.51	0.586	0.741	3.50	83.3	2.1
49	297	2.61	0.318	0.637	5.77	37.2	1.2
38	304	1.24	0.600	0.709	4.32	123	2.4
41	311	1.39	0.590	0.690	5.23	127	2.4
55	313	1.45	0.699	0.693	5.05	164	4.1
47	319	1.30	0.320	0.630	4.86	63.1	2.1
48	319	2.85	0.319	1.89	3.82	67.3	1.7
53	319	1.09	0.319	0.503	...	61.0 ^b	...
39	319	0.491	0.595	0.700	2.13	150	2.6
54	321	1.35	0.458	0.711	4.91	98.1	2.3
43	322	0.733	0.590	1.05	2.39	166	3.3
36	330	1.45	0.609	0.710	7.49	185	4.5
51	360	0.0510	0.318	0.632	4.68	155	3.9
52	381	0.383	0.320	0.632	5.41	237	8.2

^a The dose rate (eV/l. min) may be computed by multiplying the vapor density (mg/ml) by the factor 1.26×10^{18} . ^b Calculated from $G(\text{HT})$.

rent measurements in methane-hydrogen mixtures.² Corrected $G(\text{HD})$ values for the H₂O-D₂ system appear in Figure 1. $G(\text{D}_2)$ also exhibits a plateau region as a function of temperature and a dependence upon water vapor concentration at $T > 200^\circ$ similar to that exhibited by $G(\text{HD})$. We find an average of selected plateau values for $G(\text{D}_2)$ equal to 0.7 ± 0.1 molecules/100 eV in agreement with that reported previously.¹ Beyond approximately 200° both $G(\text{HD})$ and $G(\text{D}_2)$ increase abruptly with increasing temperature to values large enough to demonstrate occurrence of a thermal chain mechanism for exchange similar to that observed in light water vapor mixtures with D₂.²

No dependence of $G(\text{HD})$ or of $G(\text{D}_2)$ upon water vapor density is apparent in the plateau region, but data presented in Table I and Figure 1 demonstrate a strong dependence at 319° in the thermal chain region, independently of H₂ concentration. Figure 2 demonstrates

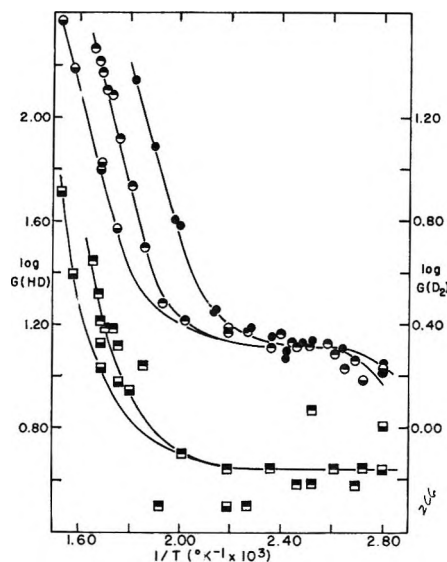


Figure 1. Variation of $\log G(\text{HD})$ and $\log G(\text{D}_2)$ with respect to temperature and water vapor density. Key: ●, $G(\text{HD})$ from H₂O-D₂, vapor density = 0.774 mg/cm³; ○, $G(\text{HD})$ from D₂O-H₂, vapor density = 0.586–0.609 mg/cm³; ○, $G(\text{HD})$ from D₂O-H₂, vapor density = 0.318–0.320 mg/cm³; □, $G(\text{D}_2)$ from D₂O-H₂, vapor density = 0.586–0.609 mg/cm³; □, $G(\text{D}_2)$ from D₂O-H₂, vapor density = 0.318–0.320 mg/cm³.

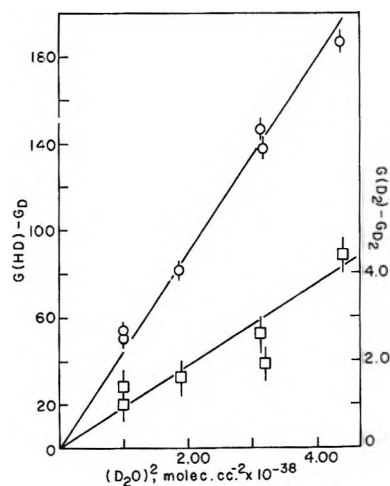


Figure 2. Variation of $G(\text{HD})$ and $G(\text{D}_2)$ from D₂O-H₂ with respect to the second power of the water vapor density at 319° . Key: ○, $G(\text{HD}) - G_{\text{D}_1}$; □, $G(\text{D}_2) - G_{\text{D}_2}$.

that the thermal chain contributions, $[G(\text{HD}) - G_{\text{D}_1}]$ and $[G(\text{D}_2) - G_{\text{D}_2}]$, are directly proportional to the second power of the water vapor concentration.

Figure 3 shows that HD is formed by a thermal chain reaction with an apparent activation energy of 19.2 ± 0.5 kcal/mol at D₂O concentrations equal to 0.016 and 0.030 M, that D₂ is formed by a thermal chain reaction with an activation energy equal to 21 ± 1 kcal/mol at the same vapor densities, and that HD is formed in H₂O-D₂ mixtures with an activation energy equal to 19 ± 1 kcal/mol at a light water concentration of

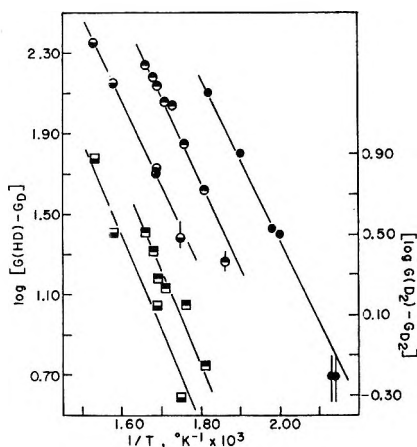


Figure 3. Arrhenius plots of the chain contributions to formation of HD and D₂. Key: ●, $G(\text{HD}) - G_{\text{H}}$ from H₂O-D₂, vapor density = 0.774 mg/cm³; ○, $G(\text{HD}) - G_{\text{D}}$ from D₂O-H₂, vapor density = 0.586-0.609 mg/cm³; ◐, $G(\text{HD}) - G_{\text{D}}$ from D₂O-H₂, vapor density = 0.318-0.320 mg/cm³; ▤, $G(\text{D}_2) - G_{\text{D}_2}$ from D₂O-H₂, vapor density = 0.586-0.609 mg/cm³; ▥, $G(\text{D}_2) - G_{\text{D}_2}$ from D₂O-H₂, vapor density = 0.318-0.320 mg/cm³.

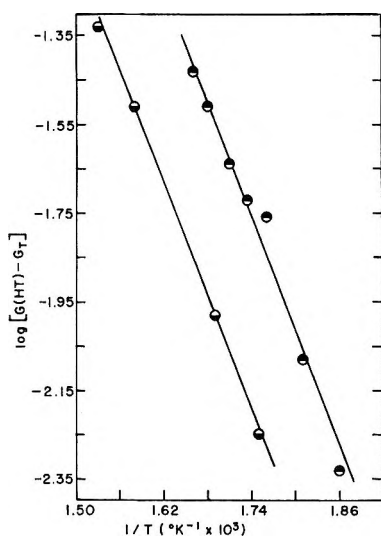


Figure 4. Arrhenius plots of the chain contributions to formation of HT in D₂O-H₂ mixtures. Key: ●, $G(\text{HT}) - G_{\text{T}}$, vapor density = 0.586-0.609 mg/cm³; ○, $G(\text{HT}) - G_{\text{T}}$, vapor density = 0.318-0.320 mg/cm³.

0.043 *M*. Figure 4 shows that HT is formed with an activation energy equal to 19.2 ± 0.5 kcal/mol at 0.016 *M* and 0.030 *M* heavy water. It is apparent that isotope effects on the activation energies for HD and DT formation in D₂O-HD and for HD formation in H₂O-D₂ are negligible within several tenths of 1 kcal/mol.

Product Yields from TOD, DOD, CO Mixtures. The presence of CO at approximately 1 mol % and higher concentrations in irradiated D₂O leads principally to formation of CO₂ and D₂ and to formation of a variety of partially deuterated minor organic products at temperatures below 218°. The data of Table II demon-

Table II: 100-eV Yields from Gaseous TOD-D₂O-CO Mixtures

Vapor density, mg cm ⁻³	Dose, eV/g × 10 ⁻¹⁹	Mol % CO	100-eV yields, molecules/100 eV			
<i>T</i> , °C			CO ₂	D ₂	Methane	DT
0.544	213	6.70	1.51	9	<i>a</i>	<i>a</i>
0.548	215	5.46	1.59	<i>a</i>	7	<i>a</i>
0.556	217	6.88	3.42	<i>a</i>	8.0 ^b	<i>a</i>
0.556	215	6.80	5.03	7	8.2	0.60
0.558	218	6.76	6.47	12	10	0.64
0.563	278	3.40	1.61	31	32	0.06
0.554	319	1.33	1.63	93	95	0.00

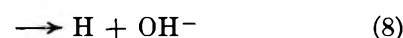
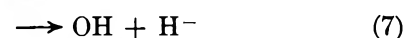
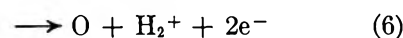
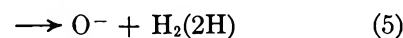
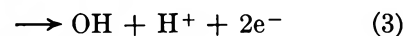
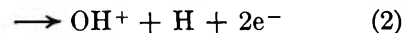
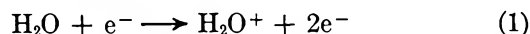
^a Presence detected, but not determined quantitatively.

^b Yield calculated from $G(\text{D}_2) = 2.6(\pm 0.2) \times 10^3 G(\text{DT})$ as in experiments 4, 6, 7 and 8.

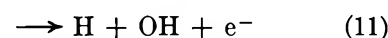
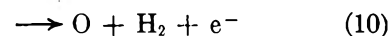
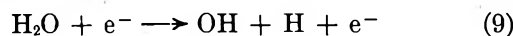
strate that $G(\text{CO}_2)$ and $G(\text{D}_2)$ increase abruptly with increasing temperature in the vicinity of 218° and that they are formed at equal rates by a thermal chain mechanism above 218°. Organic fragments tend to vanish from the mass spectrum of the gaseous products at higher temperatures as reflected by the sharp decrease in $G(\text{methane})$ between 218 and 319° shown in Table II.

Discussion

Evidence demonstrating or strongly suggesting the occurrence of the following ion forming electron impact processes in water vapor has been observed with 60-100 eV electrons at pressures up to about 10⁻⁵ Torr.^{4,9}

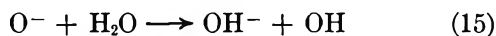
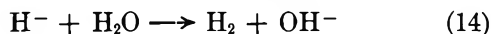
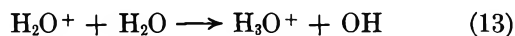


Unimolecular decomposition of excited water molecules produces neutral fragments by means of the following steps under the same conditions.⁹

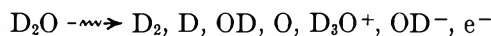


Ion-molecule reactions known to occur in pure water vapor are³

(9) C. E. Melton, *J. Phys. Chem.*, **74**, 582 (1970).

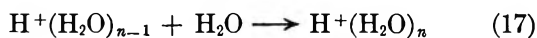


Reactions 13–16 are very efficient at thermal ion energies. Thus, the immediate result of electron impact and rapid secondary reactions in heavy-water vapor is summarized qualitatively, as follows

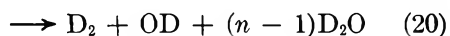
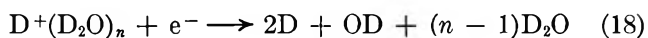


wherein the abundance of OD^- relative to other charged fragments is negligibly small.⁹

The fate of D_3O^+ may be either neutralization or hydration to form $\text{D}^+(\text{D}_2\text{O})_2$. Formation of neutral molecule clusters about the proton have been observed by several groups,^{10–14} and cluster equilibria appear likely to be established very rapidly, indeed, at water vapor pressures in the vicinity of 1 atm. Each of the successive equilibrium steps is reported to be exothermic through $n = 8$ or thereabouts.^{11–14}



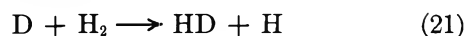
Assuming any reasonable high pressure limiting value for the second order neutralization coefficient and estimating a value of the order $10^{-8} \text{ cm}^3 \text{ molecule}^{-1} \text{ sec}^{-1}$ for the second order rate constant for formation of $\text{H}^+(\text{H}_2\text{O})_2$ in the high pressure limit,¹⁵ it is clear that neutralization is many orders of magnitude slower than cluster formation for H_3O^+ (or D_3O^+) at water vapor densities and dose rates employed in the present work. It is likely that the entire set of positive ion cluster equilibria is established without interference from neutralization steps. It follows that the neutralization steps may be represented by reactions 18–20.



Reaction 20 can occur only at very low relative frequency, because the yield of D_2 is small relative to that of HD in the presence of protium under all conditions of temperature, dose rate, vapor density, and protium concentration employed and may also be formed wholly or in part by one or all of reactions 4, 10, and 14, as well as by successive conversion of HD. The net result of electron impact steps, rapid secondary reactions, and neutralization reactions appears to be simply, $\text{D}_2\text{O} \xrightarrow{\text{e}^-} \text{D}_2, \text{D}, \text{OD}$, neglecting the small yield of O atoms formed in primary events in very low yield and by reaction 16; $G(\text{O}) \leq 0.6 \text{ atoms}/100 \text{ eV}$.^{3,9}

Mechanism for HD Formation in the Thermal Plateau Region. The lowest temperature at which $G(\text{HD})$ becomes independent of temperature in $\text{D}_2\text{O}-\text{H}_2$ mixtures

is determined by competition between reaction 21 and loss of D atoms to radical combination steps.



Under conditions employed in this and previous work³ the HD yield plateau begins at approximately 110° in both $\text{D}_2\text{O}-\text{H}_2$ and $\text{H}_2\text{O}-\text{D}_2$ mixtures. Under the same conditions the range over which $G(\text{HD})$ remains independent of temperature is determined by competition between first order removal of H atoms at the walls of the reaction vessel in $\text{D}_2\text{O}-\text{H}_2$ mixtures (loss of D atoms to the walls in $\text{H}_2\text{O}-\text{D}_2$)² and thermally activated reactions of hydrogen atoms with water molecules which lead to chain formation of HD by means discussed below. In the plateau region it is, therefore, apparent that the hydrogen additive effectively "counts" D atoms and, perhaps, other precursors of HD and that it does so at mole fractions of the order 10^{-3} . Figure 1 illustrates the observation that $G(\text{HD})$ in the plateau region is equal to $13.1 \pm 0.3 \text{ molecules}/100 \text{ eV}$ (average deviation from the mean) in both $\text{D}_2\text{O}-\text{H}_2$ and $\text{H}_2\text{O}-\text{D}_2$ mixtures, independently of water vapor density, dose rate and temperature. The average plateau yield may be up to 4 percent larger in $\text{D}_2\text{O}-\text{H}_2$ mixtures. This is within the limits of precision of measurement, but may be a reflection of the slightly greater ionization efficiency of D_2O observed by Jesse.¹⁶

In the absence of compelling evidence to the contrary it is reasonable to assume that the immediate precursor of HD in the plateau region as well as at higher temperatures is the hydrogen atom. The magnitude of the plateau yield of HD suggests, however, an efficiency of utilization of electron kinetic energy for hydrogen atom production which is difficult to rationalize on the basis of current knowledge of the excited states of water and the behavior of electrons and other species known to be present in irradiated water vapor. The yield of hydrogen atoms from neutralization events must lie in the range $100/W-200/W \text{ atoms}/100 \text{ eV}$ (~ 3 to ~ 7) depending upon the relative frequencies of reactions 18 and 19. Available data^{11–13} indicate that reaction 18 is endoergic for thermal electrons at 300°K for clusters of $n > 3$. Estimated standard free energies for ion cluster formation^{11–13} indicate that less than one positive ion cluster per thousand in homogeneous equilibrium has $n \leq 3$ at water vapor densities used in this and

(10) P. F. Knewstubb and A. W. Tickner, *Proc. Roy. Soc. Ser. A*, **255**, 520 (1960).

(11) P. Kebarle, S. K. Searles, A. Zolla, J. Scarborough, and M. Arshadi, *J. Amer. Chem. Soc.*, **89**, 6393 (1967).

(12) D. P. Beggs and F. H. Field, *ibid.*, **93**, 1567 (1971).

(13) D. P. Beggs and F. H. Field, *ibid.*, **93**, 1576 (1971).

(14) M. DePaz, J. J. Leventhal, and L. Friedman, *J. Chem. Phys.*, **51**, 3748 (1969).

(15) A. Good, P. A. Durden, and P. Kebarle, *ibid.*, **52**, 212 (1970).

(16) W. P. Jesse, *ibid.*, **41**, 2060 (1964).

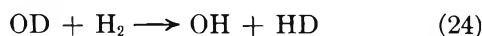
previous work in the middle of the plateau region (400°K), assuming that the enthalpies of formation do not become markedly more positive between 300 and 400°K. Conservation of energy and available information concerning the appearance potentials of positive ions and the energy levels of excited states of water molecules^{17,18} including triplet states^{18,19} appear to preclude the possibility that $G(\text{HD})$ can be as large as 13 molecules/100 eV unless (i) the yield of HD from neutralization events and electron attachment processes is significantly greater than $100/W$, (ii) an immediate precursor other than the hydrogen atom is responsible for a significant fraction of the HD yield, and/or (iii) mechanisms which produce more than one HD molecule per D atom contribute significantly. We first examine the latter two of these possibilities.

The possibility that HD has an immediate ionic precursor, *i.e.*, D_2O^+ or $\text{D}^+(\text{D}_2\text{O})_n$, is readily dismissed. A fast reaction of D_2O^+ with H_2 is most improbable, because of the low relative abundance of H_2 and near equality of the rate constants for reactions 13 and 23.^{20,21}



The apparent enthalpies of successive cluster forming steps become independent of the total energy of the hydronium ion beyond $n = 4$, at very low pressure,¹² and the clustering steps are very fast below $n = 4$, indicating that clustering and thermal equilibration processes will predominate over interactions with H_2 , which might otherwise be possible. Thus, the possibility that D_3O^+ or $\text{D}^+(\text{D}_2\text{O})_n$, which may be formed with up to 23 kcal/mol of excitation energy¹²⁻¹⁴ depending upon the value of n , may utilize this energy to exchange with H_2 before thermal equilibration can also be ruled out at high water vapor densities.

The possibility that HD has an immediate thermalized neutral precursor other than the D atom can also be dismissed, because OD is the only alternative neutral fragment of appreciable abundance. If OD were able to form HD by reaction with H_2



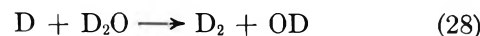
in competition with reaction 22, $G(\text{HD})$ would exceed G_{D} by the factor $k_{24}/(k_{24} + k_{22})$ in the plateau region. It is firmly established, however, that reaction 22 has a large frequency factor (10^{-11} cm³ molecule⁻¹ sec⁻¹) and a low activation energy (4.0 kcal/mol) and that it proceeds 100–1000 times as efficiently at 400°K as reaction 21.²² Reaction 24 would appear, *a priori*, to be much less efficient on the ground that it must proceed through a four-center intermediate structure, placing it in a class of elementary reaction for which there is little solid evidence and which, if they occur, require very much higher thermal activation energies than reaction 22.²⁵⁻²⁸

The possibility that HD has an immediate excited neutral precursor, such as D_2O^* , which is not a precursor of D atoms and which may exchange directly with H_2 , requires a cross section for collision induced de-excitation relative to that for exchange which seems unrealistically small, because $G(\text{HD})$ is independent of the mole fraction of H_2 above, at most, 0.004 at 400°K and because the requirements of direct bimolecular exchange are not likely to be "energetically modest" relative to H atom abstraction, as has been suggested.²³ The only such species which is, therefore, seemingly possible is a low lying triplet state molecule which is anomalously stable with respect to collision induced intersystem crossing and dissociation, because direct exchange between H_2 and a triplet state water molecule must violate the Wigner spin conservation rule. The possibility that HD has an immediate precursor (ionic, neutral, excited or thermalized) other than the hydrogen atom has no evidence in its favor and seems, in summary, to be slight.

Two schemes by means of which a hydrogen atom may form more than one HD molecule have been proposed. Santar and Bednar²³ have suggested a chain type exchange mechanism initiated by electronically excited hydrogen atoms and propagated by translationally hot hydrogen atoms, *viz.*



wherein chain termination would be effected by thermalization of the species H' and D' . This scheme is highly unlikely under our experimental conditions. A translationally hot D atom cannot reasonably be expected to run a gauntlet of several thousand collisions with D_2O while retaining in excess of 24 kcal/mol of translational energy and failing to be removed by reaction 28 (see discussion of thermal chain region below)



Johnson has proposed²⁴ that $G(\text{HD})$ in the plateau region may exceed G_{D} as a result of the use of vibrational energy made available by hydrogen atom combination

(17) F. Fiquet-Fayard, *J. Chim. Phys.*, **57**, 453 (1960).

(18) L. M. Hunter, D. Lewis and W. H. Hamill, *J. Chem. Phys.*, **52**, 1733 (1970).

(19) R. N. Compton, R. H. Heubner, P. W. Reinhardt and L. B. Christophorou, *ibid.*, **48**, 901 (1968).

(20) S. K. Gupta, E. G. Jones, A. G. Harrison, and J. J. Myher, *Can. J. Chem.*, **45**, 3107 (1967).

(21) F. W. Lampe, J. L. Franklin, and F. H. Field, *J. Amer. Chem. Soc.*, **79**, 6132 (1957).

(22) N. Greiner, *J. Chem. Phys.*, **51**, 5049 (1969).

(23) I. Santar and J. Bednar, *Collect. Czech. Chem. Commun.*, **32**, 953 (1967).

(24) G. R. A. Johnson, private communication (1968).

to promote isotopic exchange with water, *i.e.*, *via* reaction 29 as an alternative to collisional deexcitation



The occurrence of homogeneous vibrationally activated exchange reactions seems to have been tentatively established by shock tube experiments ($\text{H}_2\text{-D}_2\text{-Ar}$,²⁵ $\text{D}_2\text{-H}_2\text{S-Ar}$,²⁶ $\text{D}_2\text{-CH}_4\text{-Ar}$,²⁷ $\text{D}_2\text{-NH}_3\text{-Ar}$ ²⁸), in each of which bimolecular exchange of hydrogen atoms appears to be much more probable than collisional deexcitation for $\text{D}_2(v \simeq 5)$. There is no evidence for occurrence of reactions of this kind when the excited species can be formed only by atom combination. Thus, for example, $\text{D}_2(v) + \text{CH}_4 \rightarrow \text{HD} + \text{CH}_3\text{D}$ appears to proceed rapidly in shock heated mixtures of D_2 and CH_4 in argon,²⁷ but there is nothing to suggest that recombination of D atoms leads to formation of CH_3D in irradiated mixtures of D_2 and CH_4 at temperatures below the detectable onset of the hydrogen atom abstraction mechanism.²⁹ This is, at first glance, surprising in view of the observation in all shock tube investigations cited that the probability of exchange per collision is an order of magnitude or more greater than that of collisional deexcitation (*i.e.*, removal of one quantum at $v = 5$), whereas $\text{D}_2(v)$ will be formed in the $v = 17$ level by atom combination. A very significant difference, of course, is that the site of atom combination in photolytic and radiolytic vessels is often the wall of the vessel. In the present and previously reported work hydrogen atoms which are formed in reaction 21 (and its counterpart in $\text{H}_2\text{O-D}_2$ mixtures) are removed by a first order process, *i.e.*, at the wall, and the discrete species, $\text{H}_2(v)$, does not appear under such conditions.

Let us now return to what is known and what is possible concerning the yield of hydrogen atoms whose precursors are ions. The so-called ionic yield includes hydrogen atoms formed in neutralization reactions 18 and 19 and those which may be formed by interactions of subexcitation electrons with the medium. Assuming that the high pressure limiting values of the second order neutralization rate constants of the positive ion clusters are independent of n , *i.e.*, of cluster size, one must conclude that the neutralization yield cannot exceed one atom per neutralization event. Of the neutralization kinetics it is known only that the second order rate constant for neutralization of H_2O^+ is of the order $10^{-7} \text{ cm}^3 \text{ ion pair}^{-1} \text{ sec}^{-1}$ in high temperature hydrocarbon flames.³⁰ Nothing is known of the effect of a filled first hydration shell ($n \geq 4$) on neutralization efficiency, but one may postulate that it functions as a dielectric sheath and appreciably lessens the attractive potential between proton and electron. Smaller clusters may, accordingly, be removed preferentially in neutralization events and, in spite of their apparently low relative abundance at equilibrium, may play a significant part in the neutralization process.

It has been shown that in irradiated gaseous mixtures

of D_2O and C_3H_8 the value of $G(\text{HD})$ extrapolated to the pure C_3H_8 limit is roughly equal to $100/W_{\text{C}_3\text{H}_8}$.³¹ This observation has been interpreted to mean that the average neutralization yield of D atoms is close to one atom per ion pair in pure water vapor on the assumption that each organic ion transfers a proton to D_2O and produces ultimately one D_3O^+ (or ion cluster) by means of some plausible mechanism, such as $\text{HD}_2\text{O}^+ + \text{D}_2\text{O} \rightarrow \text{D}_3\text{O}^+ + \text{HOD}$. Currently available data now indicate, however, that the most abundant ion in irradiated C_3H_8 at high pressures (~ 1 to 760 Torr) is C_3H_7^+ ^{32,33} that it is formed by fast hydride ion transfer reactions of fragment ions with C_3H_8 ,³² and that C_3H_7^+ does not transfer a proton to a water molecule at thermal energies.³⁴ Thus, one may either conclude that the number of D atoms formed per neutralization event equals $1/f$, where f is equal to the fraction of organic ions which transfer protons to D_2O in propane rich mixtures and is probably much less than one, or seek other means to explain the observation. Similar attempts to estimate the neutralization yield have been made by measuring decrements in $G(\text{H}_2)$ caused by addition of electron scavengers to water-alcohol mixtures.^{35,36} It has been shown, however, that the presence of alcohol molecules drastically alters the positive ion clusters in water vapor and that methanol, *e.g.*, is preferentially taken up in all clusters of the type $\text{H}^+(\text{CH}_3\text{OH})_m(\text{H}_2\text{O})_n$ for $(m+n) \leq 9$ wherein the ratio of CH_3OH to H_2O molecules in the clusters ranges up to 350 times ($m+n=3$) that in the whole sample.³⁷ Thus, in one significant respect experiments of this kind are not studies of the radiolysis of water vapor, *per se*, and the yield of hydrogen atoms per neutralization event cannot be determined in the presence of foreign polar molecules.

The yield of hydrogen atoms formed by subexcitation electrons is also unknown. No electron attachment

(25) S. H. Bauer and E. Ossa, *J. Chem. Phys.*, **45**, 434 (1966).

(26) A. Burcat, A. Lifshitz, D. Lewis, and S. H. Bauer, *ibid.*, **49**, 1449 (1968).

(27) W. S. Watt, P. Borrell, D. Lewis, and S. H. Bauer, *ibid.*, **45**, 444 (1966).

(28) A. Lifshitz, C. Lifshitz, and S. H. Bauer, *J. Amer. Chem. Soc.*, **87**, 143 (1965).

(29) R. H. Lawrence, Jr., and R. F. Firestone, *ibid.*, **88**, 4564 (1966).

(30) H. F. Calcote, 26th Meeting of AGARD Propulsion and Energetics Panel, Pisa, Italy, Sept., 1965.

(31) G. R. A. Johnson and M. Simic, *J. Phys. Chem.*, **71**, 1118 (1967).

(32) L. I. Bone and J. H. Futrell, *J. Chem. Phys.*, **46**, 4084 (1967).

(33) M. S. B. Munson, J. L. Franklin, and F. H. Field, *J. Phys. Chem.*, **68**, 3098 (1964); G. A. W. Derwish, A. Galli, A. Giardini-Guidoni, and G. G. Volpi, *J. Chem. Phys.*, **41**, 2998 (1964).

(34) J. Long and M. S. B. Munson, *ibid.*, **53**, 1356 (1970); D. P. Beggs and F. H. Field, *J. Amer. Chem. Soc.*, **93**, 1577 (1971).

(35) J. H. Baxendale and G. F. Gilbert, *Science*, **147**, 1571 (1965).

(36) R. S. Dixon and M. G. Bailey, *Advan. Chem. Ser.*, **No. 82**, 247 (1968).

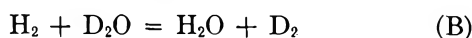
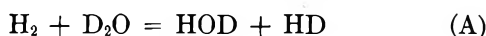
(37) P. Kebarle, R. N. Haynes, and J. G. Collins, *J. Amer. Chem. Soc.*, **89**, 5753 (1967).

processes which lead to hydrogen atom formation are known to occur for isolated molecules at electron energies below at least 7.5 eV.³⁸ Studies of electron attachment at water vapor pressures up to 10 Torr suggest,³⁹ however, that lower energy electrons may attach to aggregates of water molecules with an apparent probability in excess of 10^{-4} /collision at about 2 eV, for example, and that the probability of capture at low energies increases rapidly with pressure in the 3 to 10 Torr range. Hydrated hydroxyl ions of the form $\text{OH}^-(\text{H}_2\text{O})_n$, ($n \leq 5$) have been observed in water vapor.⁴⁰

If half or more of the liquid phase energy of hydration⁴¹ is realized, the reaction $e^- + (\text{D}_2\text{O})_n \rightarrow \text{OD}^-(\text{D}_2\text{O})_n + \text{D}$ could have a threshold energy of 4–5 eV. There is as yet no evidence that hydroxyl ion clusters are formed by this means in irradiated water vapor, but it is quite possible that this process occurs homogeneously at moderate to high pressures and among molecular aggregates at the vessel walls.

In summary, it is considered unlikely that HD has an immediate precursor other than the hydrogen atom or that mechanisms which produce more than one HD molecule per hydrogen atom are operative under conditions of these experiments. We tentatively conclude that $G(\text{HD})_{\text{plateau}}$ is equal to G_{D} in $\text{D}_2\text{O}-\text{H}_2$ and G_{H} in $\text{H}_2\text{O}-\text{D}_2$ in the absence of evidence to the contrary. Subdivision of the total yield of hydrogen atoms into ionic and nonionic portions cannot be done with precision on the strength of currently available information, but it is reasonably clear^{17,23} that the ionic yield must include a substantial combined contribution from reaction 18 and reactions of subexcitation electrons.

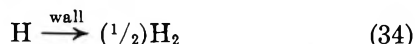
Mechanism in the Chain Region. It is apparent that two chain exchange reactions, A and B, occur at temperatures higher than the plateau region of Figure 1



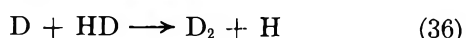
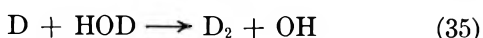
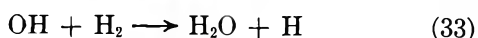
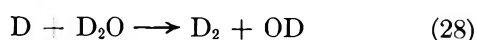
Reaction A must proceed by means of a combination of chain propagating steps 21, 22, 30, and/or 32;



and termination step 34



Reaction B must proceed *via* a combination of, in addition, 28, 33, 35, 36, and/or 31,



Rate law expressions for $G(\text{HD})$ and $G(\text{D}_2)$ must, furthermore, be consistent with the following observations: (i) $G(\text{HD})$ and $G(\text{D}_2)$ are independent of (H_2) at constant water vapor density. (ii) $[G(\text{HD}) - G_{\text{D}}]$ and $[G(\text{D}_2) - G_{\text{D}_2}]$ are directly proportional to $[\text{D}_2\text{O}]^2$ (*cf.*, Figure 2). (iii) $G(\text{D}_2)$ and $G(\text{HD})$ are independent of the fraction of H_2 consumed below, at least, 0.12.

Observation (i) demonstrates that $k_{21}[\text{H}_2] \gg k_{28}[\text{D}_2\text{O}]$, thus ruling out reaction 28. Observation (iii) rules out reactions 35 and 36. Rate law expressions follow directly from the assumption that steady-state conditions prevail for D, H, OD, and OH for all except a negligible fraction of the reaction time. Thus

$$G(\text{HD}) - G_{\text{D}} = \frac{(k_{30} + k_{32})(G_{\text{D}} + G_{\text{OD}})[\text{D}_2\text{O}]}{k_{34}}$$

$$G(\text{D}_2) - G_{\text{D}_2} = \frac{k_{31}(G_{\text{D}} + G_{\text{OD}})[\text{D}_2\text{O}]}{k_{34}}$$

The termination rate constant, k_{34} , will be of the form, $k_{34}^\circ(\text{D}_2\text{O})^{-1}$ for diffusion controlled loss of hydrogen atoms to the walls. Loss to the walls will be diffusion limited, if the termination step is first order with respect to the hydrogen atom concentration (as it is),² and, if the water vapor pressure is greater than or equal to $(4D_0)/(3r\bar{c})$, where $D = D_0/(\text{D}_2\text{O})$, r is the radius of the spherical vessel, \bar{c} is the average speed of the atoms, and e is the probability of removal per collision at the wall.⁴² Since D_0/\bar{c} is of the order 10^{-5} , $r = 4$ cm, and e has been found to lie in the range 10^{-4} to 10^{-6} for hydrogen atoms on Pyrex,⁴³ it is clear that both conditions are met and we may write the rate laws, as

$$[G(\text{HD}) - G_{\text{D}}] = \frac{(k_{30} + k_{32})(G_{\text{D}} + G_{\text{OD}})[\text{D}_2\text{O}]^2}{k_{34}^\circ}$$

$$[G(\text{D}_2) - G_{\text{D}_2}] = \frac{k_{31}(G_{\text{D}} + G_{\text{OD}})[\text{D}_2\text{O}]^2}{k_{34}^\circ}$$

in accord with observation (ii). It is, therefore, evident that the chain contribution to exchange reaction A is effected by reaction 30 and/or 32 and that chain exchange reaction B is propagated by reaction 31.

The ratio of slopes of plots of Figure 2 indicate that $k_{31}/(k_{30} + k_{32}) = 0.021$ at 319° . Absence of systematic

(38) R. N. Compton and L. G. Christophorou, *Phys. Rev.*, **154**, 110 (1967).

(39) N. E. Bradbury and H. E. Tatel, *J. Chem. Phys.*, **2**, 835 (1934); E. Kuffel, *Proc. Phys. Soc.*, **74**, 297 (1959).

(40) J. L. Moruzzi and A. V. Phelps, *J. Chem. Phys.*, **45**, 4617 (1966).

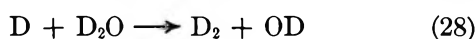
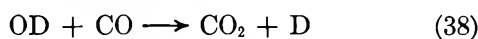
(41) F. D. Rossini, *et al.*, *Nat. Bur. Stand. (U. S.) Circ.*, **500**, 1952; W. M. Latimer, "The Oxidation States of the Elements and Their Potentials in Aqueous Solutions," 2nd ed., Prentice-Hall, Englewood Cliffs, N. J., 1952; A. F. Vorobev, *et al.*, *Vestn. Mosk. Univ. Khim.*, **18**, 48 (1963); F. N. Field and J. L. Franklin, "Electron Impact Phenomena," Academic Press, New York, N. Y., 1957.

(42) S. W. Benson, "The Foundations of Chemical Kinetics," McGraw-Hill, New York, N. Y., 1960, pp 327, 447.

(43) W. V. Smith, *J. Chem. Phys.*, **11**, 111 (1943); B. J. Wood and H. Wise, *J. Phys. Chem.*, **66**, 1049 (1962); W. Steiner, *Trans. Faraday Soc.*, **31**, 962 (1935).

variations of $[G(D_2) - G_{D_2}]/[G(HD) - G_D]$ with respect to temperature show that this ratio is independent of temperature within experimental error.

The magnitude of $k_{28}/(k_{30} + k_{31})$ is determined by the rates of formation of CO_2 (and D_2) in D_2O - CO mixtures and HD in D_2O - H_2 mixtures. The mechanism for CO_2 formation in D_2O - CO mixtures above 218° is



The rate law for CO_2 formation is

$$[G(CO_2) - G_{OD}] = \frac{k_{28}(G_D + G_{OD})[D_2O]^2}{k_{37}^\circ}$$

Thus, since $k_{34}^\circ/k_{37}^\circ = (\mu_{H,D_2O}/\mu_{D,D_2O})^{1/2}$

$$k_{28}/(k_{30} + k_{32}) = (\mu_{H,D_2O}/\mu_{D,D_2O})^{1/2} \frac{[G(CO_2) - G_{OD}]}{[G(HD) - G_D]}$$

at equal vapor densities and temperatures. Data from Table II and Figure 2 show that $k_{28}/(k_{30} + k_{32}) = 0.47 \pm 0.05$ independently of vapor density at 319° , assuming $G_D \simeq G_{OD}$, which accounts for the bulk of the stated uncertainty in this ratio.

The ratio k_{28}/k_{32} at 319° is determined by the H/D isotope effect on the rate of abstraction of D atoms from D_2O . Noting that among the reactions of H with D_2O and TOD , of D with H_2O , and of D with D_2O and TOD there are no detectable isotope effects on the activation energies for these various steps, the probable value of $E_{28} - E_{32}$ is zero with a probable uncertainty of several tenths of 1 kcal/mol. Thus, the isotope effect resides primarily or entirely in the frequency factor ratio and $k_{28}/k_{32} = (\mu_{H,D_2O}/\mu_{D,D_2O})^{1/2} = 0.72$ on the basis of the collision theory expression. It follows directly that $k_{30}/k_{32} = 0.52$ at 319° . Therefore, it must be concluded that the contributions of reactions 30 and 32 to formation of HD are comparable to all temperatures in the 218 - 381° range, because of the absence of detectable systematic curvature in the plots of Figures 1 and 3.

Assuming an empirical rule of the simple form presented by Evans and Polanyi⁴⁴ and more extensively documented by Semenov,⁴⁵ the relationship required for rough consistency between E_a and ΔH values among reactions 22, 28, 30, 31, and 32 is $E_a \simeq 14 - 0.5Q$, where Q is the exothermicity (kcal/mol) and E_{22} is set at approximately 4 kcal/mol.²² This leads to $E_{30} \simeq 15$ kcal/mol and $E_{32} \simeq 23$ kcal/mol. The expression for the observed activation energy for HD formation at temperature T is

$$E(T) = \frac{(A_{32}/A_{30})E_{32} + E_{30}e^{\Delta E/RT}}{(A_{32}/A_{30}) + e^{\Delta E/RT}}$$

It is apparent that a very large number of combinations of (A_{32}/A_{30}) , E_{32} , E_{30} , and $\Delta E = (E_{32} - E_{30})$ values will

satisfy this equation. We may, however, impose additional conditions, as follows: (1) $k_{28} = 0.72k_{32}$ for reasons presented above. (2) $E_{30} \leq 19.2 \leq E_{32}$ in deference to the Semenov rule. (3) $E(381^\circ) - E(218^\circ) \leq 0.5$ as a reasonable estimate of the systematic curvature in the Arrhenius plots which would escape detection. (4) $E(319^\circ) = 19.2$. The fraction of HD formed by reaction 30 at 319° , $f_{30}(319^\circ)$, is fixed at 0.34 by condition 1, and the expression

$$f_{30}^{-1} = 1 + (A_{32}/A_{30})e^{\Delta E/1.18}$$

is the corresponding constraint on acceptable values of ΔE and (A_{32}/A_{30}) at 319° . These conditions require that $\Delta E_{\text{max}} = 2.5$ kcal/mol, whence $E_{30,\text{min}} = 19.1 \pm 0.5$ kcal/mol and $E_{32,\text{max}} = 21.6 \pm 0.5$ kcal/mol are prescribed values consistent with all conditions imposed by our observations. This value for E_{32} is consistent with the seemingly most reliable value for E_{22} (4.0 ± 0.2 kcal/mol)²² and the estimated enthalpy of reaction 32 (16 ± 1 kcal/mol) and within the range of published estimates.⁴⁶ No evidence for occurrence of reaction 30 other than that presented above has been reported to our knowledge, and there are no estimates of E_{30} available for comparison with our value.

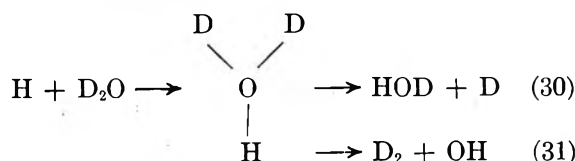
Table III is a quantitative summary of our findings.

Table III: Probable Values of the Arrhenius Parameters of Various Reactions of Hydrogen Atoms with Water Vapor (218 - 381°)

Reaction i	E_a , kcal/mol	A_i/A_{30}
(28) $D + D_2O \rightarrow D_2 + OD$	21.6 ± 0.5	4.9
(30) $H + D_2O \rightarrow HOD + D$	19.1 ± 0.5	(1.0)
(31) $H + D_2O \rightarrow D_2 + OH$	21 ± 1	0.01
(32) $H + D_2O \rightarrow HD + OD$	21.6 ± 0.5	6.8
$D + H_2O \rightarrow HOD + H$	19 ± 1	
$D + H_2O \rightarrow HD + OH$	19 ± 1	

The maximum permissible value for E_{32} is listed as the most probable value in deference, again, to the Semenov rule.

Since reactions 30 and 31 must proceed through the same intermediate structure, *viz.*



it is apparent that the requirement that two hydrogen-

(44) M. G. Evans and M. Polanyi, *Trans. Faraday Soc.*, **34**, 11 (1938).

(45) N. N. Semenov, "Some Problems of Chemical Kinetics and Reactivity," Vol. 1, Chapter 1, Pergamon Press, New York, N. Y., 1958.

(46) A. F. Trotman-Dickenson and G. S. Milne, *Nat. Stand. Ref. Data Ser., Nat. Bur. Stand.*, **9**, 8 (1967).

oxygen bonds be broken in reaction 31 is reflected primarily in the frequency factor ratio rather than in the activation energy difference.

Acknowledgment. The authors are grateful to the

U. S. Atomic Energy Commission for partial support of this work under Contract AT(11-1)-1116 and to Dr. E. J. Hart of The Argonne National Laboratory for the gift of a sample of purified heavy water.

The Effect of Ionic Dissociation of Organic Compounds on Their Rate of Reaction with Hydrated Electrons¹

by Francis A. Peter² and P. Neta*

Radiation Research Laboratories and Center for Special Studies, Mellon Institute of Science, Carnegie-Mellon University, Pittsburgh, Pennsylvania 15213 (Received October 12, 1971)

Publication costs assisted by Carnegie-Mellon University and the U. S. Atomic Energy Commission

Rate constants for the reactions of hydrated electrons with some organic compounds in γ -irradiated aqueous solutions have been measured by competition with *p*-bromophenol. The yield of bromide ions from *p*-bromophenol solutions, containing 2-propanol as a scavenger for OH and H, was used as a measure of the reaction of e_{aq}^- with this compound. From the effect of added solutes on $G(\text{Br}^-)$ the relative rate constants for the reactions of e_{aq}^- with these solutes have been calculated. This method is useful for the determination of $k_{e_{aq}^-}$ in the pH range of 2-8. The effect of pH on the rate constants for glycine, aspartic, barbituric, malonic, succinic, and lactic acids has been studied. The rate constants for these compounds at their different acid-base states were determined. In all cases the acid form was found to react much more rapidly than the basic form. The rate constant for glycine changes from $9 \times 10^6 M^{-1} \text{sec}^{-1}$ at pH 7.0 up to $2.5 \times 10^9 M^{-1} \text{sec}^{-1}$ at pH 2.1, that for barbituric acid from $9.4 \times 10^7 M^{-1} \text{sec}^{-1}$ at pH 7.6 to $9.3 \times 10^9 M^{-1} \text{sec}^{-1}$ at pH 2.6, and that for malonic acid from $1.2 \times 10^7 M^{-1} \text{sec}^{-1}$ at pH 7.2 to $1.1 \times 10^9 M^{-1} \text{sec}^{-1}$ at pH 2.1. Correlation of structure and reactivity is discussed.

Introduction

Rate constants for the reactions of the hydrated electron with many organic compounds have been measured mostly by pulse radiolysis.³ Because of the very rapid reaction of e_{aq}^- with H^+ most such measurements have been carried out in neutral or alkaline solutions. In order to follow the e_{aq}^- reaction with an organic solute in acid solution by the pulse radiolysis technique the time resolution should be improved by a few orders of magnitude over the standard microsecond detection setups. The recently developed picosecond technique has indeed been used to measure some rate constants in strongly acid solutions.⁴ To overcome the necessity for sophisticated instrumentation steady-state radiolysis competition-kinetics methods have been used (*e.g.*, ref. 5-8). The accuracy of the rate constants measured by these methods is generally poorer than that obtained with the pulse technique, and the measurements provide only relative rate constants and not absolute ones. Nevertheless, these methods proved useful in many instances and their application to the determination of e_{aq}^- rate constants in acid solutions

is being attempted in the present study. The compound used as a competitor, *p*-bromophenol, has been previously used in neutral solutions⁷ and its usefulness in acid solutions is examined here. This compound has been chosen for the present study because its rate of reaction with e_{aq}^- is expected to remain constant at all pH values below ~ 8 (pK_a of *p*-bromophenol is 9.4⁹) and because of the recent developments in ion-selective electrodes which enable accurate deter-

- (1) Supported in part by the U. S. Atomic Energy Commission.
- (2) Summer visitor from Ecole Supérieure de Physique et Chimie, Paris, France.
- (3) M. Anbar and P. Neta, *Int. J. Appl. Radiat. Isotopes*, **18**, 493 (1967).
- (4) J. E. Aldrich, M. J. Bronskill, R. K. Wolff, and J. W. Hunt, *J. Chem. Phys.*, **55**, 530 (1971).
- (5) A. Appleby, G. Scholes, and M. Simic, *J. Amer. Chem. Soc.*, **85**, 3891 (1963).
- (6) R. L. S. Willis and W. M. Garrison, *Radiat. Res.*, **32**, 452 (1967).
- (7) M. Anbar, Z. B. Alfassi, and H. Bregman-Reisler, *J. Amer. Chem. Soc.*, **89**, 1263 (1967).
- (8) O. Mičić and I. Draganić, *Int. J. Radiat. Phys. Chem.*, **1**, 287 (1969).

mination of bromide ion concentrations as low as $3 \times 10^{-6} M$.

The aim of the present study is to determine the effect of pH on the rate constants of hydrated electrons with several organic compounds. Representative compounds were chosen which exhibit pK values in the region 2–6 and the rate constants for these compounds at their different acid–base forms are determined.

Experimental Section

The organic compounds used were *p*-bromophenol (Eastman Organic Chemical and Baker Chemical), acetone (Baker Analyzed Reagent), orotic, barbituric, and aspartic acids (Cyclo Chemical Division Travenol Laboratories), glycine (Calbiochem, A grade) malonic acid (Aldrich Chemical), lactic acid (Baker Chemical), and succinic acid (Fisher Certified Reagent). All the inorganic compounds were Baker Analyzed Reagents. Water was triply distilled. The pH of solutions was adjusted using perchloric acid and potassium hydroxide. Solutions at pH 4–7 were buffered with sodium phosphates. Oxygen was removed from solutions by bubbling with argon. With solutions of acetone the argon was passed through two successive samples to check for possible losses, but no difference was detected between the results from the two solutions.

Irradiations were carried out in a ^{60}Co Gamma Cell 220 (Atomic Energy of Canada Limited) at a dose rate of $1.57 \times 10^{16} \text{ eV g}^{-1} \text{ sec}^{-1}$. Total absorbed doses were in most cases $3 \times 10^{18} \text{ eV g}^{-1}$.

The bromide ion concentration produced by the irradiation of *p*-bromophenol solutions was determined with an Orion 94-35 bromide electrode. The electrode potential relative to the reference electrode was determined with an Orion Model 801 digital pH meter capable of measuring the emf to 0.1 mV. The measured potentials were compared with those of standard solutions at the same ionic strength and pH. Bromide concentrations in the range of 1×10^{-5} to $2 \times 10^{-4} M$ were measured, which are well within the range of applicability of the electrode (1×10^{-6} to $1 \times 10^{-1} M$). Nonirradiated solutions were also examined in every case for possible hydrolysis and the concentration of bromide ions in these solutions was always below $3 \times 10^{-6} M$. The accuracy of the concentration measurements is estimated to be $\pm 2\%$.

Results and Discussion

The Radiolysis of p-Bromophenol. Bromophenol reacts very rapidly with all the primary radicals of water radiolysis, e_{aq}^- , H, and OH. Scavenging experiments have been carried out to determine the contribution of these radicals to the formation of bromide ions. Aqueous solutions of *p*-bromophenol at concentrations of 5×10^{-4} to $5 \times 10^{-2} M$ yielded $G(\text{Br}^-) = 3.4\text{--}4.8$. The increase in yield with increasing concentration must be a result of scavenging

within the spurs. The effect of added solutes on the yield of bromide is shown in Table I. Addition of *tert*-butyl alcohol as a scavenger of OH radicals (and not H) decreased $G(\text{Br}^-)$ by 0.5. This result indicates that $\sim 20\%$ of the OH radicals reacting with *p*-bromophenol lead to the formation of Br^- , most probably by addition to the ring on the carbon bearing the bromine atom followed by elimination of HBr. Addition of 2-propanol as a scavenger for both OH and H decreased $G(\text{Br}^-)$ by 0.7. The reaction of hydrogen atoms with bromophenol seems, therefore, to produce bromide only partially, probably by direct abstraction of the bromine atom, and most of the H atoms add to the ring with no consequent debromination. To further check this point solutions of bromophenol have been irradiated at pH 1 and pH 2 where all the e_{aq}^- are converted into H. The yield of Br^- dropped significantly and only $\sim 20\%$ of the H atoms form bromide (Table I).

Table I: The Effect of Added Solutes on the Yield of Bromide Ions in Irradiated Aqueous Solutions of *p*-Bromophenol^a

Added solute	Concentration	$G(\text{Br}^-)$
...	...	3.5
<i>tert</i> -BuOH	0.3	3.0
<i>i</i> -PrOH	0.3	2.8
H ⁺	0.01	0.6
{ <i>i</i> -PrOH	0.3	0.04
{ Acetone	0.1	
{ <i>i</i> -PrOH	0.3	0.1
{ Orotic acid	0.01	

^a Concentration of *p*-bromophenol $1 \times 10^{-3} M$, pH 7 was adjusted using $1 \times 10^{-3} M$ of $\text{Na}_2\text{HPO}_4 + \text{NaH}_2\text{PO}_4$.

In order to use $G(\text{Br}^-)$ as a measure of e_{aq}^- reaction it is necessary to scavenge the H and OH by an additional solute so that their contribution to the yield of bromide will be eliminated. 2-Propanol was chosen for this purpose. From the rate constants³ for the reactions of H and OH with *p*-bromophenol and with the 2-propanol it can be calculated that a concentration ratio of 50 in favor of the latter solute is sufficient for practically complete scavenging. It should be pointed out that even if scavenging is not complete the contribution of H and OH to the Br^- yield is very small. Experimental verification of this point was obtained by measuring $G(\text{Br}^-)$ at various concentration ratios.

In the presence of excess 2-propanol all the bromide yield can be attributed to the reaction of e_{aq}^- with

(9) A. Albert and E. P. Serjeant, "Ionization Constants of Acids and Bases," Wiley, New York, N. Y., 1962, and "Handbook of Organic Structural Analysis," Y. Yukawa, Ed., W. A. Benjamin, New York, N. Y., 1965.

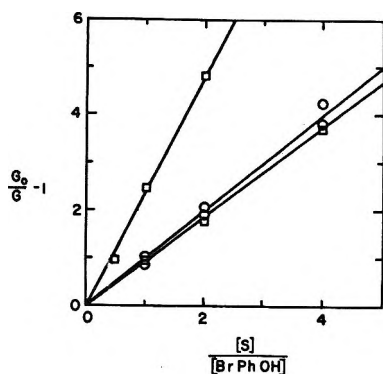


Figure 1. The dependence of the yield of bromide in irradiated solutions of *p*-bromophenol on the concentration of added electron scavengers. The upper line is for orotic acid with 1×10^{-3} *M* bromophenol and 0.3 *M* *i*-PrOH at pH 7 buffered with phosphate. The lower lines are for acetone at pH 7 (○) and pH 3 (□). The competition at pH 7 was carried out with 1×10^{-3} and 1×10^{-2} *M* bromophenol and that at pH 3 with 1×10^{-2} *M* bromophenol.

bromophenol. Indeed, the addition of a large excess of acetone or of orotic acid caused the yield of bromide to decrease down to the lowest measurable levels (Table I).

Since the acetone formed in irradiated solutions of isopropyl alcohol reacts with e_{aq}^- very rapidly, $G(\text{Br}^-)$ will decrease at high irradiation doses. The dependence of yield on total dose was, therefore, examined and was found to be linear up to at least 10^{19} eV g^{-1} , which is three times higher than the dose used in all the competition experiments.

The Competition Method. Competition experiments with acetone and with orotic acid were carried out to determine the rate constant for *p*-bromophenol in neutral solution. The rate constants can be calculated from the concentrations and the yield of bromide through equation I

$$k_s = k_{\text{BrPhOH}} \frac{[\text{BrPhOH}]}{[S]} \left(\frac{G(\text{Br}^-)_0}{G(\text{Br}^-)} - 1 \right) \quad (\text{I})$$

where k_s and $[S]$ are the rate constant and the concentration of the added solute and $G(\text{Br}^-)_0$ and $G(\text{Br}^-)$ are the yields of bromide ions in the absence and in the presence of the added solute, respectively. The competition plots for acetone and orotic acid are presented in Figure 1. In the case of acetone the experiments were carried out with various absolute concentrations (two of which are shown in Figure 1) and the same straight line is obtained for all cases. From the known rate constant for e_{aq}^- reaction with acetone, $6.0 \times 10^9 \text{ M}^{-1} \text{ sec}^{-1}$,³ the rate constant for *p*-bromophenol is calculated to be $6.0 \times 10^9 \text{ M}^{-1} \text{ sec}^{-1}$. From the competition plot for orotic acid using $k(e_{aq}^- + \text{orotic acid}) = 1.5 \times 10^{10} \text{ M}^{-1} \text{ sec}^{-1}$ ³ the rate constant for *p*-bromophenol is calculated to be $6.2 \times 10^9 \text{ M}^{-1} \text{ sec}^{-1}$ in good agreement with the value calculated from the experiments with acetone. This value is lower by a factor of two than that previously

determined at pH 5.5 by competition with nitrate⁷ and the reason for this discrepancy is not clear.

In order to check this point a pulse radiolysis experiment was carried out to measure the absolute rate constant for the reaction of e_{aq}^- with *p*-bromophenol at pH 5–6 and at pH 11. The rate constant determined at pH 11 by observing the rate of disappearance of the e_{aq}^- optical absorption at various concentrations of *p*-bromophenol is $3.4 \times 10^9 \text{ M}^{-1} \text{ sec}^{-1}$ in agreement with the previously reported value of $2.9 \times 10^9 \text{ M}^{-1} \text{ sec}^{-1}$.¹⁰ The rate constant measured at pH 5–6 (no buffer added) was found to be twice as large, namely $7 \times 10^9 \text{ M}^{-1} \text{ sec}^{-1}$, in fair agreement with the competition experiments.

The rate constant for the reaction of e_{aq}^- with *p*-bromophenol is expected to remain constant at pH < 8. This assumption was experimentally verified by competition with acetone at pH 3. Little change in the rate constant was found (Figure 1). Similar values were also obtained from the competition between bromophenol and H^+ at pH 3–5. It is, therefore, possible to use *p*-bromophenol as a reference compound for measuring e_{aq}^- rate constants in acid solutions. Two facts determine the applicability limits of this method, *i.e.*, the limited solubility of this compound and the large corrections necessary to be made for results in acid solutions. These corrections involve the difference between the percentage of e_{aq}^- scavenged by H^+ in the presence of bromophenol alone and that with added solutes. At pH < 3 the system becomes composed of three competing solutes, the rate constants for two of which are known. This complication diminishes the overall accuracy of the measurements, and no competition experiments were attempted at pH < 2.

The Effect of pH on the Rate Constants. Representative rate constants determined for the various organic compounds at different pH values are summarized in Table II. They were calculated using $k(e_{aq}^- + p\text{-BrPhOH}) = 6.0 \times 10^9 \text{ M}^{-1} \text{ sec}^{-1}$. The rate constant for the first three compounds in Table II have been reported in the literature³ and they are used here for reference as discussed above.

The rate constant for barbituric acid changes from $9.4 \times 10^7 \text{ M}^{-1} \text{ sec}^{-1}$ at pH 7.6 up to $9.3 \times 10^9 \text{ M}^{-1} \text{ sec}^{-1}$ at pH 2.6. In Figure 2 the rate constant is plotted as a function of pH. If the rate measured, k , is only a function of the concentration of the acid and the basic forms of barbituric acid ($\text{p}K_a = 4.01^9$), it can be correlated with $\text{p}K_a$ and pH by equation II

$$k = \frac{k_{\text{HA}} + k_{\text{A}} \frac{K}{[\text{H}^+]}}{1 + \frac{K}{[\text{H}^+]}} \quad (\text{II})$$

(10) M. Anbar and E. J. Hart, *J. Amer. Chem. Soc.*, **86**, 5633 (1964).

Table II: Rate Constants for the Reactions of Hydrated Electrons with Organic Compounds in Neutral and Acid Solutions^a

Compound	pH	Rate constant, $M^{-1} \text{sec}^{-1}$
Acetone	7.0	6.0×10^9
	3.0	5.6×10^9
H^+	4.0	2.5×10^{10}
Orotic acid	7.0	1.4×10^{10}
Barbituric acid	7.6	9.4×10^7
	5.0	1.0×10^8
	4.0	4.4×10^8
	2.6	9.3×10^8
Glycine	7.0	0.9×10^7
	4.0	4.6×10^7
	3.0	5.4×10^8
	2.1	2.5×10^9
Aspartic acid	7.0	1.5×10^7
	3.0	8.8×10^8
Lactic acid	7.0	5.0×10^7
	3.0	5.8×10^8
Malonic acid	7.2	1.2×10^7
	6.2	8.3×10^7
	5.1	3.9×10^8
	3.5	7.3×10^8
	2.1	1.05×10^9
Succinic acid	7.5	1.5×10^6
	6.0	1.5×10^7
	5.0	9.6×10^7
	4.0	2.7×10^8
	3.0	3.4×10^8

^a Determined by competition with *p*-bromophenol and calculated using $k_{e_{aq}^-} + p\text{-BrPhOH} = 6.0 \times 10^9$ at all pH values.

where k_{HA} and k_{A^-} are the rate constants for the acid and basic forms, respectively, and K is the dissociation constant. The theoretical plot of equation II which gives the best fit to the experimental points for barbituric acid is solid line (a) in Figure 2 and it was calculated using $k_{HA} = 9.5 \times 10^9$ and $k_{A^-} = 9.0 \times 10^7 M^{-1} \text{sec}^{-1}$. This plot clearly demonstrates that the effect of pH on the rate constant measured is due to the change in the acid-base equilibrium of the barbituric acid. The limiting rate constants of 9.5×10^9 and $9.0 \times 10^7 M^{-1} \text{sec}^{-1}$ are the rate constants for the acid and the basic forms, respectively.

Similar results were also obtained with glycine (Table II and Figure 2). The rate constant for the reaction of hydrated electrons with the glycine zwitterion at pH 7 is $9 \times 10^6 M^{-1} \text{sec}^{-1}$, in good agreement with the literature value.³ In acid solutions the rate constant increases by over two orders of magnitude. Measurements were not made at $\text{pH} < 2$ but the rate constant for the acid form of glycine can be derived from the plot in Figure 2 as $4 \times 10^9 M^{-1} \text{sec}^{-1}$. This value gives the best fit with the experimental points using $\text{p}K_a = 2.35$.⁹ The value measured at pH 3 is in agreement with a previous result obtained by competition with chloroacetic acid.⁶

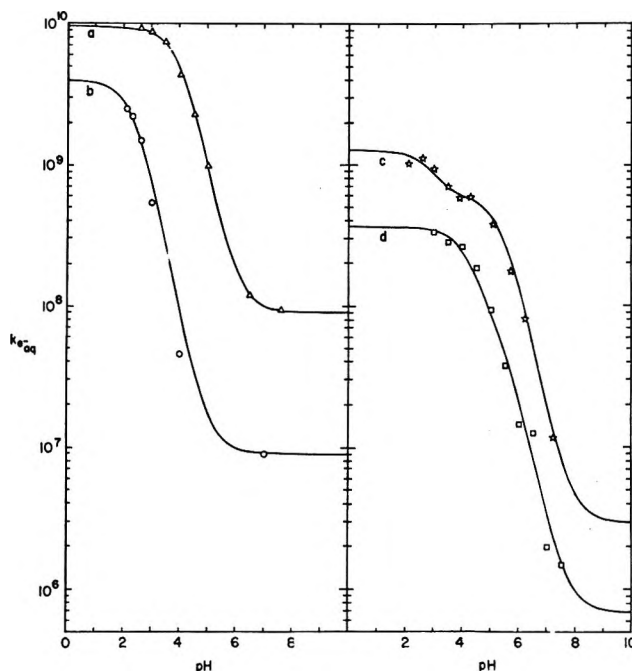


Figure 2. The effect of pH on the rate constants for the reaction of e_{aq}^- with: a, barbituric acid (Δ); b, glycine (\circ); c, malonic acid (\star); d, succinic acid (\square). The points are the experimental measurements. The curves were calculated from the $\text{p}K_a$ values for these acids and the rate constants for the different acid-base forms which give the best fit.

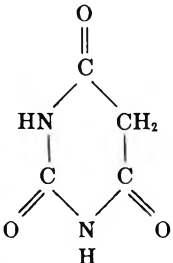
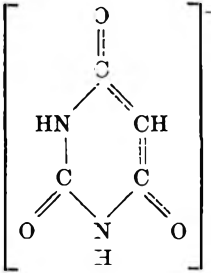
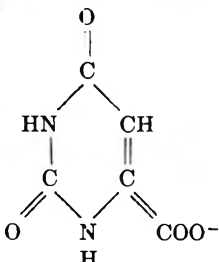
The rate constants for aspartic acid at pH 7 and pH 3 were found to be 1.5×10^7 and $8.8 \times 10^8 M^{-1} \text{sec}^{-1}$, respectively (Table II). The $\text{p}K_a$ values for aspartic acid are 2.10 and 3.86.⁹ An extended form of equation II, namely

$$k = \frac{k_{H_2A} + k_{HA^-} \frac{K_1}{[H^+]} + k_{A^{2-}} \frac{K_1 K_2}{[H^+]^2}}{1 + \frac{K_1}{[H^+]} + \frac{K_1 K_2}{[H^+]^2}} \quad (\text{III})$$

where k_{H_2A} , k_{HA^-} , and $k_{A^{2-}}$ are the rate constants for the acid, monoanion, and dianion form, respectively, and K_1 and K_2 are the dissociation constants, can be used to calculate the rate constants for the different forms of aspartic acid. The rate constant measured at pH 7 is very nearly the value for $^-OOCCH_2CH(NH_3^+)COO^-$. The value for the acid form $HOOCCH_2CH(NH_3^+)COOH$ can be estimated at $5 \times 10^9 M^{-1} \text{sec}^{-1}$ from the results for glycine and succinic acid (see below). With this assumption the rate constant for $HOOCCH_2CH(NH_3^+)COO^-$ can be calculated as $5 \times 10^8 M^{-1} \text{sec}^{-1}$.

The rate constants for lactic acid at pH 7 and pH 3 are 5×10^7 and $5.8 \times 10^8 M^{-1} \text{sec}^{-1}$ (Table II). Using equation II and $\text{p}K_a = 3.82$ ⁹ the rate constants for the basic and the acid forms can be calculated as 5×10^7 and $7 \times 10^8 M^{-1} \text{sec}^{-1}$, respectively. The value for the basic form is much higher than that reported in the literature.³ If the previous value of $< 2 \times 10^6$

Table III: Rate Constants for the Reactions of Hydrated Electrons with the Various Acid-Base Forms of Some Organic Acids

Compound	Form	pK _a	Rate Const., M ⁻¹ sec ⁻¹
Acetic acid	CH ₃ COOH		1.8 × 10 ^{8a}
		4.75	
Oxalic acid	CH ₃ COO ⁻		<10 ^{6a}
	HOOC ⁻ COOH	1.27	2.5 × 10 ^{10b}
	HOOC ⁻ COO ⁻	4.27	3.4 × 10 ^{9b}
Malonic	-OOC ⁻ COO ⁻		4.8 × 10 ^{7b}
	HOOCCH ₂ COOH	2.86	1.3 × 10 ⁹
	HOOCCH ₂ COO ⁻	5.5	6 × 10 ⁸
Succinic acid	-OOCCH ₂ COO ⁻		3 × 10 ⁸
	HOOCCH ₂ CH ₂ COOH	4.16	3.7 × 10 ⁸
	HOOCCH ₂ CH ₂ COO ⁻	5.64	7 × 10 ⁷
Lactic acid	-OOCCH ₂ CH ₂ COO ⁻		7 × 10 ⁶
	CH ₃ CHOHCOOH	3.82	7 × 10 ⁸
Glycine	CH ₃ CHCHCOO ⁻		(5 × 10 ⁷) ^c
	+H ₃ NCH ₂ COOH	2.35	4 × 10 ⁹
Aspartic acid	+H ₃ NCH ₂ COO ⁻		9 × 10 ⁸
	HOOCCH ₂ CH(NH ₃ ⁺)COOH	2.10	5 × 10 ⁹
	HOOCCH ₂ CH(NH ₃ ⁺)COO ⁻	3.86	5 × 10 ⁸
	-OOCCH ₂ CH(NH ₃ ⁺)COO ⁻		1.5 × 10 ⁷
Barbituric acid			9.5 × 10 ⁹
		4.01	
			9 × 10 ⁷
Orotic acid		(2.8)	1.5 × 10 ^{10a}

^a Taken from ref 3. ^b Taken from ref 8. ^c This value could be much lower (see text).

M⁻¹ sec⁻¹ measured at pH 11 is correct, the present result must be due to a reactive impurity in the lactic acid. The presence of 1% pyruvic acid would account for the measurement. The rate constant in acid solution cannot be affected to that extent and can be accepted as accurate to ± 20%.

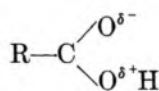
Measurements for malonic and succinic acid were carried out at 10 different pH values in each case. The results are summarized in Table II and Figure 2. Curves c and d in this figure were calculated from equation III to give the best agreement with the experimental points. In these calculations the known pK_a values for these acids⁹ have been used and the rate constants for the various acid-base forms have been varied until the best fit was achieved. The values used for the curves shown in Figure 2 are summarized in Table III together with the rate constants for the acid-base forms of the other compounds studied.

The agreement between the experimental points for malonic acid and the theoretical curve is satisfactory. A change in the rate constants could not give a better fit. However, using pK₂ = 5.7⁹ the curve deviated from the experimental points by about 0.3 pH units. This fact suggested a possible error in the literature value of pK₂. This value has been, therefore, determined again from a titration curve and found to be 5.5 which gives a much better agreement with the rate constants as seen in Figure 2. In the case of succinic acid there seems to be a larger scatter of the experimental points around the calculated curve. This mainly results from the decreased accuracy in the measurement of very low rate constants and, therefore, the value used for the basic form is accurate only to about ± 50%. The values for the other two forms of succinic acid are more accurate, about ± 20%.

Correlation of Structure and Reactivity. From the rate constants summarized in Table III it is clear that dissociation of a carboxyl group has a strong effect on its rate of reaction with e_{aq}⁻. The nonreactivity of the carboxylate ion toward e_{aq}⁻ has been explained by the resonance stabilization of these ions.¹¹ The undissociated acids are much more reactive as is seen in Table III and as has been found previously for several simple acids.³ The rate constants for the reaction of e_{aq}⁻ with formic and acetic acid are 1.4 and 1.8 × 10⁸ M⁻¹ sec⁻¹, respectively,³ and this reactivity could be taken as that of an isolated COOH group. The results for succinic acid support this suggestion. The rate for the acid form containing two COOH groups is 3.7 × 10⁸ M⁻¹ sec⁻¹ and that for the monoanion containing only one COOH group is 7 × 10⁷ M⁻¹ sec⁻¹ (Table III). In this case there is an additional electrostatic repulsion which diminishes the rate. The dianion is, of course, nonreactive. Comparing these results with those for malonic acid (Table III) and oxalic acid⁸ it is clear that

(11) M. Anbar, *Advan. Phys. Org. Chem.*, **7**, 115 (1969).

the proximity of two carboxyl groups largely affects their rates. Malonic acid reacts 3.5 times more rapidly than succinic acid, and oxalic acid reacts 19 times more rapidly than malonic acid. These changes are most probably due to the electron withdrawing effect of one carboxyl group on the other. Since electron withdrawing groups decrease the rate constant for the reaction of e_{aq}^- with a carbonyl group,¹¹ it can be concluded that the reactivity of carboxylic acids cannot be assigned to the carbonyl part and the electron is probably not adding to the C=O double bond. Increase in reactivity caused by electron withdrawing groups was found for esters and amides and explained by the mesomeric effect.¹¹ It is, therefore, plausible that carboxylic acids react similarly and the electron adds to the OH part which bears a partial positive charge in the mesomeric form



Electron withdrawing groups on the R substituent, such as another COOH, will increase the electron affinity of this OH. These suggestions are also supported by the results for glycine, where the electron withdrawing property of the NH_3^+ group increases the rate constant up to $4 \times 10^9 M^{-1} \text{sec}^{-1}$ (Table III). The OH in lactic acid is expected to exert a smaller activating effect, which indeed it does. Quantitative correlation of the electron withdrawing properties (Taft's σ^* function) with the rate constants measured in the present study is difficult because of the small number of rates available and because of lack of knowledge of some σ^* values. However, it is clear that the rate constant for e_{aq}^- with COOH increases with the increase in electron withdrawing from this group, *i.e.*, the behavior of carboxylic acids toward e_{aq}^- is similar to that of esters and amides and not to that of carbonyl compounds.

The rate constants for e_{aq}^- with barbituric and orotic acid can be discussed together in terms of the reactivity of the carbonyl groups and the 5,6 double bond. The carbonyl group at position 2 is comparable to that in

urea ($3 \times 10^5 M^{-1} \text{sec}^{-1}$) and is expected to be similarly unreactive. The carbonyl group at positions 4 and 6 of barbituric acid are comparable to that in acetamide ($1.7 \times 10^7 M^{-1} \text{sec}^{-1}$) and, therefore, the observed rate constant of $9.5 \times 10^9 M^{-1} \text{sec}^{-1}$ must be a result of the effect of one carbonyl group on the other. This effect is similar in nature to that in the case of malonic acid but it is considerably greater. The high reactivity of orotic acid is the sum of the reactivity of the carbonyl group at position 4, activated by the electron withdrawing property of the carboxyl through the double bond, and the reactivity of the 5,6 double bond activated by the carbonyl and the carboxyl groups (compare, for example, ethylene: $<10^6$ with acrylamide: 2×10^{10} and fumarate ion: $7.5 \times 10^9 M^{-1} \text{sec}^{-1}$). The situation changes completely when barbituric acid undergoes dissociation. The anion is in a resonance structure (Table III) which does not contain any of the reactive sites. The 5,6 double bond loses some of its olefinic character through resonance and in addition it is deactivated by a hydroxyl group (vinyl alcohol, for example, is also unreactive). The carbonyl groups in barbituric acid, which become partially alkoxide ions, are not reactive. These changes explain why the dissociated form of barbituric acid is two orders of magnitude less reactive than the undissociated form and than orotic acid. It should be noted that the charge has also a significant effect on the rate constant of e_{aq}^- (*cf.* propionic acid *vs.* succinic monoanion) and it contributes to the differences in the reactivities of dissociated and undissociated forms of acids.

In conclusion it has been demonstrated that *p*-bromophenol can be successfully used for the measurement of rate constants for reaction of e_{aq}^- at pH 2–8. The effect of pH on the rate constant for various organic acids has been studied and the rates for the different acid–base forms have been derived. It has been found that dissociation of a carboxyl group decreases the rate constant by at least two orders of magnitude. The rates for carboxylic acids are increased by electron withdrawing groups. The rate for barbituric acid also decreases by two orders of magnitude with dissociation and the effect of structure on rate constant was discussed.

Optical Bleaching Effects on the Paramagnetic Relaxation of Trapped Electrons in Methyltetrahydrofuran at 77°K

D. P. Lin and Larry Kevan*

Department of Chemistry, Wayne State University, Detroit, Michigan 48202 (Received October 26, 1971)

Publication costs assisted by the U. S. Atomic Energy Commission

The effect of optical bleaching on the characteristic relaxation time, $(T_1T_2)^{1/2}$, of trapped electrons (e_t^-) in methyltetrahydrofuran (MTHF) glass at 77°K has been measured for different doses corresponding to different initial spatial distributions. At low radiation doses $(T_1T_2)^{1/2}$ increases as e_t^- are bleached. This confirms the spur model of electron trapping in this matrix and indicates that the spurs contain more than one e_t^- on the average. At high radiation doses $(T_1T_2)^{1/2}$ remains constant as e_t^- are bleached. This is interpreted in terms of spin-spin relaxation of e_t^- with MTHF as well as with other e_t^- . A quantitative treatment of T_1T_2 data vs. total spin concentration confirms this latter interpretation.

Introduction

The spatial distribution of trapped species produced by γ -irradiation is of interest in radiation chemistry because radiation energy is deposited inhomogeneously in condensed systems. For paramagnetic species the study of spin-spin interactions provides a method to examine local spatial distribution of the spins. Previous work has shown how changes in T_2 , the spin-spin relaxation time, measured by microwave saturation can indicate changes in the spatial distribution of the trapped spins.¹ Trapped electrons in aqueous¹⁻³ and organic glasses⁴⁻⁶ are distributed inhomogeneously in spurs with a spur size that increases with decreasing matrix polarity.⁶ The effect of thermal decay on the spatial distribution of radicals in poly(methylmethacrylate) has also been studied by paramagnetic relaxation methods.⁷

Optical bleaching of electrons trapped in glassy matrices is expected to remove electrons homogeneously throughout the system. This should have a predictable effect on the relaxation time of the electrons as measured by T_2 depending on the initial spatial distribution. In this work we test this conjecture on electrons trapped in methyltetrahydrofuran (MTHF) at 77°K and confirm the spur model of electron trapping in this matrix. It is also shown that the spin-spin relaxation of trapped electrons in MTHF involves interaction with the MTHF radicals as well as with other trapped electrons.

Experimental Section

Matheson, Coleman and Bell chromatography 2-MTHF was purified as described previously.⁶ Samples were prepared into 2 mm diameter glassy (*i.e.*, transparent) spheres by dropping drops of MTHF into liquid nitrogen in a nitrogen atmosphere.

Irradiation was carried out in liquid nitrogen in a ⁶⁰Co γ -irradiator at a dose rate of ~ 0.4 Mrad hr⁻¹.

Actual doses to the samples were corrected for the ⁶⁰Co decay rate.

Epr measurements were made with a Varian 4502 X-band spectrometer. The magnetic field modulation frequency was 400 Hz and the modulation amplitude was 0.6 G. Saturation curves were determined by measuring the epr derivative signal intensity, V (height \times width²), vs. the microwave magnetic field, H_1 . Slow passage conditions as defined by $H_1/(\omega_m H_m) \gg (T_1T_2)^{1/2}$ were approximated. H_m is the magnetic field modulation amplitude in gauss and ω_m is the modulation angular frequency in radians sec⁻¹. Adiabatic passage conditions as defined by $1/\gamma H_1 \ll H_1/\omega_m H_m$ were fulfilled at higher microwave power in the saturation region. The value of H_1 for the spectrometer used⁸ is given by: $H_1 = 2.22P^{1/2}$ G, where P is the measured incident power to the cavity in watts.

Direct light, without any filter, from a 500-W tungsten bulb in a slide projector was used to bleach the electrons in the epr cavity. It took only a few seconds to bleach the initial 10% of the electrons. The radical signal was not affected by the bleaching light. Because of overlap between the trapped electrons and the radical signals the trapped electron signal height was obtained by subtracting 1.2 times the radical hyperfine line adjacent to the center line from the center line.

Spin concentrations were determined by double integration of unsaturated first derivative spectra.

- (1) J. Zimbrick and L. Kevan, *J. Chem. Phys.*, **47**, 2364 (1967).
- (2) H. Hase and L. Kevan, *J. Amer. Chem. Soc.*, **90**, 6875 (1968).
- (3) B. G. Ershov, G. P. Chernova, O. Ya Grinberg, and Ya. S. Lebedev, *Izv. Akad. Nauk SSSR, Ser. Khim.*, 2439 (1968).
- (4) D. Smith and J. J. Pieroni, *Can. J. Chem.*, **43**, 876 (1965).
- (5) L. Kevan and D. H. Chen, *J. Chem. Phys.*, **49**, 1970 (1968).
- (6) D. P. Lin and L. Kevan, *ibid.*, **55**, 2629 (1971).
- (7) W. Kaul and L. Kevan, *J. Phys. Chem.*, **75**, 2443 (1971).
- (8) B. L. Bales and L. Kevan, *J. Chem. Phys.*, **52**, 4644 (1970).

The spin concentrations are all relative to $G(e_t^-) = 2.0$ for e_t^- in irradiated 10 M NaOH at 77°K.

Results

The epr spectrum of γ -irradiated MTHF at 77°K gives a narrow singlet due to e_t^- superimposed on a septet due to a MTHF radical. The assignment of the spectra is the same as in previous work.^{4,6}

Figure 1 shows the yield-dose curve for e_t^- in MTHF glass at 77°K. Previous studies⁶ on the change of the characteristic relaxation time of e_t^- in MTHF, $(T_1T_2)^{1/2}$ where T_1 is the spin-lattice relaxation time, with dose have shown the following about the spatial distribution of e_t^- . At doses up to about 1.4 Mrad the e_t^- are trapped nonuniformly in regions of high local spin concentration called spurs. Above 1.4 Mrad the spurs begin to overlap and as higher doses are attained the overall spatial distribution of e_t^- becomes more and more uniform. It can be noted that the yield-dose curve in Figure 1 becomes nonlinear in the region of spur overlap. With these facts in mind, radiation doses for optical bleaching experiments were selected for four regions representing different amounts of spur overlap. These doses were (1) 0.52 Mrad at which the spurs do not overlap, (2) 1.75 Mrad at which the spurs just overlap, (3) 3.15 Mrad at which the spurs overlap and which is the dose near the maximum e_t^- yield, and (4) 6.30 Mrad at which the spurs overlap but the e_t^- yield is less than its maximum. Figure 2 shows the effect of optical bleaching on the characteristic relaxation time for the four different dose regions. The characteristic relaxation time corresponding to each point on Figure 2 is determined from a complete saturation curve, and the percentages shown refer to the percent e_t^- remaining after optical bleaching relative to the unbleached sample.

The relaxation times were determined from analysis of the saturation curve according to eq 1 where $\gamma = 1.76 \times 10^7 \text{ G}^{-1} \text{ sec}^{-1}$ and $H_{1/2}$ is the value of H_1 for which the signal is one-half of what it would be in the absence of saturation. The method is described in detail in ref 6.

$$T_1T_2 = \frac{3}{\gamma^2 H_{1/2}^2} \quad (1)$$

Discussion

A. Confirmation of the Spur Model. Curves (1) and (2) in Figure 2 are clearcut confirmations of the spur model for e_t^- in MTHF. In the isolated spur region of curve (1) the relaxation time of a given e_t^- is determined by interactions with other spins (e_t^- and radicals) in the same spur and is approximately independent of the number of spurs. Optical bleaching of e_t^- will remove e_t^- homogeneously throughout the matrix and thus will only remove one e_t^- from any given spur on the average. The local spin concentration is inversely related to T_2 . So if the number of e_t^- in a spur is a

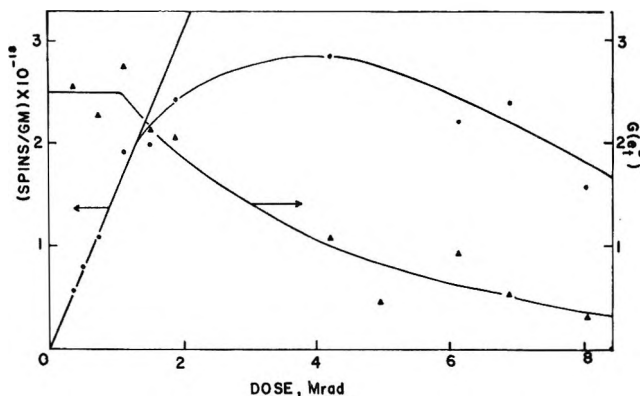


Figure 1. Yield of trapped electrons in MTHF at 77°K vs. radiation dose. $G(e_t^-)$ refers to the yield per 100 eV of absorbed radiation energy.

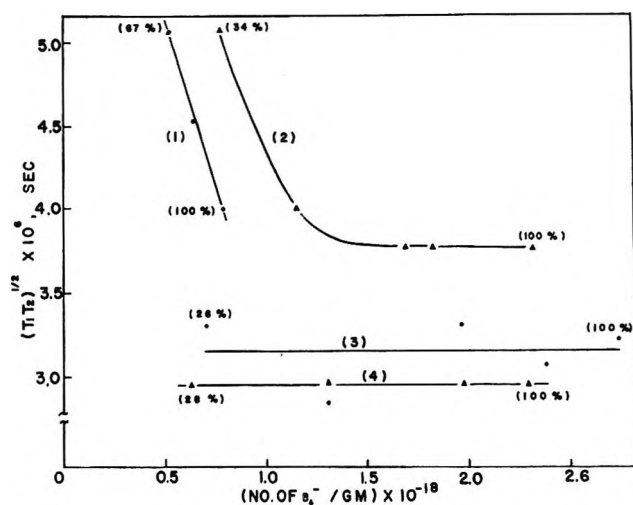


Figure 2. Partial optical bleaching effects on the characteristic relaxation time of e_t^- in MTHF at 77°K by a 500 W slide projector: (1), 0.52 Mrad; (2), 1.75 Mrad; (3), 3.15 Mrad; (4), 6.30 Mrad.

small number, optical bleaching will increase the average relaxation time for e_t^- that is measured experimentally. This increase is observed and shown by curve (1) in Figure 2. It can also be noted that if only one e_t^- were present in each spur, then optical bleaching in the isolated spur region would not change the relaxation time.

Curve (2) is consistent with the onset of spur overlap. As the first 30% of e_t^- are bleached the relaxation time remains constant. Since the spurs overlap, the removal of one e_t^- causes little change in the average relaxation time of any other given e_t^- . However, as a greater percentage of the e_t^- are bleached the relaxation time increases for the same reason that curve (1) increased.

The spur model is also confirmed by looking at the difference in relaxation time between curves (1) and (2) at a constant e_t^- concentration of 0.75×10^{18} spins/g. The 34% point on curve (2) has a longer relaxation time and thus a lower local spin concentration than the 100% point of curve (1). Isolated spurs obtain in both cases

but the number of spurs is greater for curve (2) because it received a higher dose. Since the total electron concentration is the same for both points the local spin concentration is lower and the relaxation time is higher for the 34% point in curve (2).

An e_t^- concentration gradient may be established within the sample during optical bleaching and may possibly affect the validity of the above interpretation of the results. The concentration gradient has been calculated for the conditions of the present experiments and is negligible with respect to spur dimensions.⁹

B. Evidence for Spin-Spin Relaxation between Electrons and Radicals. Curves (3) and (4) apply to the situation where considerable spur overlap occurs. It is apparent that the same spin concentrations of e_t^- do not have the same relaxation times. The initial e_t^- concentration in curve (4) at 6.30 Mrad is less than the initial e_t^- concentration in curve (3) at 3.15 Mrad as shown in Figure 1, yet the relaxation time is lower at the higher dose. This indicates that the e_t^- spin interacts with the radical spins as well as other e_t^- spins. At high doses the radical spin concentration continues to increase and does not pass through a maximum as does the e_t^- concentration.⁶ So at doses above 3 Mrad the spin relaxation of e_t^- is dominated by interactions with the radicals over interactions with other e_t^- . When some of the e_t^- are bleached, there is no change in relaxation time because the radicals dominate the relaxation.

The spin-spin interaction between e_t^- and MTHF radicals that is supported by curves 3 and 4 contrasts with the conclusion that the spin-spin relaxation mechanism is only dependent on e_t^- and not on the O^- radicals in the alkaline ice matrix (10 M NaOH) at high dose.¹⁰ Thus there seems to be a real difference between these two matrices. In the MTHF matrix the overlap between the e_t^- and radical spectra is complete, but in the alkaline ice matrix the overlap is only partial. This difference may be related to these observations.

More quantitative evidence for spin-spin relaxation between trapped electrons and radicals in MTHF is provided by the expression for T_2 in terms of the local spin concentration. Kittel and Abrahams¹¹ calculated the frequency moments for spin-spin dipolar broadening from spins randomly distributed on a cubic lattice with the external magnetic field along the 100 axis. For nonequivalent magnetic centers (*i.e.*, different g -factors or g -anisotropy) and for a glassy or polycrystalline sample in which the species are oriented randomly with respect to the magnetic field the dipolar width is reduced by 0.67 and 0.71, respectively.¹² When the fractional spin population is less than 0.01, as it is for radiation-produced species, the dipolar line is Lorentzian and characterized by a frequency half-width at half-height of T_2^{-1} . The relationship between T_2 and $n\rho$ where n is the number of spins per gram and ρ is the matrix density is then given by eq 2 which can be rewritten as eq 3

$$T_2 = (0.82 \times 10^{-12} n\rho)^{-1} \quad (2)$$

$$(T_1 T_2)^{-1} = (0.82 \times 10^{-12} n\rho) T_1^{-1} \quad (3)$$

The data for $(T_1 T_2)^{-1}$ vs. dose taken from ref 6 is plotted according to eq 3 in Figures 3 and 4. In Figure 3 n is taken as the total bulk spin concentration of e_t^- plus radicals while in Figure 4 n is taken as only the e_t^- concentration. Now, n is the local-spin concentration, but as the spurs overlap at high doses the local

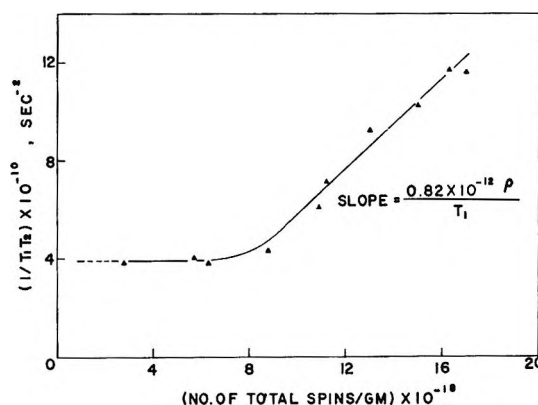


Figure 3. $(T_1 T_2)^{-1}$ of e_t^- in MTHF vs. total spin concentration of e_t^- plus radicals: a test of eq 3 in the text.

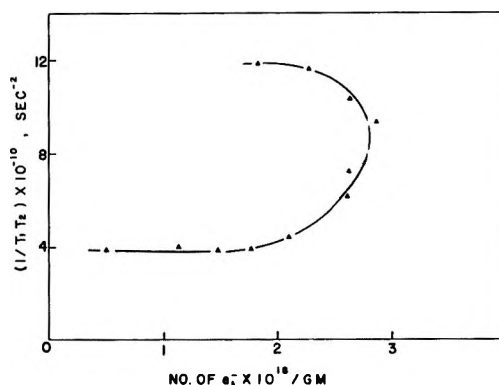


Figure 4. $(T_1 T_2)^{-1}$ of e_t^- in MTHF vs. the spin concentration of e_t^- only: a test of eq 3 in the text.

concentration approaches the bulk concentration. So eq 3 is expected to hold at high doses or higher total spin concentration. It can be seen that Figure 3 does fit eq 3 while Figure 4 does not at all. This confirms that the spin-spin relaxation of e_t^- involves the total spin concentration of both e_t^- and radicals. Furthermore, if T_1 is calculated from the slope in Figure 3 a value of 1.1×10^{-4} sec is obtained which is in reasonable agreement with the T_1 values previously measured.⁶

Acknowledgment. This research was supported by

- (9) D. P. Lin, Ph. D. Thesis, Wayne State University, 1971.
- (10) H. Hase and L. Kevan, *J. Chem. Phys.*, **52**, 3183 (1970).
- (11) C. Kittel and E. Abrahams, *Phys. Rev.*, **90**, 238 (1953).
- (12) S. J. Wyard, *Proc. Phys. Soc., London, Sect. A*, **86**, 587 (1965).

the U. S. Atomic Energy Commission under Contract No. AT(11-1)-2086. In addition equipment support

was received from the Air Force Office of Scientific Research under Grant No. AFOSR-70-1852.

Visible-Light Effects on Electronic Absorption Bands of Some Cation Radicals Produced by Photoionization at 77°K

by **Katsumi Kimura,* Shunji Katsumata, and Kazutoshi Sawada**

*Physical Chemistry Laboratory, Institute of Applied Electricity, Hokkaido University, Sapporo, Japan
(Received July 16, 1971)*

Publication costs assisted by the Institute of Applied Electricity, Hokkaido University

In an EPA rigid glass at 77°K, we have carried out photoionization experiments of some aromatic amines (*m*-aminophenol, *m*-anisidine, and *m*-phenylenediamine) yielding radical cations and trapped electrons located in their vicinity, and have observed appreciable blue shift and sharpening of electronic absorption bands of the cations by visible-light bleaching of the trapped electrons. When the biphenyl anions instead of the trapped electrons are located near the cations, the almost same spectral changes have also been observed. The observed cation-band shifts may be explained quantitatively by a perturbation theory, in which Coulomb potential terms due to the trapped electron are taken into account in the Fock Hamiltonian of the cations, suggesting that the photoejected electrons are trapped at a mean distance of about 30 Å from the partner cations.

Recently we have studied electronic absorption spectra of free radicals produced by uv irradiation of substituted benzenes in rigid glasses at 77°K.¹⁻⁴ When photolyzed in an EPA glass, some meta-disubstituted benzenes have been found to give very broad absorption bands peaking at about 670 nm owing to trapped electrons with an intensity as strong as the visible bands of the cations.⁴ It has also been shown that the trapped-electron band disappears completely by irradiation with red light without significantly affecting the intensity of the cation spectra.⁴ This experimental fact seems to indicate that most of the trapped electrons react with the solvent molecule by near-ir excitation to yield a secondary negative species, *e.g.*, C₂H₅O⁻, which does not show any detectable visible absorption bands. According to recent photoionization studies⁵⁻⁷ on some aromatic amines in rigid glasses, it has been indicated that photoejected electrons are trapped at a mean distance of 30 to 70 Å apart from the partner cations depending on polarity of rigid solvents used. For instance, the mean distance is reported to be 30 Å in a rigid EPA glass.⁶ Therefore, it seems interesting to determine whether a secondary negative ion species could be located at a similar distance.

While reinvestigating the 77°K photolysis of the meta-disubstituted benzenes, we noticed that their cation radicals showed small blue shifts and considerable band sharpenings of the visible bands when ir-

radiated by the visible light of 550-620 nm. This did not come to our attention in the previous study.⁴ In this note it is indicated that the spectral changes observed here may tentatively be explained in terms of a difference in electrostatic interaction between the cation-trapped electron system and the cation-secondary anion system.

Experimental Section

Samples studied here are *m*-aminophenol, *m*-anisidine, and *m*-phenylenediamine which were purified by the same method as previously.⁴ Photoirradiation experiments of these compounds were carefully carried out using glass and solution filters in the two following steps. The rigid EPA glasses containing these compounds (about 5×10^{-4} M) were first irradiated by uv light of 270-370 nm for 5-6 min in order to produce their cation radicals as well as the trapped electrons.

- (1) K. Kimura, K. Yoshinaga and H. Tsubomura, *J. Phys. Chem.*, **71**, 4485 (1967).
- (2) K. Kimura, H. Yamada, and H. Tsubomura, *J. Chem. Phys.*, **48**, 440 (1968).
- (3) S. Arimitsu, K. Kimura, and H. Tsubomura, *Bull. Chem. Soc. Jap.*, **42**, 1858 (1969).
- (4) A. Egawa, K. Kimura, and H. Tsubomura, *ibid.*, **43**, 944 (1970).
- (5) W. M. McClain and A. C. Albrecht, *J. Chem. Phys.*, **44**, 1594 (1966).
- (6) N. Yamamoto, Y. Nakato, and H. Tsubomura, *Bull. Chem. Soc. Jap.*, **40**, 451 (1967).
- (7) K. Tsuji and F. Williams, *Trans. Faraday Soc.*, **65**, 1718 (1969).

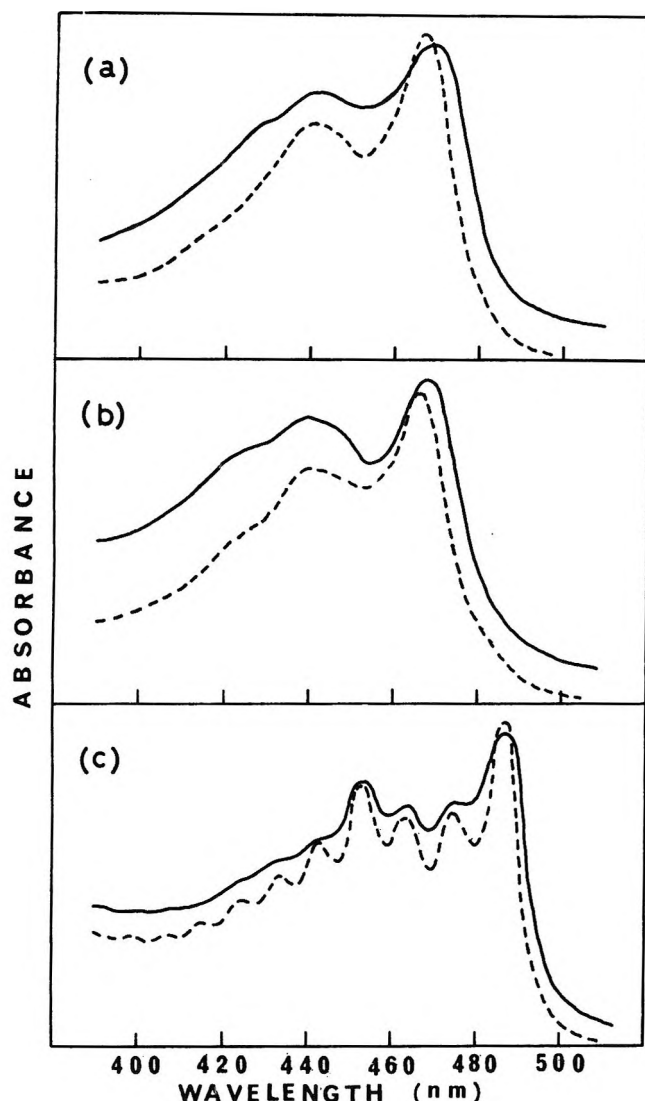


Figure 1. The longest wavelength cation bands observed before (—) and after (-----) the visible-light irradiation: a, *m*-aminophenol⁺; b, *m*-anisidine⁺; c, *m*-phenylenediamine⁺.

Then these uv-irradiated samples were illuminated by visible light of 550–620 nm for 2–3 min in order to bleach mainly trapped electrons without significantly affecting the cation band intensities.

Absorption spectrum measurements were carried out with a Cary Model 15 spectrophotometer, using a quartz cell of 15-mm path length. The solutions in the quartz cells were degassed by the freeze-pump-thaw technique and then were sealed.

Results and Discussion

In Figure 1, the absorption bands of the three cations measured before and after the photobleaching of the trapped electron are compared. Magnitudes of the observed band shifts are shown in Table I. From the previous studies, it may be sure that the electrons ejected from the molecules upon uv irradiation are trapped in the rigid glass.^{4,5}

Table I: Blue Shifts of the Longest Wavelength Cation Bands by the Visible-Light Irradiation

Systems	$\Delta\sigma$, cm ⁻¹
<i>m</i> -Aminophenol ⁺ + e ⁻	139
<i>m</i> -Aminophenol ⁺ + biphenyl ⁻	139
<i>m</i> -Anisidine ⁺ + e ⁻	73
<i>m</i> -Anisidine ⁺ + biphenyl ⁻	77
<i>m</i> -Phenylenediamine ⁺ + e ⁻	~0
<i>m</i> -Phenylenediamine ⁺ + biphenyl ⁻	~0

Similar spectral changes were also observed when the biphenyl anion is located in the vicinity of the cation. When biphenyl (about 1×10^{-3} M) as an electron scavenger is added into the EPA solutions of the compounds studied here, the absorption bands of not only the cation but also the biphenyl anion appear by the uv irradiation. The successive photobleaching of the biphenyl anion by using the visible light of the 600-nm region gives rise to essentially the same spectral change observed in the case of the trapped electron, again without affecting the cation-band intensities. The resulting cation band shifts are also included in Table I, for comparison.

Since as far as the cation remains the opposite charge should exist somewhere, the photobleaching of the trapped electron or of the biphenyl anion seems to transform an electron into, *e.g.*, C₂H₅O⁻, not showing any detectable visible absorption band. If the resulting negative charge retains in the same position as that of the original one (the trapped electron or the biphenyl anion), no spectral change may take place. The considerable cation-band sharpenings⁸ observed here could indicate a reduction in electrostatic field strength acting on the cation. Therefore, the secondary negative ion should locate in a much longer distance from the cation than the initial one. (Another possibility of an ion-pair formation between the cation and anion might be considered upon the visible-light irradiation, but this may be ruled out since such an ion-pair formation will shift the cation band to the opposite side.)

Let us estimate the average strength of electric field acting on the cation by the charge of an electron trapped in the EPA glass as follows. Using the Lorentz field for the effective field strength⁹ and the coulombic field for the external field, then the effective field (F) is given by $(D + 2)e/3Dr^2$, where D is the dielectric con-

(8) To investigate how much the cation-band sharpening takes place, the *m*-phenylenediamine⁺ band with vibrational structure obtained before and after the visible-light irradiation was analyzed in terms of a superposition of Gaussian functions. From such a spectrum simulation, it was found that the bandwidth (at 1/e of the peak height) becomes narrower from 600 to 500 cm⁻¹ by 20%. Similar band sharpenings were also observed for the other two cations.

(9) H. Labhart in "Advances in Chemical Physics," I. Prigogine, Ed., Interscience, New York, N. Y., 1967, p 179; K. Seibold, H. Navangul, and H. Labhart, *Chem. Phys. Lett.*, **3**, 275 (1969).

stant and r is the distance between the cation and the trapped electron. With a reasonable value of $D = 2$ for the 77°K glass, the effective field strength is estimated to be about 1070 kV/cm when at $r = 30 \text{ \AA}$. This may be compared with an external field of 500 kV/cm used by Sauter and Albrecht¹⁰ for studying an electronic absorption broadening of azulene in 3-methylpentane glass at 77°K.

With the model mentioned above for the secondary negative ion, the observed cation-band shifts (Table I) may be interpreted qualitatively by the following simple theoretical treatment. For simplicity, here, the secondary negative ion is assumed to be at a far distance from the cation so that its electric field acting on the cation is negligibly weak compared to that due to the initial negative charge. Since perturbation terms are given by $\sum_{\mu} Z_{\mu} e^2 / Dr_{\mu X}$ in the Fock Hamiltonian, the excitation energies are approximately given by

$$\Delta E_{i \rightarrow j} = \Delta \epsilon_i - \Delta \epsilon_j = \sum_{\mu} (c_{i\mu}^2 - c_{j\mu}^2) Z_{\mu X} e^2 / Dr_{\mu X} \quad (1)$$

Here $\Delta \epsilon_i = \epsilon_i' - \epsilon_i$, and ϵ_i' and ϵ_i are i th molecular orbital energies expressed by the use of the perturbed and nonperturbed Hamiltonian, respectively, and μ and X denote the μ th atomic orbital and the trapped electron, respectively. In this approximation, the transition-energy shifts can be calculated from a relation of

$$\Delta W = \sum_{ij} a_{ij} \Delta E_{i \rightarrow j} \quad (2)$$

in which a_{ij} 's are coefficients in the state wave functions. According to our recent theoretical calculation¹¹ with the open shell SCF-MO CI method, the cation bands under consideration are assigned to electronic transitions to the second excited states from the ground one. This calculation also indicates that the transitions to the first excited states may occur at 0.782 and 0.724 eV for m -aminophenol⁺ and m -phenylenediamine⁺, respectively, with very small oscillator strengths (0.004 and 0.010, respectively). No absorption bands assigned to these first transitions have been observed in the near-infrared region.

Taking these spectral assignments into account, the above eq 2, in which a main contribution comes from $\Delta E_{3 \rightarrow 5}$, yields the cation-band shifts plotted in Figure 2 with $D = 2$. The marked differences of curves a and b arise from mainly the differences of the coefficients in the third and fifth MO's of the two cations.¹²

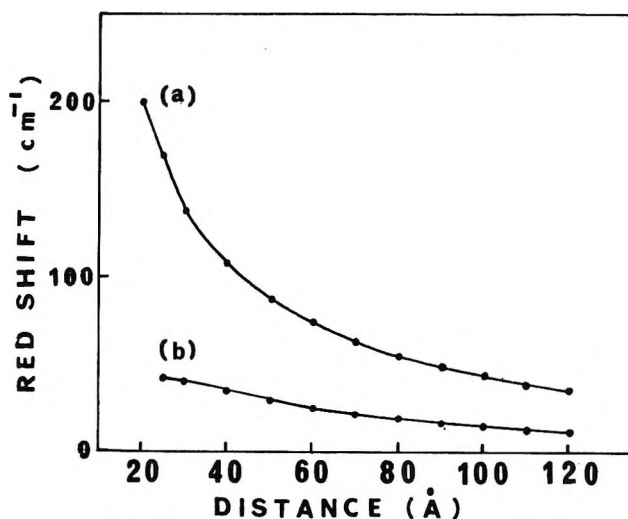


Figure 2. Calculated shifts of the cation bands plotted against distance between the cation and the trapped electron (or the biphenyl anion): a, m -aminophenol⁺; b, m -phenylenediamine⁺.

It is of interest to indicate that red shifts of 130 and 30 cm^{-1} are estimated at a distance of $r = 30 \text{ \AA}$ for m -aminophenol⁺ and m -phenylenediamine⁺, respectively, in fairly good agreement with the experimental shifts. The present experimental information seems thus to support that the photoejected electron is located in the vicinity of the partner cation, and by the visible light irradiation it reacts with the solvent molecule giving rise to a secondary anion species which is finally located at far distance from the cation.

Changes in the dipole moment between the ground and excited states of the cations ($\Delta \mu = \mu_e - \mu_g$) may roughly be estimated from the band shifts ($\Delta \sigma$) by the following equation: $\Delta \mu = (hc/F)\Delta \sigma$, with neglect of a polarizability change in the both states. Then, from the band shifts observed here, the dipole moment changes were evaluated to be about 7.8, 4.2, and 0 D for m -aminophenol⁺, m -anisidine⁺, and m -phenylenediamine⁺, respectively.

Acknowledgment. We wish to thank Mrs. T. Yamazaki for her help in the spectral measurement and Mr. Y. Achiba for his help in computation.

(10) H. Sauter and A. C. Albrecht, *Chem. Phys. Lett.*, **2**, 8 (1968).

(11) S. Katsumata and K. Kimura, to be published.

(12) Our calculation (ref 11) has shown that $c_{2N} = -0.38$, $c_{5O} = -0.29$, $c_{5N} = +0.41$, $c_{5O} = +0.19$ for m -aminophenol⁺, and $c_{2N} = -0.32$, $c_{5N} = +0.33$ for m -phenylenediamine⁺.

Barriers to Rotation around the Amide Bond and the Central Carbon–Carbon Bond in Tetrabenzoyloxamide and Its Monothio and Dithio Analogs

by Robert E. Carter* and Jan Sandström

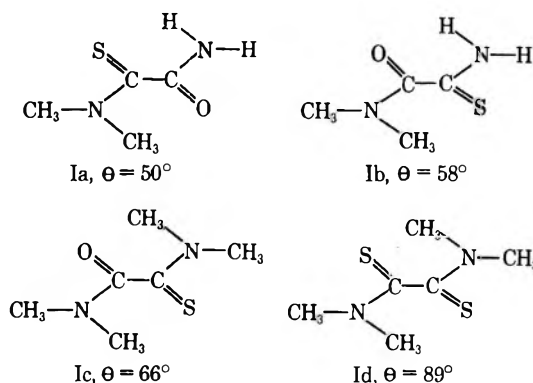
Divisions of Organic Chemistry 2 and 1, Chemical Center, S-220 07, Lund 7, Sweden (Received August 12, 1971)

Publication costs assisted by the Swedish Natural Sciences Research Council

By a study of the temperature-dependent nmr spectra of the title compounds, the barrier to rotation around the central carbon–carbon bond has been found to increase in the order oxamide (9.7 kcal/mol), thioxamide (17.6 kcal/mol), and dithioxamide (>24 kcal/mol). The barriers are predominantly steric in origin, and they result from repulsions between the oxygen or sulphur atom in one half of the molecule and the benzylic methylene group in the E position in the other. The barrier to rotation of the dibenzylamino group in the oxamide is similar to the analogous barrier in dimethylformamide, and the corresponding barriers in the thioamide parts are at least as high as in dimethylthioformamide, indicating that the molecule is free from strain in the initial state. The equilibrium conformations calculated by a nonbonded 6–12 potential function are in good agreement with dipole moment data. The INDOR technique proved very valuable in unraveling the four overlapping AB quartets in the nmr spectrum of the monothioxamide.

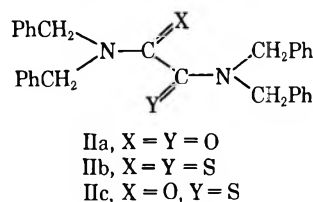
An earlier investigation of the ultraviolet spectra of mono- and dithioxamide and their N-methyl derivatives¹ showed that in the N,N-dimethyl derivatives the planar trans configuration is energetically unfavorable and that the steric strain is relieved by rotation mainly around the central carbon–carbon bond (the pivot bond). From the shifts of the uv maxima on N-methylation, it was possible to calculate approximate angles of twist (θ), and it was found that an $-\text{N}(\text{CH}_3)_2 \cdots \text{O}=\text{C}$ interaction gave a smaller twist than an $-\text{N}(\text{CH}_3)_2 \cdots \text{S}=\text{C}$ interaction, and that two $-\text{N}(\text{CH}_3)_2 \cdots \text{S}=\text{C}$ interactions caused a larger twist than one, as exemplified by the compounds Ia–d.

Such twisted molecules are chiral, and provided the



barriers to rotation around the pivot bond fall in the appropriate range, they can be estimated by a variable temperature study of the nmr spectra of suitable prochiral groups attached to the molecule. Siddall and Good² studied tetraisopropyloxamide and observed a rotation which was slow on the nmr time scale below -15° . We have chosen to study tetrabenzoyloxamide and its mono- and dithio analogs (IIa–c) in the hope of

obtaining a quantitative estimate of the difference in steric effect between oxygen and sulfur. For comparison, the temperature dependence of the nmr spectra of tetramethyloxamide and its dithio analog (Id) were also studied.



Experimental Section

Tetrabenzoyloxamide (IIa) was prepared according to Armbrrecht, *et al.*,³ from dibenzylamine and oxalyl chloride in benzene–triethylamine. It crystallized from 1-butanol as colorless rod-shaped prisms, mp $132\text{--}132.5^\circ$ (lit. $130\text{--}131^\circ$).

Tetrabenzylmonothioxamide (IIc). Tetrabenzoyloxamide (10 g) was reacted with phosphorus pentasulfide (10 g) in refluxing dry toluene (200 ml) for 10 hr with mechanical stirring. The solution was filtered hot, the residue extracted with hot toluene, and the combined toluene solutions were evaporated. Extraction with chloroform left an undissolved residue of phosphorus pentasulfide, and addition of light petroleum (bp $40\text{--}60^\circ$) to the chloroform solution precipitated a pale yellow crystalline product (8.5 g), mp $128\text{--}129^\circ$, consisting of a mixture of the mono- and dithioamides with unreacted starting material according to nmr anal-

(1) B. Persson and J. Sandström, *Acta Chem. Scand.*, **18**, 1059 (1964).

(2) T. H. Siddall, III, and M. L. Good, *Bull. Soc. Chem. Jap.*, **39**, 1619 (1966).

(3) B. H. Armbrrecht, L. M. Rise, C. H. Grogan, and E. Emmett Reid, *J. Amer. Chem. Soc.*, **75**, 4829 (1953).

ysis. Due to the very similar solubility properties of these compounds, fractional crystallization proved to be inefficient for separation, but on chromatography of the crude product (2.5 g) on alumina, benzene eluted the dithiooxamide (0.20 g), and benzene containing 5% diethyl ether, the monothiooxamide (1.61 g), which was obtained as pale yellow prisms, mp 134–136°, after recrystallization from toluene. (Calcd for $C_{30}H_{28}N_2OS$ (464.60): C, 77.6; H, 6.07; N, 6.03; S, 6.90. Found: C, 78.1; H, 6.02; N, 6.02; S, 7.03.)

Tetrabenzylidithiooxamide (IIb) was most conveniently prepared by reacting tetrabenzylloxamide (5 g) with phosphorus pentasulfide (6 g) in refluxing dry xylene (100 ml) for 26 hr with mechanical stirring. The solution was filtered hot, and on cooling the product separated (4.6 g, 84% yield) as pale yellow, flattened rods, mp 177–178° after recrystallization from toluene. (Calcd for $C_{36}H_{28}N_2S_2$ (480.67): C, 75.0; H, 5.87; N, 5.83; S, 13.3. Found: C, 74.3; H, 5.89; N, 5.81; S, 13.4.)

Tetramethyldithiooxamide was prepared according to Klöpping and van der Kerk.⁴

Nmr spectra were recorded on Varian A60, A60-A, HA-100, and/or XL-100 instruments, equipped with variable temperature probes and V-6040 temperature controllers. INDOR experiments⁵ were performed on the HA-100 instrument operating in the frequency sweep mode and locked on the signal from internal TMS or hexamethyldisiloxane. The irradiation radio-frequency field was generated by modulation of the magnetic field using a Hewlett-Packard 200 CD Audio Oscillator.

Temperature measurements were made by the replacement technique, using the Varian methanol or ethylene-glycol samples, calibrated with the aid of a thermocouple as previously described.⁶ Temperatures measured in this way are assumed to be accurate to within $\pm 2^\circ$, which is considered acceptable for the present purposes in view of the difficulty in an exact determination of the coalescence point in spectra with several overlapping AB quartets.

Free energies of activation were estimated by the approximate formulas appropriate for a coalescing doublet (1)⁷ or for a coalescing AB quartet (2),⁸ derived from the expressions given in references 7 and 8 in conjunction with the Eyring equation.⁹ The accuracy of

$$\Delta G^\ddagger = \frac{4.57T_c}{1000} \left(9.97 + \log \frac{T_c}{\Delta\nu_0} \right) \text{ kcal/mol} \quad (1)$$

$$\Delta G^\ddagger = \frac{4.57T_c}{1000} \times \left(9.97 + \log \frac{T_c}{\sqrt{\Delta\nu_{AB}^2 + 6J_{AB}^2}} \right) \text{ kcal/mol} \quad (2)$$

the ΔG^\ddagger determinations is governed mainly by the accuracy of the temperature measurements (*vide supra*). The estimated limits of error are given in Table I.

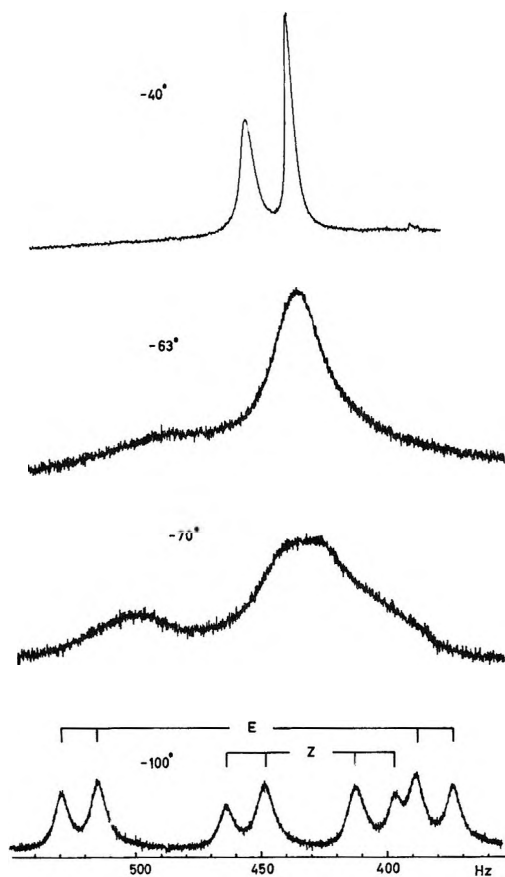


Figure 1. Nmr spectra of IIa in dichlorofluoromethane at 100 MHz, methylene protons.

Results and Discussion

Tetrabenzylloxamide (IIa). The 100 MHz spectra of this compound were recorded on 0.3–0.5 molal dichlorofluoromethane and deuteriochloroform solutions. At low temperatures (-90° to -100°) in dichlorofluoromethane solution, the spectrum of the benzylic protons consisted of two overlapping AB quartets (Table I and Figure 1), and the signals due to the aromatic protons were two well-resolved singlets. On increasing the temperature, first the downfield and then the upfield AB quartet coalesced (at -70° and at -63° , respectively), and at probe temperature the benzylic protons gave rise to two singlets at $\delta = 4.27$ and 4.42 (ppm from TMS). It is worth noting that the AB coupling constant in the high-field quartet (at -100°) is about 1 Hz greater than that in the low-field one. This may be a

(4) H. L. Klöpping and G. J. M. van der Kerk, *Rec. Trav. Chim. Pays-Bas*, **70**, 917 (1951).

(5) V. J. Kowalewski in *Progr. Nucl. Magn. Res. Spectrosc.*, **5**, 1 (1969).

(6) G. Isaksson and J. Sandström, *Acta Chem. Scand.*, **24**, 2565 (1970).

(7) H. S. Gutowsky and C. H. Holm, *J. Chem. Phys.*, **25**, 1228 (1956).

(8) R. J. Kurland, M. B. Rubin, and W. B. Wise, *J. Chem. Phys.*, **40**, 2426 (1964).

(9) S. Glasstone, K. J. Laidler, and H. Eyring, "Theory of Rate Processes," McGraw-Hill, New York, N. Y., 1941, p 195 ff.

Table I: Nmr Parameters (100 MHz) for Aromatic Protons and AB Spectra, and Barriers to Rotation around the Pivot Bond

Compound	ν_{Ar} , Hz ^a	$\nu_{CH_2} - Z$			T_c , °K	ΔG_0^\ddagger kcal/mol	$\nu_{CH_2} - E$			T_c , °K	ΔG_0^\ddagger kcal/mol
		ν_A^b	ν_B	J_{AB}			ν_A^b	ν_B	J_{AB}		
IIa ^c	725.6; 749.6	454.7	405.4	15.5	203	9.7 ± 0.2	521.6	381.0	14.5	210	9.7 ± 0.2
IIb ^d	727.7	495.7	441.7	15.2	546.4	492.2	14.4
IIb ^e	...	483.7	437.9	15.3	518.6	500.5	14.1
IIb ^f	718.5; 722.7	489.2	446.4	15.1	>473	>24	514.7	508.1	14.5
IIc ^d	<i>g</i> 721.0; 722.4	462.1	436.2	15.8	469.3	446.4	14.4
	<i>h</i> 729.7; 732.1	478.8	425.3	15.3	568.8	449.6	14.5	373	17.9 ± 0.5

^a No assignment to specific phenyl groups has been attempted. ^b Arbitrarily assigned to the low-field resonances. ^c In dichlorofluoromethane at -100° . ^d In deuteriochloroform at probe temperature. ^e In *o*-dichlorobenzene at probe temperature. ^f In hexamethylphosphoric triamide at $+60^\circ$. ^g Amide part. ^h Thioamide part.

reflection of different spatial orientations of the benzylic protons with respect to adjacent π bonds.¹⁰ The aromatic protons gave rise to two broad singlets at low temperatures ($\Delta\nu_{1/2} = 6-7$ Hz at *ca.* -100°). Between -80° and -60° the upfield signal was resolved into a broad, unsymmetrical "triplet," (Figure 2) while the downfield signal remained a singlet with $\Delta\nu_{1/2}$ of the order of 1.5 Hz between -50° and probe temperature. It is quite plausible that the differences in appearance of the two aromatic signals are due to different dispositions of the aryl rings with respect to the anisotropic carbonyl groups.

In deuteriochloroform solution at probe temperature, the singlets from the benzylic protons were at $\delta = 4.38$ and 4.51, and those due to the aromatic protons were at $\delta = 7.18$ ($\Delta\nu_{1/2} = 1.7$ Hz) and 7.28 ($\Delta\nu_{1/2} = 1.4$ Hz). On increasing the temperature, the benzylic singlets broadened and then coalesced at 127° (spectra run at 100 MHz with the sample in a sealed tube). The difference in width of the aromatic proton singlets disappeared as the temperature was increased, and the signals coalesced at 121° (spectra run at 100 MHz).

A reasonable interpretation of the appearance of the AB type spectra at low temperatures is hindered rota-



tion around the $-\text{C}-\text{C}-$ (pivot) bond. From the observed coalescence temperatures a value of 9.7 kcal/mol for ΔG^\ddagger may be estimated by the use of eq 2. The coalescence of the benzylic and aromatic singlet pairs at higher temperatures is of course due to rapid rotation on the nmr time scale around the $-\text{C}-\text{N}$ bonds. Use of eq 1 allows the estimation of a value of 21 kcal/mol for ΔG^\ddagger in this case.

Solvent effects seem to be of no great consequence for the amide rotation in IIa, since the same ΔG^\ddagger value (within the experimental error) was obtained in both hexamethylphosphoric triamide (HMPT) and *o*-dichlorobenzene (ODC) solution.

Tetrabenzylthiooxamide (IIb). In deuteriochloroform solution at probe temperature (100 MHz), the benzylic protons gave rise to two well-resolved AB

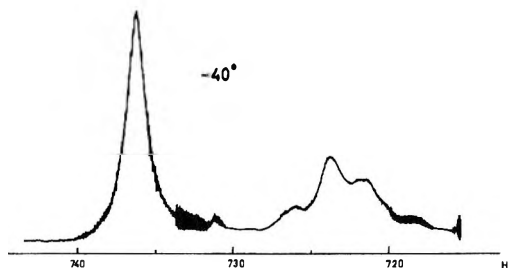


Figure 2. Aromatic protons of IIa in dichlorofluoromethane at 100 MHz.

quartets (see Table I). As noted above in the case of IIa, the AB coupling constant in the high-field quartet was about 1 Hz greater than that in the low-field one. Furthermore, the line width of the downfield pair of lines in each quartet in the spectrum of IIb was greater than that of the upfield pair. This is most plausibly explained as the result of stereospecific long-range coupling between the benzylic and aromatic protons. The resonance due to the aromatic protons was a broad band consisting of at least three poorly resolved peaks.

Spectra of this compound were recorded at various temperatures in HMPT and ODC solutions. In both of these solvents, the internal shift of the low-field benzylic AB quartet had been considerably diminished (see Table I). As the temperature was increased, all of the resonances due to the benzylic protons slowly broadened, but even at 188° , the highest temperature reached in ODC solution, the AB structure was still discernible. In HMPT solution, at about 200° (60 MHz), a broad structureless absorption was observed. In this case, it is unfortunately impossible to distinguish between the effects of thioamide rotation and rotation around the pivot bond on the line shape. A lower limit of 24 kcal/mol for ΔG^\ddagger for both rotations may be roughly estimated.

Tetrabenzylmonothiooxamide (IIc). A 100-MHz spectrum in deuteriochloroform solution at probe tempera-

(10) M. Barfield and D. M. Grant, *J. Amer. Chem. Soc.*, **85**, 1899 (1963); see S. Sternhell, *Quart. Rev., Chem. Soc.*, **23**, 236 (1969).

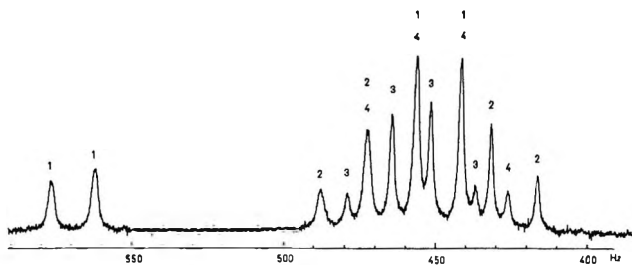


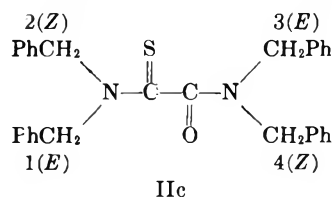
Figure 3. Methylene protons of IIc in deuteriochloroform at 100 MHz, probe temperature.

ture contained thirteen peaks between $\delta = 4.1$ and 5.8 ppm due to the benzylic protons (Figure 3), arising from four partially overlapping AB quartets (Table I), and four peaks due to the aromatic protons between $\delta = 7.1$ and 7.4 ppm. The four lines of each AB quartet were disclosed with the aid of the INDOR technique;⁵ the resulting assignments are indicated in Figure 3 and Table I. It should be pointed out that the chemical shifts of the benzylic protons of IIa and IIc are highly temperature dependent. As the temperature was increased, a gradual broadening of all signals was observed. Due to considerable overlap of the peaks from the various AB spectra at higher temperatures, the separate coalescence of each AB system was not discernible. However, since the line shape of the low-field half of the quartet denoted 1 (assigned to the thioamide half of the molecule; *vide infra*) could be observed undisturbed by the other benzylic signals, a coalescence temperature of about 100° could be estimated for this quartet. All four lines of the quartet denoted 2 (also assigned to the thioamide half of the molecule) were observable up to about 70°. Between this temperature and *ca.* 95°, the 2 quartet was transformed into a broad shoulder on the high-field side of the relatively sharp singlet arising from the coalescence of the 3 and 4 quartets (assigned to the amide half of the molecule). It is obvious that the line shapes of the 3 and 4 quartets must be influenced by both the rotation around the pivot bond and that around the acyl-nitrogen bond in the amide group. A coupling of these two rotations is an attractive possibility, since a rotation around the amide bond alleviates the $\text{CH}_2 \cdots \text{S}$ interaction (*vide infra*) which is responsible for the twist around the pivot bond. At *ca.* 130°, the highest temperature reached in deuteriochloroform solution (sealed tube), the benzylic proton resonances consisted of a strongly broadened doublet arising from the collapsed 1 and 2 quartets and, overlapping the "2-component" of the doublet, a relatively sharp singlet from the collapsed 3 and 4 quartets. The same general appearance of the spectrum was observed at higher temperatures in HMPT solution, but even at 200°, the 1-2 doublet had not coalesced. This allows the estimation of a rough value of 24 kcal/mol as a lower limit for the barrier to acyl-nitrogen rotation in the thioamide group. A

tentative assignment of the quartets 1-4 to the four methylene groups in the monothiooxamide may be made on the basis of the following observations.

(a) In the 100-MHz spectrum of the oxamide in dichlorofluoromethane and in that of the monothiooxamide in deuteriochloroform solution, the protons of one of the benzylic methylenes show AB shifts of 140.6 Hz and 119.2 Hz, respectively, whereas the AB shifts of the other benzylic protons in these molecules fall in the region 20-55 Hz. The large shifts may be attributed to the proximity of a methylene group in one half of the molecule to a carbonyl group in the other half. An indication that this interpretation is correct may be obtained from the fact that both of the AB shifts in the dithiooxamide spectrum are only 54 Hz (at 100 MHz in deuteriochloroform solution; see Table I).

(b) Of the four AB coupling constants in the monothiooxamide spectrum, two fall in the region 14.1-14.5 Hz and two in the region 15.3-15.8 Hz. As noted above, there is a similar difference between the coupling constants in the oxamide (IIa) and dithiooxamide (IIb) spectra. With the aid of a molecular model it becomes clear that the methylene group with the large shift is most likely the E group¹¹ in the thioamide half of the molecule (1). From the behavior of the spectrum with increasing temperature, it can be concluded that the signals of quartet 2 (in compound IIc below)



are attributable to the thioamide Z-methylene group. The smaller of the two "thioamide" AB coupling constants is thus associated with the E-methylene group, and the larger with the Z group. It seems reasonable to assume that the same relation holds in the amide half of the molecule. Accordingly, the signals of quartet 3 are assigned to the amide Z-methylene group, and those of 4 to the E group. Also for the oxamide and dithiooxamide, the AB quartet with the large coupling constant is assigned to the Z methylene group, and that with the small coupling constant to the E group.

Amide Rotations and Equilibrium Conformations. The barrier to rotation of the dibenzylamino group in the oxamide IIa (Table II) is close to the values given for the corresponding rotation in *N,N*-dimethylformamide (20.8-21.1 kcal/mol in carbon tetrachloride¹²). The analogous barriers in the dithiooxamide IIb and in the thioamide group of IIc are at least not signifi-

(11) J. E. Blackwood, C. L. Gladys, K. L. Loening, A. E. Petrarca, and J. E. Rush, *J. Amer. Chem. Soc.*, **90**, 509 (1968).

(12) M. Rabinowitz and A. Pines, *J. Amer. Chem. Soc.*, **91**, 1585 (1969).

Table II: Nmr Parameters (at 100 MHz unless Otherwise Noted) for Amide and Thioamide Rotations

Compound	Solvent	$ \nu_E - \nu_Z ^a$, Hz	$ \nu_E - \nu_Z ^b$, Hz	T_c , °K	ΔG_0^\ddagger , kcal/mol
IIa	CDCl ₃	14.9		400	20.8
			9.3	394	20.9
	ODC	10.8	...	395	20.8
	HMPT	9.8		395	20.9
			10.8	397	20.9
IIb	HMPT	22.5 ^c	...	>473	>24
IIc	HMPT	47 ^c	...	>473	>24
Tetramethyloxamide	HMPT	1.2	...	373	21.2
Tetramethyldithio-oxamide	ODC	10.2	...	451	23.9

^a Methyl and methylene protons ^b Aromatic protons. ^c At 60 MHz.

cantly lower than in *N,N*-dimethylthioformamide (24 kcal/mol¹³) or *N*-methyl-*N*-benzylthioformamide (25.1 kcal/mol¹⁴). This is to be expected, if the two halves of the molecules II are independent of each other in the equilibrium conformation. To clarify this point, we have calculated the conformational energy of the molecule as a function of the dihedral angle θ . Starting from the *s*-*trans* conformation ($\theta = 0$), we have computed the atom pair interactions that are affected by the rotation around the pivot bond, employing the technique described by Scheraga.¹⁵ Molecular models indicate that the benzene rings are turned away from the opposite half of the molecule in all reasonable conformations (Figure 4), and consequently all repulsions involving these groups were neglected. An idealized geometry was assumed, with all bond angles equal to 120° and the bond lengths taken from the X-ray crystallographic studies of oxamide¹⁶ and dithiooxamide,¹⁷ though with the pivot bond assumed to be 1.48 Å in all three systems. The atom-atom interactions were calculated by a Lennard-Jones potential (eq 3). The coefficients e_{ij} depend on the atoms involved and were

$$U_{ij} = \frac{d_{ij}}{r^{12}} - \frac{e_{ij}}{r^6} \quad (3)$$

obtained using the Slater-Kirkwood equation¹⁵

$$e_{ij} = \frac{1.5 e \hbar \alpha_i \alpha_j}{\sqrt{m} \left(\sqrt{\frac{\alpha_i}{N_i}} + \sqrt{\frac{\alpha_j}{N_j}} \right)} = \frac{362.32 \alpha_i \alpha_j}{\sqrt{\frac{\alpha_i}{N_i}} + \sqrt{\frac{\alpha_j}{N_j}}} \quad (4)$$

where α_i is the polarizability of atom i (in Å³) and N_i is the "effective" number of outer shell electrons. N_i was obtained by a graphic method devised by Scott and Scheraga.¹⁸ The coefficient for the r^{-12} term is obtained by minimizing the energy for a distance equal to the sum of the van der Waals radii of atoms i and j . The parameters employed are found in Table III.

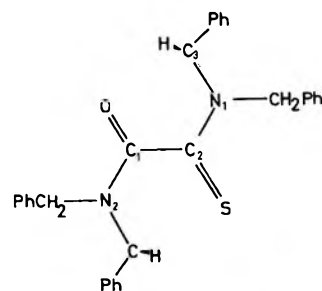


Figure 4. The *s*-*trans* conformation of IIc, used for interaction calculations.

Table III: Parameters for Calculating Nonbonded Potentials; from Ref 15 unless Otherwise Stated

Atom or group	N_i	r_{\min} , Å	α , Å ³	Interaction	e_{ij} Å ⁶ , kcal/mol	d_{ij} 10 ⁻³ Å ¹² , kcal/mol
C	5.2	1.70	0.93	CO	367	205
				CS	1409	1295
				HN	125	27
H	0.9	1.20	0.42	HO	125	25
				HS	498	181
N	6.1	1.55	0.87	NN	363	161
				NO	365	153
O	7.0	1.52	0.84	NS	1385	979
				OO	367	145
S	15.0 ^a	1.80	3.90 ^b	OS	1387	928
				SS	5405	5883
				CH ₂ CH ₂	1129	1448
CH ₂	7.0 ^c	1.85 ^c	1.77 ^c	OS	1387	928
				SS	5405	5883
				CH ₂ CH ₂	1129	1448

^a Calculated according to ref 18. ^b Average polarizability, $1/3 (\alpha_{\parallel} + 2 \alpha_{\perp})$, calculated from the value for carbon disulfide (K. G. Denbigh, *Trans. Faraday Soc.*, **36**, 936 (1940)). ^c From D. A. Brandt, W. G. Miller, and P. J. Flory, *J. Mol. Biol.*, **23**, 47 (1967).

The conformations of the benzylic methylene groups were chosen so that both hydrogen atoms had the same distance to the opposite oxygen or sulfur atom, and the individual H...O(S) and C...O(S) interactions were computed. They were found to vary in a parallel manner throughout the entire range of dihedral angles, and they were the only repulsive interactions in the range $0 \leq \theta \leq 100^\circ$. The methylene groups were treated as united particles ("extended atoms" according to Scheraga¹⁵) in the CH₂...CH₂ interaction, which

(13) A. Loewenstein, A. Melera, P. Rigny, and W. Walter, *J. Phys. Chem.*, **68**, 1597 (1964).

(14) W. Walter, G. Maerten, and H. Rose, *Justus Liebig's Ann. Chem.*, **691**, 25 (1966).

(15) H. A. Scheraga, *Advan. Phys. Org. Chem.*, **6**, 103 (1968).

(16) C. Romers, *Acta Crystallogr.*, **6**, 429 (1953).

(17) P. J. Wheatley, *J. Chem. Soc.*, 396 (1965).

(18) R. A. Scott and H. A. Scheraga, *J. Chem. Phys.*, **42**, 2209 (1965).

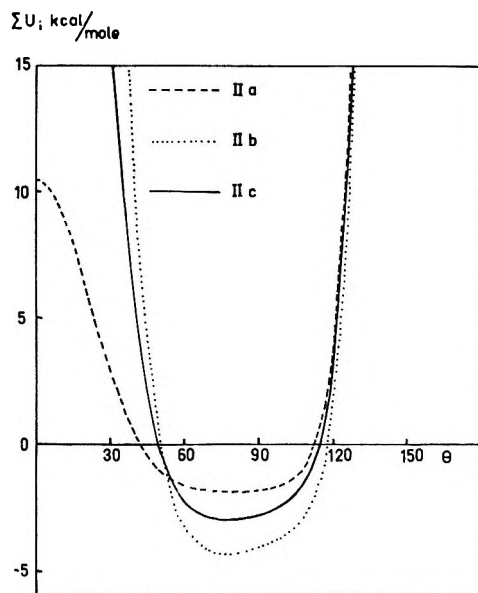


Figure 5. Nonbonded interactions in compounds II as a function of the dihedral angle θ .

was repulsive beginning at $\theta = 100^\circ$ with an energy that increased rapidly with increasing dihedral angle.

Since our aim has not been to calculate the barrier to rotation around the pivot bond, we have omitted all considerations of bond bending and compression, as well as electrostatic interactions and π -electron interaction across the pivot bond. Consequently, the calculated differences in strain energy between the equilibrium conformations and the transition states for rotation around the pivot bond are more or less unrealistic. It is evident, however, that the transition state must have the *s*-trans conformation, since the

corresponding barriers are 12.3 kcal/mol for IIa, 116.1 kcal/mol for IIb, and 64.2 kcal/mol for IIc, whereas the energies for the *s*-cis conformations are extraordinarily high. It also appears that the two halves of the molecule are independent of each other in the range $50^\circ \leq \theta \leq 110^\circ$, and this conclusion is not affected by the approximations made in the calculations. Therefore, we concluded that the initial state of the amide (thioamide) rotation is free from steric strain in the equilibrium conformation. This must also apply to tetramethyldithiooxamide, and is reflected in the good agreement between the thioamide barriers in this compound (Table II) and in dimethylthioformamide. As mentioned above, only a lower limit to the thioamide barriers in IIb and IIc could be determined. If these barriers are indeed higher than that in dimethylthioformamide, this could most reasonably be ascribed to steric strain in the transition state. The similarity of the amide barriers in IIa, tetramethyloxamide (Table II), and dimethylformamide indicates that this effect must be small.

It is worth noting (Figure 5) that the equilibrium values for the dihedral angle obtained for the oxamide ($\theta = 80^\circ$) and dithiooxamide ($\theta = 77^\circ$) systems agree well with the values found by Lumbroso¹⁹ by an analysis of the dipole moments of tetramethyloxamide ($\theta = 85^\circ$) and tetramethyldithiooxamide ($\theta = 82^\circ$).

Acknowledgments. We wish to thank Miss Eva Ericsson for able experimental assistance. This work was supported in part by the Swedish Natural Sciences Research Council.

(19) H. Lumbroso in a paper presented at the Fourth Symposium on Organic Sulphur Chemistry in Venice, 1970.

The Infrared Spectrum of Matrix Isolated $\text{UO}_2(\text{g})$ and Its Thermodynamic Properties¹

by S. Abramowitz* and N. Acquista

National Bureau of Standards, Washington, D. C. 20234 (Received September 29, 1971)

Publication costs assisted by the National Bureau of Standards

The far-infrared spectrum of U^{16}O_2 and U^{18}O_2 has been observed and assigned. A value of the missing stretching fundamental has been estimated. These vibrational frequencies have been utilized to estimate the S°_{2000} for reasonable molecular models. A value of S°_{2000} of 93.9 ± 2.0 eu is estimated for $\text{UO}_2(\text{g})$ to the harmonic oscillator rigid rotor approximation. Any electronic contributions to the S°_{2000} have been neglected and a singlet ground state has been assumed.

The infrared spectrum of matrix isolated UO_2 has recently been observed.² In this study we observed one stretching fundamental for U^{16}O_2 , $\text{U}^{16}\text{O}^{18}\text{O}$, and U^{18}O_2 and we also reported observing ν_2 , the bending mode of UO_2 at 81 cm^{-1} for U^{16}O_2 and at 73 cm^{-1} for U^{18}O_2 . The observation of ν_2 of U^{18}O_2 was somewhat obscured by the absorption band of the polyethylene windows (used as outer windows in our cryostat) in this region. Having observed ν_2 , and a stretching mode of $\text{U}^{16}\text{O}^{18}\text{O}$, it seemed worthwhile to try to estimate the missing stretching fundamental in order to have reasonable values for the calculation of thermal functions for this species.

We calculated the value of the missing fundamental by using the observed stretching modes of U^{16}O_2 , $\text{U}^{16}\text{O}^{18}\text{O}$, and U^{18}O_2 , and the bending mode of U^{16}O_2 and U^{18}O_2 . An angle of 105° yields very good agreement with the observed frequencies if one assigns the observed fundamental to ν_1 , the symmetric stretching frequency. A variation of $F_{12} = \sqrt{2}fr\alpha$ over values from $+0.5$ to -0.5 mdyne/Å does not materially affect the calculated value of ν_3 . (The calculated value of ν_3 varies from 753.8 to 756.3 cm^{-1} .) Reversing the assignment of the stretching modes requires the change in the angle to about 90° and results in a calculated frequency for ν_1 varying from 754.2 to 757.3 for a similar variation in F_{12} . A drastic change of the angle from the 90 – 110° range to 160° results in a somewhat poorer fit in the calculated frequencies, but does not materially change the value of the calculated missing fundamental. Values of about $755 \pm 5 \text{ cm}^{-1}$ are calculated for the fundamental for a suitable variation of F_{12} . The difficulty of estimating the angles for a molecule such as UO_2 was noted in ref 1. However, we feel that an angle of about 105° is consistent with the observed data. In conclusion we prefer a value of 755 cm^{-1} for the unobserved stretching fundamental and an angle of 105° for the OOU angle. An uncertainty in this frequency of about 15 cm^{-1} is indicated by the calculations, but as

noted below, an error of 10% in this frequency will not seriously alter the calculated entropy. A summary of some of the calculations is given in Table I. Linevsky has observed ThO_2 in an argon matrix at liquid helium temperatures.³ He observed both ν_1 and ν_3 for Th^{16}O_2 , Th^{18}O_2 , and $\text{Th}^{16}\text{O}^{18}\text{O}$. His data are consistent with an angle of 106° with ν_1 higher in frequency than ν_3 ($\nu_1 = 786.8 \text{ cm}^{-1}$, $\nu_3 = 734.5 \text{ cm}^{-1}$). The similarity of these results with those in our study is very good and lends confidence to our conclusions.

The calculation of the thermal functions of $\text{UO}_2(\text{g})$ to the rigid rotor harmonic oscillator approximation was performed. To test the sensitivity of the calculation to our choice of molecular parameters we varied α , the value of the calculated stretching frequency, and R , the interatomic distance. The S°_{2000} is given in Table II for some of the models chosen assuming a nondegenerate electronic ground state and no low-lying electronic states which would contribute to the entropy at 2000 K. The number of significant figures is given for comparison purposes and does not reflect the accuracy of the value reported.

As one can see, a variation in R of 0.25 \AA from 1.75 to 2.00 \AA at a constant value of α changes the entropy by 0.80 eu; a change in the vibrational frequency from 755 to 680 cm^{-1} effects the entropy to the extent of 0.20 eu, while a change in α from 105 to 160° gives a difference of 2.02 eu. Therefore, we feel that a S°_{2000} of $\text{UO}_2(\text{g})$ is 93.9 ± 2.0 eu assuming the matrix frequencies reflect the gas phase frequencies. In this connection it should be noted that a change in vibrational frequency for ν_2 from 81 to 100 cm^{-1} changes the entropy by about 0.54 eu.

We prefer a value of 93.9 eu which is in good agree-

(1) This research was supported in part by the Defense Nuclear Agency, Washington, D. C.

(2) S. Abramowitz, N. Acquista, and K. R. Thompson, *J. Phys. Chem.*, **75**, 2283 (1971).

(3) M. Linevsky, private communication.

Table I: Force Constants and Frequencies for Various Molecular Models of UO_2

F_{11}^a $f_r + f_{rr}$	F_{12}^a $\sqrt{2}f_{r\alpha}$	F_{22}^a f_α	F_{33}^a $f_r - f_{rr}$	α	$\nu_1,^b \text{ cm}^{-1}$	$\nu_2,^b \text{ cm}^{-1}$	$\nu_3,^b \text{ cm}^{-1}$	Species
6.859	0.0	0.027	4.936	105	874.2 (0.1)	79.1 (1.9)	753.8	U^{16}O_2
					826.7 (-0.1)	74.9 (-1.9)	714.1	U^{18}O_2
					854.4 (0.0)	77.0	730.0	$\text{U}^{16}\text{O}^{18}\text{O}$
5.11	0.0	0.027	6.63	105	757.5	79.1 (1.9)	873.4 (0.9)	U^{16}O_2
					713.5	74.9 (-1.9)	827.5 (-0.9)	U^{18}O_2
					730.1	77.0	854.4 (0.0)	$\text{U}^{16}\text{O}^{18}\text{O}$
5.02	0.0	0.028	6.741	90	754.2	79.1 (1.9)	873.8 (0.5)	U^{16}O_2
					713.8	74.8 (-1.8)	827.1 (-0.5)	U^{18}O_2
					730.1	77.0	854.4 (0.0)	$\text{U}^{16}\text{O}^{18}\text{O}$
5.02	0.0	0.028	6.741	90	873.8 (0.5)	79.1 (1.9)	754.2	U^{16}O_2
					827.1 (-0.5)	74.8 (-1.8)	713.8	U^{18}O_2
					854.4 (0.0)	77.0	730.1	$\text{U}^{16}\text{O}^{18}\text{O}$
5.33	0.0	0.026	6.34	160	755.7	79.0 (2.0)	872.5 (1.8)	U^{16}O_2
					712.8	75.0 (-2.0)	828.4 (-1.8)	U^{18}O_2
					730.4	77.0	854.4 (0.0)	$\text{U}^{16}\text{O}^{18}\text{O}$

^a All force constants in $\text{mdyn}/\text{\AA}$. ^b The $(\nu_{\text{obsd}} - \nu_{\text{calcd}})$ is given parenthetically. The error in ν_2 of about 2 cm^{-1} probably reflects the error in measuring ν_2 of U^{18}O_2 as discussed.

Table II: S°_{2000} for Various Models of UO_2^a

α	Vibrational frequencies, cm^{-1}			$R, \text{\AA}$	$S^\circ_{2000}, \text{ cal mol}^{-1} \text{ K}^{-1}$
105	755	81	874.3	1.75	93.882
160	755	81	874.3	1.75	91.859
90	755	81	874.3	1.75	93.934
105	680	81	874.3	1.75	94.085
105	755	81	874.3	2.00	94.678
105	755	81	874.3	1.60	93.347
105	755	100	874.3	1.75	93.463
105	740	81	874.3	1.75	93.920

^a Any electronic contributions to the entropy have been neglected and a singlet ground state has been assumed.

ment with the S°_{2000} for PuO_2 and CeO_2^4 which have been determined by standard calorimetric means to be 93.3 and 92.7, respectively, with an uncertainty of about

1 to 2 eu. This value is also in agreement with entropy values computed from vapor pressure and calorimetric data. It should be noted that this estimated value of the entropy, unlike previous ones, neglects any contribution from excited electronic states and further assumes a singlet ground state for UO_2 . Since the UO_2 molecule has a C_{2v} structure with a preferred angle of 105° one expects both valence and ionic bonding between the U and O atoms. This type of bonding may be expected to yield low multiplicities for UO_2 . The addition of $R \ln 3$ to the entropy values given in Table II would be required if the ground state of UO_2 is a triplet instead of a singlet. No data exist on the electronic states of UO_2 making estimates of entropy contributions from the excited levels difficult.

(4) R. J. Ackermann, *J. Chem. Thermodynamics*, in press.

Location of Univalent Cations in Synthetic Zeolites of the Y and X Type with Varying Silicon to Aluminum Ratio. II. Dehydrated Potassium Exchanged Forms

by W. J. Mortier,* H. J. Bosmans, and J. B. Uytterhoeven

Laboratorium voor Oppervlaktischeikunde, 3030 Heverlee, Belgium (Received August 30, 1971)

Publication costs assisted by the Katholieke Universiteit Leuven

The structure of four dehydrated, potassium exchanged Y and X zeolites (Si:Al ratio 2.98, 2.51, 1.75, and 1.22 respectively) was studied using X-ray powder methods. The cations seem to be distributed over the highest charged sites. The total occupancy of the sites I and I' approaches a maximum amount, imposed by the rule that no sites sharing the same six-membered ring shall be occupied simultaneously. The occupancy of site II also reaches its maximum. A comparison was made with the hydrated state, for which the structure parameters were determined in previous work.

Introduction

The occupancy of the different exchange positions in the synthetic zeolites X and Y is not fixed and is to be considered as a parameter in minimizing the free energy of the structure. The occupancy of the cation sites is influenced by, *e.g.*, the Si:Al ratio, the nature and the charge of neutralizing cations, and the presence or absence of hydration water or other ligands.

In the first part of this work¹ we investigated a series of synthetic zeolites X and Y, with Si:Al ratios of 2.98, 2.51, 1.75, and 1.22, saturated with K⁺ ions and hydrated. It was shown that there are gradual changes in the occupancy of the different ion sites from sample to sample.

In the present work the same samples are investigated in the dehydrated form: important changes in the occupancy of the ion sites were observed and will be discussed.

Thus far, it was mainly for the location of the multivalent cations in the zeolites X and Y that a comparison was made between the hydrated and dehydrated state. A general observation was an increased population of the sites inside the small cavities (I and I') in the dehydrated state with respect to the hydrated samples. Smith² made an excellent review on that subject.

Within the composition range of our zeolites, K exchanged and dehydrated samples were only studied by Eulenberger,³ *et al.*, who investigated a dehydrated KY sample (Si:Al = 2.36), and by Pluth and Schomaker (see Smith²) who studied a single crystal of a K⁺ exchanged and dehydrated natural faujasite (Si:Al = 2.3). Their results will be included in our discussion.

In this paper we provide a systematic survey of the changes in the occupancy of the different ion loca-

tion sites in relation with the Si:Al ratio for a series of dehydrated samples saturated with the same monovalent ion: K⁺. A comparison with part I of this work¹ will provide an insight in the influence of hydration water on the ion location.

Experimental Section

Four samples of synthetic faujasite with Si:Al ratios of 2.98, 2.51, 1.75, and 1.22 were kindly supplied by the Linde Company. The chemical composition and a full description of the analytical methods are given in part I.¹ For this work a vacuum camera was constructed in which the samples could be heated to a temperature over 300° and evacuated at a pressure of 10⁻⁵ to 10⁻⁶ Torr. The windows of the camera consisted of two layers of milar, and the vacuum-tight sealing was realized with epoxy resin araldite. The camera was mounted on the axis of the Philips powder diffractometer and carefully adjusted using Si powder as a standard.

The pretreatment of the sample in the camera consisted of an overnight evacuation at 80 to 100°. The temperature was then raised slowly to 300° and kept at that level for at least 1 hr. Subsequently, the sample was cooled to room temperature. During this procedure a pressure of 10⁻⁵ Torr was maintained by continuous pumping. Comparison with thermogravimetric experiments revealed that this procedure delivers a completely dehydrated sample. Rehydration of the sample was prevented by continuing the evacuation during the diffraction experiment.

(1) W. J. Mortier and H. J. Bosmans, *J. Phys. Chem.*, **75**, 3327 (1971).

(2) J. V. Smith, 2nd International Conference on Molecular Sieve Zeolites at Worcester, Mass., 1970.

(3) G. R. Eulenberger, D. P. Shoemaker, and J. G. Keil, *J. Phys. Chem.*, **71**, 1812 (1967).

Table I: Dehydrated K Zeolites X and Y

		Atomic parameters ^a			
		F 48.2	F 54.7	F 69.3	F 86.5
(Si, Al)	<i>x</i>	0.1244 (2)	0.1262 (2)	0.1250 (2)	0.1246 (2)
	<i>y</i>	0.9456 (2)	0.9450 (2)	0.9459 (2)	0.9456 (2)
192 (i)	<i>z</i>	0.0376 (2)	0.0368 (2)	0.0369 (2)	0.0372 (2)
	<i>B</i> , Å ²	2.26 (11)	2.48 (13)	0.94 (14)	1.78 (14)
O ₁	<i>x</i> = - <i>y</i>	0.1063 (9)	0.1056 (11)	0.1070 (12)	0.1075 (11)
	<i>z</i>	0.0	0.0	0.0	0.0
96 (h)	<i>B</i> , Å ²	5.68 (43)	6.62 (51)	6.05 (58)	6.08 (52)
O ₂	<i>x</i> = <i>y</i>	0.2521 (8)	0.2507 (10)	0.2506 (10)	0.2504 (13)
	<i>z</i>	0.1355 (5)	0.1398 (6)	0.1358 (6)	0.1373 (8)
96 (g)	<i>B</i> , Å ²	3.67 (33)	3.93 (39)	2.03 (38)	5.94 (51)
O ₃	<i>x</i> = <i>y</i>	0.1718 (7)	0.1714 (8)	0.1737 (8)	0.1745 (8)
	<i>z</i>	0.9673 (5)	0.9639 (5)	0.9642 (6)	0.9615 (6)
96 (g)	<i>B</i> , Å ²	1.47 (31)	1.74 (33)	0.00 (33)	1.51 (39)
O ₄	<i>x</i> = <i>y</i>	0.1801 (8)	0.1798 (8)	0.1797 (8)	0.1803 (8)
	<i>z</i>	0.3202 (5)	0.3224 (6)	0.3225 (6)	0.3233 (6)
96 (g)	<i>B</i> , Å ²	1.88 (31)	2.02 (36)	1.04 (38)	1.55 (37)
K(I)	<i>x</i> = <i>y</i> = <i>z</i>	0.0	0.0	0.0	0.0
	occupancy	0.402 (32)	0.335 (35)	0.590 (38)	0.573 (35)
16 (c)	<i>B</i> , Å ²	8.13 (1.26)	8.48 (1.78)	6.41 (1.00)	6.83 (1.06)
K(I')	<i>x</i> = <i>y</i> = <i>z</i>	0.0749 (18)	0.0768 (15)	0.0751 (19)	0.0760 (20)
	occupancy	0.441 (20)	0.566 (20)	0.518 (24)	0.430 (22)
32 (e)	<i>B</i> , Å ²	4.61 (63)	4.52 (50)	4.51 (69)	3.21 (65)
K(II)	<i>x</i> = <i>y</i> = <i>z</i>	0.2535 (7)	0.2510 (8)	0.2502 (7)	0.2473 (10)
	occupancy	0.815 (14)	0.838 (17)	0.903 (19)	0.799 (18)
32 (e)	<i>B</i> , Å ²	1.27 (21)	2.13 (27)	0.98 (26)	2.44 (30)
K ⁺	<i>x</i> = <i>y</i> = <i>z</i>	0.3750	0.3750	0.3750	0.3750
	<i>R</i> , Å	5.4	5.3	5.4	5.4
	<i>n</i> ⁰ molecules	1.58	4.42	14.88	38.19
8 (b)	<i>B</i> , Å ²	10.0	10.0	10.0	10.0
Final	<i>R</i> _I	0.1983	0.1967	0.2018	0.1958
	<i>R</i> _F	0.1231	0.1259	0.1299	0.1321

^a The standard deviations are indicated in parentheses.

The unit cell parameters were obtained by extrapolation of about 20 a_0 values, calculated from the strongest Cu $K\alpha_1$ peaks, against $\cos^2 \theta / \sin \theta$.⁴ (λ of Cu $K\alpha_1$ was taken 1.54050 Å). The extrapolated a_0 values are given below. The samples are indicated by the letter F followed by the number of cations per unit cell. The chemical compositions are given in parentheses: F 48.2, (K_{48.2}Al_{48.2}Si_{143.8}O₃₈₄) $a_0 = 24.776$ (1) Å; F 54.7, (K_{54.7}Al_{54.7}Si_{134.3}O₃₈₄) $a_0 = 24.896$ (6) Å; F 69.8, (K_{69.8}Al_{69.8}Si_{122.2}O₃₈₄) $a_0 = 24.973$ (3) Å; F 86.5, (K_{86.5}Al_{86.5}Si_{105.5}O₃₈₄) $a_0 = 25.076$ (3) Å.

For each sample, four diffractometer diagrams were recorded. The intensities of the peaks were estimated from the weights of paper cuts, made in tracing paper, and obtained as the mean of the four independent measurements. They were measured up to $N = h^2 + k^2 + l^2 = 396$, *i.e.*, 128 reflections. Unobserved intensities were taken as $I_{\min}/2$. Absorption corrections were not needed, since the samples were sufficiently thick (sample holder: 38 × 11 × 4 mm).

With the slit system used, a certain amount of the incident radiation fell outside the sample holder for the first diffracted peak. Therefore, the observed intensity of this peak was multiplied by a factor to

take into account the loss of incident radiation. Nevertheless, for the least-squares refinement the weight of this peak was put equal to zero.

In the least-squares refinement, a block-diagonal approximation was used. The coordinates and the temperature factor B of each framework atom were taken in a separate block. For the exchangeable cations, the temperature factors and the occupancy factors were refined alternately together with the positional parameters in another single block. The scaling was adjusted every four cycles, and obtained from a plot of $\ln (\sum_{10} I_0 / \sum_{10} I_c)$, against $\sin^2 \theta / \lambda^2$ for every ten lines. The main reason for this procedure of calculation was to eliminate the correlation between the temperature factor on one hand, and the occupancy and scale factors at the other.

The same weighting scheme as in part I was used. The application of liquid scattering functions⁵ to unlocated scattering material was shown to be success-

(4) W. Parrish, J. Taylor, and M. Mack, *Advan. X-ray Anal.*, **7**, 66 (1964).

(5) H. D. Simpson and H. Steinfink, *Acta Crystallogr.*, **A26**, 158 (1970).

Table II: Dehydrated Potassium Zeolites X and Y

	Interatomic distances (Å) and bond angles (deg) ^a			
	F 48.2	F 54.7	F 69.8	F 86.5
Tetrahedron				
T-O ₁	1.65 (2)	1.63 (2)	1.67 (3)	1.68 (2)
T-O ₂	1.65 (2)	1.67 (2)	1.65 (3)	1.68 (3)
T-O ₃	1.62 (2)	1.64 (2)	1.63 (2)	1.61 (2)
T-O ₄	1.64 (2)	1.63 (2)	1.67 (2)	1.69 (2)
Mean	1.64	1.64	1.66	1.67
T-O ₁ -T	137.9 (1.5)	142.4 (1.8)	136.8 (1.9)	135.4 (1.8)
T-O ₂ -T	155.3 (1.1)	148.9 (1.3)	152.7 (1.4)	150.3 (1.8)
T-O ₃ -T	140.5 (9)	146.0 (9)	145.3 (1.1)	148.1 (1.1)
T-O ₄ -T	139.6 (1.1)	139.8 (1.1)	138.2 (1.1)	136.3 (1.1)
Mean	143.3	144.3	143.3	142.5
O ₁ -O ₂	2.68 (3)	2.74 (4)	2.75 (4)	2.79 (4)
O ₁ -O ₃	2.75 (2)	2.69 (3)	2.72 (3)	2.69 (3)
O ₁ -O ₄	2.67 (3)	2.67 (3)	2.67 (3)	2.67 (3)
O ₂ -O ₃	2.56 (2)	2.64 (3)	2.58 (3)	2.63 (3)
O ₂ -O ₄	2.69 (3)	2.69 (3)	2.75 (3)	2.76 (3)
O ₃ -O ₄	2.70 (3)	2.68 (3)	2.74 (3)	2.77 (3)
Mean	2.68	2.68	2.70	2.72
O ₁ -T-O ₂	108.7 (9)	111.8 (1.0)	111.7 (1.1)	112.0 (1.2)
O ₁ -T-O ₃	114.7 (9)	110.3 (1.1)	110.7 (1.1)	109.4 (1.1)
O ₁ -T-O ₄	108.5 (9)	109.7 (1.1)	106.2 (1.1)	104.9 (1.1)
O ₂ -T-O ₃	103.2 (8)	105.5 (9)	103.7 (9)	106.3 (1.1)
O ₂ -T-O ₄	109.7 (8)	109.4 (9)	111.9 (9)	109.9 (1.0)
O ₃ -T-O ₄	111.8 (1.0)	110.0 (1.0)	112.8 (1.0)	114.5 (1.0)
Mean	109.5	109.5	109.5	109.5
Cations				
K(I)-O ₁	3.73 (2)	3.71 (3)	3.78 (3)	3.81 (3)
-O ₂	3.36 (1)	3.47 (1)	3.39 (1)	3.44 (2)
-O ₃	2.86 (2)	2.90 (2)	2.84 (2)	2.85 (2)
-K(I')	3.21 (4)	3.30 (4)	3.25 (5)	3.30 (5)
K(I')-O ₂	3.09 (5)	3.14 (4)	3.07 (5)	3.12 (6)
-O ₃	2.67 (5)	2.80 (4)	2.77 (5)	2.87 (5)
-K(I')	3.51 (9)	3.38 (7)	3.53 (9)	3.48 (10)
K(II)-O ₂	2.92 (2)	2.76 (2)	2.86 (2)	2.76 (3)
-O ₄	3.06 (2)	3.06 (3)	3.08 (3)	3.05 (3)
Framework ^b				
Center cubooctahedron				
-K(I')	2.15	2.07	2.16	2.13
-O ₃	4.24	4.32	4.37	4.46
-O ₂	4.46	4.43	4.44	4.46
-T	4.94	4.97	4.99	5.01
-O ₄	5.21	5.26	5.30	5.35
-K(II)	5.51	5.42	5.42	5.31
-O ₁	6.53	6.53	6.60	6.63
Center large cage				
-K(II)	5.21	5.33	5.40	5.55
-O ₄	6.96	6.97	7.02	7.03
-O ₂	7.33	7.29	7.42	7.42
-O ₁	7.36	7.39	7.40	7.42
-T	7.61	7.57	7.65	7.69

^a The standard deviations are indicated in parentheses. ^b The standard deviations were not computed.

ful in the study of the hydrated samples.¹ A similar procedure was applied to the unlocated potassium ions in this work. Their centers were supposed to be located randomly at the surface of a sphere with a radius obtained by trial calculations, using the first 20 reflec-

tions. An additional temperature factor of 10 \AA^2 was always applied. Difference fourier analysis gave a good agreement with the cation occupancy obtained by the least-squares procedure. The space group Fd3m (no. 227) was used.

Table III: Location of Potassium Ions in the Dehydrated Samples and Comparison with Other Data^a

	KF 48.2	KF 54.7	KF 69.8	KF 86.5
1. Cations that could be located (in % of total amount)	96.7	91.9	78.7	55.9
2. Cations located in the hydrated samples (in % of total amount) ¹	65.2	63.2	62.2	45.5
3. Ions on site S _I	6.4 (0.0)	5.4 (1.3)	9.4 (7.0)	9.2 (8.9)
4. Ions on site S _{I'}	14.1 (13.6)	18.1 (13.3)	16.6 (12.0)	13.6 (7.2)
5. Ions on site S _{II}	26.1 (17.8)	26.8 (20.0)	28.9 (24.3)	25.6 (23.2)
6. Ions on sites S _I + S _{I'}	20.5 (13.6)	23.5 (14.6)	26.0 (19.0)	22.7 (16.1)
7. Unlocated ions (near S _{III'})	1.6 (16.8)	4.4 (20.1)	14.9 (26.5)	38.2 (47.2)
8. $n(I) + 0.5n(I')$	13.5	14.6	17.7	16.0

^a The numbers in parentheses are the values obtained for the hydrated samples in part I.

The residuals were defined by

$$R_F = \sum_{hkl} |k|F_o| - |F_c| / \sum_{hkl} k|F_o|$$

$$R_I = \sum_N |kI_o - I_c| / \sum_N kI_o$$

where I_o was the observed intensity, corrected for the continuously varying factors.

The following charges were given to the framework atoms: Si²⁺, Al²⁺, O⁻. To the cations the real charge +1 was attributed. The atomic scattering factors were taken from the international tables for X-ray crystallography III. The interatomic distances and bond angles were calculated using the program ORFFE.⁶

Results

In Table I, the parameters describing the structure are given. We followed the cation site indication proposed by Smith.² The sites I (16 per unit cell) and I' (32 per unit cell) share the six-ring of oxygen ions of the hexagonal prism. Site II and II' (both 32 per unit cell) share the other six-rings of the cubooctahedron facing the large cage. The accents indicate a cation site inside the cubooctahedron. In part I site III' was defined as a four-ring composed of two oxygen ions O₁ and two ions O₄. The prime is used here to distinguish this site from the site III proposed by Breck.⁷ The R_F and R_I values are also indicated in Table I. For the first three reflections a large deviation is observed between observed and calculated intensities. If these three reflections are not included in the calculations the R_I and R_F values are 0.1710, 0.1105; 0.1730, 0.1150; 0.1877, 0.1211; and 0.1822, 0.1258. A list of I_o and I_c values for part I and II can be obtained from the National Auxiliary Publications Service.^{7a}

Table II gives the interatomic distances and bond angles; the distances from the center of the cubooctahedron and the large cage to the surrounding atoms are given also. A survey of the occupancy of the different sites is given in Table III. Figure 1 gives a plot of the occupancy of the sites as a function of the number of cations per unit cell.

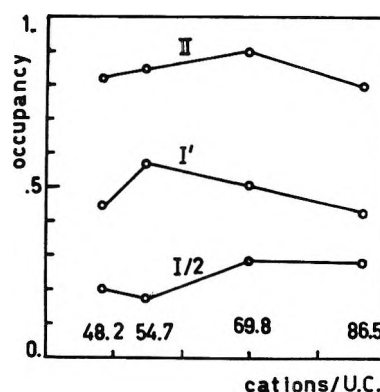


Figure 1. Dehydrated K-zeolites X and Y vs. occupancy of the cation sites. These occupancy figures are proportional to the number of ions at the different sites by a factor of 32.

Discussion

The results show that the framework coordinates remain essentially identical with those of the hydrated samples.¹ The occupancy of the cation exchange sites and the distance between the coordinating oxygen ions and the exchangeable cations are the main points of difference between the hydrated and the dehydrated samples.

Like in the hydrated state, the variation of the T-O distances follows the sequence of increasing aluminum content. Assuming the distances Si-O = 1.61 Å and Al-O = 1.75 Å (Smith and Bailey⁸) the average T-O distances, for the samples F 48.2, F 45.7, F 69.8, and F 86.5 would be, respectively, 1.645, 1.649, 1.661, and 1.673 Å. This corresponds closely to our experimental values 1.640, 1.644, 1.655, and 1.665 Å for the average of the four different T-O distances of the Si, Al tetrahedron.

(6) W. R. Busing, K. O. Martin, and H. A. Levy, ORFFE, Oak Ridge National Laboratory, Oak Ridge, Tenn., 1964.

(7) D. W. Breck, *J. Chem. Educ.*, **41**, 678 (1964).

(7a) For this list, order document NAPS-01694, from ASIS-National Auxiliary Publications Service, c/o CCM Information Corporation, 866 Third Avenue, New York, N. Y., 10022, remitting \$2.00 for each microfiche or \$5.00 for each photocopy.

(8) J. V. Smith and S. W. Bailey, *Acta Crystallogr.*, **16**, 801 (1963).

The cations at site I are surrounded by six oxygens in an octahedral arrangement ($3m$). This is the only site in the dehydrated framework which provides full coordination of the framework oxygens to the potassium ions. The K(I)-O₃ distance seems to be longer in the dehydrated as compared to the hydrated state. A higher potassium content in the hexagonal prisms and stronger lattice distortions are probable reasons for this variation. Going from F 48.2 to F 86.5 the values of the K(I)-O₃ distances for the hydrated samples are 2.74, 2.80, 2.82, and 2.76 and for the dehydrated ones 2.84, 2.90, 2.85, and 2.84 Å. The cations at the sites I' and II are closer to the coordinating oxygens than they are in the hydrated samples. This is certainly due to the one-sided coordination with three framework oxygens. In zeolites X and Y, saturated with Ca²⁺ or Sr²⁺ ions, cations on sites II' were reported in partly dehydrated samples.² In our work cations on sites II' were never detected.

The most interesting features and at the same time the main objective of this study are the data on the cation site occupancies, related to the number of cations per unit cell, and their comparison with the hydrated samples.

In the hydrated samples¹ the relative occupancy of the different ion exchange sites could be more or less explained on the basis of a statistical distribution of the cations. In the dehydrated samples the absence of the water molecules with a high dielectric constant will most likely result in a less homogeneous charge distribution. Therefore, the exchangeable cations will be fixed preferentially on the sites with the highest charge density or in the sites I where the most favorable coordination conditions are realized.

As compared to the series of hydrated samples more cations could be located in this work. The comparison is made in Table III: lines 1 and 2 compare the total fraction of the cations that could be located in the hydrated and in the dehydrated samples. These variations are due to an increase, upon dehydration, of the population in sites S_I, S_{I'}, and S_{II}, and a corresponding decrease of the number of ions on sites S_{III}, where they were not detectable by XR diffraction. One of the most striking changes upon dehydration is the filling of site I for the samples KF 48.2 and KF 54.7. In the hydrated samples¹ these sites were almost empty, where in the dehydrated state the occupancy is close to 40%. For the samples KF 69.8 and KF 86.5 the filling of site I is over 50% but this is only slightly higher than in the hydrated samples.

Smith suggested² that the best way to distribute 58 monovalent cations in zeolite Y or in faujasite is to put 32 in S_{II}, 20 in S_{I'}, and 6 in S_I. Our values obtained with KF 54.7 seem to substantiate this suggestion since we found, respectively, 26.8, 18.1, and 5.4. However, Smith's suggestion is based mainly on electrostatic considerations, and applicable to Y zeolite.

On the basis of our data more general rules can be formulated, as explained in the next paragraphs, which seem to be applicable to the complete composition range of the synthetic faujasites.

At first it is observed that the number of ions on site I' is not higher than two cations per cuboctahedron which corresponds to 16 cations per unit cell. The value 18.1, obtained for KF 54.7, is somewhat high but still considered reasonably close to the limit 16.

It also seems to be a rule that neighboring sites S_I and S_{I'} are not occupied simultaneously. This was assumed yet in most works on this field, and the only real exception in the literature were the figures by Eulenberger, *et al.*³ This will be discussed further.

In a more general way we can formulate the rule that the maximum occupancy of sites I and I' is such that the sum of the number of cations on site S_I and half the number on site S_{I'} is never higher than 16. This can be expressed by the formula

$$n(\text{I}) - 0.5n(\text{I}') \leq 16$$

The application of this rule to our samples, going from KF 48.2 to KF 86.5, yields the values 13.5, 14.6, 17.7, and 16.0. The figure obtained for F 69.8 (17.7) is somewhat high, but within the limits of experimental errors still in agreement with this rule. The figures obtained by Pluth and Schomaker (see Smith²) on KY are in agreement with this rule since they add up to 15.1. Application of this rule to Eulenberger's³ data gives a value of 19.3 which is improbably high and at variance with our data on KF 54.7, a sample comparable to Eulenberger's KY.

In fact, the foregoing equation is another expression of the complementarity rule given by Dempsey and Olson⁹ for zeolites X saturated with divalent ions ($N_{\text{I}} = 2(16 - N_{\text{I}'})$). The formulation used by us was suggested earlier by Smith.² Our results just show that it can be generally applied to a wide variety of compositions by introducing the inequality sign. The value 16 is only realized for the X like members of the series. For our two Y-type samples almost all the cations are located without realizing the maximum filling of the small cavities.

In the four samples, the sites S_{II} are occupied for at least 80%. This is in agreement with earlier determinations on dehydrated samples.²

There are still a number of unlocated cations. Since the samples were completely dry, these cations must be close to the walls in the large cavities. In part I,¹ the four-membered rings of oxygen ions composed of two ions O₁ and two O₄ were discussed to be the most probable sites. They were indicated as sites S_{III}. The negative charge that can be associated with these sites depends on the aluminum content of the sample. The highest possible charge will be realized when three of

(9) E. Dempsey and D. H. Olson, *J. Phys. Chem.*, **74**, 305 (1970).

the six T atoms surrounding site III' are aluminum (local Si:Al ordering 1:1). The probable number of such highly charged sites can be calculated as follows. The charge at two neighboring sites III' is determined by the sequence of four pairs of T atoms. This charge can adequately be described by the Al content of the two four-rings of the hexagonal prism. To take into account all the T atoms (192 per U.C.), only 48 four-rings must be considered. If a given four-ring contains two Al atoms, the site III' to which it belongs will be highly charged if the adjacent four-ring contains also two Al atoms. When the adjacent four-ring contains only one Al atom, a highly charged site III' is generated in 50% of the cases, *i.e.*, when the Al occupies a position close to the first four-ring. If p_2 is the probability to have a four-ring containing two Al atoms and p_1 is the probability that it contains only one Al atom, the probability for a site III' to be highly charged is given by $p = (p_2)^2 + 0.5p_1p_2$. We must subtract from this $0.5(p_2)^2$ if we exclude a double occupancy of two adjacent highly charged sites III'. We obtain then $p = 0.5p_2(p_1 + p_2) = 0.5p_2$, and per unit cell, this yields $(0.5p_2)96$, or $48p_2$. Using the Al content of the different samples, the number of four-membered rings containing two Al atoms were calculated and given in part I.¹ The numbers of highly charged sites III' derived from these figures, excluding double occupancy are as follows

Samples	KF 48.2	KF 54.7	KF 69.8	KF 86.5
Number of sites	0.0	6.6	21.8	38.5

the total number of sites $S_{III'}$, being 96 per unit cell. Comparing these figures to the number of unlocated cations (1.6, 4.4, 14.9, and 38.2) we observe a very close agreement. This seems to us a reasonable speculation, but no direct X-ray evidence was found. Site III' might be a not as well defined site, as the sites I, I', and II, resulting in no strictly localized ions. Disorder in the Si:Al distribution, local lattice distortions in the dehydrated state (the O_1 oxygens have unusually high temperature factors), and four oxygens instead of three can be a reason for this.

In the hydrated samples¹ systematic variations of the occupancy of the different sites as a function of the aluminum content of the samples could be drawn. A gradual increase of the population on S_{II} with increasing aluminum content was observed, and also a decrease of the occupancy on sites $S_{I'}$ and a concomitant increase on S_I going from KF 48.2 to KF 86.5. These correlations (see Figure 1) were not observed for the dehydrated samples. Within narrow limits the occupancy of the site S_{II} is the same in all the samples. The only significant variations were observed in the Y type samples (KF 48.2 and KF 54.7) for the sites S_I and $S_{I'}$. This is due to the fact that these two sites are still below maximum filling.

The question arises whether the cation migration is reversible or not. In order to investigate this, a sample of KF 54.7 was strongly dehydrated and subsequently exposed to the air. After 24 hr, the diffractometer diagram was identical with that of the original hydrated sample, but after 1 hr exposure the diagram was still very similar to that of the dry material. Therefore we may assume that, for our samples, the cation migration is reversible.

Conclusion

In this and in a preceding work¹ a study was made of the distribution of the potassium ions over the different cation sites in a series of four synthetic zeolites of type X and Y with different aluminum contents. The study was realized on dehydrated and hydrated samples. Some general rules can now be formulated.

In the dehydrated samples the cations seem to be distributed in such a way that they occupy the sites with the highest charge. For the sites inside the small cavities there are some restrictive rules due to space requirements and electrostatic interactions. The site S_I , although it provides optimum coordination possibilities, is never completely filled. This is due to the fact that neighboring sites S_I and $S_{I'}$ are never occupied simultaneously. The occupancy of site $S_{I'}$ is never higher than 2 potassium ions per cuboctahedron. For the Y zeolites the occupancy of the sites S_I and $S_{I'}$ is lower than the maximum values allowed by these rules.

In the dehydrated samples the occupancy of the sites S_{II} approaches the maximum value, 32 per ions cell, for all the samples.

A number of ions cannot be located, and this number increases with the total amount of potassium ions. In dehydrated samples these cations are likely to be close to the walls of the large cavities: the geometrically favorable sites for these locations, indicated as $S_{III'}$, are composed of two oxygen ions of type O_1 and two of type O_4 . No experimental evidence was found for the presence of ions exactly on these sites, but it could be shown that the number of unlocated cations corresponds to the number of $S_{III'}$ sites carrying the highest possible charge.

In the hydrated state the number of cations that could be located is lower than in the dehydrated samples, and the difference increases with the aluminum content. The difference in occupancy for the sites inside the small cages is most pronounced in S_I for the samples KF 48.2 and KF 54.7 (Y type) and in $S_{I'}$ for the samples KF 69.8 and KF 86.5 (X type). The action of the water molecules probably results from the combined effect of the hydration of the cations, which offers a more favorable coordination, and a lowering of the electrostatic field by the dielectric properties of the water. The effect of the hydration is a more statistical distribution of the cations. Nevertheless, a tendency

can still be observed towards a preferential occupancy of the sites with the highest charge density.

Acknowledgments. W. J. M. gratefully thanks the "Belgisch Nationaal Fonds voor Wetenschappelijk Onderzoek" for a research grant as "Aspirant." We

thank Prof. W. M. Meier for his interest and valuable advice on our work. The calculations were performed in the calculation center of the "Katholieke Universiteit Leuven." We acknowledge the gifts of the samples by the Linde Company.

A Potential Energy Surface for the Addition of Benzyne to Ethylene

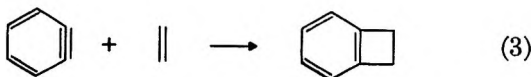
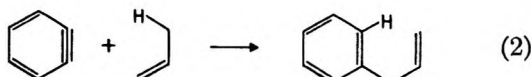
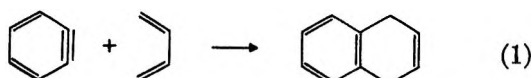
by David M. Hayes and Roald Hoffmann*

Department of Chemistry, Cornell University, Ithaca, N. Y. 14850 (Received April 13, 1971)

Publication costs assisted by the National Science Foundation

A potential energy surface for the cycloaddition of benzyne to ethylene, calculated by the extended Hückel method, is presented. The least-motion $2_s + 2_s$ approach is forbidden, while the allowed $2_s + 2_a$ process is at high energy. The computed reaction path is shown in Figure 3. It has as one important feature a dead end valley in which the ethylene polarizes the benzyne and interacts in a typical carbonium ion manner with the electrophilic terminus of the polarized bond. We believe this valley will simulate an intermediate. The reaction terminates by a complex rotation and relaxation leading to benzocyclobutene. The calculated potential energy surface does not at this time appear completely consistent with the experimental facts concerning energetics and stereochemistry.

Rapid reactions of unstable intermediates are no guarantee that such processes are concerted. The most common reactions of *o*-benzyne are the Diels-Alder and "ene" type additions (1) and (2).¹ These are both



symmetry-allowed $4 + 2$ cycloadditions,² anticipated to proceed in a stereospecific concerted manner. The stereochemical supporting evidence for concertedness has been obtained in both cases.³⁻⁵ When neither reaction 1 nor 2 is available to a benzyne, but there is offered up to this reactive species a simple ethylene, there takes place a $2 + 2$ cycloaddition resulting in benzocyclobutene (3).¹ This cycloaddition is highly exothermic. Though no kinetic information is available the reaction appears to take place readily at room temperature. We estimate an experimental upper limit of 15 kcal/mol for the activation energy to reaction 3.

The least motion $2_s + 2_s$ cycloaddition,^{2a} in which the two reactants approach each other maintaining the C_{2v} geometry shown in Figure 1a, is a symmetry-forbidden process. This may easily be shown from a correlation diagram for the reaction or from our general arguments concerning concerted cycloadditions.² Despite the exothermicity of the process we would not expect a reaction following the forbidden path to proceed as readily as the actual reaction does.

$2_s + 2_a$ cycloadditions^{2a} are symmetry-allowed and we turn to considering these. A benzyne adding in a 2_a manner is a stereoelectronic impossibility, since it would lead to a trans double bond or disruption of bonding in the benzene ring. A $2_s + 2_a$ cycloaddition, 2_s on the benzyne, 2_a on the ethylene, (approach geometry of Figure 1b) at first sight offers an attractive pathway. But a $2_s + 2_a$ cycloaddition appears to re-

(1) Benzyne chemistry is reviewed by Reinhard W. Hoffmann, "Dehydrobenzene and Cycloalkynes," Academic Press, New York, 1967, and T. L. Gilchrist and C. W. Rees, "Carbenes, Nitrenes, and Benzyne," Nelson, London, 1969.

(2) (a) For a definition of the 2_s , 2_a nomenclature see ref 2c, p 824; (b) R. Hoffmann and R. B. Woodward, *J. Amer. Chem. Soc.*, **87**, 2046 (1965); (c) R. B. Woodward and R. Hoffmann, *Angew. Chem.*, **81**, 797 (1965).

(3) R. W. Atkin and C. W. Rees, *Chem. Commun.*, 152 (1969).

(4) M. Jones, Jr., and R. H. Levin, *J. Amer. Chem. Soc.*, **91**, 6411 (1969).

(5) L. Friedman, private communication.

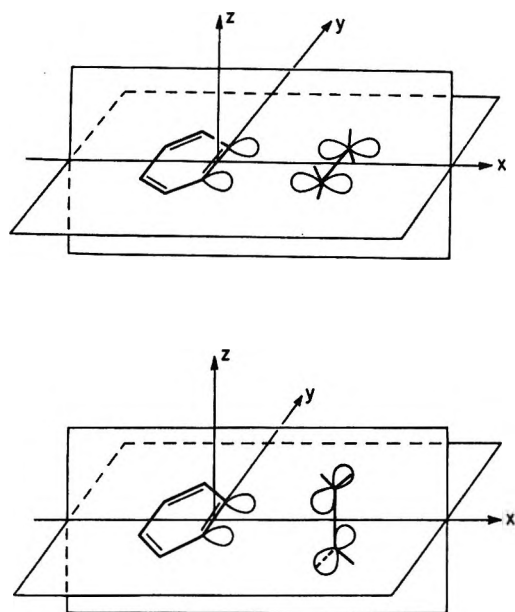


Figure 1. (a) Top. An approach geometry for the least motion $2s + 2s$ cycloaddition of benzyne to ethylene. (b) Bottom. One possible approach geometry for the $2s + 2s$ cycloaddition.

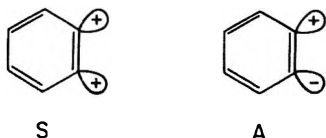
quire torsion in both components,⁶ and such torsion is prohibitive for the benzyne which is constrained to a planar geometry.

We are left with postulating a nonconcerted process for this facile cycloaddition. Several groups have in fact found that the $2 + 2$ cycloaddition of benzyne to cis or trans-substituted ethylenes is somewhat stereoselective but not stereospecific.^{4,7-11} Whatever stereoselectivity is exhibited is not in the direction of a $2s + 2s$ addition.

In this paper we present an extended Hückel study of the potential surface for the addition of benzyne to ethylene. Our findings point up the complexities of many-dimensional potential surface explorations and reinforce the necessity of revising our naive view of nonconcerted reactions.

Benzyne

Before we begin our discussion of the potential energy surface we review our knowledge of the electronic structure of benzyne.^{1,12-14} The two localized σ hybrids which one may imagine are left behind when two hydrogens are removed from benzene combine into a symmetric (S) and antisymmetric (A) pair. Any differentiation in energy between S and A is the conse-



quence of interaction of the two hybrids with each other. The overlap of the hybrid lobes is relatively inefficient, and the splitting between S and A is consequently small.

Configuration interaction mixes strongly the configurations $(S)^2$ and $(A)^2$. The resulting lowest singlet, of the form $c_1(S)^2 + c_2(A)^2$, $c_1 > c_2$, and the triplet of the configuration $(S)^1(A)^1$ compete for being the ground state of benzyne. The interaction between the hybrids appears to be just large enough to guarantee that the ground state of the *o*-benzyne is a singlet. The essential facts of the electronic structure of benzyne are the following. (1) The molecule possesses a singlet ground state with a low-lying triplet state an unknown energy above it. (2) There is in benzyne a high-lying occupied S level and a low-lying unoccupied A level. (3) The ground state singlet may be described as arising primarily from the configuration $(S)^2$, with a sizable admixture of $(A)^2$. (4) A weak third bond is a consequence of this description. We also anticipate good electron donor and electron acceptor properties from this easily polarizable third bond. In the introduction we mentioned that the least-motion cycloaddition of benzyne to ethylene is a symmetry forbidden process. This conclusion is based on the primacy of the configuration $(S)^2$ in the ground state wave function of benzyne.

Calculations

We carried out semiempirical molecular orbital calculations of the extended Hückel type.¹⁵ Some seven degrees of freedom were allowed in our study. Three spherical coordinates D, θ, ϕ and three Euler angles¹⁶ $\epsilon\phi, \epsilon\theta, \epsilon\psi$ were used to define the location and orientation of ethylene relative to benzyne. The origin of the spherical polar coordinate system coincided with the origin of the body-centered cartesian coordinates at the center of the benzyne triple bond (see Figure 2). The spherical polar vector D was directed to the origin of the body-centered coordinate system of ethylene (Figure 2).

The seventh degree of freedom studied was the "relaxation" of ethylene as it approaches the benzyne ring.

- (6) Reference 2c p 828.
- (7) I. Tabushi and R. Oda, *Tetrahedron Lett.*, 3743 (1968).
- (8) L. Friedman, R. J. Osiewicz, and P. W. Rabideau, *ibid.*, 5735 (1968).
- (9) M. Jones, Jr., and R. H. Levin, *ibid.*, 5593 (1968).
- (10) H. H. Wasserman, A. J. Solodar, and L. S. Keller, *ibid.*, 5597 (1968).
- (11) P. G. Gassman and H. P. Benecke, *ibid.*, 1089 (1969).
- (12) T. Yonezawa, H. Knoishi, H. Kato, K. Morokuma, and K. Fukui, *Kogyo Kagaku Zasshi*, 69, 869 (1966); T. Yonezawa, H. Knoishi, and H. Kato, *Bull. Chem. Soc. Jap.*, 41, 1031 (1968); T. Yonezawa, H. Knoishi, and H. Kato, *ibid.*, 42, 933 (1969).
- (13) R. W. Atkin and T. A. Claxton, *Trans. Faraday Soc.*, 66, 257 (1970).
- (14) R. Hoffmann, A. Imamura, and W. J. Hehre, *J. Amer. Chem. Soc.*, 90, 1499 (1968); M. D. Gheorghiu and R. Hoffmann, *Rev. Roum. Chim.*, 14, 947 (1969).
- (15) R. Hoffmann, *J. Chem. Phys.*, 39, 1397 (1963); R. Hoffmann and W. N. Lipscomb, *ibid.*, 36, 2179, 3489 (1962); R. Hoffmann and W. N. Lipscomb, *ibid.*, 37, 2872 (1962). The hydrogen 1s exponent was 1.3.
- (16) See H. Goldstein "Classical Mechanics," Addison-Wesley, New York, N. Y., 1950, p 107 for definition and sign convention of Euler angles.

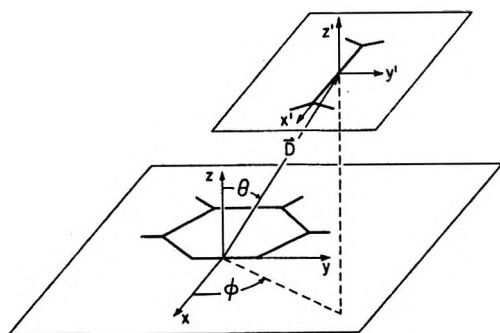


Figure 2. The coordinate system for benzyne and ethylene. Spherical coordinates $D(=r)$, θ , and ϕ locate the origin of the ethylene body-centered cartesian system with respect to the origin of the benzyne body-centered axes.

At large distances the molecular geometry of ethylene should remain unperturbed. As the molecule approaches benzyne we would anticipate the ethylene carbon-carbon bond to lengthen and the CH_2 groups to become pyramidal, culminating in a benzocyclobutene fragment geometry. We initially studied three stages of relaxation: "planar" (P), "partially relaxed" (PR), "relaxed" (R). Our results then forced us further to consider a fourth geometry "planar-partially relaxed" (PPR) in which the degree of relaxation differed at each carbon. The geometrical parameters for these four ethylenes are listed in Table I.

Table I: Geometrical Parameters of Various Stages of Relaxation of Ethylene

Relaxation state	C-C, Å	Angles HCH, deg	Pyramidalities, ^a deg
Planar (P)	1.34	120, 120	0, 0
Planar-Partially Relaxed (PPR)	1.44	120, 115	0, 22.5
Partially Relaxed (PR)	1.44	115, 115	22.5, 22.5
Relaxed (R)	1.54	110, 110	45, 45

^a Acute dihedral angle between the HCH plane and the body-centered $x'y'$ plane.

Benzyne was maintained as an idealized regular hexagon with all C-C, 1.40 Å; all C-H, 1.10 Å; all HCC and CCC angles, 120°. The C-H distance in ethylene was also maintained at 1.10 Å.

No attempt has been made to map the entire potential energy surface for the benzyne and ethylene system. Rather, the aim of this work has been to determine the reaction path and its vicinity. In our exploration of this path we were aided by an automatic minimum seeking program which utilized a procedure due to Rosenbrock¹⁷ for finding those values of θ , ϕ , $\epsilon\phi$, $\epsilon\theta$, $\epsilon\psi$ which for a given D gave the lowest energy.

We present our computed reaction path in Figure 3—a sequence of snapshots of the two molecules at various separations.

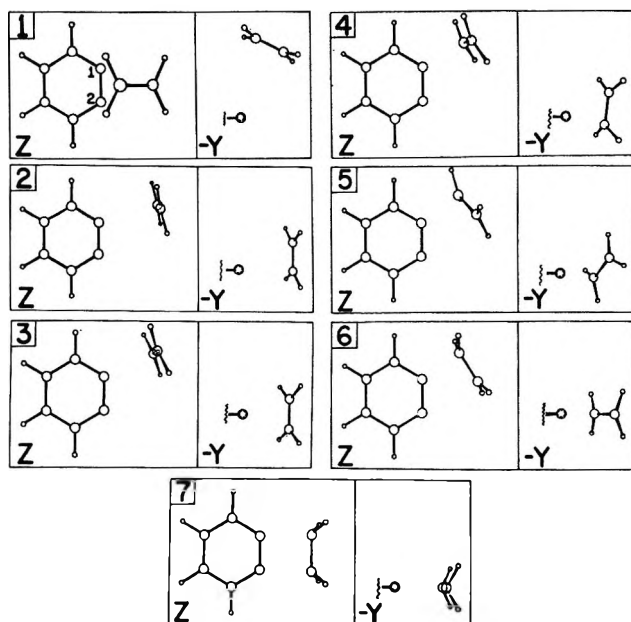


Figure 3. The computed reaction path presented as a series of snapshots. Each picture is presented as two views (not projections) from along the benzyne z and y axes. The snapshots are at $D = 3.25, 3.00, 2.75, 2.50, 2.45, 2.28$, and 2.25 Å in sequence. In the side view, only the carbons 1 and 2 of benzyne are shown, the rest of the molecule referred to by a wavy line. Pictures 1-3 are discussed in the "Distant Approach" section and pictures 4-7 are discussed in the "Terminating Approach" section. Picture 1 illustrates the "center" approach and picture 3 the "upright-side" approach. These illustrations were produced by a computer program due to C. K. Johnson, "ORTEP, a Fortran Thermal Ellipsoid Plot Program for Crystal Structure Illustrations," ORNL Report No. 3794, Oak Ridge National Laboratory, Oak Ridge, Tenn., 1965.

The Distant Approach

We first confirmed some of the qualitative conclusions reached in the introduction. Figure 4 shows how the energy varies along the least motion $2_s + 2_s$ approach for P and R ethylene. The degree of relaxation can influence the value of D at which level crossing occurs, but it cannot prevent that level crossing. The calculated activation energy for the forbidden reaction is approximately 1.7 eV.

In the $2_s + 2_s$ approach there takes place an effective torsion of 180° around the ethylene CC bond. Our study of the $2_s + 2_s$ approach was restricted to three degrees of freedom consistent with the twofold symmetry axis shown in Figure 1b: D , a torsional angle around the CC bond of ethylene, α , and a twist angle around the twofold axis, β . All geometries considered were even less stable than those in the $2_s + 2_s$ approach. Thus although the level crossing is avoided by joint rotation in α and β , there is not enough return in the bonding to make up for the energetic cost of twisting

(17) H. H. Rosenbrock and C. Storey, "Computational Techniques for Chemical Engineers," Pergamon Press, New York, N. Y., 1966.

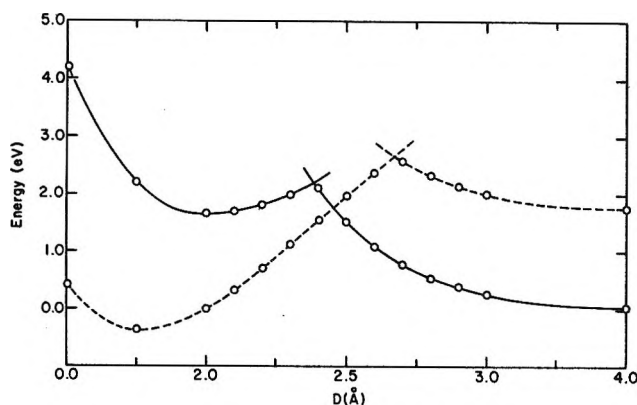


Figure 4. Computed potential energy curves for the least-motion approach of ethylene to benzyne. The solid line is for a planar P ethylene, the dashed line for a fully relaxed R ethylene.

the ethylene. We attribute this to the previously mentioned fact that a $2_s + 2_a$ cycloaddition requires torsion in the 2_s as well as the 2_a component, and that this torsion, which was not allowed in our calculations, is unlikely in a benzyne.

The optimum orientation of an ethylene at large separation is not contained in the above two approaches. We searched the coordinate space at various D by varying independently the angles θ , ϕ , $\epsilon\phi$, $\epsilon\theta$, $\epsilon\psi$. A rough grid covered (at great cost) the entire range of these angles. The automatic minimization program allowed us then to home in on the true minima. In the region $D > 2.50$ Å we located two distinct potential energy valleys, corresponding to geometries which we will call "center" and "upright-side." These are illustrated in snapshots 1 and 3 of Figure 3. In the "center" geometry the ethylene is above the benzyne plane, tilted, but with its CC bond in the xz plane. The benzyne carbons are equivalent but the ethylene carbon atoms are not. In the "upright-side" geometry the ethylene orients itself off to one side, interacting more with one benzyne carbon than with the other. The ethylene carbons are now equivalent but those of the benzyne are not.

The optimized energies of the center and upright-side valleys are compared in Figure 5. At $D > 3.0$ Å the center minimum is at lower energy, while at $D < 3.0$ Å the upright-side minimum is at lower energy. We have confirmed that these are nevertheless independent valleys. The center valley persists until $D \cong 2.5$ Å, at which point a minimization procedure sends the molecule to the upright-side minimum. The upright-side minimum does not persist for $D > 3.2$ Å. The barrier between the two valleys was studied in some detail. It is very small at $D = 3.0$ Å; in fact the upright-side minimum at this point is slightly distorted (snapshot 2 of Figure 3) compared to its subsequent appearance (snapshot 3) in such a way as to take it partway toward the center minimum.

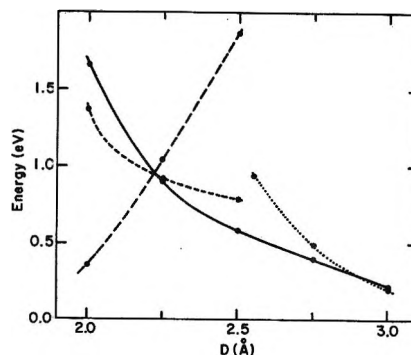


Figure 5. Potential energy vs. D for several ethylene approaches: "center" valley; — "upright-side" approach of a planar ethylene; - - - - "upright-side" approach of a PR ethylene; — — $2_s + 2_a$ least motion approach for partially relaxed ethylene.

Figure 5 also contains a curve for an upright-side approach of a partially relaxed ethylene. At $D < 2.25$ Å this geometry is favored.

The Effective Intermediate

We are next faced with the problem of how the upright-side valley is converted to the benzocyclobutene. The upright-side valley, to whose extremely interesting electronic structure we will return in a moment, is clearly a *cul-de-sac*. Figure 5 indicates that partially relaxed or not the energy rises steeply as D is decreased. Also reproduced in Figure 5 is the energy of a partially relaxed ethylene $2_s + 2_a$ approach, taken from Figure 4. At $D < 2.25$ the PR approach, terminating in benzocyclobutene, is more stable than the PR "upright-side." Yet the latter continues to be a true local minimum, with respect to the angular parameters, at smaller D .

Molecules exploring this surface will probably usually proceed into the "upright-side" valley past $D = 2.25$ Å, even though such motion cannot lead to reaction. Reaction must occur by initiating in the region $2.3 \lesssim D \lesssim 2.6$ a rotatory motion by which the upright-side geometry is transformed into benzocyclobutene. It should be noted that the value of D at which rotation can take place is severely restricted. If we rotate at $D > 2.50$ Å then we find ourselves in-plane right at the point where the forbiddenness of the reaction is most strongly felt (see Figure 4). If we rotate at $D < 2.25$ Å we have already climbed within the upright-side valley to too high an energy.

The rotatory motion encounters initially a steeper portion of the potential surface than progress up the valley, but whereas the latter meets with increasingly stiffer resistance, the former leads to reaction. The situation is shown in a highly schematic two-dimensional contour map in Figure 6. Path A corresponds to the initially easy but ultimately nonproductive ascent into the valley of the upright-side geometry. Path B is the initially steep but ultimately productive

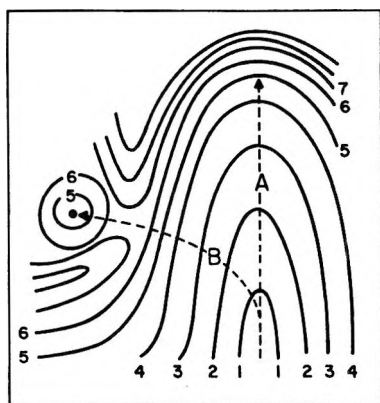


Figure 6. Schematic contour diagram. The vertical scale represents progress into the "upright-side" valley, while the horizontal scale models a rotation leading to benzocyclobutene. The contour values are arbitrary, indicating only the rise and fall of the energy.

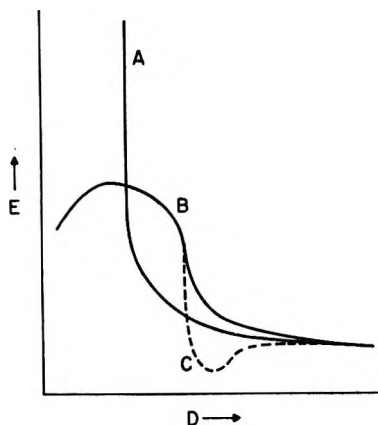


Figure 7. Schematic representation of the energy along paths A and B described in the "Effective Intermediate" section of the text. Curve C corresponds to the formation of a true intermediate.

optimum ascent. The energy variation along these paths is schematically drawn in Figure 7.

We think that typical molecular trajectories will unproductively explore the "dead-end" valley. The average molecule should then have a long residence time in the "upright-side" valley before it finds its way over to the product. Such long residence times would also result if the valley did not exist but instead there were a true local minimum, an intermediate, at a position close to where the optimum ascent out of the valley begins (curve C in Figure 7). It is clear that detailed trajectory calculations¹⁸ are required to check our intuition on dynamic effects. We think that a dead-end valley such as the one we discern here will be operationally indistinguishable from a true intermediate, and as such constitutes another example of a *twixtyl*.¹⁹

The electronic structure of a typical "upright-side" geometry becomes then of utmost interest as a model for such an intermediate. Figure 8 shows the important charges and overlap populations for such a model. It

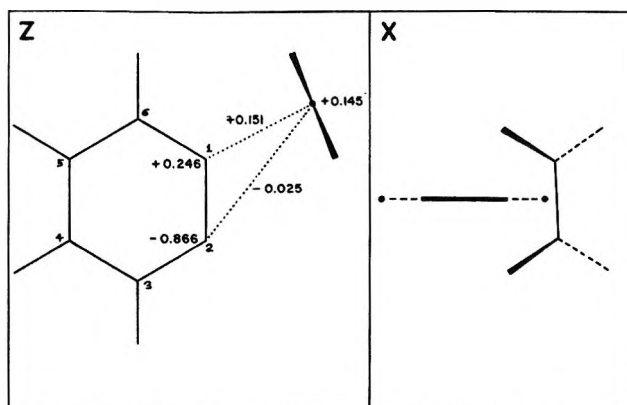
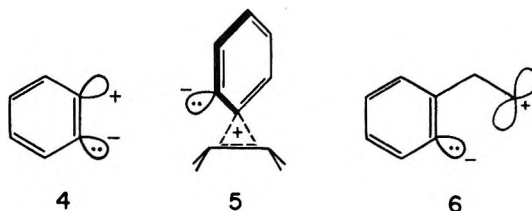


Figure 8. Two projections of a planar ethylene in "upright-side" valley at $D = 2.50 \text{ \AA}$. The significant overlap populations and charges are indicated. Note that one of the views is along the x axis, unlike the second views of Figures 3 and 9.

is not surprising to find some bonding to the near benzyne carbon, little bonding to the other. Note, however, the remarkable polarization of the benzyne, and the significant positive charge transfer to the ethylene. We may imagine that as the ethylene approaches it polarizes the benzyne third bond to a charge distribution corresponding to 4, and that the polarized benzyne interacts in a typical electrophilic manner with ethylene



to produce the species 5. The electronic distribution of 5 is consistent with our computational results (Figure 8); this effective intermediate is rationally described as an internally compensated zwitterionic σ -phenonium ion. While it bears an obvious resemblance to other phenonium ions,²⁰ it carries its own counterion within itself.

In some of the experimental studies on the benzyne-ethylene cycloaddition the possibility of an intermediate closely related to 5, namely the "classical" zwitterionic structure 6, was considered.¹⁰ The absence of major solvent effects on the observed stereochemical preferences was considered as partial evidence against the involvement of a species such as 6.¹¹ We are not sure if the usual solvation arguments are applicable to a

(18) P. J. Kuntz, M. H. Mok, and J. C. Polanyi, *J. Chem. Phys.*, **50**, 4623 (1969); L. M. Raff and M. Karplus, *ibid.*, **44**, 1212 (1966); D. L. Bunker and N. C. Blais, *ibid.*, **41**, 2377 (1964), and related work by these and other research groups.

(19) R. Hoffmann, S. Swaminathan, B. G. Odell, and R. Gleiter, *J. Amer. Chem. Soc.*, **92**, 7091 (1970).

(20) D. J. Cram, *J. Amer. Chem. Soc.*, **86**, 3767 (1964); D. J. Cram in "Carbonium Ions," Vol. III, G. A. Olah and P. v. R. Schleyer, Ed., Wiley-Interscience, New York, N. Y., 1971.

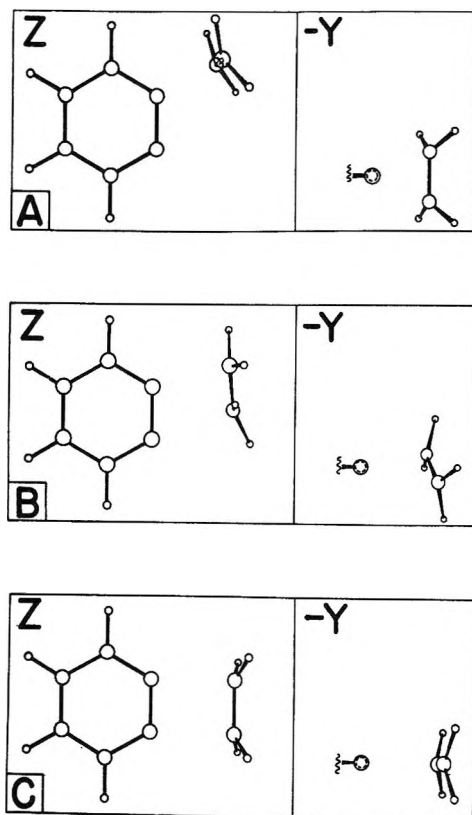


Figure 9. Views from along the z and y axes of benzyne of a transformation of PR ethylene from the "upright-side" valley to the product geometry. D is fixed at 2.25 \AA while the motion is carried out with all five angular degrees of freedom changing by the same fractional amount in each step. A = beginning, B = middle point, C = end of rotation.

species such as **5**; since the positive and negative charges are held so close to each other, the species might appear neutral to an external solvent molecule.

The Terminating Approach

We turn to the final stages of the reaction, the transformation of the upright-side geometry into the product benzocyclobutene. Our first attempt involved a continuous transformation, treating all the angular parameters as varying in a correlated fashion, from the upright-side geometry to the benzocyclobutene structure for a partially relaxed ethylene at $D = 2.25 \text{ \AA}$. The beginning, midway, and end points of this motion are shown in projection in Figure 9. The potential energy along this path rose to a maximum of 1.7 eV above the separated molecules, a disappointingly large value in view of the potentially lower activation energy implied in Figure 5.

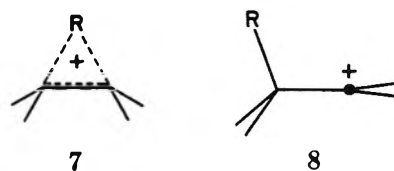
We found a lower activation energy path by two different procedures.²¹ In the first process we began with planar ethylene in the upright-side valley at $D = 2.50 \text{ \AA}$ at an energy of 0.58 eV (this and all subsequent un-referenced energies are relative to separated ethylene and benzyne). We rotated the ethylene by 90° around the line joining carbons 1 and 4 of benzyne (see Figure

8 for labeling convention). Since the perpendicular to the ethylene plane was very nearly collinear with the 1-4 axis, such a rotation keeps D approximately constant at 2.50 \AA . The energy rises uniformly along with this motion, to a value of 0.90 eV when the ethylene carbons reach the benzyne plane. Optimization of the angular variables ϕ and $\epsilon\phi$ only, *i.e.*, restricting the ethylene CC bond to lie in the benzyne plane and the ethylene hydrogens symmetrically above and below that plane, led to a minor readjustment in geometry with a correspondingly small reduction in excitation to 0.87 eV .

In the next stage of the reaction the ethylene moves in to somewhat smaller D with the ethylene carbons in the benzyne plane but still off to the side. The energy climbs slowly along this stage of the approach. Since C(7) of ethylene is more strongly bonded than C(8) to benzyne carbon 1, we allowed partial relaxation at C(7), while keeping C(8) trigonal (see PPR geometry of Table I). The optimized P and PPR ethylenes are of nearly identical energy between $D = 2.40$ and 2.50 \AA . At $D \cong 2.28 \text{ \AA}$, which turns out to be the high energy point on our reaction path, the PPR ethylene (shown in snapshot 6 of Figure 3) is definitely more stable. The energy at this point is 1.19 eV above separated molecules.

The reaction terminates by an energetically downhill sequence. At $D \cong 2.25 \text{ \AA}$ the PPR geometry simultaneously partially relaxes the planar end and moves to a symmetric benzocyclobutene conformation. This spontaneously fully relaxes both ends as it descends in energy to a true benzocyclobutene (snapshot 7 of Figure 3).

The second pathway from the upright-side valley to the product derives from the observation that at $D = 2.25 \text{ \AA}$ less than 0.1 eV is required to move the ethylene in the positive z -direction until the lower ethylene carbon is in the benzyne plane. This motion corresponds to converting a "nonclassical" geometry, **7**, to a "classical" conformation, **8**, of an ethyl cation. The calcu-



lated "softness" of the surface of this motion is consistent with the results of other calculations on model systems such as the ethyl cation.²²

Moving the ethylene vertically up makes the ethylene carbon atoms nonequivalent. The lower in-plane car-

(21) Details for the energy surface search may be found in the Ph.D. Dissertation of D. M. Hayes, Cornell University, 1971.

(22) J. E. Williams, V. Buss, L. C. Allen, P. v. R. Schleyer, W. A. Lathan, W. J. Hehre, and J. A. Pople, *J. Amer. Chem. Soc.*, **92**, 2141 (1970); G. V. Pfeiffer and J. G. Jewett, *ibid.*, **92**, 2143 (1970); R. Sustmann, J. E. Williams, M. J. S. Dewar, L. C. Allen, and P. v. R. Schleyer, *ibid.*, **91**, 5350 (1969).

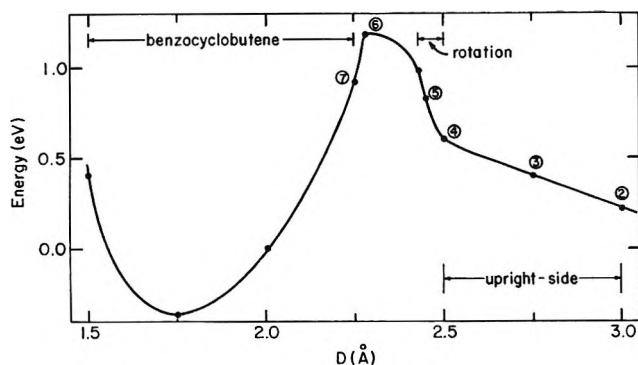


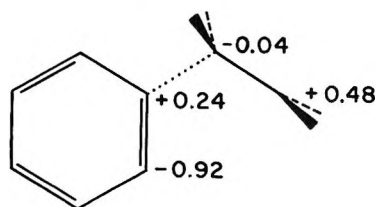
Figure 10. The calculated potential energy along the reaction path. The circled numbers correspond to the snapshots of Figure 3.

bon atom is expected to relax faster than the dangling upper carbon. Accordingly we changed the ethylene geometry to planar-partially relaxed and optimized its orientation at $D = 2.50 \text{ \AA}$. The resulting geometry, snapshot 4 of Figure 3, differs by only 0.02 eV from the symmetrical planar upright-side geometry. We now rotated the ethylene around the 1-4 axis of benzyne, until the carbon atoms of the ethylene were in the benzyne plane. The midway point of this rotation is snapshot 5 of Figure 3. At the termination of the rotation we optimized the geometrical parameters again, which resulted in a trivial displacement, and an excitation energy of 0.99 eV. It should be noted that, in the process of rotation into plane, D decreases from 2.50 to 2.43 Å.

At this point the alternative reaction path merges with the first one. The closure to benzocyclobutene proceeds as before, through an activation energy of 1.19 eV. The energy along the entire reaction path, previously illustrated in Figure 3, is shown in Figure 10.

It seems that the necessity to consider two branching pathways for the approach to the transition state is a consequence of our inadequate treatment of the degree of freedom of relaxation. Ideally, we should allow a continuous series of relaxations independently at each ethylene carbon. It may be that one clear reaction path would emerge in that case. But our computational resources do not allow us eight degrees of freedom, and the resolution of this problem remains for the future.

The transition state for the cycloaddition, approximated by snapshot 6 of Figure 3, possesses a highly unsymmetrical charge distribution shown below. The correspondence to a dipolar intermediate, 6, is obvious,



and the same questions regarding the absence of solvent effects on this reaction¹¹ that were discussed above

can be raised. It should be noted that the true charge imbalance in this geometry will be less than that shown above. First, extended Hückel calculations tend to exaggerate charge distributions. Second and more important, we are dealing with a formal diradical situation, meaning that we have two energy levels not far split in one-electron energy.²³ Let us call these levels HO and LU, for highest occupied and lowest unoccupied. HO is essentially a C_2 lone pair, while LU is heavily concentrated at C_8 . The EH calculation considers only the configuration $\dots (HO)^2$. To the extent that HO and LU are close in energy a more elaborate calculation will introduce configuration interaction and yield a ground state $c_1(HO)^2 + c_2(LU)^2$ which is much more balanced in the charge distribution.

We next studied the barriers to internal rotation in the ethylene fragment along the reaction path, in order to account for the observed nonstereospecificity of the cycloaddition. It is obvious that there should be a high barrier in the reactant ethylene and the product cyclobutene. The expectation that very low barriers would be found in PPR geometries near the transition state, where π -overlap between ethylene carbons is decreased, were however not met. The calculated barriers to twisting the terminal methylene group by 90° were certainly lower in the region between snapshots 4 and 7. However, they did not fall below 25 kcal/mol, much too high to account for the observed nonstereospecificity. The barrier can be lowered significantly by reoptimizing the angular parameters for a twisted ethylene fragment, and we believe that if greater flexibility is allowed to the ethylene the barrier will decrease further.

The Reaction Path

The benzyne-ethylene potential surface is a complicated one. We have identified three distinct potential energy valleys. These are (1) the distant centered approach, (2) the upright-side valley—a *cul-de-sac* simulating an intermediate, and (3) the product valley.

The reaction path for this cycloaddition is not easily defined. D —the distance between the center of the benzyne triple bond and the center of the ethylene—is a good reaction coordinate for large distances. Further in it is not at all clear that D serves as well. The minima of the potential surface are off to one side while D is basically a symmetrical coordinate. To move from the upright-side geometry to the transition state we were led to a rotation around the benzyne 1-4 axis—a motion which keeps D constant only for some special cases.

The lowest energy pass between reactants and prod-

(23) R. Hoffmann, *J. Amer. Chem. Soc.*, **90**, 1475 (1968); R. Hoffmann, G. D. Zeiss, and G. W. VanDine, *ibid.*, **90**, 1485 (1968); R. Hoffmann, A. Imamura, and W. J. Hehre, *ibid.*, **90**, 1499 (1968); R. Gleiter and R. Hoffmann, *ibid.*, **90**, 5457 (1968); *Tetrahedron*, **24**, 5899 (1968); *Angew. Chem.*, **81**, 225 (1969); R. Hoffmann, *Chem. Commun.*, 240 (1969).

ucts on this surface is fairly well defined. It occurs at the beginning of the product valley, corresponding to snapshot 6 of Figure 3. The calculated energy of this transition state is 1.19 eV or approximately 27 kcal/mol above separated products. This number is somewhat high, but in a reasonable range given the deficiencies of the computational method.

There is a wide range of reactive trajectories for this reaction. The one we think most closely approximates the true reaction path is given by the series of snapshots in Figure 3. The energy along this pathway was shown in Figure 10. An alternative trajectory which would encounter the same transition state but differ in the region of "rotation" is described in the previous section. Still another family of trajectories may be constructed by taking the transition state and pulling the ethylene off to infinity while maintaining the C(1)-C(7)-C(8) angle constant. If at the proper stages in this path relaxation is allowed for, such a motion would proceed along a path of uniformly decreasing energy on the large D side of the barrier. However these alternate trajectories, which could be followed by some specific molecule, do not constitute the reaction path, as classically defined. All the points along this trajectory, other than the transition state, would move to lower energy "upright-side" or "center" geometries

at the same D . Nevertheless it is clear that a multiplicity of reactive paths with the same activation energy on this surface implies the importance of dynamic effects and reinforces the need for trajectory calculations.

It is important here to reiterate the deficiencies of our calculation. The computed activation energy is too high by approximately a factor of 2. The computed barrier to rotation of the ethylene along the reaction path is also too high to account for the lack of stereospecificity. While some of the disagreement may be due to lack of optimization of all degrees of freedom, we fear that the major source of discrepancy is to be traced to the inadequacies of the extended Hückel method. While there is some reason to believe, on the basis of our experience with many other systems, that the qualitative reaction path is reliably predicted, the results must be viewed with reservation until much better calculations are performed.

Acknowledgment. We are grateful to M. Jones, Jr., and the referees of the paper for their comments. Our research was supported by the donors of the Petroleum Research Fund, administered by the American Chemical Society, the National Science Foundation, and the National Institutes of Health.

Potential Surfaces for the Addition of CH_2 and CF_2 to Ethylene and Isobutene

by Roald Hoffmann,* David M. Hayes,

Department of Chemistry, Cornell University, Ithaca, New York

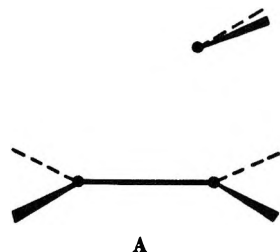
and Philip S. Skell

Department of Chemistry, Pennsylvania State University, University Park, Pennsylvania (Received June 28, 1971)

Publication costs assisted by the Petroleum Research Fund

Molecular orbital calculations favor an attack of singlet CH_2 and CF_2 on ethylene in which the methylene approaches slightly off-center and with its plane approximately parallel to the ethylene plane. The carbene substituents are canted in such a way as to optimally maintain three-center overlap, with corollary symmetry of bond formation and charge transfer. In an approach to an isobutene these pathways are modified for steric reasons, and the possibility of two separated reactive channels arises. A detailed study of the methylene + ethylene surface shows that special care must be taken in the choice of the computational reaction coordinate.

Some fifteen years ago, in the early days of modern carbene chemistry, Skell and coworkers came to the conclusion that the transition state for the addition of methylenes to ethylenes was characterized by the geometrical arrangement shown below as **A**.¹ Methylenes



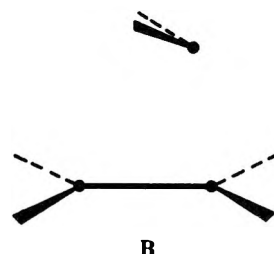
exhibited carbonium or halonium ion type selectivity in their additions to substituted ethylenes. The approach of carbonium ions or other two-electron-deficient species to olefins is likely to begin with an interaction of an unoccupied orbital (*e.g.*, the p orbital in carbonium ion **1a**) with the olefin π system. This line of reasoning led to transition state **A**, whose primary feature is the interaction of the unoccupied methylene p orbital (**1b**), rather than its in-plane "lone pair,"² with the π -system of the ethylene.



The direct experimental probes of transition state geometry are not yet available, and the first test of Skell's conclusion came from a semiempirical molecular orbital calculation of the potential surface for the approach of a methylene to an ethylene.³ Figure 1 shows some superimposed snapshots of a side view of the reaction path thus computed. The calculated reaction path clearly shows the initial approach of the

two molecules in parallel planes, and the concomitant interaction of the methylene p orbital with the ethylene π system.⁴ The insight of the previous workers was thus confirmed.

The transition state for the computed attack, which we may approximate in **B**, differs in a minor but inter-



esting way from transition state **A**. This is in the position of the methylene hydrogens. In **A** they are tilted up and to the right, in **B** up and to the left. Were the methylene carbon directly over the midpoint of the ethylene C=C bond then these distortions would be indistinguishable. To the extent that the methylene carbon is off-center they are distinct.

This preference for approach **B** over approach **A** is a detail of the potential surface worthy of further consideration. First we would like to review the procedure utilized for obtaining the computed reaction path.³

(1) P. S. Skell and A. Y. Garner, *J. Amer. Chem. Soc.*, **78**, 3409 (1956). See also P. S. Skell and M. S. Cholod, *ibid.*, **91**, 7131 (1969) and W. R. Moore, W. R. Moser and J. E. La Prade, *J. Org. Chem.*, **28**, 22 (1963).

(2) (a) The electronic structure of methylenes is discussed by P. P. Gaspar and G. S. Hammond, in "Carbene Chemistry," W. Kirmse, Ed., Academic Press, New York, N. Y., 1964, p 235; R. Hoffmann, G. D. Zeiss, and G. W. Van Dine, *J. Amer. Chem. Soc.*, **90**, 1485 (1968); (b) Excellent discussions of the present state of carbene reactivity studies may be found in the papers by G. L. Closs, *Top. Stereochem.*, **3**, 193 (1968); and R. A. Moss in "Carbene Chemistry," L. Friedman, Ed., Wiley-Interscience, New York, N. Y., 1971.

(3) R. Hoffmann, *J. Amer. Chem. Soc.*, **90**, 1475 (1968).

(4) An alternative approach, involving a symmetrical attack of a linear singlet methylene, has been suggested by A. G. Anastassiou, *Chem. Commun.*, 991 (1968).

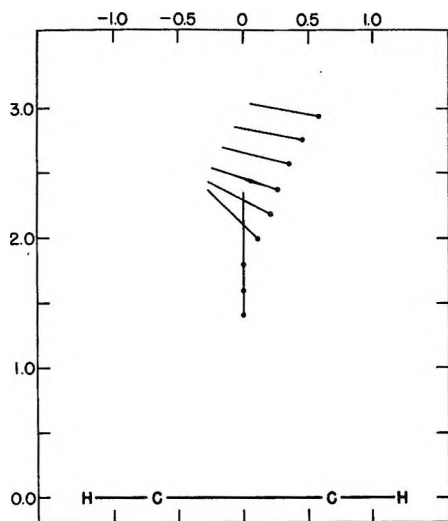


Figure 1. Snapshots of the reaction path for methylene adding to ethylene. The fixed ethylene and the moving methylene are both seen in projection upon the mirror plane of symmetry maintained in the reaction. The tilt of the approaching methylene is that yielding the lowest energy for a given value of R , the distance from the center of the ethylene to the methylene carbon. The scales are in Å. Further details may be found in reference 3.

The full potential surface for the system $C_2H_4 + CH_2$ spans 21 internal degrees of freedom. Chemically reasonable constraints must be applied to reduce this number to a magnitude which we can reasonably handle. With extended Hückel computation times of 2–3 sec per geometry we are able to deal with an estimated maximum of eight degrees of freedom. In the case at hand, a highly exothermic reaction, we concentrated on the distant approach, in which we could assume that the reactant geometries were not severely affected. The problem reduced to one of the relative motion of two solid bodies, an ethylene and a methylene. A convenient coordinate system for describing this motion could be obtained by freezing the ethylene with the origin at its inversion center, using three spherical coordinates R, θ, φ to locate the methylene carbon and three Euler angles $\epsilon\varphi, \epsilon\theta, \epsilon\psi$ to specify the orientation of the methylene.

Our computer program automatically searched for those $\theta, \varphi, \epsilon\varphi, \epsilon\theta, \epsilon\psi$ which gave the minimum energy at a given R .⁵ The result is a computed reaction path. We believe this path approximates the true reaction path, though it must be realized by the reader that in the absence of a view of the whole surface the choice of origin for R remains more or less arbitrary. The final section of this paper will discuss this point further. It was found that the computed reaction path could be described in less than six degrees of freedom. A mirror plane of symmetry was chosen by the molecule along the computed reaction path, thus reducing the number of degrees of freedom to three— $R, \theta, \epsilon\theta$. Figure 1 shows the projection of the reactants on the mirror plane which is maintained.

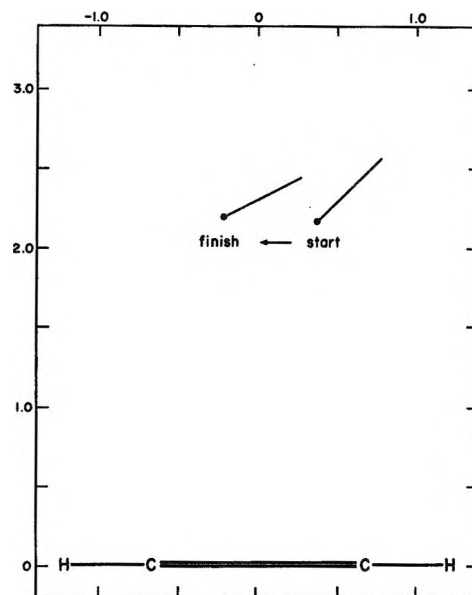


Figure 2. One numerical experiment on the methylene-ethylene potential surface. A methylene with the initial geometry marked "start" moves by an energetically uniformly decreasing path to "finish." The view is the same as in Figure 1.

There is no doubt that the path shown in Figure 1 and symbolized by the snapshot **B** is the favored computed reaction path. In particular if a methylene molecule is placed initially in a geometry resembling **A** and is allowed three to six degrees of freedom in its motion then it moves directly over along a path of uniformly decreasing energy to a mirror image of geometry **B**, designated as **B***. One such numerical experiment, at $R = 2.2$ Å, is shown in Figure 2. At this distance the motion from **A** to **B*** gains 6 kcal in energy. At larger distances the energy gain for a corresponding motion would of course be smaller still.

There are two obvious pathways from **A** to **B** or **B***, and their identification will become important to the sequel. The first pathway, the one chosen in the computed potential surface, is a simple sideways sliding of the CH_2 unit from **A** to **B***.



The second pathway is a pivoting in place of the CH_2 group leading from **A** to **B**.



(5) The optimizing procedure was one due to H. H. Rosenbrock, *Comput. J.*, 3, 175 (1960), and was adapted by K. D. Gibson.

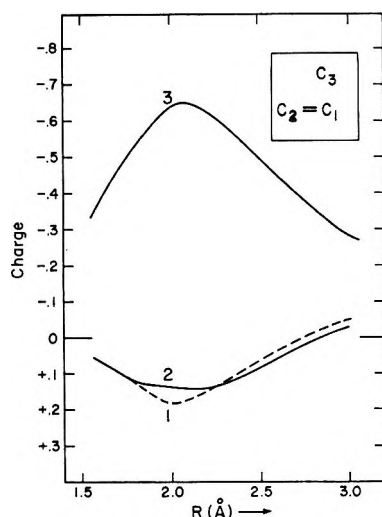


Figure 3. Charge distribution on the carbons along the reaction path of figure 1. C_3 , the methylene carbon, is closer to C_1 at intermediate stages in the reaction.

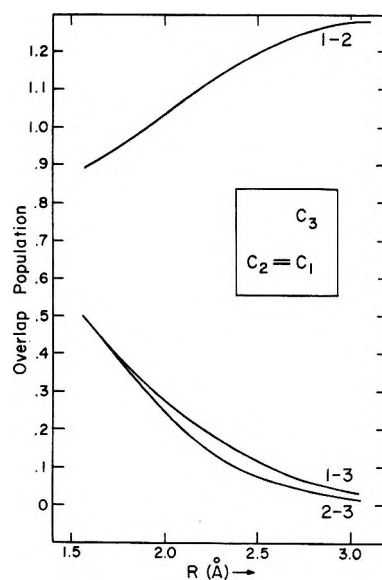


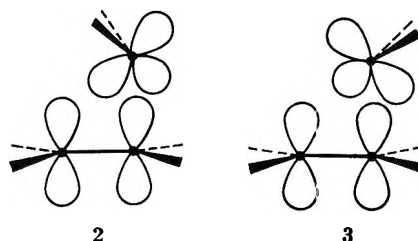
Figure 4. Overlap populations between carbon atoms along the reaction path of Figure 1.

Whereas the sliding over process is energetically downhill, we always find a barrier to the pivoting process. Presumably this is due to the fact that the midpoint in the pivoting motion has the methylene "lone pair" or σ orbital interacting with the π system, approaching the situation for the high energy forbidden reaction.³

What makes transition state **B** better than **A**? Let us first look at the charge distribution on the three carbons as the reaction proceeds (Figure 3). The most striking feature of the charge distribution is the charge transfer from olefin to methylene, consistent with the primary interaction of a filled ethylene molecular orbital with an empty methylene acceptor level. The second remarkable feature of the charge distribution is the extent to which both ethylene carbons are similarly

charged. Examination of the overlap populations (related to bond orders) along the reaction path (Figure 4) shows that while the new CC bonds are forming at unequal rates, with the proximal C_1 - C_3 bond forming first, there is never any great disparity in the rate of bond formation.

Both the charge distribution and the bond orders are consistent with as symmetrical as possible an interaction of the methylene carbon with the ethylene, and yet the methylene carbon is significantly off center most of the reaction path. The symmetry in charge transfer and in bonding is accomplished by tilting the methylene in just the sense required by **B**. That is, given that methylene carbon is off center it can restore approximate symmetry in the p - π interaction by tilting as in **2** (**B**), but makes the electronic interaction still more unsymmetrical if it tilts as in **3** (**A**).



This conclusion is confirmed by examination of charge distributions for geometries like **3**. The occasion for a quantitative comparison will arise below.

Our calculated potential energy surface for the addition of methylene to ethylene shows no activation energy for the process. In reality there must be an activation energy, but it also must be small,¹ less than 3 kcal/mol. We wanted to confirm our computed reaction path for a carbene addition with a larger activation energy. The species chosen was CF_2 , which is known to possess an activation energy of approximately 11-12 kcal/mol⁶ to addition to ethylene. Our computed reaction path for CF_2 addition is shown in Figure 5. It clearly is very similar to the CH_2 reaction path. Figure 6 shows the energy along the forbidden least motion path^{3,7} as well as the energy along the reaction path of Figure 5. The calculated activation energy of slightly more than 20 kcal/mol is, of course, an upper limit; were we to allow some additional degrees of freedom such as relaxation of the ethylene fragment by bending the hydrogens out of plane we would surely lower the activation energy. Extended Hückel calculations, while qualitatively reliable, typically err by a factor of two on activation energies.

The transition state, marked \ddagger in Figure 5, occurs at a distance of approximately 1.8 Å. Every geometry

(6) See S. W. Benson and H. E. O'Neal, "Kinetic Data on Gas Phase Unimolecular Reactions," *Nat. Stand. Ref. Data Ser., Nat. Bur. Stand.*, **21**, 248 (1970); also R. A. Mitsch and A. S. Rodgers, *Int. J. Chem. Kin.*, **1**, 439 (1969).

(7) R. B. Woodward and R. Hoffmann, *Angew. Chem.*, **81**, 797 (1969).

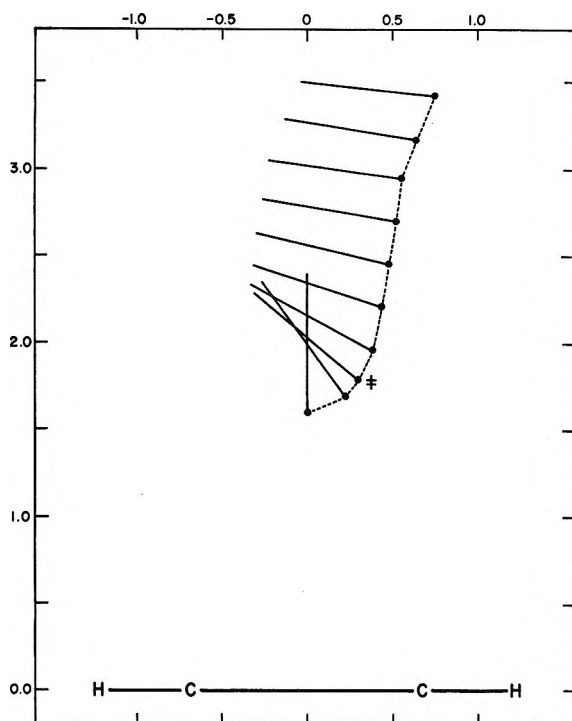


Figure 5. Snapshots of the reaction path for difluoromethylene adding to ethylene. The conventions and view are specified in the caption to Figure 1. The transition state is marked by the symbol ‡.

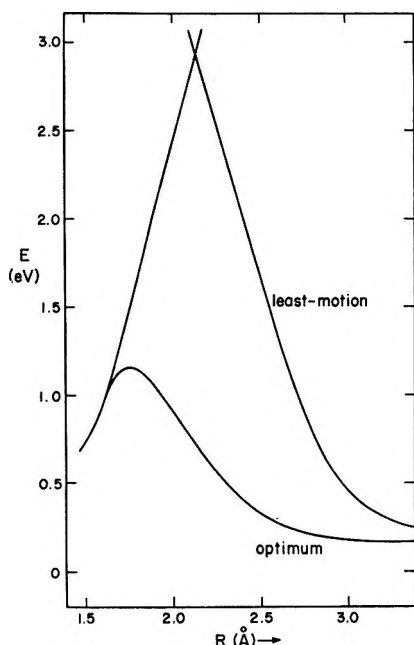
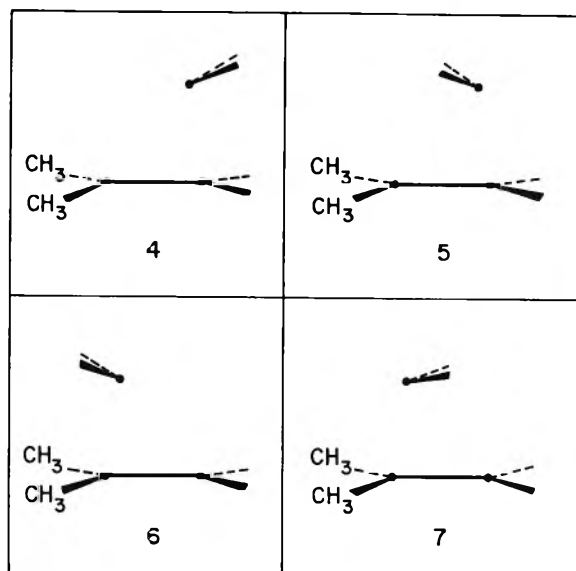


Figure 6. Energy along the reaction path of Figure 5 (marked optimum), as well as along the least-motion approach of C_{2v} symmetry. The energy zero is arbitrary.

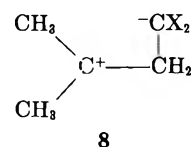
of type A slides over smoothly to one of type B. Electron density is still transferred to the methylene in the course of the reaction, but in accord with the lower electrophilicity of difluorocarbene much less charge transfer occurs than in the methylene case.⁸ Inter-

estingly enough, there is now an imbalance in the source of the electron transfer, most of it originating at C₁, the carbon closest to the CF₂ during the approach.

We next turned to a study of an unsymmetrical olefin substrate, isobutylene. For an unsymmetrical olefin of this type, conformation B is no longer identical with its mirror image B*, nor A with A*. Let us write down the four possible transition state geometries 4 (A), 5 (B), 6 (A*), 7 (B*).



We had noticed that the ethylene carbons were symmetrically participating in the charge transfer to the methylene. However in the case of isobutylene, where there exists the opportunity for very favorable cation stabilization at the methyl substituted end, it seems reasonable that the methylene would take advantage of this fact and accordingly favor conformations 4 and 5. These correspond most closely in geometry to the important valence structure 8.



Moreover there is a possible steric destabilization of conformations 6 and 7.

The interesting case is then conformation 4. This is A type, and in the case of methylene adding to ethylene we have noted that such a conformation slides easily over to B*. However in this case B* is 7, destabilized for the above mentioned reasons. Since in-place pivoting of 4 to attain 5 is also energetically costly, there is here a real possibility that there are two distinct reaction paths, represented by 4 and 5, leading to dimethylcyclopropane.

(8) For some studies on dichlorocarbene related to this point see P. S. Skell and M. S. Cholod, *J. Amer. Chem. Soc.*, **91**, 7131 (1969); I. A. Dyakonov, R. R. Kostikov, and V. S. Aksenov, *Reakts. Sposobnost Org. Soedin.*, **7**, 557 (1970); I. H. Sadler, *J. Chem. Soc. B*, 1024 (1969).

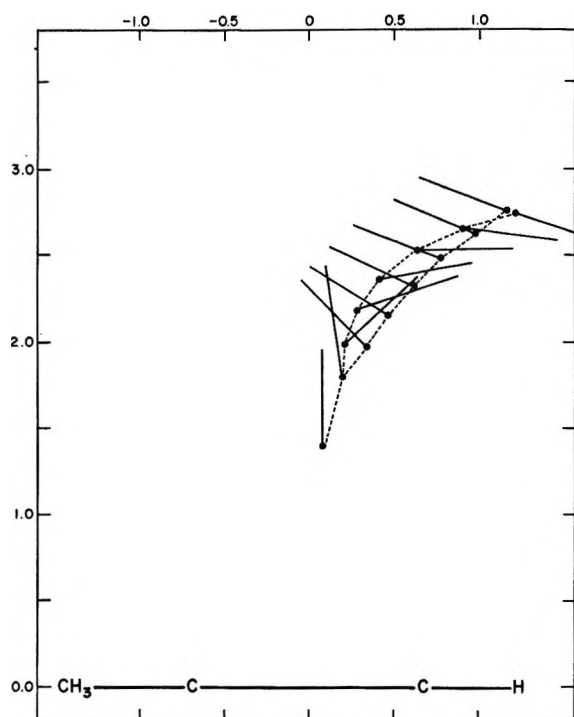


Figure 7. Snapshots of the reaction paths for the addition of methylene to isobutylene. The conventions and view are specified in the caption to Figure 1. The isobutylene methyl groups are at left. Dashed lines connect the independent reaction paths described in the text.

The presence of two such distinct paths is confirmed by the molecular orbital calculations. Figure 7 shows a superposition of snapshots of the reaction paths. For large R there are two conformations, each of them a local minimum in the five angular dimensions. At $R \sim 1.9 \text{ \AA}$ these merge, close to the product cyclopropane. At each R the minimum corresponding to 4 is at higher energy than that corresponding to 5, as we would have expected from our experience with methylene plus ethylene. The destabilization of 4 is not great, amounting to a maximum of 2 kcal/mol. Potential curves for 4 or 5 show no activation energy for the reaction. One might also note the increasing parallelism of the 4 and 5 methylene planes at large R , terminating in a geometry for 4 in which the hydrogens come below the carbon. Clearly at these long distances all that seems to matter is that the methylene p orbital be directed toward the center of the ethylene π bond. Starting geometries corresponding to 6 and 7 are not local minima, but slide over to 5 and 4, respectively.⁹

The theoretical presence of two computed reaction paths allowed us to compare the electron density changes along approaches A and B (4 and 5) more precisely. This is accomplished in Figure 8. It will be noted that the lower energy B approach necessitates somewhat less charge transfer, as well as less charge imbalance among the ethylene carbons.

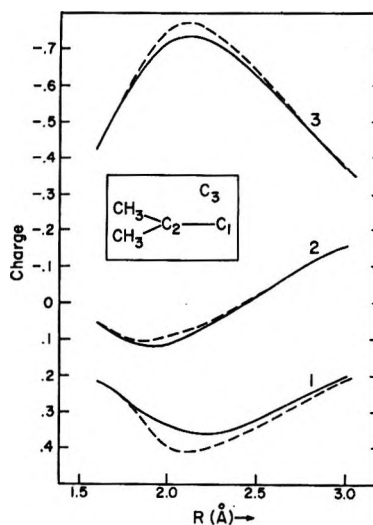


Figure 8. Charge distribution along the two reaction paths of Figure 7. The solid line is for the reaction path of type B, the dashed line for that of type A.

We have also calculated a potential surface for CF_2 and isobutylene. This shows the combined features of the $\text{CF}_2 + \text{C}_2\text{H}_4$ and $\text{CH}_2 + (\text{CH}_3)_2\text{C}=\text{CH}_2$ surfaces. There are two distinct reaction paths of type 4 and 5. There is also present a sizable activation energy.

Importance of Proper Choice of Computational Reaction Coordinate. In the process of studying the methylene-ethylene surface we came across a problem of some significance in the general computation of potential surfaces. The reaction path of Figure 1 was calculated by optimizing θ , φ , $\epsilon\varphi$, $\epsilon\theta$, $\epsilon\psi$ for a given value of the computational reaction coordinate R . R was chosen as the distance between the ethylene center and the methylene carbon.

Suppose the computed reaction coordinate R is chosen in a different way, for instance as the distance between the methylene carbon and one of the ethylene carbon atoms. The computed reaction path is shown in Figure 9. The distance R is here measured from the right-hand ethylene carbon. This second calculated reaction path is primarily of type A, and the optimum approach brings the methylene closer to the left-hand carbon. If bond formation is to be a consequence of reaction then this seems to be a poor choice for a reaction coordinate, since bonding is first established with a carbon other than the one from which the reaction coordinate is measured.

What is needed here is a view not only of the reaction path but a substantial section of the entire potential surface. Without such an examination the true reaction path cannot really be said to have been established.

(9) Some interesting stereochemical consequences of the favored paths of approach of alkylidenecarbenes to unsymmetrical olefins are given by M. S. Newman and T. B. Patrick, *J. Amer. Chem. Soc.*, **91**, 6461 (1969); **92**, 4312 (1970).

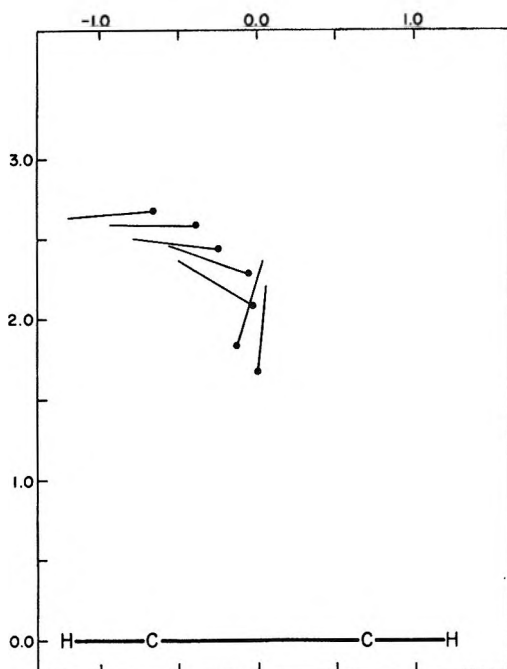


Figure 9. Snapshots of reaction path for the addition of methylene to ethylene when the reaction coordinate R is chosen as the distance from the *right-hand* carbon of ethylene.

In Figure 10 we show an enlarged section of the area covered by Figure 1. The methylene carbon is fixed at the indicated y and z coordinates (the horizontal and vertical coordinates of Figure 1) and the optimum tilt of the methylene group is computed. This tilt is indicated by a slant line and its energy is specified below this line.¹⁰

The figure illustrates clearly why if motion is constrained to be along an arc of equal distance from the center of the ethylene the **B** geometry is preferred, while if the motion is along an arc measured from an ethylene carbon, an **A** geometry is favored. More energy is gained from moving down to the ethylene than from moving sideways. The general features of the potential surface revealed in Figure 10 confirm our original choice of reaction coordinate and provide

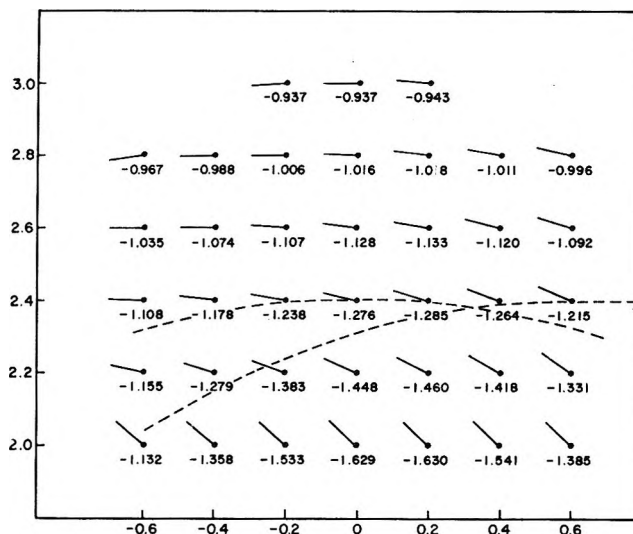


Figure 10. A section of the area of Figure 1, for altitudes 2 to 3 Å above the ethylene. The methylene carbon is fixed at the indicated point and the optimum tilt of the methylene is computed. The tilt is indicated by the slope of the line—which is not of sufficient length to be a true projection of the methylene. Associated energies are in electron volts relative to an arbitrary zero. The dashed curves are loci of points 2.4 Å from the center of the ethylene and from the right-hand ethylene carbon.

a better picture of the energy attached to various impact geometries. Finally we would like to emphasize that we have included the numerical experiments in this section not because they yield any chemical insight but because they are instructive in demonstrating the dangers of arbitrary choice of computational reaction coordinate in limited searches of a complex potential surface.

Acknowledgment. This work was supported at Cornell by the Petroleum Research Fund and the National Science Foundation. P. S. S. acknowledges the support of the Air Force Office of Scientific Research.

(10) Only nonequivalent geometries are specified. For each point there are **A** and **B** type minima, if methylene tilt is the only degree of freedom allowed.

A CNDO/2 Calculation on the Helical Conformations of a Tetrapeptide of Glycine.¹ III. The ϕ - ψ Energy Surface

by Robert Schor,*

Department of Physics and Institute of Materials Science, The University of Connecticut, Storrs, Connecticut 06268

Hans Stymne, Gunnar Wettermark,

Division of Physical Chemistry, The Royal Institute of Technology, Stockholm 70, Sweden

and Carl W. David

Department of Chemistry, University of Connecticut, Storrs, Connecticut 06268 (Received September 7, 1971)

Publication costs assisted by the University of Connecticut Research Foundation

The ground-state potential energy surface for the helical conformations of a tetrapeptide of glycine has been calculated using the CNDO/2 method. The potential energy surface contains three nonequivalent minima. The absolute minimum is found in a region close to both the α helix and the 3_{10} helix. The other two local minima are found in the region of the 2_7 helix and near the fully extended conformation, respectively. The results are compared to those obtained in our previous extended Hückel calculations on the same system.

Introduction

Theoretical studies of the conformations of isolated helices (under vacuum) of polypeptide chains with intramolecular interactions have been carried out by many workers^{2,3} using semiempirical potential functions for barriers to rotation around single bonds, non-bonded interactions, dipole-dipole interactions between amide groups, and hydrogen bonding potential energy functions. More recently semiempirical quantum mechanical techniques have been used to study glycylic and alanyl residues,⁴ polypeptide chains⁵ and model peptide molecules.⁶ We⁷ have presented the results of a detailed study by extended Hückel theory (EHT) of the stereochemistry of a polypeptide chain long enough to incorporate an intramolecular hydrogen bond (see Figure 1). In the present work, we present the corresponding results obtained by using the CNDO/2 method.

Method

Santry's modification¹² of the CNDO/2 method⁸⁻¹² was applied. The CNDO/2 method provides an approximate SCF solution to the LCAO molecular Hartree-Fock equations, in which all valence electrons are included and in which electronic repulsion is explicitly introduced.

The method for determining the coordinates of the atoms in the helical conformations of the polypeptide chain as shown in Figure 1 is due to Némethy and Scheraga.¹³ The peptide unit is considered to have a rigid planar structure with fixed bond angles and bond lengths. The coordinates of the atoms in a peptide unit for the bond angles and distances taken from Leach, Némethy, and Scheraga¹⁴ are given in Table I.

The new conventions¹⁶ for the rotation angles ϕ and ψ are used in the present work. (The rotation angles ϕ and ψ as given by the former convention¹⁶ are related to the new rotation angles ϕ and ψ by: $\phi_{\text{new}} = \phi_{\text{old}} - \pi$, $\psi_{\text{new}} = \psi_{\text{old}} - \pi$.) The calculations were performed on an IBM 360/75 computer. (The execution time for a tetrapeptide of glycine was approximately 8 min for each point on the potential energy surface.) The largest grid width was taken to be 30° ,

(1) This work was supported by Grant No. 2741-6 from the Swedish Natural Science Research Council.

(2) (a) D. A. Brant and P. J. Flory, *J. Amer. Chem. Soc.*, **87**, 633, 2791 (1965); (b) G. N. Ramachandran, C. M. Venkatachalam, and S. Krimm, *Biophys. J.*, **6**, 849 (1966).

(3) R. A. Scott and H. A. Scheraga, *J. Chem. Phys.*, **45**, 2091 (1966).

(4) R. Hoffmann and A. Imamura, *Biopolymers*, **7**, 207 (1969).

(5) A. Rossi, C. W. David, and R. Schor, *Theoret. Chim. Acta*, **14**, 429 (1969).

(6) J. F. Yan, F. A. Momany, R. Hoffmann, and H. A. Scheraga, *J. Phys. Chem.*, **74**, 420 (1970).

(7) A. Rossi, C. W. David, and R. Schor, *J. Phys. Chem.*, **74**, 4551 (1970).

(8) J. A. Pople, D. P. Santry, and G. A. Segal, *J. Chem. Phys.*, **43**, 129 (1965).

(9) J. A. Pople and G. A. Segal, *ibid.*, **43**, 136 (1965).

(10) J. A. Pople and G. A. Segal, *ibid.*, **44**, 3289 (1966).

(11) D. P. Santry and G. A. Segal, *ibid.*, **47**, 158 (1967).

(12) D. P. Santry, *J. Amer. Chem. Soc.*, **90**, 3309 (1968).

(13) G. N. Némethy and H. A. Scheraga, *Biopolymers*, **4**, 369 (1966).

(14) S. J. Leach, G. Némethy, and H. A. Scheraga, *Biopolymers*, **4**, 369 (1966).

(15) IUPAC-IUB Commission on Biochemical Nomenclature, *Biochemistry*, **9**, 3471 (1970).

(16) J. T. Edsall, P. J. Flory, J. C. Kendrew, A. M. Liquori, G. Némethy, G. N. Ramachandran, and H. A. Scheraga, *Biopolymers*, **4**, 121 (1966); *J. Biol. Chem.*, **241**, 1004 (1966); *J. Mol. Biol.*, **15**, 399 (1966).

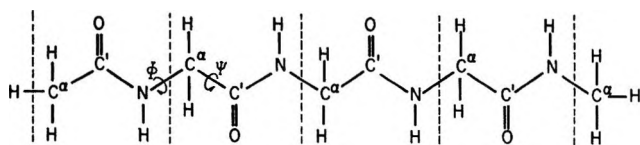


Figure 1. Diagrammatic representation of a tetrapeptide of glycine including the rotation angles ϕ ($N-C^\alpha$) and ψ ($C^\alpha-C'$) around the single bonds.

Table I: Coordinates for the Atoms in a Planar Peptide Unit of Glycine¹⁴

Atom	j	$z_j, \text{Å}$	$y_j, \text{Å}$	$x_j, \text{Å}$
C'	1	1.42	0.58	0.00
O	2	1.61	1.80	0.00
N	3	2.37	-0.34	0.00
H (amide)	4	2.18	-1.32	0.00
C $^\alpha$	5	3.80	0.00	0.00
H $^\alpha$ ^a	6	0.36	0.54	0.89
H $^\alpha$ ^a	7	0.36	0.54	-0.89

^a The C $^\alpha$ -H distance was taken to be 1.09 Å which is an average of the data on aliphatic hydrocarbons.

but a width as small as 5° was used for studying certain energy contours which varied more rapidly with ϕ and ψ .

Results

The ground-state potential energy surface for four peptide units (three residues) is displayed in Figure 2. Since $R = H$, the map is centrosymmetric about the point $\phi = 0, \psi = 0$.

There are three nonequivalent minima in the contour map: (1) the absolute minimum around $\phi = -20^\circ, \psi = -60^\circ$ whose energy has been set equal to zero. It should be noted that the minimum is quite shallow in this region and the interpolation is uncertain. Hence, the estimated uncertainty in the minimum is about $\pm 15^\circ$; (2) a local minimum about $\phi = -60^\circ, \psi = 60^\circ$ of 4 kcal/mol of residue; and (3) one local minimum at the fully extended chain conformation $\phi = -180^\circ, \psi = -180^\circ$ of 5 kcal/mol of residue.

The absolute minimum is reasonably close to and about equidistant from both the 3_{10} helix $\phi = -49^\circ, \psi = -26^\circ$ ¹⁷ and the α helix $\phi = -48^\circ, \psi = -57^\circ$. The minimum at $\phi = -60^\circ, \psi = 60^\circ$ corresponds to a seven membered hydrogen bonded ring. Two postulated conformations in this region are the 2_7 helix and the 2_7 helix at $\phi = -75^\circ, \psi = 70^\circ$.¹⁷ Maigret, *et al.*,¹⁸ found this to be the most stable conformation in their calculation on *N*-acetyl-*N'*-Methylglycylamide V.

Additionally, one notes the suggestion of a valley at $\phi \cong -60^\circ, \psi \cong -50^\circ$ which would correspond to the α helix.¹⁷

The general features of our present map (particularly in the regions of high steric repulsion) are similar to those obtained in our previous (EHT) calculations on

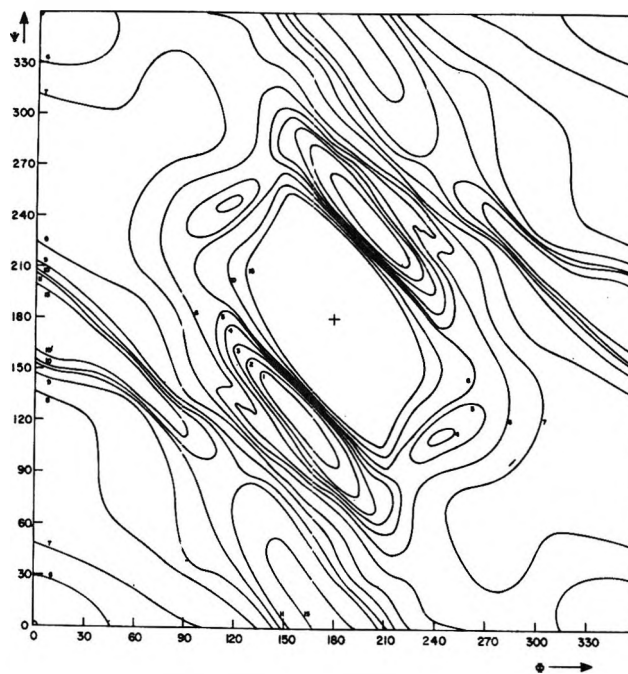


Figure 2. Ground-state potential energy surface for a tetrapeptide of glycine calculated by the CNDO/2 method. The contours of constant energy are relative to the most stable conformation chosen as zero energy and are in units of kcal/mol of residue.

the same system. The most significant differences are: (1) the absolute minimum occurs much closer to the α helix and the 3_{10} helix than in the previous computations; (2) there is a shift of the local minimum in the β region to the fully extended chain conformation; and (3) the appearance of a new minimum conformation which corresponds to the formation of a seven membered hydrogen bonded ring.

The partial charges, which are sensibly independent of the rotation angles ϕ and ψ , are given in Table II for the extended chain and the α helical conformations. The charges, although taken from the first and fourth peptide units, are representative of the atoms in the entire chain. The present results for the charge distribution around the peptide bond should be compared to those obtained by using Extended Hückel Theory (EHT) on *N*-methyl acetamide⁶ and on the tetrapeptide of glycine.⁷ On the basis of the CNDO/2 method, there is no longer an exaggerated charge separation for the atoms in the C-O bond.

Conclusion

The present CNDO/2 calculations on the helical calculations of a tetrapeptide of glycine are consistent with recent calculations in protein stereochemistry. An extension of the calculation to longer chain lengths may result in a more definite assignment of the absolute

(17) G. N. Ramachandran and V. Sasisekharan, *Advan. Protein Chem.*, **23**, 323 (1968).

(18) B. Maigret, B. Pullman, and M. Dreyfus, *J. Theor. Biol.*, **26**, 321 (1970).

Table II: Gross Charges on the Atoms in a Planar Peptide Unit for Various Helical Conformations of the Tetrapeptide of Glycine

Conformation	Atomic charges						
	N ^a	H ^a	O ^b	C ^b	C ^b	H ^a	H ^a
Fully extended chain	-0.19	+0.12	-0.37	+0.36	-0.09	+0.03	+0.01
Antiparallel-chain pleated sheet	-0.19	+0.12	-0.37	+0.36	-0.09	+0.03	+0.01
Parallel-chain pleated sheet	-0.20	+0.12	-0.37	+0.36	-0.09	+0.03	+0.01
Right-handed α helix	-0.20	+0.15	-0.37	+0.37	-0.10	+0.03	+0.00
Neighboring helix	-0.22	+0.17	-0.37	+0.37	-0.10	+0.03	0.00

^a Atomic charge taken from fourth peptide unit. ^b Atomic charge taken from first peptide unit.

minimum to a region around the α -helical conformation. Such calculations on longer chains would require extended computer space and computer time which is unfortunately not readily available to us at the present time.

Acknowledgments. The authors wish to thank Dr. Angelo Rossi for kindly supplying us with the set of coordinates used in these calculations. We wish also to acknowledge fruitful discussions with Drs. Björn Roos, F. A. Momany, and R. F. McGuire.

A Model for the Simulation of the Electron Spin Resonance Spectra of Nitroxide-Type Probe Molecules in a Nematic Mesophase

by Theodore Pietrzak

Department of Chemistry, University of Alabama, University, Alabama 35486 (Received September 2, 1971)

Publication costs borne completely by The Journal of Physical Chemistry

A model for simulating the esr spectrum of nitroxide-type molecules in nematic mesophases is developed which includes nuclear spin-flip transitions in the reorientation process. A typical nitroxide, $A_{zz} = 32$ G, $A_{yy} = A_{xx} = 6$ G and $g_{zz} = 2.0027$, $g_{yy} = 2.0061$, $g_{xx} = 2.0089$, is used as an example and the variation of the g value and hyperfine splitting (A) of the resulting three-line spectrum (isotropic line shape) is calculated as dependent on an ordering parameter (S_{zz}) which corresponds to a maximum angular deviation (θ_{\max}) of the length of the nitroxide molecule from the static magnetic field direction. Spin-flips of the nucleus in the reorientation process are included due to the anisotropy in the hyperfine tensor (A) and the fast jump rates involved in isotropic averaging. Comparison is made to other treatments of the problem which yield results differing to the extent of the approximations involved.

There is current interest in electron spin resonance (esr) studies of paramagnetic molecules in liquid-crystalline solvents, especially nematic-type mesophases.¹⁻⁴ Suitable paramagnetic probe molecules are rod-like molecules with a methyl-protected nitroxide group incorporated at the terminal position. Proper choice of nitroxide incorporation ensures coplanarity of the two tertiary carbon atoms, the nitrogen and oxygen atoms⁶ and minimum departure of the N-O bond direction from the length of the molecule axis.⁴ With these conditions one may find correspondence in the degree of ordering of the probe molecules with that of the diamagnetic liquid-crystalline solvent molecules as described by ordering parameters.⁶

We wish to report results for the simulation by a motional model of the esr spectra of such nitroxide-type probe molecules hypothetically in a nematic mesophase

- (1) H. R. Falle and G. R. Luckhurst, *J. Magn. Resonance*, **3**, 161 (1970).
- (2) G. Havach, P. Ferruti, D. Gill, and M. P. Klein, *J. Amer. Chem. Soc.*, **91**, 7526 (1969).
- (3) G. C. Fryburg and E. Gelerinter, *J. Chem. Phys.*, **52**, 3378 (1970).
- (4) P. Ferruti, D. Gill, M. A. Harpold, and M. P. Klein, *ibid.*, **50**, 4545 (1969).
- (5) C. L. Hamilton and H. M. McConnell in "Structural Chemistry and Molecular Biology," Ed., A. Rich and N. Davidson, W. H. Freeman, San Francisco, Calif., 1968, p 115.
- (6) A. Saupe, *Z. Naturforsch. A*, **19**, 161 (1964); A. Saupe, *Angew. Chem. Int. Ed. Engl.*, **7**, 97 (1968).

with the z -principal axis (N-O bond direction) parallel to the static magnetic field H_0 for perfect ordering. The motion of the nitroxide probe molecules in the ordered mesophase is simulated by small discrete reorientations of less than 5° spherical angle and the esr spectra result from this simulation of motion by use of a more general treatment to simulate random motionally averaged esr spectra.⁷ This general treatment is intermediate in computational difficulty between the methods used by Griffith, *et al.*,⁸ and more recently by Freed, *et al.*,⁹ for slow-tumbling rates. In this instance, however, the nitroxide is undergoing rapid reorientation (correlation time for tumbling $< 10^{-9}$ sec) in the nematic mesophase so as to exhibit isotropic line shapes (three line spectrum) with shifts in g value and hyperfine splitting as dependent on the degree of ordering. The technique for simulating esr spectra (PW) while similar to the treatment of Itzkowitz¹⁰ differs in that a stationary-state Hamiltonian which includes all off-diagonal terms (nonsecular and pseudosecular) was solved exactly¹¹ and the time-dependent esr spectra were simulated by suitable linear combinations of the exact stationary-state solutions. A and g tensors chosen were for "typical" methyl-protected nitroxide radicals:⁵ $A_{zz} = 32$ G, $A_{yy} = A_{xx} = 6$ G and $g_{zz} = 2.0027$, $g_{yy} = 2.0061$ and $g_{xx} = 2.0089$. The $2p\pi$ orbital which contains the odd-electron lies along the x axis and the N-O bond direction and long axis of the rod-like molecule lie along the z axis (see Figure 1).

The discrete-jump model used has 93 orientations in the positive x, y, z octant. A random walk simulating molecule motion is done by allowing the magnetic field vector H_0 to jump to nearest neighbor orientations in the fixed-coordinate system but with restriction to those orientations whose $\theta < \theta_{\max}$ with θ being measured from the z axis (see Figure 1). Perfect ordering along H_0 would occur for $\theta_{\max} = 0^\circ$ and an isotropic spectrum results at $\theta_{\max} = 90^\circ$. A basis set of orientations is established for a particular θ_{\max} which describes the cone in Figure 1 and a random walk is done over a sufficient number of points in that basis set to ensure isotropic averaging of the hyperfine tensors. The esr spectrum results from a cumulation of individual spectra averaged over the orientations visited. Each orientation has an esr spectrum associated with it as a result of solving the Hamiltonian for that orientation (θ, ϕ). In the course of the random walk the ordering parameter⁶ $S_{zz} = \frac{1}{2}\langle(3 \cos^2 \theta - 1)\rangle$ was computed as an ensemble average along with S_{zz} and S_{yy} using θ and ϕ . In this model $S_{zz} = S_{yy} = -\frac{1}{2}S_{zz}$. The results for the entire range of $\theta_{\max} = 0-90^\circ$ are shown in Figure 2 as the dotted-dashed lines ($m_I = \pm 1$). The center line ($m_I = 0$) is linear with respect to S_{zz} . The results from this simulation can be nearly approximated by using the first-order expression:¹² $A^2 = 1/g^2 (g_{zz}^2 A_{zz}^2 \sin^2 \theta \cos^2 \phi + g_{yy}^2 A_{yy}^2 \sin^2 \theta \sin^2 \phi + g_{xx}^2 A_{xx}^2 \cos^2 \theta)$ and deriving an expression for $\langle A \rangle$, the hyperfine splitting, as dependent

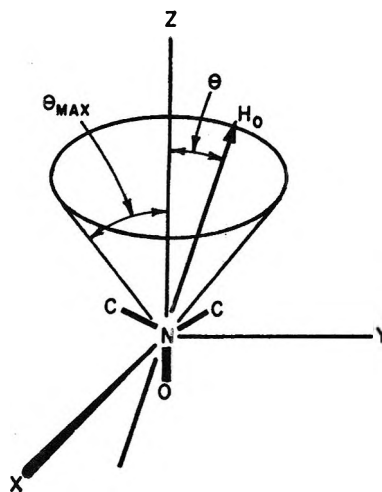


Figure 1. Principal axes of the hyperfine and coincident g tensors showing the magnetic field vector H_0 limited to a basis set formed by θ_{\max} . The $2p\pi$ orbital lies along the x axis.

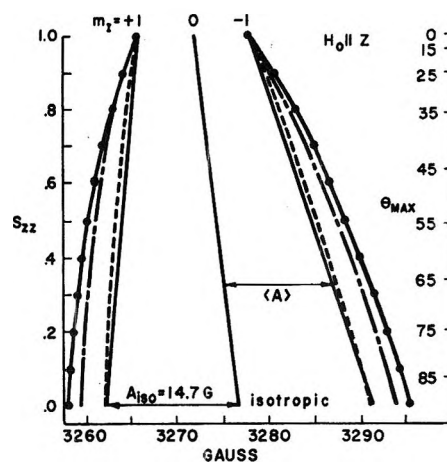


Figure 2. Positions of the three hyperfine lines plotted against S_{zz} and θ_{\max} . Results are from: —, linear approximation; ●—●, first-order expression; - - -, initial simulation; - - - - -, simulation including nuclear spin-flip transitions.

on S_{zz} . These results for $\langle A \rangle$ plotted about the $m_I = 0$ line are the connected points in Figure 2 ($m_I = \pm 1$). The expression for A^2 includes contributions from pseudosecular terms which are found to contribute significantly (up to a maximum of 4 G) to the splitting at a particular orientation.¹³

(7) T. Pietrzak and D. E. Wood, *J. Chem. Phys.*, **53**, 2454 (1970), subsequently referred to as PW.

(8) L. J. Libertini, A. S. Waggoner, P. C. Jost, and O. H. Griffith, *Proc. Nat. Acad. Sci. U. S.*, **64**, 13 (1969).

(9) J. H. Freed, G. V. Bruno, and C. Polnaszek, *J. Phys. Chem.*, **75**, 3385 (1971).

(10) M. S. Itzkowitz, *J. Chem. Phys.*, **46**, 3048 (1967).

(11) M. Kopp and J. H. Mackey, *J. Computational Phys.*, **3**, 539 (1969); J. H. Mackey, M. Kopp, and E. C. Tynan in "Electron Spin Resonance of Metal Complexes," Teh Fu Yen, Ed., Plenum, New York, N. Y., 1969.

(12) B. Bleaney, *Phil. Mag.*, **42**, 441 (1951).

(13) L. J. Libertini and O. Hayes Griffith, *J. Chem. Phys.*, **53**, 1359 (1970).

Approximate treatment for an average effective Hamiltonian which neglects pseudosecular terms and g anisotropy yields an expression⁴ for ΔA linearly dependent on S_{zz} where the average hyperfine splitting is $\langle A \rangle = A_{iso} + \Delta A$. These results as dependent on S_{zz} are plotted as the solid lines ($m_I = \pm 1$) in Figure 2. Experimental data are presumed to be well described by this linear approximation.⁴ The linear dependence of the g value as a function of S_{zz} was found to be the same from the simulations and from all the approximations discussed in this paper.

From the simulation of the isotropic spectrum at $S_{zz} = 0$, $\langle A \rangle$ is 2.5 G larger than A_{iso} (14.7 G). This is a weakness of the model at least for large anisotropy in \mathbf{A} ¹⁴ and can be due to the neglect of nuclear spin-flip transitions ($\Delta m_I = \pm 1$, $\Delta m_S = \pm 1$) which become increasingly important at fast jump rates encountered in isotropic averaging.¹⁵ Inclusion in the orientation process of the probability of such nuclear spin-flip transitions results in the dashed lines ($m_I = \pm 1$) as shown in Figure 2. These results were obtained by allowing such spin-flips to forbidden lines in the averaging process to the extent of obtaining the best value for $\langle A \rangle$ at $S_{zz} = 0$ (isotropic). This corresponded to a nuclear spin-flip occurring every third jump in the reorientation process of a single nitroxide molecule.

The results from the simulation by the discrete-jump

model incorporating nuclear spin-flip transitions suggests slightly larger $\langle A \rangle$ values at typically intermediate experimental S_{zz} values of 0.4 to 0.7.^{16,17} It also suggests that the dependence of $\langle A \rangle$ on S_{zz} is determined by the anisotropy in the hyperfine tensor (\mathbf{A}) since off-diagonal terms contribute to the intensity of these spin-flip transitions at all orientations.¹³ Both in approach and in results for $\langle A \rangle$, this treatment lies between the linear approximation (solid lines) which neglects pseudosecular terms and the initial simulation (dotted-dashed lines) and first-order results (connected points) both of which neglect nuclear spin-flips in the reorientation process. For experimental verification, independent correlation of ordering parameters with temperature in nematic mesophases is necessary along with consideration of the nitroxide probe molecules as nonideal nematic molecules in a nematic host.

(14) A hypothetical species with the same g tensor but with an A tensor of 20 G, 11 G, and 11 G as x , y , and z diagonal elements, respectively, was simulated with this model at isotropic averaging with $\langle A \rangle = 14.2$ G. This indicates that the anisotropy in A plays a role in the goodness of fit for A_{iso} as simulated from this model. This conclusion is also supported by the good agreement for A_{iso} of NO_2 in zeolite as simulated by this model (see ref 7).

(15) H. Sillescu and D. Kivelson, *J. Chem. Phys.*, **48**, 3493 (1968).

(16) A. Saupe, *Angew. Chem. Int. Ed. Engl.*, **7**, 97 (1968).

(17) A. Saupe, G. Englert, and A. Povh, *Advan. Chem. Ser.*, **No. 63**, 51 (1967).

Adsorption on Flat Surfaces. III. Adsorption of Branched-Chain Alcohols

by T. D. Blake* and W. H. Wade

Department of Chemistry, University of Texas at Austin, Austin, Texas (Received September 27, 1971)

Publication costs assisted by the Robert A. Welch Foundation

Gravimetric measurements have been made of the vapor-phase adsorption of various branched-chain alcohols on the oxidized surface of aluminum foil. All resulting isotherms are Langmuirian up to at least 0.3 relative pressure, but then rise steeply. Tertiary alcohols show a subsequent step at two to three monolayers. In the case of 2-methyl-2-propanol, as the temperature is lowered below the melting point, multilayer adsorption diminishes and the step moves towards higher relative pressures. At temperatures just below the melting point, isotherms intersect the saturation vapor pressure axis, and nucleation of the bulk phase is sufficiently delayed for isotherm measurement above saturation. This delay is attributed to a large contact angle resulting from a structural dissimilarity between the adsorbed and bulk phases. If the alumina surface is first covered with 70% of a monolayer of pentanol, then although the total adsorption of tertiary alcohols is reduced, the general shape of their isotherms is unchanged. In general, the work provides further evidence that the high energy, heterogeneous character of alumina surfaces can be masked by a monolayer of a low-molecular-weight alcohol to give a low energy surface of considerable uniformity.

Introduction

Previous work carried out in this laboratory,¹⁻³ has demonstrated that the important autophobicity concept due to Zisman and coworkers⁴⁻⁶ may be applied to the vapor-phase adsorption of low-molecular-weight *n*-aliphatic alcohols on alumina. Evidently, monolayers of alcohols having hydrocarbon chains containing as few as 3 carbon atoms per molecule are sufficient to obscure the high energy character of this surface. Incomplete monolayers of longer chain alcohols are also effective. Thus, 70% of a monolayer of pentanol reduces the surface pressure of decane from 36.2 to 7.1 dyn cm⁻¹, and increases the contact angle from 0 to about 8 deg.³

These investigations have now been extended to include various branched-chain alcohols. As in the earlier papers in this series,^{2,3} the substrate chosen was oxidized aluminum foil. The use of a planar rather than a powdered adsorbent reveals certain features of the isotherms that might otherwise be obscured by subsaturation condensation. The adsorbates investigated were cyclohexanol, 2-propanol, and the tertiary alcohols 2-methyl-2-propanol, 2-methyl-2-butanol, and 3-methyl-3-pentanol. Hereinafter, these will be designated, respectively, cyclo-C₆, *iso*-C₃, *tert*-C₄, *tert*-C₅ and *tert*-C₆. Straight chain alcohols will be referred to as C₃, C₄, etc.

Experimental Section

Details of the gravimetric adsorption apparatus and the experimental technique used in this work have been given elsewhere.^{2,3} The foil sample (package B)² comprised a stack of 200 rectangular sheets of 5- μ m aluminum foil having a total geometric area of 1.02 m² and a roughness factor of 1.08. The sheets were held in place by a light silica framework. Prior to each run, the

sample was cleaned by overnight treatment with pure oxygen at 400°, and then outgassed to 10⁻⁶ Torr before being cooled to isotherm temperature and constant weight. If required, pretreatment with C₅ was carried out as previously described.³

The alcohols (99 + mol % grade, supplied by Matheson Coleman and Bell) were exhaustively dried over molecular sieve, and outgassed and repeatedly distilled under vacuum before use.

The arrangement used to maintain the sample within 0.02° of the quoted isotherm temperature is shown in Figure 1. Ambient room temperature was either 23 or 28 ± 0.5°. Saturation vapor pressures, p_0 , (listed in Table I) were always determined with excess bulk alcohol present in the sample chamber since in most cases literature values were not considered sufficiently reliable. The presence of foreign vapors (typically air from solution) could be detected by partially evacuating the system and remeasuring p_0 .

Contact angles were measured using the sessile drop apparatus described previously.³

Results and Discussion

Up to $p/p_0 = 0.8$, all adsorption isotherms (Figures 2-5) resemble those obtained with straight-chain alco-

* Address correspondence to this author at Kodak, Ltd., Wealdstone, Harrow, Middlesex, England, HA1 4TY.

(1) J. Barto, J. L. Durham, V. F. Baston, and W. H. Wade, *J. Colloid Interface Sci.*, **22**, 491 (1966).

(2) T. D. Blake and W. H. Wade, *J. Phys. Chem.*, **75**, 1887 (1971).

(3) T. D. Blake, J. L. Cayias, W. H. Wade and J. A. Zerdecki, *J. Colloid Interface Sci.*, **37**, XXX (1971).

(4) E. F. Hare and W. A. Zisman, *J. Phys. Chem.*, **59**, 335 (1955). W. H. Fox, E. F. Hare, and W. A. Zisman, *ibid.*, **59**, 1097 (1955).

(5) O. Levine and W. A. Zisman, *ibid.*, **61**, 1068 (1957).

(6) W. A. Zisman, *Advan. Chem. Ser.*, **No. 43**, 1 (1964), and papers cited therein.

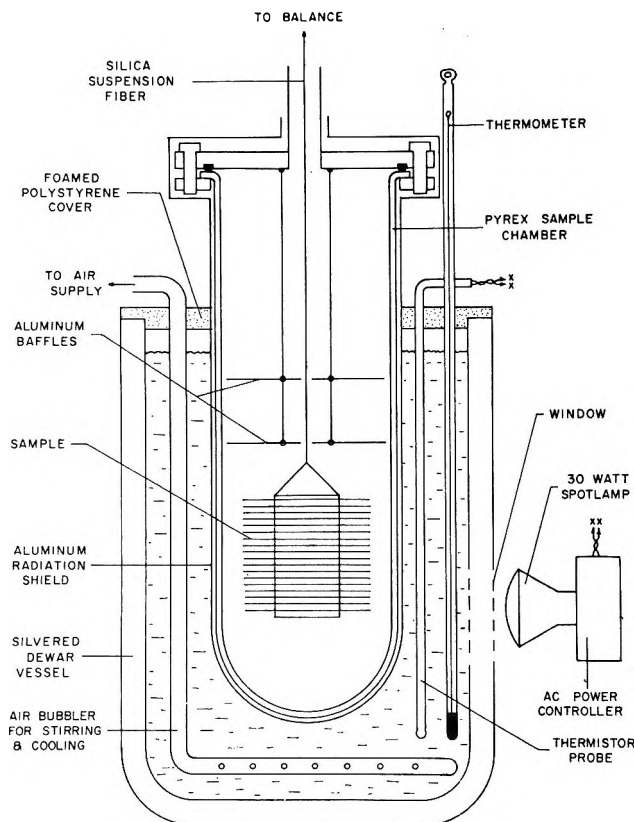


Figure 1. Details of the arrangement used to control sample temperature. For the 0° isotherm, the water bath was replaced by a larger vessel containing distilled water-ice slush.

Table I: Saturation Vapor Pressures (Torr) at T , $^\circ\text{C}$

Alcohol	T , $^\circ\text{C}$			
	0.00	13.30	20.00	26.60
cyclo- C_6			0.485	
<i>iso</i> - C_3			31.64	
<i>tert</i> - C_4 (liquid)	7.77 ^a	19.4 ^a	30.6 ^a	46.6
<i>tert</i> - C_4 (solid)	5.74	17.22	28.28	...
<i>tert</i> - C_5			11.74	
<i>tert</i> - C_6			4.61	

^a Indicates supercooled liquid (from data of Parkes and Barton, *J. Amer. Chem. Soc.*, **50**, 24 (1928)).

holds C_3 to C_5 ,^{1,2} being highly Langmuirian in character, possessing well-developed "knees" and long linear regions. Adsorption on the bare surface was reversible above $\theta = 0.65$. However, the 0.35θ remnant could not be removed even after prolonged evacuation at 10^{-6} Torr and was, presumably, dissociatively adsorbed.^{1,2}

The Langmuir molecular areas of all the alcohols so far investigated are listed in Table II together with measured contact angles and selected physical properties obtained from the literature. Assuming alignment roughly normal to the surface, the molecular areas follow a logical progression, with molecules of potentially similar cross-section having similar areas. Thus,

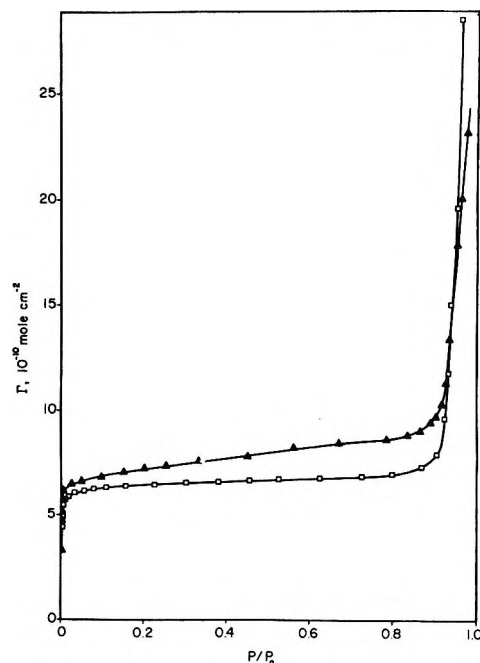


Figure 2. Adsorption of cyclo- C_6 (\square) and *iso*- C_3 (\blacktriangle) on aluminum foil at 20° .

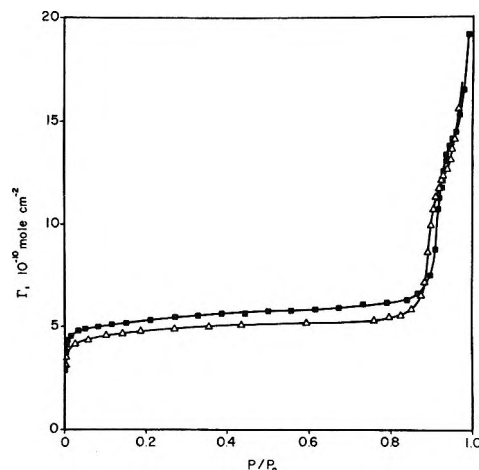


Figure 3. Adsorption of *tert*- C_5 (\blacksquare) and *tert*- C_6 (\triangle) on aluminum foil at 20° .

iso- C_3 and cyclo- C_6 differ by only 1.1 \AA^2 , whereas the introduction of two $-\text{CH}_2-$ groups in going from *tert*- C_4 to *tert*- C_6 involves an area increase of 4.7 \AA^2 .

Above $p/p_0 = 0.8$, all the isotherms rise steeply. Cyclo- C_6 adsorption exceeds five statistical monolayers at $p/p_0 = 0.97$ and appears to approach the saturation vapor pressure axis asymptotically. This suggests a zero contact angle for the bulk alcohol, which is a solid at the experimental temperature (20°). *iso*- C_3 also shows multilayer adsorption, and in this case, the contact angle was found to be less than 5° , but possibly nonzero. The fact that C_3^2 is more autophobic than *iso*- C_3 can be explained if it is assumed that the critical surface tensions of their monolayers are, respectively, lower and higher than their bulk surface tensions.

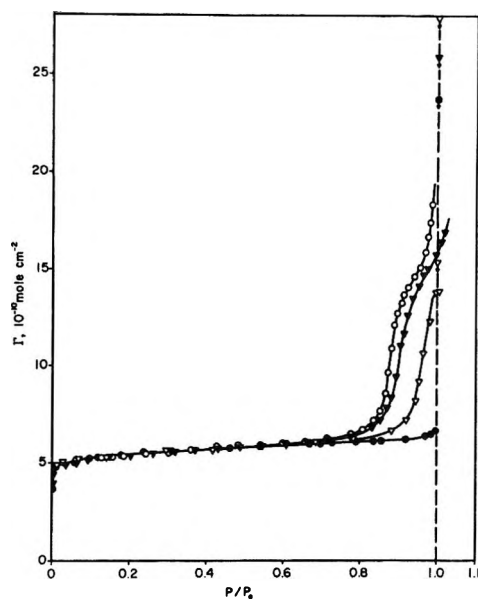


Figure 4. Adsorption of *tert*-C₄ on aluminum foil at 26.6° (○), 20° (▼), 13.3° (▽), and 0° (●).

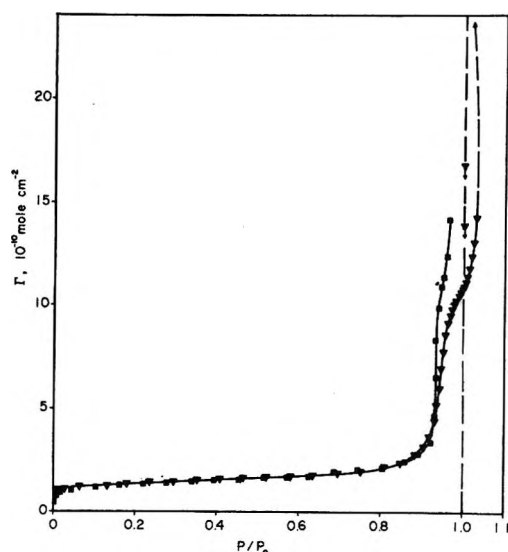


Figure 5. Adsorption of *tert*-C₄ (▼) and *tert*-C₆ (■) on C₆-treated aluminum foil at 20°.

Since the latter are 23.7 dyn cm⁻¹ (C₃) and 21.4 dyn cm⁻¹ (*iso*-C₃), the critical surface tensions would be comparable with those of solid hydrocarbon and close-packed CH₃- surfaces (22–24 dyn cm⁻¹).⁶ Furthermore, as one would not expect the surface tension of cyclo-C₆ to change significantly on freezing, the critical surface tension of a monolayer of this alcohol must be at least 34 dyn cm⁻¹, which is about the value found for CH₂- surfaces.⁶

Figures 3 and 4 show that the multilayer adsorption of the tertiary alcohols is more unusual. At about $p/p_0 = 0.93$ each of the 20° isotherms shows a definite step. In addition, the *tert*-C₄ isotherms for temperatures below the melting point intersect the saturation

Table II: Molecular Areas, Contact Angles (θ), Surface Tensions (γ_{LV}), and Boiling and Melting Points (bp and mp) of the Alcohols so far Investigated

Alcohol	Molecular area Å ²	θ , deg at 20°		γ_{LV} at 20° dyn cm ⁻¹	Bp, °C	Mp, °C
		Advanc- ing	Reced- ing			
C ₁	15.9	0	0	22.6	65	-94
C ₂	19.9	0	0	22.3	78.5	-117
C ₃	24.6	13	<5	23.7	97	-126
C ₄	24.4	16	5	24.6	118	-90
C ₅	24.8	31	21	25.6	138	-79
cyclo-C ₆	26.7	33.8 at 27°	161	+25.2
<i>iso</i> -C ₃	25.4	<5	0	21.4	82	-89.5
<i>tert</i> -C ₄	32.4	<5 at 26°		19.6	82.5	+25.5
<i>tert</i> -C ₅	33.3	11	7	22.8	102	-9
<i>tert</i> -C ₆	37.1	23.6	122	-24

vapor pressure axis and, at 20°, continue well beyond saturation. However, discussion of this latter behavior will be deferred until later. For the moment, it is sufficient to note that the inflection points on either side of the step risers correspond to completion of the first and *third* statistical monolayers (rather than first and second). Thus, it appears that the second and third monolayers adsorb concertedly, possibly with molecules in the second layer hydrogen-bonded to those in the third. Kiselev, *et al.*,⁷ who observed a concerted bimolecular adsorption of *tert*-C₄ on Graphon with the step riser at $p/p_0 = \sim 0.1$, briefly adopted a hydrogen bonded dimer explanation.

Association of alcohols in the liquid phase is well documented and is directly responsible for their high boiling point. Thomas⁸ in a series of publications has paid particular attention to the differences in the liquid state association of primary, secondary, and tertiary alcohols. His calculations show that *tert*-C₄, *tert*-C₅, and *tert*-C₆ are the most extensively associated alcohols, and, based on a finite degree of association in the low temperature limit, he favors a ring polymer configuration involving approximately four monomer units. Such a structure for *tert*-C₄ oriented to maximize vertical interactions yields a calculated (based on Dreiding models) equivalent monomer area of 13 Å². This is equivalent to a riser of $\theta = 1.8$ —very close to the observed value. Zettlemoyer, *et al.*,⁹ have observed what is close to a single step riser with $\theta = \sim 2$ for *iso*-C₃ on a graphitized black and one must wonder if the above postulate is not also applicable for his system.

(7) N. N. Avgul, A. V. Kiselev, and I. A. Lyzina, *Kolloid. Zh.*, **23**, 513 (1961).

(8) L. H. Thomas and R. Meatyard, *Proc. Roy. Soc.*, 1986, 1995 (1963).

(9) D. R. Bassett, E. A. Boucher, and A. C. Zettlemoyer, *J. Phys. Chem.*, **71**, 2787 (1967).

Pierce and Ewing^{10,11} and others have suggested that stepwise adsorption is favored by: (1) uniformity of substrate; (2) strong lateral interactions between adsorbate molecules; (3) a sufficiently low temperature such that the small energy differences that give rise to steps are not smeared out by thermal agitation. These views are consistent with the present results since: (1) a close-packed monolayer of nearly spherical $(\text{CH}_3)_3\text{C}$ - groups is likely to provide a highly uniform surface; (2) strong lateral interactions are possible with adsorbates that give Langmuirian isotherms on heterogeneous surfaces (such as alumina);² (3) the isotherm temperatures of the tertiary alcohols (especially *tert*- C_4) are reasonably close to their melting points, and at least their first monolayers will be highly localized because of strong interactions with the surface. However, it would appear wisest to recognize the specific interactions in *tert*-alcohols and modify² in recognition of the possible existence of such ring polymers.

Figure 5 reveals that if the foil is pretreated with C_5 , the amount of tertiary alcohol necessary to complete the first monolayer is much reduced, but subsequent adsorption is only slightly affected. Evidently, the appearance of steps is not determined by the detailed structure of the first monolayer, which, in these examples, comprises approximately 28 C_5 and 6 *tert*- C_4 , CH_2 , and CH_3 units per 100 \AA^2 .

The greater flexibility of the straight chain units, which is responsible for their lower, less well defined melting points, is probably the main reason why they do not also show stepped isotherms at 20° . Pierce and Ewing report that ethyl chloride adsorbs stepwise on graphite at -78° , but not at 0° ,¹⁰ and carbon tetrachloride gives steps at temperatures just below the melting point, but not above.¹¹

As the temperature is lowered still further, however, the steps in the CCl_4 isotherms move to higher relative pressures: the step originally centered at $p/p_0 = 0.75$ at -26° moving to $p/p_0 = 0.83$ at -42° . In the present work, equivalent behavior is shown by *tert*- C_4 . At 26.6° (1.1° above the melting point), the step is centered around $p/p_0 = 0.93$, but at 20° , although the step is somewhat more pronounced, it has shifted to $p/p_0 = 0.99$. At 13.3° , total adsorption in excess of a monolayer is restricted to about one and one-half monolayers; at 0° , it is almost entirely absent. Pierce and Ewing postulate that even with nearly spherical molecules such as CCl_4 , adsorbate-adsorbent interactions at temperatures below the melting point may produce a first layer structure unfavorable for further adsorption. At temperatures above the melting point, however, increased thermal agitation ultimately destroys both the ordered structure and the energetic discrimination between the molecular layers, and thereby increases the total amount of multilayer adsorption.

As noted above, the isotherms for *tert*- C_4 below its melting point intersect the saturation vapor pressure

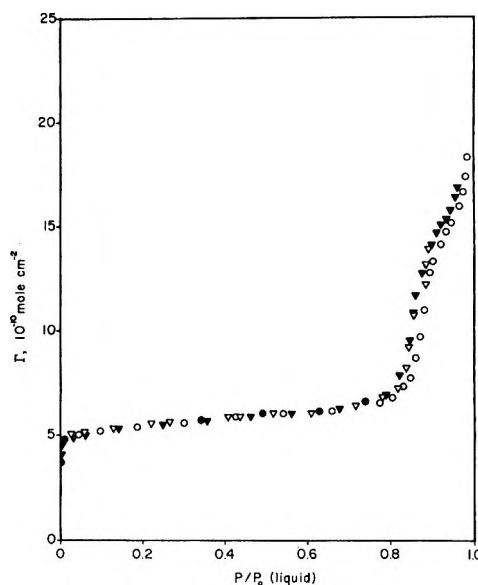


Figure 6. Adsorption of *tert*- C_4 on aluminum foil at 26.6° (\circ), 20° (\blacktriangledown), 13.3° (∇), and 0° (\bullet), with isotherms plotted as functions of $p/p_{0,L}$, where $p_{0,L}$ is the saturation vapor pressure of *tert*- C in the liquid state (supercooled at 20° , 13.3° , and 0°).

axis. This behavior is to be expected with adsorbates that exhibit nonzero contact angles, but is seldom observed because of capillary condensation. Some sub-saturation condensation at very high relative pressures was expected in the present work also—owing to the inevitable presence of some areas of foil-foil and foil-framework contact within the sample package.² Yet, with *tert*- C_4 at 20° , condensation-free equilibrium data were obtained up to $p/p_0 = 1.02$ (Figure 4) and 1.04 on the C_5 -treated surface (Figure 5). The system would remain at these relative pressures for many hours before condensation set in, Γ became unbounded, and p/p_0 dropped to 1.00.

These observations are explicable if the contact angle between bulk (*i.e.* solid) *tert*- C_4 and its adsorbed phase is sufficiently large to inhibit heterogeneous nucleation of condensate by increasing the free energy of formation of critical nuclei.¹² A large contact angle implies a structural difference between the adsorbed and bulk phases^{2,13,14} that would be consistent with the interpretation of step shifts suggested by Pierce and Ewing.

However, the above explanation is incomplete, for, as the temperature was lowered, it became increasingly difficult to obtain data above saturation: thus, at 13.3 and 0° , Γ became unbounded at only $p/p_0 = 1.005$ and 1.00, respectively. Such behavior presumably re-

(10) C. Pierce and B. Ewing, *J. Amer. Chem. Soc.*, **84**, 4070 (1962).

(11) C. Pierce and B. Ewing, *J. Phys. Chem.*, **71**, 3408 (1967).

(12) R. Defay, I. Prigogine, A. Bellemans, and D. H. Everett, "Surface Tension and Adsorption," Longmans, London, 1966.

(13) B. V. Derjaguin and Z. M. Zorin, *Proc. Int. Cong. Surf. Activ.*, **2nd**, 145 (1957).

(14) D. H. Bangham and Z. Saweris, *Trans. Faraday Soc.*, **34**, 554 (1938); D. H. Bangham, *J. Chem. Phys.*, **14**, 352 (1946).

flects a reduction in the free energy of formation of critical nuclei, and, therefore, a reduction in either the contact angle or the surface tension of the condensate. Since the latter parameter is unlikely to decrease with temperature, it is necessary to explain why the contact angle should do so.

Now, it has been found that if the *tert*-C₄ isotherms are plotted as functions of $p/p_{0,L}$, where $p_{0,L}$ is the saturation vapor pressure of the alcohol in the liquid state (supercooled at 20, 13.3, and 0°; see Table I), then, to a close approximation, they coincide with one another (Figure 6). This dictates an isosteric heat of adsorption equal to the *heat of vaporization* of the supercooled liquid and implies that the ring complexes are metastable and have the approximate degrees of freedom associated with the liquid state. It thus appears that the properties of the adsorbed phase are largely independent of both temperature and the physical state of the bulk alcohol; but, as the temperature is lowered, successively less of the total adsorption isotherm is revealed before condensation sets in. At 0°, for example, only the first monolayer is completed before the saturation vapor pressure of the solid is reached, whereas at 20° the first *three* statistical monolayers are completed. If it is supposed that the structure of the first monolayer is more solid-like (*e.g.*, has a greater density and order) than subsequent layers, then, as required, the solid condensate should exhibit a smaller contact angle at 0° than at 20°.

On the other hand, at 20°, the contact angle between the *supercooled liquid tert*-C₄ and its adsorbed phase may be sufficiently small for nucleation of liquid condensate before solid. (In this case, Ostwald's rule⁹ would

be operative for heterogeneous nucleation.) Certainly, the contact angle of *tert*-C₄ at 27° is less than 5 deg (Table II), which is consistent with the fact that its surface tension is 3–4 dyn cm⁻¹ lower than the critical surface tension of CH₃ surfaces. In comparison, *tert*-C₆, which has a surface tension of 22.8 dyn cm⁻¹, exhibits a contact angle of 7–11 deg at 20°.

It should be noted that at temperatures below the melting point, once condensation of *tert*-C₄ had set in, the pressure ultimately became stable at p_0 without reduction in Γ . If alcohol was subsequently withdrawn from the system, the equilibrium pressure remained at p_0 while Γ fell (arrowed points in Figures 4 and 5) until the adsorption branch of the isotherm was regained; desorption then proceeded reversibly. Thus, the unusual supersaturation data reported here are not due to temperature differences between the foil sample and the walls of the sample chamber; on the contrary, the quoted relative pressures should be within ± 0.005 of the actual values.

In conclusion, it is pointed out that the basic principle underlying the above discussion is that with autophobic systems, adsorbed and bulk material should be treated as *separate phases*. This principle, which may be attributed to Bangham,¹⁴ is well borne out by the work of Derjaguin, *et al.*,^{13,15} and by the results reported here.

Acknowledgments. The authors thank The Robert A. Welch Foundation and the National Science Foundation for their continued interest and financial support.

(15) B. V. Derjaguin and L. M. Shchersakov, *Kolloid. Zh.*, **23**, 40 (1961); *Colloid J. USSR*, **23**, 33 (1961).

Thermochemistry of Halide Exchange in an Anion-Exchange Resin

by G. R. Choppin,* G. Y. Markovits, and M. E. Clark

Department of Chemistry, Florida State University, Tallahassee, Florida 32306 (Received May 17, 1971)

Publication costs borne completely by The Journal of Physical Chemistry

The thermodynamic parameters for the exchange of halide ions on Dowex-1X1 have been calculated from the temperature variation of the equilibrium constant. These data for anion exchange are found to correlate with the change in the water content of the resin phase during the ion exchange. Selectivity values can be predicted for halide exchange on Dowex-1 and Dowex-2 resins of 0.5 to 4% DVB content from a knowledge of the water content of the pure resin salts and the thermodynamic values per mole of water exchanged per per cent DVB of the resin.

One theory of ion exchange proposes that selectivity is the result of specific interactions in the resin phase.¹ In contrast to this theory of resin phase ion pairing is an alternative model in which anion-exchange resin selectivity is related to differences in the hydration tendencies of the exchanging anions in the external aqueous phase.² Alternately, Reichenberg has described evidence to support a model in which the differences in hydration energies in the resin phase determine the order of halide selectivity.³

Solutions of tetraalkylammonium salts can serve as model compounds for strongly basic ion-exchange resins such as Dowex-1. It had been proposed that "water-structure enforced ion pairs" are formed between the large tetraalkylammonium cations and the heavier halides such as bromide and iodide.⁴ This would seem to provide support for the model wherein halide selectivities in anion-exchange resins reflect the effects of ion pairing in the resin phase. However, more recently the osmotic coefficients and molal heat contents of tetraalkylammonium halide solutions have been interpreted as providing no evidence for ion-pair formation but as indicating significant effects by the ions on the solvent structure.^{5,6} This would support the ion-exchange theories of Reichenberg, Chu, Whitney, and Diamond. A previous study of halide exchange with Dowex-2 resin using calorimetry considered the possibility both of site binding of the heavier halides and of ion-solvent interactions in the aqueous phase with the latter playing an ill-defined role.⁷

In this paper we report the results of the determination of the thermodynamic parameters of halide exchange with Dowex-1 resin. The nmr shifts of the water in the resin phase as well as in aqueous solutions of tetraalkylammonium salts were obtained to provide a measure of the similarity of the resin phase and its model system.

Experimental Section

Analytical grade Dowex-1 (1% DVB) resin (Bio-

Rad Laboratories, chloride form, 50–100 mesh) was washed with 1 M HCl, saturated NaCl, and then with distilled water until no further chloride could be detected in the effluent. Part of this material was converted into the fluoride, bromide, iodide, nitrate, hydroxide, and perchlorate forms. These resins were washed and then air-dried with frequent mixing and analyzed. Triplicate samples agreed within 1 ppt.

Weighed samples of halide forms of the dry resin were hydrated by submersion in distilled water. Halide exchange was accomplished by equilibrating these resin samples by stirring with standardized solutions of binary mixtures of potassium halides in which the total halide concentration in the solutions were analyzed for the concentration of the halides present. The chloride-fluoride exchange experiments were designed so that F⁻ was present in excess of Cl⁻ in solution. For the fluoride determination PbClF was precipitated along with PbF₂ in 75% acetone. All other halide analyses were done by standard methods. Comparison of total concentrations in the initial and final solutions gave the correction for final effective solution volume. From the initial and final solution data it was possible to calculate the amount of each halide present in the resin phase. Stoichiometric equilibrium constants were calculated from the molalities of the anions in each phase.

To determine the water content of the wet resins, resin samples were separated from the solution and centrifuged for 20 min on a sintered glass plate in a centrifuge cone. After weighting, the resin samples

(1) F. E. Harris and S. A. Rice, *J. Chem. Phys.*, **24**, 1258 (1956); *Z. Phys. Chem. (Frankfurt am Main)*, **8**, 207 (1956).

(2) B. Chu, D. C. Whitney, and R. M. Diamond, *J. Inorg. Nucl. Chem.*, **24**, 1405 (1962).

(3) D. Reichenberg in "Ion Exchange," Vol. I, J. Marinsky, Ed., Marcel Dekker, New York, N. Y., 1966.

(4) S. Lindenbaum and G. E. Boyd, *J. Phys. Chem.*, **68**, 911 (1964).

(5) S. Lindenbaum, L. Leifer, G. E. Boyd, and J. W. Chase, *ibid.*, **74**, 761 (1970).

(6) S. Lindenbaum, *ibid.*, **74**, 3027 (1970).

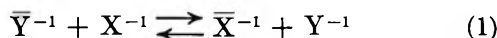
(7) F. Vaslow and G. E. Boyd, *ibid.*, **70**, 2507 (1966).

were dried in a vacuum desiccator over $\text{Mg}(\text{ClO}_4)_2$ for 24 hr and reweighed. It is possible that a small amount of water was retained by the resin after this drying technique since it has been shown that Dowex-1 resin in the chloride form retained about 0.3 mole of water per mole of chloride.⁸ An error of this magnitude would not affect our results unduly since the total water content of our resins was much greater than this. The temperature, which was controlled within $\pm 0.02^\circ$, was treated as an errorless variable.

The nmr spectra of water in tetraalkylammonium salt solutions and in Dowex-1X1 resin in the different anionic forms were recorded on a Varian HR-60 spectrometer. A sealed concentric capillary containing dioxane as an external reference was used.

Results

The exchange reaction can be written as



in which \bar{Y} and \bar{X} are the resin phase species. We define the standard state of the resin as that state which is in equilibrium with an external solution phase of 0.10 *M* potassium halide solution. This is similar to the standard state defined by Vaslow and Boyd in their thermodynamic study of halide exchange with Dowex-2 resin.⁷ Table I presents the equilibrium

Table I: Equilibrium Constants For Halide Exchange in Dowex-1X1 Resin

Ion A	Ion B	([B]/[A])	<i>K</i>	Temp, °C
F	Cl	0.258	3.32 ± 0.07	4.0
F	I	0.0945	36.76 ± 0.14	5.2
Cl	Br	0.596	2.36 ± 0.09	5.2
F	Cl	0.271	2.68 ± 0.05	25
F	I	0.127	19.3 ± 0.06	25
F	I	0.130	18.9	25
Cl	Br	0.617	2.14 ± 0.08	25
Cl	Br	1.01	2.49 ± 0.25	25
Cl	Br	1.14	2.04 ± 0.19	25
Cl	I	0.196	7.21 ± 0.03	25
Cl	I	0.207	6.4	25
Cl	I	0.425	6.67	25
F	Cl	0.286	2.36 ± 0.04	40
F	I	0.148	13.36 ± 0.04	40
Cl	Br	0.645	1.87 ± 0.08	47.5

ratios of the halide ion concentrations in the aqueous phase and the calculated equilibrium constants for the halide exchange. The error listed is the standard deviation for a single measurement calculated from the estimated errors in the volumes, concentrations, etc. Duplicate runs gave results well within the stated error limits. The values of *K* were independent of the direction from which equilibrium was approached.

The integral values of the thermodynamic functions are given by

$$\Delta G^\circ = -RT \int_0^1 \ln K dn_x \quad (2)$$

and

$$\Delta H^\circ = \int_0^1 \Delta \bar{H} dn_x \quad (3)$$

where n_x is the mole fraction of the exchanging halide anion and *K* is the equilibrium constant. In an ideal system which would exhibit a linear variation of the water content of the resins with the mole fraction composition, the thermodynamic properties measured for a resin composition of $n_{\bar{X}} = n_{\bar{Y}} = 0.5$ are numerically equal to the integral values.³ Table II lists the data

Table II: Water Content of Saturated Dowex-1 Anion Resin

Resin form	Moles H ₂ O per equivalent of resin
F ⁻	98.5 ± 0.3
Cl ⁻	71.5 ± 1
Br ⁻	53.8 ± 0.2
I ⁻	10.15 ± 0.03
ClO ₄ ⁻	17.95 ± 0.05
0.43 Cl ⁻ + 0.57 I ⁻	31.6
0.26 Cl ⁻ + 0.74 I ⁻	20.6
0.29 F ⁻ + 0.71 I ⁻	44.5
0.49 Cl ⁻ + 0.51 Br ⁻	54.7
0.37 Cl ⁻ + 0.63 Br ⁻	52.4

for our systems and indicates the possibility of large deviations from linearity in some cases. However, considering the experimental uncertainties and difficulties in measuring the water content of resins, we have assumed that the approximation of linearity is acceptable.

Accordingly, we chose initial conditions in most experiments that would give approximately unity for the ratio of halide ion concentrations in the resin phase at equilibrium. Moderate variations in this ratio did not change the values of *K* significantly as is shown in Table I. The variation of the equilibrium constant with temperature could be used to calculate the enthalpy. Within error limits linear plots were obtained for $\ln K$ vs. the reciprocal of the absolute temperature. The values calculated for ΔG° , ΔH° , and ΔS° at 25° are listed in Table III. As may be ascertained readily from Table III, internal agreement existed within the thermodynamic data for different possible combinations of exchanging ions, thereby providing additional proof that our experiments yielded the integral values.

The nmr chemical shifts of the tetraalkylammonium

(8) Y. Marcus and J. Naveh, *J. Phys. Chem.*, **73**, 591 (1969).

Table III: Thermodynamic Values for Halide Exchange With Dowex-1X1 at 25.0°

Reaction	Medium	ΔG° , kcal/mol	ΔH° , kcal/mol	ΔS , cal/deg mol
RF \rightarrow RCl	0.10 M K ⁺	-0.580 \pm 0.008	-1.6 \pm 0.1	-3.5 \pm 0.4
RF \rightarrow RI	0.10 M K ⁺	-1.763 \pm 0.003	-5.02 \pm 0.02	-10.95 \pm 0.08
RCl \rightarrow RBr	0.10 M K ⁺	-0.452 \pm 0.022	-1.0 \pm 0.2	-1.7 \pm 0.8
RCl \rightarrow RI	0.10 M K ⁺	-1.176 \pm 0.003	-3.46 \pm 0.02	-7.68 \pm 0.86
RF \rightarrow RCl	0.10 M Na ⁺	-0.775 \pm 0.007	-1.55 \pm 0.06	-2.6 \pm 0.2
RF \rightarrow RBr ^a	0.10 M K ⁺	-1.032	-2.60	-5.2
RBr \rightarrow RI ^a	0.10 M K ⁺	-0.724	-2.46	5.98

^a Calculated by Hess' law from the first four systems.

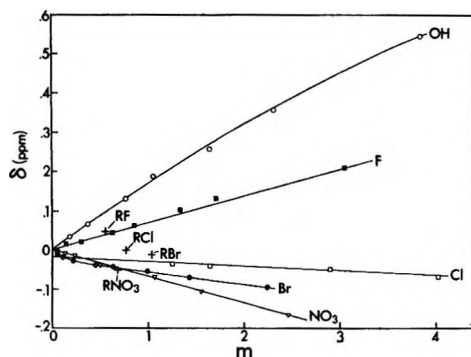


Figure 1. Observed proton chemical shifts of water as a function of the molality of solutions of $(\text{CH}_2)_4\text{NA}$ where A = OH⁻ (○), F⁻ (■), Cl⁻ (□), Br⁻ (●), and NO₃⁻ (▽). The values for analogous hydrated resins are also included.

salt solutions and of the hydrated resin relative to pure water are plotted in Figure 1.

Discussion

The thermodynamic values of Table III for halide exchange with Dowex-1X1 are in good agreement with the data for Dowex-2X0.5 and Dowex-2X2 obtained by calorimetry.⁷ The standard state in all these studies was the resin phase in equilibrium with an external aqueous phase of 0.1 M alkali halide. Our counterion was potassium rather than sodium; in Table III we have included data for one system using sodium as the counterion to show the difference.

We have recognized an interesting correlation between the enthalpy and entropy of halide exchange and the change in the number of moles of water in the resin phase when a mole of a particular resin-halide is completely converted into a mole of a different resin-halide. The number of moles of water transferred from resin to aqueous phase per mole of halide exchange is (from Table II) 27 for RF \rightarrow RCl, 45 for RF \rightarrow RBr, and 88 for RF \rightarrow RI. The ΔH value of -1.6 kcal is assumed to be related directly to the change of 27 mol of water. For 45 mol of water in the RF \rightarrow RBr exchange we would expect, then, $-1.6 \times 45/27$ or 2.7 kcal difference and for 88 mol of water in the RF \rightarrow RI exchange, the difference should be $-1.6 \times 88/27$ or

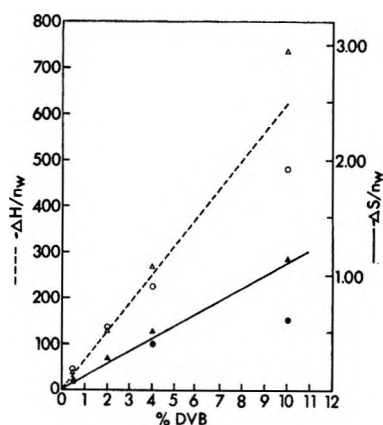


Figure 2. Plots of $\Delta H/n_w$ (○) and $\Delta S/n_w$ (▲, ●) as a function of divinylbenzene content of Dowex-2 for Cl-Br (▲) and Br-F (○) exchange.

-5.2 kcal difference. These values are very close to those in Table III. Similarly, relating the difference of -3.5 cal/deg in the entropy values of Table III for the RF \rightarrow RCl exchange to 27 mol of water results in expected differences in the entropies for the RF \rightarrow RBr and RF \rightarrow RI exchanges of -5.8 and -11 cal/deg which again agree with the observed differences within the accuracy imposed by the uncertainty in the exact values for the moles of water involved. For these three systems the enthalpy change per mole of water exchange is -57 ± 1 cal and the entropy change per mole of water exchanged is -0.12 ± 0.01 cal/deg.

The literature data available for the thermodynamic values of halide exchange in Dowex-2 resin are more extensive than that for Dowex-1. In Figure 2 the values of $\Delta H/n_w$ and $\Delta S/n_w$ (n_w = number of moles of water exchanged per mole of halide exchange) are plotted as a function of divinylbenzene content. The resins up to 4% DVB can be fitted to straight lines whose slopes are -61 cal/(mol H₂O % DVB) for $\Delta H/n_w$ and -0.11 cal/(deg mol H₂O % DVB) for $\Delta S/n_w$. Not surprisingly, the data for 10% DVB resin do not fit this line so well. As the DVB content increases, the water content decreases and relatively large uncertainties exist in the n_w values.

These results show that the thermodynamics of the exchange of the halide ions in anion-exchange resin

of relatively low DVB content can be correlated with the transfer of water between the resin and the external aqueous phase. The effect of the halide ions on the structuring of the solvent water in the resin phase must be an important factor in determining the water content of the resin. The similarity in the chemical shifts for the resin halides and tetraalkylammonium halide solutions provides additional support for the view that the observed thermodynamic parameters for anion exchange are not attributable to any specific mode of interaction of the anions within the resin phase.

Phenomenologically, the relationship between the swelling volume of resins and the types of counterions present has been related to the hydration volumes of the ions.⁹ As we noted in the introduction, selectivity has been ascribed to the difference in the hydration tendency of the ions exchanging in the external aqueous solution phase^{2,7} and in the resin phase.³ The data in this paper relate selectivity to the differences in hydration in the resin phase as ions are exchanged. From a knowledge of the water content of the pure resin salts for a resin of low DVB, we can predict the values of the selectivity constant and the enthalpy and entropy of exchange for resins of different cross linkages with the values $\Delta G/n_w/\%$ DVB, etc.

We recognize that ion exchange is a very complex

phenomenon and selectivity is unlikely to be explained by any single, simple correlation. However, the relative hydration tendencies of the ions must be one of the factors in selectivity. A possible explanation for the relative order of hydration of the pure resin salts has been suggested by Steigman and Dobrow.¹⁰ These authors proposed that "anion selectivities on ion-exchange resins in water are strongly influenced by antagonistic and cooperative interactions of two water atmospheres: that surrounding the quaternary ammonium ion of the resin and that surrounding the entering anion." Qualitatively, such a concept correlates with the greater hydration of RF compared to RCl, etc. For systems of low water content (*e.g.*, resins of higher DVB), it is unlikely that the resin and the counterion form full hydration spheres and other factors must play dominant roles in selectivity.

Acknowledgments. This research was supported by Contract 14-01-0001-2104 of the Office of Saline Water, Department of the Interior. The NSF also provided some assistance through a grant to the FSU Computer Center.

(9) F. Helfferich, "Ion Exchange," McGraw-Hill, New York, N. Y., 1962.

(10) J. Steigman and J. Dobrow, *J. Phys. Chem.*, **72**, 3424 (1968).

Thermodynamic Properties of Hydrated and Ammoniated Electrons

by Gerard Lepoutre

Laboratoire de Chimie physique (équipe associée au CNRS), 59 Lille, France

and Joshua Jortner*

Department of Chemistry, Tel-Aviv University, Tel-Aviv, Israel (Received June 18, 1971)

Publication costs borne completely by The Journal of Physical Chemistry

We have found fair agreement between the free enthalpies of solvated electrons as computed from experimental data and from theoretical models. The apparent anomalies in the entropy of the ammoniated electron are due to a looser packing in the first solvation layer relative to the pure solvent, this effect being larger at a lower temperature. Some spectroscopic results can be rationalized in terms of the thermodynamic data.

Introduction

Various thermodynamic properties have been previously computed for hydrated and ammoniated electrons on the basis of experimental data.¹⁻⁴ We wish to use these data for a comparative study of the hydrated and the ammoniated electron and for a comparison between the thermodynamic properties of solvated electrons in polar liquids and the results of

recent theoretical estimates.⁵ To achieve this goal, we require a unified choice of definitions and extra-

(1) R. M. Noyes, *J. Amer. Chem. Soc.*, **86**, 971 (1964).

(2) J. Jortner and R. M. Noyes, *J. Phys. Chem.*, **70**, 770 (1966).

(3) W. L. Jolly, *Advan. Chem. Ser.*, **No. 50**, 30 (1969).

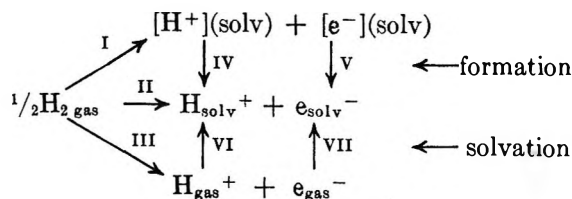
(4) G. Lepoutre and A. Demortier, to be published in *Ber. Bunsenges. Phys. Chem.*

(5) D. A. Copeland, N. R. Kestner, and J. Jortner, *J. Chem. Phys.*, **53**, 1189 (1970).

thermodynamic assumptions for the hydrated and for the ammoniated electron.

Definitions

Let us consider the following set of reactions



Let X° be any standard thermodynamic property (S, H, G, \dots) and ΔX_n° be its variation during reaction n ($n = \text{I, II}, \dots$).

Let $[\text{H}^+](\text{solv})$ and $[\text{e}^-](\text{solv})$ be protons and electrons in the solvent in hypothetical states where their X° values and the corresponding ΔX° values of formation are zero.

Then, we assert that (a) all $\Delta X_{\text{I}}^\circ$ are zero by definition; (b) the values of $\Delta X_{\text{IV}}^\circ$ and of $\Delta X_{\text{V}}^\circ$ are individual properties of "formation" of the solvated proton or the solvated electron ($\Delta X_{\text{IV}}^\circ = \Delta X_{\text{H}_{\text{solv}}^+}^\circ$; $\Delta X_{\text{V}}^\circ = \Delta X_{\text{e}_{\text{solv}}^-}^\circ$); (c) the values of $\Delta X_{\text{VI}}^\circ$ and of $\Delta X_{\text{VII}}^\circ$ represent individual properties of "solvation" of the gaseous proton or the gaseous electron.

Extrathermodynamic Assumptions

A. The ΔX_f° of formation of individual solvated ionic species and their individual standard entropies S° can be separated by reliable extrapolations schemes which involve experimental data concerning a large number of cations and anions. This assumption is quite reliable and is not expected to lead to large errors. Such a method previously applied by Jortner and Noyes to hydrated electrons^{1,2} will now be extended to ammoniated electrons. In the case of ammonia, Jolly³ and Lepoutre⁴ had indeed used individual standard entropies, but their ΔX_f° values of formation were computed on the basis of arbitrary assumption that all the ΔX_f° values of formation of the ammoniated proton are equal to zero.

B. The ΔX_f° values of formation of the gaseous electron are equal to their X° values, *i.e.*, $\Delta X_{\text{e}_{\text{g}}^-}^\circ = X_{\text{e}_{\text{g}}^-}^\circ$. As a consequence, for reaction III, we have

$$\Delta X_{\text{H}_{\text{g}}^+}^\circ = X_{\text{H}_{\text{g}}^+}^\circ - \frac{1}{2}X_{\text{H}_2\text{g}}^\circ$$

resulting in an asymmetry in the ΔX_f° values for the proton and for the electron. This asymmetry will forbid us to compare the properties of the solvated proton with the properties of the solvated electron, but we shall still be able to compare the various thermodynamic properties of the solvated electron in different solvents.

C. The X° values for the gaseous electron can be computed as for a perfect gas with translation and spin, providing a "best guess" for these quantities.

Jortner and Noyes² have applied assumptions b and c for the hydrated electron; we shall apply them here for the thermodynamic properties of the ammoniated electron.

Data

We choose the hypothetical ideal standard molal state for the solvated protons and electrons, and the standard state where the fugacity is 1 atm for the gaseous protons and electrons. We use the results of Jortner and Noyes² for the hydrated electron and the results of Lepoutre and Demortier⁴ for the ammoniated electron. Some details about our computations are given in Appendix I. We obtain the thermodynamic quantities listed in Table I. For each thermodynamic quantity, we have indicated whether assumptions a, b, and (or) c were used.

Discussion

A. *Comments on the Formation of the Solvated Electron.* Focusing attention mainly on the features of reactions II, V, and VII, we see from Table I that, although assumption c has not been invoked for the same properties in water and in ammonia, the values obtained in these two solvents are of comparable magnitude. Let us recall that assumption a is safe, that b bears the only inconvenience of forbidding a comparison between protons and electrons, and that assumption c provides a best guess. Looking more specifically at reaction V (the formation of the solvated electron) we find that the standard free enthalpy of formation of the solvated electron is lower in water than in ammonia and that it decreases with increasing temperature in ammonia; this temperature coefficient can be commented in two different ways.

The temperature coefficient of $\Delta G_{\text{e}_{\text{am}}^-}^\circ$ is due to the large decrease of $H_{\text{e}_{\text{am}}^-}^\circ$ with increasing temperature, this effect being only partially compensated by the increase of $(-T\Delta S_{\text{e}_{\text{am}}^-}^\circ)$. It may be useful to bear in mind that the enthalpies and the entropies of formation contribute with opposite signs to the temperature coefficient of the free enthalpy of formation. It may also be useful to remember that the large temperature coefficients of $\Delta H_{\text{e}_{\text{am}}^-}^\circ$ and of $\Delta S_{\text{e}_{\text{am}}^-}^\circ$ arise essentially from the experimental reaction II, and that the experimental data yield a small temperature coefficient of $\Delta G_{\text{II}}^\circ$ and a large negative temperature coefficient of $\Delta H_{\text{II}}^\circ$. Further insight into the nature of the temperature coefficient of $\Delta G_{\text{e}_{\text{am}}^-}^\circ$ is based on the following consideration. Both $-(\partial G_{\text{e}_{\text{am}}^-}^\circ/\partial T)$ and $-(\partial G_{\text{II}}^\circ/\partial T)$ are equal to $S_{\text{e}_{\text{am}}^-}^\circ$, the standard entropy of the ammoniated electron. The large positive value of $S_{\text{e}_{\text{am}}^-}^\circ$ gives rise to the negative temperature coefficient of $\Delta G_{\text{e}_{\text{am}}^-}^\circ$. It should be noted that the value of $S_{\text{e}_{\text{am}}^-}^\circ$ derived from G_{II}° and from H_{II}° without invoking assumptions b and c.

We thus conclude that the enthalpy of formation of the solvated electron is lower in water than in ammonia

Table I: Thermodynamic Data for Some Reactions Involving the Solvated Electron^a

		NH ₃ , -35°	NH ₃ , +25°	H ₂ O, +25°
II	ΔG°	+43.7	+44.4	+66.3
	ΔH°	+42.2	+37.4	+62.2 c
	ΔS°	-6.2	-24.2	-13.7 c
IV (H ⁺)	ΔG_f°	+68.6 a, b, c	+71.1 a, b, c	+103.8 a
	ΔH_f°	+58.3 a, b, c	+58.9 a, b, c	+98.8 a, b
	ΔS_f°	-42.8 a, b	-40.6 a, b	-16.8 a, b
	S_{Hsoliv}°	-28.0 a	-25.0 a	-1.2 a
V (e ⁻)	$\Delta G_f^\circ, G^\circ$	-24.9 a, b, c	-26.4 a, b, c	-37.5 a, b
	$\Delta H_f^\circ, H^\circ$	-16.1 a, b, c	-21.5 a, b, c	-36.6 a, b, c
	ΔS_f°	+36.6 a, b	+16.4 a, b	+3.1 a, b, c
	$S_{\text{e soliv}}^\circ$	+36.6 a	+16.4 a	+3.1 a, c
VII (e ⁻)	$\Delta G_{\text{soliv}}^\circ$	-25.1 a, c	-26.4 a, c	-37.5 a, b
	$\Delta H_{\text{soliv}}^\circ$	-17.3 a	-23.0 a	-38.1 a, b
	$\Delta S_{\text{soliv}}^\circ$	+32.4 a, c	+11.4 a, c	-1.9 a
III	ΔH°	+366.5	+367.1	+367.1
VI (H ⁺)	$\Delta H_{\text{soliv}}^\circ$	-300.3 a	-306.7 a	-266.8 a, b, c
	$S_{\text{e gas}}^\circ$	+4.2 c	+5.0 c	+5.0 c
	$H_{\text{e gas}}^\circ$	+1.2 c	+1.5 c	+1.5 c
	$S_{1/2, \text{H}_2 \text{ gas}}^\circ$			

^a All G° , H° , ΔG° , ΔH° are in kcal/mol. All S° , ΔS° , are in cal/(mol deg).

and is mainly responsible for the lower value of the free enthalpy of formation in liquid ammonia. The standard entropy is also lower in water than in ammonia. It was shown elsewhere⁴ that the values of S_{e}° in ammonia are exceptionally high. The low positive value of $S_{\text{e ag}}^\circ$ would yield a very small negative temperature coefficient for ΔG_f° .

B. Comparison with Theoretical Values. In a recent paper, Copeland, Kestner, and Jortner (CKJ)⁵ have computed the energies of solvated electrons. They state that the total energy, E_t , is the sum of the electronic energy, E_e , and of the medium rearrangement of energy E_M .

$$E_t = E_e + E_M \quad (1)$$

They compute these energies as functions of a configurational variable (the radius R of the cavity) and establish the configuration stability by the conditions

$$(\partial E_t / \partial R)_{R=R_0} = 0; (\partial^2 E_t / \partial R^2)_{R=R_0} > 0 \quad (2)$$

Their model accounts for the coordination number N of solvent molecules in the first shell around the electron, and a continuous dielectronic medium beyond this layer. The following comments should be made at this point. (a) E_t is a free enthalpy of the rearrangement of the medium at constant temperature and pressure. The term E_M in eq 1 is the contribution to internal energy of electrostatic interactions involving the solvent molecule. It does not include heat and work contributions to the internal energy. Therefore

$$E_M = H_M = G_M \quad (3)$$

and the total internal energy of rearrangement is

$$E_{Mt} = TS_M - PV_M + E_M \quad (4)$$

Since there are no TS or PV terms in the electronic part of the internal energy, the total internal energy is

$$E_t = E_e + E_{Mt} = E_{e1} + TS_M - PV_M + E_M \quad (5)$$

The total free enthalpy is

$$G_t = E_t - TS_M + PV_M = E_{e1} + E_M = E_t \quad (6)$$

Therefore, as we have stated, E_t is the total free enthalpy, G_t , of the solvated electron.

(b) We see that condition 2 for configurational stability is correct, since we have to write, at constant T and P

$$(\partial G_t / \partial R)_{R=R_0} = 0 \quad (7)$$

(c) Finally, let us state that in eq 4, 5, and 6, the term PV_M is negligible at ordinary pressures, so that

$$E_{Mt} = H_{Mt} \quad E_t = H_t \quad (8)$$

We can now proceed to compare theory and experiment. We take the theoretical values of $G_t = E_t$ in the CKJ paper. Equilibrium values in ammonia were given at 203 and 300°K; we interpolate them at 240°K. With CKJ, we have to make assumptions for the appropriate choice of V_0 , the electronic energy of the quasi free electron state, and of N , the coordination number. We make the reasonable assumptions that $V_0 = 0.5$ or 0.0 eV and $N = 4$ or 6. For water, instead of having an equilibrium value, we add the assumption that $R_0 = 0.5 \text{ \AA}$.

In Table II, we list these theoretical results for the total free enthalpies of the species $e^-(\text{NH}_3)_N$ and $e^-(\text{H}_2\text{O})_N$ in a polarizable continuum. These species are formed according to reactions of the type



where $(e^-)(\text{solv})$ is the electron in the hypothetical state with zero free enthalpy and zero free enthalpy of formation.

Table II: Theoretical and Experimental Values^a for G_T

$$G_T = E_t = \Delta G_{f^{\circ} e_{\text{solv}}^-} - 2N/3\Delta G_{\text{vap}}^{\circ}$$

Theory (G_T)	NH ₃ -35°	NH ₃ +25°	H ₂ O +25°
$V_0 = 0.5$ $N = 4$	-1.03	-0.99	-1.41
$N = 6$	-0.93	-0.89	-0.87
$V_0 = 0.0$ $N = 4$	-1.41	-1.37	-1.91
$N = 6$	-1.24	-1.21	-1.23
Experiment			
$\Delta G_{f^{\circ} e_{\text{solv}}^-}$	-1.08	-1.15	-1.63
$-2/3\Delta G_{\text{vap}}^{\circ}$	0.00	+0.04	-0.06
$\Delta G_{f^{\circ} e_{\text{solv}}^-} - 2N/3\Delta G_{\text{vap}}^{\circ}$			
$N = 4$	-1.08	-0.99	-1.87
$N = 6$	-1.08	-0.91	-1.99

^a All data are in eV.

The theoretical value of G_t and the experimental value of $\Delta G_{f^{\circ} e_{\text{solv}}^-}$ cannot be directly compared, as the latter value includes *all* the free enthalpy contributions required to form the electron localization center, while G_t in the CKJ model did not account for all the structural changes required to bring N molecules from the bulk to create the first coordination layer. We shall therefore set

$$G_{f^{\circ} e_{\text{solv}}^-} = G_t - N\Delta G_L^{\circ}$$

where ΔG_L° is the difference in the molal free enthalpy (due to attractive intermolecular interactions) between a molecule in the bulk of the pure liquid and in the first coordination layer. A crude estimate of this energy term may be obtained as follows. Apart from lateral interactions, included in G_t , these N molecules may still interact, in the direction of R , with neighbor solvent molecules in the outer shells. We should therefore include in ΔG_L° only about two-thirds of the intermolecular interactions in the pure liquid (or, alternatively, add one-third of this interaction term to G_t). Finally, since we can identify these intermolecular interactions with the cohesion in the liquid state, we set

$$\Delta G_L^{\circ} = 2/3\Delta G^{\circ}$$

where G_V° is the free enthalpy of vaporization, and therefore state that $G_T(\text{theor}) = (\Delta G_{f^{\circ} e_{\text{solv}}^-} - 2/3N\Delta G_V^{\circ})$ (exptl).

We list the pertinent data in Table II. Let us make the reasonable assumptions⁵ that $V_0 = 0.5$ in ammonia and $V_0 = 0.0$ in water. If we choose $N = 4$ for both solvents, the agreement between theory and experiment is fairly good for the absolute values of G_t in different solvents and for the temperature effect. The agreement in respect to the sign of the temperature

coefficient dG_t/dT is due to the large positive temperature coefficient of $-\Delta G_V^{\circ}$ which, multiplied by $2N/3$ overwhelms the negative temperature coefficient of $\Delta G_{f^{\circ} e_{\text{am}}^-}$. Further discussion should concern comparison between theoretical and experimental enthalpies and entropies. Unfortunately, direct theoretical computations of enthalpies or entropies are not presently available.

The present data for the temperature coefficient of G_t in ammonia clearly indicates that the negative temperature coefficient of $\Delta G_{f^{\circ} e_{\text{am}}^-}$ and the corresponding positive values of $S_{e_{\text{am}}^-}^{\circ}$ are mostly due to what happens to solvent molecules when they are transferred from the bulk of the solvent to the first solvation layer. The new solvent arrangement in the first coordination layer is looser than in the bulk, so that the molecules in the first solvation layer have a larger number of degrees of freedom than in the bulk. It thus seems reasonable that $S_{e^-}^{\circ}$ should be smaller in ammonia at higher temperature, when there is already more freedom in the bulk and still be smaller in water, where the first conduction shell is more tightly solvated.

The present thermochemical data presented herein may be useful to elucidate some of the peculiarities concerning the shape of the optical absorption spectrum of very dilute metal ammonia solutions. The two amazing features of the optical spectrum are (a) a pronounced asymmetry on the high energy side, (b) the half-line width is practically temperature independent.^{6,7} The theoretical calculations⁶ of the line shape for a constant N predict a practically symmetric line shape for the $1s \rightarrow 2p$ transition where the half-width should reveal a temperature dependence proportional to $T^{1/2}$. The pronounced experimentally observed asymmetry can be rationalized by invoking higher bound and bound and bound-continuum transitions; however, still the half-line width (or the second moment of the intensity distribution) should be temperature dependent. One has therefore to invoke the idea of a compound line shape where electron cavities characterized by different N values yield a different contribution at different temperatures. The values of $\delta G_t = G_t(N=4) - G_t(N=6)$ are practically temperature independent, being $\delta G_t = 0.10$ eV both at -35 and at $+25^{\circ}$ (see Table II). Although the absolute value of δG_t is by no means certain, one may conclude that at higher temperatures the contribution of the $N = 6$ clusters will increase, thus leading to an additional source of broadening which increases at higher temperature, in contrast to the experimental spectroscopic data. However, once the contribution of the ΔG_L° term is included we find that the free enthalpy difference $\delta G = \Delta G_{f^{\circ} e_{\text{solv}}^-}(N=4) - \Delta G_{f^{\circ} e_{\text{solv}}^-}(N=6)$ from $\delta G = -0.10$ eV

(6) R. K. Quinn and J. J. Lagowski, *J. Phys. Chem.*, **73**, 2326 (1969).

(7) S. Golden and T. R. Tuttle, in "Metal-Ammonia Solutions" (Colloque Weyl II, 1969), J. J. Lagowski and M. J. Sienko, Ed., Butterworths, London, 1970.

at 35° to $\delta G = -0.18$ eV at $+25^\circ$ whereupon at higher temperatures the $N = 4$ structure will be favored. Thus at lower temperatures we may expect a substantial contribution to the optical absorption band from both the $N = 4$ and the $N = 6$ species, the compound line shape will narrow with increasing temperature due to the diminished contribution of the $N = 6$ species, while each $N = 4$ and $N = 6$ component suffers phonon broadening so that the resulting line width remains constant. It appears thus that some of the puzzling spectroscopic observations can be adequately rationalized in view of the new thermodynamic data.

Acknowledgment. We are grateful to the Israeli Council for Research and Development and to the French Centre National de la Recherche Scientifique for the support under the auspices of the French-Israel Cultural Agreement to one of us (G. L.), which made this work possible.

Appendix: Details for Table I

1. Water, 25° .

Reaction IV: Reliable extrapolations¹ yield ΔG_f° and S° . Assumption b gives then ΔS_f° and ΔH_f° .

Reaction V: Reliable extrapolations¹ and comparisons² yield ΔG_f° . Reliable comparisons² and assumption c yield S° . Assumption b gives then ΔS_f° , H_f° and G° and H° .

Reaction II: Sum of IV and V; does not depend on

assumptions a and b, which are cancelled; still depends on reliable comparisons used for reaction V.

Reaction VII: Reliable comparisons² yield ΔS° . Assumptions c and b, and the data of reaction V, give ΔG° and ΔH° .

Reaction VI: Assumptions c and b, and the data of reactions IV and III, give ΔH° .

2. Ammonia, $+25$ and -35° .

Reaction II: Experimental data, no assumption.

Reaction VII: Reliable extrapolations⁸ give ΔH° at 25° . We take the revised value of ref 5. Reliable extrapolations⁴ give $S_{\text{H}^+}^\circ$ at $+25$ and at -35° . The data of reaction II at both temperatures give $S_{e^-}^\circ$. By writing $T(dS_{e^-}/dT)_p = (dH/dT)_p$ we obtain the approximate variation of ΔH° between $+25^\circ$ and -35° . This gives ΔH° at -35° . From ΔH° , S° , and assumption c, we compute ΔS° and ΔG° at both temperatures.

Reaction VI: The data of reactions II, III, and VII, give ΔH° .

Reaction V: As already stated, $S_{e^-}^\circ$ is obtained through reliable extrapolations and the data of reaction II. ΔS° is then given by assumption b. ΔG° and ΔH° are obtained with assumptions b and c and the data of reaction VII.

Reaction IV: Difference between reactions II and V.

(8) J. Jortner in "Metal Ammonia Solutions," G. Lepoutre and M. J. Sienko, Ed., W. A. Benjamin, New York, N. Y., 1964.

Polyanions and Their Complexes. VIII. Interaction of Methylene Blue with Cellulosic Polyanions in Heterogeneous Systems

by P. J. Baugh, J. B. Lawton, and G. O. Phillips*

Department of Chemistry and Applied Chemistry, University of Salford, Salford M5 4WT, Lancashire, England
(Received March 11, 1971)

Publication costs borne completely by The Journal of Physical Chemistry

Thermodynamic parameters have been evaluated for the interaction of methylene blue with cellulosic polyanions in heterogeneous systems. For a particular anionic site (carboxymethyl, phosphate, and sulfate) the free energy (ΔG°) and the enthalpy (ΔH°) changes increase with anionic site density. At a given site density ΔG° and ΔH° increase in the order carboxymethyl > phosphate > sulfate, which correlates with the photon energy of the light absorbed by the polyanion dye complexes. The reasons for selectivity are discussed, and the order of binding is rationalized in terms of the size and charge density of the anionic sites.

Introduction

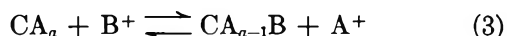
Previously, the mechanism and thermodynamics of interaction of methylene blue with synthetic and connective tissue polyanions was examined in dilute aqueous solutions, using pulse radiolysis and spectral methods. It was shown that dye aggregation rather than ion binding is mainly responsible for the spectral shifts which accompany such interactions (metachromasia).¹ The spectral shifts and ion binding which accompany the interactions are the basis of a wide range of histological methods for identifying polyanions in biological systems, particularly in tissue sections.² Whereas there is information available about the mechanisms of such interactions in aqueous solution, the comparable data about solid state systems is extremely sparse,³ despite the fact that it is such systems which are encountered in practice in biological staining procedures. To achieve reproducible solid-state systems for examination we have synthesised a range of cellulosic polyanions. Our first objective is to establish reliable thermodynamic data about the interaction of cationic dyes with solid polyanions in heterogeneous systems. Secondly, since a wide variation in anionic site density can be achieved with synthetic cellulosic polyanions, the influence of this factor can also be examined, in addition to the influence of the chemical nature of the site. No such systematic variation is possible, of course, with the naturally occurring polyanions.

Here approaches will be critically considered in order to select the most suitable procedures for evaluation of the experimental data. Following the observation that the mass action constant varied with the concentrations of the interacting ions, several empirical approaches have been evolved for investigating ion binding, based on the more extensively studied behavior of ion-exchange resins. Rothmund and Kornfeld⁴ considered two relationships to describe the ion exchange properties of permutit

$$K_1 = \frac{(C_1')^p C_2}{C_2' C_1} \quad (1)$$

$$K_2 = \frac{C_1' (C_2')^\beta}{C_2' (C_1)} \quad (2)$$

where C_1 and C_2 are the concentrations of the two (univalent) ions in the aqueous solution and C_1' and C_2' are the concentrations of the ions in the solid phase at equilibrium. Here $\beta = 1/p$, and $\log K_2 = (\log K_1)/p$, or $\log K_2 = \beta \log K_1$. Formula 2 satisfactorily accounts for the exchange of silver and sodium ions on permutit,⁴ and Davidson⁵ used this expression for solid cellulosic polyanions (oxycelluloses) in equilibrium with univalent dye cations. Equation 2 has also been used in studies on the exchange of ions of the same valency^{6,7} and for the binding of metal ions to polyanions.⁸ An expression similar in form to (2) may be derived by consideration of the ion exchange of ion B^+ for ion A^+ on an ion exchange matrix C^{a-} as a series of equilibria



etc., each represented by an equilibrium constant from $k_1, k_2 \dots k_n$. When all the ions are replaced $a = n$

(1) J. S. Moore, G. O. Phillips, D. M. Power, and J. V. Davies, *J. Chem. Soc. A*, 1155 (1970).

(2) G. Quintarelli, Ed., "The Chemistry and Physiology of Mucopolysaccharides," Little, Brown and Co., Boston, Mass., 1968.

(3) G. O. Phillips, Proc. N.A.T.O. Advanced Study Institute on "Connective Tissue Research" Santa Margherita, Italy, Academic Press, London, 1969.

(4) V. Rothmund and G. Kornfeld, *Z. Anorg. Allg. Chem.*, **103**, 129 (1918).

(5) G. F. Davidson, *J. Text. Inst.*, **41**, T361 (1950).

(6) T. Yambe, *Tokyo Daigaku Seisan Gijyutsu Kenkyujo Hokoku*, **6**, 1 (1956).

(7) O. Samuelson and R. Djurfeld, *Acta Chem. Scand.*, **11**, 1209 (1957).

(8) J. R. Dunstone, *Biochem. J.*, **85**, 336 (1962).

$$K' = k_1 \times k_2 \times \dots \times k_n \quad (5)$$

and

$$K' = \frac{\{CB_a\}\{A^+\}^a}{\{CA_a\}\{B^+\}^a} \quad (6)$$

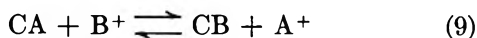
where $\{ \}$ represents the concentration of the species in appropriate units. In eq 1, 2, and 6 activity coefficients are neglected. Eisenman,⁹ working with cation selective glass electrodes, empirically derived an expression which is claimed to yield a true thermodynamic equilibrium constant

$$K'' = \frac{\{CB_a\}^m \{A^+\} \gamma_A}{\{CA_a\}^m \{B^+\} \gamma_B} \quad (7)$$

where m is dependent on the activities of the ions bound to the polyanion and γ_A, γ_B the activity coefficients of the ions A^+ and B^+ in solution. Expression 7 is very similar to eq 1 since CB_a and CA_a correspond to C_1' and C_2' , respectively. Thus

$$K'' = K_1 \frac{\gamma_A}{\gamma_B} \quad (8)$$

Generally, however, ion-exchange is described by the reduced form of eq 3¹⁰⁻¹² in which a typical site and two cations are represented



where

$$K_c = \frac{\{CB\}\{A^+\}}{\{CA\}\{B^+\}} \quad (10)$$

since

$$K_a = \frac{\{CB\}\{A^+\} \gamma_A}{\{CA\}\{B^+\} \gamma_B} \quad (11)$$

then

$$K_a = K_c \frac{\gamma_A}{\gamma_B} \quad (12)$$

Here, mole fraction of ions in the solid phase is used and molarity (or molality) of ions in solution, since only ratios of these quantities occur in (11). K_a is a "selectivity coefficient," which varies with the composition of the solid phase.

Using the Gibbs-Duhem relationship for the ions in the solid phase, assuming that the activity of water in that phase remains constant, the thermodynamic equilibrium constant (K) can be evaluated¹⁰⁻¹³ from the relationship

$$\ln K = \int_0^1 \ln K_a dN_B \quad (13)$$

where N_B is the mole fraction of ion B^+ . The activity coefficient of an ion in the solid phase is unity in the standard state, which is defined as that state in which

all the anionic sites are occupied by ions of the same type. Thus the standard free energy change

$$-\Delta G^\circ = RT \ln K \quad (14)$$

is the change in free energy when 1 mol of the ion exchanger in the form CA is transformed to the form CB . There appears to be no particular advantage in the alternative treatment of Izmailov and Mushinskaya¹⁴ where $\log K_a$ is plotted against N_B and extrapolated to $N_B = 0$ to give $\log K$.

Ion exchange of inorganic ions¹⁵⁻²⁰ have mainly been studied using these methods, but as far as we are aware no thermodynamically valid parameters have been measured for ion exchange equilibria involving dye cations. The available information relating to methylene blue indicates that a true equilibrium is established in an ion-exchange resin when the degree of cross-linking is low.²¹ More recently, Libinson, *et al.*,²² measured equilibrium constants for the exchange of methylene blue with hydroxonium ions on a polystyrenesulfonate resin. Using the assumption that the ratio of the activity coefficients in the aqueous phase is unity, selectivity coefficients were obtained by extrapolation to zero dye concentration in the polyanion. In our study we have calculated actual activity coefficients of methylene blue from previously published freezing-point depression data.²³ Using these values we have obtained thermodynamic equilibrium constants for the exchange of cellulosic polyanions with methylene blue cations.

Experimental Section

Materials. Cotton yarn supplied by Jett C. Arthur, Jr., Southern Regional Research Laboratories, U. S. Department of Agriculture, was of the Deltapine variety and was purified by extraction with hot ethanol

(9) G. Eisenman, *Biophys. J.*, **2**, 2590 (1962).

(10) O. D. Bonner, W. J. Argersinger, and A. W. Davidson, *Trans. Kans. Acad. Sci.*, **53**, 404 (1950).

(11) E. Hogfeldt, E. Ekedahl, and L. G. Sillen, *Acta Chem. Scand.*, **4**, 556 (1950).

(12) G. L. Gains and H. C. Thomas, *J. Chem. Phys.*, **21**, 714 (1953).

(13) L. H. Baetsle, "Notes on Physical Chemistry of Ion Exchange," School of Public Health, University of California, Berkeley, 1963.

(14) N. A. Izmailov and S. K. Mushinskaya, *Russ. J. Phys. Chem.*, **36**, 640 (1962).

(15) O. D. Bonner and F. L. Livingstone, *J. Phys. Chem.*, **60**, 530 (1956).

(16) O. D. Bonner and L. L. Smith, *ibid.*, **61**, 1614 (1957).

(17) J. S. Redinha and J. A. Kitchener, *Trans. Faraday Soc.*, **59**, 515 (1963).

(18) H. S. Sherry and H. F. Walton, *J. Phys. Chem.*, **71**, 1457 (1967).

(19) H. Laudelout, R. van Bladel, G. H. Bolt, and A. L. Page, *Trans. Faraday Soc.*, **64**, 1477 (1968).

(20) G. E. Boyd and F. Vaslow, *J. Phys. Chem.*, **70**, 2295 (1966).

(21) G. S. Libinson, E. M. Savitskaya, and B. P. Burns, *Dokl. Akad. Nauk SSSR*, **145**, 511 (1962).

(22) G. S. Libinson and I. M. Vagina, *Russ. J. Phys. Chem.*, **41**, 1575 (1967).

(23) J. Lange and E. Herre, *Z. Phys. Chem., Abt. A*, **181**, 329 (1937).

followed by boiling in dilute sodium hydroxide solution. At the same time precautions were taken to minimize air oxidation. The sodium hydroxide was removed by washing in distilled water, the cotton acidified with dilute acetic acid, neutralized with dilute ammonium hydroxide, and finally washed with distilled water.²⁴

Sodium carboxymethyl celluloses (CMC1–CMC4) were prepared from the cotton yarn by the method of Daul, *et al.*,²⁵ using sodium monochloroacetate instead of the free acid. Cellulose phosphates (CP) were prepared using the methods of Gallagher²⁶ (CP1) using a mixture of sodium phosphates in water, and Thomas, *et al.*²⁷ (CP2 and CP3) using phosphorus oxychloride in pyridine at 60°. Cellulose sulfates (CS1–CS3) were prepared by the method of Dingler, *et al.*,^{28,29} using chlorosulfonic acid in pyridine at 50°. Subsequently, the sodium salts of each of the cellulosic polyanions were prepared by immersing the reaction products in sodium carbonate solution prior to the final washings in deionized water.

The degree of substitution (DS) was determined by the method of the American Society for Testing and Materials.³⁰ The degree of polymerization (DP) was measured by determining the fluidity of a solution of the cotton in a solution of tetraamminecopper(II) hydroxide using the method developed at the Shirley Institute.³¹ The fluidity was related to the intrinsic viscosity³² and from this value the DP was determined.³³ These measurements showed that the anionic celluloses were similar in DP to the untreated material.

Methylene blue was obtained from E. Gurr Limited. The same sample was used for all the experiments and the purity was checked chromatographically by the methods of Bergmann and O'Konski,³⁴ and Bellin and Ronayne.³⁵ A $3.4 \times 10^{-6} M$ aqueous solution had a molar extinction coefficient (ϵ) of 9.5×10^4 at the main absorption peak of 667 nm, which is in agreement with the values of Bergmann and O'Konski.³⁴

Polyanion–Dye Equilibria. Appropriate weights of polyanion were equilibrated with aliquots (50 ml) of dye solution ($10^{-4} M$), buffered at pH 8,^{5,30} containing sodium chloride (0–15 M). Equilibration was achieved at selected temperatures, using the thermostatically controlled "Orbital Incubator" supplied by Gallenkamp Ltd. The uptake of the dye by the polyanion was measured with a Unicam SP 500 spectrophotometer, using the equilibrated solution after centrifugation to remove any suspended polyanion–dye complex. Under these conditions Davidson^{5,36} has shown that a true ion exchange equilibrium exists between methylene blue cations and sodium ions on anionic celluloses. We have verified this under our experimental conditions by gravimetric estimation of the chloride ion concentration at equilibrium for each type of polyanion studied, using CMC2, CP3, and CS2. In the absence of salt we found no decrease in the chloride ion concentration at equilibrium. Thus the dye was only taken up by ion ex-

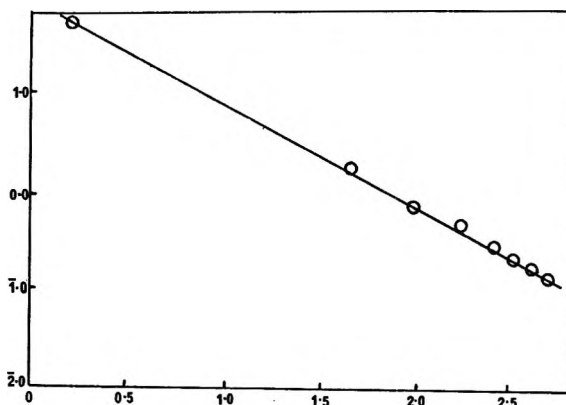


Figure 1. Evaluation of K' from the expression^{5–8} $\log K' = \log \left(\frac{[CMB]}{[CN_a]} \right) + a \log \left(\frac{[Na^+]}{[MB^+]} \right)$.

change on all three types of polyanion. In the presence of 0.15 M NaCl (the highest concentration used) the chloride ion concentrations were constant to within the experimental error of $\pm 0.1\%$.

The variation of the equilibrium with pH was studied for each type of polyanion using the buffer solutions proposed by Davidson³⁶ to maintain constant concentrations of sodium ions in all the solutions used.

Results

The experimental data were treated by both the empirical^{4–8} and thermodynamically valid methods^{10–13} described. Following the work of Davidson⁵ on the uptake of dye cations by oxycellulose, the empirical treatment given by Rothmund and Kornfeld⁴ has been used in a form which may be derived from eq 6

$$\log K' = \log \frac{\{CB_a\}}{\{CA_a\}} + a \log \frac{\{A^+\}}{\{B^+\}} \quad (15)$$

Thus a plot of $\log \left\{ \frac{CB_a}{CA_a} \right\}$ against $\log \left(\frac{[A^+]}{[B^+]} \right)$ gives $\log K'$ as the intercept. A plot of eq 15 is shown in Figure 1 ($CA_a = CN_a$ for sites occupied by sodium ions, and $CB_a = CMB$ for sites occupied by methylene blue cations).

(24) C. M. Conrad and J. H. Kettering, *Ind. Eng. Chem., Anal. Ed.*, **14**, 432 (1942).

(25) G. C. Daul and J. D. Reid, *Text. Res. J.*, **17**, 554 (1947).

(26) D. M. Gallagher, *Amer. Dye Rep.*, **53**, 361 (1964).

(27) G. A. Thomas and G. Kosolapoff, U. S. Patent, 2401440 (1946).

(28) O. Dingler, W. H. Stevens, and E. Gebauer-Fuelnegg, *Ber. Deut. Chem. Ges. A*, **61**, 2000 (1928).

(29) O. Dingler and E. Gebauer-Fuelnegg, *J. Amer. Chem. Soc.*, **52**, 2849 (1930).

(30) *Book ASTM Stand.*, **15**, (1969).

(31) Shirley Institute Test Leaflet No. Chem. 7, 3rd ed, May 1960.

(32) "Cellulose and Cellulose Derivatives," (High Polymer Series 5, Part III), Interscience, London, 1955, p 1433

(33) C. M. Conrad, V. W. Tripp, and T. Mares, *J. Phys. Colloid Chem.*, **55**, 1474 (1951).

(34) K. Bergmann and C. T. O'Konski, *J. Phys. Chem.*, **67**, 2169 (1963).

(35) J. S. Bellin and M. E. Ronayne, *J. Chromatogr.*, **24**, 131 (1966).

(36) G. F. Davidson, *J. Text. Inst.*, **39**, T59 (1948).

Table I: Determination of Activity Coefficients of Methylene Blue

{Dye}, <i>M</i>	0.001663	0.001813	0.003084	0.004046	0.005943	0.007640	0.007893	0.009292
Osmotic coefficient (<i>f</i> ₀)	0.652	0.642	0.603	0.579	0.539	0.513	0.506	0.480
Activity coefficient (γ_{\pm})	0.451	0.433	0.344	0.300	0.243	0.210	0.205	0.180

The calculations required by the thermodynamically valid method have been made on the basis of certain assumptions which have been discussed previously³⁷ and are summarized as follows: (a) the activity coefficients for methylene blue (Table I) calculated from the data of Lange and Herre²³ by the method of Kortum³⁸ may be extrapolated to lower concentrations by the Davies equation,³⁹ and are valid at the temperatures used in the experiments; (b) single ion activity coefficients may be calculated from the above values for MB⁺ using the data of Butler⁴⁰ and Stokes and Robinson⁴¹ and for Na⁺ from the data of Butler;⁴⁰ (c) that the premises underlying eq 13 are valid here; (d) that $\log K = \int_0^1 \log K_a dN_B$ (from eq 13).

In considering these assumptions, it is important to note that all our solutions were of low ionic strength, and the dye concentration was less than 10^{-4} *M* in all instances. Thus, the recent evidence of Mukerjee and Ghosh⁴² that methylene blue salts behave as ordinary electrolytes and the proof by Padday^{43,44} that no ion pairing took place in six dye chloride solutions studied by him offer justification for our calculation of single ion activity coefficients. Nevertheless, it is important to point out that the results are not significantly different if mean activity coefficients are used. Moreover, whereas the calculated activity coefficients for MBCl are strictly valid only at the freezing point of the solution, a view has been expressed by Glasstone⁴⁵ that for low concentrations, activity coefficients are unlikely to change significantly over a small temperature range. In our calculations only the ratio of γ_{MB}/γ_{Na} is used; thus it is reasonable that in our experimental solutions the activity coefficients calculated from solution data for MBCl and NaCl provide a true representation of this ratio. Baetsle¹³ points out that in dilute solutions the activity coefficients show no mutual interference. Previous authors^{16-18,22} have assumed that the ratio of activity coefficients in their solutions was unity and our results, if calculated on this basis, show no change in the relative values of $\log K_a$.

Our original calculations³⁷ were made before the publication of the paper on the activity coefficients of methylene blue by Ghosh and Mukerjee.⁴² However, their results support our calculated values. Using the new data we have calculated the concentration of monomeric dye in many of our solutions and evaluated the activity coefficient of the dye monomer at appropriate ionic strengths. Using these results we find that our ΔG° values in Table II are changed by less than 1%.

Our use of the thermodynamic method¹⁰⁻¹³ of calculating $\log K$ is supported by our experimental finding that there is no preferential uptake of anions (Cl⁻) by the ion exchange matrix. In addition, our polyanions have contained only a few anionic sites and thus each site is freely accessible to the exchanging cations. This low degree of substitution also allows us to assume that any change in solvent activity within the exchanger is negligible. Previous authors¹⁶⁻²⁰ have also used these assumptions.

Table III shows the effect of activity corrections on the data relating to a cellulose phosphate (CP3). Figure 2 shows a plot of $\log K_a$ against mole fraction of methylene blue for the same data. The area under the curve ($\int_0^1 \log K_a dN_B$) is equal to $\log K$.

The data obtained in our experiments have been used to calculate both empirical (K' , $\Delta G'$, $\Delta H'$, $\Delta S'$) and thermodynamic (K , ΔG° , ΔH° , ΔS°) parameters and the values are presented in Table II. Although we have sought to calculate true thermodynamic values, it will be seen in the subsequent discussion that our arguments depend only on true relative values being

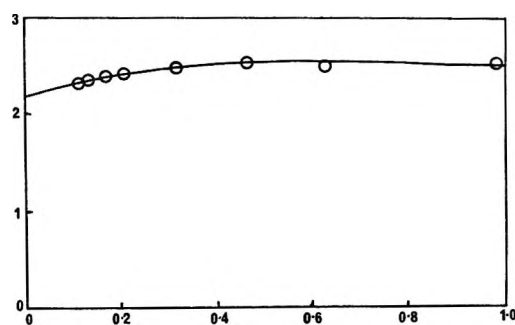


Figure 2. Evaluation of K from the expression¹⁰⁻¹³ $\log K = \int_0^1 \log K_a dN$; plot of $\log k_a$ vs. N_{MB} .

(37) J. B. Lawton, M. Sc. Thesis, University of Salford, 1970.

(38) G. Kortum, "Treatise on Electrochemistry," Elsevier, Amsterdam, 1965.

(39) C. W. Davies, *J. Chem. Soc.*, 2093 (1938).

(40) J. N. Butler, "Ionic Equilibria, Mathematical Approach," Addison-Wesley, Reading, Mass., 1964.

(41) R. H. Stokes and R. A. Robinson, "Electrolyte Solutions," Butterworths, London, 1968.

(42) A. K. Ghosh and P. Mukerjee, *J. Amer. Chem. Soc.*, **92**, 6413 (1970).

(43) J. F. Padday, *J. Phys. Chem.*, **71**, 3488 (1967).

(44) J. F. Padday, *ibid.*, **72**, 1259 (1968).

(45) S. Glasstone, "Thermodynamics for Chemists," D. van Nostrand, New York, N. Y., 1958.

Table II: Parameters for the Exchange of Methylene Blue and Sodium Ions on Cellulosic Polyanions

Polyanion	<i>T</i> , °C	Empirical treatment ⁴⁻⁸ (Rothmund-Kornfeld)					Thermodynamic treatment ^{10-11, 18-20}				Degree of substitution
		<i>K'</i>	<i>a</i>	kcal mol ⁻¹		$-\Delta S'$, cal °K ⁻¹ mol ⁻¹	<i>K</i>	kcal mol ⁻¹		$-\Delta S^\circ$, cal °K ⁻¹ mol ⁻¹	
				$-\Delta G'$	$-\Delta H'$			$-\Delta G^\circ$	$-\Delta H^\circ$		
CMC1	25	2,090	1.43	4.52		4.10	133	2.89		1.95	
					5.74				3.47		0.021
CMC1	39	1,350	1.45	4.46		4.10	102	2.86		1.96	
CMC2	26	42,600	1.70	6.32		140	331	3.44		4.75	
					54.5				4.85		0.051
CMC2	36	2,160	1.42	4.71		161	254	3.39		4.72	
CMC3	22	282	1.02	3.30			283	3.30			0.056
CP1	25	2,040,000	2.32	8.59			448	3.60			0.077 ^b
CP3	26	479	1.15	3.66		3.58	296	3.37		1.55	
					4.7				3.82		0.012
CP3	35	380	1.11	3.63		3.48	246	3.34		1.43	
CS1	24	74.5	0.38	2.54		8.05	5,620 ^a	5.08		5.05	
					5.15				6.58		0.0086
CS1	37	51.9	0.37	2.42		8.82	3,540 ^a	5.01		5.07	
CS2	25	176	0.51	3.35		57.9	7,490 ^a	5.26		6.20	
					20.6				6.60		0.0103
CS2	35	88	0.38	2.73		58.0	5,240 ^a	5.21		6.07	

^a Calculated from average values of log *K*_a. ^b As dibasic sites.

Table III: Evaluation of log *K* of Cellulose Phosphate (CP3) at 26°^a

{NaCl}, <i>M</i>	0.00024	0.0102	0.0252	0.0502	0.0752	0.1002	0.1252	0.1502
γ_{Na}	0.990	0.900	0.857	0.816	0.791	0.769	0.733	0.713
{MB}, <i>M</i> ($\times 10^{-6}$)	4.64	6.61	7.51	8.36	8.86	9.11	9.27	9.39
γ_{MB}	0.760	0.721	0.704	0.690	0.681	0.677	0.672	0.671
CMB	7.09	4.49	3.29	2.17	1.51	1.18	0.97	0.81
log <i>K</i> _c	2.3874	2.4025	2.4475	2.4103	2.3635	2.3322	2.3212	2.3050
log $\frac{\gamma_{Na}}{\gamma_{MB}}$	0.1145	0.0960	0.0860	0.0680	0.0650	0.0550	0.0380	0.0260
log <i>K</i> _a	2.5019	2.4985	2.5335	2.4783	2.4285	2.3872	2.3592	2.3310
<i>N</i> _{MB}	0.980	0.621	0.455	0.300	0.209	0.163	0.134	0.112

^a MB = methylene blue cation; Na = sodium cation; CMB = methylene blue salt of cellulose polyanion as millimoles dye per 100 g of dry polyanion.

obtained, since we are attempting to compare the properties of the three types of anionic site used in our polyanions.

The variation of dye-binding with pH is illustrated in Figure 3, which shows similar trends to those already reported for polyanions in tissue sections by Balazs and Szirmai.⁴⁶

Discussion

Using the empirical treatment of Rothmund and Kornfeld,⁴ Davidson⁶ obtained the values *K'* = 138, $-\Delta G'$ = 2.92 kcal mol⁻¹ and *a* = 0.85 for the interaction between oxycellulose (DS = 0.0058) and methylene blue at 20°. For the uptake of a similar cationic dye azure A by polyanions present in tissue sections at 4°, Goldstein⁴⁷ reported $-\Delta G'$ of 3.8–5.3 kcal mol⁻¹. Our values based on the Rothmund-Kornfeld⁴ treatment are of comparable magnitude (Table II). How-

ever, there is not always good agreement between the values calculated by this procedure and the more thermodynamically acceptable approach we have also described. When the Rothmund-Kornfeld index *a* (eq 15) is near unity, the agreement is reasonable as for CMC1 and CP3. Otherwise discrepancies are apparent, as for CP1 where *a* = 2.32, and $-\Delta G'$ = 8.59 against $-\Delta G^\circ$ = 3.60 kcal mol⁻¹. This lack of correspondence between the two approaches is particularly marked for the polyanions which show most affinity for the methylene blue. The cellulose sulfates show the greatest affinity in the presence of salt (Table II) and at low pH (Figure 3) and here there is little, if any, correlation between the values of $\Delta G'$ and ΔG° . Ne-

(46) E. A. Balazs and J. A. Szirmai, *Acta Histochem. Supp.*, **1**, 56 (1958).

(47) D. J. Goldstein, *Quart. J. Microsc. Sci.*, **104**, 413 (1962).

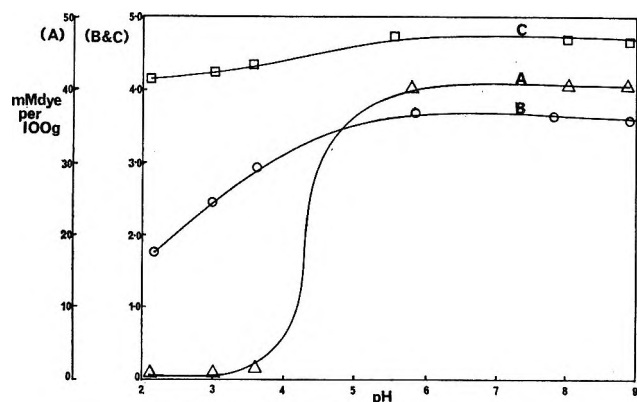


Figure 3. Variation of dye-binding with pH: A, carboxymethyl cellulose, CMC4; B, cellulose phosphate, CP2; C, cellulose sulfate, CS1.

glect of activity factors is, therefore, a serious omission in the empirical treatment. A better correlation has been obtained by use of the other empirical formula of Rothmund and Korfeld⁴ (eq 1) and Eisenman⁹ (eq 7) where $\log K_1 = (\log K')/a = \log K''$, and $\Delta G_1 = \Delta G'/a = \Delta G''$. However, this amendment offers no advantages over the thermodynamic approach and it will not be developed further here. Our comments about the cellulose polyanion-methylene blue interactions will, henceforth, be confined to the more reliable thermodynamic parameters which are summarized in Table II.

Effect of Anionic Site Density. The data in Table II demonstrates that for the carboxymethylated, phosphorylated, and sulfated celluloses the energy changes involved in exchanging sodium ions for methylene blue cations increase as the degree of substitution increases. This observation is in agreement with the predictions of Harris and Rice,⁴⁸ who indicated that the selectivity (K) of a polyelectrolyte should increase as the capacity of the polyelectrolyte for counterions increases. Our previous thermodynamic studies on polyanion-methylene blue interactions in aqueous solution employing pulse radiolysis¹ utilized polyanions with considerably higher anionic site densities (DS 0.5–1) and gave enthalpy values which were exothermic within the range 9–13.6 kcal mol⁻¹. Recently, using a direct calorimetric method in our laboratory, Armand⁴⁹ has found $-\Delta H^\circ = 11.4$ kcal mol⁻¹ for the interaction of CMC (DS 0.7; DP 200) with methylene blue in aqueous solution. The general correspondence in the results by the three methods indicates the reliability of the values and does support the trend towards higher enthalpies with increasing site density up to a maximum of ca. 13 kcal mol⁻¹.

Nature of the Site. Comparing carboxymethyl (CMC1), phosphorylated (CP3) and sulfated (CS2) cellulose, Table II shows that the energy changes increase in the order carboxymethyl < phosphate < sulfate, despite the fact that the carboxymethyl cellulose

is more highly substituted. The photon energy of the metachromatic absorption maximum in solution due to these groups also increases in this order.⁵⁰ Another parameter which has been used to indicate the strength of the interaction between polyanions and organic counterions^{2,3,50} is the salt concentration required to release all the counterion from the polyanion-counterion complex. For the various types of site considered, this limiting salt concentration⁵⁰ also increases in the same order as the energy changes. The order found is also supported by the data in Figure 3, giving the relative affinities of methylene blue towards the three types of anionic site at various pH values. Here, therefore, we are able to demonstrate the thermodynamic basis for the widely utilized procedure of fractionating naturally occurring polyanions according to the chemical nature of their anionic sites by means of the solubilization of polyanion-organic counterion complexes with salts.²

Ion Exchange Selectivities. Values of K in Table II vary from 102 (CMC1, 39°) to 7490 (CS2, 25°), showing that in all instances methylene blue cations are taken up in preference to sodium ions. Comparable values for other ion-exchange equilibria are shown in Table IV. It is significant that organic cations have a high affinity for both cellulosic polyanions and polystyrenesulfonates, and that the values of K are of the same order for each, indicating that similar energy changes are involved.

Table IV: Equilibrium Constants from Published Studies of Ion Exchange

Type of resin	Ions exchanged		K	T
	A ⁺	B ⁺		
Carboxymethyl cellulose ^a	H ₃ O ⁺	Na ⁺	398	20
Zeolite ¹⁸	Ag ⁺	Na ⁺	794	25
Polystyrenesulfonate ¹⁷	Ag ⁺	Na ⁺	12	25
Polystyrenesulfonate ¹⁴	aniline	H ₃ O ⁺	126	25
Polystyrenesulfonate ²²	aniline	H ₃ O ⁺	2.5	40
Polystyrenesulfonate ²²	neutral red	H ₃ O ⁺	795	40
Polystyrenesulfonate ²²	methylene blue	H ₃ O ⁺	2000	40
Polystyrenesulfonate ¹⁴	tetramethylammonium ion	H ₃ O ⁺	79.5	25

^a H. Sobue and Y. Tabata, *Bull. Chem. Soc. Jap.*, 29, 527 (1956).

In evaluating such energy changes it is necessary to consider not only the electrostatic interactions,⁵¹ but also the free energy changes due to the rearrangement of water molecules.^{9,52,53} A theoretical consideration

(48) F. E. Harris and S. A. Rice, *J. Phys. Chem.*, 61, 1350 (1957).

(49) G. Armand, unpublished results.

(50) G. O. Phillips, J. V. Davies, K. S. Dodgson, and J. S. Moore, *Biochem. J.*, 113, 465 (1969).

(51) L. J. Pauley, *J. Amer. Chem. Soc.*, 76, 1422 (1954).

of the exchange of one univalent ion by another has yielded the relationship

$$\Delta G_{B^A} = \frac{e^2}{D} \left[\frac{1}{r_e + r_A} - \frac{1}{r_e + r_B} \right] - \left[\Delta G_A - \Delta G_B \right] \quad (16)$$

where ΔG_{B^A} is the free energy change for the exchange of ion A by ion B, ΔG_A and ΔG_B are the free energy changes involved in rearranging the water of hydration around the ions, e is the electronic charge, r_e the effective radius of the ion exchanging grouping, r_A and r_B the radii of the ions, and D the dielectric constant of the medium.

For cellulose sulfates r_e will be considerably greater than for carboxymethyl cellulose and since the electrostatic terms will be larger for the carboxymethyl group, it would be expected to bind small cations more strongly than large ones. In keeping with this expectation, Reichenberg⁵² on ion exchange resins and Rinaudo and Milas⁵⁴ using carboxymethyl cellulose in solution have shown that polycarboxylates bind Na^+ in preference to K^+ . On the other hand, since r_e is large for cellulose sulfates, the free energy changes due to the rearrangement of the water of hydration would be the most pronounced influence. Again experiment supports this prediction, since silver ions are bound more firmly than sodium, or hydroxonium ions, and K^+ more firmly than Na^+ to polystyrene sulfonates.^{17,52} In our work we have considered only the exchange between methylene blue cations (M) and sodium ions (N), and the variables are, therefore, only the nature of the anionic sites and their distribution. Thus, if ΔG_C and ΔG_S are the free energy changes involved in the exchange of M for N on each polyanions, and it is assumed that there is no considerable difference between the ΔG values for the rearrangement of water around N and M for each of the anionic sites, then

$$\Delta G_C - \Delta G_S = \frac{e^2}{D} \left[\frac{r_M - r_N}{(r_e + r_M)(r_e + r_N)} - \frac{r_M - r_N}{(r_s + r_M)(r_s + r_N)} \right] \quad (17)$$

Thus, since $r_s > r_e$ and $r_M > r_N$, then ΔG_S will be numerically greater than ΔG_C . As experimentally observed,^{50,55-58} therefore, in dye binding and metachromasia studies, the sulfate group is a stronger binder for cationic dyes than carboxyl groups, whereas ions such as Li^+ and Na^+ are bound more strongly to carboxyl than sulfate groups.⁵⁹ The data reported in Table II are, therefore, in good agreement with theoretical predictions and experimental observations of the binding of organic and inorganic cations to polyanions in aqueous solutions.

The phosphate group is intermediate in its behavior and the change in free energy lies between that of the sulfate and carboxylate groups. This observation is in agreement with the metachromatic behavior of this

group,⁵⁷ although Booij,⁶⁰ and Bungenberg de Jong⁶¹ reported that this group bound certain other dye cations more strongly than sulfate, or carboxyl groups. These facts can be rationalized on the basis of eq 16 and 17 by considering the effect of pH on the phosphate group. At low pH values the group will be in the form $-\text{O}-\text{PO}_3\text{H}_2$, which will not bind dye cations; at intermediate pH values the group will be $-\text{O}-\text{PO}_3\text{H}^-$, which will bind dye cations more strongly than the sulfate group. At higher pH values the group will be $-\text{O}-\text{PO}_3^{2-}$ which is similar in size to $-\text{O}-\text{SO}_3^-$, but the higher electrical charge will cause the group to have binding properties intermediate between those of the carboxyl and sulfate groups. For polyanion CP3, analysis shows that the phosphate group is singly charged (doubly esterified $=\text{PO}_2^-$) and this group falls naturally between the carboxylate and the sulfate groups in size and thus in binding power, according to the predictions of eq 17. This behavior is supported by the values in Table II.

Energy Changes and Metachromasia. It was previously noted that the photon energy of the metachromatic absorption maximum decreases in solution, in the order sulfate > phosphate > carboxylate.⁵⁴⁻⁵⁷ Using diffuse reflectance, we have determined the absorption spectra of the solid polyanion-methylene blue complexes.³⁷ The comparison between the energy changes associated with shifts in spectra and $-\Delta G^\circ$ and $-\Delta H^\circ$ obtained in the present study are shown in Table V. The energy changes calculated from band centers are probably the most significant since the distribution of dye must be random within the polyanion, some being aggregated and producing strong metachromasia and some monomeric, giving only small bathochromic effects.³⁷ Thus, there is more than one absorbing system and, therefore, the maximum trend is that the energy changes calculated from the absorption spectra increase as the free energy and enthalpy changes increase (numerically). This behavior would be anticipated since the decrease of both the free energy and enthalpy of the system would lead to greater stability, making electronic transitions more difficult (*i.e.*, higher energy). Similarly, the color change on complex forma-

(52) D. Reichenberg, "Ion Exchange," Vol. 1, J. Marinsky, Ed., E. Arnold, London, 1964.

(53) G. N. Ling, "A Physical Theory of the Living State," Blaisdell, New York, N. Y., 1962.

(54) M. Rinaudo and M. Milas, *J. Chim. Phys.*, **66**, 1489 (1969).

(55) J. W. Kelly and L. Chang, *J. Histochem. Cytochem.*, **17**, 651 (1969).

(56) A. L. Stone, *Biochim. Biophys. Acta*, **148**, 193 (1968).

(57) O. Bank and H. J. Bungenberg de Jong, *Protoplasma*, **32**, 489 (1939).

(58) J. Dorling and J. E. Scott, *Histochemie*, **5**, 221 (1965).

(59) H. J. Bungenberg de Jong, "Colloid Science," Vol. 2, H. R. Kruyt, Ed., Elsevier, Amsterdam, 1949.

(60) H. L. Booij, *Acta Histochem. Suppl.*, **1**, 37 (1958).

(61) H. J. Bungenberg de Jong and C. van der Meer, *Proc. Kon. Ned. Akad. Wetensch.*, **45**, 593 (1942).

Table V: Energy Changes Associated with Metachromasia

Polyanion	Ratio of sites to dye	Energy changes ($h\nu$), ^a kcal/mol		$-\Delta G^\circ$, kcal/mol	$-\Delta H^\circ$, kcal/mol
		Band, center	Maximum ^b		
CMC1	14.2	0.6	3.1	2.9	3.5
CP3	1.10	2.5	8.4	3.4	3.8
CS1	1.00	5.6	11.3	5.1	6.6

^a Calculated by comparison with the dye in aqueous solution (maximum absorption at 665 nm). ^b Calculated on the basis of the short wavelength end of the broad absorption band.

tion (metachromasia) is predictably hypochromic since electronic transitions of higher energy are less likely to occur, thus lowering the molar extinction coefficient of the main absorption peak.

Summarizing, therefore, the thermodynamic parameters which have been obtained for the interaction of the sodium salts of cellulose sulfates, phosphates, and carboxymethyl cellulose with methylene blue satisfactorily account for the strength of ion binding and spectral characteristics of the complexes produced.

Acknowledgment. Thanks are due to Mrs. B. J. Brain for technical assistance.

Reactivities of Ion Pairs and Free Ions in Proton Abstraction Reactions.

The Reaction between Polystyryl Carbanion Salts and Triphenylmethane

by L. L. Chan and J. Smid*

Department of Chemistry, State University of New York, College of Forestry, Syracuse, New York 13210
(Received July 26, 1971)

Publication costs assisted by the Petroleum Research Fund

The proton abstraction reaction between polystyryl carbanion salts and triphenylmethane in ethereal solvents was studied spectrophotometrically. The apparent second-order rate constant as measured from the initial slope of the optical density *vs.* time curve was found to increase strongly at lower initial polystyryl concentration. The reaction mechanism resembles that found for the anionic homopolymerization of styrene, *i.e.*, the free polystyryl ion is much more reactive than the contact ion pair (in THF at 25° the reactivity of the free ion is about 1000 times that of the sodium ion pair). In more polar solvents the ion pair rate constant increases as more reactive loose ion pairs are formed. The above proton abstraction reaction is self-retarding, as the newly formed trityl carbanion salt is much more dissociated than the corresponding polystyryl salt ($K_d = 7.6 \times 10^{-6} M^{-1}$ for trityl sodium in THF at 25° *vs.* $K_d = 1.5 \times 10^{-7} M^{-1}$ for the styryl salt). Conductance measurements and optical spectra were employed to obtain more information on the solvation state of the trityl ion pairs.

The mechanisms of reactions involving carbanions as intermediates are known to be sensitive to the type of counterion, the temperature, the nature of the solvent and the presence of ion-coordinating additives.^{1,2} This can often be attributed to the variety of ionic and solvation states (such as different kinds of ion pairs) in which the reacting species can exist. In this respect, mechanistic studies of anionic polymerization of vinyl monomers have substantially contributed to a better understanding of the effects of counterion and other variables on reactivities of carbanion salts in media where ion pairing is predominant,^{1b,2} and a considerable amount of quantitative information is presently available on the reactivities of free carbanions and their ion pairs in addition and electron transfer reactions.

Proton transfer to carbanions has been studied in a variety of ways in order to establish kinetic and equilibrium acidities of hydrocarbons and the effect of solvent on these quantities.^{3,4} Absolute rate constants

(1) (a) D. J. Cram, "Fundamentals of Carbanion Chemistry," Academic Press, New York, N. Y., 1965; (b) M. Szwarc, "Carbanions, Living Polymers and Electron Transfer Processes," Interscience, New York, N. Y., 1968.

(2) J. Smid, "Structure and Mechanism in Vinyl Polymerization," T. Tsuruta and K. F. O'Driscoll, Ed., Marcel Dekker, New York, N. Y., 1969, Chapter 11.

(3) A. Streitwieser, Jr., J. H. Hammons, E. Ciuffarin, and J. I. Brauman, *J. Amer. Chem. Soc.*, **89**, 59 (1967), and many other papers by A. Streitwieser, Jr., *et al.*

(4) C. D. Ritchie and R. E. Uschold, *J. Amer. Chem. Soc.*, **90**, 3415 (1968); C. D. Ritchie, *ibid.*, **91**, 6749 (1969), C. D. Ritchie, "Solute-Solvent Interactions," Marcel Dekker, New York, N. Y., 1969, Chapter 4.

were measured by Ritchie, *et al.*,⁴ in solvents such as methanol and DMSO where the extent of ion pairing is usually small. However, not much is known about the difference in reactivities between free carbanions and their ion pairs in proton transfer reactions. The available data on the extent of dissociation of polystyryl carbanion salts ($\sim\text{CH}_2\text{CH}^-(\text{Ph})$, M^+ , and denoted by S^-, M^+) in ethereal solvents induced us to study the reaction of this carbanion with triphenylmethane, a reaction which can conveniently be followed spectrophotometrically. In order to interpret the kinetic data it was necessary to determine the extent of dissociation of the trityl salts from conductance measurements and to obtain information on the solvation state of the ion pairs from optical spectra.

Experimental Section

The polystyryl salts ("living polymers") were prepared in THF from the corresponding dicarbanion salts of α -methylstyrene dimers or tetramers by addition of an approximately tenfold excess of styrene. Details of the preparation as well as the purification of the solvents used in this study (tetrahydrofuran, tetrahydropyran, and 1,2-dimethoxyethane) have been reported elsewhere.^{5,6}

Triphenylmethyl (trityl) salts were prepared from the corresponding polystyryl salts by addition of a slight excess of triphenylmethane. The reaction proceeds to completion as indicated from the identical optical spectra of two trityllithium samples, one prepared from polystyryllithium and a second one obtained by reacting butyllithium with triphenyl methane. All spectral measurements were carried out on a Cary 14 recording spectrophotometer.

Conductance data for the trityl salts were obtained with a Leeds and Northrup A-C conductance bridge operating at 1000 Hz, with a General Radio Corp. tuned amplifier and null detector being used as a balance instrument. The all-glass enclosed conductance apparatus⁵ containing the trityl solution was constructed in such a way that the concentration could be varied between 10^{-4} and $5 \cdot 10^{-6}$ M without exposing the solution to air or moisture. Destruction of the trityl carbanions was less than 5% during the time of the measurements. Conductivities of trityl sodium in THF were measured over a temperature range of 25 to -70° , that of tritylpotassium only at 25° (for details of such measurements, see also ref 7). Salt concentrations were measured spectroscopically at room temperature, using the absorption peak in the 460–500-nm region. The extinction coefficients, ϵ_m , of Tm^-, Na^+ and Tm^-, K^+ were obtained by reacting a Tm^-, M^+ solution of known optical density with a slight excess of solid fluorene. From the known ϵ_m values of the fluorenyl salts^{6,8} the ϵ_m value for Tm^-, Na^+ at 472 nm was found to be 2.3×10^4 , while that of Tm^-, K^+ at 480 nm is 2.4×10^4 . The literature value of Tm^-, Na^+ in di-

ethyl ether is 2.3×10^4 .⁹ A slight error is introduced when these ϵ_m values are used at low salt concentration, as under these conditions the optical spectrum results from a superposition of the spectrum of the ion pair and that of the free ion. Due to the broadness of the transition and the comparatively small bathochromic shift for the free ion, the extinction coefficient measured at the apparent λ_m decreases by less than 10% compared to the ϵ_m at high concentration.

Reaction rates were obtained by a conventional batch technique, using again an all-glass enclosed evacuated apparatus. After the concentration of the polystyryl salt solution was measured spectrophotometrically (λ_m 340 nm, ϵ_m 12000), a known quantity of solid triphenylmethane was dissolved by distilling part of the solvent from the polystyryl solution onto the solid hydrocarbon. The two solutions were then rapidly mixed at 25° , the mixture transferred to an optical cell and the change in optical density recorded at the λ_m of the Tm^-, M^+ salt or at that of S^-, M^+ . Poor stability of Tm^-, Li^+ and of polystyryllithium prevented us from obtaining reliable data for this counterion. The stability of all salts is less in DME than in THF. For reactions carried out in DME or in THP, the solvent was removed from a polystyryl-THF solution, and a known quantity of DME or THP (distilled from a carbanion solution) was then added to the dry salt just prior to the reaction with triphenylmethane. The reaction rate was measured in a similar way as described for THF. Full details of the reaction apparatus and the precautions which must be taken to ensure reliable kinetic data are outlined in ref 10.

Results and Discussion

Absorption Spectra. The optical spectrum of the trityl carbanion contains a broad absorption band with a maximum in the 470–500-nm region.^{11,12} Its exact position, given in Table I under a variety of conditions, is affected by solvent, temperature, type of cation and the carbanion concentration. For example, bathochromic shifts are observed in more polar solvents or on lowering the temperature. This behavior resembles that of other carbanion salts such as the fluorenyl alkali salts^{6,13} and those of the dicarbanions of tetraphe-

(5) D. N. Bhattacharyya, C. L. Lee, J. Smid, and M. Szwarc, *J. Phys. Chem.*, **69**, 612 (1965).

(6) T. E. Hogen Esch and J. Smid, *J. Amer. Chem. Soc.*, **88**, 307 (1966).

(7) T. E. Hogen Esch and J. Smid, *ibid.*, **88**, 318 (1966).

(8) T. Ellingsen and J. Smid, *J. Phys. Chem.*, **73**, 2712 (1969).

(9) S. F. Mason, *Quart. Rev. (London)*, **15**, 336 (1961).

(10) T. Shimomura, J. Smid, and M. Szwarc, *J. Amer. Chem. Soc.*, **89**, 5743 (1967).

(11) R. Waack and M. A. Doran, *ibid.*, **85**, 1651 (1963).

(12) A. Streitwieser, Jr., J. I. Brauman, J. H. Hammons, and A. H. Pudjaatmaka, *ibid.*, **87**, 384 (1965).

(13) L. L. Chan and J. Smid, *ibid.*, **90**, 4654 (1968).

Table I: Absorption Maxima of Triphenylmethyl Salts

Cation	10 ⁶ Conc., M	Solvent	λ_m , nm		
			50°	25°	-50°
Li ⁺	300	THF		496	
	50	THF		500 ^a	
Na ⁺	300	THF		480	
	50	THF	472	480	500
	5	THF		490	
	5	THF		480 ^b	
	0.1	THF		500	
K ⁺	50	THP		470	
	50	DME		500	
	300	THF	482	485	495
Cs ⁺	50	THF		495	
	50	THF		495	
	0.1	THF		500	
	50	THF	485 ^c	495	(-75°)

^a The same value was found by Waack, *et al.*¹¹ ^b Measured in the presence of a twenty times excess sodium tetraphenylboride. ^c A λ_m of 488 nm was reported for Tm⁻, Cs⁺ in cyclohexylamine¹² and 495 nm in DMSO. (C. D. Ritchie and R. E. Uschold, *J. Amer. Chem. Soc.*, **89**, 2960 (1967)).

nylethylene^{14,16} and 1,1,4,4-tetraphenylbutane.⁶ The absorption maxima and band shapes of the latter two salts are similar to that of the trityl salts.

The solvent and temperature dependent optical changes, at least those occurring above Tm⁻, M⁺ concentrations of 10⁻³ M, can be rationalized by assuming an equilibrium between tight and loose ion pairs. No separate absorption maxima are observed in solutions containing mixtures of the two kinds of ion pair, due to the broadness of the absorption band. However, the observed change in the halfwidth of the Tm⁻, Na⁺ peak, *viz.*, 88 nm in THP, 106 nm in THF, and 96 nm in DME, indicates that the spectrum in THF is a superposition of the spectra of the two separate ion pair species. In THP, the ion pairs are essentially of the tight variety (λ_m 470 nm) while in DME only separated ion pairs exist at 25° (λ_m 500 nm). One calculates that the fraction of loose ion pairs in THF at 25° is about 0.3.

Formation of free Tm⁻ ions causes the bathochromic shifts at low salt concentration (see Table I). This can be deduced from the observation that addition of excess NaBPh₄ to a Tm⁻, M⁺ solution at low concentration causes a hypsochromic shift. It is estimated that the ratio of ion pairs to free ions in a 5 × 10⁻⁵ M solution of Tm⁻, Na⁺ in THF at 25° is close to unity (λ_m being 490 nm as compared to 500 nm for the free ion and 480 nm for the ion pair in THF). This means that $K_d \approx 10^{-5} M^{-1}$, which compares favorably with the value of $K_d = 7.6 \times 10^{-6} M$ measured by conductance (see next section).

Conductance Measurements. The various parameters of the Fuoss conductance equation, $F/\Lambda = 1/\Lambda_0 + f^2 C \Lambda / K_D F \Lambda_0^2$ were calculated by using previously published data on the temperature dependence of the den-

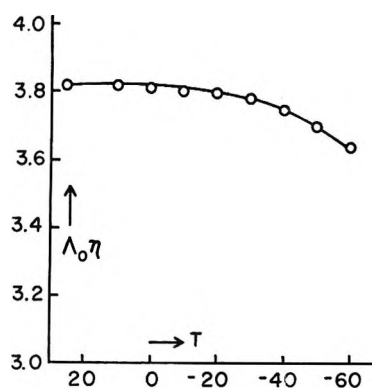


Figure 1. The effect of temperature on the Walden product Δ_{07} of triphenylmethylsodium in THF.

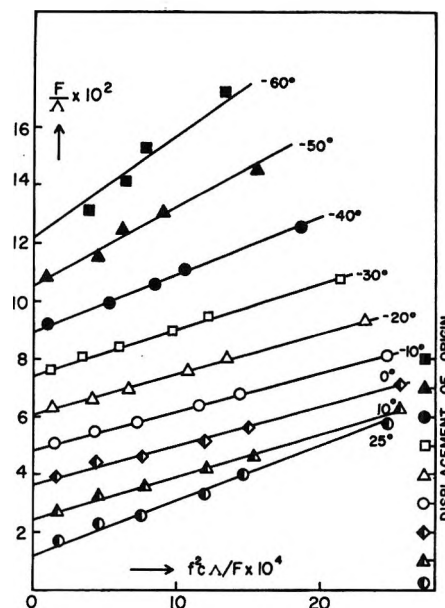


Figure 2. Fuoss plots of triphenylmethylsodium in THF (note the displacement of the origin for the various plots).

sity, viscosity, and dielectric constant of THF.⁷ Approximate values for the limiting conductances, Λ_0 , were obtained from $1/\Lambda$ vs. CA plots and inserted into the Fuoss equation. The Λ_0 values obtained from the Fuoss plots are presented in Figure 1 as a Walden plot (Δ_{07} vs. T) and are also listed in Table II, together with the dissociation constants K_d calculated from the slopes of the Fuoss plots. The latter plots are depicted in Figure 2 for Tm⁻, Na⁺ in THF. The enthalpies and entropies of dissociation of Tm⁻, Na⁺ were derived from the $\log K_d$ vs. $1/T$ plot shown in Figure 3. The following values were found

$$\Delta H^\circ_{D,298} = -6.2 \text{ kcal/mol}, \Delta S^\circ_{D,298} = -44 \text{ e.u.}$$

and

$$\Delta H^\circ_{D,213} = -0.6 \text{ kcal/mol}, \Delta S^\circ_{D,213} = -23 \text{ e.u.}$$

(14) J. F. Garst and R. S. Cole, *J. Amer. Chem. Soc.*, **84**, 4352 (1962).

(15) R. C. Roberts and M. Szwarc, *ibid.*, **87**, 5542 (1965).

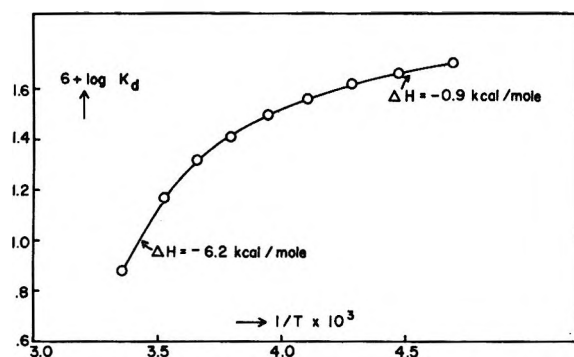


Figure 3. Temperature dependence of the dissociation constant K_d of triphenylmethylium in THF.

Table II: The Λ_0 and K_d Values of Tritylsodium and Tritylpotassium in THF

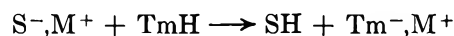
$T, ^\circ\text{C}$	Λ_0	Λ_{07}	$10^6 K_d, M$
Tritylsodium			
25.0	83.2	0.382	7.6
10.0	70.0	0.382	14.8
0.0	62.0	0.381	20.5
-10.0	54.8	0.380	25.8
-20.0	48.0	0.380	31.8
-30.0	41.5	0.377	36.0
-40.0	35.0	0.375	42.0
-50.0	29.0	0.370	45.4
-60.0	23.4	0.364	50.4
Tritylpotassium			
25	83.5	0.383	3.4

The Λ_0 and K_D values for Tm^-, M^+ appear to be reasonable. Since the Λ_0^+ values for the THF solvated Na^+ and K^+ ion at 25° were both reported to be $45 \text{ cm}^2 \text{ ohm}^{-1} \text{ equiv}^{-1}$,¹⁶ a value of 41 is calculated for the Λ_0^- of the Tm^- ion. This is similar to that found for the B-Ph_4 ion ($\Lambda_0^- = 41$ at 25° , see ref 16) and for the tetraphenylethylene monoradical anion T^- ($\Lambda_0^- = 41$ at 20° , see ref 15). The size of the latter two ions is probably not much different from that of the Tm^- ion which is reported to be a propeller shaped molecule.¹⁷ The decrease in the Walden product at lower temperature has also been found for NaBPh_4 ¹⁶ and for T^-, Na^+ ,¹⁵ the cause being enhanced solvation at lower temperatures.¹⁶

Application of the Denison-Ramsey equation $\Delta H_d^\circ = (Ne^2/aD)[1 + d \ln D/d \ln T]$ yields values for the interionic distance, a , equal to 1.2 \AA at 25° and 7.2 \AA at -60° ($d \ln D/d \ln T$ is -1.13 at 25° and -1.20 at -60° , see ref 8). The 7.2 \AA at low temperature appears to be reasonable and is indicative of a loose ion pair structure, in agreement with optical data. One calculates from the Fuoss equation $K_d = (3000/4\pi a^3) \exp(-e^2/aDkT)$ a value of $K_d = 5.5 \times 10^{-5} M$ for Tm^-, Na^+ in THF at -60° . This is close to the experimentally observed value of $K_d = 5.0 \times 10^{-5} M$.

However, the 1.2 \AA value at 25° points to the nonapplicability of the Denison-Ramsey equation at this temperature. This is not surprising since the optical data show that the fraction of tight Tm^-, Na^+ ion pairs under these conditions is about 0.7. Also, the $\Delta H_{d,298}^\circ = -6.2 \text{ kcal/mol}$ is close to that found for the ion pairs of the dianion of tetraphenylethylene (-7.2 kcal/mol) and for fluorenylsodium (-8.3 kcal/mol) both of which are predominantly tight ion pairs in THF at 25° .^{8,15} The dissociation constant for Tm^-, K^+ in THF at 25° is about twice as low as that found for Tm^-, Na^+ , in agreement with the behavior observed for polystyryl and fluorenyl salts.^{5,8}

Rate Constants of Proton Abstraction. Assuming the simple bimolecular reaction



(the reaction was found to go to completion) one can write for the rate of proton abstraction

$$-d[\text{S}^-, \text{M}^+]/dt = +d[\text{Tm}^-, \text{M}^+]/dt = k[\text{S}^-, \text{M}^+][\text{TmH}]$$

The reaction can be followed by observing either the increase in optical density at the λ_m of Tm^-, M^+ or by measuring the disappearance of S^-, M^+ at 340 nm . Since $\text{OD}_\lambda = \text{OD}_{\lambda, \text{S}^-} + \text{OD}_{\lambda, \text{T}^-}$ (λ referring to the wavelength of the measurement) one can easily show that

$$k_0 = \frac{(d[\text{OD}]/dt)_0}{[\text{TmH}]_0[\text{OD}]_{m, \text{S}^-} - \epsilon_{\lambda, \text{T}^-} - \epsilon_{\lambda, \text{S}^-}}$$

In this equation, $(d[\text{OD}]/dt)_0$ denotes the initial slope of the OD vs. time curve at the λ_m of Tm^-, M^+ (an example of such a curve is given in Figure 4). $[\text{TmH}]_0$ is the initial concentration of triphenylmethane, $\text{OD}_{m, \text{S}^-}$ is the optical density and ϵ_{m, S^-} the extinction coefficient of the polystyryl salt at its absorption maximum of 340 nm ($\text{OD}_{m, \text{S}^-}$ is measured before S^-, M^+ is mixed with the solid TmH), while $\epsilon_{\lambda, \text{T}^-}$ and $\epsilon_{\lambda, \text{S}^-}$ refer to the respective molar extinction coefficients of Tm^-, M^+ and of S^-, M^+ at the absorption maximum, λ_m , of Tm^-, M^+ . The pertinent kinetic data and the calculated k_0 values are collected in Table III.

The dependence of the apparent second-order rate constant k_0 on the initial polystyryl concentration is reminiscent of the behavior of polystyryl salts in anionic homopolymerization.⁵ It indicates a high reactivity of the free polystyryl ion, and hence, an increase in k_0 as the polystyryl salt concentration is decreased.

It should be pointed out at this stage that the overall reaction is complicated by the fact that the proton transfer between S^-, M^+ and TmH produces a new carb-

(16) C. Carvajal, K. J. Tölle, J. Smid, and M. Szwarc, *J. Amer. Chem. Soc.*, **87**, 5548 (1965).

(17) V. R. Sandel and H. H. Freeman, *ibid.*, **85**, 2328 (1963); R. Waack, M. A. Doran, E. B. Baker, and G. A. Plak, *ibid.*, **88**, 1272 (1966).

Table III: Proton Abstraction Reaction between Polystyryl Salts and Triphenylmethane at 25°

Salt	Solvent	$10^4 [S^-, M^+]_0, M$	$10^4 [TmH], M$	$k_0, M^{-1} \text{sec}^{-1}$
S^-, Na^+	THF	708	107	0.4
		72.5	6.9	2.0
		6.3	3.46	9.0
		4.5	1.54	10.0
		1.1	4.9	20.0
		9.3 ^a	81.0	0.33
	8.1 ^b	54.0	0.27	
	DME	80.0	17.9	14
40.0		7.76	20	
6.15		2.82	31	
1.45		2.08	50	
S^-, K^+	THF	96.0	12.9	1.4
		69.0	24.4	1.7
		32.0	32.2	2.3
		9.8	12.7	4.3
		8.8	7.0	4.3
		2.9	3.1	7.3

^a $[NaBPh_4]$ added = $3.1 \times 10^{-4} M$. ^b $[NaBPh_4]$ added = $1.7 \times 10^{-3} M$.

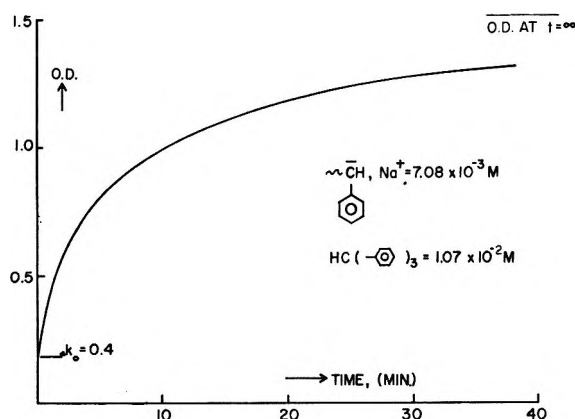


Figure 4. Plot of optical density vs. time for the reaction $S^-, Na^+ + TmH \rightarrow SH + Tm^-, Na^+$, in THF at 25°, measured at $\lambda = 480 \text{ nm}$.

anion salt Tm^-, M^+ that is considerably stronger dissociated than S^-, M^+ . (This means that the progress of the reaction can also be followed conductometrically.) At 25° in THF, the K_d of S^-, Na^+ is $1.5 \times 10^{-7} M$ and that of Tm^-, Na^+ is $7.6 \times 10^{-6} M$. Therefore, a high reactivity of the free S^- ion means that the proton abstraction reaction slows down as soon as Tm^-, M^+ is formed. This is also apparent from the observed rate curve shown in Figure 4. The apparent bimolecular rate constant as calculated from the half life time of the reaction is substantially lower than that derived from the initial slope. From the known dissociation constants of the two salts one can calculate the fraction $f = [S^-]/[S^-, M^+]$ as a function of the extent of the reaction for different initial concentrations of S^-, M^+ .

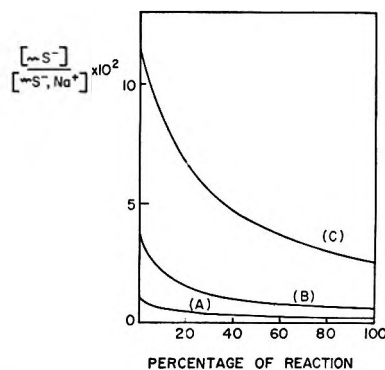


Figure 5. Dependence of the fraction of free polystyryl ions $S^-/S^-, Na^+$ on the progress of the reaction $S^-, Na^+ + TmH \rightarrow SH + Tm^-, Na^+$. Curves A, B, and C represent solutions with initial $[S^-, Na^+]$ of $10^{-3} M$, $10^{-4} M$, and $10^{-5} M$, respectively.

The results of such computer calculations are shown in Figure 5. If the Tm^-, M^+ dissociation constants were negligibly small compared to those of S^-, M^+ , the fraction $S^-/S^-, M^+$ should have increased with the progress of the reaction. The calculated decrease in the fraction $S^-/S^-, M^+$ shows that one should expect a considerable retardation of the reaction rate. However, we estimate that the rate constant as calculated from the initial slope is not affected by more than 20%.

Assuming that ion pairs and free ions are both participating in the proton abstraction reaction, one can write⁶

$$k_0 = k_i + (k_f - k_i)(K_d/[S^-, M^+]_0)^{1/2}$$

where k_i and k_f are the respective rate constants of the ion pair and free ion and $(K_d/[S^-, M^+]_0)^{1/2}$ represents the fraction of free S^- ions at the onset of the reaction, assuming that this fraction is $\ll 1$. Plots of k_0 vs. $[S^-, M^+]_0^{-1/2}$ for S^-, Na^+ and S^-, K^+ are shown in Figure 6, and the linear correlation indicates that the suggested mechanism involving ion pairs and free ions is correct. The high free ion reactivity is also apparent from the rate depression caused by the addition of $NaBPh_4$ (see Table III).

The free ion rate constant k_f can be calculated from the slopes of the plots of Figure 6, utilizing the known dissociation constants of the polystyryl salts. The ion pair rate constant k_i for S^-, Na^+ in THF cannot be reliably derived from the intercepts of the above plots. However, a reasonable value can be deduced from the experiments performed in the presence of $NaBPh_4$ by calculating the fraction of free S^- ions. In DME the intercept is much larger and yields a reliable value for k_i .

The k_i and k_f values are collected in Table IV. Considering the uncertainty in determining the apparent rate constants k_0 from the initial slopes of the reaction curves, the agreement in the k_f values in THF as derived from the two different alkali polystyryl salts is good. One finds that the free S^- ion rate constant is about 10^3

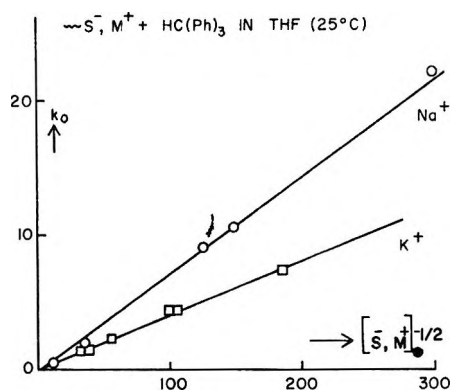


Figure 6. Plot of the apparent second-order rate constant k_0 vs. the reciprocal of the square root of the initial polystyryl salt concentration.

times higher than that of the sodium ion pair in THF at 25°. However, the ion pair reactivity is strongly enhanced in better solvating media, as shown by the increase in the k_i of S^-, Na^+ when THF is replaced by DME. An increase in the fraction of reactive loose ion pairs of S^-, Na^+ in DME is the most likely cause of the higher ion pair rate constant. A similar increase was found in the ion pair propagation rate constant of polystyryl sodium,¹⁰ which was found to increase from 11 $M^{-1} \text{sec}^{-1}$ in THP¹⁸ to 80 $M^{-1} \text{sec}^{-1}$ in THF⁵ to 3600 $M^{-1} \text{sec}^{-1}$ in DME¹⁰ all values referring to 25°. The free ion rate constant does not appear to be much affected by a change in solvent. This was also observed for the anionic polymerization of styrene in ethereal solvents.¹⁹ Generally, therefore, the mechanism of the proton abstraction reaction between polystyryl salts and triphenylmethane resembles that found in addition reactions involving carbanion intermediates such as the anionic homopolymerization of vinyl monomers.

Table IV: Absolute Rate Constants for the Reaction of Polystyryl Carbanion Salts with Triphenylmethane; Temperature 25°

Cation	Solvent	K_d, M	$k_f, M^{-1} \text{sec}^{-1}$	$k_i, M^{-1} \text{sec}^{-1}$
Na^+	THF	1.5×10^{-7a}	178	0.15
Na^+	DME	1.4×10^{-6b}	138	11
K^+	THF	8.8×10^{-8a}	142	<0.2

^a Reference 5. ^b Reference 10.

The proton transfer rate constant $k_f = 178 M^{-1} \text{sec}^{-1}$ for the reaction $S^- + TmH \rightarrow SH + Tm^-$ appears to be rather low. The ΔpK_A between triphenylmethane and $\sim CH_2CH_2\phi$ is probably close to 3.5 (the pK_A for TmH is reported to be 32.5, while that of $\sim CH_2CH_2\phi$ should be in between that of toluene, $pK_A = 35$ and cumene, $pK = 37$, all values taken from the Mc-

Ewen-Streitwieser-Appelquist-Dessy scale, see ref 1a, p 19). On the other hand, the ΔpK_A between fluorene and 9-methylfluorene is only 0.6 in DMSO²⁰ and less than 0.1 in cyclohexylamine,²¹ water²² and ethereal solvents.²³ Nevertheless, the rate constant of proton transfer of the free fluorenyl carbanion with 9- CH_3 fluorene in THF at 25° was found to be 85 $M^{-1} \text{sec}^{-1}$ and considerably higher in THP.²³ Clearly, the Bronsted equation will not hold in this case, and steric hindrance in the reaction involving triphenylmethane is the most likely cause. This has previously been suggested by Streitwieser²⁴ and by Ritchie²⁵ for the reaction of alkoxide ions with triphenylmethane. We have recently observed other cases of slow proton transfer reactions due to steric hindrance, such as the reaction between the dianion of 1,1 diphenylethylene ($C\phi_2-CH_2CH_2-C\phi_2$) and 9-propyl fluorene in THF.²⁶ The apparent second-order rate constant of this reaction is only 20 $M^{-1} \text{sec}^{-1}$ in THF at 25°, in spite of an expected ΔpK_A of at least 10.¹² Under almost identical conditions the apparent second-order rate constant of the reaction $F^-, Na^+ + 9\text{-methylfluorene}$ ($\Delta pK_A \approx 0.0$) was found to be 2.0 $M^{-1} \text{sec}^{-1}$ ²³ while that of the reaction $F^-, Na^+ + 1,2\text{ benzofluorene}$ ($\Delta pK_A \approx 2.0$) was reported to be in the order of $10^3 M^{-1} \text{sec}^{-1}$.²⁷

Recent work by Bank and Bockrath on the protonation of sodium naphthalene with water in tetrahydrofuran has produced evidence for a low reactivity of the loose ion pair as compared to that of the tight ion pair.²⁸ One hypothesis that was advanced to explain this behavior suggests that the counterion plays a catalytic role and that the ion pair reactivity is determined by the ability of the cation to facilitate the rupture of the H-OH bond. In some of our earlier work on the protonation of fluorenyl carbanions by the more acidic benzofluorenes we also had indications of a low free ion reactivity as compared to that of the tight ion pair.²⁸ More recent work shows that this is not the case when 9-methylfluorene is the protonating agent.²³ It is not unlikely, however, that a similar reactivity behavior as observed by Bank and Bockrath for radical anions will

(18) M. van Beylen, M. Fisher, J. Smid, and M. Szwarc, *Macromolecules*, **2**, 575 (1969).

(19) M. van Beylen, D. N. Bhattacharyya, J. Smid, and M. Szwarc, *J. Phys. Chem.*, **70**, 157 (1966).

(20) C. D. Ritchie and R. E. Uschold, *J. Amer. Chem. Soc.*, **89**, 1721 (1967).

(21) A. Streitwieser, Jr., E. Ciuffarin, and J. H. Hammons, *ibid.*, **89**, 63 (1967).

(22) K. Bowden and R. Stewart, *Tetrahedron*, **21**, 261 (1965).

(23) K. H. Wong, T. Ellingsen, and J. Smid, unpublished results from this laboratory.

(24) A. Streitwieser, Jr., *Progr. Phys. Org. Chem.*, **3**, 41 (1965).

(25) C. D. Ritchie and R. E. Uschold, *J. Amer. Chem. Soc.*, **89**, 2960 (1967).

(26) G. Collins and J. Smid, unpublished results from this laboratory.

(27) T. E. Hogen Esch and J. Smid, *ibid.*, **89**, 2764 (1967).

(28) S. Bank and B. Bockrath, *J. Amer. Chem. Soc.*, **93**, 430 (1971).

be found for carbanions when protonated in ethereal solvents by water or alcohols, although the studies of such reactions are likely to be complicated by the aggregation of the resulting hydroxides or alcoholates in the low polarity media.

Acknowledgment. The financial support of this research by the National Science Foundation (GP 26350) and by the Petroleum Research Fund, administered by the American Chemical Society, is gratefully acknowledged.

Comproportionation Kinetics of Stable Violen Radical Ions

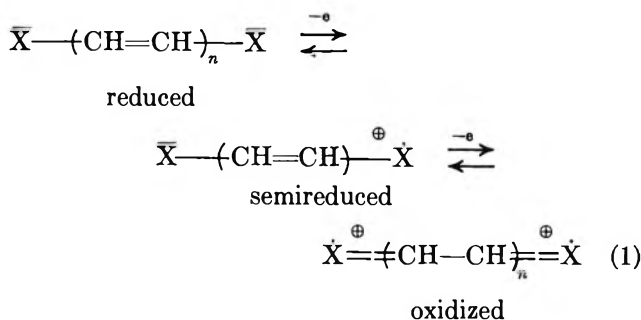
by Bruce C. Bennion, James J. Auborn, and Edward M. Eyring*

Department of Chemistry, University of Utah, Salt Lake City, Utah 84112 (Received May 20, 1971)

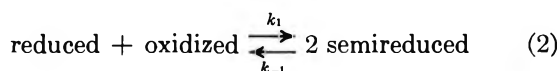
Publication costs assisted by the U. S. Air Force Office of Scientific Research

Violen radical ion systems contain highly colored oxidized, reduced, and semireduced species, all existing in simultaneous equilibrium in solution. Kinetic measurements by the stopped-flow method have enabled calculation of a rate constant for the rapid combination of the reduced and oxidized forms (comproportionation) of 1,1',2,2'-tetramethyl-(*cis*- + *trans*-)vinylene-3,3'-diindolizine: $k = (6.5 \pm 2.0) \times 10^8 M^{-1} \text{sec}^{-1}$ in acetonitrile ($\mu \leq 10^{-4} M$, 25°). The kinetics of a second violene system are just beyond the range of accessibility of the stopped-flow apparatus. The comproportionation reaction appears to be close to diffusion-controlled in acetonitrile.

A significant collection of radical ion systems, whose suggested name is the "violenes,"¹ are known to exist as part of a two-step redox system represented by



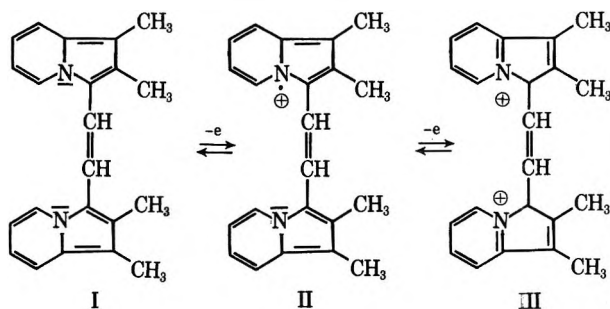
The three forms are each isolable and can exist in simultaneous equilibrium in solution as



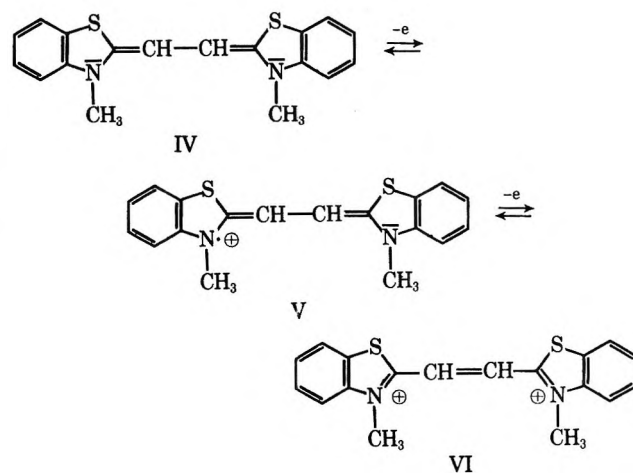
$$\frac{[\text{semireduced}]^2}{[\text{reduced}][\text{oxidized}]} = K > 100 \quad (3)$$

Because the extra electron of the semireduced form is delocalized in a π -electron system, this form is especially stable and absorbs light of longer wavelengths. Although Hünig and co-workers¹⁻⁴ have reported equilibrium constants for many of these systems, no attempts to measure the related rate constants have been reported. We report here the preparation of two violene systems and measurements of the forward and re-

verse rate constants for formation of the semireduced form. Two systems were prepared



and



1,1',2,2'-tetramethyl-(*cis*- + *trans*-)vinylene-3,3'-diindolizine and its semireduced and oxidized forms (I, II, and III) were prepared as described by Fraser and Reid.⁵ We isolated a sample of the *trans* isomer of I by chromatographing the *cis*-*trans* mixture on alumina, but the *trans* isomer gave no different kinetic results than did the original mixture of isomers. Therefore, we made no further efforts to separate isomers in other syntheses. We prepared 1,2-bis-(3'-methylbenzothiazol-2'-ylidene)ethane and its oxidized form (IV and VI) by the method of Kiprianov and Kornilov.⁶ The semireduced form (V) was prepared by dissolving equimolar quantities of (IV) and (VI) in acetonitrile and allowing them to react.

We checked the purity of each compound by comparison with melting point and spectral data from the published reports of those who first prepared them.^{5,6} Agreement was excellent in all cases, with the exception that the reported spectrum for species (IV) in ethanol⁶ does not represent that species. We dissolved a sample of (IV) in alcohol and observed that the solution changed from yellow to rose within a few minutes. This latter solution gave a visible spectrum which corresponded exactly with the published work,⁵ but we found that this solution would not react with (VI) to give the distinctly red colored intermediate (V). Compound (VI) was stable in acetonitrile only under a N₂ atmosphere. Kiprianov and Kornilov reported no melting point for the diperchlorate salt of (VI), but we found mp 208–209°.

All kinetic experiments were carried out in acetonitrile because this solvent afforded the best stability. Hünig¹ suggests that the ideal solvent for violene radical ion systems should be aprotic and exhibit neither nucleophilic nor reducing power, especially towards the oxidized forms. The indolizine system (I, II, and III) remains stable for several hours in acetonitrile, which appears to be a nearly ideal solvent. The other violene system (IV, V, and VI) is less stable in either acetonitrile deoxygenated by bubbling with N₂, or in dimethyl formamide, another good violene solvent. To ensure that instability would be no problem, all experiments were conducted within minutes after preparation of stock solutions. Immediately after each experiment, solutions were checked for decomposition by measuring optical absorbances at the maxima for each of the three species in each system. Only species (VI) decomposed appreciably during an experiment. Since for other reasons we were not able to measure a rate constant for the system of which (VI) is a part, no corrections for concentration changes were attempted.

Reagent grade acetonitrile (J. T. Baker and Eastman) containing less than 0.1% water was used in all experiments. Stock solutions of 1.00 × 10⁻⁴ M each of both the reduced and oxidized forms were prepared by weighing the respective compounds to 1 μg accuracy with a Mettler microbalance.

Kinetic experiments were conducted with a Durrum-Gibson Stopped-Flow Spectrophotometer equipped with a 2-mm optical-path-length Kel-F absorbance cuvette. The instrument was thermostated at 25 ± 0.05° by means of a Lauda K-2 circulator. The flow deadtime was determined to be less than 1 msec using the Fe³⁺ + SCN⁻ reaction and the extrapolation method recommended by the manufacturer. The triggering mechanism normally used with the temperature-jump accessory to the instrument was used in these stopped flow experiments and was set to exclude extraneous effects seen during mixing.

Equal concentrations of the freshly prepared oxidized and reduced forms of the compounds in acetonitrile were mixed in the stopped-flow apparatus and the rate of formation of the semireduced form was followed spectrophotometrically with 2-mm slits at 643 nm for (II) and 594 nm for (V). The results for the indolizine system could be checked with less sensitivity by following the rate of disappearance of either of the reactants at the wavelengths of their absorption maxima, (I) at 412 nm or (III) at 512 nm. The reaction was too rapid to permit the approximation of pseudo-first-order kinetics by increasing the concentration of one reactant significantly above that of the other. The reactants were unstable at concentrations below ~10⁻⁵ M in acetonitrile through which N₂ had been bubbled. Only the last few percent (~1–5%) of a relatively large transmittance change (up to ~80%) that occurred upon mixing could be reliably observed. With kinetic data obtained so close to equilibrium, the forward and reverse rates are nearly equal. The most obvious way to treat such data is by means of relaxation kinetics.

A characteristic relaxation time was determined from each oscilloscope photograph of transmittance *vs.* time. We developed a useful kinetic expression in the following manner. The relaxation time for reaction 2 is found by standard procedures to be

$$\tau^{-1} = 4k_1 [\text{semireduced}] + k_1 ([\text{reduced}] + [\text{oxidized}]) \quad (4)$$

Because we always mixed equal concentrations of reduced and oxidized forms in our experiments, we can write, using equation 3

$$[\text{reduced}] = [\text{oxidized}] = \frac{K^{-1/2}C_0}{1 + 2K^{-1/2}} \quad (5)$$

(1) S. Hünig in "Free Radicals in Solution." Plenary lectures presented at the International Symposium on Free Radicals in Solution, Ann Arbor, Michigan, August 21–24, 1966, pp 109–122, Butterworths, London, 1967.

(2) S. Hünig and J. Gross, *Tetrahedron Lett.*, 2599 (1968).

(3) S. Hünig, H. Schlaf, G. Kiesslich, and D. Scheutzwow, *Tetrahedron Lett.*, 2271 (1969).

(4) S. Hünig, *Angew. Chem., Int. Ed. Engl.*, 3, 286 (1969).

(5) M. Fraser and D. H. Reid, *J. Chem. Soc.*, 1421 (1963).

(6) A. I. Kiprianov and M. Yu. Kornilov, *Zh. Obshch. Khim.*, 31, 1699 (1961).

and

$$[\text{semireduced}] = \frac{C_o}{1 + 2K^{-1/2}} \quad (6)$$

where C_o represents the total violene concentration, including all three species. Substitution of eq 5 and 6 into eq 4 leads to the simplified expression

$$\tau^{-1} = 2k_1K^{-1/2}C_o \quad (7)$$

A plot of τ^{-1} vs. C_o will yield a slope from which k_1 can be readily calculated from the known equilibrium constant. These data are presented in Table I for the (I, II, III) indolizine system. A plot for this system is shown in Figure 1.

Table I: Comproportionation Kinetic Data for Indolizine Radical Ions in Acetonitrile at 25°

$C_o,^a 10^{-5} M$	$\tau^{-1},^b 10^3 \text{ sec}^{-1}$	$k_1,^c 10^8 M^{-1} \text{ sec}^{-1}$
2.5	1.33	7.5
3.0	1.75	8.2
5.0	1.64	4.6
	2.08	5.9
	2.27	6.4
10.0	4.35	6.1
	4.45	6.3

^a Total concentration of indolizine in all forms. ^b Observed relaxation time from stopped-flow experiments. ^c Calculated comproportionation rate constant.

Taking $K = 8 \times 10^2$ from a published value¹ for the same solvent, we calculate $k_1 = 6.5 \times 10^8 M^{-1} \text{ sec}^{-1}$. For the reverse rate constant we calculate $k_{-1} = k_1/K = 8.1 \times 10^5 M^{-1} \text{ sec}^{-1}$. Considering the scatter of points in Figure 1, our calculated rate constant is accurate to about $\pm 30\%$. Attempts to measure relaxation times for the second violene system (IV, V, and VI) were not successful. This reaction is apparently more rapid than the first, and is nearly completed within the mixing time of the stopped-flow instrument. Therefore, it can only be determined that k_1 for this system is within the same order of magnitude, but more rapid than for the indolizine system.

The rate constant, $k_1 = 6.5 \times 10^8 M^{-1} \text{ sec}^{-1}$, lies near the limit of accessibility of the stopped-flow method. We had attempted to measure the same kinetics using a temperature-jump relaxation method, but found that the equilibrium is quite temperature insensitive, even to a 15° perturbation. This implies a relatively low heat of reaction. The Stokes-Einstein equation for the diffusion coefficients of the reacting species taken with the Smoluchowski relation for the rate of a diffusion-controlled reaction between molecules of equal radii⁷ predicts a limiting rate constant of $1.8 \times 10^{10} M^{-1} \text{ sec}^{-1}$ in acetonitrile at 25°. Our ob-

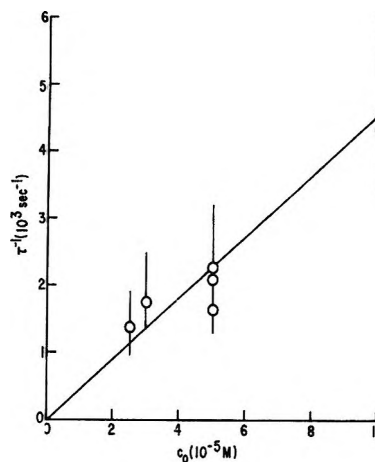


Figure 1. Plot of reciprocal relaxation time, τ^{-1} , vs. total indolizine concentration, C_o , in acetonitrile at 25°.

Circles denote experimental data points of Table I. Vertical error bars correspond to the estimated $\pm 30\%$ imprecision in measured τ values. The diagonal theoretical line is the best fit of the data subject to the constraints imposed by eq 7 that it be linear and that it pass through the origin of coordinates.

served comproportionation rate constant for the indolizine system is slightly more than one order of magnitude slower than the diffusion-controlled rate predicted by this approximate theoretical equation. This is consistent with measured rates⁸ for other presumably diffusion-controlled reactions.

Our results also compare favorably with those of Diebler, Eigen, and Matthies, who investigated the comproportionation reaction between benzoquinone and hydroquinone anion to form the semiquinone radical ion in basic aqueous solution.⁹ They reported a comproportionation rate constant $k_1 = 2.6 \times 10^8 M^{-1} \text{ sec}^{-1}$ and a disproportionation rate constant $k_{-1} = 7 \times 10^7 M^{-1} \text{ sec}^{-1}$ at 11° in aqueous solution with pH > 10 and ionic strength $\mu = 0.1$. If we correct their k_1 for the viscosity of acetonitrile and a temperature of 25° we would predict a comproportionation rate of $7.1 \times 10^8 M^{-1} \text{ sec}^{-1}$ for the benzoquinone system under the conditions of our experiments. This predicted rate is very close to that measured for the violene system considered in this paper and lies within the range of experimental error. We might expect comproportionation electron transfer reactions of other violenes and quinone-like systems to exhibit similar behavior in solvent systems where they remain stable.

Acknowledgment. This work was supported by AFOSR (SRC)-OAR, USAF, Grant No. 69-1717-F.

(7) E. F. Caldor, "Fast Reactions in Solution," Blackwell, Oxford, 1964.

(8) P. Warrick, Jr., J. J. Auborn, and E. M. Eyring, *J. Phys. Chem.*, in press.

(9) H. Diebler, M. Eigen, and P. Matthies, *Z. Naturforsch., B*, **16**, 629 (1962).

A General Solution for the Sequence of Two Competitive-Consecutive Second-Order Reactions

by Walter Y. Wen

Department of Chemistry, University of Oregon, Eugene, Oregon 97403 (Received October 21, 1971)

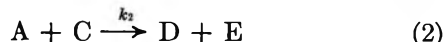
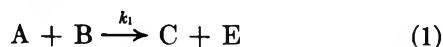
Publication costs assisted by the National Science Foundation

The kinetic equations for a sequence of two competitive-consecutive second-order reactions have been solved so that both rate constants can be evaluated from runs with any ratio of initial reactant concentrations. The technique has been successfully applied to the data of Ingold for the saponification of dimethyl glutarate by sodium hydroxide.

Methods of evaluating the rate constants from kinetic data generated by a series of two competitive-consecutive second-order reactions have been investigated by Wells,¹ recently by Saville,² and reviewed by Frost and Pearson³ and Szabó.⁴ The system is very complex and the kinetic equations cannot be handled by the conventional techniques. Assuming that the initial concentrations of the reactants are stoichiometrically equivalent, Frost and Schwemer⁵ developed a solution for this system. McMillan⁶ showed that the ratio of the rate constants can be determined easily if the simultaneous concentrations of two substances are known.

Although Frost and Schwemer's method⁵ is computationally convenient, in practice it can be difficult to prepare stoichiometric amounts of reactants. This was found to be particularly true when the reactants are gases and the reactions are rapid.⁷ To avoid this restriction we have derived a general Frost-Schwemer equation which can be applied to reactant mixtures with any proportions of the two reactants.

The chemical system consists of the reactions⁸



where k_1 and k_2 denote the rate constants of reaction 1 and 2, respectively. Although there are five possible kinetic equations for the system, only two of them are independent. Those for B and D are

$$\frac{dB}{dt} = -k_1AB \quad (3)$$

$$\frac{dD}{dt} = k_2AC \quad (4)$$

By material balance one obtains

$$A - 2B - C = A_0 - 2B_0 \quad (5)$$

$$B + C + D = B_0 \quad (6)$$

$$A + E = A_0 \quad (7)$$

where A , B , C , D , and E are the concentrations of the corresponding substances and the zero subscripts indicate initial concentrations. Since there are only three independent stoichiometric relationships for five variables, two parameters are needed to describe the system completely and one must either measure the concentrations of two species at the same time or the same species at at least two different times (besides $t = 0$) in order to obtain the two rate constants. The latter technique is developed in the present paper.

To simplify the derivations, the following dimensionless variables and parameters are introduced.

$$\alpha = \frac{A}{A_0} \quad \beta = \frac{B}{B_0} \quad \gamma = \frac{C}{B_0} \quad \delta = \frac{D}{B_0}$$

$$\epsilon = \frac{E}{A_0} \quad \tau = k_1B_0t \quad \kappa = \frac{k_2}{k_1} \quad \rho = \frac{A_0}{B_0}$$

In terms of these, C is eliminated from eq 4 using eq 6 and then the ratio of eq 4 to 3 becomes

$$\frac{d\delta}{d\beta} = -\kappa \frac{1 - \beta - \delta}{\beta} \quad (8)$$

Equation 8 can be transformed into a homogeneous first-order differential equation which can be readily solved to give⁹

(1) P. R. Wells, *J. Phys. Chem.*, **63**, 1978 (1959).

(2) B. Saville, *ibid.*, **75**, 2215 (1971).

(3) A. A. Frost and R. G. Pearson, "Kinetics and Mechanism," Wiley, New York, N. Y., 1961, p 178.

(4) Z. G. Szabó, "Comprehensive Chemical Kinetics," C. H. Bamford and C. F. H. Tipper, Ed., Vol. 2, Elsevier, New York, N. Y., 1969, p 61.

(5) A. A. Frost and W. C. Schwemer, *J. Amer. Chem. Soc.*, **74**, 1286 (1952).

(6) W. G. McMillan, *ibid.*, **79**, 4838 (1957).

(7) P. Goldfinger, R. M. Noyes, and W. Y. Wen, *ibid.*, **91**, 4003 (1969).

(8) For comparison all symbols used in the derivations are adopted from those in ref 3 and 5.

(9) W. Y. Wen, Ph.D. thesis, University of Oregon, 1971, p 116.

Table I: α , γ , δ , and ϵ as Functions ρ , κ , and β

$$\alpha = 1 - \frac{1}{\rho} \left[2 - \left(2 + \frac{1 - \beta^{\kappa-1}}{\kappa - 1} \right) \beta \right] \quad (10)$$

$$\gamma = \frac{\beta - \beta^{\kappa}}{\kappa - 1} \quad (11)$$

$$\delta = 1 - \frac{\kappa\beta - \beta^{\kappa}}{\kappa - 1} \quad (9)$$

$$\epsilon = \frac{1}{\rho} \left[2 - \left(2 + \frac{1 - \beta^{\kappa-1}}{\kappa - 1} \right) \beta \right] \quad (12)$$

$$\alpha = 1 - \frac{1}{\rho} [2 - (2 - \ln \beta)\beta] \quad (10a)$$

$$\gamma = -\beta \ln \beta \quad (11a)$$

$$\delta = 1 - (1 - \ln \beta)\beta \quad (9a)$$

$$\epsilon = \frac{1}{\rho} [2 - (2 - \ln \beta)\beta] \quad (12a)$$

$$\delta = 1 - \frac{\kappa\beta - \beta^{\kappa}}{\kappa - 1} \quad (9)$$

assuming that only A and B are present initially. For a special case of $\kappa = 1$, direct solution of eq 8 yields

$$\delta = 1 - (1 - \ln \beta)\beta \quad (9a)$$

which also can be obtained by taking the limit of eq 9 as $\kappa \rightarrow 1$. It can be shown, using eq 5, 6, 7, and 9 or 9a, that α , γ , and ϵ can be expressed as functions of ρ , κ , and β . Results of these derivations are summarized in Table I. It should be noted that if $\rho = 2$, eq 10 reduces to the Frost-Schwemer equation,⁵ that eq 11 is exactly that obtained by McMillan,⁶ and that both γ and δ are independent of ρ .

In terms of the dimensionless variables and parameters, the integrated form of eq 3 becomes

$$\tau = \frac{1}{\rho} \int_{\beta}^1 \frac{d\beta}{\alpha\beta} \quad (13)$$

By substituting eq 10 into eq 13, τ can then be evaluated if ρ , κ , and the limit of β are known.

For $\rho = 1.5$ Figure 1 shows τ and α plotted against β for various κ . τ was calculated from eq 13 by means of the trapezoidal formula using a step size for β of 0.01. Since for a particular β and κ , τ has only one value, plots similar to Figure 1 for γ , δ , and ϵ can be constructed using eq 10, 11, 9, and 12.

Because τ is defined as $k_1 B_0 t$, a plot of β vs. $\log t$ for a single run with $\rho = 1.5$ should yield a curve parallel to one of the family of β vs. $\log \tau$ curves. But κ can be more accurately determined by the time ratio (t ratio) method.⁵ It should be clear that the ratio of time for 50% of B reacted to time of 10% reacted, t_{50}/t_{10} , equals τ_{50}/τ_{10} which is a function of κ . Several results of κ as functions of t ratio, with $\rho = 1.5$, for various ratios of B reacted are shown graphically in Figure 2. Similar t -ratio plots based on A, C, D, or E also can be obtained from the related equations listed in Table I.

Using plots analogous to Figures 1 and 2, or the corresponding tables if desired, k_1 and k_2 can be determined from the results of a single run following any of

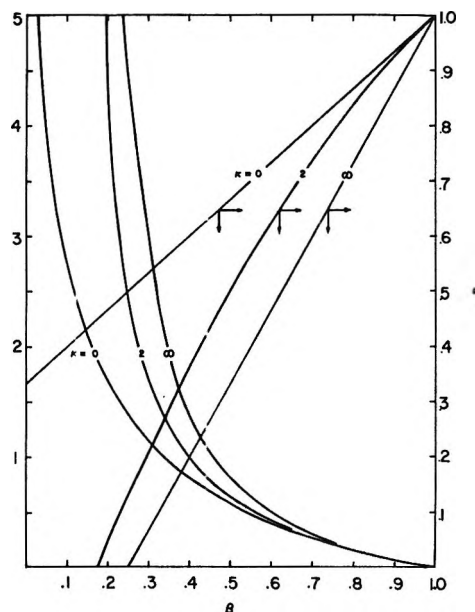


Figure 1. Plots of τ and α vs. β for various values of κ , with $\rho = 1.5$.

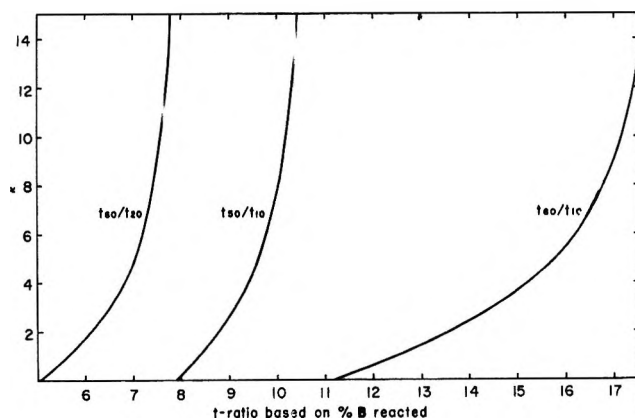


Figure 2. Plots of κ vs. t ratio for 60% and 10%, 60% and 20%, and 50% and 10% of B reacted, with $\rho = 1.5$.

the five species. The calculational procedure is described by Frost and Schwemer.⁵ However, because the relations between β and α , γ , δ , or ϵ are quite

Table II: Calculations of the Rate Constants for the Saponification of Dimethyl Glutarate by Sodium Hydroxide at 20.3° Using the Data of Ingold¹⁰ ($\rho = 1.0$)

t , min	A , 10^{-3} mol/l.	α	τ	k_1 , l./mol min)
0.0	1.999	1.000		
2.5	1.929	0.965	0.0366	7.324
4.2	1.883	0.942	0.0615	7.324
6.0	1.839	0.902	0.0877	7.320
10.0	1.743	0.872	0.1465	7.329
12.0	1.699	0.850	0.1760	7.337
14.1	1.655	0.828	0.2065	7.326
16.0	1.619	0.810	0.2340	7.316
18.0	1.577	0.789	0.2635	7.323
20.0	1.539	0.770	0.2930	7.329
23.0	1.487	0.744	0.3365	7.319
26.0	1.435	0.718	0.3810	7.331
29.0	1.387	0.694	0.4255	7.340
32.0	1.345	0.673	0.4680	7.316
35.0	1.307	0.654	0.5210	7.446

Average = 7.334

$$k_2 = 0.151 \times 7.334 = 1.107$$

Calculation of κ

α	t , min	comparison of % α reacted	t ratio	κ
0.95	3.6	35/05	9.917	0.152
0.90	7.6	35/10	4.697	0.142
0.85	12.0	35/15	2.975	0.152
0.80	16.9	35/20	2.112	0.145
0.75	22.2	30/05	7.833	0.154
0.70	28.2	30/10	3.710	0.156
0.65	35.7	30/15	2.331	0.156
		30/20	1.669	0.152

Average = 0.151

Table III: Comparison of the Rate Constants Obtained from the Data of Ingold¹⁰ by Different Methods of Calculation

Method	k_1 , l./mol min)	k_2 , l./mol min)
Ingold ⁹	7.24	1.12
Wideqvist ¹⁰	7.277	1.12
This work	7.334	1.107

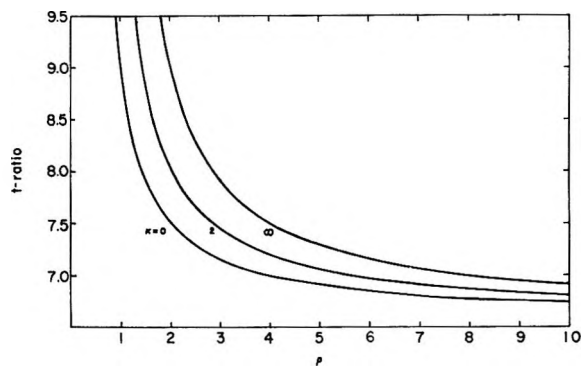


Figure 3. Plots of t ratio vs. ρ for various values of κ , with the ratio of 50% to 10% of B reacted.

complicated, data analysis becomes very tedious if the reaction is monitored by following the concentration of a species other than B.

Our calculations of α and τ vs. β covered the ranges of 0.2–20 for ρ and of 0.02–50 for κ . The cases of $\kappa = 0$ and $\kappa = \infty$ were also evaluated. Figure 3 shows plots of the ratio of the time required for 50% reaction of B to that required for 10% reaction vs. ρ for various values of κ , which indicate that the t -ratio technique is quite sensitive for values of ρ between 1 and 4. If ρ is very small, then B is in large excess and one has to sacrifice experimental precision of determining B. When ρ is in the range of 1–2, the t -ratio technique can be most conveniently applied.

The above method has been employed to interpret the data of Ingold¹⁰ for the saponification of dimethyl glutarate by sodium hydroxide at 20.3°. The results of the calculations are shown in Table II. In Table III, the calculated values of the rate constants are compared with those obtained by two other approximation techniques^{10,11} in which k_2 had to be determined by independent kinetic measurements.

Acknowledgment. The author wishes to thank Professor R. M. Noyes and Dr. R. J. Field for enlightening discussions. This research has been supported by the National Science Foundation.

(10) C. K. Ingold, *J. Chem. Soc.*, 2170 (1931).

(11) S. Wideqvist, *Acta Chem. Scand.*, 4, 1216 (1950).

The Adsorption Behavior of Tetraphenylborate Anions at a Mercury Electrode

by Claudio Giomini* and Liliana Rampazzo

Institute of Chemistry, University of Rome, Faculty of Engineering, Rome, Italy (Received June 29, 1971)

Publication costs assisted by the Consiglio Nazionale delle Ricerche

The adsorption of tetraphenylborate (BPh_4)⁻ anions at the mercury electrode was investigated by measuring differential capacity values as a function of applied potential. The solutions examined were aqueous x M $\text{NaBPh}_4 + (0.916 - x)$ M NaF. The results indicate strong adsorption of (BPh_4)⁻ in the potential range -0.15 to -1.00 V vs. a NaCl nce; at potential values more positive than -0.15 V the anion is oxidized, whereas at potential values more negative than -1.2 V the specific differential capacity values coincide with those of the pure NaF solution. The zero-frequency capacity data were back integrated to obtain specific charge q and interfacial tension values. The interfacial pressure curves vs. $\log x$ (at $q = \text{constant}$) are congruent with respect to the charge; a quadratic dependence of free energy of adsorption on the charge was found. The best fitting of experimental data was obtained with a Frumkin-type isotherm, with a repulsive interaction parameter. The result is discussed in connection with the "cluster" theory of H_2O molecules at the Hg-solution interface. The Levine, Bell, and Calvert isotherm and Frumkin isotherm are compared; the agreement between experimental and calculated isotherm parameters can be considered satisfactory.

Introduction

At the present time no study has been reported about the behavior of tetraphenylborate anions (BPh_4)⁻ at the ideally polarized mercury-aqueous solution interface. We found that (BPh_4)⁻ is strongly adsorbed; to evidence adsorption, we used differential capacity measurements because of the greater sensitivity of this method to the fine structure of the double layer.

In addition to the interest in the adsorption behavior of (BPh_4)⁻ *per se*, this system was chosen also for the following reasons. (i) (BPh_4)⁻ ion is large when compared with closed shell ions previously studied. (ii) It is centrosymmetrical, so that anisotropy in ion-electrode, ion-solvent, and ion-ion interactions can be supposed nearly absent. (iii) Its sodium salt is soluble enough to allow measurements in a reasonable concentration range; moreover, no complications deriving from hydrolysis^{1a,b} were detected. (iv) In the NaF- NaBPh_4 solutions we investigated, the electrochemical oxidation of (BPh_4)⁻ ion^{2a,b} takes place at potential values more anodic than -0.15 V, so that the Hg-solution interface from this point up to the extreme cathodic side can be considered ideally polarized.

Point ii is relevant with respect to the congruence of adsorption isotherms.³ It could be expected that our system would resemble on this respect the simpler monatomic closed shell ions like Cl^- or I^- , for which experimental data were fitted to some isotherm congruent with respect to the charge.^{4a,b} In fact, as pointed out by Parry and Parsons,^{5a,b} when the orientation of the adsorbed anions is constant, the isotherms are congruent with respect to the charge. As expected, the experimental data of (BPh_4)⁻ adsorption could be fitted to a Frumkin-type isotherm,⁶ with a charge-independent interaction parameter.

Point i is of importance, among other things, in de-

termining the charge dependence of the electrical term of the free energy of adsorption; for our system, we found a quadratic trend in such dependence, which is reminiscent of the behavior of organic neutral molecules.⁷

Experimental Section

The measurements of the mercury-solution interface capacity were performed by means of an AMEL Model 951 impedance bridge. A detailed description of this instrument and its performances can be found elsewhere.⁸

The separate measurements of the resistive and capacitive components of the cell impedance can be achieved by this apparatus, as well as a very accurate and precise determination of the instant of the bridge balance, when a dropping mercury electrode (dme) is used. The dme was a drawn-out type, and its internal bore had been made water repellent by suitable coating. The cell employed was a three-electrode type, with a platinum cylinder counter electrode, and provisions to

(1) (a) S. S. Cooper, *Anal. Chem.*, **29**, 446 (1957); (b) J. N. Cooper and R. E. Powell, *J. Amer. Chem. Soc.*, **85**, 1590 (1963).

(2) (a) D. H. Geske, *J. Phys. Chem.*, **63**, 1062 (1959); **66**, 1743 (1962); (b) W. R. Turner and P. J. Elving, *Anal. Chem.*, **37**, 207 (1965).

(3) R. Parsons, *Trans. Faraday Soc.*, **51**, 1518 (1955).

(4) (a) E. Dutkiewicz and R. Parsons, *J. Electroanal. Chem.*, **11**, 100 (1966); (b) R. Payne, *Trans. Faraday Soc.*, **64**, 1638 (1968).

(5) (a) J. M. Parry and R. Parsons, *ibid.*, **59**, 241 (1963); (b) J. M. Parry and R. Parsons, *J. Electrochem. Soc.*, **113**, 992 (1966).

(6) A. N. Frumkin, *Z. Phys.*, **35**, 792 (1926).

(7) (a) R. Parsons, *J. Electroanal. Chem.*, **7**, 136 (1964); (b) J. O'M. Bockris, M. A. V. Devanathan, and K. Müller, *Proc. Roy. Soc., Ser. A*, **274**, 55 (1963); (c) B. B. Damaskin, *J. Electroanal. Chem.*, **23**, 431 (1969); (d) V. A. Kir'yanov, V. S. Krylov, and B. B. Damaskin, *Sov. Electrochem.*, **6**, 521 (1970).

(8) C. Giomini, L. Grifone, L. Rampazzo, and P. Silvestroni, *Ann. Chim. (Rome)*, **61**, 23 (1971).

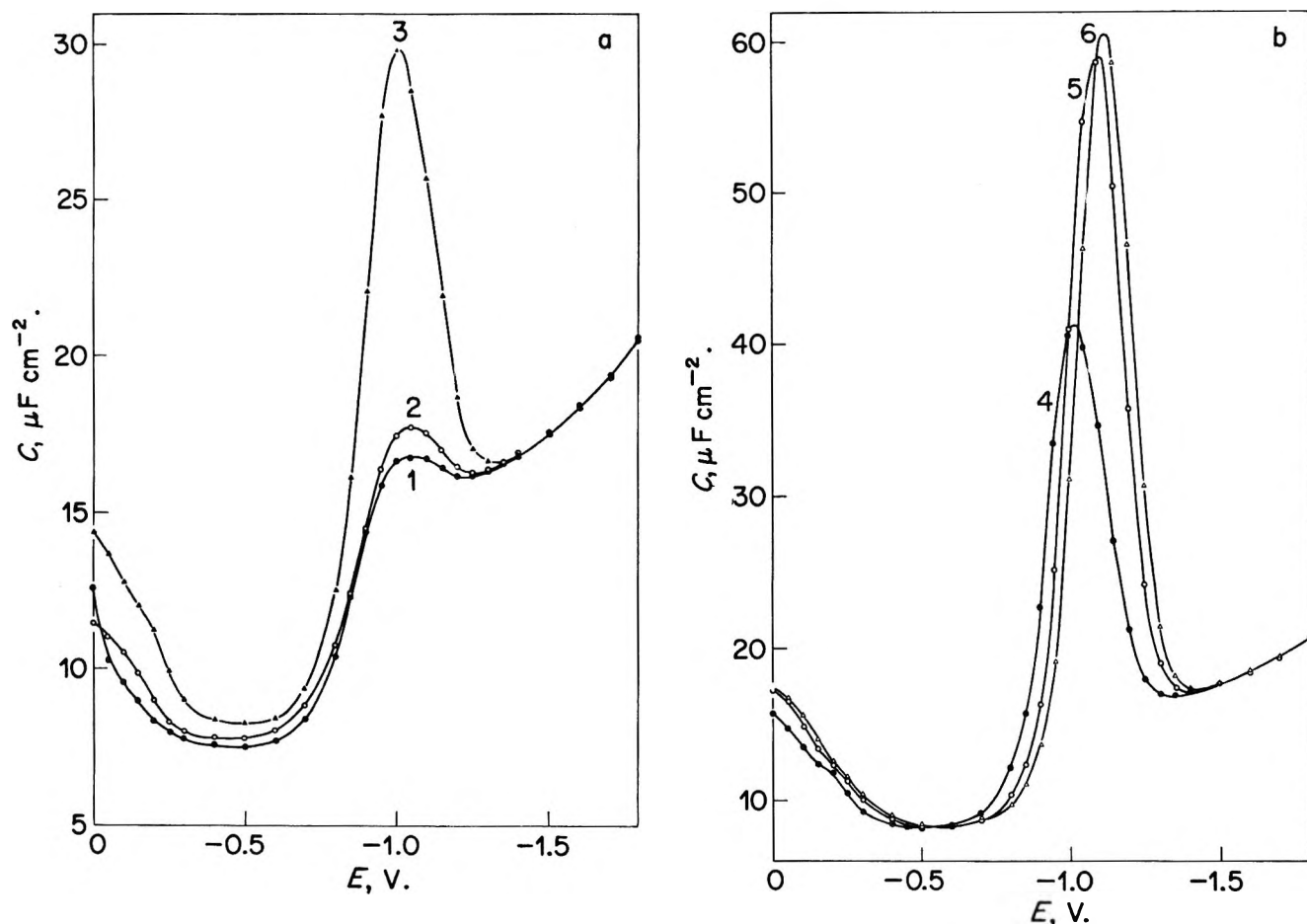


Figure 1. Specific differential capacity of a mercury electrode in contact with aqueous solutions of $x M \text{NaBPh}_4 + (0.916 - x) M \text{NaF}$ at 25° , as a function of the potential against a normal ($1 F \text{NaCl}$) calomel electrode. Values of x : (1), 5×10^{-6} ; (2), 10^{-4} ; (3), 5×10^{-4} ; (4), 10^{-2} ; (5), 5×10^{-2} ; (6), 10^{-2} . Measurements performed at 1.1 kHz on a dropping mercury electrode.

fit the drop just in the center of the counter electrode. A reservoir, containing the same solution to be examined, separated the cell from the reference electrode. The solution was never allowed to come into contact with rubber, grease, or similar matter. Teflon rings were used to make the cell air-tight, or whenever it was necessary to grant some elasticity in the apparatus.

The reference electrode was calomel type; its aqueous phase was a $1 F \text{NaCl}$ solution. NaCl instead of KCl was used because K^+ ions would have precipitated insoluble KBPh_4 from NaBPh_4 in the solution. The electrode was connected to the reservoir filled with the same solution of the cell by means of an agar bridge containing aqueous saturated NaF . The potential of such an electrode was $+0.043 \text{ V vs. sce}$.

Tridistilled water, Merck "Suprapur" NaF , and BDH or Fluka reagent grade NaBPh_4 were used to prepare the solutions. The latter product was purified according to literature methods.⁹ No difference was detected between capacity values obtained with purified and reagent grade product, so that the purification was omitted in further experiments. The mercury was subjected to the usual purification treatments, and then

tridistilled under reduced pressure; the last operation was performed a short time before the beginning of the capacity measurements. Ultrapure nitrogen was used to deoxygenate the solutions.

The solubility of NaBPh_4 in almost saturated NaF solutions is slightly more than $1 \times 10^{-2} \text{ mol/l.}$ at room temperature. Therefore the upper limit of NaBPh_4 concentration for the solution under examination was set at $1 \times 10^{-2} F$, the lower limit being $5 \times 10^{-5} F$. NaF was added to the various solutions in such a quantity to obtain a constant ionic strength of 0.916 mol/l. The pH values of such solutions ranged from 7.3 (pure NaF) to 7.6; therefore their stability was granted at least for some days after the preparation.^{1a} No evidence was reported for the existence of a tetraphenylboric acid,^{1b} so that hydrolysis of $(\text{BPh}_4)^-$ in such solutions is thought to be very small, in accordance with the measured pH values. Ion-pair formation for NaBPh_4 is reported⁹ to be absent or not relevant, at least up to moderate concentrations.

(9) A. K. Covington and M. J. Tait, *Electrochim. Acta*, 12, 113 (1967).

Generally, the instant of bridge balance was caused to occur 8.05 sec after the drop birth. To ascertain the existence of equilibrium conditions within the interfacial region at this time, specific capacity measurements were performed at different times of the drop life, for the solution containing the lowest quantity of NaBPh_4 , the potential being kept constant, at various potentials. These measurements showed that the capacity was practically constant from ~ 5 sec onwards. The time of 8.05 sec was chosen for greater convenience. The capacity measurements were made at various frequencies, from 0.8 to 5 kHz, because of their frequency dependence in the desorption peak region,¹⁰ in order to allow an extrapolation to zero frequency.¹¹ This extrapolation was made by fitting a least-squares curve through the experimental points.

Results and Discussion

Figure 1a and b shows specific differential capacity curves as a function of potential for various concentrations of NaBPh_4 in aqueous NaF solutions at constant ionic strength ($x M \text{NaBPh}_4 + (0.916 - x) M \text{NaF}$; $x = 5 \times 10^{-5}$ to 10^{-2}) at the frequency 1.1 kHz. Experimental points were taken at 50-mV intervals, except in the peak region, where more measurements were made, generally at 10-mV intervals or more, to detect the proper coordinates of the peak. Similar measurements at various frequencies permit extrapolation of the data to zero frequency.¹⁰ The corresponding curves are not very different from those of Figure 1, except that the peaks are higher; in fact, as expected,¹⁰ in the region of strong adsorption the frequency dispersion was low, not exceeding $\sim 3\%$; in the cathodic peak (desorption peak) region it was 13–5% on going from the lowest to the highest concentration.

It is clear that $(\text{BPh}_4)^-$ anion is strongly adsorbed from -0.2 to -0.8 V; desorption peaks lie in the region from -0.9 to -1.2 V depending on the concentration; at far cathodic potentials the capacity curves coincide with the curve of the pure NaF solution indicating that desorption is complete. The higher the concentration, the higher the desorption peaks and the more shifted towards more negative potentials.¹² The capacity minimum values are very low ($7\text{--}8 \mu\text{F}/\text{cm}^2$) and almost coincident for the various concentrations; therefore, it can be inferred qualitatively that the maximum coverage is nearly attained even for the lowest concentration.

In Figure 2 nonequilibrium capacity values relative to $5 \times 10^{-5} M$ solutions are reported. They refer to measurements made at 2, 3, 5, and 8 sec after the drop birth and are indicative of the fact that notable capacity depression occurs even when only 2 sec are available to $(\text{BPh}_4)^-$ ions for diffusion towards the electrode.

The zero-frequency capacity data were numerically interpolated in order to obtain values every 5 mV; specific charge q and interfacial tension γ values were

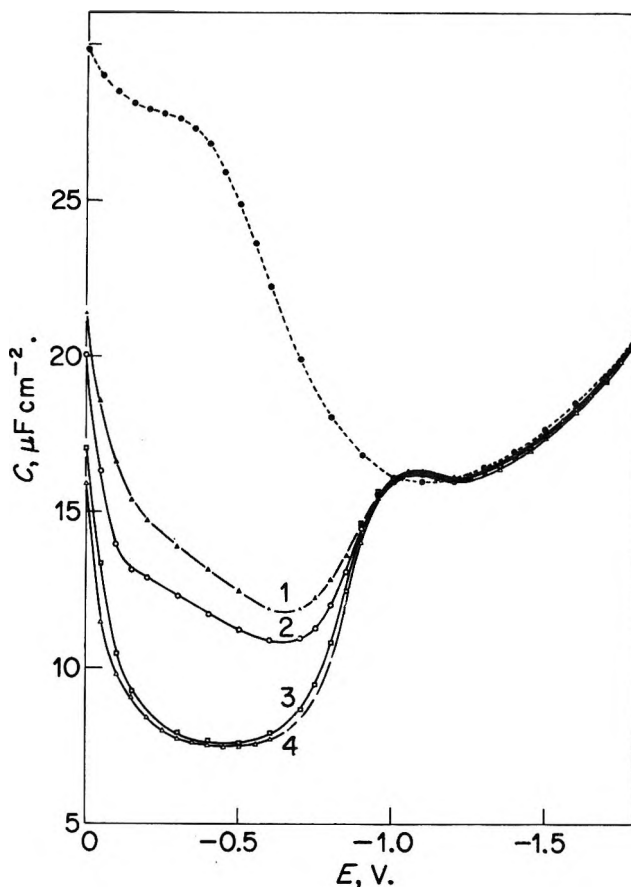


Figure 2. Specific differential capacity data of a mercury electrode, in contact with an aqueous solution of $5 \times 10^{-5} M \text{NaBPh}_4 + 0.916 M \text{NaF}$ at 25° , as a function of the potential, at various times t after the drop birth. Values of t : (1), 2.05 sec; (2), 3.05 sec; (3), 5.05 sec; (4), 8.05 sec. Dotted line: $0.916 M \text{NaF}$.

then obtained by back integration. The (known)¹³ charge and interfacial tension values relative to the pure NaF solution at -1.790 V were taken as integration constants, because of the coincidence of capacity data relative to all NaBPh_4 solutions examined with those relative to the pure NaF solution at more cathodic potential values.

The function $\zeta = \gamma + qE$ at $q = \text{const.}$ ($T, P = \text{const.}$)³ was then evaluated for each concentration of NaBPh_4 , so that the family of curves $\zeta_b - \zeta$ (index b refers to the pure NaF solution) at various q ($q = \text{integer}$) vs. $\log x$ was obtained. The various curves were congruent, *i.e.*, could be translated parallel to the $\log x$ axis, to obtain a common curve of the interfacial pressure $\Phi = \zeta_b - \zeta$ vs. $\log \beta x = \log x + f(q)$ (Figure 3).

(10) R. Parsons in "Advances in Electrochemistry and Electrochemical Engineering," Vol. I, P. Delahay and W. Tobias, Ed., Interscience, New York, N. Y., 1967, p 1 ff.

(11) R. Parsons and P. C. Symons, *Trans. Faraday Soc.*, **64**, 1077 (1968).

(12) R. Parsons, *J. Electroanal. Chem.*, **5**, 397 (1963).

(13) D. C. Grahame, Office of Naval Research, Technical Report No. 14 (1954).

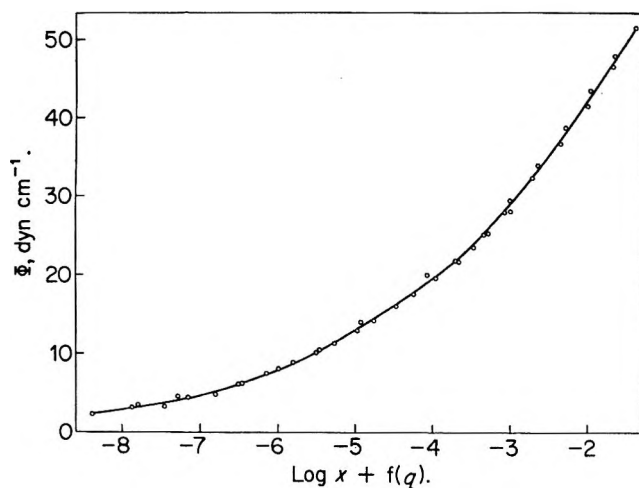


Figure 3. Composite curve relative to the interfacial pressures Φ of $(\text{BPh}_4)^-$ ion, adsorbed on a mercury electrode, as a function of $\log x$.

Figure 4 shows the function $f(q) = \log \beta(q) - \log \beta(q = 0)$, where β is the adsorption coefficient and $-RT \ln \beta = \Delta G_{\text{ads}}^\circ$. From Figure 4, the nonlinear behavior of $f(q)$ and, consequently, of $\Delta G_{\text{ads}}^\circ$ as a function of q is evident.

From the data of Figure 3, a mean-square third-order polynomial was calculated; the difference between experimental and calculated values was 0.04–0.2 dyn/cm. It is known^{4a} that, at constant ionic strength I , the (relative) interfacial excess of ions adsorbed in the inner layer Γ^i can be calculated with sufficient accuracy by means of the relation

$$\Gamma^i = \Gamma^i_{(\text{BPh}_4)^-} = [1/RT](\partial\Phi/\partial \ln x)_{q,I} \quad (1)$$

The calculated Φ vs. $\log x$ polynomial was differentiated numerically to give the corresponding Γ^i values; the maximum value of Γ^i was found to be $\Gamma_m^i = 2.6 \times 10^{-10}$ g-ion/cm².

Strictly speaking, eq 1 is valid only if it is assumed that (i) F^- ions are not specifically adsorbed (this is generally accepted); (ii) the mean activity coefficients of NaF and NaBPh_4 are constant when x is varied; this can be nearly true because I is not very high ($< 1 M$) and x itself is low ($\leq 10^{-2} M$), although the size of the ions is different;^{4a, 14–16} (iii) liquid junction potentials are constant; this can be reasonably assumed in our experimental arrangement; (iv) $\Gamma^{\text{diff}}_{(\text{BPh}_4)^-}/\Gamma_{\text{F}^-} = x/(0.916 - x)$;^{4a, 14} this implies that d , the distance between the electrode and the outer-Helmholtz plane, is constant.¹⁴

Solutions of NaBPh_4 were sufficiently dilute to allow the interfacial excesses to be identified with the interfacial concentrations.

The experimental $\log \Phi$ vs. $\log x$ plot was examined; it could be fitted to a theoretical $\log \Phi$ vs. $\log x$ plot corresponding to a Frumkin-type isotherm, with the maximum interfacial concentration $\Gamma_m^i = 2.6 \times 10^{-10}$

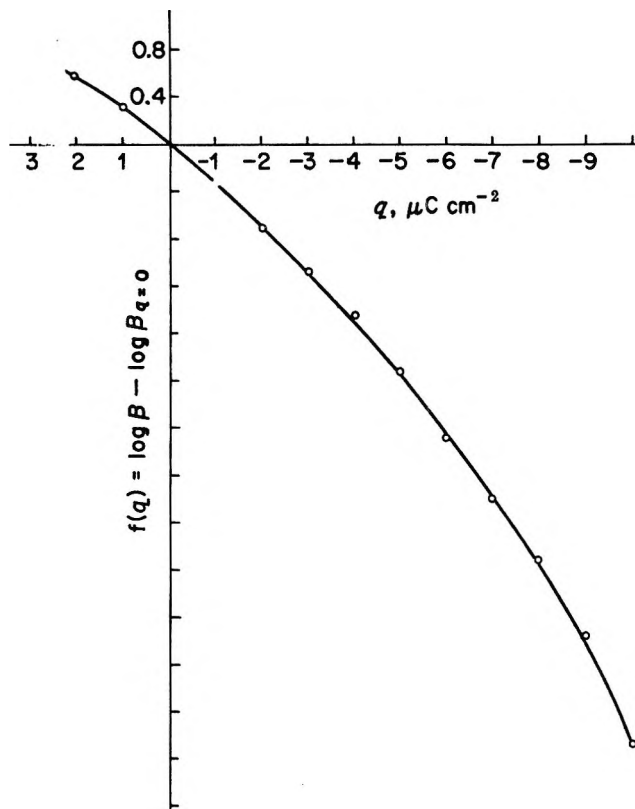


Figure 4. Values of $f(q) = \log \beta(q) - \log \beta(q = 0)$ as a function of the interfacial charge density.

g-ion/cm² and a repulsive interaction parameter $A/2.3 = 6.36$. Maximum deviation in $\log \Phi$ was 0.1 at high coverages and decreased at low coverages. Assuming a closest-hexagonal packing for $(\text{BPh}_4)^-$ anions in the inner layer, and given a mean radius of 4.2 Å¹⁷ for $(\text{BPh}_4)^-$, we calculated $\Gamma_m^i = 2.7 \times 10^{-10}$ g-ion/cm², which agrees with the experimental Γ_m^i reasonably well.

To test the validity of the Frumkin isotherm assumed before, the data were then replotted in the form of $\log [\vartheta/(r(1 - \vartheta)^r) \times 1/x]$ as a function of ϑ at $q = 0$ (modified Flory–Huggins isotherm)¹⁸ with $r = 1, 2, 3, 4, 5$, and $\vartheta = \Gamma^i/\Gamma_m^i$; $r = 5$ would correspond to the number of H_2O molecules displaced by the $(\text{BPh}_4)^-$ ion at the interface, assuming $\sim 12 \text{ \AA}^2/\text{molecule}$ of H_2O . A linear plot was obtained only if $r = 1$, which corresponds to the Frumkin isotherm, and the slope of the straight line was 6.36, the mean-square correlation coefficient being 0.99. For $r > 1$, the curve shows a minimum, *i.e.*, attractive interactions at high coverages. This can hardly be accepted for a charged species, although some kind of “hydrophobic bonding” between bulk

(14) H. D. Hurwitz, *J. Electroanal. Chem.*, **10**, 35 (1965).

(15) S. Lakshmanan and S. K. Rangarajan, *ibid.*, **27**, 127 (1970).

(16) S. Lakshmanan and S. K. Rangarajan, *ibid.*, **27**, 170 (1970).

(17) E. Grunwald, G. Baughman, and G. Kohnstam, *J. Amer. Chem. Soc.*, **82**, 5801 (1960).

(18) (a) P. J. Flory, *J. Chem. Phys.*, **10**, 51 (1942); (b) M. L. Huggins, *J. Phys. Chem.*, **46**, 151 (1942).

(BPh₄)⁻ ions has been reported.¹⁹ The modified Helfand, Frisch, and Lebowitz²⁰ isotherm was tried also and was rejected for similar reasons. From the above-mentioned plot ($r = 1$), the value of $\log \beta$ ($q = 0$, $\vartheta = 0$) of 7.4, corresponding to $\Delta G_{q=0, \vartheta=0}^{\circ} = -9.9$ kcal/g-ion was obtained.

The function $f(q) = \log \beta(q) - \log \beta(q = 0)$ of Figure 4 was well approximated by the mean-square parabola

$$f(q) - 0.022 = 0.2981q - 0.0197q^2 = \frac{A'}{2.3}q + \frac{B'}{2.3}q^2 \quad (2)$$

with $q_{\max} = 7.5 \mu\text{C}/\text{cm}^2$, which corresponds roughly to the surface pressure $\Phi = 67$ dyn/cm observed at $x = 10^{-2} M$. The descending branch of the parabola on the anodic side could not be experimentally observed because of the anion oxidation.

The more reliable value of $r = 1$ we have obtained could mean that H₂O molecules are grouped in clusters of about five units in the interphase, so that each cluster behaves as a single entity with respect to displacement by a (BPh₄)⁻ ion. Results in favor of the "cluster theory" have been obtained,²¹⁻²³ as well as contrary to it;^{24,25} the question is therefore not resolved (see also ref 26 and 27). Another way to explain $r = 1$ could be that a phenyl group of the (BPh₄)⁻ ion is normal to the surface of the electrode, the other groups being located in the outer zone of the inner double layer; in this instance the distance between the electrode and the plane of the adsorbed charges would be equal to the maximum radius of (BPh₄)⁻ ion and not to the mean radius as quoted above. But with $r_{\max} = 4.8 \text{ \AA}$ a value of $\Gamma_m = 2.2 \times 10^{-10}$ g-ion/cm² is obtained, which is somewhat lower than the experimental one. The fact that $r = 1$ gave more satisfactory results cannot be explained, at present: the proper value of r is connected with the entropy of adsorption of ions^{27,28} and is probably specific of the system under study (configuration of H₂O molecules in the neighborhood of adsorbed ion, in competition with the metal-solution field). In other words, the value of r cannot be simply calculated by the number of H₂O molecules or clusters displaced by an adsorbed particle, especially when this is large.

The Frumkin isotherm

$$\beta x = \frac{\vartheta}{1 - \vartheta} e^{A\vartheta} \quad (3)$$

i.e., $\ln \vartheta/(1 - \vartheta) = \ln \beta + \ln x - A\vartheta$ can be related to the Levine, Bell, and Calvert isotherm,^{28,29} that in our conditions can be written as (assuming $r = 1$, activity coefficient constant)

$$\ln \frac{\vartheta}{1 - \vartheta} = \ln \beta + \ln x - \frac{4\pi F^2(d - x_1)}{\epsilon_i^m RT} \left(1 - \frac{x_1}{d}\right) \Gamma_m \vartheta \quad (4)$$

where $\ln \beta$ is charge dependent, $x_1 =$ distance between the electrode and the plane of adsorbed charges, $d =$ inner layer thickness, $\epsilon_i^m =$ mean²⁸⁻³⁰ dielectric constant of the inner layer. Equation 4 holds if multiple imaging between metal and OHP is assumed; if the energy of polarization is neglected, $\ln \beta$ in (4) is expressed by

$$\ln \beta = \ln \beta_{q=0} + \frac{4\pi F(d - x_1)}{\epsilon_i^m RT} q + \frac{F}{RT} \phi_{\text{diff}} \quad (5)$$

where ϕ_{diff} = the mean potential at the CHP. The inclusion of the polarization energy turns out in a more complex dependence of $\ln \beta$ on q (ion field interaction). The term in eq 5 which is linear in q originates from the fact that the lateral (repulsive) interactions between adsorbed ions are the resultant of repulsive ion-ion and attractive ion-image forces. Comparing eq 2, 3, 4, and 5 it follows that

$$A = \frac{4\pi(d - x_1)\Gamma_m^2 F^2}{\epsilon_i^m RT} \left(1 - \frac{x_1}{d}\right) \quad (6)$$

and

$$\left(\frac{d \ln \beta}{dq}\right)_{q=0} = \frac{4\pi F(d - x_1)}{\epsilon_i^m RT} + \frac{F}{RT} \frac{d\phi_{\text{diff}}}{dq} \approx \frac{4\pi F(d - x_1)}{\epsilon_i^m RT} \quad (7)$$

if $1/C_{\text{diff}}$ is small as in our system ($I \approx 1 M$). Assuming²⁶ $\epsilon_i^m = 6$; $d = 6.3 \text{ \AA}$ and $x_1 = r_m^i = 4.2 \text{ \AA}$ for (BPh₄)⁻ we found: $A/2.3 = 6.4$ (cf. $A/2.3 = 6.36$ as found experimentally).

It is known that the major uncertainties are in the choice of the proper values of ϵ_i^m and d .²⁸ However, if the values are nearly correct, they should give a value for the coefficient of q in eq 5 at least of the correct order of magnitude. The experimental value of this coefficient is (eq 2) $(d \ln \beta/dq)_{q=0} = A'/2.3 = 0.30 \text{ cm}^2/\mu\text{C}$ and the calculated one (eq 5, 7) $A'/2.3 = 0.66 \text{ cm}^2/\mu\text{C}$. The agreement between experimental and calculated both A and A' is not so satisfactory if for instance the

(19) S. Subramanian and J. C. Ahluwalia, *J. Phys. Chem.*, **72**, 2525 (1968).

(20) D. M. Mohilner in "Electroanalytical Chemistry," Vol. I, A. J. Bard, Ed., Marcel Dekker, New York, N. Y., 1966, p 241 ff.

(21) R. Parsons, *J. Electroanal. Chem.*, **8**, 93 (1964).

(22) B. B. Damaskin, *Sov. Electrochem.*, **1**, 51 (1965).

(23) B. E. Conway and L. G. M. Gordon, *J. Phys. Chem.*, **73**, 3609 (1969).

(24) J. Lawrence and R. Parsons, *ibid.*, **73**, 3577 (1969).

(25) R. Payne, *J. Electrochem. Soc.*, **113**, 999 (1966).

(26) J. O'M. Bockris, E. Gileady, and K. Müller, *Electrochim. Acta*, **12**, 1301 (1967).

(27) B. E. Conway and L. G. M. Gordon, *J. Phys. Chem.*, **73**, 3523 (1969); see also ref 23.

(28) S. Levine, J. Mingins, and G. M. Bell, *J. Electroanal. Chem.*, **13**, 280 (1967).

(29) S. Levine, G. M. Bell, and D. Calvert, *Can. J. Chem.*, **40**, 518 (1962).

(30) V. A. Kir'yanov, *Sov. Electrochem.*, **6**, 1143 (1970).

following d and ϵ_i^m couples are assumed: $d = 2r_m^i$, $\epsilon_i^m = 6$; $d = 5.2 \text{ \AA}$, $\epsilon_i^m = 6$; $d = 6.3 \text{ \AA}$, $\epsilon_i^m = 10$; $d = 5.2 \text{ \AA}$, $\epsilon_i^m = 10$. Parry and Parsons^{6a} found that benzene-*m*-disulfonate ion is adsorbed with the benzene ring parallel to the mercury surface, the center of the negative charge being at $x_1 = 2 \text{ \AA}$ from the metal; in this case, $\ln \beta$ is linearly dependent on q . Deviations

from the linearity of $\ln \beta$ as a function of q are to be expected for large ions as $(\text{BPh}_4)^-$ ($x_1 = 4.2 \text{ \AA}$) as experimentally observed, since the polarization energy is to be taken into account in eq 5.²⁹

Acknowledgment. The authors are indebted to the Consiglio Nazionale delle Ricerche (C.N.R.), Rome, for financial support.

Transference Numbers of Potassium Chloride and Ionic Conductances in Ethylene Glycol at 25°

by M. Carmo Santos and M. Spiro*

Department of Chemistry, Imperial College of Science and Technology, London SW7 2AY, England (Received September 14, 1971)

Publication costs borne completely by The Journal of Physical Chemistry

The cation- and anion-constituent transference numbers of potassium chloride in ethylene glycol at 25° have been measured by the direct moving boundary method at 0.005, 0.01, 0.02 and 0.05 mol l.⁻¹. Small additions of water decreased the anion transference number. The limiting transference numbers were combined with literature conductances to give individual ionic conductances in ethylene glycol. Only that of Bu_4N^+ was found to be in agreement with the Zwanzig (1970) theory of ionic motion.

Introduction

In a previous study¹ we determined transference numbers, and hence individual ionic conductances, in a solvent of particularly high dielectric constant (formamide, $\epsilon = 109.5$). The present work was carried out to provide for the first time accurate transference numbers and ionic conductances in a solvent of very high viscosity. Ethylene glycol was chosen not only because it is suitably viscous ($\eta = 0.1684 \text{ P}$ at 25°)² but also because it possesses a dielectric constant sufficiently large ($40.75^{2,3}$ at 25°) to allow complete dissociation of several dissolved salts such as KCl.

Erdey-Grúz and Majthényi⁴ have reported a series of moving boundary transference numbers at 5° and 25° in ethylene glycol-water mixtures. Their lowest mol % water contents were 0.3 (for KF), 4.1 (for KCl), 0.5 (for HCl), and 0.2 (for KOH). In all cases only one concentration (0.01–0.02 *M*) of leading electrolyte was studied. It was therefore decided to use dry glycol as solvent, as many tests of internal reliability as possible—independence of current and of concentration of following electrolyte, use of both cation and anion boundaries—and to measure transference numbers at several concentrations to permit extrapolation to zero ionic strength. Potassium chloride was selected as the

leading electrolyte, for its conductances in ethylene glycol at 25° have already been accurately determined.²

Experimental Section

Materials. The relative goodness of different methods of purifying a solvent is commonly assessed by the properties of the end-product. For convenience bulk properties such as density and refractive index are normally measured even though these are extremely insensitive to the presence of small quantities of impurities. Freezing points, though better in this respect, cannot be determined very accurately in the case of glycol because of the viscous nature of the solvent and the associated supercooling. It is thus difficult to judge between most of the literature purifications of ethylene glycol. The only really sensitive tests are those that register directly the amount of the impurity. On this criterion the best literature preparation was by Accascina and Petrucci,² who distilled glycol four times at 1

- (1) J. M. Notley and M. Spiro, *J. Phys. Chem.*, **70**, 1502 (1966).
- (2) F. Accascina and S. Petrucci, *Ric. Sci.*, **30**, 808 (1960).
- (3) Interpolated from the data of N. Koizumi and T. Hanai, *J. Phys. Chem.*, **60**, 1496 (1956).
- (4) T. Erdey-Grúz and L. Majthényi, *Acta Chim. Acad. Sci. Hung.*, **20**, 175 (1959).

Torr and obtained a liquid of specific conductivity $2.2\text{--}2.7 \times 10^{-8} \text{ ohm}^{-1} \text{ cm}^{-1}$ and water content 0.3 g l^{-1} . These workers found that chemical treatment with Na_2SO_4 had no effect, although many other groups have employed distillation under reduced pressure with prior, simultaneous, or subsequent treatment with a drying agent such as Na_2SO_4 , CaO , NaOH , or drierite. We therefore carried out further purification experiments and tested the products for the presence of ions by specific conductivity (κ), for water by Karl Fischer titration with dead-stop end point, and for aldehydes by a variety of reagents (*o*-dianisidine, Tollens reagent, bisulfite + iodine,⁵ and sodium iodide⁶).

I.C.I. "S" grade ethylene glycol ($[\text{H}_2\text{O}] = 0.7 \text{ g l}^{-1}$, $\kappa = 7 \times 10^{-8} \text{ ohm}^{-1} \text{ cm}^{-1}$, $\text{fp} = -14^\circ$) served as the starting material. Allowing it to stand over 3A Molecular Sieve reduced the water content appreciably but enormously increased the conductivity. When the crude glycol was distilled at 3–5 Torr under dry oxygen-free nitrogen in an all-glass system with a 30-cm heated spiral-packed column, the middle fraction had a lower water content but the conductivity was unchanged. Distillation after standing over 3A Molecular Sieve, Na_2SO_4 , or CaSO_4 brought about some improvement in both the concentration of water and the conductivity, while the best results were obtained on distilling the solvent over CaSO_4 . This last procedure was accordingly adopted, with 150 g granular B.D.H. CaSO_4 added to 3.5 l. glycol. A calcium test by flame photometry capable of detecting 1 ppm showed that none of the salt had passed over, and all aldehyde tests were negative.

It was found essential to dry the CaSO_4 thoroughly⁷ by loading it into a 1 m long glass column of 5 cm diameter wound round with nichrome resistance wire. The column was heated to at least 360° while the contents were purged for several hours in a stream of very dry nitrogen obtained by electrically heating liquid nitrogen.⁸ The CaSO_4 was then allowed to cool in a desiccator over P_2O_5 . The same treatment was applied to the 3A Molecular Sieve employed for drying the oxygen-free cylinder nitrogen (B.O.C.) used in the glycol distillation. The purified solvent was kept under a dry nitrogen atmosphere and each batch was analyzed for water content and conductivity before use, the mean values being $[\text{H}_2\text{O}] = 0.22 \text{ g l}^{-1}$, $\kappa = 2.3 \times 10^{-8} \text{ ohm}^{-1} \text{ cm}^{-1}$. Its density was 1.1099 g cm^{-3} . No batch was kept longer than three weeks. An experiment showed that 31 g glycol in an open 100 cm^3 beaker absorbed 0.03 g water each hour, and therefore dry (cylinder) nitrogen was used to transfer purified glycol to prepare solutions, and these solutions to fill the cell.

Hopkin and Williams Analar KCl was twice recrystallized from conductivity water, dried first at 60° and then at 120° , and stored in a desiccator over P_2O_5 . Hopkin and Williams Analar BaCl_2 was purified and stored similarly but dried at 150° to remove water of crystallization. Potassium picrate (KPi) had been

prepared by Notley.¹ Eastman Kodak 2,3,5-triiodobenzoic acid (HTB) was purified and converted to the potassium salt (KTB) as described by Davies, Kay, and Gordon.⁹ B.D.H. microscopical reagent sodium fluoresceinate (NaFlu) was precipitated from its saturated aqueous solution by slowly (over 4 days) adding acetone under vigorous stirring. The crystals were dried in vacuum and stored in a brown bottle over silica gel. All solutions were made up at 25° in calibrated Pyrex volumetric flasks.

Apparatus. The experimental technique was similar to that previously employed.¹ Notley's electrical circuit was modified as described by Shamim,¹¹ and a 30 megohm resistor was placed in parallel with the cell when currents less than $30 \mu\text{A}$ were wanted. Details of the rising and falling moving boundary cells and the method of optical observation of the boundary have been published elsewhere.¹¹ The results were independent of whether the main stopcock was lubricated with Apiezon L or silicone grease, although only the latter was used when KPi was the following electrolyte. All experiments were carried out in an oil-filled thermostat at 25° .

Preliminary Experiments. KCl having been chosen as the leading electrolyte, experiments were needed to find suitable following solutions. With silver chloride cathodes and silver anodes, no falling cation boundaries were seen with LiCl, NaCl, or Et_4NCl as following salt and no rising ones with Et_4NCl , ZnCl_2 , CoCl_2 , or MnCl_2 . Rising boundaries that disappeared after a time were produced with CuCl_2 and PbCl_2 . The rising boundary between KCl and CdCl_2 was very weak and none was visible in an autogenic experiment with a cadmium anode; perhaps Erdey-Gruž and Majthényi⁴ had been able to use an autogenic cell with a cadmium anode because their glycol contained more water which helped the dissociation of CdCl_2 . A good rising boundary was formed with BaCl_2 . A series of runs with rising anion systems produced good boundaries when KCl was followed by KTB or by KPi. Two boundaries appeared with NaFlu (unpurified) but only a diffuse transition region with NaFlu (purified) suggesting that an impurity had caused the sharper visual effect, and no boundaries were seen when potassium formate, benzoate, or sulfonate acted as following electrolyte.

The boundary systems selected for quantitative

(5) F. Feigl, "Spot Tests in Organic Analysis," 6th ed, Elsevier, Amsterdam, 1960, pp 130, 213, 225.

(6) R. E. Gibson and J. F. Kincaid, *J. Amer. Chem. Soc.*, **59**, 579 (1937); R. E. Gibson, *ibid.*, **59**, 1521 (1937).

(7) J. M. Notley and M. Spiro, *J. Chem. Soc. B*, 362 (1966).

(8) J. H. Robertson, *J. Sci. Instrum.*, **40**, 506 (1963).

(9) J. A. Davies, R. L. Kay, and A. R. Gordon, *J. Chem. Phys.*, **19**, 749 (1951).

(10) M. Shamim and M. Spiro, *Trans. Faraday Soc.*, **66**, 2863 (1970).

(11) M. Spiro, "Physical Methods of Chemistry, Part IIA: Electrochemical Methods," A. Weissberger and B. W. Rossiter, Ed., Interscience, New York, N. Y., 1971, Chapter 4.

study were $\text{KCl} \leftarrow \text{BaCl}_2$, $\text{KCl} \leftarrow \text{KTB}$, and $\text{KCl} \leftarrow \text{KPi}$.

Determination of Kohlrausch Concentrations. In initial cation experiments with 0.02 *N* KCl, the Kohlrausch concentration of the following BaCl_2 solution had been estimated from aqueous conductances. The resulting potassium transference numbers, at a given current, varied over a range of ± 0.002 . The irreproducibility disappeared when the correct Kohlrausch concentration for glycol solutions, some 25% lower, was used. To measure this Kohlrausch concentration a modified rising boundary cell was constructed with a 6-mm-wide moving boundary tube that was accessible at the upper end to permit sampling. When a $\text{KCl} \leftarrow \text{BaCl}_2$ boundary reached the top of the tube the main stopcock was closed, the stopper above the tube removed, and the KCl solution sucked out with a capillary tube connected to a vacuum pump. The top layer of BaCl_2 solution, possibly by now contaminated with KCl, was similarly removed and discarded. A clean capillary tube was then inserted and a 1 cm^3 sample of BaCl_2 solution taken out for examination. Microgravimetric analysis, kindly carried out by Dr. D. A. Pantony of the Materials Science Analytical Laboratory, led to a BaCl_2 concentration of 0.013 *N*. A subsequent experiment with 0.05 *N* KCl leading showed the BaCl_2 concentration (analyzed by flame photometry) to be 0.033 *N*. The Kohlrausch ratios, 0.65 and 0.66, are in good agreement.

Similar experiments were done for the anion indicators. Here the samples were diluted 100- or 1000-fold using a microsyringe and a volumetric flask, and analyzed spectrophotometrically. The spectrum of KTB possessed a peak at 235 nm where the extinction coefficient was 2.71×10^4 l. equiv⁻¹ cm^{-1} . With a leading solution of 0.02 *N* KCl the adjusted KTB concentration was found to be 0.0066 *N* (independent of the initial KTB concentration); with 0.005 *N* KCl it was 0.0016 *N*.

The two Kohlrausch ratios of 0.33 and 0.32 are again very close. In the case of KPi the absorption spectrum displayed a maximum at 360 nm where the extinction coefficient was 1.64×10^4 l. equiv⁻¹ cm^{-1} . Leading solutions of 0.02 *N* and 0.005 *N* KCl were found to be followed by 0.0108 *N* and 0.0028 *N* KPi, respectively, and once more the Kohlrausch ratios of 0.54 and 0.56 agree well.

Volume Correction. In all cation runs the closed electrode was a silver-silver chloride cathode, with an open silver anode. The volume increased per faraday between the cathode and a point in the leading KCl solution which the boundary does not pass is then

$$\Delta V_1 = V_{\text{Ag}} - V_{\text{AgCl}} + T_{\text{K}}^{\text{KCl}} \bar{V}_{\text{KCl}}$$

The anion runs were carried out with an open silver or platinum cathode and a closed silver anode. To con-

firm that one was justified in writing the appropriate volume increase per faraday as

$$\Delta V_2 = V_{\text{AgCl}} - V_{\text{Ag}} - T_{\text{K}}^{\text{KCl}} \bar{V}_{\text{KCl}}$$

two tests were carried out on the anode process. First, had any glycol been electrochemically oxidized, acid would have been generated. Analyses of the anolyte solution before and after electrolysis proved the extent of any such reaction to be less than 0.1%. Second, an auxiliary experiment with a silver anode in 0.035 *N* KCl solution in glycol, in an H-shaped cell, showed that the electrode weighed 6.3 mg more after the passage of 16.2 C while the theoretically expected increase due to AgCl formation was 6.0 mg. The agreement is satisfactory.

Apparent molar volumes of several salts have been determined⁶ in ethylene glycol but not that of KCl. The densities of KCl solutions at several molalities (*m*) between 0.18 and 0.65 mol (kg of glycol)⁻¹ were accordingly measured, and the apparent molar volumes fitted the equation

$$\phi/\text{cm}^3 \text{ mol}^{-1} = 31.8 + 1.5\sqrt{m}$$

For 0.05 *N* KCl, $\bar{V}_{\text{KCl}} = 32.0 \text{ cm}^3 \text{ mol}^{-1}$. Hence, from the known molar volumes of Ag and AgCl , and the transference numbers in Table I

Table I: Summary of Cation Transference Measurements on KCl in Ethylene Glycol at 25°

<i>N</i>		Current μA	T_{K}		
c_{KCl}	$10^3 c_{\text{BaCl}_2}$		Mean	Zero water	Best
0.0100	6.5-6.7	50	0.4756	0.4755	0.4758
0.0200	11.7-13.6	87-124	0.4756	0.4755	0.4755
0.0500	33.2-34.8	202-327	0.4759	0.4758	0.4753

$$\Delta V_2 = -\Delta V_1 = 0.3 \text{ cm}^3 \text{ mol}^{-1}$$

The volume correction $c_{\text{KCl}}\Delta V$ is therefore negligibly small even at the highest concentration employed.

Results

Tables I and II summarize the results of 34 transference runs. The transference numbers were all independent of the concentration of the following electrolyte within the range employed. The choice of currents was restricted by poor visibility at low currents (the cation boundary was invisible for 0.005 *N* KCl and faint for 0.01 *N* KCl) and by joule heating at high ones where the boundaries became curved. The cation transference numbers were independent of current while the anion ones showed a very slight tendency to fall at greater currents. The "mean" values of T_{Cl} have therefore been biased in favor of the low current values, affecting the fourth decimal place by less than 1 on the average. At any given

concentration, the average deviation of the cation or anion results from the mean was ± 0.00015 . The solvent correction has been applied to all "mean" transference numbers.

Table II: Summary of Anion Transference Measurements on KCl in Ethylene Glycol at 25°

N		Current μA	T_{Cl}		
c_{KCl}	$10^3 c_{\text{KTB}}$		Mean	Zero water	Best
0.0050	1.7-1.8	19-34	0.5236	0.5237	0.5440
0.0100	3.2-3.4	32-52	0.5238	0.5239	0.5242
0.0200	6.5-9.8	73-123	0.5245	0.5246	0.5245
0.0500	17.1	52-320	0.5252	0.5253	0.5247

A series of experiments was carried out with 0.02 N KCl solutions to discover the effect of small quantities of water in the solvent. Both leading and following solutions were made up in the same water-containing glycol. The results are summarized in Table III and plotted in Figure 1. On the basis of these measurements the "mean" transference numbers (column 4 in Tables I and II), which were determined in glycol containing 0.012 mol l.⁻¹ of water, have been extrapolated to zero water content (column 5 of Tables I and II). Two anion runs were also done with 0.02 mol KCl dissolved directly in a liter of glycol as supplied by the manufacturers (I.C.I. Ltd., $[\text{H}_2\text{O}] = 0.04$ mol l.⁻¹). The chloride transference number was 0.5246, only 0.0003 higher than the value expected from purified glycol of the same water content. It seems ironic that distillation of the solvent affected the results so little.

Table III: Effect of the Addition of Water on Transference Numbers in 0.02 N KCl Solution

$[\text{H}_2\text{O}]$, mol l. ⁻¹	T_{K}^a	T_{Cl}^b
0.01	0.4756	0.5245
0.22		0.5233
0.48	0.4775	
0.76		0.5211
1.00	0.4794	0.5209

^a With 0.0135 N BaCl₂ solution following, at 121-122 μA .

^b With 0.0074 N KTB solution following, at 119-124 μA .

The independently measured cation and anion transference numbers, at zero water content, add up to 0.9994 (0.01 N KCl), 1.0001 (0.02 N KCl), and 1.0011 (0.05 N KCl). This provides a good check on the reliability of the results. "Best" transference numbers have been obtained by dividing the experimental figures by $(T_{\text{K}} + T_{\text{Cl}})$, and have been listed in the 6th column of Tables I and II. We estimate their un-

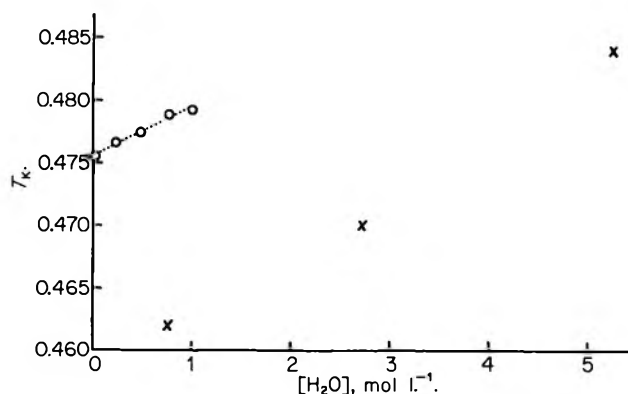


Figure 1. Variation of cation-constituent transference number in 0.02 N glycolic KCl solution with concentration of added water: O, present work; X, ref. 4.

certainties as less than $\pm 0.1\%$ and probably less than $\pm 0.05\%$.

A set of anion boundary runs was also carried out with KPi as following electrolyte. The solutions around the open platinum cathode always turned red, perhaps due to the formation of picramate or a Meisenheimer complex, but the compound did not come near the boundary region. Superficially the KCl \leftarrow KPi results seemed satisfactory, being reproducible, independent of initial indicator concentration over a 10% range, and only slightly dependent on current. The variation with water content was much the same as in Table III. The "mean" chloride transference numbers in purified glycol were 0.5284 (0.005 N KCl), 0.5264 (0.01 N KCl), 0.5274 (0.02 N KCl), and 0.5277 (0.0348 N KCl; the limited solubility of KPi in glycol made it impossible to study higher KCl concentrations). These figures, on average, are more than 0.003 higher than those obtained with KTB as following electrolyte (Table II). Moreover, addition of the picrate data and the cation transference numbers in Table I gives $(T_{\text{K}} + T_{\text{Cl}})$ values of ca. 1.003, considerably greater than the theoretical value of unity. These external criteria apart, there is a suspicious aspect within the KCl \leftarrow KPi transference numbers themselves: the value for 0.005 N KCl floats ca. 0.003 above the T_{Cl} vs. \sqrt{c} line on which the other picrate data lie. For these reasons the results obtained with KPi as boundary indicator have been rejected. Other examples of such deviant behavior are not unknown,¹² and they underline the necessity of employing every possible means of testing the reliability of transference measurements. The moving boundary method is particularly well suited for a large number of checks and cross-checks. It should be added that 3 runs with 0.02 N KCl \leftarrow 0.012 N KPi in water gave $T_{\text{Cl}} = 0.5100$, in excellent agreement with the literature values of 0.5099-0.5101.^{13,14}

(12) G. S. Kell, private communication (1961), found the hydrogen transference number of HCl in water to be 0.0025 higher with BaCl₂ following than with KCl.

Discussion

Comparison with Previous Results. The results in Tables I and II, and those of Erdey-Grúz and Majthényi,⁴ are plotted in Figure 1. The variation of transference number with water content is seen to be very similar but the transference numbers themselves are almost 4% apart. It is difficult to account for such a large difference. Erdey-Grúz and Majthényi estimate their experimental uncertainty as *ca.* $\pm 1\%$, and although they applied no solvent or volume correction these should be small for 0.02 *N* KCl. Doubts must therefore be raised about the autogenic boundaries they formed with a cadmium anode. The use of such boundaries involves the assumption that the following electrolyte automatically adjusts itself to the Kohlrausch concentration behind the boundary, and since CdCl₂ is likely to be a weak electrolyte in glycol (K_{diss} for PbCl₂ in glycol¹⁵ is 0.0026 mol l.⁻¹), joule heating may have disturbed the normal process of adjustment. This problem disappears with sheared boundaries. Here the initial concentration of following electrolyte can be varied at will, and the electrode itself—and the layers of concentrated solution above it—can be positioned sufficiently far from the moving boundary to avoid the danger of convective mixing.

Variation with Concentration. The "best" T_K values, plotted against \sqrt{c} , fall on a curve that approaches the Debye-Hückel-Onsager limiting slope from above and begins to merge with it at very low concentrations. A graph of the Longworth function¹³

$$T_{K^0}' = \frac{T_K \Lambda' + \beta \sqrt{c}}{\Lambda' + 2\beta \sqrt{c}} \quad (1)$$

where

$$\Lambda' = \Lambda^0 - (\alpha \Lambda^0 + 2\beta) \sqrt{c}$$

and $\alpha = 0.612$, $2\beta = 4.44$, $\Lambda^0 = 9.693^2$, is shown in Figure 2 to be linear in normality c . The limiting potassium transference number T_{K^0} is thus 0.47665 and the Longworth slope 0.031 l. equiv⁻¹. The Stokes¹⁶ and Kay and Dye¹⁷ equation

$$T_K = T_{K^0} + \frac{2(T_K - 0.5)\beta \sqrt{c}}{\Lambda^0(1 + \kappa a)} \quad (2)$$

where $\kappa = 0.456 \sqrt{c}$, fits the experimental data best with $a = 9 \pm 1 \text{ \AA}$. At this distance of closest approach T_{K^0} is constant, and equals 0.4766. On the other hand, the conductances of KCl in glycol require² an a value of 3.78 \AA , a figure much lower and more physically reasonable than 9 \AA . Such a result is not unexpected, for a recent critical analysis¹⁸ has shown equation 2 to be unsatisfactory for most transference number data in nonaqueous solutions.

Limiting Electrolyte Conductances. Extensive conductance measurements in ethylene glycol over a range of (low) concentrations have been carried out by two

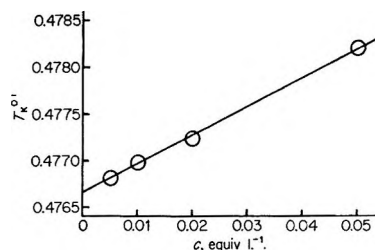


Figure 2. Plot of Longworth function T_{K^0}' vs. normality of KCl.

groups of workers, both of whom analyzed the data by the Onsager-Fuoss equation¹⁹

$$\Lambda = \Lambda^0 - (\alpha \Lambda^0 + 2\beta) \sqrt{\gamma c} + E \gamma c \log \gamma c + J \gamma c - K_A \gamma c f_{\pm}^2 \Lambda \quad (3)$$

Λ , as before, stands for equivalent conductance and c for normality, γ is the degree of dissociation, K_A the association constant, and f_{\pm} the mean ionic activity coefficient. The other symbols represent parameters of the theory.¹⁹ Accascina and his school have in this way provided limiting equivalent conductances (in cm² ohm⁻¹ equiv⁻¹) for LiCl²⁰ (7.185), NaCl²¹ (8.18), KCl² (9.693), NaBr²² (8.087), Et₄NPI²³ (4.41), and Bu₄NBr²⁴ (6.496). Only the last two compounds showed some association. No association at all was discovered by DeSieno, *et al.*,²⁵ who recently determined the conductances of tetramethyl, tetraethyl, tetrapropyl, and tetrabutyl bromides and iodides. The results are internally consistent with the exception of Bu₄NI whose conductance appears to be too low by 0.05. The limiting conductance of the only compound of overlap, Bu₄NBr, is 6.489, in good agreement with D'Aprano's value²⁴ of 6.496, which had been obtained by eq 3 with a small viscosity term. It should be mentioned that the glycol in the later study²⁵ possessed a viscosity 4% lower than that generally accepted; this affects the extrapolation slightly (as does the choice of a lower dielectric constant) and suggests that some

(13) L. G. Longworth, *J. Amer. Chem. Soc.*, **54**, 2741 (1932).

(14) R. W. Allgood, D. J. Le Roy, and A. R. Gordon, *J. Chem. Phys.*, **8**, 418 (1940).

(15) J. C. James, *J. Amer. Chem. Soc.*, **71**, 3243 (1949).

(16) R. H. Stokes, *ibid.*, **76**, 1988 (1954).

(17) R. L. Kay and J. L. Dye, *Proc. Natl. Acad. Sci. U. S.*, **49**, 5 (1963).

(18) M. Spiro, "Physical Chemistry of Organic Solvent Systems," A. K. Covington and T. Dickinson, Ed., Plenum Press, London, 1972, Chapter 5.

(19) R. M. Fuoss and F. Accascina, "Electrolytic Conductance," Interscience, New York, N. Y., 1959, p 195.

(20) F. Accascina and M. Goffredi, *Ric. Sci.*, **37**, 1126 (1967).

(21) F. Accascina, A. D'Aprano, and M. Goffredi, *ibid.*, **34**, 151 (1964).

(22) F. Accascina and A. D'Aprano, *ibid.*, **36**, 257 (1966).

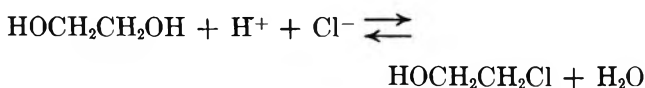
(23) F. Accascina and S. Petrucci, *ibid.*, **30**, 1164 (1960).

(24) A. D'Aprano and R. Triolo, *ibid.*, **34**, 443 (1964).

(25) R. P. DeSieno, P. W. Greco, and R. C. Mamajek, *J. Phys. Chem.*, **75**, 1722 (1971).

water may have been introduced into the solvent from the ion-exchange column that was employed.²⁵

Several other studies contain useful information. The conductances of four electrolytes over a range of glycol-water mixtures have been graphically reported²⁶ and discussed,²⁷ and Erdey-Grúz has kindly sent us²⁸ the detailed results. For 0.01 *N* solutions in glycol the equivalent conductances of KCl and KF were found to be 8.66 and 7.06 cm² ohm⁻¹ equiv⁻¹, respectively, and the figures extrapolated to dry glycol from conductances in several mixtures containing less than 1% water are 30.4 for HCl and 13.65 for KOH. By use of eq 3 with $\alpha = 4 \text{ \AA}$, we calculate the limiting conductances to be KCl 9.59, KF 7.88, HCl 32.8, and KOH 14.91. The physical significance of the KOH result is discussed later. The value for KCl is 1% smaller than Accascina and Petrucci's.² A still lower limiting conductance for KCl of 8.75 is obtained when eq 3 with $\alpha = 4 \text{ \AA}$ is applied to Kirby and Maass'²⁹ conductance at 0.05 *N*; at this concentration, however, eq 3 may no longer be exact. Their HCl figure²⁹ at 0.05 *N*, treated similarly, yields $\Lambda^\circ = 22.1$, a result so low that it suggests either the presence of water in the solvent or a chemical reaction such as



Kirby and Maass' limiting conductances for HNO₃ (29.8), KNO₃ (9.6), and NaNO₃ (7.6) (derived by simple Λ vs. \sqrt{c} extrapolations whose slopes indicate some association in the case of nitric acid) lead to Λ° (HCl) = 30.2 when combined with the alkali chloride data above. This result agrees better with that of Erdey-Grúz²⁸ than the one they obtained directly. Grave doubts must be expressed about a recent Russian paper³⁰ whose HCl conductances in glycol rise with increasing concentration and which give an extremely low limiting conductance of 16. It was claimed, moreover, that the addition of water to 1×10^{-4} *N* glycolic HCl solutions increases the equivalent conductance, in complete contradiction to all previous information.^{26, 27}

The Shedlovsky extrapolation³¹ has been used in the literature to obtain the limiting conductances in glycol of AgNO₃³² (9.14) and AgNO₂³³ (9.04), and by M. Carmo Santos³⁴ to treat published data for AgNO₃³⁵ and TlCl³⁶ to give 9.93 and 10.38 cm² ohm⁻¹ equiv⁻¹, respectively. The two silver nitrate results differ by 8%, and we shall choose the more recent value.³² A figure for PbCl₂ (7.73) was determined³⁷ from a simple phoreogram. In the case of barium and nickel perchlorates,³⁸ plots of Λ vs. \sqrt{c} were curved and extrapolation to zero concentration gave negative and thus physically meaningless intercepts. James³⁹ has obtained the limiting conductances of zinc sulfate, zinc malonate, and lanthanum ferricyanide in several water-

glycol mixtures but not in pure glycol, and an empirical method of estimating the conductances in 100% glycol has been described.³⁴

Limiting Ionic Conductances. Combination of the limiting KCl transference number with the literature conductances allows us to construct Table IV in which limiting individual ionic conductances are listed in cm² (int. ohm)⁻¹ equiv⁻¹. The accuracy of the figures relies largely on that of the electrolyte conductances involved. The conductance of the NO₃⁻ ion, in particular, depends upon whether the data for KNO₃ or NaNO₃ are employed (HNO₃ gives quite a different answer), and an uncertainty of ca. ± 0.3 must be assigned to it and to the derived conductances of Ag⁺ and NO₂⁻.

Table IV: Limiting Ionic Equivalent Conductances in Ethylene Glycol at 25°

Cation	λ_+°	Anion	λ_-°
H ⁺	27.7	OH ^{-a}	10.3
Li ⁺	2.112	F ⁻	3.26
Na ⁺	3.107	Cl ⁻	5.073
K ⁺	4.620	Br ⁻	4.980
Ag ⁺	4.4	I ⁻	4.608
Tl ⁺	5.31	NO ₃ ⁻	4.7
Me ₄ N ⁺	2.973	NO ₂ ⁻	4.6
Et ₄ N ⁺	2.197	Pi ⁻	2.213
Pr ₄ N ⁺	1.737		
Bu ₄ N ⁺	1.513		
Pb ²⁺	2.66		

^a See text for species actually involved.

Approximate limiting conductances for certain ions can be deduced from two other sources of transference data. These were all converted to limiting transference numbers by means of eq 2 with $\alpha = 4 \text{ \AA}$, and combined with the limiting conductance of either Cl⁻ or K⁺, as appropriate, from Table IV. First, the transfer-

(26) T. Erdey-Grúz, E. Kugler, and J. Hidvégi, *Acta Chim. Acad. Sci. Hung.*, **19**, 363 (1959).

(27) T. Erdey-Grúz, E. Kugler, and L. Majthényi, *Electrochim. Acta*, **13**, 947 (1968).

(28) T. Erdey-Grúz, private communication (1969).

(29) P. Kirby and O. Maass, *Can. J. Chem.*, **36**, 456 (1958).

(30) V. I. Vigdorovich and I. T. Pchelnikov, *Elektrokhimiya*, **5**, 710 (1969).

(31) T. Shedlovsky, *J. Franklin Inst.*, **225**, 739 (1938).

(32) V. S. Griffiths and K. S. Lawrence, *J. Chem. Soc.*, **473** (1956).

(33) V. S. Griffiths and M. L. Pearce, *ibid.*, **3243** (1957).

(34) M. Carmo Santos, *Rev. Port. Quím.*, **11**, 50 (1969).

(35) R. Müller, V. Raschka, and M. Wittmann, *Monatsh.*, **48**, 659 (1927).

(36) A. B. Garrett and S. J. Vellenga, *J. Amer. Chem. Soc.*, **67**, 225 (1945).

(37) J. W. Norman and A. B. Garrett, *ibid.*, **69**, 110 (1947).

(38) A. L. Chaney and C. A. Mann, *J. Phys. Chem.*, **35**, 2289 (1931).

(39) J. C. James, *J. Chem. Soc.*, 1094 (1950); *ibid.*, 153 (1951).

ence results of Erdey-Grúz and Majthényi⁴, extrapolated as well as possible to zero water content, yield 34 cm² ohm⁻¹ equiv⁻¹ for H⁺, 9.8 for OH⁻, and 3.7 for F⁻. The first two figures are rather sensitive to experimental error; for example, the 1% uncertainty mentioned by the authors⁴ in the cation transference number of HCl affects $\lambda_{\text{H}^+}^0$ by ± 2.6 . Second, the Kohlrausch ratios measured in the present work lead directly to the transference numbers of the adjusted indicator solutions, which in turn give limiting ionic conductances of 2.5 for Ba²⁺, 2.0 for Pi⁻, and 1.1 for TB⁻. In both cases the agreement with comparable figures in Table IV is fair if a reasonably generous allowance is made for experimental uncertainties.

Limiting ionic conductances can also, at least in principle, be arrived at *via* trace diffusion coefficients. That of Na⁺ in 0.1 *m* NaCl has been determined⁴⁰ in ethylene glycol at 25° and found to be 0.82×10^{-6} cm² sec⁻¹. Unfortunately the concentration is too high to permit a reliable extrapolation to zero ionic strength. If nevertheless one does apply the Onsager limiting equation for self-diffusion,⁴⁰ together with the known limiting conductance²¹ of NaCl, one obtains by successive approximations $D_{\text{Na}^+}^0 = 1.02 \times 10^{-6}$ cm² sec⁻¹ and thus, *via* Nernst's relation, $\lambda_{\text{Na}^+}^0 = 3.84$ cm² ohm⁻¹ equiv⁻¹. Not even the 5% uncertainty in the measured diffusion coefficient can cover the discrepancy between this result and that in Table IV. Reversing the procedure, however, and using the sodium conductance in the table, gives $D_{\text{Na}^+}^0 = 0.827 \times 10^{-6}$ cm² sec⁻¹. This is not an unreasonable result by comparison with the situation in aqueous,^{41a} aqueous methanolic,⁴² and ethanolic⁴² solutions where trace diffusion coefficients at an ionic strength of 0.1 are only a few units per cent less than the limiting values, and it would appear that glycol fits into the same pattern.

As in other alcoholic media,⁴³ ionic conductances increase in the order Li⁺ < Na⁺ < K⁺ because the smaller the bare ion, the more heavily solvated it is and the more resistance it offers to ionic migration. The same is true for F⁻ < Cl⁻. This picture breaks down, however, when the bare ion is large, and in the halide series the mobility passes through a maximum at Cl⁻. Despite a regular conductance rise of Cl⁻ < Br⁻ < I⁻ in most alcoholic solvents,^{43,44} a maximum conductance also exists (at Br⁻) in water^{41b} and in formamide.^{1,46} In these two solvents,^{41c,1} as in glycol,⁴⁶ there is evidence from viscosities that the higher halide ions produce structure-breaking. Our knowledge is not yet adequate to explain these features quantitatively.

Ions of sufficiently large size approximate to the hydrodynamic sphere-in-continuum model, and the tetraalkylammonium ions offer some scope for testing various theoretical relationships. The simplest is Stokes' law

$$\lambda_i^0 \eta = |z_i| eF / A_v \pi r_i \quad (4)$$

where $z_i e$ is the charge of the ion and r_i its radius, F is Faraday's constant, and the parameter A_v is 6 if the liquid adjacent to the interface "wets" the ion and moves with it (perfect sticking) and 4 if there is perfect slipping of solvent at the surface of the ion. It follows that if the ion is large enough not to be appreciably solvated, r_i equals the radius of the bare ion and then

$$\lambda_i^0 \eta = \text{constant} \quad (5)$$

which is Walden's rule. In practice even ions of the size of Bu₄N⁺ do not obey this equation. There is a tendency for the $\lambda_i^0 \eta$ product to increase with increasing viscosity, but an empirical linear relationship

$$\lambda_i^0 \eta = a + b\eta \quad (6)$$

recently proposed⁴⁷ is not confirmed by the results in Table V. In particular, extrapolation of the straight line for Bu₄N⁺ in Figure 1 of ref 47 to the viscosity of ethylene glycol predicts 0.328 as the Walden product: the measured value is 0.255, lower even than that for the solvent of next lowest viscosity (sulfolane).

Table V: Tests of Theoretical Relationships

Ion, i	$r_i, \text{\AA}^a$	λ_i^0 (Zwanzig) ^b		Exptl ^b	
		Stick	Slip	λ_i^0	$\lambda_i^0 \eta$
Li ⁺	0.60	0.32	0.16	2.11	0.356
Na ⁺	0.95	1.04	0.60	3.11	0.523
K ⁺	1.33	1.81	1.35	4.62	0.778
Cl ⁻	1.81	2.07	2.13	5.07	0.854
Me ₄ N ⁺	3.47	1.37	1.98	2.97	0.501
Et ₄ N ⁺	4.00	1.20	1.76	2.20	0.370
Pr ₄ N ⁺	4.52	1.07	1.58	1.74	0.293
Bu ₄ N ⁺	4.94	0.98	1.46	1.51	0.255

^a From ref 41, pp 125-126, 461. Later X-ray work by B. S. Gourary and F. J. Adrian, *Solid State Phys.*, **10**, 127 (1960), gives the following, rather different, radii: Li⁺, 0.94; Na⁺, 1.17; K⁺, 1.49; Cl⁻, 1.64; so that the conductance values calculated for Na⁺ could more fittingly apply to Li⁺. However, more recent work still suggests that even these radii require modification (V. Meisalo and O. Inkinen, *Acta Crystallogr.*, **22**, 58 (1967)).
^b Ionic conductances are in cm² ohm⁻¹ equiv⁻¹, viscosities in poise.

(40) A. E. Marcinkowsky, H. O. Phillips, and K. A. Kraus, *J. Phys. Chem.*, **72**, 1201 (1968).

(41) (a) R. A. Robinson and R. H. Stokes, "Electrolyte Solutions," 2nd ed, Butterworths, London, 1959, p 317; (b) pp 463, 465; (c) pp 304, 516.

(42) P. C. Carman, *J. Phys. Chem.*, **73**, 1095 (1969).

(43) Reference 18, Appendix Tables 5.7-5.9.

(44) D. F. Evans and P. Gardam, *J. Phys. Chem.*, **72**, 3281 (1968); *ibid.*, **73**, 158 (1969); M. A. Matesich, J. A. Nadas, and D. F. Evans, *ibid.*, **74**, 4568 (1970).

(45) J. Thomas and D. F. Evans, *J. Phys. Chem.*, **74**, 3812 (1970).

(46) K. Crickard and J. F. Skinner, *ibid.*, **73**, 2060 (1969).

(47) M. Della Monica and L. Senatore, *ibid.*, **74**, 205 (1970).

A more sophisticated treatment has recently been published by Zwanzig.⁴⁸ In a revision of his earlier theory⁴⁹ on the effect of dielectric as well as viscous friction on the motion of an ion, he derived the equation

$$\lambda_i^0 \eta = |z_i| eF / (A_v \pi r_i + A_D z_i^2 P^* r_i^{-3}) \quad (7)$$

where the parameter A_D equals 0.375 for perfect sticking and 0.75 for perfect slipping. The symbol P^* stands for

$$P^* \equiv \frac{e^2(\epsilon_0 - \epsilon_\infty) \tau}{\epsilon_0(2\epsilon_0 + 1) \eta}$$

in which ϵ_0 and ϵ_∞ are the static (low frequency) and optical (limiting high frequency) dielectric constants, respectively, and τ the dielectric relaxation time. Fernández-Prini and Atkinson⁵⁰ have examined how well this theory applies to a variety of ions in a range of solvents. Their calculations show that eq 7, with perfect slipping, is fairly successful for R_4N^+ ions in aprotic solvents and in protic solvents in which P^* is small (water, formamide) but that the agreement with experiment is poor for other solvents and especially for small alkali metal cations. Dielectric saturation of the solvent around the ion was suggested⁵⁰ as a likely reason. At the time no accurate data were available for a solvent of really high viscosity, and it is therefore of interest to see how well eq 7 fits the conductances in ethylene glycol.

From dielectric tabulations in the literature⁵¹ we find that for glycol at 25° $\epsilon_\infty = 5.48$ and $\tau = 11.1 \times 10^{-11}$ sec so that $P^* = 1.60 \times 10^{-30}$ cm⁴, a value not much bigger than that for water or formamide and smaller by more than an order of magnitude than those in methanol and the higher alcohols. The ionic conductances calculated by eq 7 are contrasted with the experimental results in Table V. With conditions of slip the agreement is good for the largest tetraalkylammonium ions but deteriorates rapidly as the ions become smaller. For the alkali metal ions the disagreement is less bad for "stick" than for "slip," not an unreasonable result in view of the likelihood of strong solvation. On the whole, therefore, ethylene glycol fits the pattern found for the other solvents examined,⁵⁰ being similar in behavior to formamide. It should be emphasized that the theory holds good under just those conditions (large r_i , small P^*) in which eq 7 approximates closely to eq 4 with slip, *i.e.*, to one form of Stokes' law. As soon as dielectric friction becomes comparable with viscous friction there is no longer any satisfactory concordance between theory and experiment.

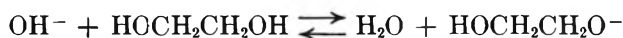
Another way of testing the Zwanzig theory is by the corollary that a plot of λ_i^0 vs. r_i must pass through a maximum,⁵² at a point

$$(\lambda_i^0)_{\max} = \frac{(27)^{1/4} |z_i| eF}{4\eta(z_i^2 A_D P^*)^{1/4} (\pi A_v)^{3/4}};$$

$$(r_i)_{\max}^4 = z_i^2 P^* \left(\frac{3A_D}{\pi A_v} \right)$$

In ethylene glycol, for univalent ions, these coordinates are $\lambda_{\max}^0 = 2.077$ cm² ohm⁻¹ equiv⁻¹ at $r_{\max} = 1.758 \text{ \AA}$ in the case of sticking and $\lambda_{\max}^0 = 2.367$ at $r_{\max} = 2.314 \text{ \AA}$ for the slip condition. It is evident by inspection of Table IV that numerous ions exist of conductance greater than that predicted by the theory.

One ion of exceptionally high conductance is H^+ , and its ability to outrun other cations in certain protic solvents as a result of proton-jumping is well known.⁵³ The reason for the decrease in proton-jumping on the addition of water has been discussed by several workers.^{26, 27, 54} The significance of the high OH^- mobility is difficult to assess in view of the possible reaction



An estimate of its equilibrium constant K can be made by writing

$$K = K_{EG} / K_{HOH}$$

The autoprotolysis constant⁵⁵ of ethylene glycol (1.445×10^{-16} mol² kg⁻²) divided by the molality of the solvent itself (15.11) gives $K_{EG} = 8.97 \times 10^{-18}$ mol kg⁻¹. A rough approximation to K_{HOH} in glycol of dielectric constant 40.75 may be obtained from data in 45 wt % dioxane-water at 25° whose dielectric constant is 38.48.⁵⁶ Here the autoprotolysis constant of water is⁵⁷ 1.809×10^{-16} mol² kg⁻² and its molality 3.053 mol (kg total solvent)⁻¹, so that $K_{HOH} = 5.93 \times 10^{-17}$. Thus $K \approx 0.15$. Crude as this estimate is, it does suggest that in dilute hydroxide solutions in ethylene glycol the equilibrium lies far over to the right. If this is so, the high conductance of OH^- in Table IV should more properly be attributed to the $HOCH_2CH_2O^-$ ion, a result of some interest since the solvate ions in methanol and ethanol show little sign of pro-

(48) R. Zwanzig, *J. Chem. Phys.*, **52**, 3625 (1970).

(49) R. Zwanzig, *ibid.*, **38**, 1603 (1963).

(50) R. Fernández-Prini and G. Atkinson, *J. Phys. Chem.*, **75**, 239 (1971).

(51) F. Buckley and A. A. Maryott, *Nat. Bur. Std. Circ.*, **589** (1958).

(52) H. S. Frank, "Chemical Physics of Ionic Solutions," B. E. Conway and R. G. Barradas, Ed., Wiley, New York, N. Y., 1966, Chapter 4.

(53) B. E. Conway, "Some Aspects of the Thermodynamic and Transport Behavior of Electrolytes," "Physical Chemistry: An Advanced Treatise," Vol. IX A, H. Eyring, Ed., Academic Press, New York, N. Y., 1970, Chapter 1.

(54) R. W. Gurney, "Ionic Processes in Solution," McGraw-Hill, New York, N. Y., 1953, Chapter 4.

(55) K. K. Kundu, P. K. Chattopadhyay, D. Jana, and M. N. Das, *J. Phys. Chem.*, **74**, 2633 (1970).

(56) H. S. Harned and B. B. Owen, "The Physical Chemistry of Electrolytic Solutions," 3rd ed, Reinhold, New York, N. Y., 1958, p 713.

(57) H. S. Harned and L. D. Fallon, *J. Amer. Chem. Soc.*, **61**, 2374 (1939).

ton jumping.¹⁸ A direct determination of the limiting conductance of a salt of ethylene glycol in the dry solvent would resolve any uncertainty.

A useful application of ionic conductances is to help select an electrolyte for salt bridges in emf work. One criterion is that the cation and anion of the salt be equimobile, and inspection of Table IV shows that in glycol NaF, TiCl₄, KI, KNO₃, and Et₄N⁺PI⁻ closely meet this requirement. Which of these electrolytes is the

most suitable will depend upon the second criterion of high solubility, and at present insufficient solubility data are available for a decision to be made.

Acknowledgments. We thank Núcleo de Química-Física (Comissão de Estudos da Energia Nuclear-I.A.C.), Lisbon, for leave of absence granted to M.C.S., N.A.T.O. for the award of a Fellowship, and the Wellcome Foundation for a grant.

A Further Description of Complete Equilibrium Constants¹

by William L. Marshall

Reactor Chemistry Division, Oak Ridge National Laboratory, Oak Ridge, Tennessee 37830 (Received November 25, 1970)

Publication costs assisted by the Oak Ridge National Laboratory, U. S. Atomic Energy Commission

A complete equilibrium constant (K^0), in which solvent species are included to reduce the number of parameters needed for describing solute ionization equilibria, is derived from a multistep solvation treatment of a conventional ionization constant (K). The previously assumed net change (k) in the number of solvent molecules in the reaction process is shown to have this mathematical form for both single and multiple solvent systems. The usefulness of K^0 and k originates from their experimental, isothermal constancy over wide ranges of solvent concentration (varied by pressure or inert diluent, where the solute concentration always approaches zero). In the present derivation, both are shown not to be exactly constant. Therefore, the experimental invariance of K^0 and k is proposed to result from only a very few solvated species of major concentration for each class of solute species, and thus the usefulness of the concept is unhindered. No additional parameters are needed for application. The use of fugacity of the solvent and the Gibbs-Duhem relation are considered in connection with this description. In an example of application, the aqueous ionization behavior of MgSO₄ is predicted both in dioxane-water solvents at saturation vapor pressure and in water to 2000 bars by combining solvent separated ion-pair theory (five constants required) with the complete constant approach, using results in water at saturation vapor pressure only. Reasonable agreement with experiment is observed, although better agreement is obtained by applying just a complete constant concept, which requires only the two constants, K^0 and k .

Introduction

A complete equilibrium constant (K^0) describing electrolyte equilibria in solvent media under isothermal conditions may be given by

$$K^0 = \frac{a_M + a_A^-}{a_{MA} a_{H_2O}^k} = \frac{K}{a_{H_2O}^k} \quad (1)$$

where a (activity) is taken to be in units of moles per liter for both solute and solvent species, all species are in solution, K is the conventional ionization constant, and k represents the net change in solvation numbers between the product and reactant solute species in the reaction process.²⁻⁴ When the solute and solvent are in reference states of infinite dilution for solute and of pure substance (or solvent mixture) for solvent, the activity coefficients (γ) of solute and solvent species are unity by definition. Under this restriction, $a =$

$\gamma C = C$ where $C =$ concentration (moles per liter), and eq 1 can be written

$$\log K = \log K^0 + k \log C_{H_2O} \quad (2)$$

$C(\text{solute}) \rightarrow 0$

The concentration of reactive solvent (C_{H_2O}) may be changed either by varying the hydrostatic pressure on the system or by diluting with a solvent assumed to be inert. In the treatment, it follows that only absolute concentration is applicable, for example, moles

(1) Work sponsored by the U. S. Atomic Energy Commission under contract with the Union Carbide Corporation. Presented before the Division of Physical Chemistry at the 160th National Meeting of the American Chemical Society, Chicago, Ill., Sept. 13-18, 1970.

(2) W. L. Marshall and A. S. Quist, *Proc. Nat. Acad. Sci., U. S.*, **58**, 901 (1967).

(3) A. S. Quist and W. L. Marshall, *J. Phys. Chem.*, **72**, 1536 (1968).

(4) W. L. Marshall, *ibid.*, **74**, 346 (1970).

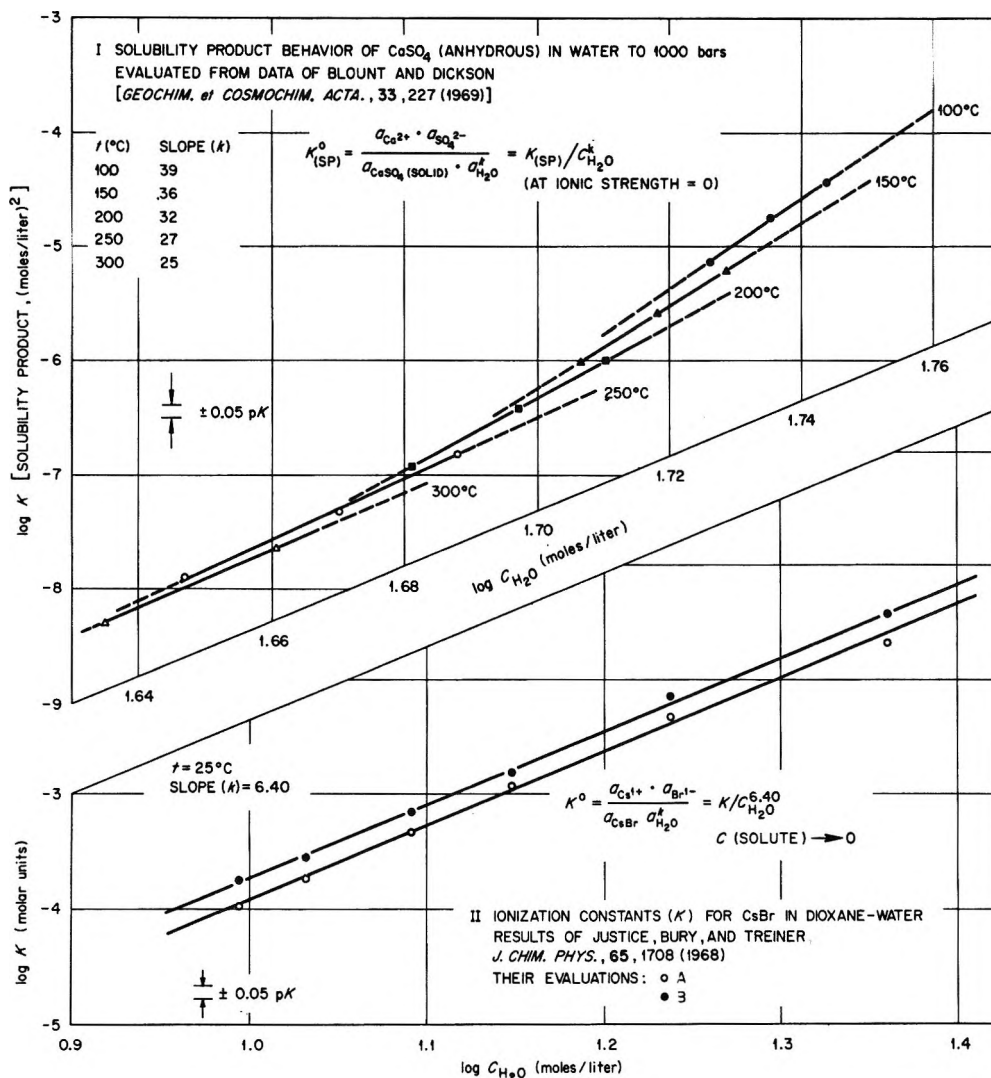


Figure 1. Recent examples of adherence to complete constant concept: I, solubility product behavior of calcium sulfate in water to 1000 bars at 100–300°, values of $\log K_{sp}$ from Table I; II, ionization behavior of cesium bromide in dioxane–water solvents at 25°.

per liter, which is proportional to the number of the given species per unit of volume. The standard states for all species, including the solvent, are the hypothetical 1 M solutions at the particular pressure (and temperature) where K and $C_{\text{H}_2\text{O}}$ are obtained. The above condition that $C(\text{solute})$ approaches zero applies to all considerations of complete constants given in this and our preceding papers.

From recent literature,^{5,6} examples of conventional ionization and solubility constants adhering to eq 2, and not included elsewhere,^{2-4,7} are shown in Figure 1. For ionization in dioxane-water solvents, the dioxane was assumed to be an inert diluent with respect to preferential solvation of solute species. For solubility, the solubility products [K_{sp} (moles/liter)²] at zero ionic strength (I), plotted as $\log K_{sp}$ (Table I) in Figure 1, were obtained by conversions and extrapolations of the molal solubilities of Blount and Dickson at 100–300°⁶ as described in the Appendix. Figure 2 shows the experimental, isothermal constancy of K^0 for various

substances over wide ranges of dioxane–water composition, pressure, and temperature. In Figure 3 the logarithms of some conventional ionization constants plotted against $\log C_{\text{H}_2\text{O}}$ are compared with $\log K$ plotted against \log fugacity (f) of H_2O to show the simple rectilinear relationships observed with $\log C_{\text{H}_2\text{O}}$ as the variable, as contrasted with the need for many parameters to describe behavior with $\log f_{\text{H}_2\text{O}}$ as a variable.⁴ Literature references to values of K used for Figures 2 and 3 are given elsewhere.³

It is the purpose of this paper to show that the form of a complete constant can be obtained directly from the description of a conventional constant in terms of multistep solvation equilibria. Multistep reaction

(5) J.-C. Justice, R. Bury, and C. Treiner, *J. Chim. Phys. Physicochim. Biol.*, 65, 1708 (1968).

(6) C. W. Blount and F. W. Dickson, *Geochim. Cosmochim. Acta.*, 33, 227 (1969).

(7) W. L. Marshall, *Rev. Pure Appl. Chem.*, 18, 167 (1968); *Rec. Chem. Progr.*, 30, 31 (1969).

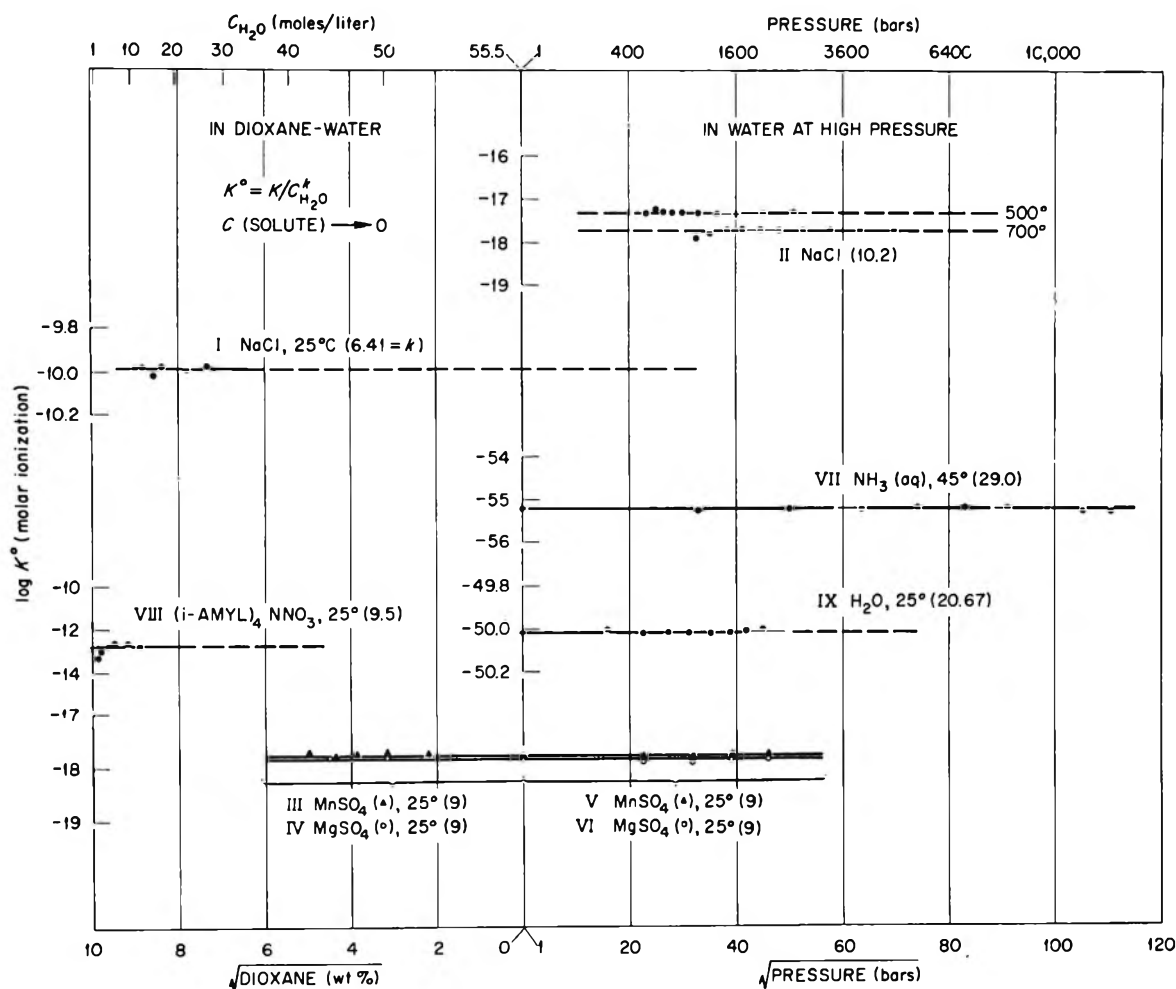


Figure 2. Examples of the invariance of the complete equilibrium constant over extreme ranges of temperature, pressure, and dioxane-water composition. From K values of (I) Kunze, Fuoss, (1963); (II) Quist, Marshall (1968); (III) Atkinson, Hallada (1962); (IV) Dunsmore, James (1951); (V) Fisher, Davis (1965); (VI) Fisher (1962); (VII) Hamann, Strauss (1955); (VIII) Fuoss, Kraus (1933); and (IX) Hamann (1963). All values of $\log K^0$ for sets V and VI were arbitrarily normalized to sets III and IV at the common boundary, solvent water at saturation vapor pressure, by adding 0.24 and 0.13 units of $\log K^0$ to each value of sets V and VI, respectively. Which sets (III and IV vs. V and VI) are more nearly correct at this boundary is not considered.

equilibria have been commonly used to describe complex reaction rates and equilibria both in theory and practice. From this usual description, the additional steps presented here to obtain the form for K^0 (the extraction of $C_{H_2O}^k$ from a conventional constant) do not appear to be initially obvious. Through the derivation, K^0 and k are found not to be exact isothermal constants, although it is self-evident that they are experimentally constant over wide ranges of solvent concentration as shown in Figures 1-3; therefore, the usefulness of K^0 is not impaired. The treatment is shown to be applicable to solute-solvent equilibria both in single and multiple solvent systems and further supports the incorporation of the activity of solvent species as a variable in these equilibrium expressions.

It is the purpose also to present several aspects of the application of complete constants related to this description. In a new application, the combined use of solvent separated ion-pair theory (which requires five

constants for its use here) and complete constants allows prediction of the aqueous ionization behavior of $MgSO_4$ at 25° both in water to 2000 bars and in dioxane-water solvent compositions at saturation vapor pressure. Comparison with experiment is reasonable, and this is accomplished with results on $MgSO_4$ only at saturation vapor pressure in water, together with the pressure-volume properties of water and the density-wt % properties of dioxane-water solvents. However, better agreement with experiment was obtained from the use only of a complete constant approach, where only two constants, K^0 and k , are required. The detailed mathematical description does not therefore limit the usefulness of K^0 , whereby a considerably smaller number of constants (or parameters) are needed to describe equilibrium (or ionization) behavior in solvent systems than by approaches where the solvent is not considered a reactant of variable activity (in moles per liter where $C(\text{solute}) \rightarrow 0$).

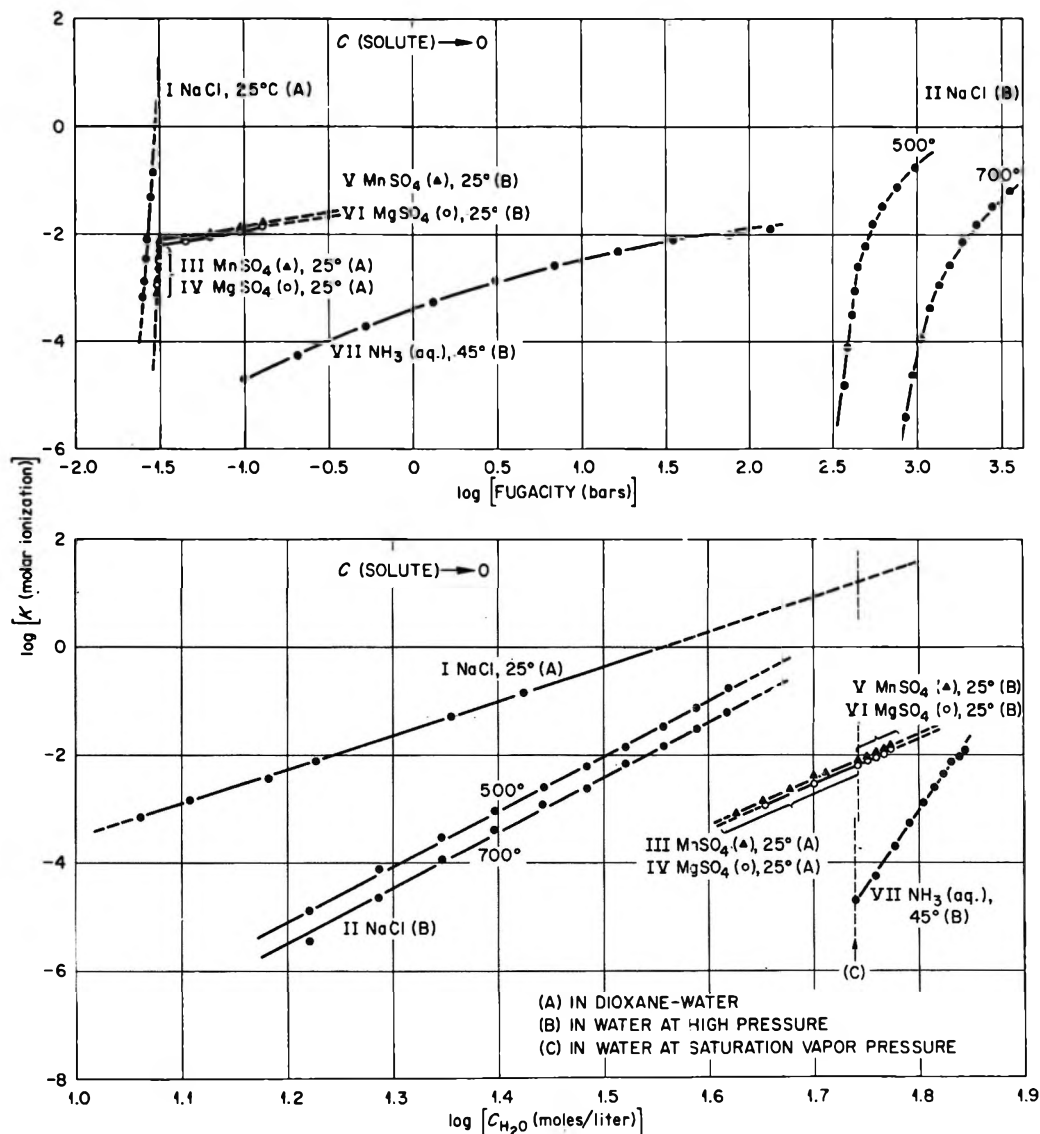
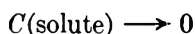


Figure 3. Contrasts in the dependence of K (molar ionization) on the fugacity and molar concentration of water over extreme ranges of temperature, pressure, and dioxane-water composition. From K values of (I) Kunze, Fuoss (1963); (II) Quist, Marshall (1968); (III) Atkinson, Hallada (1962); (IV) Dunsmore, James (1951); (V) Fisher, Davis (1965); (VI) Fisher (1962); and (VII) Hamann, Strauss (1955). All values of $\log K$ for sets V and VI were normalized to those of III and IV, as done for Figure 2.

Mathematical Description of A Complete Constant

The form of a complete constant can be obtained mathematically from a detailed description of a conventional ionization constant representing ionization equilibria in solvent media. A conventional ionization constant may be written

$$K = \frac{a_M \cdot a_{A^-}}{a_{MA^0}} = \frac{\sum_{i'} C_{i'}(M_{aq}^+) \sum_{i''} C_{i''}(A_{aq}^-)}{\sum_i C_i(MA_{aq}^0)} \quad (3)$$



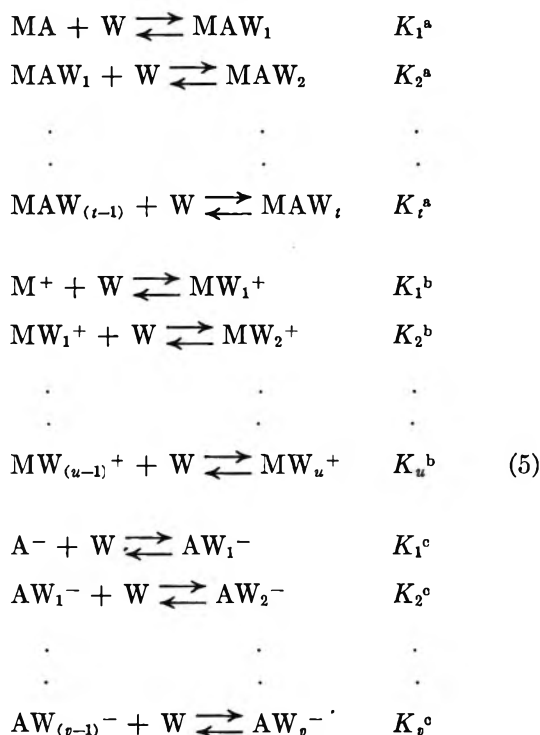
where units of concentration (C) have been substituted for activity (a) as the concentration of solute approaches zero and where each summation represents a particular class of solute species of varying extents of solvation. For example

$$\sum_{i'=0}^u C_{i'}(M_{aq}^+) = C_{M^+} + C_{MW^+} + C_{MW_2^+} + \dots + C_{MW_u^+} \quad (4)$$

where M^+ , MW^+ , MW_2^+ , ... MW_u^+ represent positive ions and W represents the solvent molecule. The usual evaluation of a conventional constant does not distinguish between these separately solvated species but rather considers only the sum of the concentrations of the separate species in each class as described by eq 4.

In order to describe explicitly a conventional ionization constant by mass action equilibria, this constant may be evaluated on the basis of stepwise solvation processes. From kinetic theory, this requirement would appear to apply for any forward (or reverse) reaction process when more than two molecules (or

ions) of reactant species form a product species. A series of solvation reactions for an initial unsolvated neutral molecule (MA), positive ion (M^+), and negative ion (A^-) can be represented by the following series of reaction equilibria, where $K_1^a, K_2^a, \dots, K_t^a, K_1^b, K_2^b, \dots, K_u^b, K_1^c, K_2^c, \dots, K_v^c$ are the separate solvation constants



The concentrations of the separate neutral solute species are given by

$$\begin{aligned}
 C_{\text{MA}} &= \text{MA} \\
 C_{\text{MAW}_1} &= K_1^a \text{MA} \cdot \text{W} \\
 C_{\text{MAW}_2} &= K_1^a K_2^a \text{MA} \cdot \text{W}^2 = K_{2^*}^a \text{MA} \cdot \text{W}^2 \\
 &\vdots \\
 &\vdots \\
 C_{\text{MAW}_t} &= k_{t^*}^a \text{MA} \cdot \text{W}^t
 \end{aligned} \quad (6)$$

where brackets denoting concentration are omitted from the right-hand terms and $K_{t^*}^a$ represents the product of the separate solvation constants up to the number t . The concentrations in the classes of positive and negative solute species are described similarly. The sums of these concentrations in the separate classes are now substituted into eq 3 to give

$$K = \frac{[\text{M}^+][1 + K_1^b \text{W} + K_2^{*b} \text{W}^2 + \dots + K_{u^*}^b \text{W}^u] \times [\text{A}^-][1 + K_1^c \text{W} + K_2^{*c} \text{W}^2 + \dots + K_{v^*}^c \text{W}^v]}{[\text{MA}][1 + K_1^a \text{W} + K_2^{*a} \text{W}^2 + \dots + K_{t^*}^a \text{W}^t]} \quad (7)$$

where $K_{2^*}^a = K_1^a \cdot K_2^a, K_{2^*}^b = K_1^b \cdot K_2^b$, etc. Taking the natural logarithm of eq 7 and rearranging yields

Table I: Calculated Values (First Treatment) of the Molar Solubility Product [K_{sp} (moles/liter)²] of Anhydrous Calcium Sulfate at Zero Ionic Strength from The Solubility in Water of Blount and Dickson,⁶ and Required Densities, Dielectric Constants, and Debye-Hückel Limiting Slopes; 100-300° at Pressures to 1000 Bars

Temp, °C	Pressure, bars	Density, g cm ⁻³	Dielectric constant ^a	Debye-Hückel slope ^b	log K_{sp} (plotted in Figure 1)
100	1.01 ^c	0.958	55.4	0.601	-5.15
100	500	0.980	57.2	0.579	-4.75
100	1000	1.000	58.8	0.561	-4.44
150	4.76 ^c	0.917	43.9	0.690	-6.02
150	500	0.942	45.5	0.663	-5.57
150	1000	0.965	47.1	0.637	-5.21
200	15.5 ^c	0.865	34.6	0.810	-6.94
200	500	0.897	36.6	0.758	-6.41
200	1000	0.924	38.0	0.727	-6.00
250	39.8 ^c	0.799	26.7	0.985	-7.90
250	500	0.842	28.8	0.905	-7.33
250	1000	0.878	30.7	0.840	-6.81
300	85.9 ^c	0.712	19.7	1.287	(-8.89) ^d
300	500	0.777	22.5	1.098	-8.26
300	1000	0.824	24.5	0.995	-7.65

^a Values of dielectric constant estimated,⁴⁶ except at saturation vapor pressure. ^b Debye-Hückel limiting slope based on ionic strength in units of molality (see text). ^c Saturation vapor pressure of pure water. ^d Value in parentheses not included in Figure 1 since the value of solubility used for its determination was obtained by a relatively long extrapolation (see Table 2 of Blount and Dickson⁶).

$$\begin{aligned}
 \ln K &= \ln \frac{[\text{M}^+][\text{A}^-]}{[\text{MA}]} + \ln [1 + K_1^b \text{W} + K_2^{*b} \text{W}^2 + \dots + K_{u^*}^b \text{W}^u] \\
 &+ \ln [1 + K_1^c \text{W} + K_2^{*c} \text{W}^2 + \dots + K_{v^*}^c \text{W}^v] - \ln [1 + K_1^a \text{W} + K_2^{*a} \text{W}^2 + \dots + K_{t^*}^a \text{W}^t] \quad (8)
 \end{aligned}$$

By differentiating eq 8 with respect to $\ln W$ at constant temperature (T), we obtain

$$\begin{aligned}
 \left(\frac{\partial \ln K}{\partial \ln W} \right)_T &= 0 + \\
 &\frac{[K_1^b \text{W} + 2K_2^{*b} \text{W}^2 + \dots + uK_{u^*}^b \text{W}^u]}{[1 + K_1^b \text{W} + K_2^{*b} \text{W}^2 + \dots + K_{u^*}^b \text{W}^u]} + \\
 &\frac{[K_1^c \text{W} + 2K_2^{*c} \text{W}^2 + \dots + vK_{v^*}^c \text{W}^v]}{[1 + K_1^c \text{W} + K_2^{*c} \text{W}^2 + \dots + K_{v^*}^c \text{W}^v]} - \\
 &\frac{[K_1^a \text{W} + 2K_2^{*a} \text{W}^2 + \dots + tK_{t^*}^a \text{W}^t]}{[1 + K_1^a \text{W} + K_2^{*a} \text{W}^2 + \dots + K_{t^*}^a \text{W}^t]} \quad (9)
 \end{aligned}$$

remembering in the differentiation that $(\partial W / \partial \ln W)_T = W$ and that the first term on the right-hand side in eq 8, representing only anhydrous species, is independent of changes in solvent concentration. Again, it should be emphasized that $C(\text{solute})$ always approaches zero.

The second, third, and fourth terms on the right-hand side of eq 9 correspond mathematically to the average number of molecules of solvation on the positive ions, negative ions, and neutral molecules, respectively. This observation follows by multiplying both the denominator and numerator of these three terms in eq 9 by $[M^+]$, $[A^-]$, and $[MA]$, respectively, with the consideration of eq 6. Thus

$$\left(\frac{\partial \ln K}{\partial \ln W}\right)_T = m + n - j = k \quad (10)$$

where m , n , and j are substituted for the corresponding terms in eq 9 representing average solvation numbers. By differentiating eq 8 with respect to hydrostatic pressure (P) at constant temperature, we obtain

$$\left(\frac{\partial \ln K}{\partial P}\right)_T = (m + n - j)\beta = k\beta \quad (11)$$

where β is the compressibility of the solvent.

Equation 9 shows that k and thus K^0 cannot be exact isothermal constants as the solvent concentration is varied where $C(\text{solute}) \rightarrow 0$. At the extreme double limit, for example, where $C(\text{solvent } W) \rightarrow 0$ in addition to $C(\text{solute}) \rightarrow 0$, we find that $(\partial \ln K / \partial \ln W)_T$ or k also approaches zero. [This double limit could be approached experimentally for solute-solvent equilibria in aqueous supercritical fluids or in gaseous mixtures in general, but of course not for liquid water as solvent at low temperature.] Nevertheless, the parameter k is now mathematically defined to represent the net difference in average solvation numbers between the product and reactant solute species in the equilibrium at the particular pressure or concentration of solvent where the differentials of eq 9-11 are obtained. Therefore, a given value of K^0 as defined by eq 1 or 2 applies exactly only at a particular pressure, or concentration of solvent [again, where $C(\text{solute}) \rightarrow 0$]; that is, the slope of $\ln K$ vs. $\ln W$ at P gives the value of k (at P) necessary to calculate K^0 (at P). The integration of eq 10 or 11 thus yields eq 1 or 2 where K^0 and k must be replaced by $K^0(P)$ or $k(P)$ to show the dependency on pressure and where the temperature is always held constant. Nevertheless, within the precision of published experimental measurements, K^0 and k have been found to remain constant over wide ranges of solvent concentration at constant temperature (Figures 1-3). A suggested reason for this approximate constancy, which makes the concept useful, is given in a later section.

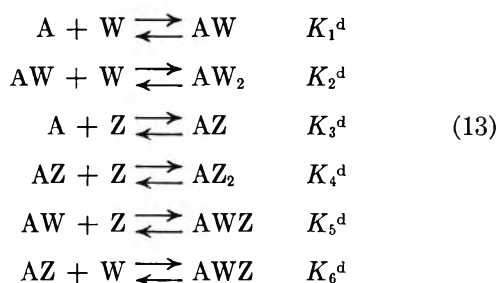
Complete Constants in Mixed Solvents. The mathematical description of K^0 for solute behavior in mixed solvents, where the several solvents selectively solvate the solute species, is considerably more complicated than the above description with a single solvent. For this paper, therefore, a simpler description of the stepwise solvation equilibria of a single solute species (A)

in a mixed solvent (W and Z) will suffice to show the mathematical form that will be obtained on treatment of ionization equilibria in multiple solvents. In this treatment, we shall assume that the analytical concentration of an anhydrous species A can be determined but that the solvated species of A of different extents of solvation are indistinguishable by our analytical method. The observed solvation constant $K(\text{solv})$ is then described by

$$K(\text{solv}) = \frac{\sum_i C_i(\text{A, solvated})}{C(\text{A, anhydrous})} \quad (12)$$

$C(\text{solute}) \rightarrow 0$

Stepwise equilibria can be written, which for simplicity are limited to a small, finite number of steps



By substituting into eq 12 the sum of the concentrations of the various solvated species defined by the above set of equilibria, we obtain

$$\begin{aligned} K(\text{solv}) &= \frac{[AW] + [AW_2] + [AZ] + [AZ_2] + [AWZ]}{[A]} = \\ &= \frac{[A](K_1^d W + K_1^d K_2^d W^2 + K_3^d Z + K_3^d K_4^d Z^2 + K_1^d K_5^d W \cdot Z)}{[A]} \\ &= K_1^d W + K_1^d K_2^d W^2 + K_3^d Z + K_3^d K_4^d Z^2 + K_1^d K_5^d W \cdot Z \end{aligned} \quad (14)$$

Taking the natural logarithm of eq 14 and differentiating with respect to $\ln W$ at constant temperature yields

$$\begin{aligned} \left(\frac{\partial \ln K(\text{solv})}{\partial \ln W}\right)_T &= \\ &= \frac{(K_1^d W + 2K_1^d K_2^d W^2 + K_1^d K_5^d W \cdot Z)}{(K_1^d W + K_1^d K_2^d W^2 + K_3^d Z + K_3^d K_4^d Z^2 + K_1^d K_5^d W \cdot Z)} + \\ &= \frac{(K_3^d Z + 2K_3^d K_4^d Z^2 + K_1^d K_5^d W \cdot Z)}{(K_1^d W + K_1^d K_2^d W^2 + K_3^d Z + K_3^d K_4^d Z^2 + K_1^d K_5^d W \cdot Z)} \left(\frac{\partial \ln Z}{\partial \ln W}\right)_T = \\ &= r + s \left(\frac{\partial \ln Z}{\partial \ln W}\right)_T \end{aligned} \quad (15)$$

remembering again that $(\partial W / \partial \ln W)_T = W$, and that $(\partial Z / \partial \ln W)_T = Z(\partial \ln Z / \partial \ln W)_T$. Thus in this simple example, the first term on the right-hand

side of eq 15 corresponds mathematically to the average extent of solvation of the solvated species by solvent W and the second term, respectively, corresponds to the average extent of solvation by solvent Z multiplied by $(\partial \ln Z / \partial \ln W)_T$. The letters r and s are used to represent these two average extents of solvation that do not include the anhydrous species A which is considered a separate, analytically distinguishable species in eq 12.

Equation 15 shows that r and s are functions of solvent concentrations and of the separate values of the various solvation constants. However, at a constant mixed solvent composition and constant pressure, r and s are constants, and eq 15 can be integrated to yield

$$\begin{aligned} \partial(\ln K(\text{solv}))_T &= r(\partial \ln W)_T + s(\partial \ln Z)_T \\ \ln K(\text{solv}) &= \ln K^0(\text{solv}) + r \ln W + s \ln Z \\ K^0(\text{solv}) &= K(\text{solv}) / (W^r Z^s) \end{aligned} \quad (16)$$

where $K^0(\text{solv})$, a complete constant, originates from the constant of integration, $\ln K^0(\text{solv})$, under the above restrictions.

The finite number of steps of solvation given by eq 13 is very small compared to the real situation where the average solvation numbers r and s will be expected to have values much greater than 2, the maximum possible number with the limited steps of eq 13. For ionization equilibria involving neutral, positive ion, and negative ion solvated species, the mathematical treatment will yield the same form as eq 15 for the separate classes (for example, the neutral solvated molecules, and positive and negative solvated ions) of solute species from which by combination of these separate equations (similar to eq 15) will yield

$$K^0 = K / (W^k Z^p) \quad (17)$$

where k and p represent net changes in the number of molecules of solvation by W and Z , respectively, on ionization of a substance $MA(\text{solvated})$ of average selective solvation to form two ions $M(\text{solvated})^+$ and $A(\text{solvated})^-$ of average selective solvation. Equation 17 is the form of the relationship given elsewhere³ for ionization behavior in a binary mixed solvent system where both solvents selectively solvate the solute species. When more than two reactive solvents are present, a relation similar to eq 17 is readily derived by the same mathematical process of eq 12–16.

Use of Concentration of Solvent Where $C(\text{Solute})$ Approaches Zero

Application of Gibbs–Duhem Relation. When the solute species are in their reference states, as defined herein, the use of concentration for the activity of a single solvent in equilibrium expressions may be justified through consideration of the Gibbs–Duhem relation. Where $(w - 1)$ components (that is, the solute

components) are treated ideally, the remaining component can also be treated to behave according to the form of an ideal substance.^{8a} To show this relationship where concentration is used in an equilibrium expression, the Gibbs–Duhem relation may be written, at constant temperature and pressure

$$n_1 d\mu_1 = - \sum_{i=2}^w n_i d\mu_i \quad (18)$$

where n_1 is the number of moles of solvent in a unit of constant volume (V) containing $n_2 + n_3 + \dots + n_w$ moles of components 2, 3, \dots , w . The chemical potentials are represented by μ . With the restriction of ideality for solute species, eq 18 may now be written

$$n_1 d\mu_1 = -RT \sum_{i=2}^w n_i d \ln \left(\frac{n_i}{V} \right) \quad (19)$$

$$= -RT \sum_{i=2}^w dn_i \quad (20)$$

$$= +RT dn_1, \text{ since } \sum_{i=1}^w dn_i = 0^{8b} \quad (21)$$

Dividing both sides by the constant volume, V , rearranging, and integrating yields

$$\left(\frac{n_1}{V} \right) d\mu_1 = RT d \left(\frac{n_1}{V} \right) \quad (22)$$

$$d\mu_1 = RT d \ln \left(\frac{n_1}{V} \right) \quad (23)$$

$$\mu_1 = \mu_1^0(P) + RT \ln C_1 \quad (24)$$

where n_1/V is equal to C_1 , the concentration of the solvent, and where the concentration of solute approaches zero. The standard state potential is given here as a function only of pressure (P) since in this paper we have considered only isothermal equilibria. If temperature also is allowed to vary, this standard state potential must be expressed as a function both of temperature and pressure [$\mu^0(T, P)$]. Reiss derives a similar relationship where mole fractions of components are used instead of concentrations.^{8a} A unique discussion of activity, of standard state potentials as functions of both pressure and temperature, and also of solvents that may be treated as inert solvents (as assumed here and previously for dioxane) is given in critical detail by Reiss.^{8a}

Defining the form of ideality for a solvent in solute–solvent equilibria in multiple solvent systems by means of the Gibbs–Duhem relation does not appear to be applicable since the mixed solvent consists of more than one component. For these solvent systems, the definition that the reference state of each solvent species

(8) (a) Howard Reiss, "Methods of Thermodynamics," Blaisdell Publishing Co., New York, N. Y., 1965, Chapter IX, pp 142–146; (b) *ibid.*, pp 129–132, eq 8.61.

will be taken as its concentration in the particular (pure) solvent mixture must suffice.

Consideration of Solvent Fugacity. For observed conventional ionization constants expressed by eq 7, or for the complete constant which is obtained directly from the variation of the conventional constant with solvent concentration, one might consider using fugacity (f) instead of concentration of the solvent species in the mass action expression. A discussion on this subject is given elsewhere.⁴ However, we now have a mathematical expression for k (eq 9, 10) into which $f(\text{solvent})$ can be substituted for W . With this substitution, $f(\text{solvent})$ must also be considered to have been contained in eq 7 for the conventional constant. Equation 2 provides a slope (k) for $\log K$ vs. $\log C_{\text{H}_2\text{O}}$ that is essentially a constant at 500–700° (See Figure 3) over a range of $C_{\text{H}_2\text{O}}$ of about 0.5 logarithmic unit (base 10). The fugacity of water over this range of $C_{\text{H}_2\text{O}}$ varies also by about 0.5 logarithmic unit but with a different form (Figure 3) that yields a widely varying slope for $\log K$ vs. $\log f_{\text{H}_2\text{O}}$. It therefore is evident that replacement by fugacity of the concentration of solvent as included in the expression for K (eq 7) increases the complexity of description.

Experimentally Observed Isothermal Constancy of K^0 and K

A value of k , although shown mathematically not to be a constant, for many equilibria is experimentally constant at constant temperature over a wide change in concentration of solvent (water). This observation of constancy must mean that only a very few solvated species of successive solvation numbers comprise the majority mole fraction of each class of solute. The existence of a very wide range of solvated species in each class would be indicated by a large change in the value of k with change in the concentration of solvent at constant temperature; this behavior is not observed. Nevertheless, it might be possible that wide ranges could exist for all classes whereby, upon changing the solvent concentration, uniquely simultaneous variations in m , n , and j of eq 10 would effectively yield a (nearly) constant value for k . This uniqueness would seem to be unlikely, and therefore the first explanation appears to be more reasonable to account for the experimental constancy of k (and of K^0) at constant temperature.

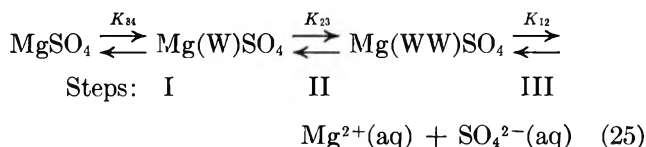
The value of k , however, changes rather rapidly with temperature, at least for the ionization of sodium chloride in water, until a temperature of about 400° is reached.⁹ From eq 9, k is considered to be a function of the concentration of water and of the many separate solvation constants; these solvation constants are taken to be independent of pressure but to vary with temperature. The marked change in k with changing temperature, but not with changing solvent concentration at constant temperature, implies that variations

with temperature of the separate solvation constants as given in eq 9 produce the major change with temperature in the value of k .

If only one solvated species exists in each class of neutral molecules, positive ions, and negative ions, k should be mathematically independent of both temperature and pressure in accordance with eq 9 (or eq 17 — k and p). In addition k (or k and p) should be an integer, representing the change in the number of molecules of solvation for a *single* reaction process. This behavior might appear to exist for the several 1–1 salts (NaCl, NaBr, NaI) in water as solvent in the range of temperature 400–800° where k is essentially an integer (10) that is independent both of temperature and pressure.¹⁰

Solvent Separated Ion-Pair Theory

Solvent separated ion-pair theory states that the ionization of a salt in solvent media may occur in three major steps, whereby one and two molecules of solvent (water) successively separate the cationic and anionic part of a neutral salt molecule to form distinguishable ion-pairs before full separation to form the two solvated ions. This theory, first proposed by Eigen and Tamm,¹¹ can be described by the following equilibria for the ionization of a salt like MgSO_4 in water solvent



where water (W) is not included as a reactant of variable concentration. From these equilibria, the following expression for a conventional ionization constant $K'_{(\text{MgSO}_4)}$ is derived

$$K'_{(\text{MgSO}_4)} = \frac{C_{\text{Mg}^{2+}(\text{aq})} C_{\text{SO}_4^{2-}(\text{aq})}}{C_{\text{Mg(WW)SO}_4} + C_{\text{Mg(W)SO}_4} + C_{\text{MgSO}_4}} \quad (26)$$

$$C(\text{solute}) \longrightarrow 0$$

$$= \frac{K_{12}K_{23}K_{34}}{1 + K_{34} + K_{23}K_{34}} \quad (27)$$

which corresponds to the reciprocal of the equation given by Atkinson and Petrucci for the conventional association constant for this process.¹² The symbols for the constants of the stepwise equilibria are the same as those presented previously;^{11,12} steps I, II, and III, however, are reversed.

To describe these stepwise equilibria in terms of separate, complete constants and $C_{\text{H}_2\text{O}}$, eq 27 can be written in the following form

(9) (a) L. A. Dunn and W. L. Marshall, *J. Phys. Chem.*, **73**, 2619 (1969); (b) A. S. Quist and W. L. Marshall, *ibid.*, **72**, 684 (1968).

(10) L. A. Dunn and W. L. Marshall, *ibid.*, **73**, 723 (1969).

(11) M. Eigen and K. Tamm, *Z. Elektrochem.*, **66**, 93, 107 (1962).

(12) G. Atkinson and S. Petrucci, *J. Phys. Chem.*, **70**, 3122 (1966); see their eq 13.

$$K'_{(\text{MgSO}_4)} = \frac{K_{12}^0 K_{23}^0 K_{34}^0 C_{\text{H}_2\text{O}}^{(e+g+h)}}{1 + K_{34}^0 C_{\text{H}_2\text{O}}^h + K_{23}^0 K_{34}^0 C_{\text{H}_2\text{O}}^{(g+h)}} \quad (28)$$

where h , g , and e represent net changes in solvation numbers that include the solvent separating the ion-pairs and K_{34}^0 , K_{23}^0 , and K_{12}^0 are complete constants that are isothermally independent of variations in $C_{\text{H}_2\text{O}}$ for each of the steps I, II, and III, respectively. The assumed variation of each stepwise conventional constant in eq 27 as described in eq 28 is analogous to that for variations in the overall conventional constant where for the ionization of MgSO_4 (aqueous)

$$K_{(\text{MgSO}_4)} = K^0 C_{\text{H}_2\text{O}}^k \quad (29)$$

and where k is the net change in solvation numbers for the overall process (see Figure 2). From the values of Eigen and Tamm for standard volume changes (ΔV) at 25° and 1 bar of -3 , -14 , and $0 \text{ cm}^3 \text{ mol}^{-1}$,¹¹ values of h , g , and e of 3.7, 13.4, and 0 were calculated for steps I, II, and III, respectively. The numbers 3.7 and 13.4 are to be contrasted with the implied numbers 1 and 1 for steps I and II, respectively. The calculations were made with the equation¹³

$$k = -\Delta V / (RT\beta) + 1 \quad (30)$$

where the integer 1 arises from the use of values of ΔV obtained from variations of K in molal units with pressure,^{13b} where h , g , or e is substituted for k , where β , the compressibility of water, was taken to be $45.89 \times 10^{-6} \text{ atm}^{-1}$ at 1 bar (25°),^{14,15} and where R is the gas constant and T is the absolute temperature.

With published values of K_{34} , K_{23} , and K_{12} at 25° and 1 bar of Atkinson and Petrucci,¹² the earlier, similar values of Eigen and Tamm,¹¹ included also in the paper of Atkinson and Petrucci,¹² and the above values of h , g , and e from which K_{34}^0 , K_{23}^0 , and K_{12}^0 are obtained with equations analogous to eq 29, values of $K'_{(\text{MgSO}_4)}$ were calculated at pressures to 2000 bars using *PVT* tables given elsewhere¹⁶ for the conversion from pressure to $C_{\text{H}_2\text{O}}$. In addition, values of $K'_{(\text{MgSO}_4)}$ were calculated with eq 28 for low concentrations of water, as in dioxane-water solvents; densities for relating $C_{\text{H}_2\text{O}}$ to wt % H_2O may be obtained from several sources.¹⁷ A curve describing these calculated values of $K'_{(\text{MgSO}_4)}$ is compared in Figure 4 with experimentally determined values of Fisher in water at pressures to 2000 bars¹⁸ and with some values of Dunsmore and James in dioxane-water solvents at saturation vapor pressure.¹⁹ Included also is a straight line obtained from calculated values of $K_{(\text{MgSO}_4)}$ with eq 29 where the value of k has been adjusted to give the best overall fit to both sets of experimental values of $K_{(\text{MgSO}_4)}$. [In Figure 2, $k = 9$ was selected to fit both $K_{(\text{MgSO}_4)}$ and $K_{(\text{MnSO}_4)}$ for the best consistency. However, with greater weighting of the two values of $K_{(\text{MgSO}_4)}$ in dioxane-water, $k = 8.2$ appeared to give the best fit for $K_{(\text{MgSO}_4)}$ alone.] In Figure 4, all calculated and experimental values of

$K_{(\text{MgSO}_4)}$ (or $K'_{(\text{MgSO}_4)}$) were normalized to a $\log K_{(\text{MgSO}_4)}$ of -2.40 and -2.42 , respectively, at 1 bar by addition of a constant $\Delta(\log K_{(\text{MgSO}_4)})$ to each $\log K_{(\text{MgSO}_4)}$ in a particular set. Many separately published values of $\log K_{\text{MgSO}_4}$ at 25° and 1 bar have varied between -2.2 and -2.4 as referenced elsewhere;²⁰ a value of -2.40 , however, appears to provide the best consistency with values at other temperatures.²⁰

There appears to be reasonably good agreement between the three-step (five constants required, K_{34}^0 , K_{23}^0 , K_{12}^0 , h and g ; e is zero) and the multistep (undefined number, but with only two constants, K^0 and k^0 , required) complete constant approaches, although additional water molecules of solvation must be added in reaction steps I and II of the three-step process (eq 25). However, between the two treatments a better fit to experiment is obtained through the use of the multistep approach with only K^0 and k required (line A of Figure 4). A lack of full agreement could be explained by some errors in the assigned values of K_{34} , K_{23} , K_{12} , ΔV_{34} , ΔV_{23} , and ΔV_{12} at 1 bar of the Eigen-Tamm theory. Disagreement would also be expected if species other than, or in addition to, those given by eq 25 are present in significant concentration at equilibrium. Additional steps would need to be added to the equilibria of eq 25, with the necessity for additional constants in eq 27 and 28. Nevertheless, calculations by both approaches fit experimental values relatively well, with somewhat better agreement by the two-constant treatment.

Concluding Comments

The consideration of equilibrium behavior of solutes in terms of interactions with solvent probably is the most important aspect of electrolyte and nonelectrolyte solute chemistry. In recent years, many authors have considered and discussed the solvent as a reactant under the above circumstances both in experimental studies and in theory.^{2-4,21-31} The distinguished theoretic-

(13) (a) See ref 4, eq 13; (b) see ref 4, p 348.

(14) F. J. Millero, R. W. Curry, and W. Drost-Hansen, *J. Chem. Eng. Data*, **14**, 422 (1969).

(15) G. S. Kell and E. Whalley, *Phil. Trans. Roy. Soc. London*, **258**, 565 (1965).

(16) (a) W. E. Sharp, University of California Report No. UCRL-7118 (1962); (b) C. W. F. T. Pistorius and W. E. Sharp, *Amer. J. Sci.*, **258**, 757 (1960).

(17) I. D. McKenzie and R. M. Fuoss, *J. Phys. Chem.*, **73**, 1501 (1969) plus previous papers by R. M. Fuoss and coworkers; V. S. Griffiths, *J. Chem. Soc.*, 1326 (1952); E. Tommila and A. Koivisto, *Suom. Kemistilehti B*, **21**, 18 (1948); F. Hovorka, R. A. Schaefer, and D. Dreisbach, *J. Amer. Chem. Soc.*, **58**, 2264 (1936); *ibid.*, **59**, 2753 (1937); J. A. Geddis, *ibid.*, **55**, 4832 (1933).

(18) F. H. Fisher, *J. Phys. Chem.*, **66**, 1607 (1962).

(19) H. S. Dunsmore and J. C. James, *J. Chem. Soc.*, 2925 (1951).

(20) W. L. Marshall, *J. Phys. Chem.*, **71**, 3584 (1967).

(21) E. U. Franck, *Z. Phys. Chem. (Frankfurt am Main)*, **8**, 107, 192 (1956).

(22) M. Levy, *C. R. Trav. Lab. Carlsberg, Ser. Chim.*, **30**, 291, 301 (1958); M. Levy and J. P. Magoulas, *J. Amer. Chem. Soc.*, **84**, 1345 (1962).

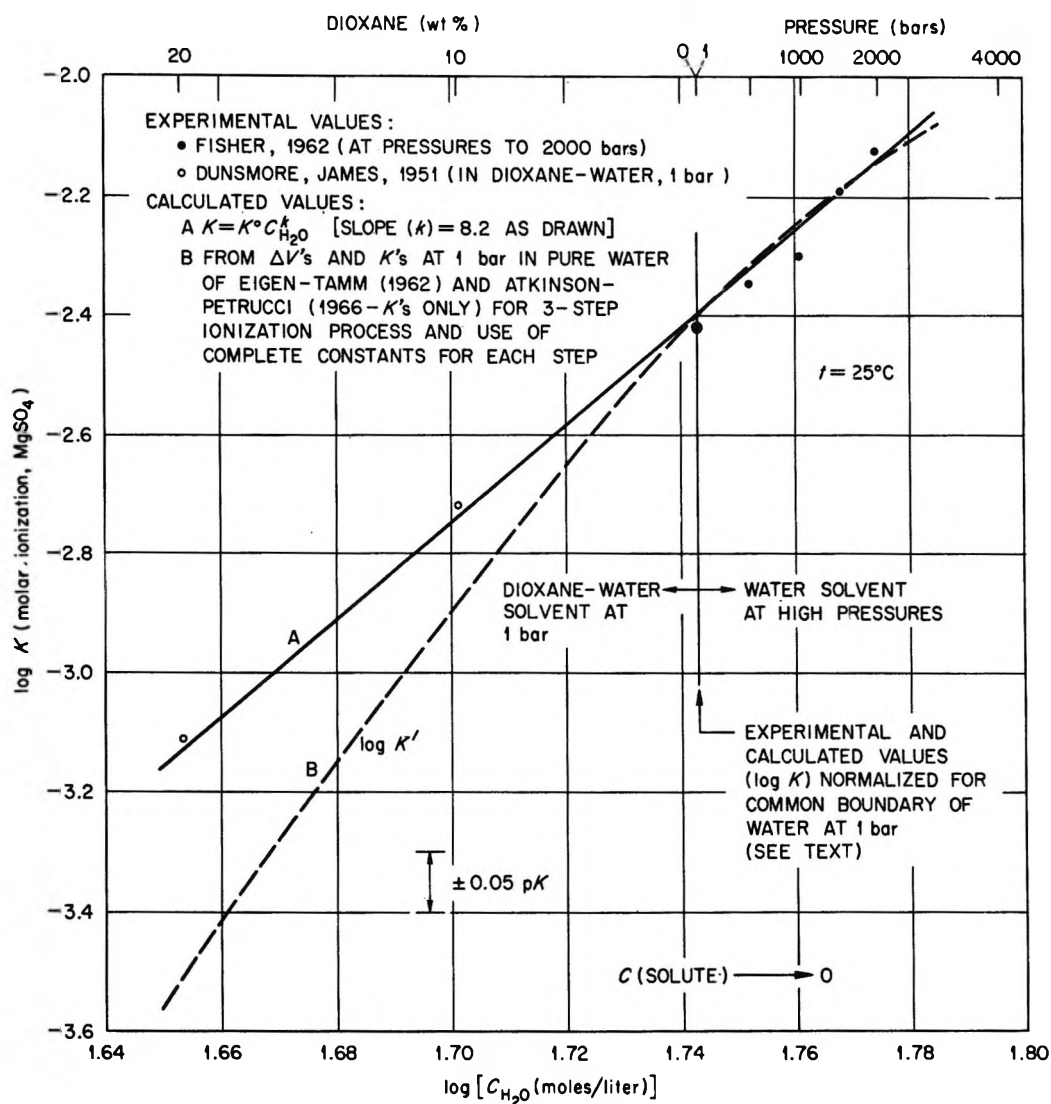


Figure 4. Complete constant concept (Line A) compared with use of complete constants combined with solvent-separated ion-pair theory (three step process of Eigen and Tamm, 1962) (Line B) for calculating ionization constants (aqueous) of MgSO_4 in dioxane-water solvents at saturation vapor pressure and in water to 2000 bars at 25° .

cal treatment of McMillan and Mayer³² is concerned principally with multicomponent interactions that include the solvent as a component, where the theoretical equations are based on numbers of "set" species per unit of volume. Most recently, several authors and books have reviewed the literature on solute-solvent interactions in great detail.³³⁻³⁶ It is believed, however, that the introduction of successive, mass action solvation reactions (like the sets of eq 5) to obtain a mathematically defined net change in solvation numbers has not been presented previously for solute-solvent equilibria. While the description of the activities of particular classes of solute species as described in eq 3 may be self-evident, the quantitative result of this multiple, mass action approach (eq 3-9) seems to stress further the importance of incorporating the solvent as a reactant of variable activity into a complete equilibrium expression.

In all differentiations with respect to pressure (or $\ln W$) in this paper, the temperature was held constant be-

- (23) D. J. Glover, *J. Amer. Chem. Soc.*, **87**, 5275, 5279 (1965).
- (24) R. Gaboriaud, *Ann. Chim. (Paris)*, **2**, 201 (1967).
- (25) Y. Kondo, H. Tojima, and N. Tokura, *Bull. Chem. Soc. Jap.*, **40**, 1408 (1967); Y. Kondo, Y. Honjo, and N. Tokura, *ibid.*, **41**, 987 (1968); Y. Kondo, M. Uchida, and N. Tokura, *ibid.*, **41**, 992 (1968).
- (26) F. Aufauvre, "Etude du Comportement des Anilines dans l'eau, l'acetone et les melanges eau-acetone," Doctor of Physical Sciences Thesis, Faculty of Sciences, Univ. of Clermond-Ferrand, France, Oct., 1969.
- (27) H. C. Helgeson, *Amer. J. Sci.*, **267**, 729 (1969).
- (28) R. V. James and E. L. King, *Inorg. Chem.*, **9**, 1301 (1970).
- (29) R. L. McDonald and T. H. Hufen, *J. Phys. Chem.*, **74**, 1926 (1970).
- (30) E. M. Woolley, D. G. Hurkot, and L. G. Hepler, *ibid.*, **74**, 3908 (1970); K. P. Anderson, E. A. Butler, and E. M. Woolley, *ibid.*, **75**, 93 (1971).
- (31) R. G. Bates, *Electroanal. Chem. Interfacial Electrochem.*, **29**, 1 (1971); S. Goldman, P. Sagner, and R. G. Bates, *J. Phys. Chem.*, **75**, 826 (1971).

cause under this condition the many separate solvation constants of eq 5 could be taken to remain constant. Equation 8 can also be differentiated with respect to $1/(T, ^\circ\text{K})$ at constant pressure for substitution into the van't Hoff isochore, $(\partial \ln K/\partial(1/T))_P = -\Delta H/R$, where ΔH is the standard change in enthalpy and R is the gas constant. The final equation, however, is considerably complex because all separate solvation constants must also be taken to vary with temperature; therefore, this derivation was not presented. In addition, the expected large change in k with temperature (at 25–300°) introduces a question concerning the actual significance of the determined values of the conventional thermodynamic function ΔH (and also of ΔS , the standard change in entropy). By correct application of the van't Hoff isochore, it must be accepted that the reaction stoichiometry does not vary with temperature. For complete equilibria the above expected large change in k with temperature would not satisfy this restriction.⁴ Determined values of ΔH and of ΔS provide not only the differences in these standard state thermodynamic functions between solute reactants and products but reflect also differences in solute-solvent interactions between reactants and products. These effects of solvent are qualitatively evident from the diversity of behavior of ΔH and of ΔS that are obtained from the variation with temperature of conventional ionization constants of aqueous electrolytes.

The treatment of solute-solvent equilibria presented here provides a description by many separate solvation constants. However, experimental observations show that these many constants are not required for a satisfactory description of solute-solvent equilibria over wide ranges of pressure and mixed solvent composition. The experimental constancy of k (and of K^0) certainly indicates that there must not be a wide range of solvated species for each of the various classes of species as defined by equations like eq 4. Only the net change in solvation numbers (k) and K^0 for a given electrolyte at a given temperature appears to be required for most applications. Consequently, the complete mass action, or chemical, approach should continue to be useful for describing isothermal behavior of solute ionization constants and for providing additional insight into solute-solvent interactions.

Appendix

The Solubility Product (K_{sp}) of Calcium Sulfate at Zero Ionic Strength from Its Solubility. Blount and Dickson recently have published molal solubilities (s') of anhydrous calcium sulfate in water and in aqueous solutions of sodium chloride at temperatures from 100 to 450° and at pressures from vapor saturation to 1000 bars.⁶ In order to test a $\log [K_{sp}(\text{moles/liter})^2]$ vs. $\log C_{\text{H}_2\text{O}}$ relationship for obtaining a complete constant, their molal solubilities (s') to 300° were converted to solubility products $[Q'_{sp}(\text{mole}/1000 \text{ g of solvent})^2 =$

$(s')^2]$ at the various ionic strengths (I), which were then extrapolated by means of extended Debye-Hückel theory to values $[K'_{sp}(\text{mol}/1000 \text{ g of solvent})^2]$ at zero ionic strength.³⁷ With densities of water as a function of temperature and pressure,¹⁶ the values of K'_{sp} obtained were converted to molar solubility products $[K_{sp}(\text{moles per liter})^2]$ for plotting as shown in Figure 1. Several papers have been published recently on the above type of extrapolation from experimentally obtained molal solubilities of CaSO_4 (and its two hydrates) at 0–350° and saturation vapor pressure in water and in 1–1 electrolyte salt solutions.^{38–41} In these studies, the solubilities of CaSO_4 were fitted to the following equation at constant temperature

$$\log [Q'_{sp} \text{ at } I] = \log [K'_{sp}, I = 0] + 8S\sqrt{I}/(1 + A_{sp}\sqrt{I}) + BI - CI^2 \quad (31)$$

where the ionic strength I is in units of molality, S is the Debye-Hückel limiting slope based on I in molal units for a monovalent ion [$8S$ is the combined value for a 2–2 electrolyte], and A_{sp} , B and C are adjustable parameters that vary only with temperature. From the previous studies^{38–41,42} the parameters B and C were taken to be essentially zero at 100–350°, and values of A_{sp} were given as 1.59 at 100° and 1.60 at 125–350°.

For making the above calculations of $\log K_{sp}$ from the solubilities of CaSO_4 of Blount and Dickson, values of the Debye-Hückel slopes (based on molal units for I) at the various temperatures and pressures were obtained from the theoretical expression for $S(\text{molal})$, as included in the treatise of Harned and Owen,⁴³ with the use of densities¹⁶ and experimental⁴⁴ and estimated⁴⁵

(32) W. G. McMillan and J. E. Mayer, *J. Chem. Phys.*, **13**, 276 (1945).

(33) B. E. Conway, "Physical Chemistry, An Advanced Treatise," Vol. IXA, Henry Eyring, Ed., Academic Press, New York, N. Y., Chapter 1, 1970.

(34) J. E. Desnoyers and C. Jolicoeur, "Modern Aspects of Electrochemistry," No. 5, J. O'M. Bockris and B. E. Conway, Ed., Plenum Press, New York, N. Y., Chapter 1, 1969.

(35) J. F. Coetzee and C. D. Ritchie, Ed., "Solute-Solvent Interactions," Marcel Dekker, New York, N. Y., 1969.

(36) S. Petrucci, Ed., "Ionic Interactions from Dilute Solutions to Fused Salts," Vol. 1, Academic Press, New York, N. Y., 1971.

(37) Note: In a previous paper (ref 3), extrapolations to zero ionic strength of relatively low solubilities of particular salts were not made, and these solubilities probably should have been evaluated on the basis of zero ionic strength.

(38) W. L. Marshall, R. Slusher, and E. V. Jones, *J. Chem. Eng. Data*, **9**, 187 (1964).

(39) W. L. Marshall and R. Slusher, *J. Phys. Chem.*, **70**, 4015 (1966).

(40) C. C. Templeton and J. C. Rodgers, *J. Chem. Eng. Data*, **12**, 536 (1967).

(41) W. L. Marshall and R. Slusher, *ibid.*, **13**, 83 (1968).

(42) W. L. Marshall and E. V. Jones, *J. Phys. Chem.*, **70**, 4028 (1966).

(43) H. S. Harned and B. B. Owen, "The Physical Chemistry of Electrolytic Solutions," Reinhold, New York, N. Y., 1958, pp 164–166.

(44) G. C. Akerlöf and H. I. Oshry, *J. Amer. Chem. Soc.*, **72**, 2844 (1950).

(45) A. S. Quist and W. L. Marshall, *J. Phys. Chem.*, **69**, 3165 (1965).

dielectric constants at the separate temperatures and pressures. The values of $\log K_{sp}$ believed to be the best were calculated from the smoothed (with fitted equation) solubility values of Blount and Dickson in water only for each condition of constant temperature and pressure through the use of eq 31, with the values of A_{sp} given above and B and C equal to zero (first treatment). These calculated values of $\log K_{sp}$, which are plotted in Figure 1, are given in Table I together with the calculated values of the Debye-Hückel slopes and evaluated densities and dielectric constants that were used. When the Blount-Dickson solubilities in sodium chloride solutions were included, with the use of eq 31 and a nonlinear least-squares (NLLS) treatment, all calculated values of $\log K_{sp}$ were about 0.1–0.2 logarithmic units less negative than those from the first treatment. In this second treatment, all four parameters (K'_{sp} , A_{sp} , B , C) were allowed to adjust to give the best fit at each temperature and pressure. When A_{sp} was restricted to 1.60 (1.59 at 100°) and B and C allowed to adjust, the calculated values of $\log K_{sp}$ obtained from the use of all solubilities at a constant temperature and pressure were about 0.1–0.2 logarithmic units more negative than those from the first treatment. Since there were no reported smoothed solubilities in

solutions containing between 0 and 1 *m* NaCl, the first treatment was preferred. Many solubilities in solutions of added electrolyte molality between 0 and 1 *m* would appear to be required for a relatively valid treatment by eq 31 where A_{sp} , B , and C are also determined simultaneously.

Inclusion of an associated species, $\text{CaSO}_4^?$, did not appear to be justified under the circumstances of these calculations, although association constants for the formation of CaSO_4^0 at saturation vapor pressures and temperatures of 0–350° have been considered and given elsewhere.^{39,46,47} However, it is believed that the solubility of anhydrous calcium sulfate is sufficiently low at the high temperatures (100–350°) that this association behavior does not have an appreciable effect on the values of $\log K_{sp}$ given in Table I and plotted in Figure 1. Comparisons of published values for the ion solubility product^{46,47} with the formal solubility constant (where association is not included)^{38,40–42} of CaSO_4 at 100–300° show agreement within about 0.2–0.4 logarithmic units.

(46) L. B. Yeatts and W. L. Marshall, *J. Phys. Chem.*, **73**, 81 (1969).

(47) A. W. Gardner and E. Glueckauf, *Trans. Faraday Soc.*, **66**, 1081 (1970).

Application of Significant Structures Theory to Some Hydrocarbon Liquids

by G. L. Faerber, S. M. Breitling, A. MacKnight, and H. Eyring*

Department of Chemistry, University of Utah, Salt Lake City, Utah 84112 (Received January 29, 1971)

Publication costs assisted by the National Science Foundation

Using significant structures theory, the thermodynamic properties of benzene, *o*-xylene, *m*-xylene, and *p*-xylene have been calculated in the normal liquid region (melting point to critical point). With the use of a single partition function the thermodynamic properties of toluene and ethylbenzene have also been calculated for the normal as well as the supercooled liquid region. The entropy of melting disappears near the glass transition temperature for the supercooled liquids. A new method of parameter determination is proposed for liquids comprised of complex molecules.

Introduction

Significant structures theory has been successfully applied to a large number of liquids and liquid mixtures containing relatively simple molecules.^{1–5} This work investigates the thermodynamic properties of the normal liquid and supercooled liquid regions of a family of benzene ring-containing compounds: benzene, toluene, ethylbenzene, *o*-xylene, *m*-xylene, and *p*-xylene. In an earlier paper⁶ the viscous flow and glass transition temperatures of the supercooled mono-

substituted alkylbenzenes were discussed. This leads to an interesting possibility that a single partition

(1) H. Eyring and M. S. Jhon, "Significant Liquid Structures," Wiley, New York, N. Y., 1969.

(2) E. J. Fuller, T. Ree, and H. Eyring, *Proc. Nat. Acad. Sci. U. S.*, **45**, 1594 (1959).

(3) S. Chang, H. Pak, W. Paik, S. H. Park, M. S. Jhon, and W. S. Ahn, *J. Korean Chem. Soc.*, **8**, 33 (1964).

(4) K. Liang, H. Eyring, and R. P. Marchi, *Proc. Nat. Acad. Sci. U. S.*, **52**, 1107 (1964).

function may possibly extend significant structures theory to the supercooled liquid region.

Significant structures theory (see ref 1) recognized the following as the most important contributions to liquid structure: (1) oscillating or solidlike molecules; (2) the positional degeneracy of the solidlike molecules; and (3) translating or gaslike molecules.

The partition function f_1 for a mole of liquid can be written as

$$f_1 = (f_s)^{NV_s/V} (f_g)^{N(V-V_s)/V} \quad (1)$$

where N is Avogadro's number, f_s and f_g are the partition functions for the solidlike and gaslike molecules, respectively. V and V_s are the molar volumes of the liquid and solid, respectively. V_s/V represents the fraction of solidlike molecules while $(V - V_s)/V$ represents the fraction of gaslike molecules.

Since the temperatures considered were far from 0°K, even for the supercooled regions, the Einstein perfect crystal oscillator partition function⁷ was used for the solid. However, Pauling⁸ suggested that below a certain transition temperature rotational degrees of freedom in the solid are frozen into librational modes for solids that exhibit high entropies of fusion (*i.e.*, 8–9 eu). Since all the compounds studied exhibit high entropies of fusion, the number of degrees of freedom assigned to Einstein oscillators was increased from three to six. The partition function for the solidlike molecules then becomes

$$f_s = \exp(E_s/RT) [1 - \exp(-\theta/T)]^{-6} [1 + n(V - V_s)/V_s \exp(-aE_s V_s / (V - V_s) RT)] \prod_{i=1}^{NI} (8\pi^3 I_i kT)^{1/2} / \sigma_m h \prod_{j=1}^{NII} [1 - \exp(-h\nu_j/kT)] \quad (2)$$

E_s is the sublimation energy; R is the gas constant; T is absolute temperature; θ is the Einstein characteristic temperature; n and a are dimensionless parameters in the solidlike degeneracy term. NI is the number of side chain rotors; I_i is the reduced moment of inertia of the alkyl side chain rotor; σ_m is the symmetry number of the side chain rotors; k is Boltzmann's constant; and h is Planck's constant. NII is the number of vibrational degrees of freedom and the ν_j 's are the internal vibrational frequencies.

The partition function for the gaslike molecules is

$$f_g = (2\pi mkT)^{3/2} / h^3 (eV/N) [8\pi^2 (8\pi^3 ABC)^{1/2}] (kT)^{3/2} / \sigma h^3 \prod_{i=1}^{NI} (8\pi^3 I_i kT)^{1/2} / \sigma_m h \prod_{j=1}^{NII} [1 - \exp(-h\nu_j/kT)] \quad (3)$$

where m is the mass of the molecule; A , B , and C are the moments of inertia for the molecule; and σ is the symmetry of the molecule.

From thermodynamics,⁹ Helmholtz free energy, A , is

$$A = -kT \ln f_1 \quad (4)$$

Helmholtz free energy can then be differentiated with respect to temperature and volume and yield the vapor pressure, P , entropy, S , heat capacity at constant volume and pressure, C_v and C_p , respectively, coefficient of thermal volume expansion, α , and the coefficient of volume compressibility, β .

Determination of Parameters

The partition function, f_1 , depends on five parameters: E_s , θ , V_s , a , and n . For the simplest systems these parameters can be calculated *a priori*,¹ or experimental values may be used. In more complex systems the experimental values may not be adequately known or, as in the case of water,¹⁰ the experimental crystalline solid values do not represent the "solidlike" structures in the fluid. This is not surprising since crystalline solids frequently exhibit polymorphic phase transitions as a function of temperature and pressure. It is not unlikely that a "solidlike" array of molecules in a liquid would have considerably different properties than the same molecules in a crystal. Therefore some method of parameter determination must be used. To date the "Seoul technique"^{3,10} has proved the most popular. This method requires good experimental triple point data that are not available for the compounds studied here.

A new parameter determining method is proposed that relies on the fact that the liquid partition function is very dependent on the "solidlike" degeneracy term

$$1 + n(V - V_s)/V_s \exp[-aE_s V_s / (V - V_s) RT] \quad (5)$$

since without this term the condition $G_l = G_s$ cannot be satisfied. By examining eq 4 for several simple compounds previously studied,¹ it was found that the ratio n/V_s was nearly a constant for the inert gases, methane and nitrogen (av $n/V_s = 0.473$). The value of $aE_s V_s / RT$ was also nearly a constant (av $aE_s V_s / RT = 1.55$). Since argon is the model compound for the theory and a substance for which n and a have been theoretically calculated, it was decided to use the argon values of these ratios.

We therefore use the experimental V_s and the ratio for argon to determine n_{cpd} .

$$n_{cpd} = n_{argon} V_{s(cpd)} / V_{s(argon)} = 0.432 V_{s(cpd)} \quad (6)$$

To determine a , the experimental values of E_s , V_s , and T_m , the melting temperature of the compounds was

(5) M. S. Jhon, J. Grosh, T. Ree, and H. Eyring, *Proc. Nat. Acad. Sci. U. S.*, **54**, 1419 (1965).

(6) G. L. Faerber, S. W. Kim, and H. Eyring, *J. Phys. Chem.*, **74**, 3510 (1970).

(7) A. Einstein, *Am. Phys.*, **22**, 180 (1907).

(8) L. Pauling, *Phys. Rev.*, **36**, 430 (1930).

(9) H. Eyring, D. Henderson, B. Stover, and E. M. Eyring, "Statistical Mechanics and Dynamics," Wiley, New York, N. Y., 1964.

(10) M. S. Jhon, J. Grosh, T. Ree, and H. Eyring, *J. Chem. Phys.*, **44**, 1465 (1966).

used. In the following relationship 1.472 is the value of $aE_s V_s / RT$ for argon.

$$a_{\text{cpd}} = 1.472RT_m / E_s V_{s(\text{cpd})} \quad (7)$$

Note that n_{epd} increases with $V_{s(\text{cpd})}$, approximately as the number of atoms in a molecule, and a increases as $1/V_{s(\text{cpd})}$.

With the experimental value of θ , a trial set of parameters are available with which the physical and thermodynamic properties can be calculated. θ is adjusted to give the correct entropy at the melting point. E_s is adjusted to give 1 atm pressure at the experimental boiling temperature. Finally, $V_{s(\text{cpd})}$ is adjusted to give the best volumes of the liquid.

Since the molal volume of the "solidlike" part of the liquid is temperature and pressure dependent, the following correction is made

$$V_{s\text{PT}} = V_{s(\text{cpd})} [1 + \alpha_s(T - T_m) - \beta_s(P - 1)] \quad (8)$$

where $V_{s\text{PT}}$ is the molar volume of the "solidlike" part of the liquid at temperature T and pressure P . α_s and β_s are the coefficients of thermal expansion and compressibility, respectively. For benzene, α_s is about 4.5×10^{-4} ($^\circ\text{K}^{-1}$) and β_s is about 8.36×10^{-8} (atm^{-1}).¹¹ The compressibility is so small that at 1 atm the pressure term in eq 8 can be neglected.

The values of n for complex molecules are found to be larger than the number of nearest neighbors. The degeneracy factor $n(V_m - V_s)/V_m$ for a large molecule is not only due to translation, but the extra volume simultaneously increases the freedom of rotation which shows up as an increase in n leading to values greater than 10.7.

Results of Thermodynamic Calculations

Significant structures theory was applied to benzene, *o*-xylene, *m*-xylene, *p*-xylene, toluene, and ethylbenzene. Thermodynamic calculations were made from the melting point to the critical point. Since toluene and ethylbenzene are known to supercool,¹² the theory was extended down in temperature to the experimental glass transition point.

The parameters used for the calculations are found in Table I.¹³⁻¹⁸ Table II lists the per cent standard deviation between observed and calculated results for the thermodynamic properties over the liquid range. Table III lists the calculated and observed properties of toluene and ethylbenzene as typical results in this study. Table IV¹⁹ lists the calculated and observed critical properties. Table V lists the calculated and observed molar volumes and entropies of toluene and ethylbenzene in the supercooled region. Figure 1 shows the calculated and observed molar volume *vs.* temperature for benzene, toluene, and ethylbenzene. Figure 2 gives plots of \log (vapor pressure) *vs.* $1/T$ for benzene, toluene, and ethylbenzene. The experimental data used to check the calculations were gathered from many sources.²⁰⁻⁴⁰

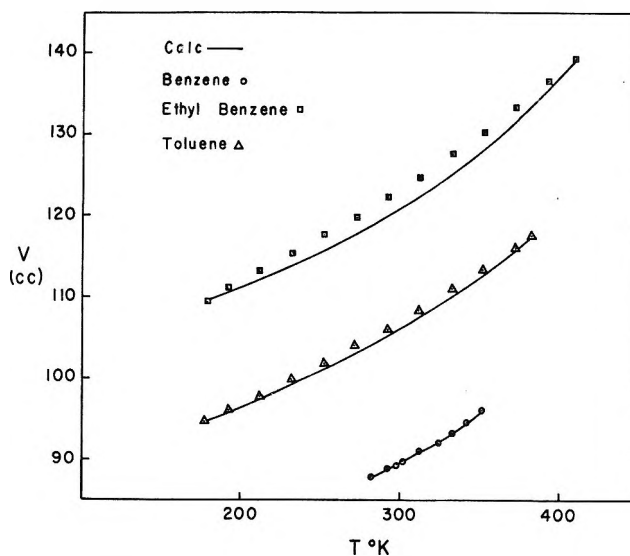


Figure 1. Molar volumes of benzene, toluene, and ethylbenzene *vs.* temperature.

- (11) P. W. Bridgman, *Proc. Amer. Acad. Arts Sci.*, **74**, 399 (1942).
- (12) A. J. Barlow, J. Lamb, and A. J. Matheson, *Proc. Roy. Soc., Ser. A*, **292**, 322 (1966).
- (13) E. R. Andrews and R. G. Eades, *ibid.*, **218**, 537 (1953).
- (14) J. H. Hildebrand and G. Archer, *Proc. Natl. Acad. Sci. U. S.*, **47**, 1881 (1961).
- (15) S. G. Biswas and S. C. Sirkar, *Indian J. Phys.*, **31**, 141 (1957).
- (16) F. D. Rossini, *et al.*, "Selected Values of Physical and Thermodynamic Properties of Hydrocarbons and Related Compounds," Carnegie Press, Pittsburgh, Pa., 1953.
- (17) A. I. Kitaigorodskii, B. D. Koreshkov, and E. I. Pikus, *Fiz. Tverd. Tela.*, **7**, 2843 (1965).
- (18) A. I. Kitaigorodskii, *Sov. Phys. Cryst.*, **7**, 152 (1962).
- (19) K. A. Kobe and R. E. Lynch, Jr., *Chem. Rev.*, **52**, 117 (1953).
- (20) J. S. Rowlinson, "Liquids and Liquid Mixtures," Butterworths, London, 1959, p 37.
- (21) L. A. K. Staveley, W. J. Tupman, and K. R. Hart, *Trans. Faraday Soc.*, **51**, 323 (1955).
- (22) J. S. Burlow, *J. Amer. Chem. Soc.*, **62**, 696 (1940).
- (23) R. C. Lord, Jr., and D. H. Andrews, *J. Phys. Chem.*, **41**, 149 (1937).
- (24) G. D. Oliver, M. Eaton, and H. M. Huffman, *J. Amer. Chem. Soc.*, **70**, 1502 (1948).
- (25) E. B. Freyer, J. C. Hubbard, and D. H. Andrews, *ibid.*, **51**, 759 (1929).
- (26) W. Schaafs, *Z. Phys. Chem. (Leipzig)*, **194**, 28 (1944).
- (27) K. S. Pitzer and D. W. Scott, *J. Amer. Chem. Soc.*, **65**, 803 (1943).
- (28) L. S. Kassel, *ibid.*, **58**, 670 (1936).
- (29) W. D. Felix, "Technique and Application of the Significant Structure Theory to Simple Liquids," Ph.D. Thesis, University of Utah, Salt Lake City, Utah, 1962.
- (30) V. Ya. Kurvatov, *J. Gen. Chem. (USSR)*, **17**, 1999 (1947).
- (31) G. Allen, G. Gee, and G. J. Wilson, *Polymer*, **1**, 456 (1960).
- (32) E. W. Washburn, Ed., "International Critical Tables," Vol. 3, McGraw-Hill, New York, N. Y., 1928, pp 223, 224.
- (33) R. J. Corruccini and D. C. Ginnings, *J. Amer. Chem. Soc.*, **69**, 2291 (1947).
- (34) C. Drucker, E. Jimeno, and W. Kangro, *Z. Phys. Chem. (Leipzig)*, **90**, 513 (1915).
- (35) D. Tyrer, *ibid.*, **87**, 169 (1914).
- (36) K. K. Kelley, *J. Amer. Chem. Soc.*, **51**, 2738 (1929).
- (37) J. C. Marshall, L. A. K. Staveley, and K. R. Hunt, *Trans. Faraday Soc.*, **52**, 19 (1956).

Table I: Summary of Liquid Parameters

Compound	n	a	V_s	V_s (obsd)	E_s	E_s (obsd) ^d	θ °K	θ (obsd), ^f °K
Benzene	33.00	0.00101	78.16	76.88 ^a	10,035.7	10,383	56.9	95 ^g
<i>o</i> -Xylene	46.00	0.0006038	108.14		12,987.6	13,140	46.8	61-84
<i>m</i> -Xylene	46.00	0.0005498	108.76	106.9 ^b	12,215.7	13,243 ^e	38.2	58-68
<i>p</i> -Xylene	43.80	0.0007376	111.53	101.9 ^b	11,857.5	13,797 ^e	39.9	72-91
Toluene (supercooled)	38.00	0.0005686	91.21	87.48 ^c	11,117.3	10,070	39.3	66-84
					7,250.0		57.0	
Ethylbenzene (supercooled)	43.60	0.000440	105.85		12,395.8	11,695	46.0	58-84
					9,200.0		88.3	

^a See ref 13. ^b See ref 14. ^c See ref 15. ^d See ref 16. ^e See ref 5. ^f See ref 17. ^g See ref 18.

Table II: Per Cent Standard Deviation^a between Observed^b and Calculated Properties

Compound	V_s cc/mol	P_s atm	S , eu	C_v , cal deg ⁻¹ mol ⁻¹	C_p , cal deg ⁻¹ mol ⁻¹	$\alpha \times 10^3$, °K ⁻¹	$\beta \times 10^6$, atm ⁻¹
Benzene	0.051	1.03	0.87	1.17	9.56	24.1	17.9
Toluene	0.85	51.6	6.20	1.75	13.59	31.0	29.1
<i>o</i> -Xylene	0.54	21.6	1.69	...	11.84	24.3	31.1
<i>m</i> -Xylene	0.644	1.58	2.47	...	14.03	25.7	26.4
<i>p</i> -Xylene	0.505	31.27	1.25	...	16.16	29.3	29.0
Ethylbenzene	1.43	50.2	6.34	...	13.6	26.5	9.85

^a Per cent standard deviation defined as

$$\sigma = \left[\sum_{i=1}^n \left(\frac{X_{\text{obsd}} - X_{\text{calcd}}}{X_{\text{obsd}}} \right)^2 / n \right]^{1/2} \times 100$$

^b For references to experimental data consult G. Faerber, Ph.D. Dissertation, University of Utah, Salt Lake City, Utah, 1971. ^c No experimental data available.

Table III: Calculated and Observed Properties

T , °K	P , atm	V_s cc/mol	C_v , cal deg ⁻¹ mol ⁻¹	C_p , cal deg ⁻¹ mol ⁻¹	S , eu	$\alpha \times 10^3$, °K ⁻¹	$\beta \times 10^6$, atm ⁻¹
Toluene							
178.16 calcd	5.73×10^{-7}	94.67	18.89	23.99	37.99	0.544	23.7
obsd	...	94.59	34.91
298.16 calcd	3.77×10^{-2}	105.57	28.07	34.25	52.39	0.749	69.3
obsd	3.78×10^{-2}	106.84	...	37.53	52.40	1.08	90.6
383.77 calcd	1.036	117.45	34.97	43.52	62.17	1.160	171.9
obsd	1.00	117.62	...	44.09	...	1.18	...
Ethylbenzene							
179.26 calcd	8.887×10^{-8}	109.65	20.06	25.09	44.74	0.480	21.8
obsd	...	109.65	40.30
298.16 calcd	2.069×10^{-2}	120.53	30.90	38.15	60.94	0.764	70.16
obsd	2.013×10^{-2}	43.9	60.95	1.01	81.2
409.10 calcd	1.89	139.62	41.43	54.21	75.83	1.583	271.3
obsd	1.00	139.68

Discussion and Conclusions

The rotors on the benzene ring have been assumed to be free in our partition function. This is certainly justifiable in the case of toluene, *m*- and *p*-xylene. The barriers for the methyl rotor of toluene has been calculated to be 67 cal/mol.⁴¹ This is in accord with

(38) G. Jones and F. C. Jelen, *J. Amer. Chem. Soc.*, **57**, 2532 (1935).

(39) G. B. Guthrie, Jr., R. W. Spitzer, and H. M. Huffman, *ibid.*, **66**, 2120 (1944).

(40) F. E. Blacet, P. A. Leighton, and E. P. Bartlett, *J. Phys. Chem.*, **35**, 1935 (1931).

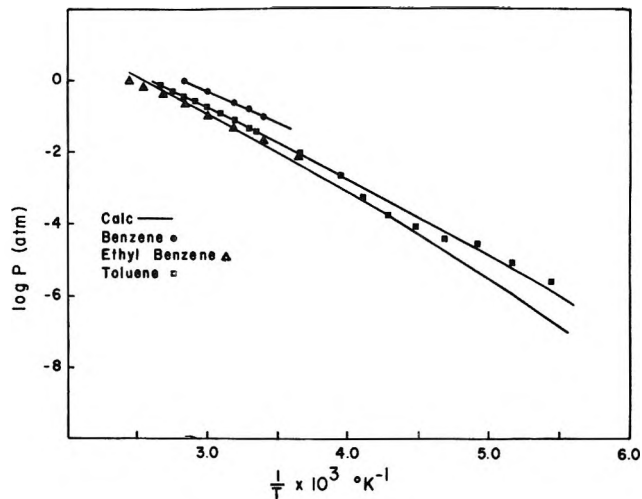
(41) W. R. Woolfenden, "Carbon-13 Magnetic Resonance Analysis of Some Alkylbenzenes," Ph.D. Thesis, University of Utah, Salt Lake City, Utah, 1965.

Table IV: Critical Properties

		Calculated	Observed ^a	% deviation
Benzene	T_c , °K	590	562	+5.0
	V_c , cc	294	260	+13.1
	P_c , atm	59.6	48.6	+22.6
Toluene	T_c , °K	618	594	+4.0
	V_c , cc	358	316	+13.3
	P_c , atm	51.2	41.0	+24.9
<i>o</i> -Xylene	T_c , °K	607	631	-3.8
	V_c , cc	409	379	+7.9
	P_c , atm	44.1	36.9	+19.5
<i>m</i> -Xylene	T_c , °K	644	619	+4.0
	V_c , cc	422	393	+7.4
	P_c , atm	45.4	36.0	+26.1
<i>p</i> -Xylene	T_c , °K	664	618	+7.4
	V_c , cc	421	366	+15.0
	P_c , atm	46.9	35.0	+34.0
Ethylbenzene	T_c , °K	573	619	-7.4
	V_c , cc	398	374	+6.4
	P_c , atm	42.8	38.0	+12.6

^a See ref 19.**Table V:** Results of Volume and Entropy Values in the Supercooled Region^a

	T , °K	Volume, cc ^b		Entropy, cal deg ⁻¹ mol ⁻¹	
		Toluene	Ethylbenzene	Toluene	Ethylbenzene
Calcd	179.26 (mp)	...	117.1	...	40.6
Obsd		...	109.9	...	40.6 ^d
Calcd	178.17	97.0	...	34.9	...
Obsd		94.7	...	34.9 ^c	...
Calcd	170	96.1	115.3	33.8	38.9
Obsd		93.9	108.9
Calcd	160	95.0	113.4	32.5	37.1
Obsd		93.0	107.8
Calcd	150	93.9	111.7	31.1	35.4
Obsd		92.1	106.9
Calcd	140	92.8	110.3	29.7	33.6
Obsd		91.2	105.8
Calcd	130	91.7	108.9	28.2	31.7
Obsd		90.3	104.8
Calcd	120	90.7	107.6	26.6	29.8
Obsd		89.4	103.7
Calcd	113 (T _g)	87.8	...	25.4	...
Obsd		83.8
Calcd	111 (T _g)	...	106.3	...	27.8
Obsd		...	102.8

^a New parameters for supercooled region: toluene, $E_s = 7250$ cal, $\theta = 57.0^\circ\text{K}$; ethylbenzene, $E_s = 9200$ cal, $\theta = 88.3^\circ\text{K}$.^b See ref 12. ^c See ref 36. ^d See ref 39.Figure 2. Log of vapor pressure (benzene, toluene, and ethylbenzene vs. $1/T$).

value of 1080 cal/mol.⁴² In this case the methyl group is clearly not free.

Although no literature values of α_s are available for any of the compounds studied except benzene, the ranges of values of 1.6 to 4.5 ($\times 10^{-4}$ deg⁻¹) seem reasonable since benzene has an $\alpha_s = 4.5 \times 10^{-4}$ deg⁻¹.¹¹

The values of n , as expected, increase with larger molecules. Large values of n arise from the rotational degeneracy as well as translational degeneracy in the liquid. To get a rough idea of the rotational contribution to the degeneracy, we examined the degeneracy factor using the parameters for viscosity (a measure of the translational degeneracy).⁶ This value was then subtracted from the average degeneracy factor obtained for the thermodynamic properties ($g_{av} = g_{trans} \cdot g_{rot}$). The contribution of g_{av} for toluene and ethylbenzene is about twice as much as for translation alone. The V_s values are consistently larger than the observed V_s for the solid at the melting point. This corresponds to a change in packing near the melting point. θ values are not unreasonable when we look at the range of observed values (see Table I). While the values of E_s differ from observed values, they are not unreasonable if we remember that they apply to the solidlike structure in the liquid.

In Table II it can be seen that the calculated and observed results are in good agreement for molar volume, entropy, and (for the observed) cases of heat capacity at constant volume. Since the heat capacity at constant pressure, coefficients of thermal expansion and compressibility involve the second derivatives of the Helmholtz free energy surface, the range of per cent

(42) W. J. Taylor, D. D. Wagman, M. G. Williams, K. S. Pitzer, and F. B. Rossini, *J. Res. Nat. Bur. Stand.*, **37**, 95 (1946).(43) D. W. Scott, G. B. Guthrie, J. S. Messerly, S. S. Todd, W. T. Berg, I. A. Hossenlopp, and J. P. McCullough, *J. Phys. Chem.*, **66**, 911 (1962).

earlier workers who claim a low barrier.^{42,43} The barriers in calories per mole for the xylenes are meta 550, para 600, and ortho 2200.⁴² So in the case of *o*-xylene our approximation is not strictly valid. For ethylbenzene the methyl rotor is assumed to have a barrier of 3400 cal/mol, and the ethyl rotor is given a

standard deviations between 9.6 and 31.1% seems acceptable. The vapor pressure predictions of the substances studied are less satisfactory. From Table III and Figure 2 it can be seen that the deviation between calculated and experimental, although not small, is something like 10% at higher temperatures, while the greatest deviation is at lower temperatures. The results for benzene and *m*-xylene are entirely acceptable, but the vapor pressure results for the remaining compounds lie in the region of 20–52% deviation and the vapor pressure of complex molecules must be further studied. In the case of toluene the low temperature vapor pressure measurements may stand reinvestigation since they show a larger deviation than the high temperature measurements.

The calculated critical properties offer a severe test for the theory. Comparing these results with those obtained previously¹ on other substances the results are somewhat improved with the critical pressure being the most difficult to obtain.

Significant structure theory was extended some 68° into the supercooled region for toluene and ethylbenzene. Toluene and ethylbenzene undergo a glass transition at 113 and 111°K, respectively. To obtain convergence of slopes down to the experimental glass point, it was necessary to vary E_s and θ . It was necessary to decrease E_s , which is consistent with the poorer packing which occurs in a supercooled liquid. Since the intermolecular bonds are not as strong and there is wasted space, E_s decreases. Since θ decreases with an increase in temperature,^{17,18,44} it is reasonable to find that in the supercooled region θ increases. This is consistent with a tightening of the solidlike structure. The calculated entropy at the glass point is higher than the entropy of the solid at that temperature. The calculated entropies of supercooled toluene at 113°K and ethylbenzene at 111°K are 25.4 and 27.9 eu, respectively. From integrated plots of C_p vs. $\ln T$ the entropy of solid toluene is about 18 eu³⁶ and for ethylbenzene the entropy is also about 18 eu.³⁹ This difference allows for the residual entropy that a glass has above the entropy of a crystal at the same temperature. The difference in entropy from the melting point to the glass point is 9.52 eu for toluene and 12.74 eu for ethylbenzene. The entropies of fusion are 8.89 and 12.29 eu, respectively. Thus we see that all of

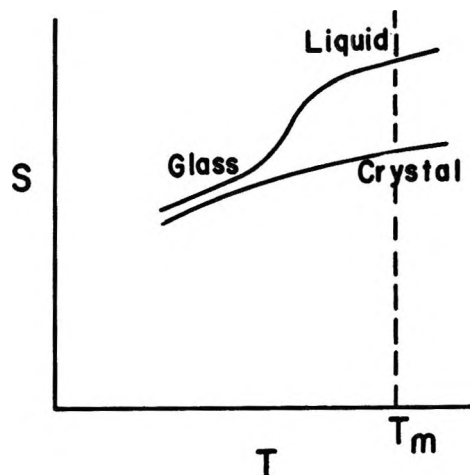


Figure 3. Schematic representation of the isobaric dependence of entropy of a substance, in various states, on temperature (after ref 45).

the entropy of melting has been lost when the liquid is supercooled to its glass point. Extensive quantitative comparisons in this region are not possible at this time. Since as Turnbull⁴⁵ states, "There is some but not much information on the thermodynamic properties of substances in their undercooled liquid and glass states." This information seems consistent with the entropy representation in Figure 3.

In summary we conclude that significant structure theory successfully calculates the thermodynamic and physical properties of the six compounds investigated. The new method of fixing parameters works successfully for large polyatomic molecules. This method of parameter determination can be readily applied to other series of compounds. The necessarily limited extension into the supercooled region yielded qualitatively good results. We conclude that significant structure theory gives good results for complex liquids.

Acknowledgment. The authors wish to thank the National Institutes of Health, Grant GM 12862, National Science Foundation, Grant GP 28631, and Army Research-Durham, Contract DA-ARO-D-31-124-72-G15, for support of this work.

(44) E. A. Guggenheim, "Thermodynamics," 5th ed, North-Holland Publishing Co., Amsterdam, 1967, p 117.

(45) D. Turnbull, "Liquids," T. J. Hughel, Ed., Elsevier, Amsterdam, 1965.

The Relationship of Crystalline Forms I, III, IV, and V of Anhydrous Sodium Sulfate as Determined by the Third Law of Thermodynamics¹

by G. E. Brodale and W. F. Giaque*

Low Temperature Laboratory, Departments of Chemistry and Chemical Engineering,
University of California, Berkeley, California 94720 (Received August 2, 1971)

Publication costs assisted by the National Science Foundation

The heat capacity of metastable $\text{Na}_2\text{SO}_4(\text{III})$ has been measured from 15 to 300°K. These data, in combination with the calorimetric heat of transition from stable $\text{Na}_2\text{SO}_4(\text{V})$ to $\text{Na}_2\text{SO}_4(\text{III})$, and available calorimetric data at temperatures above 300°K, have been used with the third law of thermodynamics to show that $\text{Na}_2\text{SO}_4(\text{III})$ is metastable at all temperatures from 0 to 517°K, where it is in equilibrium with $\text{Na}_2\text{SO}_4(\text{V})$, which has itself become metastable. $\text{Na}_2\text{SO}_4(\text{III})$ has previously been considered to be a stable phase at temperatures above 458°K. A phase $\text{Na}_2\text{SO}_4(\text{IV})$ was found to have an enthalpy content 75 cal/mcl above that of $\text{Na}_2\text{SO}_4(\text{V})$ and this has been taken as the heat of transition from stable $\text{Na}_2\text{SO}_4(\text{V})$ to stable $\text{Na}_2\text{SO}_4(\text{IV})$ at 458°K. The upper limit of stability for $\text{Na}_2\text{SO}_4(\text{IV})$ was taken as 514°K. These two temperatures, 458 and 514°K, had been found to be the only stable transition temperatures by Kracek and Gibson, who used a bomb containing the solid in contact with aqueous solution to obtain equilibrium. Heat capacity, entropy, enthalpy, and free energy functions have been tabulated for $\text{Na}_2\text{SO}_4(\text{V}, \text{IV}, \text{III}, \text{and I})$. These data predict that $\text{Na}_2\text{SO}_4(\text{I})$, the form stable between 514°K and the melting point, can undergo a transition, $\text{Na}_2\text{SO}_4(\text{I})$ to $\text{Na}_2\text{SO}_4(\text{III})$ at 509°K, in which both phases are metastable. This transition temperature had also been noted by Kracek and Gibson, using dry Na_2SO_4 , although they ascribed it to the transition $\text{Na}_2\text{SO}_4(\text{I}) \rightarrow \text{Na}_2\text{SO}_4(\text{II})$.

Interest in the relationship of the sodium sulfate system to the third law of thermodynamics in this laboratory started with the discovery of Pitzer and Coulter,² that the decahydrate has residual entropy when cooled to limiting low temperatures. After many other hydrates had been investigated here without the discovery of other cases of such residual entropy it seemed desirable to check the work on $\text{Na}_2\text{SO}_4 \cdot 10\text{H}_2\text{O}$. The principal reason for this was the accumulated experience in this laboratory relating to the difficulty which can be caused by assuming that the overall analysis for water in a hydrated crystal gives a true account of the phases present. Brodale and Giaque³ repeated the work on $\text{Na}_2\text{SO}_4 \cdot 10\text{H}_2\text{O}$, including the heats of aqueous solution under conditions such that the phases were definitely known. Their experiments confirmed the residual entropy result of Pitzer and Coulter.² There was and is no reason to question the low temperature heat capacity measurements of Pitzer and Coulter on the form of anhydrous Na_2SO_4 (Form V) stable at ordinary temperatures. However, Brodale and Giaque decided that it would be of interest to measure the heat capacity of a thermodynamically unstable form of anhydrous Na_2SO_4 (Form III) which was believed to resist transition due to slow reaction rate. The relationship between the $\text{Na}_2\text{SO}_4(\text{III})$ and $\text{Na}_2\text{SO}_4(\text{V})$ forms appeared to offer an interesting third law comparison. Although the heat capacities and heats of solution were completed, attempts to combine the results with the then available information at higher temperatures indicated some lack of understanding with respect to the high temperature

data. All of our data on $\text{Na}_2\text{SO}_4(\text{III})$ were withheld from publication, especially since it was generally realized that the transitions above ordinary temperatures were slow and may have caused error in the available high temperature data.

Much of the earlier work designed to establish phase relationships of Na_2SO_4 was done by Kracek and his collaborators.⁴⁻⁶ Kracek³ studied the Na_2SO_4 system using differential thermal analysis and microscopic examination of the dry (no more than 0.1% H_2O) salt, and postulated the existence of five different forms of anhydrous Na_2SO_4 in order to explain all the features of his observations. He labeled these modifications with Roman numerals from $\text{Na}_2\text{SO}_4(\text{I})$ which crystallizes from the molten salt to $\text{Na}_2\text{SO}_4(\text{V})$ which crystallizes from aqueous solution. Upon cooling $\text{Na}_2\text{SO}_4(\text{I})$ in the absence of moisture one always obtains metastable $\text{Na}_2\text{SO}_4(\text{III})$ which can apparently be kept indefinitely at room temperature if kept absolutely dry, and which is easily detected by its high heat content relative to $\text{Na}_2\text{SO}_4(\text{V})$ as was shown by Pickering,⁷ who made heat of solution measurements in water.

(1) This work was supported in part by the National Science Foundation.

(2) K. S. Pitzer and L. V. Coulter, *J. Amer. Chem. Soc.*, **60**, 1310 (1938).

(3) G. E. Brodale and W. F. Giaque, *ibid.*, **80**, 2042 (1958).

(4) F. C. Kracek, *J. Phys. Chem.*, **33**, 1281 (1929).

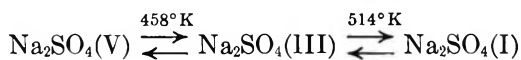
(5) (a) F. C. Kracek and R. E. Gibson, *ibid.*, **33**, 1304 (1929);

(b) F. C. Kracek and R. E. Gibson, *ibid.*, **34**, 188 (1930).

(6) F. C. Kracek and C. J. Ksanda, *ibid.*, **34**, 1741 (1930).

(7) S. U. Pickering, *J. Chem. Soc.*, **XLV**, 686 (1884).

Measurements on the dry salt are adversely affected by slow equilibrium and superheating, and it was not possible for Kracek to assign accurate temperatures to the various transitions. Kracek and Gibson,^{5a} using dilatometry, found that the presence of aqueous solution substantially speeds up the transformations and reduces the hysteresis. The liquid apparently provides a mechanism for recrystallization, thus enabling easier attainment of equilibrium. In the presence of aqueous solution they observed only two transformations corresponding to three stable phases. The two observed temperatures were $458 \pm 1^\circ\text{K}$ and $514 \pm 1^\circ\text{K}$. X-Ray analysis by Kracek and Ksanda⁸ also detected only three forms of Na_2SO_4 . Since it had been well established from heat of solution measurements that $\text{Na}_2\text{SO}_4(\text{III})$ is formed when $\text{Na}_2\text{SO}_4(\text{I})$ is cooled in the absence of moisture, Kracek and Ksanda suggested that the system could be represented by the relationship



with $\text{Na}_2\text{SO}_4(\text{II})$ and $\text{Na}_2\text{SO}_4(\text{IV})$ existing only as unstable phases. However, the present results utilize the third law of thermodynamics to show that $\text{Na}_2\text{SO}_4(\text{III})$ is metastable with respect to $\text{Na}_2\text{SO}_4(\text{V})$ at all temperatures from 0 to 517°K . New observations also indicate that $\text{Na}_2\text{SO}_4(\text{IV})$ is the stable phase between 458 and 514°K .

Schroeder, Gabriel, and Partridge⁸ made solubility measurements of Na_2SO_4 in water between 413 and 623°K , and subjected the residual solid phases to microscopic examination which confirmed Kracek and Gibson's observations that in the presence of aqueous solution Na_2SO_4 undergoes only two transformations near 458 and 514°K corresponding to three stable phases.

Recently Paukov and Lavrent'eva⁹ heated Na_2SO_4 to 350° for 1 hr and measured the low temperature heat capacity over the range 13.5 to 296°K on the assumption that it had been converted to $\text{Na}_2\text{SO}_4(\text{III})$. Their results are intermediate between our measurements on $\text{Na}_2\text{SO}_4(\text{III})$ and the data of Pitzer and Coulter on $\text{Na}_2\text{SO}_4(\text{V})$. Paukov and Lavrent'eva report that thermographic analysis was used to demonstrate that their sample of $\text{Na}_2\text{SO}_4(\text{III})$ contained only traces of $\text{Na}_2\text{SO}_4(\text{V})$. We have little confidence in thermographic analysis at the rates ordinarily used (not stated by P. & L.), and especially in a case where the transition is sluggish. Thus we decided to test our hypothesis, that the composition of the sample of P. & L. was intermediate between phases III and V, by the heat of solution method.

Following the procedure of P. & L., $\text{Na}_2\text{SO}_4(\text{V})$ was heated for exactly 1 hr at 350° . A heat of solution measurement of a portion in water, at 25° , 2.5 hr later showed that the sample contained about 96% $\text{Na}_2\text{SO}_4(\text{III})$. The Na_2SO_4 was allowed to stand for 8 days,

after which another heat of solution measurement showed that it contained only 10% $\text{Na}_2\text{SO}_4(\text{III})$.

The above statements are based on an accurate knowledge of the heat of transition at 25° between phases (V) and (III). This has been most accurately determined by Coughlin,¹⁰ whose sample of $\text{Na}_2\text{SO}_4(\text{III})$ was "ignited at 880° for 6 hr," followed by a measurement of the heat of solution in water at 30° . Similar heat of solution measurements by Coughlin¹⁰ on stable $\text{Na}_2\text{SO}_4(\text{V})$ contain an erroneous correction for the "0.105%" water content of his sample. Before correction his average value for the ΔH of solution to a final concentration of 0.0543 *M* at 30° was -628.2 ± 1.6 cal/mol. The correction should have been -17.1 cal/mol instead of the -1.4 cal/mol given by Coughlin,¹⁰ leading to a value $\Delta H = -628.2 - 17.1 = -645 \pm 1.6$ cal/mol. When this value is combined with Coughlin's ΔH of solution for $\text{Na}_2\text{SO}_4(\text{III})$, -1363 ± 3.3 cal/mol the ΔH of transition is found to be

$$\text{Na}_2\text{SO}_4(\text{V}) = \text{Na}_2\text{SO}_4(\text{III}) \quad (1)$$

$$\Delta H_{303.15} = -1363 + 645 = -718 \pm 4 \text{ cal/mol}$$

Using the small ΔC_p for reaction 1 from the present results

$$\Delta H_{298.15} = 716 \pm 4 \text{ cal/mol} \quad (2)$$

We may also combine the heat of solution of $\text{Na}_2\text{SO}_4(\text{V})$ from Pitzer and Coulter² with the heat of solution of $\text{Na}_2\text{SO}_4(\text{III})$ measured during the present work. This involved the heat of aqueous solution and low temperature heat capacities on a sample which had been heated at $\sim 780^\circ$ for 4 days, followed by cooling in a drybox to produce $\text{Na}_2\text{SO}_4(\text{III})$. The resulting heat of transition was in substantial agreement (713 ± 10 cal/mol) with Coughlin's¹⁰ value of the above heat of transition at 25° .

It would appear that heating Na_2SO_4 to temperatures near or above the melting point, followed by cooling, produces metastable $\text{Na}_2\text{SO}_4(\text{III})$ which resists conversion to $\text{Na}_2\text{SO}_4(\text{V})$. However, holding the substance at a temperature such as 350° may leave many nuclei of $\text{Na}_2\text{SO}_4(\text{V})$, which cause recrystallization of the $\text{Na}_2\text{SO}_4(\text{III})$. Such a situation is not at all unusual and extra heating to destroy nuclei of an unwanted phase is a standard procedure in producing a wide variety of unstable phases. Also, it is difficult to remove all of the water from Na_2SO_4 by heating for a short time such as an hour in an environment at 350° , especially when the heating delay caused by transition heat absorption near 250° is considered. Analysis of our sample after it had been in an oven at 350° for exactly 1 hr showed

(8) W. C. Schroeder, A. Gabriel, and E. P. Partridge, *J. Amer. Chem. Soc.*, **57**, 1539 (1935).

(9) T. E. Paukov and M. N. Lavrent'eva, *Zh. Fiz. Khim. Tsiklu Vseukr. Akad. Nauk*, **43**, 2116 (1969); *Russ. J. Phys. Chem.*, **43**, 1185 (1969).

(10) J. P. Coughlin, *J. Amer. Chem. Soc.*, **77**, 868 (1955).

0.03% of H₂O, whereas Paukov and Lavrent'eva⁹ report 0.008% of H₂O. Since there is evidence that water has a catalytic effect on the Na₂SO₄ transitions we consider that heating to 350° is insufficient to ensure the stability of Na₂SO₄(III) due to water content.

Preparation of Na₂SO₄

Na₂SO₄(III) was prepared by heating reagent grade Na₂SO₄ at ~780° in a platinum dish for 4 days. The hot sample was removed to a drybox where it was allowed to cool to room temperature. The low temperature calorimeter and the sample tubes A and B for the heat of solution were all filled and sealed in the drybox on March 4, 1958. Since the experiments extended over a considerable period they present an unusual opportunity to observe the substantial stability of Na₂SO₄(III) when Na₂SO₄(I) has been heated to a sufficiently high temperature to remove water and to destroy nuclei of Na₂SO₄(V). The significant dates of experiments will be given.

Low Temperature Heat Capacity of Na₂SO₄(III)

The low temperature calorimeter was the one used for our measurements on Na₂SO₄·10H₂O.³ References to the type of calorimeter and thermometry were given.³ The most complete description of our low temperature calorimeters and techniques is included in "Notes on Assembly and Experimental Procedure with Low Temperature Calorimeters."¹¹ The experimental data on Na₂SO₄(III) are given in Table I. The

sample weighed 172.1049 g corrected to *in vacuo* weight. The molecular weight was taken as 142.04.

The heat capacity of Na₂SO₄(III) was measured over the range 15–300°K during the period March 31 to April 16, 1958. It was left at room temperature until September 11, 1958, at which time a sample was removed from the calorimeter and examined by X-ray. The examination showed the characteristic structure of Na₂SO₄(III) and gave no evidence of Na₂SO₄(V). This in itself does not rule out the presence of a few percent of Na₂SO₄(V), but if the low temperature had triggered conversion, the period from April to September 1958 should have produced a detectable amount of Na₂SO₄(V). After the sample for X-ray examination had been removed the calorimeter was stoppered. On May 20, 1959 the sodium sulfate was transferred to a stoppered glass bottle. Probably neither the stoppered calorimeter nor the glass bottle was completely airtight against "breathing" during the period until Nov 4, 1959, although the temperature was very uniform and any "breathing" should have been minimized. After the sealed heat of solution samples A and B had been examined, as will be discussed below, it was considered of some interest to test the low temperature sample that had been allowed to come into contact with the undried atmosphere. The heat of solution on Nov 4, 1959, corrected to infinite dilution at 25°, was found to be –574 cal/mol in good agreement with the –560 ± 10 cal/mol result of Pitzer and Coulter² for Na₂SO₄(V). It is probable that moisture caused complete conversion of the Na₂SO₄(III) sample to Na₂SO₄(V) although the chance of Na₂SO₄(V) nucleation starting should be proportional to the some 100 g of the original sample which remained on Nov 4, 1959.

To supplement the data in Table I by results above 300°K we prefer measurements by adiabatic calorimetry over those obtained by dropping capsule enclosed samples from temperature *T* to a calorimeter at ordinary temperatures. In fact, the several metastable states and severe hysteresis of Na₂SO₄, make it an exceptionally poor subject for the drop method. Thus, we give no weight to the enthalpy differences obtained by Coughlin,¹⁰ using that technique. We have given full weight to the data of Shmidt and Sokolov,¹² who used adiabatic calorimetry for both Na₂SO₄(III) and (V). They prepared Na₂SO₄(III) from Na₂SO₄(I), and since they made measurements on Na₂SO₄(I) to 748° in a platinum capsule which was not "airtight,"¹² we may assume that this sample could lose water and thus was very dry. They state: "On cooling in the absence of moisture, this modification is transformed into Na₂SO₄ (III)." The data of Pitzer and Coulter² on Na₂SO₄(V) were used below 300°K.

Table I: Heat Capacity of Na₂SO₄(III)^a

<i>T</i> , °K	<i>C_p</i>	<i>T</i> , °K	<i>C_p</i>
13.16	0.250	129.03	19.66
15.18	0.383	135.62	20.29
16.83	0.524	142.68	20.94
18.99	0.767	150.73	21.62
21.63	1.104	159.41	22.32
24.42	1.574	167.92	22.97
27.79	2.200	175.94	23.55
31.97	3.077	183.54	24.05
36.23	4.003	191.20	24.58
40.39	4.944	199.24	25.17
44.80	5.982	207.67	25.77
49.74	7.133	215.89	26.29
55.64	8.481	223.71	26.79
62.21	9.912	231.32	27.23
68.15	11.14	238.65	27.64
74.61	12.33	245.93	28.07
82.09	13.66	253.27	28.58
89.78	14.84	260.34	28.88
97.67	15.97	266.99	29.27
105.27	16.96	274.05	29.62
112.64	17.86	281.22	29.93
120.38	18.73	288.72	30.32
127.90	19.54	297.71	30.71

^a *C_p* in gibbs/mol; M.W. 142.04; 0° = 273.15°K. (gibbs ≡ defined calorie/defined degree.)

(11) "The Scientific Papers of William F. GIAUQUE," Vol. I, Dover Publications, New York, N. Y., 1969, pp 332–368.

(12) N. E. Shmidt and V. A. Sokolov, *Zh. Neorg. Khim.*, 6, 2319 (1961); *Russ. J. Inorg. Chem.*, 6, 12 (1961).

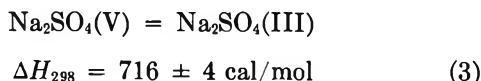
Table II: Thermodynamic Properties of Na₂SO₄^a

T	(H-H ₀) ^o - (F-H ₀) ^o					(H-H ₀) ^o - (F-H ₀) ^o					(H-H ₀) ^o - (F-H ₀) ^o					(H-H ₀) ^o - (F-H ₀) ^o																																											
	T	C _p	S	T	T	T	C _p	S	T	T	T	C _p	S	T	T	T	C _p	S	T	T	T	C _p	S	T	T																																		
Stable Na ₂ SO ₄ (V)					Stable Na ₂ SO ₄ (V) (contd)					Metastable Na ₂ SO ₄ (III) (contd)					Metastable Na ₂ SO ₄ (III) (contd)																																												
15	.222	.072	.054	.018	400	34.710	45.343	22.203	23.140	50	7.189	3.354	2.379	.975	460	38.784	52.003	24.477	27.525	470	39.369	52.842	24.788	28.055	480	40.021	53.678	25.098	28.580	490	40.772	54.511	25.410	29.101	500	41.667	55.343	25.726	29.617	509	42.644	56.095	26.016	30.079	510	42.755	56.179	26.049	30.130	517	43.696	56.768	26.281	30.487	520	44.147	57.022	26.383	30.639
20	.581	.179	.135	.043	410	35.064	46.204	22.512	23.692	55	8.342	4.094	2.869	1.225	470	39.369	52.842	24.788	28.055	480	40.021	53.678	25.098	28.580	490	40.772	54.511	25.410	29.101	500	41.667	55.343	25.726	29.617	509	42.644	56.095	26.016	30.079	510	42.755	56.179	26.049	30.130	517	43.696	56.768	26.281	30.487	520	44.147	57.022	26.383	30.639					
25	1.213	.372	.284	.089	420	35.411	47.053	22.815	24.238	60	9.436	4.867	3.370	1.496	480	40.021	53.678	25.098	28.580	490	40.772	54.511	25.410	29.101	500	41.667	55.343	25.726	29.617	509	42.644	56.095	26.016	30.079	510	42.755	56.179	26.049	30.130	517	43.696	56.768	26.281	30.487	520	44.147	57.022	26.383	30.639										
30	2.026	.663	.504	.159	430	35.751	47.891	23.112	24.779	70	11.506	6.479	4.387	2.092	490	40.772	54.511	25.410	29.101	500	41.667	55.343	25.726	29.617	509	42.644	56.095	26.016	30.079	510	42.755	56.179	26.049	30.130	517	43.696	56.768	26.281	30.487	520	44.147	57.022	26.383	30.639															
35	2.981	1.045	.788	.258	440	36.085	48.716	23.403	25.313	80	13.318	8.137	5.393	2.744	500	41.667	55.343	25.726	29.617	509	42.644	56.095	26.016	30.079	510	42.755	56.179	26.049	30.130	517	43.696	56.768	26.281	30.487	520	44.147	57.022	26.383	30.639																				
40	4.054	1.512	1.127	.385	450	36.413	49.531	23.689	25.842	90	14.879	9.798	6.362	3.435	510	42.755	56.179	26.049	30.130	517	43.696	56.768	26.281	30.487	520	44.147	57.022	26.383	30.639	520	44.147	57.022	26.383	30.639	520	44.147	57.022	26.383	30.639	520	44.147	57.022	26.383	30.639															
45	5.206	2.056	1.516	.540	458	36.672	50.175	23.913	26.262	100	16.280	11.439	7.285	4.154	517	43.696	56.768	26.281	30.487	520	44.147	57.022	26.383	30.639	520	44.147	57.022	26.383	30.639	520	44.147	57.022	26.383	30.639	520	44.147	57.022	26.383	30.639	520	44.147	57.022	26.383	30.639															
50	6.402	2.666	1.944	.722	458	36.672	50.175	23.913	26.262	110	17.540	13.050	8.161	4.890	520	44.147	57.022	26.383	30.639	520	44.147	57.022	26.383	30.639	520	44.147	57.022	26.383	30.639	520	44.147	57.022	26.383	30.639	520	44.147	57.022	26.383	30.639	520	44.147	57.022	26.383	30.639															
55	7.595	3.332	2.403	.929	458	36.672	50.175	23.913	26.262	120	18.698	14.627	8.991	5.636	520	44.147	57.022	26.383	30.639	520	44.147	57.022	26.383	30.639	520	44.147	57.022	26.383	30.639	520	44.147	57.022	26.383	30.639	520	44.147	57.022	26.383	30.639	520	44.147	57.022	26.383	30.639															
60	8.746	4.043	2.884	1.159	458	36.672	50.175	23.913	26.262	130	19.747	16.166	9.779	6.387	520	44.147	57.022	26.383	30.639	520	44.147	57.022	26.383	30.639	520	44.147	57.022	26.383	30.639	520	44.147	57.022	26.383	30.639	520	44.147	57.022	26.383	30.639	520	44.147	57.022	26.383	30.639															
70	10.851	5.552	3.874	1.678	458	36.672	50.175	23.913	26.262	140	20.695	17.664	10.525	7.139	520	44.147	57.022	26.383	30.639	520	44.147	57.022	26.383	30.639	520	44.147	57.022	26.383	30.639	520	44.147	57.022	26.383	30.639	520	44.147	57.022	26.383	30.639	520	44.147	57.022	26.383	30.639															
80	12.754	7.128	4.868	2.260	458	36.672	50.175	23.913	26.262	150	21.546	19.122	11.232	7.889	520	44.147	57.022	26.383	30.639	520	44.147	57.022	26.383	30.639	520	44.147	57.022	26.383	30.639	520	44.147	57.022	26.383	30.639	520	44.147	57.022	26.383	30.639	520	44.147	57.022	26.383	30.639															
90	14.439	8.729	5.839	2.890	460	36.736	50.335	23.969	26.366	160	22.349	20.538	11.902	8.636	520	44.147	57.022	26.383	30.639	520	44.147	57.022	26.383	30.639	520	44.147	57.022	26.383	30.639	520	44.147	57.022	26.383	30.639	520	44.147	57.022	26.383	30.639	520	44.147	57.022	26.383	30.639															
100	15.941	10.330	6.776	3.554	470	37.055	51.128	24.244	26.884	170	23.105	21.916	12.539	9.377	520	44.147	57.022	26.383	30.639	520	44.147	57.022	26.383	30.639	520	44.147	57.022	26.383	30.639	520	44.147	57.022	26.383	30.639	520	44.147	57.022	26.383	30.639	520	44.147	57.022	26.383	30.639															
110	17.258	11.912	7.670	4.242	480	37.369	51.912	24.514	27.398	180	23.829	23.257	13.146	10.111	520	44.147	57.022	26.383	30.639	520	44.147	57.022	26.383	30.639	520	44.147	57.022	26.383	30.639	520	44.147	57.022	26.383	30.639	520	44.147	57.022	26.383	30.639	520	44.147	57.022	26.383	30.639															
120	18.441	13.465	8.519	4.946	490	37.681	52.686	24.780	27.906	190	24.535	24.564	13.727	10.837	520	44.147	57.022	26.383	30.639	520	44.147	57.022	26.383	30.639	520	44.147	57.022	26.383	30.639	520	44.147	57.022	26.383	30.639	520	44.147	57.022	26.383	30.639	520	44.147	57.022	26.383	30.639															
130	19.520	14.985	9.325	5.660	500	37.989	53.450	25.040	28.409	200	25.236	25.841	14.285	11.556	520	44.147	57.022	26.383	30.639	520	44.147	57.022	26.383	30.639	520	44.147	57.022	26.383	30.639	520	44.147	57.022	26.383	30.639	520	44.147	57.022	26.383	30.639	520	44.147	57.022	26.383	30.639															
140	20.502	16.468	10.088	6.379	510	38.295	54.205	25.297	28.908	210	25.910	27.088	14.823	12.266	520	44.147	57.022	26.383	30.639	520	44.147	57.022	26.383	30.639	520	44.147	57.022	26.383	30.639	520	44.147	57.022	26.383	30.639	520	44.147	57.022	26.383	30.639	520	44.147	57.022	26.383	30.639															
150	21.397	17.913	10.813	7.100	512	38.356	54.355	25.348	29.007	220	26.548	28.309	15.341	12.968	520	44.147	57.022	26.383	30.639	520	44.147	57.022	26.383	30.639	520	44.147	57.022	26.383	30.639	520	44.147	57.022	26.383	30.639	520	44.147	57.022	26.383	30.639	520	44.147	57.022	26.383	30.639															
160	22.232	19.321	11.501	7.820	517	38.509	54.728	25.475	29.254	230	27.160	29.503	15.841	13.661	520	44.147	57.022	26.383	30.639	520	44.147	57.022	26.383	30.639	520	44.147	57.022	26.383	30.639	520	44.147	57.022	26.383	30.639	520	44.147	57.022	26.383	30.639	520	44.147	57.022	26.383	30.639															
170	23.030	20.693	12.156	8.537	520	38.600	54.952	25.550	29.401	240	27.751	30.670	16.325	14.346	520	44.147	57.022	26.383	30.639	520	44.147	57.022	26.383	30.639	520	44.147	57.022	26.383	30.639	520	44.147	57.022	26.383	30.639	520	44.147	57.022	26.383	30.639	520	44.147	57.022	26.383	30.639															
180	23.793	22.031	12.781	9.250	520	38.600	54.952	25.550	29.401	250	28.322	31.815	16.793	15.022	520	44.147	57.022	26.383	30.639	520	44.147	57.022	26.383	30.639	520	44.147	57.022	26.383	30.639	520	44.147	57.022	26.383	30.639	520	44.147	57.022	26.383	30.639	520	44.147	57.022	26.383	30.639															
190	24.515	23.337	13.380	9.957	520	38.600	54.952	25.550	29.401	260	28.877	32.936	17.247	15.689	520	44.147	57.022	26.383	30.639	520	44.147	57.022	26.383	30.639	520	44.147	57.022	26.383	30.639	520	44.147	57.022	26.383	30.639	520	44.147	57.022	26.383	30.639	520	44.147	57.022	26.383	30.639															
200	25.217	24.612	13.954	10.658	520	38.600	54.952	25.550	29.401	270	29.421	34.036	17.688	16.349	520	44.147	57.022	26.383	30.639	520	44.147	57.022	26.383	30.639	520	44.147	57.022	26.383	30.639	520	44.147	57.022	26.383	30.639	520	44.147	57.022	26.383	30.639	520	44.147	57.022	26.383	30.639															
210	25.871	25.858	14.506	11.352	520	38.600	54.952	25.550	29.401	280	29.955	35.116	18.117	17.000	520	44.147	5																																										

18 months later, before solution. The agreement of the ΔH 's of solution of the two samples leaves no doubt concerning the stability of the dry Na₂SO₄(III) over the above period.

Determination of the Transition Temperature of Na₂SO₄(V) → Na₂SO₄(III)

The ΔH of solution of Na₂SO₄(III) given in Table III was used above in combination with the data of Pitzer and Coulter² on Na₂SO₄(V) to give 713 ± 10 cal for the transition (V) → (III) at 298°K, as mentioned above. The data of Coughlin^{5a} have been corrected above to give the value 716 ± 4 cal/mol for this transition at 298°K. We prefer to give total weight to the result of Coughlin because he made six determinations with a very small mean deviation. Also the former Berkeley Bureau of Mines Laboratory had long previous experience in aqueous solution calorimetry. Since the heat of transition is obtained as a difference, it is preferable to give complete weight to the work of the one experimenter, with one calorimeter, in eliminating errors which might be systematically high or low. In addition, the combined work in this laboratory by Pitzer and Coulter² and the present authors gives a result, 713 ± 10 cal/mol, within Coughlin's small deviation although its possible limit of error is somewhat greater. Thus, we accept the value 716 ± 4 cal/mol as the heat of transition.



Using the enthalpy values in Table II

$$\Delta H^\circ_0 = 638 \text{ cal/mol} \quad (4)$$

The $(F^\circ - H^\circ_0)/T$ values in Table II may now be used to determine the transition temperature of Na₂SO₄(V) → Na₂SO₄(III).

$$\frac{\Delta F}{T} = 0 = \frac{\Delta H^\circ_0}{T} + \frac{\Delta(F^\circ - H^\circ_0)}{T} \quad (5)$$

The temperature at which the above equality is valid is found to be 517°K.

As mentioned above, Kracek and Gibson^{5a} studied the transitions and volume changes in Na₂SO₄ in the presence of water in a bomb, because they had found that water enabled the attainment of equilibrium conditions. In the dry state the system displays marked hysteresis. On the basis of their results in the presence of water they suggested^{5a} that a phase to which they assigned the designation of Na₂SO₄(IV) was stable over a small region below 458°K. We prefer to believe and will offer evidence in support of the idea that Na₂SO₄(IV) is stable above 458°K, having been produced by a stable transition from Na₂SO₄(V) at 458°K. Kracek and Gibson found that a stable transition to Na₂SO₄(I) occurred at 514°K and consistency with

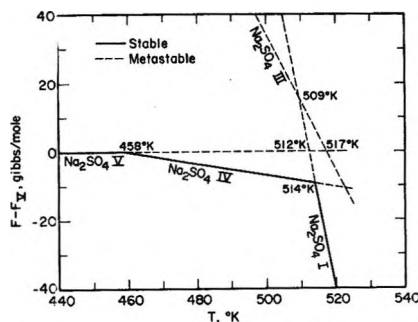


Figure 1. Free energy diagrams for Na₂SO₄ phases I, III, IV, and V.

the above requires that this temperature be assigned to the transition Na₂SO₄(IV) = Na₂SO₄(I).

Before proceeding further in the orderly analysis of the several transitions it is desirable to construct a diagram for free energy *vs.* temperature for the several phases. Na₂SO₄(V) will be taken as a zero reference for free energy at all temperatures, as is shown in Figure 1.

The horizontal solid line terminating at 458°K, in Figure 1, represents the stable region of Na₂SO₄(V). The dashed extension above 458°K represents metastable Na₂SO₄(V). This condition is readily realizable in the dry state, as has been demonstrated by the calorimetric measurements of Shmidt and Sokolov,¹² to which we have referred above.

The dashed line for Na₂SO₄(III), is drawn from the third law treatment of the calorimetric data. It shows the equilibrium between metastable Na₂SO₄(V) and metastable Na₂SO₄(III) at 517°K, which serves as an anchor for drawing the Na₂SO₄(III) curve.

Kracek and Gibson^{5a} show in their Figure 11 a transition in the presence of a saturated water solution which has a volume increase at 514°K. There seems to be little doubt that this is a transition between equilibrium phases and we assign it to Na₂SO₄(IV) = Na₂SO₄(I) as mentioned above.

We have stated above that new observations have indicated that Na₂SO₄(IV) is the equilibrium phase over the range 458–514°K. It was evident from the overall thermodynamic data and particularly the proximity of the several assignable transition points in the short range above 500°K, that an assumed Na₂SO₄(IV) phase must have an enthalpy content and a heat capacity very similar to those of Na₂SO₄(V). The following experiment was carried out: Na₂SO₄ was crystallized from solution in the range 40–45°. It was then held for 19 days at a temperature of 470–475°K. This temperature was selected because it was above the transition temperature, 458°K. Two hr and 40 min after removal the ΔH of solution of a sample at 298.15°K was found to be -636 cal/mol at infinite dilution. A second sample was held for 16 days at room temperature and another ΔH of solution mea-

surement gave a result of -634 cal/mol, confirming the first result. A sample was shown to have a water content of 0.04% . This indicates that the state produced by holding Na_2SO_4 at a temperature above the 458°K transition acquired an increased enthalpy of about 75 cal/mol and that it had a substantial stability when held at room temperature. It will now be assumed that the heat of transition of $\text{Na}_2\text{SO}_4(\text{V}) \rightarrow \text{Na}_2\text{SO}_4(\text{IV})$ is 75 cal/mol and the consequences investigated.

The entropy of transition at 458°K is then $75/458 = 0.163$ gibbs/mol, and the value of ΔF for $\text{Na}_2\text{SO}_4(\text{IV})$ minus $\text{Na}_2\text{SO}_4(\text{V})$ by $-0.163 \times (T - 458)$ between 458 and 514°K . This line has been drawn straight in Figure 1 because of our assumption that the heat capacities of $\text{Na}_2\text{SO}_4(\text{V})$ and (IV) are identical.

In extending the $(F^\circ - H^\circ_0/T)$ function for $\text{Na}_2\text{SO}_4(\text{I})$ beyond the 514°K transition point of $\text{Na}_2\text{SO}_4(\text{IV})$ and $\text{Na}_2\text{SO}_4(\text{I})$, the $\Delta H_{514^\circ\text{K}}$ of this transition is required. This is the sum of $\Delta H(\text{V} \rightarrow \text{III}) + \Delta H(\text{III} \rightarrow \text{I}) - \Delta H(\text{V} \rightarrow \text{IV})$, all calculated to 514°K . $\Delta H(\text{V} \rightarrow \text{III})$ is available by combining the enthalpy data in Table II with the $\Delta H^\circ_0 = 638$ cal/mol. The result is $\Delta H(\text{V} \rightarrow \text{III})_{514^\circ\text{K}} = 1040$ cal/mol.

$\Delta H(\text{III} \rightarrow \text{I})$ is given by Shmidt and Sokolov¹² as 1630 cal/mol (1629 , 1626 , 1636) at about 521.7°K . They comment on the severe hysteresis. We will present evidence later which indicates that this transition is superheated from 509°K . Using the ΔC_p of the transition to calculate the heat at 514°K , the 1630 cal/mol becomes $\Delta H(\text{III} \rightarrow \text{I})_{514^\circ\text{K}} = 1646$ cal/mol.

The $\Delta H(\text{V} \rightarrow \text{IV})$ over the range 458°K to 514°K has been taken as 75 cal/mol, thus $\Delta H(\text{V} \rightarrow \text{IV})_{514^\circ\text{K}} = 75$ cal/mol.

The above sum $\Delta H(\text{IV} \rightarrow \text{I})_{514^\circ\text{K}} = 1040 + 1646 - 75 = 2611$ cal/mol.

This heat of transition and the heat capacities of Shmidt and Sokolov¹² enable the calculation of the thermodynamic properties of $\text{Na}_2\text{SO}_4(\text{I})$, as given in Table II and shown near the transition region in Figure 1. The data have been extrapolated a short distance and are found to intersect the free energy curve of $\text{Na}_2\text{SO}_4(\text{III})$ at 509°K , as shown in Figure 1. This temperature, $509^\circ\text{K} = 236^\circ$, is of interest because Kracek and Gibson⁴ found a break near this temperature during their dilatometer experiments on "dry" Na_2SO_4 . They state, "This break at 235° was one of the most definite and reproducible points we encountered in all the investigation." They found that the dry Na_2SO_4 could be cycled through a rather small hysteresis loop as the substance was alternately heated and cooled a little when it was near 509°K (236°) and ascribed a transition to this temperature. We have used the term "dry Na_2SO_4 ," although we believe that most of the work on Na_2SO_4 , which did not involve heating to very high temperatures, was carried out on Na_2SO_4 which must have contained a small concentra-

tion of water. In fact, this may have had a part in reducing the superheating of transitions while preserving substantial amounts of unstable states as a fortunate compromise. However, when dry Na_2SO_4 was being heated from lower temperatures it did not begin to undergo the transition until a temperature of about 248° (521°K), as is shown by Figure 5 of Kracek and Gibson.^{5a} This is apparently the reason why Shmidt and Sokolov¹² observed the $(\text{III} \rightarrow \text{I})$ transition at the higher temperature, as heat was added during their calorimetric measurements. Perhaps one should not be surprised that there are crystal structures which act like traps, that spring easily only in one direction. An interesting example is the carefully studied case of phosphine, PH_3 .¹⁵ This substance has a transition point at 49.43°K , where it should transform on cooling to the form stable below 49.43°K ; however, the rate was immeasurably slow at 48 – 49°K even when a mixture of the stable and unstable forms was known to be present. When the PH_3 was cooled to 40°K , the optimum temperature, conversion to the stable form could be accomplished in 2 or 3 days. However, in this case, when the stable form was heated, transition at 49.43°K occurred with no detected hysteresis.

Table II also gives the thermodynamic properties of $\text{Na}_2\text{SO}_4(\text{V})$ and $\text{Na}_2\text{SO}_4(\text{I})$ in short regions where these phases are metastable.

We can make a comment on the two heats of transition of Shmidt and Sokolov¹² which they assign to the process $\text{Na}_2\text{SO}_4(\text{V}) \rightarrow \text{Na}_2\text{SO}_4(\text{I})$. They found 2584 ± 15 cal/mol at 516°K for Na_2SO_4 which had been crystallized from aqueous solution at 42 – 45° . They also found 2673 ± 5 cal/mole at 521°K for effloresced Na_2SO_4 , which had been prepared by dehydrating $\text{Na}_2\text{SO}_4 \cdot 10\text{H}_2\text{O}$ in a vacuum at room temperature. Several experiments in this laboratory have shown that there is no appreciable difference in enthalpy when Na_2SO_4 prepared in each of these ways is dissolved in water at 25° . This means that Na_2SO_4 prepared by vacuum efflorescence of the decahydrate is not sufficiently microscopic to affect the enthalpy. The difference in the above measurements, $2673 - 2584 = 89 \pm 20$ cal/mol, is suspiciously near to the difference in enthalpy between $\text{Na}_2\text{SO}_4(\text{V})$ and $\text{Na}_2\text{SO}_4(\text{IV})$.

The higher value is approximately equal to that obtainable from Table II for $\text{Na}_2\text{SO}_4(\text{V}) = \text{Na}_2\text{SO}_4(\text{I})$

$$\Delta H_{512^\circ\text{K}} = 2681 \text{ cal/mol}$$

It seems reasonable that the finely divided effloresced salt can lose water much more effectively and thus could be more readily obtained as the metastable $\text{Na}_2\text{SO}_4(\text{V})$ in the relatively dry state. The coarse particles of ground salt should retain more water and thus it is more likely to transform to $\text{Na}_2\text{SO}_4(\text{IV})$ which has a

(15) C. C. Stephenson and W. F. Giauque, *J. Chem. Phys.*, **5**, 149 (1937).

higher enthalpy and thus a lower heat of transition, $\Delta H = 2611$ cal/mol, to $\text{Na}_2\text{SO}_4(\text{I})$ at 514°K .

Since $\text{Na}_2\text{SO}_4(\text{IV})$ with a substantial stability below 458°K can be prepared it should be possible to compare its entropy with that of $\text{Na}_2\text{SO}_4(\text{V})$ by using the third law. From Table II, $S(\text{Na}_2\text{SO}_4, \text{V})_{458^\circ\text{K}} = 50.175$ gibbs/mol; thus, $S(\text{Na}_2\text{SO}_4, \text{IV})_{458^\circ\text{K}} = 50.175 + 0.163 = 50.338$ gibbs/mol. The small difference, 0.163 gibbs/mol, in a total entropy of 50.338 gibbs/mol,

means that on the average the heat capacity of $\text{Na}_2\text{SO}_4(\text{IV})$ should exceed the heat capacity of $\text{Na}_2\text{SO}_4(\text{V})$ by only about 0.3% over the range 0 – 458°K . This should help convey the reason why we are willing to assume that the heat capacities of these two phases can be taken as identical over the range 458 to 514°K .

Acknowledgment. We thank Helena W. Ruben for the X-ray analysis.

The Vapor Pressure Isotope Effect in Aqueous Systems. I. H_2O – D_2O (-64° to 100°) and H_2^{16}O – H_2^{18}O (-17° to 16°); Ice and Liquid.¹ II.

Alkali Metal Chloride Solution in H_2O and D_2O (-5° to 100°)

by Jovan Pupezin, Gyorgy Jakli, Gabor Jancso, and W. Alexander Van Hook*

Chemistry Department, University of Tennessee, Knoxville, Tennessee 37916 (Received August 31, 1970)

Publication costs assisted by the Petroleum Research Fund

High precision data are reported over a broad temperature range for the vapor pressure isotope effects displayed by the systems H_2^{16}O – H_2^{18}O ; H_2O – D_2O ; H_2O – D_2O – NaCl (1.1, 2.9, 4.0, and 5.5 m); H_2O – D_2O – KCl (3.5 and 4.5 m); H_2O – D_2O – CsCl (1.0, 3.0, 4.5, and 6.0 m); and H_2O – D_2O – LiCl (3.0, 5.0, 7.0, and 15.0 m). Here m is the concentration in aquamolality. The results are summarized with analytical expressions reported in the text and are good to ± 0.0003 ln R unit or better (R is the isotopic pressure ratio). For the solutions the data extend from about 0 to 90° except for KCl where the lower bound is 20° . The pure deuterium oxide system was investigated in both the ice and liquid phases in the region between -64 and 100° , but the measurements on oxygen-18 labeled water were limited to a narrower temperature range. For the pure waters, agreement with earlier workers was satisfactory and extends to the predicted triple points and ice–liquid fractionation factors. The analytical expressions for the temperature dependence of the vapor pressure isotope effects reported here are regarded as the best now available. For the salt solutions expressions for the change in the vapor pressure isotope effect as a function of concentration and temperature and expressions for the isotope effects on the excess thermodynamic properties of solution are extracted from the data (including isotope effects on the osmotic and the activity coefficients, and the excess free energies, enthalpies, entropies, and heat capacities of solution). The isotope effects on the standard thermodynamic properties of solution are also determined where possible (NaCl and KCl). A useful minor facet of the work is the least-square analysis of literature data on the osmotic and activity coefficients of KCl and CsCl to give expressions for these quantities reliable within ± 0.01 unit between 0.5 m and saturation over our temperature range. The solution data are compared with those from other laboratories where available (almost all only at 25°). They are discussed briefly in terms of models of solution structure.

Introduction

There is a great deal of current interest in theories of water and aqueous solution structure. In this context it is useful to compare isotope effects on the physical properties of aqueous solutions with the pure solvents. The vapor pressure isotope effect (VPIE) is particularly useful here because essentially it measures the isotopic free energy ratios. [Thus it is well established^{2,3} that the VPIE is a model sensitive property. In fact the

statistical theory of isotope effects in condensed phase systems⁴ has already been applied with some success

(1) Presented in part at the 159th National Meeting of the American Chemical Society, Houston, Texas, 1970.

(2) (a) J. Bigeleisen, C. B. Cragg, and M. Jeevanandam, *J. Chem. Phys.*, **47**, 4335 (1967); (b) J. Bigeleisen, S. V. Ribnikar, and W. A. Van Hook, *ibid.*, **38**, 489 (1963); (c) J. Bigeleisen, M. J. Stern, and W. A. Van Hook, *ibid.*, **38**, 497 (1963); (d) J. Bigeleisen and T. Ishida, *ibid.*, **45**, 5498 (1968); (e) M. J. Stern, W. A. Van Hook, and M. Wolfsberg, *ibid.*, **39**, 3179 (1963).

to the H₂O–D₂O system by Van Hook,⁵ by Wolff,⁶ and by Jones.⁷] A number of authors have therefore considered isotope effects on the properties of aqueous solutions but progress has been hindered by the fact that the differences between solvent and solution are quite small, that the VPIE for the H₂O–D₂O solvent system itself is not precisely established below about 50°, and that almost all of the pertinent data on solutions is limited to a single temperature (25°) or a narrow temperature range.

The present paper is the first of a series which will report on solvent isotope effects on activity coefficients in aqueous solutions over a broad temperature range. In this paper we will describe new high precision measurements of the vapor pressure isotope effect of the pure solvents and compare them with new measurements of the VPIE's of alkali metal chloride solutions. The differences are small and we shall find that high precision is required if a meaningful interpretation of the solution effects is to be given. Some data on the H₂¹⁶O–H₂¹⁸O system as well as data on the VPIE for H₂¹⁸O and D₂O ices are also presented. In later papers we shall report measurements on other series of salts, and/or make comparisons with statistical mechanical model calculations. In fact the eventual goal of the experimental program is to test models of solvent and solution structure with data on the VPIE.

This is not the appropriate place to review in any depth the voluminous literature concerned with proposed structures and model calculations on water and aqueous solutions which has been adequately covered in a number of recent reviews.^{8–10}

A number of earlier investigators have recognized the utility of activity coefficient differences between H₂O and D₂O solvent systems. Thus Googin and Smith¹¹ and Selecki, Tyminski, and Wolkowski,¹² have examined H₂O–HDO separation factors over saline solutions, and Robinson¹³ and Frank and Kerwin¹⁴ have made isopiestic measurements in D₂O. Also Salomaa and Aalto¹⁵ and Greyson, and Greyson and Snell¹⁶ and earlier La Mer and Noonan¹⁷ have made transfer EMF studies. Friedman and Wu and Krishnan¹⁸ and Greyson and Snell,¹⁶ Davies and Benson,¹⁹ and Wood, Rooney, and Braddock,²⁰ and Kresheck, Schneider, and Scheraga, and Kresheck²¹ recently, and Lange and coworkers²² many years ago, have measured heats of transfer from H₂O to D₂O. The enthalpy data have been reviewed by Arnett and McKelvey.²³ Rabinovitch²⁴ has also reviewed these and other topics of interest in the present context. Gold and Lowe²⁵ have investigated solvent isotope effects with the glass electrode. Solubility isotope effects have also been determined²⁶ and vapor pressures of saturated salt solutions in H₂O and D₂O have been compared.²⁷ Unfortunately a number of the above studies are not consistent with each other (especially references 11, 12, 13, and 14) and almost all of them focus only on a single temperature

(usually 25°), or a narrow temperature range. This last point we consider to be important and particularly unfortunate in view of the significant changes in the properties and structure of water which occur between its freezing and boiling points. For example the logarithm of the VPIE ratio changes by more than a factor of three over that temperature range. With almost all previous solution data restricted to a single temperature much structural information was lost.

We therefore felt it appropriate to measure solvent VPIE's over broad temperature and concentration ranges with high precision. Our planned approach is

(3) (a) W. A. Van Hook, *ibid.*, **44**, 234 (1966); (b) W. A. Van Hook and J. T. Phillips, *J. Phys. Chem.*, **70**, 1515 (1966); (c) W. A. Van Hook, *J. Chem. Phys.*, **46**, 1907 (1967); (d) W. A. Van Hook and J. T. Phillips, *J. Chromatogr.*, **30**, 211 (1967); (e) W. A. Van Hook, *J. Phys. Chem.*, **71**, 3270 (1967); (f) J. T. Phillips and W. A. Van Hook, *ibid.*, **71**, 3276 (1967); (g) J. T. Phillips and W. A. Van Hook, *J. Chem. Phys.*, **52**, 495 (1970); (h) R. L. McDaniel and W. A. Van Hook, *ibid.*, **52**, 4027 (1970).

(4) J. Bigeleisen, *ibid.*, **34**, 1485 (1961).

(5) W. A. Van Hook, *J. Phys. Chem.*, **72**, 1234 (1968).

(6) (a) H. Wolf in "Physics of Ice," N. Riehl, B. Bullemer, and H. Engelhardt, Ed., Plenum Press, New York, N. Y., 1969, p 305; (b) H. Wolf and A. Höpfner, *Ber. Bunsenges. Phys. Chem.*, **71**, 730 (1967).

(7) W. M. Jones, *J. Chem. Phys.*, **48**, 207 (1968).

(8) (a) J. L. Kavanau, "Water and Solute Water Interactions," Holden-Day, San Francisco, Calif., 1964; (b) D. Eisenberg and W. Kanzmann, "The Structure and Properties of Water," Oxford University Press, Oxford, 1969.

(9) O. Ya. Samoilov, "Structure of Aqueous Electrolyte Solutions and the Hydration of Ions," Consultants Bureau, New York, N. Y., 1965.

(10) A. K. Covington and P. Jones, Ed., "Hydrogen-Bonded Solvent Systems," Taylor and Francis, London, 1968.

(11) J. M. Googin and H. A. Smith, *J. Phys. Chem.*, **61**, 345 (1957).

(12) A. Selecki, B. Tyminski, and G. Z. Wolkowski, *Nukleonika*, **12**, 739 (1967).

(13) (a) R. A. Robinson, *J. Phys. Chem.*, **73**, 3165 (1969); (b) R. A. Robinson, *Trans. Faraday Soc.*, **35**, 1220 (1939).

(14) R. E. Kerwin, Thesis, University of Pittsburgh (1964).

(15) P. Salomaa and V. Aalto, *Acta Chem. Scand.*, **20**, 2035 (1966).

(16) (a) J. Greyson, *J. Phys. Chem.*, **71**, 259, 2210 (1967); (b) J. Greyson and H. Snell, *ibid.*, **73**, 3208, 4423 (1969); **74**, 2148 (1970).

(17) V. K. La Mer and E. Noonan, *J. Amer. Chem. Soc.*, **61**, 1487 (1939).

(18) (a) Y. C. Wu and H. L. Friedman, *J. Phys. Chem.*, **70**, 166 (1966); (b) C. V. Krishnan and H. L. Friedman, *J. Phys. Chem.*, **73**, 3934 (1969); **74**, 2356 (1970); **74**, 3900 (1970).

(19) D. H. Davies and G. G. Benson, *Can. J. Chem.*, **43**, 3100 (1965).

(20) R. H. Wood, R. A. Rooney, and J. N. Braddock, *J. Phys. Chem.*, **73**, 1673 (1969).

(21) (a) G. C. Kresheck, H. Schneider, and H. A. Scheraga, *ibid.*, **69**, 3132 (1965); (b) G. C. Kresheck, *J. Chem. Phys.*, **52**, 5966 (1970).

(22) (a) W. Birnthaler and E. Lange, *Z. Elektrochem.*, **43**, 643 (1937); **44**, 679 (1938); (b) E. Lange and W. Martin, *Z. Phys. Chem. Abt. A*, **180**, 233 (1970).

(23) E. M. Arnett and D. R. McKelvey, in "Solute-Solvent Interactions," J. F. Coetzee and C. D. Ritchie, Ed., Interscience Publishers, New York, N. Y., 1969.

(24) B. S. Rabinovitch, "Influence of Isotopy on the Physicochemical Properties of Liquids," Consultants Bureau, New York, N. Y., 1970.

(25) V. Gold and B. M. Lowe, *J. Chem. Soc., A*, **1967**, 1936.

(26) (a) E. C. Noonan, *J. Amer. Chem. Soc.*, **70**, 2915 (1948); (b) R. D. Eddy and A. W. C. Menzies, *J. Phys. Chem.*, **44**, 207 (1940); (c) R. W. Shearman and A. W. C. Menzies, *J. Amer. Chem. Soc.*, **59**, 185 (1937); (d) R. D. Eddy, R. Machemer, and A. W. C. Menzies, *J. Phys. Chem.*, **45**, 908 (1941).

(27) M. Becker, W. Schalike, and D. Zirwer, *Z. Naturforsch.*, **24**, 684 (1969).

to look at changes in the ratio $P_{\text{H}_2\text{O}}/P_{\text{D}_2\text{O}}$ at a given temperature as equivalent amounts of salt are added to the two solvents. The differences, $\Delta \ln R = \ln (P_{\text{H}_2\text{O}}^\circ/P_{\text{D}_2\text{O}}^\circ) - \ln (P_{\text{H}_2\text{O}}^{(m)}/P_{\text{D}_2\text{O}}^{(m)})$ are direct measures of the solvent activity ratios, $\Delta \ln R = \ln (a_{\text{D}_2\text{O}}/a_{\text{H}_2\text{O}}) = (\nu m/55.51)(\phi_{\text{H}_2\text{O}} - \phi_{\text{D}_2\text{O}})$; ($a_{\text{D}_2\text{O}}$ or $a_{\text{H}_2\text{O}}$ is solvent activity, m , molality, ν is particles per formula and the ϕ 's are osmotic coefficients). The initial step involves remeasurement of the VPIE of the pure solvents.

Experimental Section

In barest outline the experimental procedure consists in measuring the pressure difference between two samples kept at equal temperature and in the case of solutions equal aquamolalities.²⁸ The effects are small and high precision is required. The total pressure of the common isotope may be determined either by direct measurement or from the temperature using the best literature data which relate the pressure and temperature and (for solutions) osmotic coefficients. For the systems discussed in this paper the latter route was taken because quite precise osmotic coefficient data are available in the literature. The apparatus and thermometer calibration have been previously described.^{29,30} Very briefly, it consists of a thermostat for the samples which can be controlled to 0.001° over the range -10° to 100°. The temperature is measured by resistance thermometry (Leeds and Northrup G-1 Mueller Bridge), the total pressure (when necessary) with a Texas Instrument Company quartz Bourdon gauge (from 0 to 1000 mm to ~0.02 mm), and the isotopic differential pressure to several parts in 10⁴ with a Data-metrics Division, CGS Corporation, capacitance type differential manometer. (This instrument operates on any of four ranges, 10-100 mm to 10⁻² mm, 1-10 mm to 10⁻³ mm, 0.1-1 mm to 10⁻⁴ mm, 0.01-0.1 mm to 10⁻⁵ mm.) The factor limiting the precision of the data lies neither in the temperature control nor in the pressure measurement, but rather in the design of the sample cell, connecting lines, etc., and in the sample handling technique. This we feel is because of parasitic condensation and adsorption-desorption hysteresis of the water vapor in the different parts of the apparatus. Nonetheless the precision is considerably improved over that available to earlier authors, particularly in the lower temperature regions. We have found it necessary to thoroughly degas the samples with many (5 or 6) repeated melt-freeze-pump cycles. A good deal of patience is required to thoroughly complete the freeze portion of the cycle before pumping so that no concentration change occurs. In a later observation we found that if the final pumping cycle on the last degassing was made after the sample had been warmed up to -100°, improved precision resulted. This is most likely because we then pump off an amount of air which otherwise would have been adsorbed on the cold portions of the apparatus. It

is interesting to note that the experimental precision over most of the temperature range is better when saline solutions are being measured than it is for the pure solvents. This is no doubt due to the drying action of the salt solution whose vapor pressure is depressed with respect to the solvent. As a result parasitic condensation, etc., is appreciably decreased. This allows the solution data to be employed to refine the pure solvent VPIE's.

For the solvent measurements the H₂O was doubly distilled tap water; 100.0% D₂O was obtained from Diaprep Inc., Atlanta, Ga. This sample was distilled by them from 99.8% D₂O directly into our containers. The 0.75 cm³ sample of H₂¹⁸O (H normalized) was supplied to us by The Central Research Institute for Physics, Hungarian Academy of Sciences, Budapest. Mass spectrometric analysis gave for oxygen, ¹⁸O = 69.0 ± 0.5%, ¹⁷O = 1.4 ± 0.2%, ¹⁶O by difference. The deuterium concentration was only 1.03 ± 0.01 times normal abundance; 99.8% D₂O obtained from BioRad Laboratories, Richmond, Calif., was used as the solvent in the solution work. In all experiments the pressure differences were corrected to 100% D₂O or H₂¹⁸O assuming Raoult's law and the law of the geometric mean. The measured pressure differences were also corrected for the zero shift in the pressure gage as a function of total pressure and for the concentration change due to the finite vapor volume. Both of the latter corrections were small, never more than several ten-thousandths in the logarithm of the VPIE. The corrections applied in proceeding from the bridge readings to the temperature have already been described.³⁰ The temperatures reported in this paper are on the international practical Celsius (or Kelvin) scales of 1968.^{31,32}

Normal precautions were taken in drying and weighing the salts. NaCl and KCl were reagent grade and vacuum dried material. Reagent grade CsCl was recrystallized twice and vacuum dried. LiCl was prepared at Oak Ridge National Laboratory from the metal under anhydrous conditions. It was very kindly made available to us by J. Braunstein and H. Braunstein of Oak Ridge. The solutions were made up to the reported integer or half integer aquamolalities within 0.0002 unit. Concentrations were checked gravimetrically with AgNO₃ precipitation for the LiCl stock solutions.

Some Thermodynamics

Consider first the solvent isotope effect on the osmotic coefficient

(28) R. E. Kerwin, ref 14, appears to have coined the phrase "aquamolality" which refers to moles of solute per 55.508 mol of solvent.

(29) J. Pupezin, G. Jancso, and W. A. Van Hook, *Isotopenpraxis*, **9**, 319 (1970).

(30) G. Jancso, J. Pupezin, and W. A. Van Hook, *J. Phys. Chem.*, **74**, 2984 (1970).

(31) C. R. Barber, *Metrologia*, **5**, 35 (1969).

$$\phi_H - \phi_D = \frac{-55.508}{\nu m} [\ln a_H - \ln a_D] \quad (1)$$

Here ν is the number of ions per formula of solute, m is the aquamolality, and H refers to H₂O solvent, D to D₂O solvent. Rewriting eq 1 in terms of the pressure ratios, we obtain

$$\phi_H - \phi_D = \frac{-55.508}{\nu m} \left[\ln \frac{P_H}{P_H^0} - \ln \frac{P_D}{P_D^0} + \text{Cor} \right] \quad (2)$$

where the superscript 0's refer to the pure solvents and Cor is a small corrective term which takes account of the compressibilities of the condensed and vapor phases. It is given to more than sufficient precision by

$$RT \text{Cor} = \bar{V}_H'(P_H^0 - P_H) - V_D'(P_D^0 - P_D) + b_H[P_H - P_H^0] - b_D[P_D - P_D^0] \quad (3)$$

Cor was evaluated using the liquid molar volume data \bar{V}_H' and V_D' of Whalley³³ and virial coefficients, b_H , from Eisenberg and Kauzmann.^{3b} Then b_H/b_D , and thus b_D , was estimated using the relation given by Kell, McLaurin, and Whalley.³⁴ The isotope effect on the solution densities was assumed to be equal to that on the solvents. The correction was found to be negligible as compared to our experimental precision over the range of the experiment. Equation 2 may now be rearranged

$$\phi_H - \phi_D = \frac{55.508}{\nu m} \left[\ln \frac{P_H^0}{P_D^0} - \ln \frac{P_H}{P_D} \right] \quad (4)$$

Here the first term within the brackets is the VPIE for the pure solvents, R_0 , the second is the VPIE for the solution, R_m . Thus

$$\phi_H - \phi_D = \frac{55.508}{\nu m} [\ln R_0 - \ln R_m] \quad (5)$$

Phenomenologically ϕ_H or ϕ_D may be conveniently expressed using an equation of the form of the extended Debye-Hückel equation

$$\phi = 1 - \frac{S}{A^3 I} \left[(1 + AI^{1/2}) - 2 \ln [1 + AI^{1/2}] - \frac{1}{1 + AI^{1/2}} \right] + BI + CI^2 + \dots \quad (6)$$

In this equation S is the limiting slope, I is the ionic strength, B, C, \dots are parameters, and A is given by $50.29(\epsilon T)^{-1/2}a$. Parameter a enters the Debye theory as a characteristic length and ϵ is the dielectric constant. Also the limiting slope, S , is given by $1.8246 \times 10^6 (\epsilon T)^{3/2}$.³⁵ We assume the distance of closest approach of the ions is the same in D₂O as it is in H₂O, $a_{H_2O} = a_{D_2O}$. Then the contribution of the term in $S/A^3 I$ is readily found from the tabulated dielectric constants for H₂O and D₂O,³⁶ and values for a in H₂O. For $A = 1.5$, $\phi_H - \phi_D$ from this term is on the order of 10^{-6} over the entire temperature and concentration

range of the experiment, about two orders of magnitude less than our experimental precision. [Also note that the isotope effects on the temperature derivative of the leading term are negligible as well.] Therefore

$$\phi_H - \phi_D = \frac{55.508}{\nu m} [\ln R_0 - \ln R_m] = (B_H - B_D)I + (C_H - C_D)I^2 \dots \quad (7)$$

or, noting that for the 1:1 systems discussed in this paper $m = I$, $\nu = 2$, and letting $b = B_H - B_D$, etc., we have

$$\Delta \ln R = \ln R_0 - \ln R_m = \frac{2}{55.508} bm^2 + \frac{2}{55.508} cm^3 + \dots = \frac{2m}{55.508} (\phi_H - \phi_D) \quad (8)$$

Also

$$\ln \frac{\gamma_{\pm}(\text{H}_2\text{O})}{\gamma_{\pm}(\text{D}_2\text{O})} = 2bm + 3cm^2 + \dots \quad (9)$$

Generally b, c , etc., will be functions of temperature.

In the development so far we have implicitly assumed the validity of the extended Debye-Hückel equation (eq 6). This equation is only semiempirical and if in fact the corrective terms take a different concentration dependence than $BI + CI^2, \dots$, then the resulting concentration dependence obtained by our Gibbs-Duhem integration (*i.e.*, the analogue of eq 8, 9) will be different. Our data are certainly not capable of determining the validity of the general form of eq 6. It may well be that they (the data) are consistent with other limiting behaviors in addition to that given by $\Delta \ln R = Km^2 + \dots$. We, however, have chosen to focus on a development based on eq 6, since that equation is a theoretically based and widely accepted form.

In proceeding from the osmotic coefficients or the activity coefficients to the isotope effects on the thermodynamic properties of solution it is convenient to use the excess thermodynamic functions as developed by Friedman.³⁷ Here the chemical potential of the solute is referenced to the hypothetical one molal reference state at the same T and P as the solution. Then

$$\Delta G_{\text{total}}^{\text{ex}} = G_H^{\text{ex}} - G_D^{\text{ex}} = \nu m RT \left[-(\phi_H - \phi_D) + \ln \frac{\gamma_{\pm}(\text{H}_2\text{O})}{\gamma_{\pm}(\text{D}_2\text{O})} \right] \quad (10)$$

(32) T. B. Douglas, *J. Res. Natl. Bur. Stand., Sect. A*, **73**, 468 (1969).

(33) E. Whalley, "Proceedings of the Joint Conference on the Thermodynamic Properties of Fluids, 1957," Institute of Mechanical Engineering, London, 1958, pp 15-26.

(34) G. Kell, G. E. McLaurin, and E. Whalley, *J. Chem. Phys.*, **49**, 2839 (1968).

(35) See for example: G. Kortüm, "Electrochemistry," 2nd ed, Elsevier, Amsterdam, 1965, p 183.

(36) Reference 8b, pp 189-191.

(37) H. L. Friedman, *J. Chem. Phys.*, **32**, 1351 (1960).

$$\Delta G_{\text{total}}^{\text{ex}} = \nu RT [bm^2 + 1/2cm^3 + \dots] \quad (11)$$

The isotope effect on the excess free energy of the salt, $\Delta G_{\text{S}}^{\text{ex}}$, is given by

$$\Delta G_{\text{S}}^{\text{ex}} = 1/\nu \frac{d\Delta G_{\text{total}}^{\text{ex}}}{dm} = \mu_{\pm}^{\text{ex}} = RT \ln \gamma_{\pm} = RT [2bm + 3/2cm^2 + \dots] \quad (12)$$

and that on the solvent, $\Delta G_{\text{water}}^{\text{ex}} = \Delta G_{\text{total}}^{\text{ex}} - 2m\Delta G_{\text{S}}^{\text{ex}}$, by

$$\Delta G_{\text{water}}^{\text{ex}} = \frac{d\Delta G_{\text{total}}^{\text{ex}}/m}{d(1/m)} = -2RT \{bm^2 + cm^3 + \dots\} \quad (13)$$

The isotope effects on the excess enthalpies of solution may be determined from the temperature coefficient of the pressure measurements, although the effects are quite small and the derivatives are not expected to be precise. Thus for the salt we obtain

$$\Delta H_{\text{S}}^{\text{ex}} = -T^2 \frac{d(\Delta G_{\text{S}}^{\text{ex}}/T)}{dT} = -RT^2 \left(2m \frac{db}{dT} + \frac{3}{2} m^2 \frac{dc}{dT} + \dots \right) \quad (14)$$

Similar equations for $\Delta H_{\text{water}}^{\text{ex}}$ and $\Delta H_{\text{total}}^{\text{ex}}$ are readily derived.

In the process of data fitting (see below) we have taken the temperature dependence of b and c to be consistent with the simple assumption of a constant isotope effect on the excess heat capacity for each of the salts studied.

$$b(T) = \frac{\Delta B_{\text{MCl}}^{(1)}}{T} + \Delta B_{\text{MCl}}^{(2)} \ln T + \Delta B_{\text{MCl}}^{(3)} \quad (15)$$

$$c(T) = \frac{\Delta C_{\text{MCl}}^{(1)}}{T} + \Delta C_{\text{MCl}}^{(2)} \ln T + \Delta C_{\text{MCl}}^{(3)}$$

This assumption gave data fits within the experimental error. Still the measurements are not precise enough to rule out other plausible functional forms which could replace eq 15. Equations 14 and 15 combine to yield

$$\Delta H_{\text{total}}^{\text{ex}} = 2Rm^2(\Delta B^{(1)} - \Delta B^{(2)}T) + Rm^3(\Delta C^{(1)} - \Delta C^{(2)}T) + \dots \quad (16)$$

$$\Delta H_{\text{S}}^{\text{ex}} = 2Rm(\Delta B^{(1)} - \Delta B^{(2)}T) + 3/2 Rm^2(\Delta C^{(1)} - \Delta C^{(2)}T) + \dots$$

and

$$\Delta H_{\text{water}}^{\text{ex}} = \Delta H_{\text{total}}^{\text{ex}} - 2m\Delta H_{\text{S}}^{\text{ex}}$$

The various isotope effects on the excess entropies are found by combining eq 11-13 and 16 according to

$$T\Delta S^{\text{ex}} = -\Delta G^{\text{ex}} + \Delta H^{\text{ex}} \quad (17)$$

and the isotope effects on the excess heat capacities

(quite unreliable in the present case) are obtained by differentiating eq 16.

In addition to the isotope effects on the excess properties, those on the standard state thermodynamic properties are of interest. They can be obtained from data like the present only if additional information is available. In the case where the solubility and the isotope effect on the solubility are known, and if there are no complications (such as hydrate formation) we have

$$G_{\text{salt}}^0(\text{H}) - G_{\text{salt}}^0(\text{D}) = \Delta G_{\text{salt}}^0 = -2RT \ln \frac{m_{\text{H}}\gamma_{\text{H}}(\text{H})}{m_{\text{D}}\gamma_{\text{D}}(\text{D})} = -2RT \left[\ln \frac{m_{\text{H}}}{m_{\text{D}}} + \ln \frac{\gamma_{\text{H}}(\text{H})}{\gamma_{\text{H}}(\text{D})} + \ln \frac{\gamma_{\text{H}}(\text{D})}{\gamma_{\text{D}}(\text{D})} \right] \quad (18)$$

In eq 18 $m_{\text{H}}/m_{\text{D}}$ is the solubility isotope effect and $\gamma_{\text{H}}(\text{D})$ refers to the activity coefficient in H_2O at concentration m_{D} , etc. On the extreme right the effect is approximately broken down into a contribution attributed to the solubility measurements, $-2RT[\ln(m_{\text{H}}/m_{\text{D}}) - \ln(\gamma_{\text{H}}(\text{H})/\gamma_{\text{H}}(\text{D}))]$ and one attributed to the activity measurements, $-2RT[\ln(\gamma_{\text{H}}(\text{D})/\gamma_{\text{D}}(\text{D}))]$. This approximate factoring is useful when estimating the reliability of ΔG_{salt}^0 from the experimental errors in the different measurements. For present purposes we note that Shearman and Menzies, and Eddy and Menzies²⁶ have determined the solubilities of KCl and NaCl as a function of temperature. For both these salts the contribution to ΔG_{S}^0 is principally determined through the solubility measurements. Solubility isotope effect data are not available for CsCl or LiCl; additionally the latter system is complicated by hydrate formation.

Results and Discussion

A. Reference Pressures. In order to convert the corrected pressure differences $P_{\text{H}} - P_{\text{D}}$ to the vapor pressure ratios $P_{\text{H}}/P_{\text{D}}$ it is necessary to know the total pressure, P_{H} or P_{D} . Very accurate and highly precise vapor pressure data are available for normal ice, water, and the salt solutions.

Ice. We have used the equation proposed by Jancso, Pupezin, and Van Hook³⁰ for the reference pressure of ice. The estimated uncertainty in the pressure varies from 5 parts in 10^4 at 0° to 11 parts in 10^4 at -60° . At the higher temperatures the uncertainty is almost entirely due to the imprecision with which the triple point reference pressure has been established (4.585 ± 0.002 mm at 0.01°).^{30,38}

Water. For the pressure-temperature curve of liquid water we have used the equation given by Goff.³⁹

(38) J. Pupezin, G. Jancso, and W. A. Van Hook, *J. Chem. Ed.*, **48**, 114 (1971).

(39) J. A. Goff in "Humidity and Moisture," A. Wexler, Ed., Reinhold, New York, N. Y., 1963, Vol. 3, p 289.

$$P_{\text{mm}} = 760 \exp \left[2.302585 \left\{ 10.79586 \left(1 - \frac{273.16}{T} \right) - 5.02808 \log \frac{T}{273.16} + 1.5047 \times 10^{-4} \left(\left(1 - \exp 19.10436 \left[1 - \frac{T}{273.16} \right] \right) + 0.42873 \times 10^{-3} \left[\left\{ \exp 10.98229 \left(1 - \frac{273.16}{T} \right) \right\} - 1 \right] - 2.2195983 \right\} \right] \quad (19)$$

This equation was selected because of the excellent agreement between its predictions and the recent high precision data of Stimson⁴⁰ between 25 and 100°. The agreement between the (1963) calculated and the (1969) measured values is about 5 parts in 100,000. This is a good deal better than the old commonly employed Washburn calculation⁴¹ or the equations reported in the most recent editions of the steam tables.^{42,43}

Salt Solutions. In the calculation of the total pressure over the H₂O solutions we first fit literature osmotic coefficient data to the extended Debye-Hückel equation with a nonlinear least-squares computer program^{44a} (except for NaCl which was previously treated by Stoughton and Lietzke).^{44,45} In the fitting process eq 6 was employed with the linear (B), square (C), and cubic (D), parameters taken to be of the general form

$$B = B_1/T + B_2 \ln T + B_3 + B_4 T + \dots \quad (20)$$

In the fitting of data to eq 6, S , the limiting slope, is given by

$$S = 1.17202 \left(\frac{\sum m_i z_i^2}{\sum m_i} \right) \rho^{1/2} (\epsilon_{25} T_{25} / \epsilon T)^{3/2} \quad (21)$$

The temperature dependence of ϵ , the dielectric constant, and ρ , the density, were taken from Akerlöf and Oshry⁴⁶ and Lange,⁴⁷ and A was set equal to 1.5 for all of the salts.

The results are given in Table I to sufficient precision to allow the ϕ 's to be recorded to the nearest 0.001 after dropping the last digit to allow for round off. We regard these equations purely as empirical fits to the available data. They should not be extrapolated beyond the limits indicated in Table I. The data selected for fitting were restricted to concentrations 0.5 m or above, *i.e.*, to the concentration range specifically of interest to us. The parameters which result are highly correlated and in our opinion it would not be useful to quote standard deviations without citing the entire error matrix. Instead, for the individual salts discussed below we cite the variance.

Potassium Chloride. Data from a number of different laboratories⁴⁸⁻⁵⁵ between 0 and 100° and 0.5 to 5.0 molal were fit with good precision. The value of $\sigma = (\text{variance})^{1/2}$ obtained was 5×10^{-3} ; a few points deviated in ϕ as much as 1×10^{-2} but these only at

Table I: Osmotic Coefficients of NaCl,⁴⁶ KCl (0.5 to 5 m), CsCl (0.5 to 7 m) and LiCl (0.5 to 15 m) in H₂O between 0 and 100°^a

	B_1	B_2	B_3	B_4
KCl	-1438.0	-7.6311	45.263	0.01008
CsCl	-4385.9	-24.518	144.104	0.03435
LiCl	46.94	0.3840	-1.9621	0.00097
NaCl ⁴⁶	-330.33	0.9094	6.3145	...
	C_1	C_2	C_3	C_4
K	100.9	0.2929	-1.9820	...
Cs	5.064	...	0.00348	...
Li	5.618	...	-0.00674	...
Na ⁴⁶	32.681	0.0790	-0.5537	...
	D_1	D_2	D_3	D_4
K	-0.497	...	-0.00167	...
Cs	0.142	...	-0.00204	...
Li	-0.184	...	-0.00001	...
Na ⁴⁶

$$^a \phi = 1 - \frac{S}{A^2 I} \left\{ (1 + A\sqrt{I}) - 2 \ln (1 + A\sqrt{I}) - \frac{1}{1 + A\sqrt{I}} \right\} + BI + CI^2 + DI^3$$

where $A = 1.5$ and $B, C,$ and D take the form $B = B_1/T + B_2 \ln(T) + B_3 + B_4 T$. S is the Debye-Hückel limiting slope.

the highest temperatures and concentrations. It therefore appears unlikely that any of the calculated

(40) H. F. Stimson, *J. Res. Natl. Bur. Stand., Sect. A*, **73**, 493 (1969).

(41) E. W. Washburn, *Mon. Weather Rev.*, **52**, 488 (1924).

(42) (a) J. H. Keenan, F. G. Keyes, P. G. Hill, and J. G. Moore, "Steam Tables (Int. ed.)," Wiley, New York, N. Y., 1969; (b) R. W. Bain, "Steam Tables 1964," Her Majesty's Stationery Office (Edinburgh), 1964.

(43) Note that there is a small inconsistency (but one which is within the experimental precision) between the equations in ref 30 and 39 which should intersect at the triple point. We find $P(\text{ice}) = 4.585$ mm and $P(\text{liq}) = 4.584$ mm. The difference is within the precision with which the triple point pressure is established, 4.585 ± 0.002 mm.³⁸

(44) (a) M. H. Lietzke, ORNL 3259; (b) M. H. Lietzke and R. W. Stoughton, *J. Phys. Chem.*, **65**, 508 (1961); *J. Chem. Eng. Data*, **10**, 254 (1965).

(45) R. W. Stoughton and M. H. Lietzke, *J. Chem. Eng. Data*, **12**, 101 (1967).

(46) G. C. Akerlöf and H. I. Oshry, *J. Amer. Chem. Soc.*, **72**, 2844 (1950).

(47) N. A. Lange, Ed., "Handbook of Chemistry," 7th ed, Handbook Publishers, Inc., Sandusky, Ohio, 1949.

(48) R. Caramazza, *Gazz. Chem. Ital.*, **90**, 1721 (1960).

(49) C. S. Patterson, L. O. Gilpatrick, and B. A. Soldano, *J. Chem. Soc.*, 2730 (1960).

(50) R. P. Smith, *J. Amer. Chem. Soc.*, **61**, 500 (1939); R. P. Smith and D. S. Hirtle, **61**, 1123 (1939).

(51) M. H. Lietzke and R. W. Stoughton, *J. Tenn. Acad. Sci.*, **42**, 26 (1967).

(52) H. S. Harned and M. A. Cook, *J. Chem. Soc.*, **59**, 1920 (1937).

(53) R. H. Stokes, *Trans. Faraday Soc.*, **44**, 295 (1948).

(54) G. Scatchard and S. S. Prentiss, *J. Amer. Chem. Soc.*, **55**, 4355 (1933).

(55) R. Caramazza, *Ann. Chim. (Rome)*, **53**, 481 (1963).

osmotic coefficients are in error by as much as 0.01 under any condition of interest to us. This upper limit corresponds to an error of less than 0.0001 in the VPIE and is negligible for our purposes.

Cesium Chloride. The data of Caramazza⁵⁵ and of Soldano and coworkers^{49,56,57} between 0 and 121° and 0.5 to 7 *m* were fit. σ was determined as 4×10^{-3} and the largest single deviation was 1.0×10^{-2} . Again, these errors correspond to less than ± 0.0001 in the VPIE and may be neglected.

Sodium Chloride. The fit of Stoughton and Lietzke⁴⁵ was employed. For the temperature and concentration range described in the present work it does not appear that the calculated osmotic coefficients can be in error by as much as 0.01 even at the highest concentration and temperatures. A $\Delta\phi$ of 0.01 corresponds to an error of 0.0001 in the VPIE and is within the experimental precision.

Lithium Chloride. F. H. Gibbard, Jr., of Southern Illinois University has kindly supplied us with smoothed osmotic coefficients taken from a recent analysis⁵⁸ principally of the data Gibbard and Scatchard.⁵⁹ These are fit (Table I) well within 0.01 and we regard them as reliable to within that bound, except at the highest concentrations where the deviations may be as large as 0.02.⁵⁸ These errors may be translated into the uncertainties to be expected on $\Delta \ln R$ where they correspond to 0.0001 unit or less (negligible) except at the higher concentrations (10 and 15 *m*) at lower temperatures. Thus at 0° for the 15 *m* solution (the worst case) the anticipated error is large, 0.001 unit. Even so, this amounts to only 3% of the effect measured for $\Delta \ln R$ which is large at high concentrations.

The Absolute Pressure. With the ϕ 's established the vapor pressure may be calculated using eq 22.

$$\phi = \frac{-55.508}{\nu m} (\ln P/P^0 + (b(T)/RT)(P - P^0) + \bar{V}_1(P^0 - P)) \quad (22)$$

The symbols have already been defined. In obtaining eq 22 the real gas correction term, $(1/RT) \int_{P^0}^P (V_g - RT/P)dP$, has been evaluated assuming a virial equation of state with terms beyond the second virial coefficient neglected. The last term is negligibly small for aqueous solutions below 100°. $b(T)$ was evaluated from the relation due to Keyes⁶⁰ as quoted by Eisenberg and Kauzman,^{8b} P^0 from eq 19, ϕ for the solutions calculated from the parameters in Table I, and eq 22 solved for P by an iterative technique.⁶¹

B. Pure Water VPIE's. 1. H₂¹⁶O-H₂¹⁸O Results. A preliminary report of these results has been given.⁶² The data are presented in Table IIa.⁶³ They are suitably fit with two parameter least-square equations

$$\ln R^{18}_{\text{solid}} = \ln \left(\frac{P_{\text{H}_2^{16}\text{O}}}{P_{\text{H}_2^{18}\text{O}}} \right)_{\text{solid}} = \frac{2.110}{T} + 0.00656 \quad (256 < T < 273) \quad (23)$$

$$\ln R^{18}_{\text{liquid}} = \ln \left(\frac{P_{\text{H}_2^{16}\text{O}}}{P_{\text{H}_2^{18}\text{O}}} \right)_{\text{liquid}} = \frac{13.764}{T} - 0.03872 \quad (273 < T < 289) \quad (24)$$

The parameters are highly correlated but the variances of the fits are small. Thus the precision of eq 23 as calculated from the least-square error matrix and expressed as the square root of the variance lies between 0.7×10^{-4} and 0.4×10^{-4} $\ln R$ units. For eq 24 the figures are 1.2×10^{-4} and 0.6×10^{-4} . The uncertainty in the isotopic analysis adds another 1×10^{-4} $\ln R$ units and we feel that the calculated logarithms from eq 23 and 24 are good to $\pm 0.0002 \ln R$ unit.

The data are plotted in Figure 1 where they are compared with earlier work. Our initial reason for undertaking these measurements was to resolve a discrepancy between the manometric ice VPIE data of Matsuo and Matsubaya⁶⁴ and the liquid-solid fractionation factor reported by O'Neil.⁶⁵ Because we were thus primarily interested in the low-temperature region, because the precision of our pure solvent data suffers slightly around room temperature (see below), and because of the very high quality of the data of Szapiro and Steckel⁶⁶ above 15° we did not take data above 16°. Similarly we did not take data below our region of good temperature control (-17°). Thus the temperature range for each phase is short and the slopes of the VPIE temperature curves are not at all well determined from the present data alone (that for the liquid appears high, for the solid low).

Consider first the liquid data (Figure 1). Comparison is best made on a $\ln R$ vs. $(1/T)^2$ plot⁴ because the

(56) B. A. Soldano and C. S. Patterson, *J. Chem. Soc.*, 937 (1962).

(57) B. A. Soldano, *ibid.*, 4424 (1963).

(58) F. H. Gibbard, Jr., personal communication.

(59) F. H. Gibbard, Jr., Thesis, Massachusetts Institute of Technology, 1962.

(60) F. G. Keyes, *Trans. Amer. Soc. Mech. Eng.*, 78, 555 (1958).

(61) We are indebted to Dr. Lietzke for his suggestions on this matter and on several other points in regard to our data fitting procedures.

(62) G. Jancso, J. Pupezin, and W. A. Van Hook, *Nature (London)*, 225, 723 (1970).

(63) Listings of vapor pressure isotope effects as measured at the different experimental temperatures will appear immediately following this article in the microfilm edition of this volume of the journal. Single copies may be obtained from the Business Operations Office, Books and Journal Division, American Chemical Society, 1155 Sixteenth Street, N. W., Washington, D. C. 20036. Remit check or money order for \$3.00 for photocopy or \$2.00 for microfilm.

(64) (a) S. Matsuo and O. Matsubaya, *Nature (London)*, 221, 463 (1969); (b) M. Majoube, *Nature (London)*, 226, 1242 (1970); *J. Chim. Phys.* 68, 625 (1971).

(65) R. O'Neil, *J. Phys. Chem.*, 72, 3683 (1968).

(66) S. Szapiro and F. Steckel, *Trans. Faraday Soc.*, 63, 883 (1967).

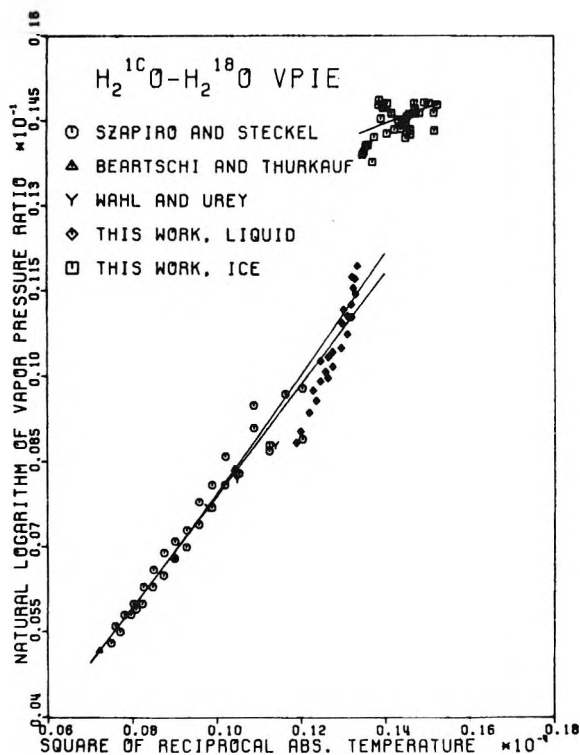


Figure 1. Vapor pressure isotope effects for the system $\text{H}_2^{16}\text{O} - \text{H}_2^{18}\text{O}$.

present effect should be principally due to the isotope effect on the hindered translational lattice modes.⁵ The data shown in Figure 1, including the present points, and literature values from Szapiro and Steckel,⁶⁶ (SS), Baertschi and Thürkauf,⁶⁷ and Wahl and Urey⁶⁸ have been least squared and the result is reported as eq 25. Other literature data⁶⁹ were not included in the least squaring because they were significantly different from the superior (in our estimation) data of SS. The agreement between the present data points and those of SS is satisfactory in the overlap region although the empirical slope of (eq 24) is much too large. There are no other data with which a direct comparison can be made below 15°.

$$\ln R^{18}_{\text{liquid}} = \frac{982.4 \pm 19.6}{T^2} - 0.00193 \pm 0.00018 \quad (373 < T < 273) \quad (25)$$

We feel that values of $\ln R$ calculated from eq 25 are the best available over the liquid range. The uncertainties can be conservatively set as $\pm 0.0002 \ln R$ unit. With these limits eq 24 and 25 overlap within the stated uncertainties over the range $0^\circ < t < 11^\circ$.

The upper line in the liquid region of Figure 1 is taken from a calculation due to Van Hook⁴ (case II) where the parameters were assigned on spectroscopic grounds. Only the lattice hindered translational frequencies contribute significantly to the ^{18}O effects and the good agreement between the calculated and observed VPIE's indicates that this frequency was reasonably assigned.

Data available for comparison on the solid phase are manometric measurements due to Matsuo and Matsubaya^{64a} and the recent mass spectrometric ones of Majoube.^{64b} The Japanese line lies nearly 20% below the fit to present data which is itself about 5% below the French results at the melting point. The larger slope displayed by the latter appears more reasonable from theoretical considerations. Solution of equations 23 and 25 at the melting point (0°) gives a figure for the solid-liquid fractionation of 0.0030 ± 0.0003 to be compared with O'Neil's⁶⁵ directly measured value of 0.0030 ± 0.0002 and Majoube's value of 0.0034 ± 0.0003 taken from his ice and liquid data.^{64b} The agreement is satisfactory and supports the present results as compared to those of the Japanese. Accepting for the moment the oversimplified model used in the earlier calculations of Van Hook⁴ we can estimate an effective average translational frequency in ice from that used for the liquid and the VPIE's for liquid and solid. Thus, $\ln(R^{18}_{\text{solid}})/\ln(R^{18}_{\text{liquid}}) = (0.01438/0.01124) \cong (\bar{\nu}^2_{\text{solid}}/\bar{\nu}^2_{\text{liquid}}) \cong (\bar{\nu}^2_{\text{solid}}/162.5^2)$, which gives $\nu_{\text{solid}} \cong 183 \text{ cm}^{-1}$ and $\Delta\nu = \nu_{\text{solid}} - \nu_{\text{liquid}} \cong 20 \text{ cm}^{-1}$. This contrasts sharply with the figure $\Delta\nu = 113 \text{ cm}^{-1}$ which was estimated earlier⁵ from the spectroscopic literature.^{70,71} The present data definitively establishes that earlier assignment as wrong.

Finally the isotope effect on the triple point is calculated from these data as $T_{\text{triple}}(\text{H}_2^{18}\text{O}) - T_{\text{triple}}(\text{H}_2^{16}\text{O}) = (0.32 \pm 0.03)^\circ\text{K}$. The only other experimental measurement is due to Kuhn and Thürkauf⁷² who estimated $\Delta T_t = (0.05 \pm 0.01)^\circ\text{K}$ from a measured ice-liquid fractionation factor of $(5 \pm 1) \times 10^{-4}$. The present data (and those of ref 64b and 65) indicate that this value is much too low.

2. $\text{H}_2\text{O}-\text{D}_2\text{O}$ Results. The $\text{H}_2\text{O}-\text{D}_2\text{O}$ data are presented in Table IIb.⁶³ The least-square fits for the three different regions examined follow. (An alternative fit to the liquid data in which the solution effects are also employed is given below in section C.) The parameters obtained are highly correlated. Enough significant figures are given so that the effects can be calculated to 0.00001 and rounded to the nearest 0.0001. This entails reporting the parameters to well beyond their confidence limits (as expressed by the standard deviations on the derived values of the parameters

(67) P. Baertschi and M. Thürkauf, *Helv. Chim. Acta*, **43**, 80 (1960).

(68) M. H. Wahl and H. C. Urey, *J. Chem. Phys.*, **3**, 411 (1935).

(69) J. L. Borowitz, *J. Phys. Chem.*, **66**, 1412 (1962); A. E. Brodsky and O. C. Skarre, *Acta Phys. Chim. USSR*, **10**, 729 (1939); I. Dostrovsky, J. Gillis, D. R. Llewellyn, and B. H. Vromen, *J. Chem. Soc.*, 3517 (1952); E. H. Riesenfeld and T. L. Chang, *Z. Phys. Chem.*, **33**, 120 (1936); S. Sakata and N. Morita, *Bull. Chem. Soc. Jap.*, **29**, 284 (1956); O. V. Uvarov, N. M. Sokolov, and N. M. Zhavoronkov, *Kernergie*, **5**, 323 (1962); H. E. Watson, *J. Appl. Chem.*, **3**, 556 (1953); McWilliams, Pratt, Dell, and Jones, *Trans. Inst. Chem. Eng.*, **34**, 24 (1956).

(70) G. E. Walrafen, *J. Chem. Phys.*, **36**, 1036 (1962); **47**, 114 (1967).

(71) N. Ockman, *Advan. Phys.*, **7**, 199 (1958).

(72) W. Kuhn and M. Thürkauf, *Helv. Chim. Acta*, **41**, 938 (1958).

Table III: Values of $10^3 \ln (P_{\text{H}_2\text{O}}/P_{\text{D}_2\text{O}})$ between 0 and 100°

	0	10	20	30	40	50	60	70	80	90	100
(1) Present work (± 0.3)	204.2	178.2	155.6	135.9	118.8	103.8	90.7	79.2	69.2	60.3	52.6
(2) Jones ⁷		169	150	132	117	102.7	90.3	79.1	69.0	59.9	51.6
(3) Zieborak ⁸²									69.4	60.2	52.0
(4) Lewis and McDonald ⁸⁰			152	134	118	103.8	91.0	79.6	69.4	60.2	52.0
(5) Riesenfeld and Chang ⁷⁹		158	138	122	109	96.5	85.5	75.8	67.2	58.7	51.0
(6) Kiss, Jakli and Illy ^a	198	171									
(7) Miles and Menzies ⁸¹		173	153	135	119	104.0	90.8	79.2	68.5	59.1	50.9
(8) Combs, Googin, and Smith ^{83a}		179	158	138	122	106.2					
(9) From salt solution data (± 0.3)	204.1	177.9	155.2	135.5	118.4	103.5	90.4	79.1	69.2	60.5	53.0

^a See ref 73. The liquid data were plotted as $\log P$ vs. $1/T$ and fit with a straight line which was extrapolated to 0 and 10°.

themselves), because the linear combination which expresses the effect is known to a much higher order of precision than are the parameters themselves.

$$\ln R_{\text{liq}} = \ln \left(\frac{P_{\text{H}_2\text{O}}}{P_{\text{D}_2\text{O}}} \right)_{\text{liquid}} =$$

$$(0.17416 \pm 0.01175) - \frac{(191.70 \pm 7.372)}{T} +$$

$$\frac{(54587 \pm 1143)}{T^2} \quad (270 < T < 373) \quad (26)$$

$$\ln R_{\text{s1}} = \ln \left(\frac{P_{\text{H}_2\text{O}}(\text{liquid})}{P_{\text{D}_2\text{O}}(\text{ice})} \right) =$$

$$-(14.9472 \pm 1.4355) + \frac{(7405.4 \pm 786.7)}{T} -$$

$$\frac{(889582 \pm 107790)}{T^2} \quad (270 < T < 277) \quad (27)$$

$$\ln R_{\text{solid}} = \ln \left(\frac{P_{\text{H}_2\text{O}}}{P_{\text{D}_2\text{O}}} \right)_{\text{ice}} =$$

$$(0.23688 \pm 0.1435) - \frac{(206.62 \pm 75.6)}{T} +$$

$$\frac{(56783 \pm 9957)}{T^2} \quad (209 < T < 273) \quad (28)$$

The data are plotted in Figure 2. The lines are the least-square fits. That for the liquid-ice data is reported as a three parameter equation for consistency but there is very little difference between the fits of the two and three parameter equations over this very short temperature range. Some comparisons with earlier work are given in Table III. To our knowledge no previous authors have reported measurements in the super-cooled region or in the region between the melting points. We consider the liquid, solid, and liquid-solid regions below.

H₂O-D₂O Ices. Previous measurements on ice I VPIE's to -40° have been reported by Kiss, Jakli, and Illy⁷³ and Matsuo, Kuniyoshi, and Miyake.⁷⁴ These

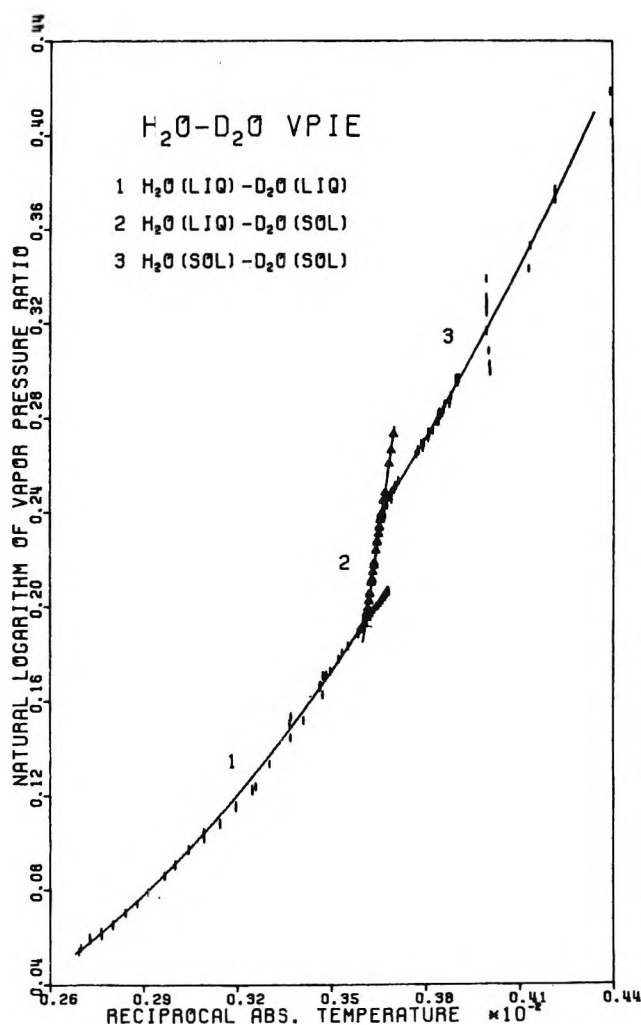


Figure 2. Vapor pressure isotope effects for the system $\text{H}_2\text{O}-\text{D}_2\text{O}$.

are in good agreement with the present data but are not plotted because of our considerably better precision above -20° . [Below -20° we could no longer use the

(73) I. Kiss, G. Jakli, and H. Illy, *Acta Chim. Acad. Sci. Hung.*, **47**, 379 (1966).

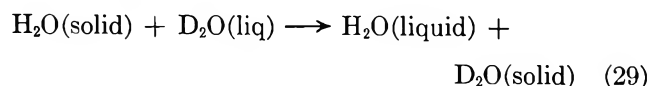
(74) S. Matsuo, H. Kuniyoshi, and Y. Miyake, *Science*, **145**, 1454 (1964).

automatic thermostat and were forced to use various organic slush baths. These were satisfactorily stable except for the CCl_4 slush, -23° , which gave poor results. No substitute was located, however, and the results using CCl_4 are reported.] The calculated line from ref 5 is also in agreement with the present results. In particular there is good correspondence between calculation and experiment in both the slope and the curvature although the two curves are displaced from each other by a small amount ($\sim 0.003 \ln R$ unit). [Note, however, that the ice phase translational assignments used in (5) have been criticized above on the strength of the H_2^{18}O results. For D_2O , however, the external translations contribute only a minor part of the VP/IE.]

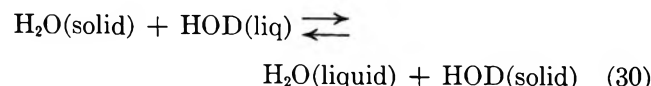
The Region between $+5^\circ$ and -5° . We have singled this region out for separate attention because to our knowledge no other measurements have been reported between the D_2O and H_2O triple points or in the supercooled region (although Merlivat and Nief have measured the $\text{HOD-H}_2\text{O}$ fractionation factor for the supercooled liquid to -15° ⁷⁵). The data over this region together with the fits are plotted in Figure 3, which thus amounts to an enlargement of a portion of Figure 2. The lines labeled A, B, C correspond to $\text{H}_2\text{O}(\text{liq})-\text{D}_2\text{O}(\text{liq})$, $\text{H}_2\text{O}(\text{liq})-\text{D}_2\text{O}(\text{solid})$ and $\text{H}_2\text{O}(\text{solid})-\text{D}_2\text{O}(\text{solid})$, respectively. Most of line A refers to supercooled D_2O and parts of line A and line B refer to supercooled H_2O . Notice that there is no evidence for the branch $\text{H}_2\text{O}(\text{solid})-\text{D}_2\text{O}(\text{supercooled})$ which is expected. However, our equipment design is such that we were unable to selectively nucleate just one of the samples and so this portion was not observed.

The curves A and B, and C and B, should intersect at the triple points of D_2O and H_2O , respectively. Simultaneous solution of equations 26 and 27 and 27 and 28 give $3.83 \pm 0.04^\circ$ for the triple point of D_2O and $-0.03 \pm 0.04^\circ$ for the triple point of H_2O ⁷⁶ in good agreement with the accepted values, 3.83° and 0.01° .

Simultaneous solutions of eq 26 and 28 at 0° gives a calculated fractionation factor of 1.0381 ± 0.0004 for the hypothetical process



in agreement within experimental error with the value 1.0384 ± 0.0002 which Weston⁷⁷ calculated from the heats of fusion and heat capacities of H_2O and D_2O . If we assume the law of the geometric mean⁷⁸ for the series HOH, HOD, DOD we obtain a fractionation factor of 1.0189 ± 0.004 (compared to Weston's calculated value of 1.0192 ± 0.002 and Kuhn and Thürkauf's,⁷² 1.0188) for the process.



It is interesting to compare these results with the direct

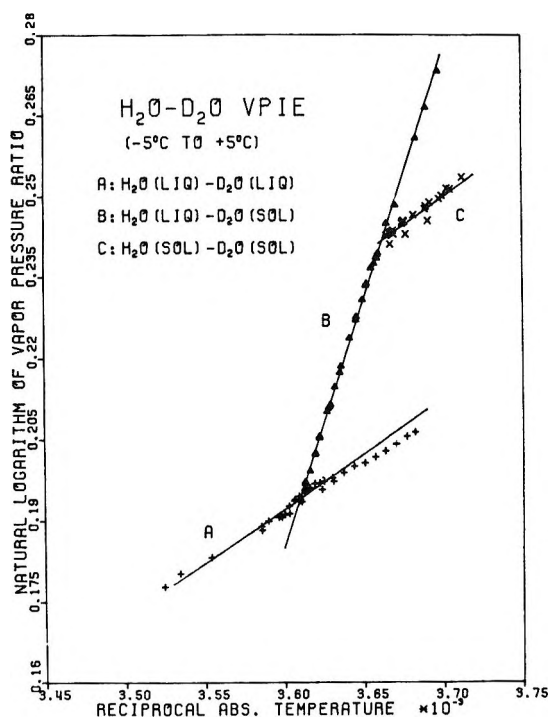


Figure 3. The vapor pressure isotope effects for $\text{H}_2\text{O}-\text{D}_2\text{O}$ between -5 and $+5^\circ$.

measurements of other workers. This is done in Table IV. Of the entries in the table Merlivat and Nief appear to be high, Kuhn and Thürkauf low. With these points disregarded the remainder average to 1.0202 ± 0.0008 when equally weighted. Within one standard deviation there is no overlap between the experimental results and the predictions of the law of the mean. However, the conclusion that the law of the mean is not obeyed is tenuous since overlap occurs within two standard deviations of either the experimental average or the calculated prediction. This near congruence is interesting in view of the fact that there is no *a priori* reason for the law of the mean to hold for water in the condensed phase.⁵

$\text{H}_2\text{O}-\text{D}_2\text{O}$ Liquids. The analysis of the $\text{H}_2\text{O}-\text{D}_2\text{O}$ liquid data is a most important portion of the present paper, at least as far as our projected experimental program is concerned. The data have already been presented in Figure 2, Table IIb, and equation 26. The reliability of the data is best judged from an examination of the variance of fit of eq 26. For the solvents σ_f ($\sigma_f = \sqrt{\text{variance of fit}}$) is about 2×10^{-4} . This is slightly improved for the individual salt solutions, probably because the vapor pressure is depressed and fluctuations due to incipient condensation, etc., are minimized. We have considered this statistical error and the pos-

(75) L. Merlivat and G. Nief, *Tellus*, **19**, 122 (1967).

(76) The effects (both for D_2O and H_2^{18}O) reported here have been corrected for the artifact mentioned in ref 43.

(77) R. E. Weston, *Geochim. Cosmochim. Acta*, **8**, 281 (1955).

(78) J. Bigeleisen, *J. Chem. Phys.*, **23**, 2264 (1955).

Table IV: Fractionation Factors at 0° for the Reaction $\text{H}_2\text{O}(\text{solid}) + \text{HOD}(\text{liq}) \rightleftharpoons \text{H}_2\text{O}(\text{liq}) + \text{HOD}(\text{solid})$

a. Calculated from the Law of the Geometric Mean and	
(1) Thermodynamic quantities	
Weston ⁷⁷	1.0192 ± 0.0002
Kuhn and Thürkauf ⁷²	1.0188
(2) VPIE measurements on D ₂ O liquid and ice	
Present work	1.0189 ± 0.0004
b. Directly Measured	
Posey and Smith ^a	1.0211 ± 0.0007
Kuhn and Thürkauf ⁷²	1.0171 ± 0.0005
Merlivat and Nief ⁷⁵	1.0235
O'Neil ^b	1.0195
Craig ^c	1.0195
Arnason ^d	1.0208 ± 0.0007

^a J. C. Posey and H. A. Smith, *J. Amer. Chem. Soc.*, **79**, 555 (1957). ^b J. R. O'Neil, *J. Phys. Chem.*, **72**, 3683 (1968). ^c H. Craig, *Trans. Amer. Geophys. Union*, **49**, 1, 216 (1968). ^d B. Arnason, *J. Phys. Chem.*, **73**, 3491 (1969).

sible systematic errors in assigning an uncertainty of ±0.0003 ln *R* units to the VPIE's which we report. The data are compared with the results of some earlier workers in Table III. The ninth row in Table III shows the results obtained below by fitting data on the solvents and on LiCl, NaCl, KCl and CsCl solutions all together in order to determine the best fit zero concentration intercept. This lies consistently just about one standard deviation below the present fit. Hopefully the true value lies between the values quoted in the first and ninth rows.

There are a number of important points of comparison in Table III. First there is excellent agreement at the higher temperatures between most of the workers in the table. [Riesefeld and Chang⁷⁹ are consistently low and will not be considered further.] Thus there is agreement within 1% with Jones⁷ from 60 to 90°, with Lewis and McDonald⁸⁰ from 40 to 90°, with Miles and Menzies⁸¹ from 30 to 80°, and with Zieborak⁸² at 80 and 90°. [The present data could well be a little (as much as 1%) high at 100° which is almost 5° beyond our actual last point and so involves some extrapolation.] *The most important difference between the present work and earlier papers is the fact that the present results are significantly higher at lower temperatures, i.e., that there is a good deal more curvature in the VPIE-temperature curve than was to be expected from the earlier work.*⁸³ This definite conclusion is only made possible by our improved precision at the lower temperatures. An important consequence which follows is that equations of the type $\ln R = A/T + B/T^2$ simply do not display enough curvature to fit over the entire range and one must either go to temperature dependent *A* and *B*'s or to extended equations, for example of type 26. Experimentally our high (as compared to other

workers) results at low temperature are substantiated by the excellent agreement between the calculated^{72,77} and observed ice-liquid fractionation factor and the present and literature^{73,74} values of the ice VPIE's.

3. *Solution Data.* The experimental results are presented in Tables: IIc (NaCl; 1.1024, 2.9000, 4.0000, and 5.5000 *m*), IIId (KCl; 3.5000 and 4.5000 *m*), IIe (CsCl; 1.0000, 3.0000, 4.5000, and 6.0000 *m*), and IIIf (LiCl; 3.0000, 5.0000, 7.0000, 10.0000, and 15.0000 *m*).⁶³ The concentrations are good to ±0.0002 *m*. The natural logarithms of the observed effect together with the associated temperatures are given. Except for KCl which was limited at the low end to room temperature by the solubility, the data generally extend from 0° or slightly below, up to about 90° for each of the salts studied. Many of the concentrations were scanned with two different, separately prepared, samples.

We chose to work the solution data up in two different ways. Large scale plots of the data gave smooth curves more or less parallel to the H₂O-D₂O pure solvent effect. In method A, the VPIE's were least squared⁸⁴ to equations of the form, $\ln R = A_1/T^2 + A_2/T + A_3$, for each different solution. The equations and data points were graphed so that any unusual behavior could be easily detected. A comparison of the *A* parameters for a given salt at different concentrations always showed a regular progression. The *A* equations were then solved at regular temperature intervals and these solutions (at a given temperature) were in turn fit to equation 8.

$$\Delta \ln R = \ln R_0 - \ln R_m = \frac{2}{55.508} bm^2 + \frac{2}{55.508} cm^3 + \dots \quad (8)$$

$$= Km^2 + Lm^3 + \dots \quad (31)$$

This process is exemplified for NaCl in Figure 4. For this salt the quadratic term alone is sufficient. (The plots show the 2.9 *m* solution apparently low below 50°.) *K* is given as a function of temperature in Figure 5.

Method A is thus straightforward, but, because it

(79) E. A. Riesefeld and T. L. Chang, *Z. Phys. Chem., Abt. B*, **33**, 120(1936).

(80) G. N. Lewis and R. T. McDonald, *J. Amer. Chem. Soc.*, **55**, 3057 (1933). [The original data were fit with our programs to an eq of type 26.]

(81) F. T. Miles and A. W. Menzies, *J. Amer. Chem. Soc.*, **58**, 1067 (1936).

(82) K. Zieborak, *Z. Phys. Chem.*, **231**, 248 (1966).

(83) (a) R. L. Combs, J. M. Googin, and H. A. Smith, *J. Phys. Chem.*, **58**, 1009 (1954). (b) The results of ref 83a at the lower temperatures are higher than those of most earlier workers in agreement with us, but do not fall off with increasing temperature as steeply as do our data and so do not show the enhanced curvature referred to in the text.

(84) M. H. Lietzke, ORNL 3259. See ref 61.

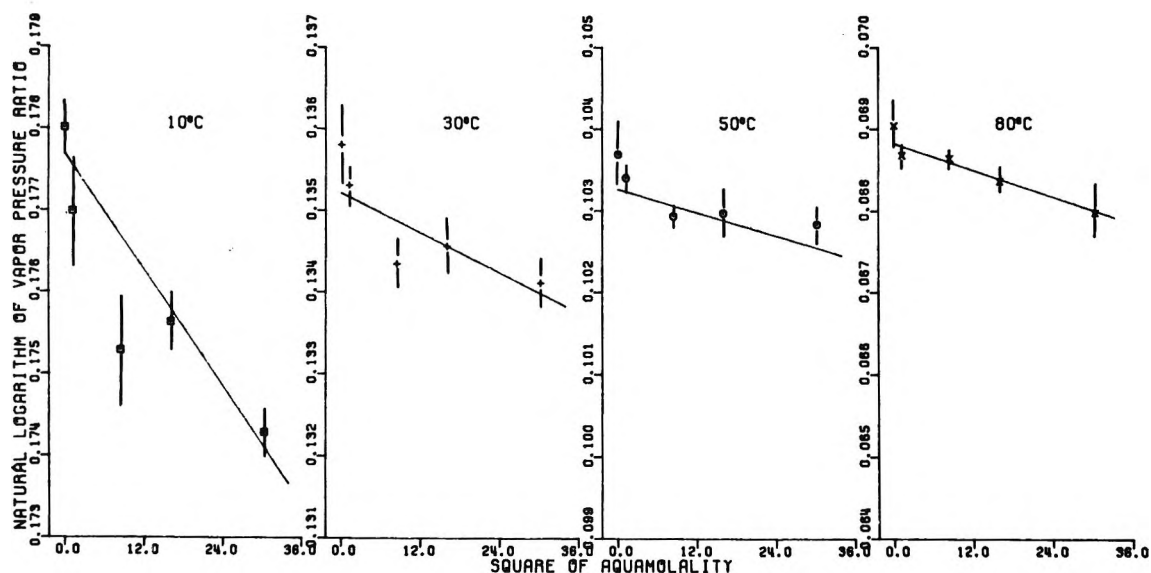


Figure 4. The concentration dependence of $\ln R$ at several different temperatures.

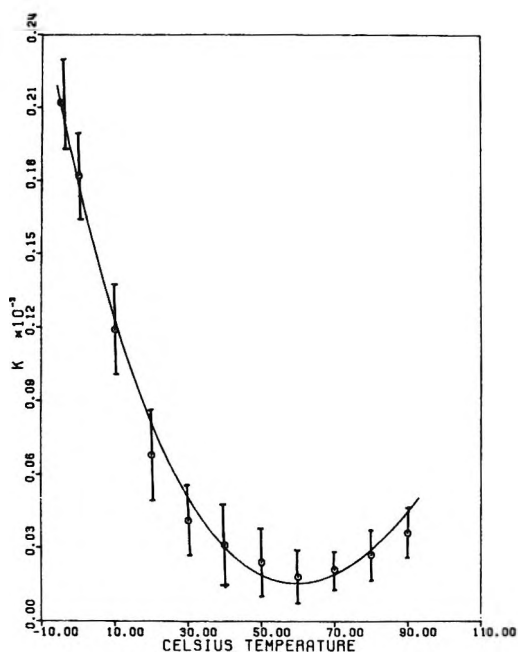


Figure 5. The temperature dependence of K_{NaCl} .

involves a threefold least squaring in finally arriving at the temperature coefficient of K , does not permit a straightforward analysis of the error to be assigned to the thermodynamic parameters. We consider it an important part of our data treatment, however, because it allows a simple graphic comparison between calculated and observed values which in the rather more abstract method B is not practical.

In method B all of the data are treated together. We have seen that the quantity of experimental interest is $\Delta \ln R_{\text{XCl}}^m = \ln R_0 - \ln R_{\text{XCl}}^m$, for each of the salts, XCl , at each concentration, m . We therefore elected to redetermine the intercept, $\ln R_0 = A_1/T^2 + A_2/T + A_3$, by employing all of the pure solvent and pertinent

Table V: The Parameters of Eq 34

	LiCl	NaCl	KCl	CsCl
ΔB_1	0.7330	3.4468	0.7326	8.5001
ΔB_2	0.002696	0.010535	0.002016	0.025315
ΔB_3	-0.017853	-0.071519	-0.013831	-0.172304
ΔC_1	7.0722×10^{-4}	-1.0512
ΔC_2	-3.1999×10^{-6}	-0.003213
ΔC_3	1.8917×10^{-4}	0.021789

solution data simultaneously. Thus, we made one single least-square fit of all of the different salt systems plus the solvent data to a single equation.

$$\ln R = \frac{A_1}{T^2} + \frac{A_2}{T} + A_3 - \sum_{i=1}^4 \left[\frac{\Delta B_1(i)}{T} + \Delta B_2(i) \ln T + \Delta B_3(i) \right] m_i^2 \quad (i = \text{Li, Na, K, Cs}) \quad (32)$$

The input data for eq 32 was limited to those concentrations at or below which the data were found to be satisfactorily fit by the quadratic term alone. These were found in the preliminary least-square runs to include all of the water, NaCl and KCl data, the 1 and 3 m CsCl data and the 3 and 5 m LiCl data. Altogether 832 data points were fit to the 15 parameters in eq 32. The expression for the intercept which was obtained is

$$\ln R_0 = \frac{57321}{T^2} - \frac{209.41}{T} + 0.20252 \quad (33)$$

The variance was 1.3×10^{-6} and the variance of fit 1.6×10^{-9} . We have reported vapor pressure isotope effects for $\text{H}_2\text{O}-\text{D}_2\text{O}$ as calculated with equation 33 to

Table VI: Error Matrix (Inverse Matrix of Normal Equations) Associated with Parameters in Table V

	LiCl	NaCl	KCl	CsCl
B_{11}	1.34×10^5	6.93×10^4	1.49×10^6	5.02×10^6
$B_{12} = B_{21}$	4.30×10^2	2.28×10^2	4.49×10^3	1.61×10^4
$B_{13} = B_{31}$	-2.90×10^3	-1.54×10^3	-3.06×10^4	-1.09×10^5
B_{22}	1.38×10^0	7.54×10^{-1}	1.36×10^1	5.17×10^1
$B_{23} = B_{32}$	-9.33×10^0	-5.06×10^0	-9.23×10^1	-3.49×10^2
B_{33}	6.29×10^1	3.40×10^1	6.28×10^2	2.35×10^3
C_{44}	7.33×10^2	1.65×10^5
$C_{45} = C_{54}$	2.35×10^0	5.28×10^2
$C_{43} = C_{44}$	-1.59×10^1	-3.56×10^3
C_{55}	7.57×10^{-3}	1.69×10^0
$C_{56} = C_{65}$	-5.11×10^{-2}	-1.14×10^1
C_{66}	3.44×10^{-1}	7.71×10^1
$b_{14} = b_{41}$	-9.70×10^3	-8.97×10^6
$b_{15} = b_{51}$	-3.12×10^1	-2.88×10^3
$b_{16} = b_{61}$	2.10×10^2	1.94×10^4
$b_{24} = b_{42}$	-3.12×10^1	-2.88×10^3
$b_{25} = b_{52}$	-1.00×10^{-1}	-9.23×10^0
$b_{26} = b_{62}$	6.76×10^{-1}	6.23×10^1
$b_{34} = b_{43}$	2.10×10^2	1.94×10^4
$b_{35} = b_{53}$	6.76×10^{-1}	6.23×10^1
$b_{36} = b_{63}$	-4.56×10^0	-4.20×10^2

± 0.0003 . They are compared with those obtained from the fit to the solvent data alone in Table III. The present results are about one standard deviation below those calculated from the solvent data alone. We prefer them for the present application. The true VPIE is hopefully bracketed by these two separate fitting procedures.

With R_0 determined as a function of temperature we returned and fit all of the salt data to the equation

$$\ln R = \ln R_0 - \sum_{i=1}^4 \left[\frac{\Delta B_1(i)}{T} + \Delta B_2(i) \ln T + \Delta B_3(i) \right] m_i^2 - \sum_{i=1}^4 \left[\frac{\Delta C_T(i)}{T} + \Delta C_2(i) \ln T + \Delta C_3(i) \right] m_i^3 \quad (i = \text{Li, Na, K, Cs}) \quad (34)$$

The 18 parameters which were obtained are reported in Table V. Enough significant figures are included so that the effects can be calculated to 0.00001 and rounded to the nearest 0.0001, even at the highest concentrations. This entails reporting the parameters to well beyond their confidence limits (as expressed by standard deviation) because the linear combination which expresses the effect is known to a much higher order of precision than are the parameters themselves. The parameters contain all of the thermodynamic information derived from the present study and therefore the associated errors are of real interest. Since the individual parameters for each salt are highly correlated with each other (but not at all with any of the other salts) we have elected to report the entire error matrix, together with the variance, rather than (more conven-

tionally) just the diagonal elements from which standard deviations are obtained. These matrices are found in Table VI. The variance was 1.0×10^{-6} and the variance of fit 1.3×10^{-9} ; 761 solution data points were included in the analysis.

Even though all the information obtained in the present study is contained in eq 34 and Tables IIa-f,⁶³ we believe it is instructive to examine some numerical values of the effects and the associated thermodynamic properties at representative temperatures. In this way comparisons are facilitated, as is the discussion of later paragraphs. This is done in Table VII where values for $\Delta \ln R$, $\Delta \phi$, $\Delta G_{\text{salt}}^{\text{ex}}/m$, $\Delta H_{\text{salt}}^{\text{ex}}/m$, $\Delta S_{\text{salt}}^{\text{ex}}/m$ and $\Delta C_p^{\text{ex}}(\text{salt})$ are shown at 0, 25, 50, 75, and 100° together with the associated errors as calculated from Table VI. Although the values for the functions themselves are readily obtained from Table V, obtaining the errors is a more involved process and we feel that the entries in the table are particularly valuable in reflecting an accurate picture of the errors across the entire temperature-concentration range of the study. For the fourth column, $10^4 \Delta \ln R$, the errors are those calculated with Table VI, or 0.0002, whichever is greater. Errors entered in the remaining columns are those calculated from Table VI except for the last column (heat capacities) where they are calculated from the error bounds on the enthalpies.

Even a casual look at Table VI or VII reveals striking differences in the errors assigned to the thermodynamic functions of the different salts. This is in spite of the fact that the precision for individual measurements was nearly the same for each data point. It is a consequence of the necessarily more restricted temperature

Table VII: Solvent Isotope Effects on Excess Properties of Aqueous Alkali Metal Chloride Solutions

m	$t, ^\circ\text{C}$	$10^4 \Delta \ln R$	$10^4 (\phi_H - \phi_D)$	$\Delta G_{\text{salt}}^{\text{ex}}/m$	$\Delta H_{\text{salt}}^{\text{ex}}/m$	$\Delta S_{\text{salt}}^{\text{ex}}/m$	$\Delta C_p^{\text{ex}}/m$
LiCl							
2	0	-1 ± 2	-11 ± 6	-0.8 ± 0.4	1 ± 6	0.01 ± 0.02	
	25	-1 ± 2	-8 ± 4	-0.6 ± 0.3	-6 ± 7	-0.02 ± 0.02	
	50	0 ± 2	3 ± 3	0.1 ± 0.1	-13 ± 7	-0.04 ± 0.02	-0.29 ± 0.13
	75	2 ± 2	22 ± 3	1.4 ± 0.2	-21 ± 7	-0.06 ± 0.02	
	100	3 ± 2	45 ± 4	3.3 ± 0.3	-28 ± 8	-0.08 ± 0.02	
4	0	1 ± 2	5 ± 4	-0.2 ± 0.2	3 ± 6	0.01 ± 0.02	
	25	1 ± 2	4 ± 2	-0.2 ± 0.1	-4 ± 6	-0.01 ± 0.02	
	50	3 ± 2	21 ± 3	0.45 ± 0.07	-12 ± 6	-0.04 ± 0.02	-0.29 ± 0.11
	75	8 ± 2	52 ± 3	1.65 ± 0.09	-19 ± 6	-0.06 ± 0.02	
	100	13 ± 2	93 ± 4	3.37 ± 0.13	-26 ± 7	-0.08 ± 0.02	
6	0	10 ± 2	48 ± 4	0.31 ± 0.03	4 ± 5	0.01 ± 0.02	
	25	8 ± 2	36 ± 5	0.26 ± 0.03	-3 ± 5	-0.01 ± 0.02	
	50	12 ± 2	53 ± 5	0.80 ± 0.07	-10 ± 5	-0.03 ± 0.02	-0.28 ± 0.10
	75	20 ± 2	91 ± 5	1.88 ± 0.10	-17 ± 6	-0.05 ± 0.02	
	100	31 ± 2	144 ± 5	3.47 ± 0.13	-24 ± 6	-0.07 ± 0.02	
10	0	78 ± 2	216 ± 5	1.42 ± 0.03	7 ± 3	0.02 ± 0.01	
	25	59 ± 2	163 ± 4	1.17 ± 0.03	1 ± 4	0.00 ± 0.01	
	50	58 ± 2	161 ± 4	1.49 ± 0.04	-6 ± 4	-0.02 ± 0.01	-0.27 ± 0.07
	75	70 ± 2	196 ± 5	2.33 ± 0.05	-13 ± 4	-0.04 ± 0.01	
	100	93 ± 2	258 ± 5	3.66 ± 0.07	-20 ± 4	-0.06 ± 0.01	
15	0	313 ± 2	578 ± 5	2.80 ± 0.02	11 ± 2	0.03 ± 0.01	
	25	236 ± 3	436 ± 6	2.31 ± 0.03	5 ± 2	0.01 ± 0.01	
	50	203 ± 3	375 ± 5	2.35 ± 0.03	-2 ± 2	-0.01 ± 0.01	-0.26 ± 0.04
	75	203 ± 3	375 ± 5	2.89 ± 0.04	-8 ± 2	-0.03 ± 0.01	
	100	226 ± 3	419 ± 5	3.90 ± 0.05	-14 ± 2	-0.05 ± 0.01	
NaCl							
2	0	8 ± 2	111 ± 5	6.00 ± 0.05	63 ± 5	0.21 ± 0.02	
	25	3 ± 2	35 ± 2	2.10 ± 0.07	34 ± 6	0.11 ± 0.02	
	50	1 ± 2	10 ± 1	0.63 ± 0.07	5 ± 6	0.01 ± 0.02	-1.2 ± 0.1
	75	1 ± 2	20 ± 1	1.41 ± 0.07	-24 ± 6	-0.07 ± 0.02	
	100	4 ± 2	58 ± 4	4.3 ± 0.3	-53 ± 6	-0.15 ± 0.02	
4	0	32 ± 2	221 ± 3	6.00 ± 0.03	63 ± 5	0.21 ± 0.02	
	25	10 ± 2	71 ± 1	2.10 ± 0.03	34 ± 6	0.11 ± 0.02	
	50	3 ± 2	20 ± 1	0.63 ± 0.03	5 ± 6	0.01 ± 0.02	-1.2 ± 0.1
	75	6 ± 2	41 ± 1	1.41 ± 0.05	-24 ± 6	-0.07 ± 0.02	
	100	17 ± 2	115 ± 4	4.3 ± 0.2	-53 ± 6	-0.15 ± 0.02	
6	0	72 ± 3	332 ± 4	6.00 ± 0.02	63 ± 5	0.21 ± 0.02	
	25	23 ± 2	106 ± 2	2.10 ± 0.02	34 ± 6	0.11 ± 0.02	
	50	6 ± 2	29 ± 1	0.63 ± 0.02	5 ± 6	0.01 ± 0.02	-1.2 ± 0.1
	75	13 ± 2	61 ± 2	1.41 ± 0.04	-24 ± 6	-0.07 ± 0.02	
	100	26 ± 2	144 ± 4	4.3 ± 0.01	-53 ± 6	-0.15 ± 0.02	
KCl							
2	25	4 ± 2	62 ± 13	3.7 ± 0.8	15 ± 24	0.04 ± 0.08	
	50	3 ± 2	47 ± 12	3.0 ± 0.8	9 ± 25	0.02 ± 0.08	
	75	3 ± 2	40 ± 11	2.8 ± 0.8	4 ± 26	0.00 ± 0.08	-0.2 ± 0.8
	100	3 ± 2	39 ± 15	2.9 ± 1.1	-2 ± 27	-0.01 ± 0.07	
	4	25	18 ± 2	125 ± 13	3.7 ± 0.4	15 ± 24	0.04 ± 0.08
50		14 ± 2	94 ± 11	3.0 ± 0.4	9 ± 25	0.02 ± 0.08	
75		12 ± 2	80 ± 11	2.8 ± 0.4	4 ± 26	0.00 ± 0.08	-0.2 ± 0.8
100		11 ± 2	79 ± 14	2.9 ± 0.5	-2 ± 27	-0.01 ± 0.08	
CsCl							
2	0	27 ± 2	371 ± 31	21.4 ± 1.8	146 ± 33	0.46 ± 0.12	
	25	14 ± 2	199 ± 31	12.5 ± 1.9	90 ± 34	0.26 ± 0.11	
	50	9 ± 2	122 ± 31	8.3 ± 2.1	33 ± 35	0.08 ± 0.11	-2.3 ± 0.7
	75	8 ± 2	114 ± 31	8.5 ± 2.3	-23 ± 37	-0.09 ± 0.11	
	100	11 ± 2	158 ± 26	12.8 ± 2.1	-80 ± 38	-0.25 ± 0.10	
4	0	81 ± 6	561 ± 42	17.7 ± 1.3	117 ± 21	0.37 ± 0.08	
	25	44 ± 6	309 ± 42	10.5 ± 1.4	74 ± 22	0.21 ± 0.07	
	50	27 ± 6	186 ± 42	6.9 ± 1.6	31 ± 23	0.07 ± 0.07	-1.7 ± 0.4
	75	23 ± 6	157 ± 41	6.7 ± 1.8	-12 ± 24	-0.05 ± 0.07	
	100	29 ± 6	199 ± 40	9.5 ± 1.9	-56 ± 25	-0.17 ± 0.07	

Table VII (Continued)

m	$t, ^\circ\text{C}$	$10^4 \Delta \ln R$	$10^4 (\phi_H - \phi_D)$	$\Delta G_{\text{salt}}^{\text{ex}}/m$	$\Delta H_{\text{salt}}^{\text{ex}}/m$	$\Delta S_{\text{salt}}^{\text{ex}}/m$	C_p^{ex}/m
6	0	123 ± 11	569 ± 52	14.0 ± 1.3	89 ± 11	0.27 ± 0.04	
	25	71 ± 11	329 ± 52	8.5 ± 1.3	59 ± 11	0.17 ± 0.04	
	50	41 ± 11	192 ± 51	5.5 ± 1.5	29 ± 11	0.07 ± 0.04	-1.2 ± 0.2
	75	28 ± 11	130 ± 52	4.8 ± 1.9	-1 ± 12	-0.02 ± 0.03	
	100	27 ± 11	125 ± 49	6.3 ± 2.5	-31 ± 12	-0.10 ± 0.03	

or concentration range for some of the salts. Thus KCl, limited to 4.5 m ($m^2 = 20$) and to temperatures above about 20°, shows very large errors in the derived functions as compared to NaCl ($m^2 = 36$) which covers the entire temperature range, even though both sets of data are nicely fit by the three parameter quadratic term alone (eq 34). Similarly CsCl shows large errors in its derived functions as compared to NaCl even though both sets of data cover identical temperature and concentration ranges. The reason is due to the fact that the CsCl displays significant curvature even at low concentrations. This demands that additional parameters be included in the fit with a concomitant larger uncertainty in the variance of fit. It is interesting to compare the CsCl with the LiCl data which extends all the way to 15 m ($m^2 = 225$). Here the wide concentration range permits the curvature to be much more precisely defined than it was for the CsCl data and the errors in the derived functions are again small (about the same as for the NaCl), even though the fit employs six parameters as compared to three for NaCl.

Finally we have calculated the standard state thermodynamic functions for transfer of NaCl and KCl from D₂O to H₂O from equation 18 and its derivatives. To do so we made empirical fits to the smoothed solubility and solubility isotope effect data reported by Menzies and coworkers.²⁶ No solubility isotope effect data are available for CsCl. The LiCl system is complicated by hydrate formation. The empirical least-square fits follow; m is used to signify the solubility.

$$\text{NaCl} \left\{ \begin{aligned} \ln m_H &= \frac{280.0}{T} + 1.0097 \ln T - 5.9034 \\ &(\sigma = 4 \times 10^{-4}) \quad (35) \end{aligned} \right.$$

$$\text{NaCl} \left\{ \begin{aligned} \ln \frac{m_H}{m_D} &= \frac{349.8}{T} + 0.9424 \ln T - 6.4759 \\ &(\sigma = 1 \times 10^{-3}) \quad (36) \end{aligned} \right.$$

$$\text{KCl} \left\{ \begin{aligned} \ln m_H &= \frac{-509.5}{T} - 0.6532 \ln T + 6.1102 \\ &(\sigma = 2 \times 10^{-3}) \quad (37) \end{aligned} \right.$$

$$\text{KCl} \left\{ \begin{aligned} \ln \frac{m_H}{m_D} &= \frac{1015}{T} + 2.754 \ln T - 18.997 \\ &(\sigma = 7 \times 10^{-3}) \quad (38) \end{aligned} \right.$$

These relations may be combined with our results (eq 34) to obtain the results of Table VIII. Here the enthalpies were obtained numerically. The errors in the tables were arbitrarily set, mostly at 20%. This was necessary since we had no good method of analyzing the uncertainties of Menzies' data. This, the solubility isotope effect, makes the most important contribution to the isotope effects on the standard state properties of transfer. The second column in Table VIII shows the approximate fractional contribution of the isotope effect on the activity coefficients to the free energy of transfer (*i.e.*, the contribution of the present data). It is as small as 6% for the NaCl system at 50° and in fact never rises above 50%.

Table VIII: Isotope Effects on Standard Properties of Transfer (D₂O to H₂O) Calculated from the Present Data and Ref 26

$t, ^\circ\text{C}$	$\Delta G_\gamma^\circ/\Delta G^\circ$	ΔG°	ΔH°	ΔS°
NaCl				
0	(0.27)	-260 ± 53	-1450 ± 300	-4.4 ± 0.9
25	(0.15)	-170 ± 30	-960 ± 200	-2.6 ± 0.5
50	(0.06)	-130 ± 25	-450 ± 100	-1.0 ± 0.5
75	(0.14)	-130 ± 25	80 ± 100	+0.6 ± 0.5
100	(0.34)	-170 ± 30	650 ± 130	+2.2 ± 0.5
KCl				
25	(0.24)	-140 ± 30	-909 ± 200	-2.6 ± 0.5
50	(0.37)	-90 ± 20	-540 ± 100	-1.4 ± 0.5
75	(0.48)	-75 ± 20	-110 ± 100	-0.1 ± 0.5
100	(0.47)	-90 ± 20	+430 ± 100	+1.4 ± 0.5

Comparisons. There are no data in the literature with which comparisons can be made except at the standard, 25°, temperature. Even there, very little work has been reported.

The most direct comparisons that can be made are with the isopiestic data of Kerwin¹⁴ and Robinson,¹³ and the glass electrode data of Schrier and Robinson.⁸⁵ These are shown in Table IX. The agreement with Schrier is quantitative. Kerwin finds the same relative ordering as do we, but it appears likely that his isopiestic reference, ZnSO₄,⁸⁶ is in error and that his scale

(85) Private communication, Drs. E. E. Schrier and R. A. Robinson.

(86) J. C. Rasiyah, Thesis, University of Pittsburgh, 1965.

Table IX: Comparison of Reported Isotope Effects on Osmotic Coefficients at 25° and 2 *m*

	$\phi_H - \phi_D = 10^{-3} Km$			
	Present work, <i>K</i>	Kerwin, <i>K</i>	Schrier and Robinson, <i>K</i>	Robinson, <i>K</i>
LiCl	-0.4 ± 0.1	-5.8	...	
NaCl	+1.8 ± 0.1	-1.2	2.0	
KCl	+3.1 ± 0.5	0.0	...	
CsCl	+10.0 ± 1.5	0.8	...	
	$K_{MCl} - K_{NaCl}$			
LiCl-NaCl	-2.2	-4.6		
NaCl-NaCl
KCl-NaCl	1.3	1.2 ⁸⁷		3.0, 1.2
CsCl-NaCl	8.2	2.0		
Reference		14	85	13

is displaced. A comparison of differences, made at the bottom of the table, shows excellent agreement with the NaCl-KCl pairs,⁸⁷ but significant differences with the LiCl and CsCl systems remain. Googin and Smith¹¹ were interested in H₂O-HDO separation factors over saline solutions. They examined a large number of salt solutions in mixed H₂O-D₂O solvents at 27° using the technique of Rayleigh distillation. They invariably found that the separation factor was lower than the pure solvent value in agreement with the positive signs on ($\phi_H - \phi_D$) quoted above. A value of *K* (above, Table IX) may be estimated from their data using an average concentration. We obtain from their data

Table X: Comparison of Reported Excess Enthalpies of Transfer as a Function of Concentration at 25°

	$\Delta H_{\text{salt}}^{\text{ex}}/m$		
	Present work	Wood and coworkers ²⁰	Wu and Friedman ¹⁸
	LiCl		
2	-6 ± 7	11.6	
4	-4 ± 6	11.4	
6	-3 ± 5	...	47 ± 8
10	1 ± 4	...	
15	5 ± 2	...	
	NaCl		
2		39.4	
4	34 ± 6	25.2	34 ± 5
6		...	
	KCl		
2	15 ± 24	39.5	
4		32.1	
	CsCl		
2	90 ± 34		
4	74 ± 22		
6	59 ± 11		

LiCl (20 *m*), *K* = 0.3 to be compared with our value (15 *m*), *K* = 3; for KCl (6.2 *m*), *K* = 14 ± 3 compares with our value of 3.1 ± 0.5 and for CsCl (7 *m*), *K* = 20 ± 3 compares with our value (6 *m*) of *K* = 10 ± 2.

It is also interesting to look at literature results for the excess enthalpy isotope effects. These are shown in Table X. The agreement is satisfactory, particularly when it is recalled that the present enthalpies are obtained only indirectly by differentiation.

Finally in Table XI we show comparisons between the Thermodynamic Functions for transfer between the standard state solutions of NaCl and KCl. The ΔG° 's appear reasonable. However, the agreement is not good between the different laboratories. The enthalpies derived from the present study appear high, particularly for the NaCl solution. We feel that this is a result of uncertainties in the literature solubility and solubility isotope effect data²⁶ because of the rather better agreement which we observe between our data and other reported excess enthalpy isotope effect data (Table X).

Table XI: Comparison of Standard State Thermodynamic Function of Transfer from D₂O to H₂O at 25°

	ΔG°	ΔH°	ΔS°
	NaCl		
Greyson ¹⁶	-110 ± 12		
Lange and Martin ^{22b}		-560	-1.51 ± 0.04
Salomaa and Aalto ¹⁵	-212 ± 9		
Kerwin ¹⁴	-116		
Wu and Friedman ¹⁸		-545 ± 30	
Davies and Benson ¹⁹		-535	
Arnett and McKelvey ²³		-590 ± 50	
This work and ref 26	-174 ± 30	-950 ± 200	-2.6 ± 0.5
	KCl		
Greyson ¹⁶	-130 ± 12		
Lange and Martin ^{22b}		-615	-1.63 ± 0.04
Salomaa and Aalto ¹⁵	-219 ± 9		
La Mer and Noonan ¹⁷	-225	-750	-1.76
Arnett and McKelvey ²³		-730 ± 90	
This work and ref 26	-140 ± 30	-909 ± 200	-2.6 ± 0.5

We conclude from the comparisons at 25° that the present data are reliable within the quoted error limits and expect that this conclusion is valid at other temperatures as well.

Discussion

There is a good deal of new information which can be extracted from eq 34 and Table VII. The trend of the

(87) It seems that in this portion of his thesis Kerwin is analyzing data due to Robinson.¹³

results with temperature is of particular interest. We have already noted that there is more curvature in the VPIE-temperature curve for the pure solvents than was to be expected from the reports of earlier workers. An important consequence is the fact that approximate equations of the form $\ln R = A/T^2 + B/T$ are experimentally ruled out for aqueous systems.

The chief features of the results for the solutions are displayed in Figure 6, where the isotope effects on the excess free energy per mole and on the excess enthalpy per mole of salt added are shown at three different temperatures. Statements concerning some of the qualitative features of the results follow.

(a) The isotope effects on the excess free energies (IEEG) are quite small (in agreement with the observations of previous workers at 25°) and they are all positive within experimental error (column 3, Table VII). Thus to the extent that the IEEG serves as a criteria for solution structure all of the salts studied here are structure breakers (although LiCl shows essentially no effect out to above 5 *m*).

(b) The IEEG data are apparently tending toward a roughly common value at very high salt concentration at each temperature and this value seems to be about the same across the whole temperature range ($\sim 3 \pm 2$ cal/mol of salt added):

(c) The ordering of the IEEG effects is that expected. Around room temperature that is $\text{Cs}^+ > \text{K}^+ > \text{Na}^+ > \text{Li}^+$.

(d) The isotope effects on the excess enthalpies (IEEE) are large. They are definitely temperature dependent and the IEEE's all change sign in the region 50 to 75° except for LiCl which has a small IEEE and apparently changes sign at a lower temperature.

(e) At very high salt concentrations the IEEE data are apparently tending to a roughly common value of 0 ± 20 cal/mol.

(f) The IEEG's and the IEEE's are of the opposite sign and smaller than the standard state free energies and enthalpies of transfer (for NaCl and KCl at least).

A number of different approaches to the interpretation of data such as the above have been made but all share (implicitly or explicitly) the ideas of ionic hydration. In this approach⁹ several different kinds of water molecules are postulated. These include molecules directly bound to the ion (hydration in the first layer), those not immediately adjacent but still which have had some modification from the bulk solution structure (hydration in outer layers), and finally unchanged water molecules. Friedman¹⁸ calls the region of water molecules of changed structure the *cosphere*. In the simplest model the different kinds of hydrations may be lumped together and one is then faced with what is essentially a two state model consisting of "changed" and "unchanged" solvent molecules. In addition we must not forget the complication that the "unchanged" solvent molecules (*i.e.*, those far from any ion) must

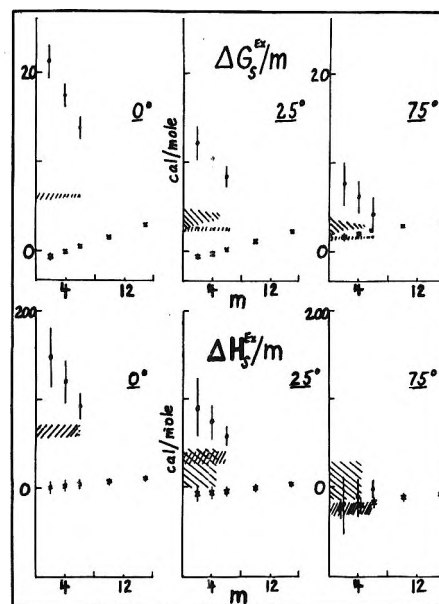
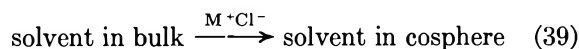


Figure 6. Isotope effects on excess free energies of solution $\Delta G_s^{\text{ex}} = G_s^{\text{ex}}(\text{H}_2\text{O}) - G_s^{\text{ex}}(\text{D}_2\text{O})$ and excess enthalpies of solution $\Delta H_s^{\text{ex}} = H_s^{\text{ex}}(\text{H}_2\text{O}) - H_s^{\text{ex}}(\text{D}_2\text{O})$. Key: CsCl, ϕ ; KCl, $\backslash\backslash$; NaCl, $////$; LiCl, \ddagger .

themselves be treated with at least a two state model so as to account for both the hydrogen bonded and the nonhydrogen bonded species.

The simplest possible model then is one where but one kind of cosphere water is assumed.



If in addition one assumes that there is no isotope effect on the hydration number (the number of solvent molecules in the cosphere) one can proceed to numerical results. A calculation of this kind was carried through by Swain and Bader⁸⁸ more than ten years ago. They assumed an isotope independent ion coordination number of four, and concentrated *all* of the isotope effects into the librational degrees of freedom of the water molecule. They focused attention exclusively on the standard state (infinite dilution properties) at 25° and were able to predict free energies and entropies in rough agreement with experiment. Input data to the calculation consisted of the solvent-solution shifts of the rather broad infrared bands assigned to the water librations.

The alternate approach, that of lumping all of the isotope effects into a (temperature dependent) isotope effect on hydration number, does not appear to be a fruitful path at present. The application of this approach to the theory of concentrated electrolyte solutions has a long history of difficulties.

Our particular interest is in the change in the isotopic ratio of water activities as measured by the vapor pressures. Following the method developed in ref 4 it

(88) C. G. Swain and R. F. W. Bader, *Tetrahedron*, **10**, 182 (1960).

is a simple matter to show that this is given in terms of the pure solvent and the solution partition functions by eq 40.

$$\ln R^0 - \ln R = -\frac{1}{N} \left[\ln \left(\frac{\bar{Q}_H}{\bar{Q}_D} \right)_{\text{solvent}}^N - \ln \left(\frac{\bar{Q}_H}{\bar{Q}_D} \right)_{\text{solution}}^N \right] \quad (40)$$

In this equation the molar volume and gas nonideality corrections have been neglected. The last term is the one of interest. If we adopt the two state model discussed above, the partition functions for the solvent in the solution will be of the general form

$$\bar{Q}_{\text{soln}}^N = \bar{Q}_1^{N_1} \cdot \bar{Q}_2^{N_2} \quad (41)$$

so that

$$\Delta \ln R = -\frac{1}{N} \left[\ln \left(\frac{\bar{Q}_{1H}}{\bar{Q}_{1D}} \right)^N - \left\{ \ln \left(\frac{\bar{Q}_{1H}^{(N-n_{2H})}}{\bar{Q}_{1D}^{(N-n_{2D})}} \right) - \ln \left(\frac{\bar{Q}_2^{n_{2H}}}{\bar{Q}_2^{n_{2D}}} \right) \right\} \right] \quad (42)$$

where N is the total number of water molecules in the system, and n_{2H} and n_{2D} are the number of cosphere waters in the H_2O and D_2O solutions, respectively. We are employing the notation 1 for unchanged (solvent) water, 2 for cosphere water. If the total number of water molecules is 55.508 mol then $n_{2H} = m_i z_{iH} L$ and $n_{2D} = m_i z_{iD} L$, where z_{iH} and z_{iD} are the respective coordination numbers and L is Avogadro's number. Thus at low enough concentrations the first and second terms in equation 42 are effectively equal. A second trivial case is found when $Q_2 = Q_1$, *i.e.*, when the structure is not affected by the solute. The simplest interesting case occurs when the water in the cosphere is tightly bound. Then we expect little or no isotope effect on the coordination numbers, and predict small effects (at low enough m_i only, notice that we are additionally using the assumption that the Q_2 ratio is not too different from the Q_1 ratio. This is the case treated in a special way in ref 88. In the context of equation 42 it appears that $\ln R$ is most sensitive to an isotope effect on the coordination numbers because this parameter enters exponentially). The model cannot hold to a very high concentration but nonetheless this set of assumptions does rationalize our observations on LiCl. These solutions show no change in the VPIE (within experimental error) all the way to about 5 m at temperatures of 50° and below. In this region of low concentration, therefore, the only interesting isotope effect data are those on the standard state thermodynamic functions of transfer. It is interesting that the standard state free energy of transfer for LiCl is reported (albeit imprecisely) as only 32 ± 92 cal/mol.^{16, 23, 89}

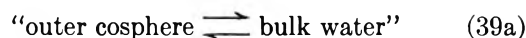
As the concentration of salt is increased some interaction between cospheres is anticipated and the excess

effects begin to play a role. We have seen for LiCl that this does not begin (at 50° or below) until about 5 m . Here the water/ion ratio is already down to 6 and as the concentration of salt is increased the ratio drops further and one must postulate that coordinated waters in the cosphere are being replaced with counterions. The isotope effect drops indicating that the structure in the cosphere is being broken down by this process. We would expect that if the concentration could be made very large (say ion/water ratios of one or so) that the effect should again level off to another concentration invariant standard state level, this time for the water dissolved in salt reference state. Therefore one expects the VPIE-concentration curve to be S shaped. Our high concentration data show no evidence of this anticipated leveling off even though they extend to 15 m . Instead $\Delta G^E/m$ is found monotonously increasing. (However, we are planning to investigate this point by making measurements on very concentrated $CaCl_2$ solutions.) Due to the high concentration rather large depressions of the VPIE are observed for the LiCl solutions ($R_0 - R_{15} = 0.024$ at 25°, $R_0 = 0.145$). Also the excess enthalpies are small, an observation which is consistent with the remarks above.

At higher temperatures the measured excess properties for LiCl are significantly different from zero even at low concentrations and it would appear that the hypothesized tightly structured cosphere is breaking down due to thermal energy input.

The remarks directed above to LiCl appear plausible as far as the Li^+ ion is concerned. This ion is well known to tightly complex its hydration sphere. With respect to the Cl^- ion, however, it is difficult to understand just why there should be only a very small effect, or a fortuitous cancellation. One would not guess that Cl^- would complex its waters of hydration tightly and the most plausible remaining hypothesis is that for this ion $Q^0 \approx Q_{\text{soln}}$.

Data for the other salts, CsCl, KCl, and NaCl, do not extend over such a wide concentration range as for LiCl. Still these salts show much larger effects per mole on the excess properties. We hypothesize that this is because their cospheres are much larger than the LiCl cosphere and more loosely bound. In this situation the assumption of just one kind of cosphere water seems unnecessarily restrictive. The larger excess effects must be due to overlap between the cospheres which must contain several layers (because the effects are measurable even at fairly low concentrations). In other words the studies on the excess properties focuses attention on the



(89) One point which is hard to understand is that we would expect the postulated tightly bound H_2O in the LiCl cosphere to have undergone a significant perturbation from the electric field of the ion. Hence it is a puzzle why the standard free energy of transfer is so small.

equilibria. Phrased in a slightly different fashion, one anticipates isotope effects on both the Q 's and the n 's, in eq 42. The net effect is that Na^+ , K^+ , and Cs^+ exert considerably greater structural effects than Li^+ . These effects correlate with size, polarizability, and a number of other parameters. The salts are all structure breakers, the VPIE is lowered in every solution. The excess thermodynamic properties seem to be tending towards salt independence at very high concentration and/or high temperature. This we would expect, since under these conditions the solvent structure is rapidly disappearing. It is also consistent with the observation that the IEE's are tending toward zero at very high concentration. Under conditions of high temperature and/or concentration, the residual effects are most likely due primarily to simple ionic polarization of single (*i.e.*, unstructured) water molecules.

The temperature dependence of the effects is interesting. The excess free energies per mole go through minima between 50 and 75°. The isotope effects on the excess heat capacities are substantial.

The simplest model for the calculation of the VPIE of water has been described by Van Hook.⁵ It consists of an "average molecule" cell model calculation and is a refinement on the calculation due to Swain and Bader⁸⁸ in that each molecule is modelled with a complete set of nine frequencies, not just the three degenerate librations. The major portion of the effect is contributed by the two internal stretches and the librations. These sets of frequencies contribute with opposite signs since the stretching force constant is considerably decreased on condensation from the gas ($\Delta\nu_1 + \Delta\nu_3 \approx -330 \text{ cm}^{-1}$ at 40°) but the librational constants are increased (from zero in the gas phase) due to the hydrogen bonding ($3\nu_{\text{lib}} \approx 1500 \text{ cm}^{-1}$ at 40°). It is likely that these frequency shifts are related and that an increase in the hydrogen bond frequency is partially compensated by a decrease in the internal stretching frequencies. Thus the complex temperature dependence of the VPIE was rationalized on terms of the observed⁹⁰ temperature dependence of the spectral absorption bands. Note that contribution of the internal (high frequency) modes goes roughly proportional to $1/T$, while that from the considerably lower frequency external modes goes roughly as $1/T^2$. The two effects partially compensate one another.

If one should apply basically the same model to the cosphere \rightleftharpoons bulk equilibrium (eq 39) he would assume no isotope effect on the hydration numbers and then develop the theory in terms of the cosphere-bulk spectral frequency shifts in an analogous fashion to the vapor-liquid shifts used for the VPIE itself. In the absence of refined measurements of the solution spectra and in the context of the remarks above under eq 42, it does not appear useful to pursue this approach quantitatively and in great detail at this time. Nonetheless it is of interest to demonstrate certain consistencies be-

tween the data and this model. The temperature dependence is of particular interest in this regard.

Accepting the basic ideas above, one is led to an approximate expression of the form (43) for the isotope effect on the equilibrium in eq 39.

$$(\Delta \ln R) = -\frac{A}{T^2} + \frac{B}{T} \quad (43)$$

Here the B term arises from the shifts in the internal (stretching) modes and the A from the shifts in the librations for the cosphere \rightleftharpoons bulk equilibria. The Swain-Bader calculation is equivalent to restricting attention to the first term. This term alone is not sufficient to account for the temperature dependency. It predicts that the isotopic enthalpy difference will be very small, proportional to (temperature)⁻¹, and sign invariant. This is not in accord with our data. Davies and Benson¹⁹ have also pointed out this limitation of the Swain-Bader model. Notice that the situation is not really improved with the addition of the second or B term. It simply amounts to introducing a constant term to the expression for the enthalpy which again is not in accord with the data. Thus it appears that if the effect is to be understood within this construct, temperature dependent A and B parameters are needed.

This can be seen another way from eq 43. If A and B are constants and if $\Delta \ln R$ is positive and does not change sign over the region of interest then it follows that $\Delta \ln R$ must decrease monotonously as the temperature is raised (if A and B be constant). The data, however, show a distinct minimum in $\Delta \ln R$ between 50 and 75° and we must therefore conclude that equation 43 does not apply. Alternatively, in the absence of spectral data, one could empirically assign appropriate temperature dependencies to the A and B parameters. This is equivalent to suggesting that the frequency shifts from bulk to cosphere are temperature dependent.

The result is not surprising. When the approach outlined above was applied to water itself⁵ it was necessary to introduce such temperature dependencies (in agreement with the spectroscopic observations). It seems only reasonable to expect that as the solvent structure changes with the temperature (as is well established), the differences between the solvent and cosphere will also change. In the modelling, these frequencies are expressed in terms of frequencies or force constants which are therefore expected to be temperature dependent. The appearance of the minimum is then most easily rationalized in terms of two (or more) different temperature dependent frequencies which contribute to the different terms in eq 43.

(It is worthwhile pointing out that the existence of the minimum we have been discussing is substantiated

(90) M. Falk and T. A. Ford, *Can. J. Chem.*, **44**, 1699 (1966); G. E. Walrafen, *J. Chem. Phys.*, **47**, 114 (1967).

by independent experimental evidence. Combs and Smith⁹¹ studied the effect of some different salts (including KCl) on the crossover temperature, T_c . At the crossover temperature $P_{H_2O} = P_{D_2O}$. T_c was found to decrease by some tens of degrees with added salt. A rough estimate of $\Delta\phi/m$ may be made from their data (for the region 150–200°). The values so estimated are significantly higher than those which we observe at the minimum.)

We conclude that data of the present kind are of real interest as an aid in unraveling details of solution structure. Information on other systems will be of benefit so that systematics can be established. We are currently employed in obtaining such data.

Acknowledgments. This work was supported by the U. S. Department of the Interior, Office of Water Resources Research, A-012 Tenn., and The Petroleum Research Fund, American Chemical Society. Grateful acknowledgment is made to the donors. Computing time was donated by the University of Tennessee computing center which has been generously supported by the National Science Foundation. We wish to thank Professor F. H. Gibbard, Jr., for permission to use his osmotic coefficient data for LiCl prior to publication, and Dr. and Mrs. J. Braunstein of Oak Ridge National Laboratory for the sample of anhydrous LiCl.

(91) R. L. Combs and H. A. Smith, *J. Phys. Chem.*, **61**, 441 (1957)

Aggregation Equilibria of Xanthene Dyes¹

by Judith E. Selwyn and Jeffrey I. Steinfeld*

Department of Chemistry, Massachusetts Institute of Technology, Cambridge, Massachusetts 02139
(Received June 25, 1971)

Publication costs assisted by the Petroleum Research Fund and the U. S. Army Research Office (Durham)

The absorption spectra of the laser-active dyes rhodamine B, rhodamine 6G and acridine red in aqueous, ethanolic and EPA solutions were studied as a function of concentration and temperature. The observed absorbance of the aqueous solutions of rhodamine B and rhodamine 6G is analyzed in terms of a monomer-dimer equilibrium. The dissociation constant, $K = c^2(\text{monomer})/c(\text{dimer})$, is 6.8×10^{-4} and 5.9×10^{-4} mol/l. at 22° for rhodamine B-H₂O and rhodamine 6G-H₂O solutions, respectively. The absorption spectra of the pure monomer and pure dimer are obtained for these two systems. Acridine red-H₂O is monomeric up to 3.38×10^{-6} M. Rhodamine B-ethanol solutions form dimers for which the equilibrium constant for dissociation is 1.1×10^{-4} mol/l. at 62° and 4.9×10^{-5} mol/l. at 22°. Calculation of the thermodynamic function for the process gives $\Delta H \simeq 4$ kcal/mol and $\Delta S_{315} \simeq -6$ eu. At -78.5° higher aggregates form in ethanolic rhodamine B solutions. 2×10^{-4} M rhodamine 6G-ethanol solutions show no evidence for the formation of aggregates, even when cooled to -78.5°. Small amounts of dimer are noted in acridine red-ethanol solutions under the same conditions. Solutions of rhodamine B-EPA are totally dimeric at 77°K. At 22° the equilibrium constant is 6.2×10^{-5} mol/l.; at -78.5° it is 3.1×10^{-5} mol/l. Thus, $\Delta H \approx 0.8$ kcal/mol and $\Delta S_{245} \approx -1.6$ eu. The low value of ΔH in this solvent gives strength to the hypothesis that hydrogen bonding is important in dimer formation. Rhodamine 6G-EPA fails to aggregate when cooled to 77°K. Acridine red-EPA is predominately monomeric at 22°; at -78.5° an equilibrium constant for the dissociation of dimers of 4.4×10^{-4} mol/l. is calculated. At 77°K higher aggregates also contribute to the observed absorption. Resolved monomer-dimer spectra are presented for the various nonaqueous systems.

I. Introduction

Convenient, continuously tunable lasers can now be produced to cover the entire visible spectrum using organic dyes as the lasing medium.²⁻¹⁰ Temperature¹¹ and concentration¹² tuning of these lasers has been thoroughly established and exploited. Basic to a complete understanding of these lasers is knowledge of the absorption and emission properties of the dyes used. All too often, theories have been generated using incomplete or erroneous spectral information.

It is known¹³⁻¹⁷ that these dyes tend to aggregate in solution, leading to a non-Beer's law concentration

(1) Taken in part from J. E. Selwyn, Ph.D. Thesis, M.I.T., June 1971.

(2) (a) P. P. Sorokin, J. R. Lankard, E. C. Hammond, and V. L. Morruzzi, *IBM J. Res. Develop.*, **11**, 130 (1967); (b) B. B. McFarland, *Appl. Phys. Lett.*, **10**, 208 (1967).

(3) P. P. Sorokin and J. R. Lankard, *IBM J. Res. Dev.*, **10**, 162 (1966).

(4) P. P. Sorokin, W. H. Culver, E. C. Hammond, and J. R. Lankard, *ibid.*, **10**, 401 (1966).

dependence of absorbance. However, in most cases the aggregation equilibrium, and the monomer and dimer spectra, have not been well characterized. This work presents a systematic study of the concentration and temperature dependence of the absorption spectra of the commonly used laser dyes rhodamine B, rhodamine 6G, and acridine red, in aqueous, ethanolic, and EPA (2 parts ethanol:5 parts isopentane:5 parts ethyl ether by volume) solutions.

II. Experimental Section

Spectra were recorded on a Cary 14M automatic spectrophotometer, using matched quartz absorption cells of 0.01, 0.1, 1.0, 2.0, 5.0, and 10.0-cm path lengths. Non-room temperature measurements were performed with the aid of a specially constructed Pyrex glass dewar which was fitted into the sample compartment of the Cary 14M in place of the usual cell holders. The entire sample chamber was flushed with dry nitrogen to prevent condensation on the optical windows at low temperatures. For measurements at 77°K and -78.5° the dewar was filled with baths of liquid nitrogen and Dry Ice-acetone, respectively, to a level such that the bottom of the sample cell was just touching the cryogenic fluid. For measurements at 0° or above room temperature, the samples were immersed within the dewar in ice water and warm water, respectively.

The rhodamine B and acridine red were obtained from Eastman Organic, and rhodamine 6G from Matheson Coleman and Bell. All dyes were used without further purification. In part, this was done to reproduce the conditions under which the dyes are used in practical laser devices; furthermore, ordinary purification procedures appear to produce little alteration in the spectra of these dyes.¹⁴ EPA solvent, specially prepared and dried, from American Instrument Co., 100% ethanol from U. S. Industrial Chemicals, or distilled water were used as solvents. All solvents employed showed no absorption over the range 4500-6000 Å. The most concentrated solution in each set of measurements was prepared by direct weighing of the solute into a measured volume of solvent. These were then diluted to obtain the other concentrations. Little, if any, change in absorption was noted in cases where solutions were stored in the dark at room temperature even after several days.

III. Analysis of Data

In the case where aggregation is principally to the dimer we may write

$$a(\lambda, c_j) = a_m(\lambda)X + a_d(\lambda) \frac{(1-X)}{2} \quad (1)$$

where $a(\lambda, c_j)$ represents the effective solution extinction coefficient for a solution of total concentration c_j (based on the monomer molecular weight) at wavelength λ , $a_m(\lambda)$ and $a_d(\lambda)$ are the extinction coefficients

at this wavelength for the pure monomer and dimer, respectively, and X is the mole fraction of monomer. Equation 1 assumes that each component of the solution separately obeys Beer's law. The mass action expression for the dissociation equilibrium gives

$$K = \frac{2X^2c}{1-X} \quad (2)$$

In our analysis we guess various values for K and calculate the corresponding X for a concentration, c . Using these values, $a_m(\lambda)$ and $a_d(\lambda)$ are obtained from eq 1 using a linear least-squares fit. For the correct value of K , we would expect all of the values of $a(\lambda, c_j)$ measured experimentally to fall on the straight line defined by the conditions

$$\begin{aligned} a(\lambda, c_j) &= a_m(\lambda) \text{ when } X = 1 \\ a(\lambda, c_j) &= a_d(\lambda)/2 \text{ when } X = 0 \end{aligned} \quad (3)$$

The best value of K was picked on the basis of the goodness of fit to eq 3 as measured by a linear correlation coefficient. The presence of higher n -mers in solution would make it impossible to obtain a fit to these equations.

Only the dimer dissociation equilibrium has been considered in this treatment. In one of the cases studied, *viz.*, rhodamine B in water, the ionization of a carboxyl group could be significant. Since prior work¹⁸ had shown, however, that the dye spectra are pH independent, this process was not considered further in analyzing the data.

IV. Results

A. Aqueous Systems. 1. Rhodamine B. This system was first studied in 1924 by Holmes.¹⁹ From this study it was concluded that a dynamic equilibrium

- (5) F. P. Schafer, W. Schmidt, and J. Volze, *Appl. Phys. Lett.*, **9**, 306 (1966).
- (6) M. L. Spaeth and D. P. Bortfeld, *ibid.*, **9**, 179 (1966).
- (7) G. I. Farmer, B. G. Huth, L. M. Taylor, and M. R. Kagan, *ibid.*, **12**, 136 (1968).
- (8) T. F. Deutsch, M. Bass, P. Meyer, and S. Protopappa, *ibid.*, **11**, 379 (1967).
- (9) B. H. Soffer and B. B. McFarland, *ibid.*, **10**, 266 (1967).
- (10) B. B. Snavely, *Proc. IEEE*, **57**, 1374 (1969).
- (11) G. T. Schappert, K. W. Billman, and D. C. Burnham, *Appl. Phys. Lett.*, **13**, 124 (1968).
- (12) G. I. Farmer, B. G. Huth, L. M. Taylor, and M. R. Kagan, *Appl. Optics*, **8**, 363 (1969).
- (13) G. S. Levinson, W. T. Simpson, and W. Curtis, *J. Amer. Chem. Soc.*, **79**, 4314 (1957).
- (14) (a) K. K. Rohatgi and G. S. Singhal, *J. Phys. Chem.*, **70**, 1695 (1966); (b) K. K. Rohatgi and G. S. Singhal, *ibid.*, **67**, 2844 (1963).
- (15) E. S. Emerson, M. A. Conlin, A. E. Rosenoff, K. S. Norland, H. Rodriguez, D. Chin, and G. R. Bird, *J. Phys. Chem.*, **71**, 2396 (1967).
- (16) W. West and S. Pearce, *J. Phys. Chem.*, **69**, 1894 (1965).
- (17) K. Bergmann and C. T. O'Konski, *ibid.*, **67**, 2169 (1963).
- (18) (a) L. V. Levshin and V. K. Gorshkov, *Opt. Spectrosc.*, **10**, 401 (1960); (b) L. V. Levshin and V. G. Bocharov, *ibid.*, **10**, 330 (1960).
- (19) W. C. Holmes, *Ind. Eng. Chem.*, **16**, 35 (1924).

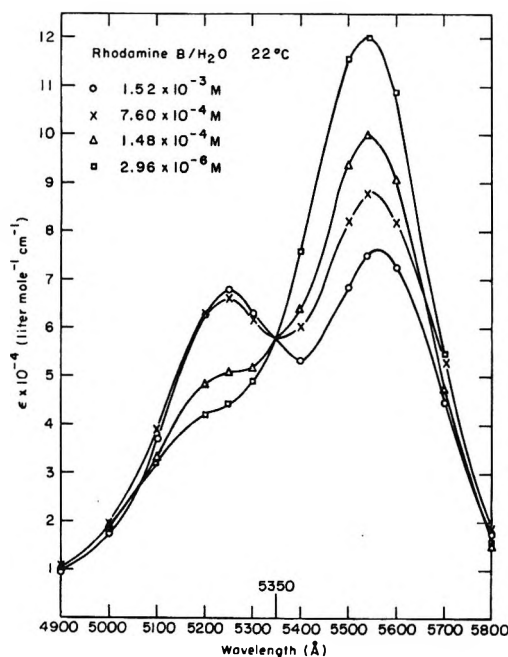


Figure 1. Absorption spectra of aqueous solutions of rhodamine B at 22°.

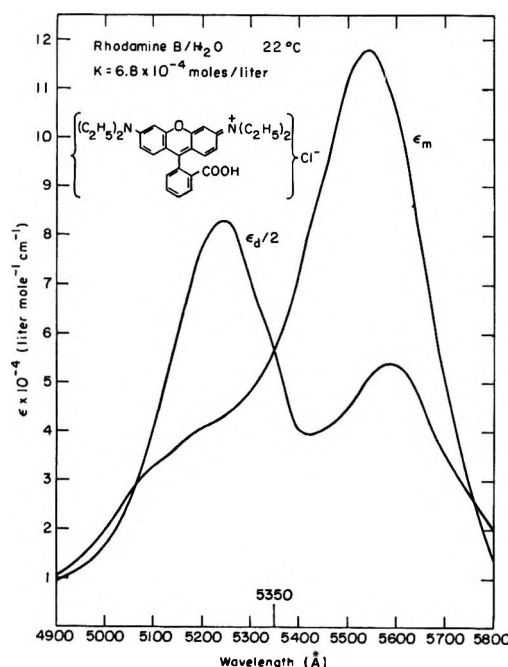
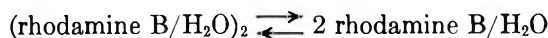


Figure 2. Resolved monomer and dimer extinction coefficients for aqueous rhodamine B.

between "constitutional forms" was responsible for the observed spectra. In the present work the concentration dependence of the absorbance of aqueous solutions was studied over the concentration range $1.52 \times 10^{-3} M$ to $4.93 \times 10^{-7} M$, at an ambient temperature of $22 \pm 1^\circ$. The observed spectra are presented in Figure 1. All spectra pass through an isobestic point at 5350 \AA . The resolved monomer and

dimer spectra are shown in Figure 2. We find an equilibrium constant for the process



of $6.8 \times 10^{-4} \text{ mol/l}$. From the equation

$$\Delta G^\circ = -RT \ln K \quad (4)$$

we obtain a free energy at 295°K of -4.2 kcal/mol for the dissociation. Rohatgi and Singhal¹⁴ report an equilibrium constant of $7.3 \times 10^{-4} \text{ mol/l}$. The closeness of these two figures may in fact be accidental in view of the questions that we raise regarding their data in the following discussion.

Since the data for this system give a good fit to eq 1, it is likely that we are dealing with a system containing only monomer and dimer, and that higher polymers have no appreciable concentration in this solution. This is in accord with the results of Levshin and Gorshkov¹⁸ in their studies of the bond energy of aqueous rhodamine B dimers (referred to as rhodamine C in the Russian literature). They find a relatively constant bond energy for the dimer of approximately 10 kcal/mol up to concentrations of $4 \times 10^{-3} M$. Our resolved monomer and dimer spectra are in substantial agreement with dilute concentration spectra and "absorption spectrum of the complexes" as presented by Levshin and Gorshkov. These authors obtain the dimer spectrum by a method that involves fitting the equilibrium constant at only a single wavelength. Our method of analysis is to be preferred as we fit the data over the entire absorption band and thereby have a larger statistical sample over which to average experimental deviations. Rohatgi and Singhal¹⁴ investigated rhodamine B-water using a glass slide sandwich as an absorption cell, so that they are unable to determine directly the path lengths of their samples. They determined the extinction coefficients of their solutions by a method of successive approximation to fit the ratio of absorption at the short and long wavelength maxima. A long extrapolation to a small intercept is involved in the process. As a result, it is not at all surprising that the dimer spectrum they obtained is markedly different from ours. The wavelength of the dimer maximum is different, as is the overall shape of the band. Their absorption spectrum for the monomer, the spectrum of a $10^{-6} M$ solution, has the same shape as ours. However, our extinction coefficients are about 20% higher. This may be a function of the fact that these authors are unable to measure the path length of their samples directly. At least part of the discrepancy (but not the entire magnitude of the difference) may be attributed to the fact that the measurements reported here were made at a temperature of approximately 22° whereas these authors worked at 30° . It is also known that dilute aqueous solutions of rhodamine B show hypochromic behavior upon heating.¹⁸

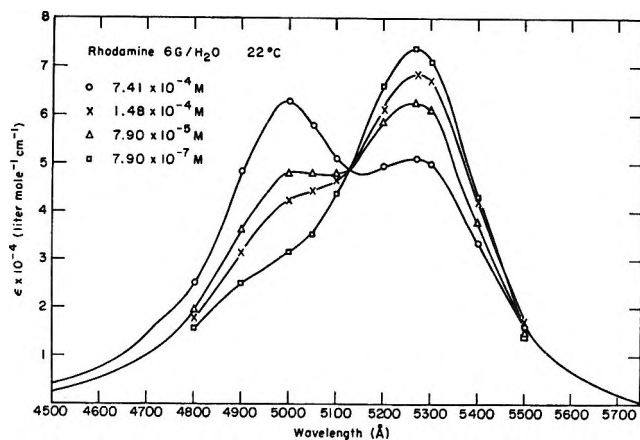


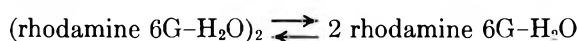
Figure 3. Absorption spectra of aqueous solutions of rhodamine 6G at 22°.

The thermodynamic data presented by Rohatgi and Singhal fail to take the hypochromic nature of the monomer into account. This invalidates their analysis of the functional dependence of the equilibrium constant on temperature for a $10^{-3} M$ solution. Thus, their values for ΔH and ΔS are probably unreliable.

2. *Rhodamine 6G-Water.* The rhodamine 6G-water system is of particular interest from the laser point of view as this solution has been used to produce the first continuous-wave dye laser.²⁰ In the production of this laser a detergent, Triton X, was added to the active medium to prevent dimerization. Our spectral studies show that 1.5% Triton X added to an aqueous solution effectively destroys dimers at concentrations typically used in dye lasers, approximately $10^{-5} M$.

We have studied the absorption of aqueous rhodamine 6G from extreme dilution, less than $10^{-6} M$, up to $7.41 \times 10^{-4} M$. Since the heat of dissociation for the dimer has been shown to be constant over this range,²¹ we may consider our solutions as binary monomer-dimer systems (no higher aggregates). Our observed spectra, shown in Figure 3, show a decrease in the low energy absorption and a new peak at high energy with increasing concentration. The solutions are isosbestic at 5130 Å. The observed spectra are in excellent agreement with those predicted based on the dimer mass action expression analysis.

For the system



we obtain an equilibrium constant of $5.9 \times 10^{-4} \text{ mol/l.}$ and $\Delta G^\circ = 4.3 \text{ kcal/mol.}$ From the work of Levshin and Baranova²² a similar value of $4 \times 10^{-4} \text{ mol/l.}$ can be computed. Again, these authors obtain this value from calculations carried out only at the wavelength of the monomer absorption maximum.

The best fit monomer and dimer spectra are presented in Figure 4. Rhodamine 6G, like rhodamine B, forms an aggregate that is blue shifted from the

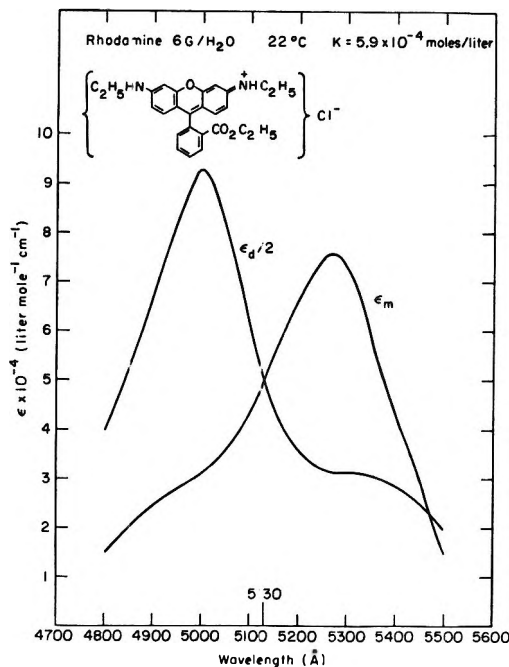


Figure 4. Resolved monomer and dimer extinction coefficients for aqueous rhodamine 6G.

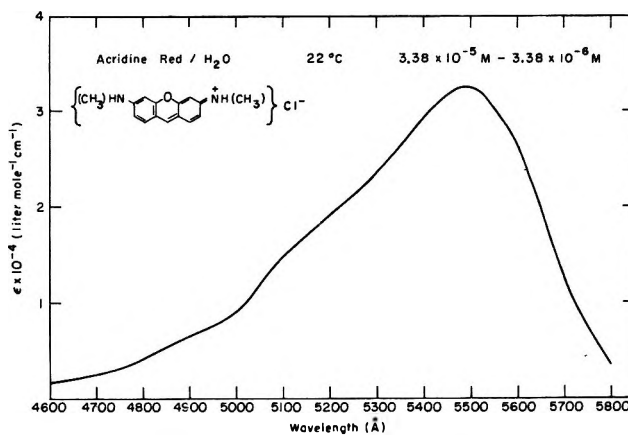


Figure 5. Absorption spectra of aqueous solutions of acridine red at 22°.

monomer peak. The low energy shoulder of the rhodamine 6G dimer is of low intensity and overlaps the high energy absorption.

3. *Acridine Red-Water.* Acridine red is very insoluble in water. Indeed, it is difficult to prepare a solution containing as little as 10 mg/l. As a result, only very dilute solutions were studied. Beer's law is obeyed by these solutions. The most concentrated solution studied was $3.38 \times 10^{-5} M$. The absorption spectrum of the acridine red monomer is shown in Figure 5 along with the molecular structure of the dye.

(20) O. G. Peterson, S. A. Tuccio, and B. B. Snavely, *Appl. Phys. Lett.*, **17**, 245 (1970).

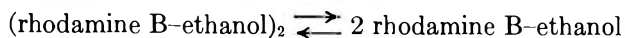
(21) E. G. Baranova and V. L. Levshin, *Opt. Spectrosc. (USSR)*, **10**, 182 (1960).

(22) V. L. Levshin and E. G. Baranova, *ibid.*, **6**, 31 (1959).

No other spectra for this system can be found in the literature.

B. Nonaqueous Systems. 1. Rhodamine B-Ethanol. Solutions of rhodamine B in ethanol were studied at 62, 22, and -78.5° . This material seems to be somewhat unusual in that dilute solutions aggregate in ethanol even at elevated temperature. As we shall see shortly, rhodamine 6G, which is structurally very similar to rhodamine B, remains monomeric in ethanol until high concentrations ($\sim 10^{-2} M$) are reached. Rhodamine 3B, the ester of rhodamine B, also fails to aggregate in dilute solutions.²² Usually, the addition of small amounts of ethanol to aggregated aqueous solutions causes considerable disaggregation. This has been shown to be the case for methylene blue, thionine²³ and cyanines.²⁴ The existence of dimers in alcoholic solutions at low temperature is documented by Stensby and Rosenberg in the case of the chlorophylls.²⁵ Dimers at room temperatures have been noted in other alcohols, principally bonadur red in methanol²⁶ and pinacyanol in glycerol.²⁷ Pyridocyanine aggregation, while not evident at room temperature in methanol, becomes obvious at $77^\circ K$ in isopropyl alcohol-isopentane mixtures.¹³ (It should be noted that the dyes are practically insoluble in hydrocarbons.) Cyanine, thiocarbocyanine, xanthenes (including rhodamine B), triphenylmethane, and acridine dyes in ethanol have been studied at $77^\circ K$ by Permogorov, Serdyukova, and Frank-Kamenetskii.²⁸ These authors attribute secondary maxima in the absorption to vibrational structure, and deny the existence of dimers in the solutions they study. Although they claim their spectra to be invariant to concentration changes, no indication is made about the range of concentrations over which spectra were recorded. They neglect the possibility that the solutions may, indeed, be composed solely of aggregates. These authors assume that the absorption spectra are temperature independent. This assumption, it should be pointed out, is contrary to the data graphically displayed in their paper. The spectra of pseudocyanine and pinacyanol clearly change shape and exhibit a large hyperchromic effect at low temperature. Therefore, we are forced to reject the analysis of these authors. Rather, we must view their solutions as being principally composed of dimers at $77^\circ K$. Thus, we regard our finding the existence of dimers in alcoholic solutions of rhodamine B as unusual, but certainly not unique.

A series of spectra isosbestic at 5440 \AA (Figure 6) were obtained from our study of solutions ranging from 6.64×10^{-4} to $6.64 \times 10^{-7} M$ at room temperature. We note that the main absorptions are at 5535 and 5440 \AA in dimer and monomer solutions, respectively. The equilibrium constant for the process



is found to be $4.9 \times 10^{-5} \text{ mol/l}$, with a ΔG° of 5.8 kcal/

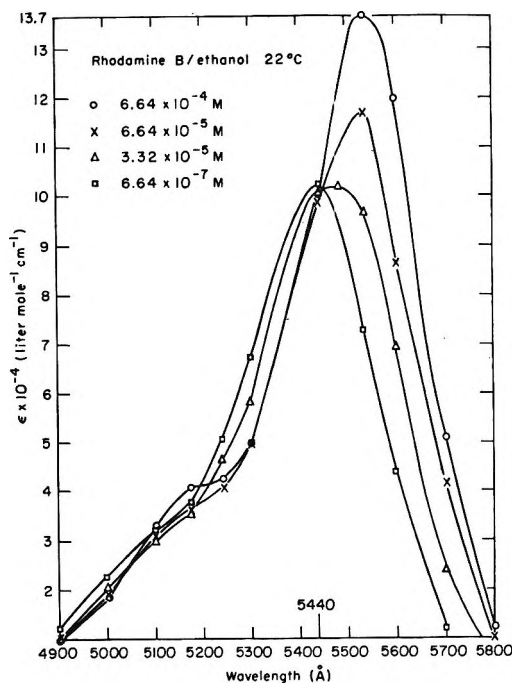


Figure 6. Absorption spectra of ethanolic solutions of rhodamine B at 22° .

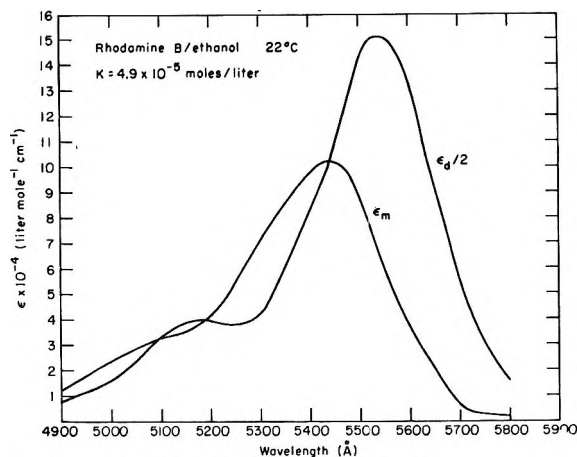


Figure 7. Resolved monomer and dimer extinction coefficients for ethanolic rhodamine B.

mol at $295^\circ K$. The best fit monomer and dimer spectra are presented in Figure 7.

A concentration correction to account for solvent volume expansion or compression must be applied to all solutions in order to calculate extinction coefficients

(23) E. Rabinowitch and L. F. Epstein, *J. Amer. Chem. Soc.*, **63**, 69 (1941).

(24) R. B. McKay and P. J. Hillson, *Trans. Faraday Soc.*, **63**, 777 (1967).

(25) P. S. Stensby and J. L. Rosenberg, *J. Phys. Chem.*, **65**, 906 (1961).

(26) A. R. Monahan and D. F. Blossey, *ibid.*, **74**, 4014 (1970).

(27) Kh. L. Arvan and N. E. Zaitseva, *Opt. Spectrosc.*, **10**, 137 (1961).

(28) V. I. Permogorov, L. A. Serdyukova, and M. D. Frank-Kamenetskii, *Opt. Spectrosc.*, **25**, 38 (1968).

at temperatures removed from that at which volumetric glassware is usually calibrated, *i.e.*, 20°. This correction amounts to a 5% volume expansion for ethanol between 0 and 50° and a 10% contraction at -78.5°. In the case of EPA solvent, substantial errors result if this factor is not considered. EPA shrinks to 88% of its room temperature volume at -78.5°K, and to 73% at 77°K. Although previous low temperature dye spectra have been reported, no account seems to have been taken of this volumetric effect. If this correction is not made, erroneous results regarding integrated intensity are obtained.

Measurements made at 62° were analyzed in a manner analogous to that used for the room temperature data. A look at the spectra (Figure 8) immediately reveals that the solutions are no longer isosbestic at 5440 Å. As a result, the decomposition of the spectra into monomer and dimer components shown in Figure 14 is not identical to that obtained at room temperature (Figure 7). Comparison of these figures reveals that although the dimer spectra are practically identical, the monomer shows a decrease in intensity at high temperature. The monomer spectrum is shown as a function of temperature in Figure 9. The factors that may result in such an intensity decrease will be discussed shortly.

At 62°, we obtain an equilibrium constant of 1.1×10^{-4} mol/l. and $\Delta G^\circ_{335} = 6.1$ kcal/mol for the dissociation process. Thus, as anticipated, our solution is enriched in dimer at lower temperatures. We may take advantage of our knowledge of the equilibrium constant at two temperatures to obtain approximate values for the other thermodynamic function of the dimerization process. If we assume ΔG to be linear between 22 and 62°, then we obtain $\Delta H \approx 4$ kcal/mol and $\Delta S_{315} \approx -6$ eu. It should be noted that this value of ΔH is substantially lower than that obtained by Levshin and Gorshkov^{18a} for aqueous solutions of rhodamine B. They attribute the large value of ΔH in this system to the hydrogen bonded nature of the dimer. The possibility of an O-H bridged dimer structure in which the water molecule participates has been proposed for the aqueous dimers.²⁹ Thus, it is consistent to expect that ΔH should be lower in ethanol than in water as ethanol does not form hydrogen bonds as readily as does water.

We see a new phenomenon developing when we cool our system to -78.5°. At this temperature, the shape of the spectra leads us to conclude that even our most dilute solutions contain a good deal of dimer. We were unable to fit our data to the binary equilibrium model. We attribute this to two factors. Firstly, we do not study solutions that are sufficiently dilute to contain mostly monomer. Secondly, at concentrations of 4.64×10^{-4} M and above we find that our spectra increase in intensity but show no marked change in shape. Two possible explanations exist for this hyperchromic shift at high concentration. It may be

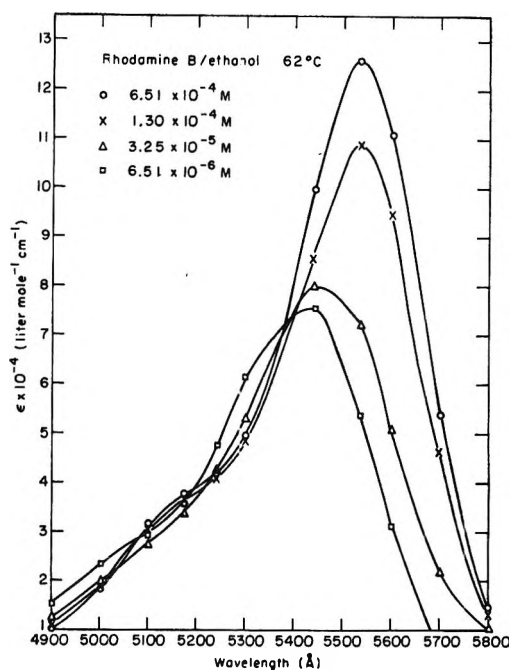


Figure 8. Absorption spectra of ethanolic solutions of rhodamine B at 62°.

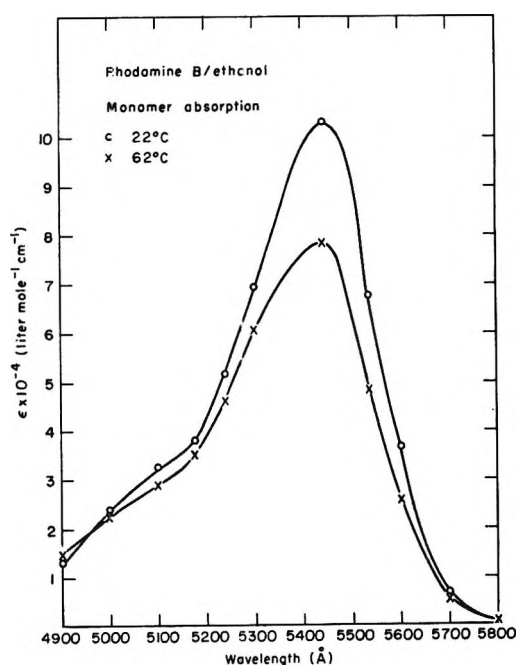


Figure 9. Comparison of the extinction coefficients of ethanolic rhodamine B at 22 and 62°.

due to a change in the actual oscillator strength of the dimer transition, or, alternatively it may be evidence for the presence of higher aggregates.

In 1928, Speas³⁰ presented a brief qualitative treatment of ethanolic rhodamine B, including spectra for a

(29) S. E. Sheppard and A. L. Geddes, *J. Amer. Chem. Soc.*, **66**, 2003 (1944).

(30) W. E. Speas, *Phys. Rev.*, **31**, 569 (1928).

dilute and a concentrated solution at room temperature. The shape of these curves and the position of the maximum is in excellent agreement with ours. He noted the changes in dilute solutions at low temperatures, as well as the hyperchromic shift that occurs when concentrated solutions are cooled.

No satisfactory explanation is available for the observed temperature dependence of the monomer absorption. Perhaps the intensity shifts in the monomer are a result of intensity borrowing from other absorption bands.

2. *Rhodamine 6G-Ethanol*. Frequent application has been made of flashlamp-excited ethanolic rhodamine 6G lasers. Our concern was, therefore, centered on the range of concentrations used in these lasers, 10^{-4} to 10^{-5} M. Both the temperature and concentration dependence of the absorption spectrum was observed. Measurements were made at 50, 22, 0, and -78.5° on solutions with room temperature concentrations from 1.65×10^{-4} M down to 3.31×10^{-7} M. The results of our study are presented in Figure 10. At room temperature, we found that the absorbance was independent of concentration, *i.e.*, Beer's law is followed. The addition of detergent to the most concentrated solution did not affect the absorption. Therefore, we conclude that our spectrum corresponds to the monomeric rhodamine 6G. The monomer spectrum is very similar to the one for rhodamine 6G in water at high dilution. A red shift of 40 Å is noted in ethanol compared to water.

At temperatures other than 22° , a volume correction was again applied to the solvent to obtain the true concentration dependent absorption of the solutions. Again, we find that the extinction is independent of concentration, but increases in intensity at low temperature. We find a steady increase in ϵ at λ_{\max} 5310 Å as the temperature is lowered. A slight narrowing of the main absorption feature is noted at -78.5° .

Baranova's study³¹ of this system at low concentrations agrees with our data. In his study of 2×10^{-6} M (monomer) solutions, he also finds that the long wavelength maximum decreases in intensity with increasing temperature between 20 and 69° . Spectral alterations are noted when very high concentrations are reached. At 2×10^{-2} M, the integrated spectral intensity is much smaller than in the monomer. The shape of the absorption curve is slightly altered and the temperature effect, although small, is in the opposite direction from that seen in dilute solutions. Increasing the concentration still more causes a larger decrease in absorption, further alteration in shape, and a large temperature effect. At very high concentrations the high energy secondary peak becomes somewhat better defined. Baranova interprets these facts as indicative of a system containing large aggregates. The dimer stage is quickly passed through in favor of high polymers. In addition, the polymers have lower absorption intensity

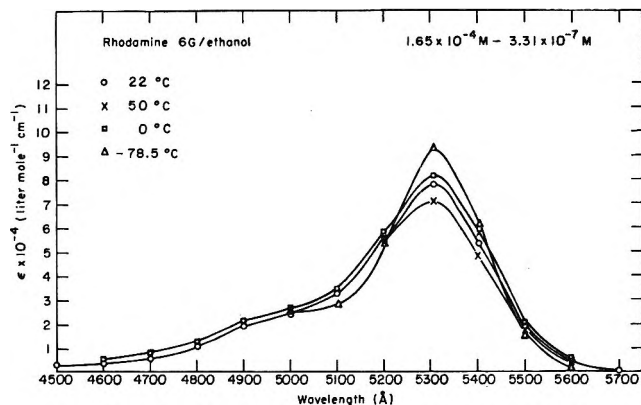


Figure 10. Temperature dependence of the concentration-independent extinction coefficient of ethanolic rhodamine 6G.

than the monomers. It appears as though the oscillator strength of the aggregates decreases as the number of units composing the polymer increases.

We predict that the rhodamine 6G dimers are fluorescent. Preliminary studies in our laboratory on the gain characteristics of a rhodamine 6G-ethanol dye laser are in accord with this conclusion, since the output power of the dye laser is increased at low temperatures. This phenomenon has previously been reported for DTTC-ethanol lasers.¹¹ We believe that the analysis proposed by Schappert to explain his observations on this system is inadequate, however, since it does not take into account the changes in absorption and fluorescence known to take place in cyanine dyes in alcoholic as well as aqueous solvents at low temperature.

3. *Acridine Red-Ethanol*. Like many other dyes, acridine red aggregates to a very small degree in ethanol. Our observations at 22° over the concentration range 1.07×10^{-4} to 5.35×10^{-6} M are presented in Figure 11. All the solutions studied are primarily monomer and the peak extinction increases only very slightly with increasing concentration. The red shift noted with increasing concentration is an indication of the presence of some dimer admixture. As we shall see later, the dimer absorption of this dye in EPA solution is also shifted to lower energy than the monomer absorption. Indeed, the monomer peak is at approximately the same wavelength (5380 Å) in these two systems. It should be noted that the monomer peak is shifted to higher wavelength by approximately 100 Å in water as compared to these two nonaqueous solvents. A comparison of the absorption spectra for ethanolic solutions of acridine red, all approximately 10^{-4} M, at various temperatures (Figure 12) again shows an increase in intensity at lower temperatures. This may be attributable to dimer admixture.

In ethanol, acridine red aggregates to a lesser extent than does rhodamine B. Qualitatively similar changes

(31) E. G. Baranova, *Opt. Spectrosc.*, **13**, 452 (1962).

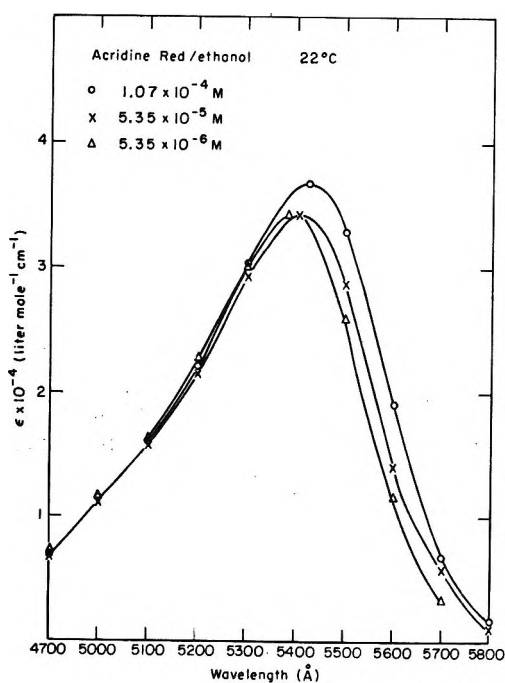


Figure 11. Absorption spectra of ethanolic solutions of acridine red at 22°.

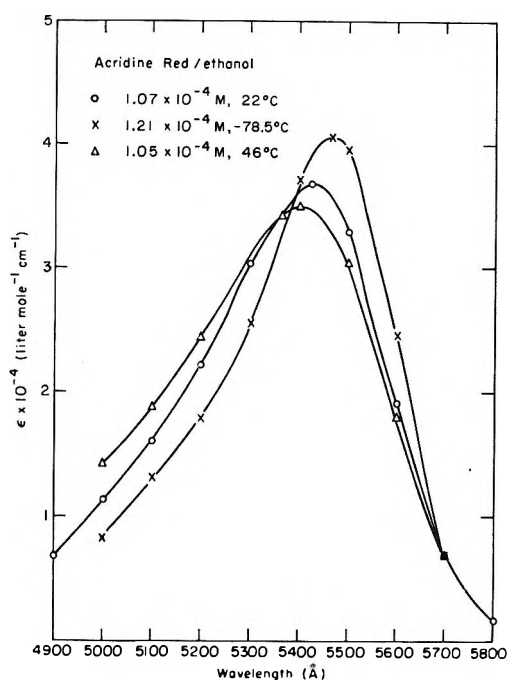


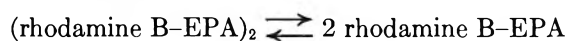
Figure 12. Temperature dependence of the extinction coefficient of ethanolic acridine red, which is nearly concentration independent.

are observed as the temperature and concentration are varied in these systems. Rhodamine 6G shows the least tendency of three dyes to aggregate in ethanol. The ethanolic aggregates are all shifted to shorter wavelength and have different intensity than the monomers.

4. *Rhodamine B-EPA*. We chose to study the

spectra of dyes in EPA because this solvent forms a clear glass at 77°K. Other solvents have been used previously for spectral analysis in the visible region at this temperature.¹³ Unfortunately, spectra obtained in solvents that solidify above liquid nitrogen temperature may not be truly representative of the ambient temperature of the sample. Indeed, it has been found that dye spectra recorded in alcohol were independent of temperature below 77°K, and probably also somewhat above this temperature.²⁸ Our previous work on the spectra of dyes in plastic matrices illustrates that spectra undergo little or no alteration with temperature once the dye solvent solidifies.³² The use of EPA eliminates this configurational freezing at temperatures above 77°K. Unfortunately, EPA is not a very good solvent for most ionic organic dyes.

At room temperature, we note a very strong concentration dependence of the rhodamine B-EPA (Figure 13) absorption spectrum even at very low concentrations, with no isosbestic point. Applying our binary equilibrium model, we find that we can fit the data reasonably well with the monomer and dimer spectra presented in Figure 14. The best fit equilibrium constant for the process



is 6.2×10^{-5} mol/l. Thus, $\Delta G_{295}^{\circ} = 5.7$ kcal/mol.

It should be pointed out that this value for the equilibrium constant is larger than the value obtained at room temperature in ethanol. Rhodamine B aggregates to a greater extent in alcohol than in the mixed solvent. This may be due to increased solubility of the dimer in alcohol due to delocalization of ionic charge. The resolved spectra have approximately the same shape in these two solvents, although the secondary maximum of the dimer is not well resolved in EPA.

The absorption in dilute solutions increases dramatically when the system is cooled to -78.5° . Comparison of Figures 13 and 15 illustrates this point very well. Indeed, the extinction maximum for a 3.51×10^{-5} M solution EPA at 22° is less than one third that of a 2.49×10^{-6} M solution at -78.5° . This change is a result of two factors that become obvious when the monomer and dimer components are resolved (Figure 16). First, the equilibrium constant, $K_{194.5} = 3.1 \times 10^{-5}$ mol/l., is smaller than at room temperature. The free energy change for dissociation of the dimer is 4 kcal/mol at this temperature. Thus, the dimer concentration in a given solution is enhanced at lower temperature. Secondly, the monomer shows a large hyperchromic shift at low temperature, analogous to our observations on this dye in alcohol. It is interesting to note that at -78.5° in EPA the rhodamine B monomer still absorbs slightly less strongly than it does at 62° in alcohol.

(32) F. M. Giroud, M.S. Thesis, M.I.T., Sept 1969.

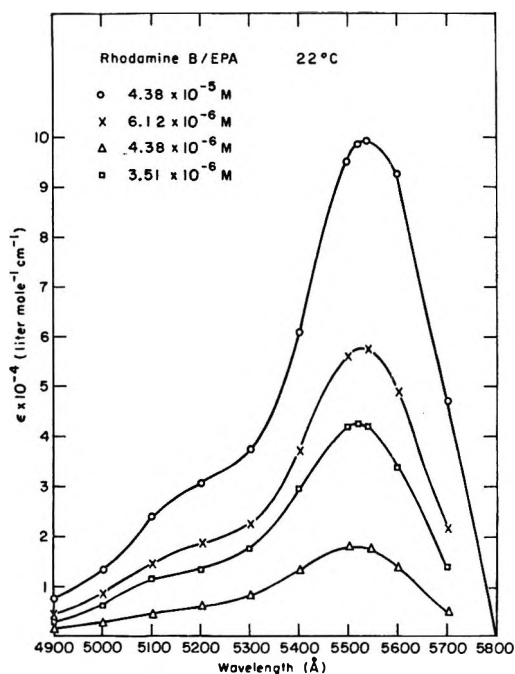


Figure 13. Absorption spectra of EPA solutions of rhodamine B at 22°.

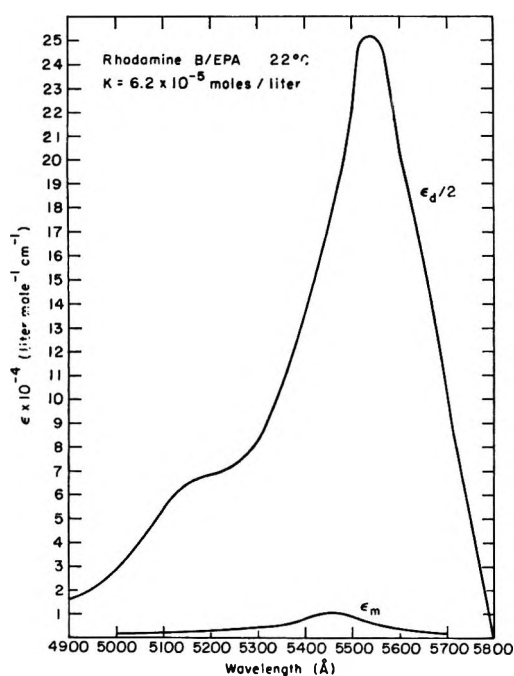


Figure 14. Resolved monomer and dimer extinction coefficients for EPA solutions of rhodamine B at 22°.

Using the equilibrium constants at 22 and -78.5° , we may obtain some information about the heat of formation of the dimer. Assuming that ΔG is linear between these two temperatures, we find that the dissociation reaction is endothermic by 0.8 kcal/mol and $\Delta S_{245} \approx -1.6$ eu. This value of ΔH should be contrasted with the value of 4 kcal/mol obtained for this dye in ethanol. This diminution of the heat of dimeri-

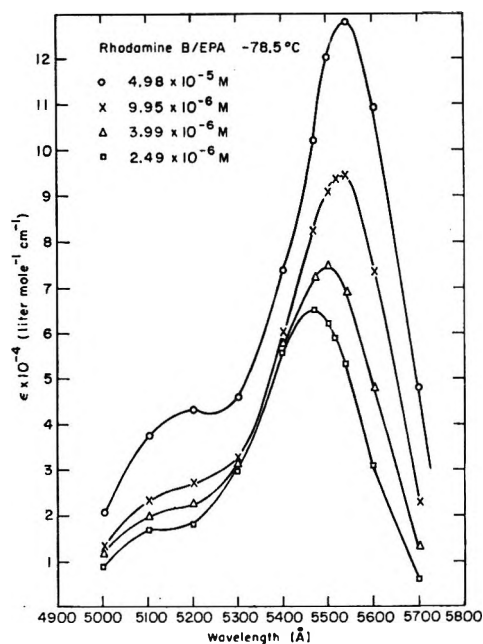


Figure 15. Absorption spectra of EPA solution of rhodamine B at -78.5° .

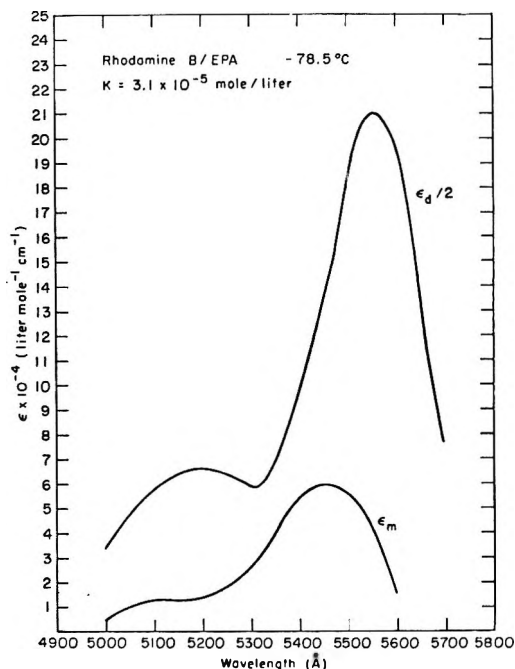


Figure 16. Resolved monomer and dimer extinction coefficients for EPA solutions of rhodamine B at -78.5° .

zation gives added weight to the theory that hydrogen bonding is important in stabilizing organic dye dimers. The bond energy obtained in EPA is of the order anticipated for a dispersion force interaction.

Studies at liquid nitrogen temperature, 77°K , reveal that the absorption of rhodamine B-EPA solutions is concentration independent over the range of concentrations 6.15×10^{-5} to 4.64×10^{-6} M (Figure 17). These concentrations have, of course, been corrected

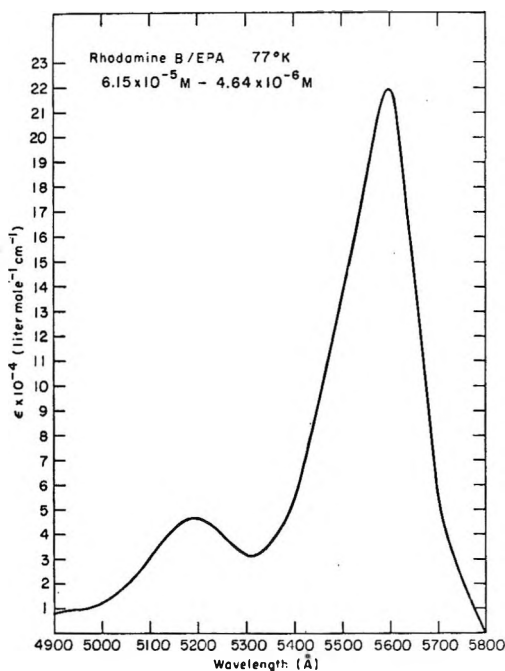


Figure 17. Concentration-independent dimer spectrum of EPA solutions of rhodamine B at 77°K.

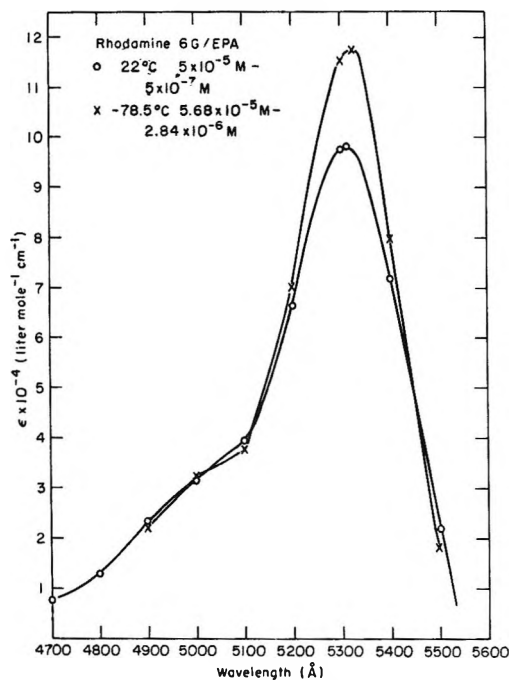


Figure 18. Concentration-independent absorption spectra of EPA solutions of rhodamine 6G at 22 and -78.5° .

for volume contraction. The spectra characteristic of these solutions strongly resemble the computer generated dimer spectrum at higher temperatures.

5. *Rhodamine 6G-EPA*. The absorption behavior of dilute solutions of rhodamine 6G in EPA at temperatures down to 77°K is adequately described by Beer's law. Since the shape of the absorption is analogous to that observed in dilute aqueous and

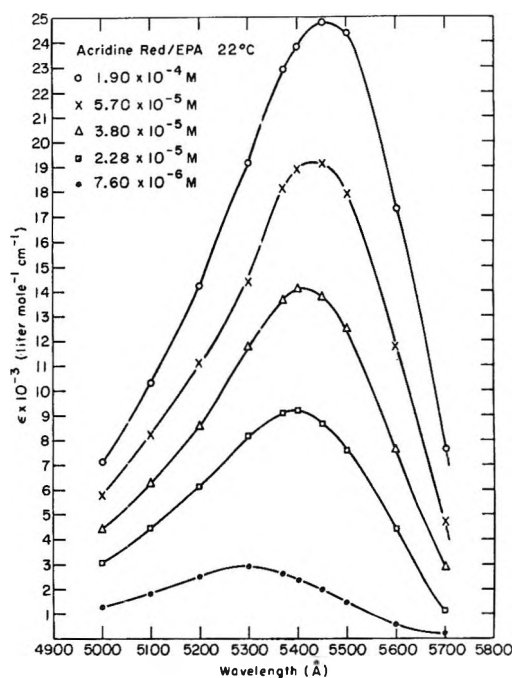


Figure 19. Absorption spectra of EPA solutions of acridine red at 22°.

ethanolic solutions, it is undoubtedly attributable to the monomeric species in solution. The spectra are presented for 22 and -78.5° in Figure 18. A marked hyperchromic shift in intensity, similar to that observed for this dye in ethanol, is seen. The width at half-height decreases with temperature for this series of spectra. The absorption at each temperature is somewhat stronger in EPA than in ethanol.

Arvan and Zaitseva²⁷ have considered the effect of solvent dielectric constant on the extent of aggregation at room temperature. Aggregation is shown to be much less in formamide than in water, although the former has a larger dielectric constant. Mixtures of water-glycerol and water-acetone with the same dielectric constant display different degrees of aggregation. As a result, the authors conclude that the chemical nature of the solvent has a much larger effect on aggregation than does the dielectric constant. They believe that the hydroxyl group present in water and alcohols, but absent in the other solvents that they studied, may play a prominent role in aggregation.

6. *Acridine Red-EPA*. As in the case of rhodamine B, acridine red absorption shows a strong concentration dependence in EPA at room temperature. As Figure 19 illustrates, the spectra show a marked change in intensity, but little alteration in shape, as the solution concentration is varied. A binary monomer-dimer model cannot be constructed which adequately predicts the observed absorption of the solutions over the concentration range studied. We attribute this to the fact that all of these solutions are largely composed of monomers with only a very small dimer concentration. Since, as we shall see shortly, the dimer absorbs much

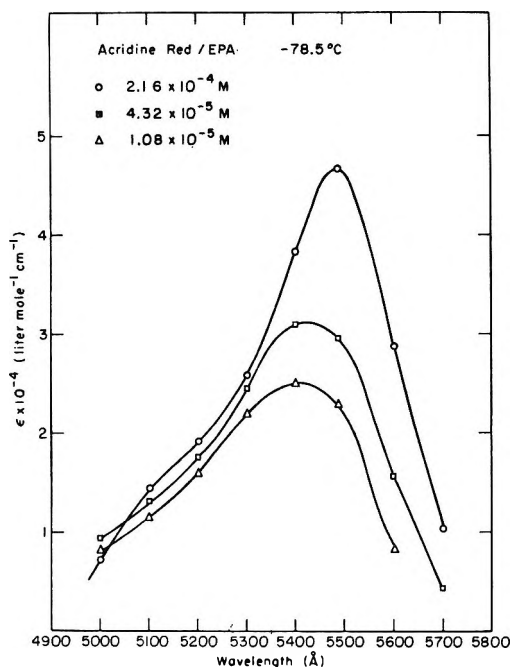
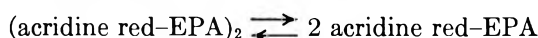


Figure 20. Absorption spectra of EPA solutions of acridine red at -78.5° .

more strongly than the monomer does, small amounts of dimer cause large spectral alterations. Also, it appears as though the monomer itself has a concentration (and temperature) dependent absorption. The intensity of the monomer absorption appears to be directly proportional to the solution concentration at low concentrations.

Acridine red-EPA shows a marked increase in absorption intensity when solutions are cooled to -78.5° . Spectra obtained at this temperature are presented in Figure 20. Comparison of these spectra illustrates that dilute solutions show the largest concentration effects. The spectral shape is concentration dependent, although no isosbestic point is noted. The monomer-dimer spectra presented in Figure 21 correspond to a best fit equilibrium constant of 4.4×10^{-4} mol/l. Thus for the process



$$\Delta G^{\circ}_{194.5} = 3 \text{ kcal/mol.}$$

Figure 22 gives the results of our observations on this system at 77°K . Unlike the other dyes that we have studied, acridine red shows a concentration-dependent absorption spectrum even at 77°K .

V. Discussion

A strong coupling molecular exciton model has been used to interpret the energy level splitting observed under conditions favoring dye aggregation.^{13,33,34} In this analysis the ground state energies and wave functions are considered as identical with those characteristic of the monomer. The first excited singlet, which corresponds to the main absorption feature of the dye

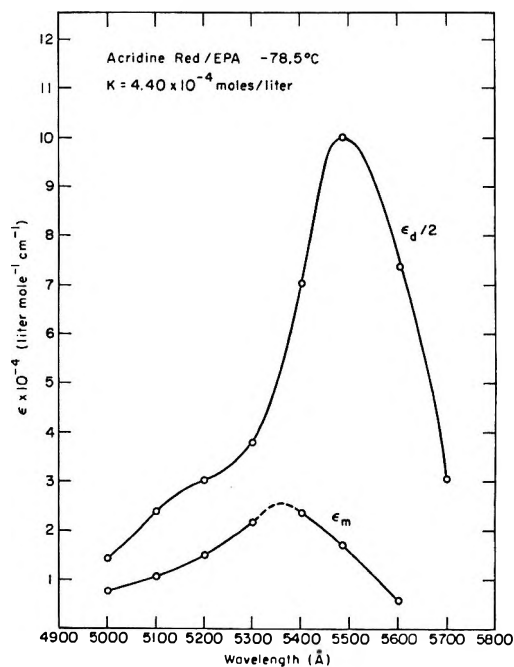


Figure 21. Resolved monomer and dimer extinction coefficients of EPA solutions of acridine red at -78.5° .

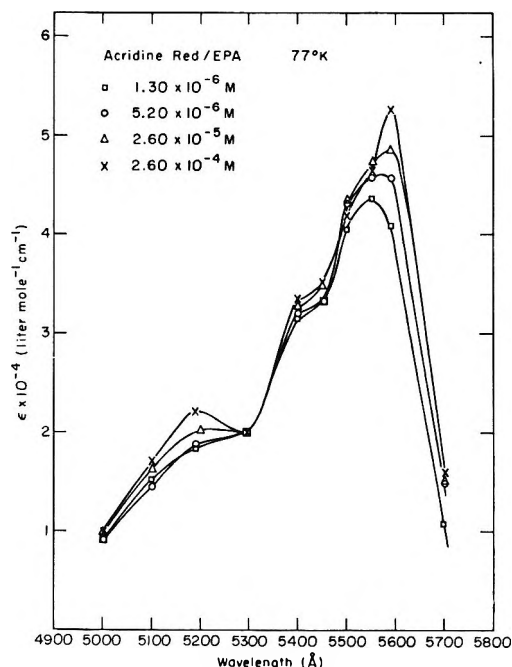


Figure 22. Absorption spectra of EPA solutions of acridine red at 77°K .

spectrum, is split N -fold when N molecules aggregate. Naturally, the energies and symmetries of the molecules in the aggregate depend on the geometrical arrangement of the molecules.^{13,34,35}

(33) I. Tinoco, Jr., *J. Chem. Phys.*, **33**, 1332 (1960); **34**, 1067 (1961).

(34) M. Kasha, M. A. El-Bayouti, and W. Rhodes, *J. Chem. Phys.*, **58**, 916 (1961).

(35) E. G. McRae and M. Kasha, *ibid.*, **28**, 721 (1958).

Table I: Dissociation Equilibria for Xanthene Dyes

Dye-solvent maximum concn	Temp. °C				Thermodynamic data
	46-62	22	-78.5	-196 (77°K)	
Rhodamine B-H ₂ O 1.52 × 10 ⁻³ M		$K = (6.8 \pm 0.5) \times 10^{-4} M$			
Rhodamine 6G-H ₂ O 7.41 × 10 ⁻⁴ M		$K = (5.9 \pm 0.4) \times 10^{-4} M$			
Acridine Red-H ₂ O 3.38 × 10 ⁻⁵ M		Monomer			
Rhodamine B-ethanol 6.64 × 10 ⁻⁴ M	$K = (1.1 \pm 0.3) \times 10^{-4} M$	$K = (4.9 \pm 0.2) \times 10^{-6} M$	Monomer, dimer, N-mer ($c > 10^{-4} M$)		$\Delta H \approx 4$ kcal/mol $\Delta S_{215} \approx -6$ eu
Rhodamine 6G-ethanol 1.65 × 10 ⁻⁴ M	Monomer	Monomer	Monomer		
Acridine Red-ethanol 1.07 × 10 ⁻⁴ M	Mainly monomer	Mainly monomer	Mainly monomer		
Rhodamine B-EPA 4.38 × 10 ⁻⁵ M		$K = (6.2 \pm 0.1) \times 10^{-5} M$	$K = (3.1 \pm 0.3) \times 10^{-5} M$	All dimer	$\Delta H \approx 0.8$ kcal/mol $\Delta S_{254} \approx -1.6$ eu
Rhodamine 6G-EPA 5.0 × 10 ⁻⁵ M		Monomer	Monomer	Monomer	
Acridine Red-EPA 1.90 × 10 ⁻⁴ M		Mainly monomer	$K = (4.4 \pm 0.1) \times 10^{-4} M$	Monomer, dimer, N-mer	

Dimer spectra are characterized as "H band" or "J band" according to whether the absorption is predominately to the upper or lower energy level of the exciton-split state. The existence of two types of dimer presents interesting consequences relevant to the dye laser. Consider the decay of the twofold upper singlet level of the dimer. The observed concentration dependence of the dye fluorescence can be qualitatively explained with the aid of the exciton model.³⁵ Aggregation creates a broad band of excited singlet levels; the band width is proportional to the dipole strength of the $S_1 \leftarrow S_0$ transition of the monomer. This band is much wider than the triplet bands as a result of the fact that the $T \leftarrow S$ transition is not spin-allowed. In the dimer, intersystem crossing may compete more successfully with fluorescence because of this broadening. Spreading of the excited singlet effectively increases the rate of intersystem crossing although the "intrinsic rate" need not be changed. Since the singlet splitting in the dye aggregate is comparable in magnitude to the singlet-triplet splitting in the monomer, intersystem crossing is greatly enhanced. This buildup of triplet state molecules leads to an increase in phosphorescent intensity in the dimer. This additional phosphorescence is at the expense of fluorescence. An increase in the concentration of triplet state molecules is detrimental to laser action not only because it depletes the population of the upper laser level, but also as a result of the possibility of laser quenching arising from $T \leftarrow T$ absorption. The $T \leftarrow T$ transitions overlap the fluorescence spectrum.

Most important, it should be observed that an "H" aggregate will not be fluorescent. This is a result of the fact that only the higher member of the excited

singlet band is populated in absorption. These molecules then relax nonradiatively to the lower level. However, the fluorescent transition to the ground state from the "J" level is not allowed. Most of the dye dimers that have been observed in aqueous solution have been of the nonfluorescent "H" class. We have noted the formation of "J" dimers in alcoholic and EPA solutions. These fluorescent dimer solutions may, indeed, be suitable for use as lasers.

Hypochromic shifts in dye solutions have frequently been described under conditions favoring aggregation. These shifts, which represent a decrease in integrated absorption intensity, have been observed in aggregates involving numerous dyes in aqueous solutions.^{14-16,26} In the present work we find large increases in intensity (hyperchromic shifts) upon dimer formation in nonaqueous systems. This fact makes an increase in fluorescence yield over the corresponding monomer not unlikely. For this reason, the formation of "J type" dimers may enhance the laser potential of these solutions. A theory involving the alignment of nonresonant moments, often applied to polynucleotides, is helpful in explaining the intensity changes accompanying aggregation.^{34,36,37}

A summary of our findings is presented in Table I. The absorption spectra of acridine red, rhodamine B and rhodamine 6G in aqueous and nonaqueous solutions has been shown to be both concentration and temperature dependent. The rhodamines form nonfluorescent dimers in aqueous solution. Very dilute solutions of acridine red are monomeric. In ethanolic solution,

(36) I. Tinoco, Jr., *J. Amer. Chem. Soc.*, **82**, 4785 (1960); **83**, 5047 (1961).

(37) H. DeVoe, *J. Chem. Phys.*, **37**, 1534 (1962).

only rhodamine B shows appreciable dimer concentration even at -78.5° . Evidence for aggregate formation in EPA solutions of rhodamine B and acridine red is presented. The dimers that are formed in nonaqueous solvents are expected to show appreciable fluorescence. Neglecting triplet losses, we expect these dimers to lase. Dilute (monomeric) nonaqueous dye solutions exhibit temperature (and possibly concentration) dependent absorption spectra which cannot be adequately explained by current theory.

Some comment as to the width of the observed absorption bands may be in order. Our previous investigation³² of these dyes in polymethylmethacrylate matrices down to 12°K showed very little narrowing of the absorption bands. However, spectra of fluid solutions show considerable narrowing as the temperature is lowered [see especially Figures 10, 12; 13, 15, and 16; and

19, 20, and 22]. These results reflect the fact that the molecules are frozen into various orientations as the plastic matrix hardens at room temperature. This continuum of orientations gives rise to the unresolved broad bands observed. Indeed, previous researchers have reached similar conclusions regarding the spectra of solid cyanine dye solutions at temperatures below that at which the solvent solidifies.¹³ Thus, at least a part of the broadening is inhomogeneous, reflecting the different solvent sites in which the dye molecule finds itself, rather than intrinsic vibrational structure of the molecule itself.

Acknowledgments. This research was supported by the U. S. Army Research Office under Contract DA-HCO4-70-C-0015, and by the Petroleum Research Fund of the American Chemical Society.

The Association of Formic Acid in Carbon Tetrachloride Solution

by Claybourne C. Snead

Department of Chemistry, Gallaudet College, Washington, D. C. 20002 (Received September 9, 1971)

Publication costs borne completely by The Journal of Physical Chemistry

The association of formic acid in dilute solutions of anhydrous and wet carbon tetrachloride has been studied at 25° , using infrared intensity measurements and partition data, respectively. Studies were also made of the solubility of water in formic acid-carbon tetrachloride solutions. The data are consistent with a simple monomer-dimer equilibrium occurring in both the anhydrous and moist carbon tetrachloride, there being no indication of hydration of the formic acid in the moist solvent. The average value of the equilibrium constant was found to be $1.44 (\pm 0.14) \times 10^3 \text{ l./mol.}$

Of the variety of experimental methods used for studying hydrogen bonding equilibria, infrared intensity measurements and partition techniques have been among the most common. There have been, however, considerable differences in the reported values of the association constants, as determined by the two methods.¹ In recent years, considerable experimental data²⁻⁸ have been obtained in partition experiments which have been interpreted in terms of hydration equilibria, as well as association equilibria, occurring in the moist organic layer. Neglect of these hydration equilibria in prior partition experiments has been proposed by these workers²⁻⁸ as the major reason for the discrepancies in the values of the association constants, as determined by the two methods.

It is the purpose of this work to test the hydration idea for a simple system (water-carboxylic acid-inert solvent). This work reports the results of

studies of formic acid in carbon tetrachloride solution using infrared intensity measurements, and partition data for formic acid between carbon tetrachloride and water. Formic acid was chosen as it has been little

(1) G. C. Pimentel and A. C. McClellan, "The Hydrogen Bond," W. H. Freeman, San Francisco, Calif., 1960.

(2) R. M. Badger and R. C. Greenough, *J. Phys. Chem.*, **65**, 2088 (1961).

(3) S. D. Christian, H. E. Affsprung, and S. A. Taylor, *J. Phys. Chem.*, **67**, 187 (1963).

(4) T. F. Lin, S. D. Christian, and H. E. Affsprung, *J. Phys. Chem.*, **69**, 2980 (1965).

(5) G. O. Wood, D. D. Mueller, S. D. Christian, and H. E. Affsprung, *J. Phys. Chem.*, **70**, 2691 (1966).

(6) Roger van Dyne, S. A. Taylor, S. D. Christian, and H. E. Affsprung, *J. Phys. Chem.*, **71**, 3427 (1967).

(7) J. R. Johnson, P. J. Kilpatrick, S. D. Christian, and H. E. Affsprung, *J. Phys. Chem.*, **72**, 3223 (1968).

(8) S. D. Christian, A. A. Taha, and B. W. Gash, *Quart. Rev.*, **24**, 20 (1970).

studied in solution⁹⁻¹¹ although it has been studied rather extensively in the pure liquid and vapor states.¹²⁻¹⁷ Carbon tetrachloride was chosen as the solvent as it is a nonhydrogen-bonding solvent.

Experimental Section

In the infrared absorption measurements, the intensity of the absorption maximum of the O-H stretching vibration of the formic acid monomer was measured in a series of solutions of formic acid in CCl₄. The measurements were made on a Perkin-Elmer 221 Double Beam recording infrared spectrophotometer; 1.00-cm cells were used. The concentration of the formic acid in the solutions ranged from about 0.002 to 0.02 *F*.

In the partition experiments, the formic acid-CCl₄-water systems were equilibrated in a constant temperature bath at 25°. The aqueous layers were titrated with standard sodium hydroxide solution. The CCl₄ layers were titrated with very dilute sodium hydroxide (approximately 0.01 *F*).

The formic acid used was Eastman 97+ % grade that was purified as described in Weissberger.¹⁸ It was stored over anhydrous copper sulfate for several days and distilled over anhydrous CuSO₄ in an all glass apparatus under reduced pressure at a temperature of 26-28°.

Eastman white label CCl₄ was dried over CaCl₂ and distilled prior to use. CCl₄ treated in this manner had negligible absorption at the maximum of the formic acid monomer frequency.

Treatment of Data

A. Infrared Intensity Measurements. The treatment is basically that of Harris and Hobbs,¹⁹ which they developed for their studies of the dimerization of carboxylic acids in CCl₄, with some changes in notation. The treatment assumes: (a) the equilibrium involves only a monomer and dimer, 2[M] ⇌ [D], with a dimerization constant

$$K = [D]/[M]^2 \quad (1)$$

(b) the Beer-Lambert law is valid for the monomer

$$A = \epsilon[M]l \quad (2)$$

and (c) the dimer does not absorb at the same frequency that the monomer does. Expressing the total concentration of the acid as monomer

$$C_o = [M] + 2[D] \quad (3)$$

and combining eq 1-3, the equation

$$A = \frac{\epsilon^2 l^2 (C_o)}{2K} \left(\frac{C_o}{A} \right) - \frac{\epsilon l}{2K} \quad (4)$$

is obtained. A plot of *A* vs. (*C*_o/*A*) should be linear with a slope of $\epsilon^2 l^2 / 2K$ and an intercept, $\epsilon l / 2K$. In these equations, [M] is the monomer concentration,

[D] is the dimer concentration, *A* is the absorbance at the monomer peak maximum, ϵ is the extinction coefficient at the maximum, *K* is the dimerization constant, and *l* is the cell-path length.

B. Partition Data. The distribution constant for the equilibrium of the acid monomer between the aqueous phase and the CCl₄ layer may be expressed as

$$K_d = \frac{[M]}{C_w(1 - \alpha - f)} \quad (5)$$

where *C*_w and [M] are the concentrations of the acid in the aqueous layer and organic (CCl₄) layer, respectively, *K*_d is the distribution constant, α is the fraction of acid dissociated in the aqueous layer, and *f* is the fraction of acid dimerized in the aqueous phase. Assuming that only a simple monomer-dimer equilibrium occurs in the CCl₄ phase and combining equations 1, 3, 5 in a manner similar to that of Moelwyn-Hughes,²⁰ the equation

$$\frac{C_o}{C_w(1 - \alpha - f)} = K_d + 2K_d^2 K C_w(1 - \alpha - f) \quad (6)$$

is obtained. A plot of $C_o / C_w(1 - \alpha - f)$ vs. $C_w(1 - \alpha - f)$ should be linear with a slope of $2K_d^2 K$ and intercept *K*_d, if this interpretation is valid. Equations 5 and 6 differ from the usual equations for treating partition data due to the presence of the additional term representing the dimerization of the monomer in the aqueous layer, *f*. Normally, it is not necessary to correct for dimerization in the aqueous layer, since in dilute solutions the amount of acid dimerized is very small. But, in concentrated solutions (on the order of several formal) the amount of acid that is dimerized is no longer negligible and such a correction is necessary. α may be calculated from the known value of the acid dissociation constant and *f* may be calculated from the value of the dimerization constant.

Results and Discussion

Infrared Absorption Measurements. The maximum

(9) H. A. Pohl, M. E. Hobbs, and P. M. Gross, *J. Chem. Phys.*, **9**, 408 (1941).

(10) A. A. Maryott, M. E. Hobbs, and P. M. Gross, *J. Amer. Chem. Soc.*, **71**, 1671 (1949).

(11) D. R. Cartwright and C. B. Monk, *J. Chem. Soc.*, 2500 (1955).

(12) A. S. Coolidge, *J. Amer. Chem. Soc.*, **50**, 2166 (1928).

(13) J. C. Halford, *J. Chem. Phys.*, **10**, 582 (1942).

(14) R. C. Herman, *J. Chem. Phys.*, **8**, 252 (1940).

(15) H. C. Ramsperger and C. W. Porter, *J. Amer. Chem. Soc.*, **48**, 1267 (1926).

(16) A. A. Shubin, *Izv. Akad. Nauk SSSR, Ser. Fiz.*, **14**, 442 (1950).

(17) M. D. Taylor and J. B. Upton, *J. Amer. Chem. Soc.*, **74**, 4151 (1952).

(18) A. Weissberger, E. S. Proskauer, J. A. Riddick, and E. S. Toops, Jr., Ed., "Techniques of Organic Chemistry," Vol. VII, (2nd edition), Interscience, New York, N. Y., 1955.

(19) J. T. Harris, Jr., and M. E. Hobbs, *J. Amer. Chem. Soc.*, **76**, 1419 (1954).

(20) E. A. Moelwyn-Hughes "Physical Chemistry," 2nd ed, Pergamon Press, Oxford, 1961, pp 1078-1082.

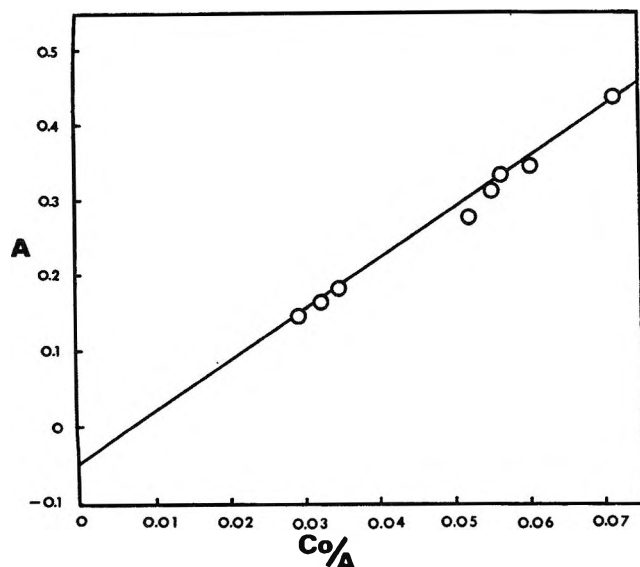


Figure 1. Infrared data: plot of A vs. C_o/A .

of the O-H stretching band of the monomer in CCl_4 solution was found to be near 3519 cm^{-1} . A plot of the data according to equation 4 is shown in Figure 1. The data may be represented by the equation

$$A = 6.67(C_o/A) - 0.0490$$

which was obtained by the least-squares procedure. The average deviation of the experimental points from the least squares line is 3.1%. From this equation, the value of the dimerization constant is $K = 1.39 (\pm 0.09) \times 10^3\text{ l./mol}$ and the extinction coefficient of the monomer is $136 (\pm 10)\text{ l./mol cm}$. The uncertainties are the estimated errors.

Partition Experiments. In the partition experiments, it became evident that the equilibrium for the distribution of formic acid between the water and CCl_4 phases was very unfavorable toward the CCl_4 layer (for an acid concentration of $7.38 F$ in the aqueous layer, the acid concentration in the CCl_4 layer was found to be only 0.01097). It was necessary, therefore, to use systems containing formic acid concentrations in the aqueous layer up to $7.38 F$. The minimum concentration of formic acid used in the aqueous layer was about $2 F$. The values of α were calculated using the value of $K_i = 1.77 \times 10^{-4}\text{ l./mol}$ for the dissociation constant²¹ and the values of f were calculated from the value of $K = 8.33 \times 10^{-3}\text{ l./mol}$ for dimerization in the aqueous layer.¹¹ Assuming that the interpretation of a monomer-dimer equilibrium is valid for the CCl_4 layer, the data are plotted in Figure 2. The least-squares equation for the data is $C_o/C_w(1 - \alpha - f) = 2.54 \times 10^{-4} + 1.91 \times 10^{-4}C_w(1 - \alpha - f)$. The average deviation of the experimental points from this line is 1.6%. From the slope and intercept, the values of the dimerization constant, $K = 1.48 (\pm 0.05) \times 10^3\text{ l./mol}$, and distribution constant, $K_d = 2.54 (\pm 0.04) \times$

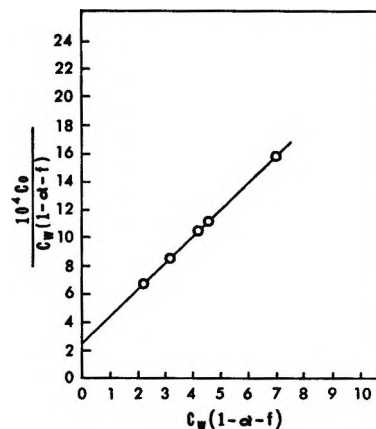


Figure 2. Partition data: plot of $C_o/C_w(1 - \alpha - f)$ vs. $C_w(1 - \alpha - f)$.

10^{-4} , along with their respective estimated errors, are obtained.

To determine if hydration of the formic acid was occurring in the CCl_4 layer, the effect of the formic acid upon the solubility of water in the CCl_4 layer was studied. This was done by equilibrating CCl_4 with aqueous formic acid solutions at 25° and determining the water concentrations in the CCl_4 layers by Karl Fischer titrations, using a Labindustries Aquameter. The Karl Fischer reagent was standardized against water saturated CCl_4 . The saturation solubility of water in CCl_4 is $0.00087 \pm 0.0003 F$ at 25° .²² In these experiments, the formic acid concentration ranged up to $10.34 F$ in the aqueous layer (corresponding to an acid concentration of $0.01764 F$ in the CCl_4 layer). No increase in water solubility was noted in these solutions. It would seem, therefore, that no detectable hydration of the formic acid in dilute, moist CCl_4 is occurring. Hence, the interpretation of a simple monomer-dimer equilibrium in the CCl_4 layer seems justified.

Combining the value of the equilibrium constant from the infrared data with that obtained from the partition method, therefore, gives the value, $K = 1.44 (\pm 0.14) \times 10^3\text{ l./mol}$ for the dimerization constant of formic acid in dilute CCl_4 solution at 25° .

Comparing these results with those of the workers who have presented evidence for hydration equilibria,²⁻⁸ there is no reason to question their results at present. Many of the systems they studied contain aromatic nuclei and since aromatic nuclei are known to participate in hydrogen bonding equilibria,¹ it is possible that the aromatic nucleus itself could be involved in hydration equilibria. Since there are no aromatic nuclei nor carbon-carbon unsaturated bonds

(21) "Handbook of Chemistry and Physics," 38th ed, Chemical Rubber Co., Cleveland, Ohio, 1956, p 1646.

(22) J. R. Johnson, S. D. Christian, and H. E. Affsprung, *J. Chem. Soc.*, 77 (1966).

in the system water-formic acid-carbon tetrachloride, this complicating factor would play no role.

Acknowledgments. The author wishes to thank the staff of the Department of Chemistry of the George

Washington University, especially Dr. Charles R. Naeser, Chairman, for permitting him to use the facilities for a portion of this work. He also wishes to thank Dr. Daniel Vomhof of the National Bureau of Standards for the use of their facilities.

The Effects of Pressure and Thermodynamic Nonideality on the Sedimentation Equilibrium of Chemically Reacting Systems: Results with Lysozyme at pH 6.7 and 8.0

by G. J. Howlett, P. D. Jeffrey, and L. W. Nichol*

Department of Physical Biochemistry, John Curtin School of Medical Research, Australian National University, Canberra, Australia (Received August 5, 1971)

Publication costs borne completely by The Journal of Physical Chemistry

Sedimentation equilibrium is considered of a polymerizing system comprising monomer in chemical equilibrium with a single higher polymer, where the activity coefficients of both species are functions of total concentration and the polymerization reaction is accompanied by a volume change. Equations are derived which describe the concentration distribution of each solute species and the relation between the actual weight-average molecular weight at a particular radial distance in the cell and the corresponding apparent value which is experimentally determinable. A method based on these equations for obtaining the nonideality coefficient, the volume change, and the equilibrium constant at 1 atm from sedimentation equilibrium experiments is illustrated with results obtained with lysozyme. Values found for these parameters at pH 6.7 in phosphate buffer agree with those reported by other workers, notably in that the volume change is essentially zero. It is found that a change of environment to pH 8.0 (diethylbarbiturate buffer) little affects the nonideality coefficient or equilibrium constant at 1 atm, but results in an *apparent* finite and negative volume change.

Introduction

In a previous communication¹ attention was given to the effects of pressure on the concentration distributions at sedimentation equilibrium of species involved in a chemical interaction (such as a protein polymerization), which was accompanied by a volume change. Equations were derived which allowed theoretical concentration distributions at sedimentation equilibrium to be calculated for the individual species. It was thereby shown for a model system consisting of monomer in equilibrium with its dimer that the experimental manifestation of a volume change accompanying the reaction could be nonsuperposition of weight-average molecular weight *vs.* concentration curves determined in experiments conducted at different angular velocities and/or with different initial concentrations. A method was suggested for analyzing experimental results of this kind to determine the magnitude of the volume change and the equilibrium constant at atmospheric pressure. However, in practice, application of the

method would be restricted to results obtained at low total concentrations, since the theory, on which it was based, assumed that the activity coefficient of each solute species was unity. On the other hand, the effects of thermodynamic nonideality in the sedimentation equilibrium of systems reacting chemically *without a volume change* have been examined in detail.²⁻⁷

The purpose of the present work is to extend the previous treatment¹ of the sedimentation equilibrium of interacting systems in which there is a volume change

(1) G. J. Howlett, P. D. Jeffrey, and L. W. Nichol, *J. Phys. Chem.*, **74**, 3607 (1970).

(2) E. T. Adams, Jr., and H. Fujita in "Ultracentrifugal Analysis in Theory and Experiment," J. W. Williams, Ed., Academic Press, New York, N. Y., 1963, p 119.

(3) E. T. Adams, Jr., and J. W. Williams, *J. Amer. Chem. Soc.*, **86**, 3454 (1964).

(4) E. T. Adams, Jr., *Biochemistry*, **4**, 1646 (1965).

(5) E. T. Adams, Jr., and D. L. Filmer, *ibid.*, **5**, 2971 (1966).

(6) E. T. Adams, Jr., *ibid.*, **6**, 1864 (1967).

(7) E. T. Adams, Jr., and M. S. Lewis, *ibid.*, **7**, 1044 (1968).

to include the effects of thermodynamic nonideality as well as those of pressure. The extension permits analysis of sedimentation equilibrium results obtained with lysozyme in aqueous environments where the protein exists as an equilibrium mixture of monomeric and dimeric species.^{5,8} The general utility of the approach is thereby illustrated with a real system.

Theory

Consider a solution containing monomer A in chemical equilibrium with a polymer C. It is assumed that the density of the solution, ρ , and the density increment for each solute species, $\partial\rho/\partial c_i$ (i denotes A or C) are not functions of pressure.⁹ It is convenient to replace the conventional $(1 - \bar{v}_i\rho)$ term with $\partial\rho/\partial c_i$ (c_i in g/ml) in what follows even though the substitution is strictly valid only in the limit $c_i \rightarrow 0$.¹⁰ It is also assumed that the activity coefficients, y_i , on the weight concentration scale are independent of pressure. Fujita¹¹ has pointed out that a necessary consequence of the latter assumption is that the partial specific volumes of both solute and solvent in an incompressible binary solution at constant temperature are independent of concentration. Fujita¹¹ also notes that concentrations on the weight-scale can only be taken as variables independent of pressure if the partial specific volumes of solute and solvent are independent of pressure. The present assumptions are consistent with these requirements. The molar volume of reaction ΔV is given by

$$\Delta V = \frac{mM_A(\partial\rho/\partial c_A) - M_C(\partial\rho/\partial c_C)}{\rho} \quad (1)$$

where M_A is the molecular weight of the monomer and $M_C = mM_A$. Equation 1 shows that ΔV is independent of pressure if the present assumptions are fulfilled and is zero only when the $\partial\rho/\partial c_i$ are identical.

At sedimentation equilibrium, the activity of each solute species, a_i , is related to the radial distance, r , by¹²

$$a_i(r_1) = a_i(r_2)e^{\phi_i M_i(r_1^2 - r_2^2)} \quad (2a)$$

$$\phi_i = \omega^2(\partial\rho/\partial c_i)/2RT \quad (2b)$$

where ω is the constant angular velocity, R the gas constant, T the absolute temperature, and r_1 and r_2 are any radial distances between or at r_m and r_b , the positions of the meniscus and base of the cell, respectively. Combination of eq 1 and 2 together with the definition of the equilibrium constant, $K(r) = a_C(r)/a_A^m(r)$, yields

$$K(r_1) = K(r_2)e^{-\{\Delta V\omega^2\rho(r_1^2 - r_2^2)\}/2RT} \quad (3)$$

Equation 3 is entirely consistent with that derived by integrating the expression $(\partial \ln K/\partial P)_T = -\Delta V/RT$ with the use of the equation describing the variation of pressure with radial distance, *viz.* $dP = r\omega^2\rho dr$. This observation serves to emphasize that the use of

eq 2a to describe the equilibrium distribution of each solute species individually is consistent with the requirement that chemical equilibrium must also be maintained throughout the cell. Previous treatments have established this point in situations where *either* nonideality¹ and/or pressure effects^{2,13} were ignored. The activity $a_i(r) = y_i(r)c_i(r)$, where $c_i(r)$ is the concentration in grams per unit volume at any position r and $y_i(r)$ is the corresponding activity coefficient on the same concentration scale. Thus, eq 2a may be rewritten as

$$c_i(r_1) = c_i(r_2)e^{\phi_i M_i(r_1^2 - r_2^2) + \ln \{y_i(r_2)/y_i(r_1)\}} \quad (4)$$

or in differential form as

$$\frac{dc_i(r)}{d(r^2)} = \frac{\phi_i M_i c_i(r)}{1 + \frac{d \ln y_i(r)}{d \ln c_i(r)}} \quad (5)$$

Following previous treatments,²⁻⁷ we express the activity coefficient as a function of the *total* solute concentration, $\bar{c}(r)$

$$y_i(r) = e^{BM_i\bar{c}(r)} \quad (6)$$

where B is a constant expressing nonideality: it is implicitly assumed in eq 6 that the expansion of $\ln y_i(r)$ as a power series in total concentration is truncated after the first term. As Adams⁴ has noted, an important consequence of this formulation is that

$$y_C(r)/y_A^m(r) = e^{BM_C\bar{c}(r)}/e^{mBM_A\bar{c}(r)} = 1 \quad (7)$$

and hence that the equilibrium constants evaluated from the concentrations of the reacting species are thermodynamic equilibrium constants. Substitution of eq 6 into eq 4 gives

$$c_i(r_1) = c_i(r_2)e^{\phi_i M_i(r_1^2 - r_2^2) + BM_i\{\bar{c}(r_2) - \bar{c}(r_1)\}} \quad (8)$$

which permits the formulation of the following simultaneous equations

$$\bar{c}(r_1) = c_A(r_1) + c_C(r_1) \quad (9a)$$

$$\bar{c}(r_2) = c_A(r_1)e^{\phi_A M_A(r_2^2 - r_1^2) - BM_A\{\bar{c}(r_2) - \bar{c}(r_1)\}} + c_C(r_1)e^{\phi_C M_C(r_2^2 - r_1^2) - BM_C\{\bar{c}(r_2) - \bar{c}(r_1)\}} \quad (9b)$$

Equation 9b is equivalent to that presented by Haschemeyer and Bowers,¹² who did not develop it explicitly in terms of reacting systems involving a vol-

(8) A. J. Sophianopoulos and K. E. Van Holde, *J. Biol. Chem.*, **239**, 2516 (1964).

(9) P. F. Fahey, D. W. Kupke, and J. W. Beams, *Proc. Nat. Acad. Sci. U. S.*, **63**, 548 (1969).

(10) E. F. Casassa and H. Eisenberg, *Advan. Protein Chem.*, **19**, 287 (1964).

(11) H. Fujita in "Mathematical Theory of Sedimentation Analysis," Academic Press, New York, N. Y., 1962, pp 247-254.

(12) R. H. Haschemeyer and W. F. Bowers, *Biochemistry*, **9**, 435 (1970).

(13) L. W. Nichol and A. G. Ogston, *J. Phys. Chem.*, **69**, 4365 (1965).

ume change. The differential form of eq 9b may be obtained simply from eq 5

$$\frac{d\bar{c}(r)}{d(r^2)} = \sum_i \frac{\phi_i M_i c_i(r)}{1 + \{d \ln y_i(r)/d \ln c_i(r)\}} \quad (10)$$

From eq 6

$$\frac{d \ln y_A(r)}{dc_A(r)} = BM_A \frac{d\bar{c}(r)}{dc_A(r)} = BM_A \left\{ 1 + \frac{dc_C(r)}{dc_A(r)} \right\} \quad (11a)$$

$$\frac{d \ln y_C(r)}{dc_C(r)} = BM_C \frac{d\bar{c}(r)}{dc_C(r)} = BM_C \left\{ 1 + \frac{dc_A(r)}{dc_C(r)} \right\} \quad (11b)$$

Differentiation of the definition of the equilibrium constant gives

$$\frac{dc_C(r)}{dc_A(r)} = m c_A^{m-1}(r) K(r) = \frac{m c_C(r)}{c_A(r)} \quad (12)$$

Combination of eq 11 and 12 shows that

$$\frac{d \ln y_A(r)}{d \ln c_A(r)} = \frac{d \ln y_C(r)}{d \ln c_C(r)} = BM_{AC_A}(r) + BM_{CC_C}(r) \quad (13)$$

Thus, eq 10 becomes

$$\frac{d\bar{c}(r)}{d(r^2)} = \frac{\phi_A M_{AC_A}(r) + \phi_C M_{CC_C}(r)}{1 + BM_{AC_A}(r) + BM_{CC_C}(r)} \quad (14)$$

We now wish to rewrite eq 14 in terms of an apparent weight-average molecular weight, which could be evaluated experimentally when the density increment of the monomer is known. This quantity is defined by

$$M_w(r)_{app} = \frac{d \ln \bar{c}(r)}{d(r^2)} \cdot \frac{1}{\phi_A} \quad (15)$$

On noting that an expression for ϕ_C in terms of $\partial \rho / \partial c_A$ is available by combining eq 1 and 2b, it follows that eq 14 becomes

$$M_w(r)_{app} = \frac{\frac{M_{AC_A}(r) + M_{CC_C}(r)}{\bar{c}(r)} - \frac{\Delta V \rho c_C(r)}{(\partial \rho / \partial c_A) \bar{c}(r)}}{1 + BM_{AC_A}(r) + BM_{CC_C}(r)} \quad (16)$$

Since the actual weight-average molecular weight at a position r in the cell is $\{M_{AC_A}(r) + M_{CC_C}(r)\} / \bar{c}(r)$, eq 16 expresses the relation between this quantity and the experimentally available parameter, $M_w(r)_{app}$, in terms of the volume change ΔV and the nonideality coefficient B . When $\Delta V = 0$ and $B = 0$, eq 16 shows that the molecular weight measured at r is the actual weight-average molecular weight at this position; whereas, when $\Delta V = 0$ and $B \neq 0$ (thermodynamic nonideality is considered in the absence of a pressure effect), eq 16 reduces to eq 9a of Adams.⁴ In either of these situations it is clear that $M_w(r)_{app}$ would be a continuous function of $\bar{c}(r)$ regardless of the value of ω selected or of the initial loading concentration used. On the other hand, as previously discussed,¹ when $\Delta V \neq 0$, discontinuities in such plots are expected and in

the event that also $B \neq 0$, the final result will depend on the signs and magnitudes of ΔV and B ; thus, the effects may oppose or reinforce each other.

Experimental Section

Materials. Salt-free lysozyme (hens' egg white) was obtained from Worthington Biochemical Corp. Polyacrylamide gel electrophoresis of this preparation in the presence of sodium dodecyl sulfate showed the presence of a single protein band, which while not excluding the possibility of microheterogeneity with respect to charge¹⁴ does suggest that the sample is homogeneous with regard to molecular weight. In this connection, it is not implied that the electrophoretic method yields a reliable estimate of the molecular weight.¹⁵ Buffer solutions used in sedimentation equilibrium experiments were prepared with analytical reagent grade chemicals and glass distilled water and were of the following compositions: pH 6.7, ionic strength 0.17 (0.005 *M* sodium dihydrogen phosphate, 0.005 *M* disodium hydrogen phosphate, 0.15 *M* sodium chloride) and pH 8.0, ionic strength 0.15 (0.02 *M* sodium diethylbarbiturate, 0.01 *M* diethylbarbituric acid, 0.13 *M* sodium chloride). Protein solutions were dialyzed overnight at room temperature against approximately 25 volumes of the same buffer. Visking 8/32 cellophane tubing which had been cleaned by immersion in 3% acetic acid at 60°, allowed to cool, and then washed exhaustively with distilled water, was used for the dialysis. The dialyzate was checked spectrophotometrically to confirm that no protein had escaped from the sac during dialysis. The partial specific volume, \bar{v} , of lysozyme was taken as 0.726 ml/g.¹⁶ The densities of the buffer solutions at the temperature of the sedimentation equilibrium experiments were interpolated from tables given by Svedberg and Pedersen¹⁷ and the densities, ρ , of protein solutions were calculated from the expression $\rho = \rho_0 + (1 - \bar{v}\rho_0)c$, where ρ_0 is the solvent density and c is the concentration of protein in grams per milliliter.

Sedimentation Experiments. Experiments were performed with a Spinco Model E ultracentrifuge fitted with electronic speed control. The temperature was controlled within $\pm 0.1^\circ$ by means of the RTIC unit and refrigerator. The Rayleigh interference optical system with offset upper limiting aperture was used throughout. The initial concentrations of protein solutions, used in sedimentation equilibrium experiments, were determined from separate experiments employing a capillary-type synthetic boundary cell

(14) C. O. Stevens and G. R. Bergstrom, *Proc. Soc. Exptl. Biol. Med.*, **124**, 187 (1967).

(15) A. K. Dunker and R. R. Rueckert, *J. Biol. Chem.*, **244**, 5074 (1969).

(16) R. C. Deonier and J. W. Williams, *Biochemistry*, **9**, 4260 (1970).

(17) T. Svedberg and K. O. Pedersen in "The Ultracentrifuge," Oxford Clarendon Press, New York, N. Y., 1940.

of 12-mm path length. Dialyzed protein solution and dialyzate were placed in the solution and solvent sectors, respectively. The rotor was initially accelerated to 10,000 rpm to equalize the menisci in the two sectors and then the speed was decreased to 5600 rpm. A photograph of the interference fringe pattern was taken as soon as the latter speed was attained and another immediately after the fringes in the boundary region had resolved. The fringe fraction was determined from the first photograph and the whole number of fringes from the second.

Sedimentation equilibrium experiments were performed with a 12-mm double-sector filled-epon centerpiece and sapphire windows. Equal amounts by weight of the fluorochemical FC 43 (0.02 g) were introduced into each sector followed by equal weights (0.1 g) of dialyzed solution and dialyzate in the solution and solvent sectors, respectively. These quantities were chosen to give column heights of about 3 mm. Care was taken to avoid mixing of the two phases, and no interaction of the lysozyme with the oil was observed throughout the experiment as judged from the optical appearance of the oil-solution interface. The use of dialyzed solution and dialyzate conforms to the requirements specified by Casassa and Eisenberg¹⁰ for the correct interpretation of sedimentation equilibrium experiments with charged macromolecules in aqueous solutions containing buffer ions. To shorten the time required to attain sedimentation equilibrium, the procedure suggested by Richards, Teller, and Schachman¹⁸ was adopted which involves overspeeding for a time before setting the speed to the desired value. It was found that no change in the concentration distributions in any of the experiments was detectable after 6 hr of centrifugation, but all of the results reported are derived from measurements taken after 10 hr. A photograph of the Rayleigh interference fringe pattern was also taken at the speed of the sedimentation equilibrium experiment before the overspeeding and before any detectable redistribution of solute had occurred. This was used to provide a baseline correction and in the labeling of fringes in the equilibrium interference pattern.

Evaluation of Molecular Weights. The photographic plates were measured on a two-dimensional microcomparator (Gaertner Scientific Corp). The plates were aligned by means of the inner and outer reference fringe patterns generated by the slits in the counterbalance. The radial reference position was obtained by measuring the inner edges of the two reference fringe patterns and taking the mean. This position corresponds to a radial distance, r , 6.50 cm from the axis of rotation. The measurements of the patterns obtained in synthetic boundary and sedimentation equilibrium experiments, in terms of fringe numbers, j , and their use in determining apparent weight-average molecular weight *vs.* concentration graphs followed a method described in

detail by Richards, *et al.*¹⁸ In outline, the photograph taken before any solute redistribution has occurred is used to provide a baseline correction and also to determine the vertical level (perpendicular to the fringes) on the equilibrium pattern along which the hinge point (corresponding to the initial concentration measured in the synthetic boundary experiment) must be located. Measurements of the radial positions of fringes across the equilibrium interference pattern at this vertical setting together with the application of the conservation of mass condition provides, after baseline corrections have been made, the first estimate of the concentration at the meniscus. This allows all the fringes in the pattern from the meniscus to the cell bottom to be labeled. A plot of $\ln j$ *vs.* r^2 can then be made and extrapolated to the meniscus and cell bottom to provide more accurate values of the meniscus concentration and the concentration change across the solution column. If these values differ significantly from the first estimate, the fringes are relabeled and the process repeated until no further change is obtained. A further refinement is available by making use of the fact that the concentration at one radial position (the hinge point) must now be equal to the initial concentration because of the way the interference pattern was measured. The concentration nearest in value to the initial concentration is thus adjusted to be precisely equal to it and all the other fringes relabeled accordingly. An advantage of this refinement is that it provides a method of labeling accurately the interference fringes which does not rely on precise determinations of the positions of the meniscus and cell bottom.

The concentration *vs.* radial distance data obtained as above were fitted by least-squares regression analysis to a polynomial of the form

$$\ln J = \sum_{i=0}^n \alpha_i r^{2i}$$

where J is the actual total concentration in terms of Rayleigh interference fringes at radial distance r from the axis of rotation. Differentiation of the resulting polynomial gives the values of $d \ln J(r)/d(r^2)$ which are required for the evaluation of apparent weight-average molecular weights as a function of concentration according to eq 15. Values for the concentration are in terms of fringes, J , but may be expressed on the more familiar weight-concentration scale by assuming a linear dependence of refractive index increment on concentration. In the treatment which follows it is also assumed that the specific refractive increments of A and C are identical, with the value¹⁶ of 0.00185 dl/g. On this basis, the relation $c = 2.46 \times 10^{-4} J$ applied, where c is in grams per milliliter. All calculations were performed with the use of an IBM 360 com-

(18) E. G. Richards, D. C. Teller, and H. K. Schachman, *Biochemistry*, **7**, 1054 (1968).

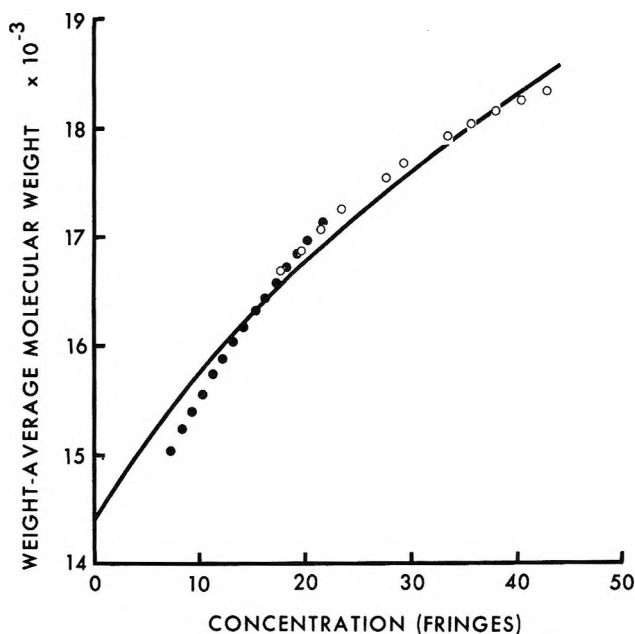


Figure 1. Sedimentation equilibrium results obtained with lysozyme in phosphate buffer pH 6.7, ionic strength 0.17 at 15°. The ordinate axis gives values of $M_w(r)_{app}$ defined in eq 16 of the text while the abscissa presents corresponding concentrations in terms of Rayleigh interference fringes. ●, initial concentration 11.64 fringes, 20,000 rpm; ○, initial concentration 28.48 fringes, 15,000 rpm. The solid line was calculated from the results of Adams and Filmer⁵ as described in the text with $K = 0.44$ dl/g and $B = -1.4 \times 10^{-6}$ dl/mol of monomer of molecular weight 14,400.

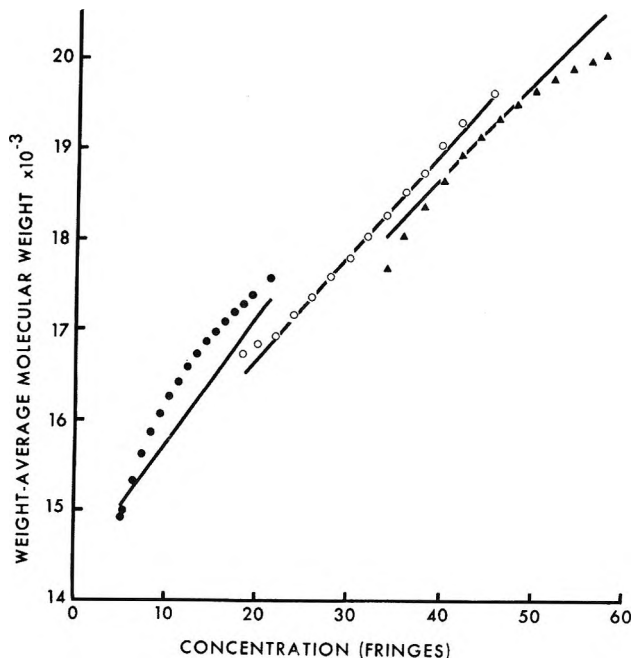


Figure 2. Sedimentation equilibrium results obtained with lysozyme in diethylbarbiturate buffer pH 8.0, ionic strength 0.15 at 15°. ●, initial concentration 11.40 fringes, 20,000 rpm; ○, initial concentration 29.42 fringes, 15,000 rpm; ▲, initial concentration 44.99 fringes, 11,000 rpm. The solid lines were computed as described in the text employing values of $K(1 \text{ atm}) = 0.24$ dl/g, $B = -4 \times 10^{-6}$ dl/mol of monomer of molecular weight 14,400, and $\Delta V = -0.03$ ml/g.

puter, and the program was tested with simulated data, which it reproduced with a precision better than 0.1%.

Results

Adams and Filmer⁵ have analyzed sedimentation equilibrium experiments performed with lysozyme at 15° in pH 6.7 phosphate buffer of ionic strength 0.17 in terms of a dimerization reaction and nonideality effects. They obtained the following values for the parameters defined earlier: $M_A = 14,400$, $K = 0.44$ dl/g, and $B = -1.4 \times 10^{-6}$ dl/mol of monomer. It was of interest in relation to the present work to confirm that plots of $M_w(r)_{app}$ vs. total concentration found in this environment superimposed. The results of two sedimentation equilibrium experiments performed with lysozyme in the same environment are presented in Figure 1. It is clear that the results from the two different experiments fall on a smooth curve which may be extrapolated to yield a value of 14,400 for M_A . As noted earlier, the superposition of the data strongly suggests that ΔV is essentially zero. Moreover, it is possible to demonstrate directly that the present results are in other respects in close agreement with those given by Adams and Filmer.⁵ This is achieved by utilizing their parameters, reported above, to construct the solid line shown in Figure 1.

In contrast to the smooth plots obtained at pH 6.7 and shown in Figure 1, the results in Figure 2 pertaining

to the sedimentation equilibrium of lysozyme at pH 8.0 show that data obtained from experiments in which the speed and initial concentration were varied do not superimpose. Many factors may contribute to this type of nonsuperposition including the following: (a) heterogeneity of the sample with respect to molecular weight (inherent¹⁹ or arising as a result of oil denaturing effects⁷); (b) errors in measurement and in the numerical differentiation procedures employed to obtain $M_w(r)_{app}$ values;²⁰ (c) a pressure dependence of the partial specific volumes of the monomer and dimer; (d) adsorption of the protein to cell walls;⁵ (e) buffer-protein interactions leading to a different distribution of buffer components in the solution and reference channels; and (f) a difference in the partial specific volumes of the monomer and dimer¹ ($\Delta V \neq 0$) and/or a difference in their specific refractive index increments. In view of the diverse range of possible contributing factors, it may seem impossible, at first sight, to analyze the results presented in Figure 2. On the other hand, it is noted that the absence of nonoverlap in Figure 1 implies that possibilities a-d are unlikely to be contributing causes of the effect shown in Figure 2. Thus, it was felt reasonable to explore the applicability of the theo-

(19) D. E. Roark and D. A. Yphantis, *Ann. N. Y. Acad. Sci.*, **164**, 245 (1969).

(20) P. D. Jeffrey and J. H. Coates, *Biochemistry*, **5**, 489 (1966).

retical relations developed herein as a first attempt in analyzing the results.

First, it was assumed initially that the plots of $\bar{c}(r)$ vs. r obtained experimentally with the lowest initial concentration (11.40 fringes) were unaffected by nonideality. This permitted simultaneous solution of eq 9a and b, written with $B = 0$ and with assumed values of ϕ_A and ϕ_C , to yield apparent values of $c_A(r_1)$ and $c_C(r_1)$ and hence an apparent value of $K(r_1)$. Values of $K(r)_{\text{app}}$ at other radial positions were similarly determined and converted into apparent values of $K(r_m) = K(1 \text{ atm})$ using eq 3. The process was repeated using a fixed value of ϕ_A , corresponding to a partial specific volume¹⁶ of 0.726 ml/g, and varying ϕ_C until the calculated values of $K(1 \text{ atm})$ became constant. A partial specific volume for the dimer, C, of 0.696 ml/g was indicated, corresponding to an apparent value of -0.03 ml/g for ΔV . When the same procedure was applied to results obtained with the higher initial concentrations (29.42 and 44.99 fringes), it was found that this value of ΔV did not lead to constant values of $K(1 \text{ atm})$ calculated from eq 3, suggesting that nonideality effects were appreciable at these concentrations. On the other hand, solution of eq 9a and b as written with $\Delta V = -0.03 \text{ ml/g}$ and selected values of B yielded a satisfactory result when $B = -4 \times 10^{-6} \text{ dl/mol}$, in that the calculated values of $K(1 \text{ atm})$ were 0.237 and 0.243 dl/g for $J = 29.42$ and 44.99, respectively, the standard deviation of six points from the mean in each case being ± 0.003 . To show that the indicated values of the relevant parameters adequately describe the experimental results obtained with the initial concentrations of 29.42 and 44.99 fringes, the solid lines in Figure 2 were constructed in the following way. Equation 3 was used to calculate $K(r)$ at each relevant r position, and hence values of $c_A(r)$ and $c_C(r)$ were evaluated employing the definition of the equilibrium constant and the experimentally observed $\bar{c}(r)$ at r . Equation 16 provided the corresponding value of $M_w(r)_{\text{app}}$.

Although the results obtained with the higher initial concentrations are seen in Figure 2 to be satisfactorily described by the reported parameters, it is now relevant to ask whether the value of B found satisfies the requirement that terms containing it do not contribute significantly to the concentration distribution observed with the lowest initial concentration. Indeed, this assumption was made initially in order to estimate the apparent ΔV . If the requirement is satisfied, the value of $K(1 \text{ atm})$ calculated as above employing the same values of ΔV and B should be constant and agree with that obtained from the analysis of the experiments at the higher initial concentrations. It was found that $K(1 \text{ atm}) = 0.341 \pm 0.003 \text{ dl/g}$, the standard deviation indicating reasonable constancy for six determinations. Although this value differs from that pertaining to the higher concentrations (*viz.* 0.24 dl/g), the difference is

within experimental error. For example, Adams and Filmer⁵ quote equilibrium constants in the range 0.44 to 0.52 dl/g for lysozyme at pH 6.7 over a concentration range of 45 to 60 fringes. This point is emphasized in Figure 2 where the solid line referring to the lowest initial concentration was calculated employing the same values of $K(1 \text{ atm})$, ΔV , and B as were used for the higher concentrations; the fit is adequate and was improved only slightly when $K(1 \text{ atm})$ was set to equal to 0.34 dl/g.

Discussion

In the analysis of sedimentation equilibrium results involving nonideality effects it seems unavoidable that use must be made of a procedure involving arbitrary selection and subsequent refinement of values of the virial coefficient(s).⁴⁻⁷ This arises as a consequence of the definition of the activity coefficient given in eq 6 in terms of the total solute concentration, which in turn introduces into eq 8, describing the distribution of individual solute species, an exponential term in total solute concentration. It is for the same reason that it does not seem possible to compute plots of $\bar{c}(r)$ vs. r employing the conservation of mass equation

$$(Q_i)_{\text{cell}} = \theta b c_i(r_b) e^{BM\bar{c}(r_b) - \phi_i M_i r_b^2} \int_{r_m}^{r_b} r e^{\phi_i M_i r^2 - BM\bar{c}(r)} dr \quad (17)$$

where $(Q_i)_{\text{cell}}$ is the amount of solute species i in the cell of thickness b and sector angle θ . When $B = 0$, Howlett, *et al.*,¹ have described in detail how use may be made of the ratio $(Q_C)_{\text{cell}} / (Q_A)_{\text{cell}}^m$ to compute plots of $\bar{c}(r)$ vs. r for model systems even when $\Delta V \neq 0$. However, when $B \neq 0$, the integrand in eq 17 contains a term in $\bar{c}(r)$ which cannot be written explicitly in terms of r . It follows that it is a practical approach to calculate from the original $\bar{c}(r)$ vs. r results the quantity $M_w(r)_{\text{app}}$, for not only is this quantity experimentally available but also an explicit expression for it in terms of the required parameters is given by eq 16.

In relation to the results obtained with lysozyme, it is noted that the magnitudes of the nonideality coefficient and the equilibrium constant at 1 atm seem to be little affected by a change in pH from 6.7 to 8.0 in the specified environments. Certainly, the present results confirm⁵ that the sign of B is negative at pH 6.7 and show that the sign remains unchanged at pH 8.0. Moreover, the results in Figure 1 agree with those of Adams and Filmer⁵ in all other respects including the contention that ΔV is essentially zero. The nonsuperposition of the curves in Figure 2 and the ability to fit these curves on the basis of eq 16 suggests, at first sight, that at pH 8.0 in diethylbarbiturate buffer and under the conditions of sedimentation equilibrium, ΔV is not only finite but also negative (-0.03 ml/g). This observation is somewhat surprising since certain other polymerizing systems^{21,22} are associated with

volume changes per mole of monomer of comparable magnitude but of opposite sign and hence tend to dissociate on an increase of pressure. While it is indeed possible that the dimerization of lysozyme at pH 8.0 is accompanied by a negative volume change as suggested by the present analysis, it is stressed that the derived value must be regarded as apparent in view of the neglect of certain other factors (previously listed) which may contribute to the nonsuperposition. Particular mention should be made of the neglect of charge effects and specific ion binding effects and of the assumption that specific refractive index increments of the monomer and dimer are identical. It is clear that the indicated negative volume change at pH 8.0 requires investigation by alternative methods;^{9,22} for, if it were substantiated, it would detract from general-

izations made in relation to the effects of pressure on enzymic activity.²³

In conclusion, it is hoped that the present theoretical development and the illustration of its use in analyzing experimental results may assist in the interpretation of sedimentation equilibrium results obtained with other polymerizing protein systems where volume changes and nonideality effects operate.

Acknowledgment. The authors are grateful to P. A. Baghurst for assistance with the computer programs.

(21) R. Josephs and W. F. Harrington, *Proc. Nat. Acad. Sci. U. S.*, **58**, 1587 (1967).

(22) T. A. J. Payens and K. Heremans, *Biopolymers*, **8**, 335 (1969).

(23) J. T. Penniston, *Arch. Biochem. Biophys.*, **142**, 322 (1971).

Formation of Dynamic Patterns in a Fluid Layer

by F. Gambale and A. Gliozzi*

Laboratorio di Cibernetica e Biofisica-Camogli (Genova), Italy and Istituto di Scienze Fisiche dell'Università di Genova, Genoa, Italy (Received September 16, 1971)

Publication costs assisted by Consiglio Nazionale delle Ricerche

The formation of convection cells induced by a vertical concentration gradient has been analyzed. The experimental system is realized spreading a polymer solution (few mm thick) on a membrane swollen with water. The critical value of concentration above which the onset of convection cells occurs has been experimentally determined and is found to be in good agreement with the theoretical expectations of a linear perturbative analysis. A study of the statistics of the cell dimensions as function of the thickness of the fluid layer is performed and a linear dependence is found to hold as from the theoretical expectations.

Introduction

The problem of instabilities causing pattern formation became of great interest for many physicists¹⁻⁴ when the experiments performed by Bénard⁵ showed the occurrence of hexagonal convection cells in a horizontal layer of fluid heated from below. The formation of Bénard cells has generally been ascribed to the buoyancy forces driving the convective flows^{1,2} although, more recently, the possible role of surface tension forces in determining such cellular convection has also been analyzed.⁶⁻⁹ The possibility of pattern formation, in systems which are initially homogeneous and where the chemical species can react and diffuse, was stressed by Turing.¹⁰ First, he underlined the possible importance of such a behavior in the functional processes of biological systems. While the Bénard phenomenon can be ascribed to the coupling between heat flow and flow of matter, the system analyzed

by Turing deals with coupling between chemical reactions and diffusion. However, both systems are examples showing that coupling between different flows makes the flows themselves organize, giving rise to a dynamic structure.¹¹⁻¹³

(1) Lord Rayleigh, *Phil. Mag.*, **32**, 529 (1916).

(2) H. Jeffreys, *ibid.*, **2**, 833 (1926); and *Proc. Roy. Soc. Ser. A*, **118**, 195 (1928).

(3) A. R. Low, *Proc. Roy. Soc. Ser. A*, **125**, 180 (1929).

(4) A. Pellew and R. V. Southwell, *Proc. Roy. Soc. Ser. A*, **176**, 312 (1940).

(5) H. Bénard, *Rev. Gen. Sci. Pures Appl.*, **11**, 1261, 1309 (1900).

(6) J. R. A. Pearson, *J. Fluid Mech.*, **4**, 489 (1958).

(7) M. J. Block, *Nature (London)*, **178**, 650 (1956).

(8) D. A. Nield, *J. Fluid Mech.*, **19**, 341 (1964).

(9) L. E. Scriven and C. V. Sternling, *ibid.*, **19**, 321 (1964).

(10) A. M. Turing, *Phil. Trans. Roy. Soc. London, Ser. B*, **237**, 37 (1952).

(11) J. I. Gmitro and L. E. Scriven, "Intracellular Transport," Academic Press, New York, N. Y., 1966.

The aim of this work is to present a phenomenon where convective and diffusive flows are coupled yielding an organized dynamic pattern. The first part of this paper is devoted to the theoretical analysis of the phenomenon. Since the basic equations are similar to those describing the Bénard system, we have given only a summary of the method, with the proper changes (for the details the reader is referred to Chandrasekar's book¹⁴). The study of the temporal evolution of the system and the numerical computation are treated with greater detail.

The second part deals with the experimental realization of the system and the comparison of the results with the theoretical expectations.

Description of the Phenomenon

The phenomenon under consideration is realized in a fluid layer subjected to a concentration gradient. The experimental system consists of a thin layer of polymer solution (usually polyethylene glycol 6000, POEG) spread on a dialysis membrane swollen with water and clamped in a cylindrical frame. A small amount of water is released by the membrane, owing to the osmotic pressure difference between the solvent inside the membrane and the external solution. In this way the membrane behaves like a solvent source and a gradient of concentration is established in the fluid layer. The density variation, due to the concentration gradient, causes buoyancy forces. The system displays ascending and descending convective flows which form a stationary polygonal pattern in the horizontal plane. Depressions and elevations on the free surface correspond to descending and ascending flows, respectively. The dimensions of the cells are linearly related to the depth of the fluid layer. Figure 1 shows a picture of such a polygonal pattern.

The behavior of a fluid layer subjected to a vertical temperature gradient, combined with a salinity gradient, has already been investigated.¹⁵⁻¹⁷ Also this system displays convective flows organized into thin columns

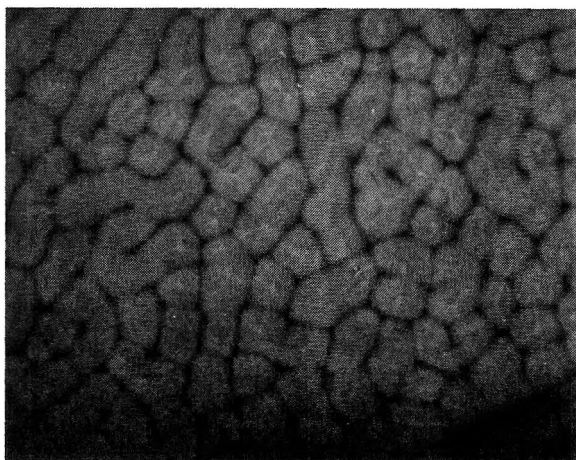


Figure 1. The pattern obtained with a 30% solution of POEG, 2 mm thick.

of fluid, alternatively ascending and descending. However a regular organization comparable to that of the presently studied phenomenon in the horizontal plane has not been observed. This fact can be due (*cf. seq.*) to the large depth of the fluid layer, about 25 cm, and to the difficulty in maintaining constant the boundary conditions.

Theoretical Considerations

The Equations of Continuity and of Motion. The system under study is an infinite horizontal layer of a water solution, at uniform temperature T , bounded by the planes $z = -1/2d$, $z = 1/2d$; the lower boundary is maintained at a fixed concentration, while the upper boundary is at a higher concentration value.

The continuity equation, with the aid of the Fick's law, can be written as

$$\frac{\partial \rho}{\partial t} = -\rho \frac{\partial v_i}{\partial x_i} - v_i \frac{\partial \rho}{\partial x_i} + \frac{\partial}{\partial x_i} D \frac{\partial c}{\partial x_i} \quad (1)$$

where ρ denotes the density of the solution, v_i the i -component of the velocity, D the diffusion coefficient and c the concentration of solute in g/l.

We shall make use here of some results contained in the Experimental Section, in order to make reasonable assumptions for our system. First of all we shall assume that the density of the solution is a linear function of concentration (*cf.* Figure 6a)

$$\rho = \rho_0(1 + \tau c) \quad (2)$$

where ρ_0 is the density of the water at temperature T , and τ is of the order of 10^{-4} l./g when $c \leq 10$ g/l. (*cf.* Experimental Section). Moreover we shall assume that in this range of concentration the diffusion coefficient D and the viscosity η may be considered constant in the whole system.

Substituting (2) in (1) we obtain

$$\frac{\partial c}{\partial t} + v_i \frac{\partial c}{\partial x_i} - \mathfrak{D} \nabla^2 c = 0 \quad (3)$$

where $\mathfrak{D} = D/\rho_0\tau$, and the velocity field has been assumed solenoidal, since, from the actual value of τ , the term $\partial v_i/\partial x_i$ of eq 1 appears to be 10^4 times smaller than the others.

On the basis of the above considerations, the equation of motion, under the Boussinesq approximation, can be written as

(12) I. Prigogine and G. Nicolis, *J. Chem. Phys.*, **46**, 3542 (1967).

(13) A. Katchalsky and R. Spangler, *Quart. Rev. Biophys.*, **1**, 127 (1968).

(14) S. Chandrasekar, "Hydrodynamic and Hydromagnetic Stability," Clarendon Press, Oxford, England, 1961.

(15) G. Veronis, *J. Mar. Res.*, **23**, 1 (1965).

(16) J. S. Turner and H. Stommel, *Proc. Nat. Acad. Sci. U. S.*, **52**, 49 (1964).

(17) M. E. Stern, *Tellus*, **12**, 172 (1960).

$$\frac{\partial v_i}{\partial t} + v_j \frac{\partial v_i}{\partial x_j} = -\frac{1}{\rho_0} \frac{\partial p}{\partial x_i} + \frac{\rho}{\rho_0} X_i + \nu \nabla^2 v_i \quad (4)$$

where ν is the kinematic viscosity defined as η/ρ_0 , X_i is the i -component of the external specific force (in this case $\vec{X} \equiv (0, 0, -g)$), and p is the static fluid pressure.

Perturbative Equations. Let us suppose our infinite horizontal layer in a stationary state without any convective motion. In this state from eq 3 we obtain that the stationary distribution of concentration, c' , is a linear function of the quota z , *i.e.*

$$c'(z) = c_0 + \beta z \quad (5)$$

where β is the concentration gradient.

Let us denote with θ a microscopical perturbation of c' and V_i the i -component of the velocity of the fluid in the perturbed state.

Neglecting all the second order terms of the perturbative variations θ and \vec{V} in eq 3 and 4 and rearranging, we get the two perturbative equations

$$\frac{\partial \theta}{\partial t} = -\beta w + \mathfrak{D} \nabla^2 \theta \quad (6)$$

where w is the z -component of the velocity *i.e.*, $w = V_z$, and

$$\frac{\partial \nabla^2 w}{\partial t} = -g \tau \left(\frac{\partial^2 \theta}{\partial x^2} + \frac{\partial^2 \theta}{\partial y^2} \right) + \nu \nabla^4 w \quad (7)$$

Equation 7 is derived by taking the double curl of eq 4.

Solutions of the Equations. Since the system has no preferential points or directions in the (x, y) plane, one can express the solution of eq 6 and 7 as a superposition of terms of the kind

$$\theta = \Theta(z) \exp(ik_x x + ik_y y + \lambda_k t) \quad (8)$$

$$w = W(z) \exp(ik_x x + ik_y y + \lambda_k t) \quad (9)$$

where

$$k = (k_x^2 + k_y^2)^{1/2} = \frac{2\pi}{l} \quad (10)$$

is the wave number associated with the k th disturbance. It can be shown¹⁴ that in our case λ_k is a real number; therefore when $\lambda_k < 0$ the disturbance will decrease exponentially with time, while when $\lambda_k > 0$ the disturbance will increase with time. It follows that the system will pass from a stable to an unstable state *via* a marginal state characterized by a wave number k_c .

Substituting eq 8 and 9 in eq 6 and 7 and introducing the dimensionless numbers

$$a = kd \quad \sigma = \lambda_k \frac{d^2}{\nu} \quad s = \frac{\nu}{\mathfrak{D}} \quad (11)$$

one gets¹⁴

$$\left(\frac{d^2}{dz^2} - a^2 \right) \left(\frac{d^2}{dz^2} - a^2 - \sigma \right) \times \left(\frac{d^2}{dz^2} - a^2 - s\sigma \right) W = -Ra^2 W \quad (12)$$

and

$$\left(\frac{d^2}{dz^2} - a^2 \right) \left(\frac{d^2}{dz^2} - a^2 - \sigma \right) \times \left(\frac{d^2}{dz^2} - a^2 - s\sigma \right) \Theta = -Ra^2 \Theta \quad (13)$$

where R is a dimensionless number defined as

$$R = \frac{\tau g \beta d^4}{\mathfrak{D} \nu} \quad (14)$$

Equations 12 and 13 have been deduced by eliminating Θ and W respectively between eq 6 and 7. In what follows we shall look for a solution of eq 12 in $W(z)$; the corresponding solution for $\Theta(z)$ can be deduced by the equations relating Θ and W .⁴

Setting $\lambda_k = 0$ in eq 12 we have a differential equation of order six, which governs the marginal state. This equation must satisfy the following six boundary conditions at the lower (rigid) and upper (free) surfaces¹⁴

$$W = 0 \quad z = \pm \frac{1}{2}d \quad (15)$$

$$\left(\frac{d^2}{dz^2} - a^2 \right)^2 W = 0 \quad z = \pm \frac{1}{2}d \quad (16)$$

$$\frac{dW}{dz} = 0 \quad z = -\frac{1}{2}d \quad (17)$$

$$\frac{d^2 W}{dz^2} = 0 \quad z = +\frac{1}{2}d \quad (18)$$

Equation 15 is obvious, while eq 16 is derived¹⁴ from the equation relating Θ and W , under the simplifying assumption that $\Theta = 0$ at $z = \pm 1/2d$. Equations 17 and 18 are both derived¹⁴ from the solenoidality condition of the velocity field (by recalling that the horizontal components of the velocity must vanish at the rigid boundary (eq 17) and by deriving with respect to z the solenoidality equation, and imposing the vanishing of the components P_{zz} , P_{yz} of the stress tensor at the free surface (eq 18)).

We are interested to determine the functional relationship between R and a which satisfies the differential equations with the proper boundary conditions. We are omitting here all the procedure^{4,14} and give only the results, summarized in Figure 2, where the curve $R^* = R^*(a)$ corresponding to the case of the marginal stability is reported.

The minimum value of R for which the system is marginally stable is $R_c^* = 1100.65$. The corresponding value of the wave number is $a_c = 2.68$.

Therefore for $R < R_c^*$ the system is stable, while when R slightly exceeds R_c^* the system is unstable with respect to the disturbance characterized by the wave number a_c .

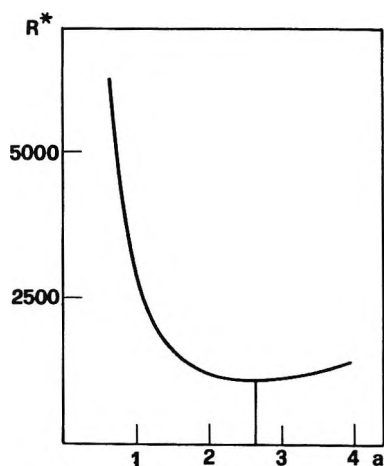


Figure 2. The curve of marginal stability, $R^*(a)$, as function of the wave number a .

Actually the wave number a defines only the modulus of a vector \vec{a} which is unspecified since the components a_x and a_y may be chosen in infinite ways. However we can argue that, since the system has no preferential points or directions in the horizontal plane, the fluid layer will be tassellated by polygonal convection cells which will be equilateral triangles, squares, or regular hexagons.

In order to define the pattern dimension we shall suppose that a hexagonal distribution occurs. In this case the side of the hexagon l and the wave number a are related by the relationship¹⁴

$$a = \frac{4}{3} \pi \frac{d}{l} \quad (19)$$

We shall use equation 19 to compare the experimental and the theoretical results.

Temporal Evolution of the Disturbances. When the system is characterized by a value of R greater than R_c^* , many disturbances will grow with time; among these, the one which has the greatest temporal factor will prevail over the others. In other words the evolution of our system will be given by the functional dependence of the temporal factor σ (defined in eq 11) on R and a . We shall therefore look for a solution of eq 12 which will satisfy the proper boundary conditions, eq 15–18. This solution may be written as a superposition of functions of the form

$$W(z) = \exp(\pm qz) \quad (20)$$

which substituted in eq 12 gives

$$(q^2 - a^2)(q^2 - a^2 - \sigma)(q^2 - a^2 - s\sigma) = -Ra^2 \quad (21)$$

Setting $\sigma = 0$ in eq 21, we get

$$(q^2 - a^2)^3 = -R^*a^2 \quad (22)$$

where $R^* = R^*(a)$ is, as already defined, the dimensionless function characterizing the marginally stable state, which has been plotted in Figure 2.

The roots $q(R^*, a)$ of eq 22 satisfy the boundary conditions but no longer satisfy eq 21 for any value of σ .

It can be easily shown that the relationship

$$\sigma = -\frac{(R^*a^2)^{1/3}}{2s} \left[(s+1) - \sqrt{(s+1)^2 + 4s\left(\frac{R}{R^*} - 1\right)} \right] \quad (23)$$

satisfies eq 24 as well as the boundary conditions and it therefore defines the functional dependence between σ , R , and a that we are looking for. In the Experimental Section a numerical analysis of eq 23 with the proper values of the parameters is performed. The results are shown in Figures 8 and 7c.

Relation 23 shows that only those disturbances characterized by a wave number a for which $R > R^*(a)$ will have a temporal factor greater than zero, as expected from the definition of marginal stability.

The fact that in relation 20 we have chosen the same values of q as in the case for the marginal stability means that the velocity as well as the concentration distribution has been supposed unaltered even when the system is far from the state of marginal stability.

It should be stressed that we have analyzed only how the system displaces from the initial state. When $R \gg R_c$ solutions are growing like $\exp(\sigma t)$ and therefore a linear analysis is no longer valid. However we shall suppose that the disturbance which has initially the greatest temporal factor will be the one prevailing in the system.^{10,11} This kind of hypothesis is supported by the experimental results, where a linear dependence between the hexagon sides and the thickness of the fluid layer is found to hold, as from the theoretical expectation (*cf. seq.*),

Experimental Section

Description of the Method. A dialysis membrane was immersed in an aqueous solution of methylene blue or neutral red for about 30 min. After this treatment the membrane was gently blotted and clamped in a perspex cylindrical cell (14 cm diameter). Great care was devoted to keep the membrane flat and in a horizontal plane. A few millimeters thick polyethylene glycol 6000 solution was then spread over the membrane. The concentration of the polymer solution varied from 0.1 to 30 g/dl in different experiments. After some minutes convective flows appeared, which were made evident by the color released by the membrane. In some experiments the solution itself was colored instead of the membrane and the convective flows appeared as transparent lines.

The formation of a cellular structure in the horizontal plane could be easily followed and recorded by means of a photographic chamber placed over the system. In order to observe the flows in the vertical plane a schlieren method was employed, and the flows were

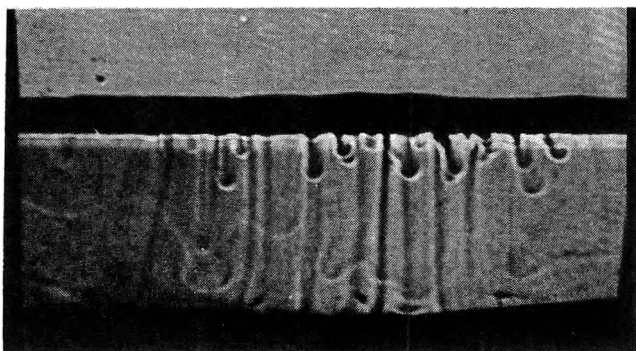


Figure 3. Descending and ascending flows photographed with a schlieren method using a 2×7 cm² glass cell. Depressions on the free surface correspond to the descending flows.

photographed with a telescopic system. Figure 3 shows a picture of these flows, in a 10% solution, 14 mm thick.

The Pattern Formation. For a 30% solution the convective flows began to be evident about 2–3 min after the spreading of the solution over the membrane (this time increases on decreasing the polymer concentration). After about 10 min the horizontal plane was tassellated with polygons whose regularity requires the control of the external conditions. These cells lasted for about 1 hr; the pattern obtained was mainly composed of quadrangular, pentagonal, and hexagonal cells (*cf.* Figure 1).

Similar cells were obtained using a concentrated solution ($\sim 3 M$) of CaCl_2 or KCl instead of a polymer solution; in this case however, the sensitivity to environmental variations was much greater owing to the lower viscosity of the solution. Therefore a regular pattern could hardly be obtained.

In Figure 4 an ordered sequence of photographs shows the pattern formation, while Figure 5 shows two different patterns at two different thicknesses of the layer. Besides the cells, which are due to the ascending colored flows, other cells, less evident, due to the descending flows, can be observed on the free surface (see Figure 1). The vertices of these cells correspond to the centers of the polygonal forms due to the rising flows.

The phenomenon can be qualitatively explained in the following way: the osmotic pressure gradient between membrane and solution causes a water flow from the membrane to the solution. Therefore the solution will be more diluted in the lower layer and the onset of convective flows is due to the tendency of the system to get a more stable configuration, provided the viscosity forces do not overcome the buoyancy forces.

Several experiments were performed to confirm this kind of interpretation; first of all the membrane was dehydrated and prevented from absorbing water from the external medium; in this case convective flows did not appear. Instead we could observe the organized flows either with a dry membrane which could absorb water vapor from the external medium, or with a swol-

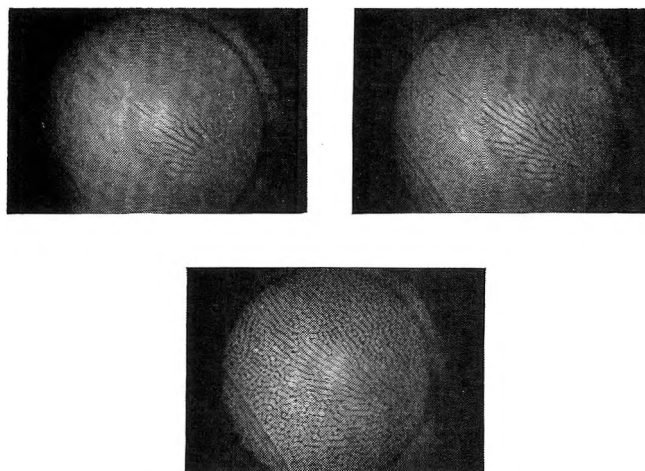


Figure 4. Typical formation of a pattern for a 30% solution 2 mm thick.

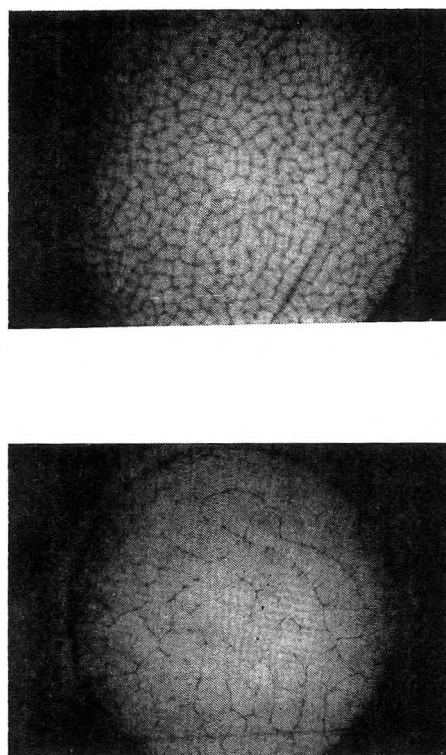


Figure 5. Two different patterns for a 30% solution 2 mm and 8 mm thick, respectively.

len membrane isolated from the external atmosphere. However in the former case the time required for the formation of the pattern was much longer. Moreover convective cells could be obtained with several kinds of membrane presenting a hydrophilic character of the matrix (*e.g.*, cellophane, collagen films), while no pattern formation was observed employing a hydrophobic membrane (*e.g.*, a teflon film).

A further test was performed to investigate whether temperature gradients were present and were playing an important role in the pattern formation. To check this the temperature difference between the lower and upper layer was measured by means of an Alumel-

Cromel thermocouple. No appreciable thermal gradient was observed. A further proof of the minor role played by possible thermal gradients was obtained by applying a small inverse temperature difference ($\sim 1^\circ$) to a 30% solution of POEG and observing that the convective flows were not disturbed.

Comparison with the Theory. A quantitative comparison between the experimental results and the theoretical expectations requires a knowledge of the physical parameters characterizing the system. For this purpose isothermal measurements of density and viscosity as a function of concentration have been performed. Figure 6a reports the relative density variation $\Delta\rho/\rho_0$ as a function of concentration. The slope of the straight line, τ , has the value 1.28×10^{-4} l./g, which is of the order of magnitude assumed in the theoretical considerations.

One can observe that the condition required by the theoretical treatment of a linear dependence between the density of the POEG solution and the concentration (cf. eq 2) is satisfied.

Figure 6 reports the kinematic viscosity as a function of concentration. The diffusion coefficient (available only at low concentrations) has been derived from previously reported values.¹⁸

From eq 14 it is possible to derive the critical value of the concentration difference Δc_r above which the instability should occur

$$\Delta c_r = \frac{R_c^* \mathcal{D} \nu}{\tau g d^3} \quad (24)$$

where the relationship $\beta = \Delta c/d$ has been employed.

Substituting the actual values of $\tau = 1.28 \times 10^{-4}$ l./g, $\mathcal{D} = 7.81 \times 10^{-6}$ cm²/sec, and $\nu = 10^{-2}$ cm²/sec in relation 24, for a thickness $d = 1.5$ mm, and choosing for R_c^* the value 1100.65 (given by the theoretical treatment as the minimum value of R above which the instability occurs), one gets $\Delta c_r = 0.02$ g/dl.

In order to calculate the difference in concentration which is established when the membrane releases water, we shall make use of the simple relationship

$$\frac{\Delta c}{d} = 2c(\delta) \left[1 - \frac{d}{\delta} \right] \quad (25)$$

where $c(\delta)$ is the concentration at the upper boundary, which is assumed equal to that of the employed solution, and δ is the actual thickness of the fluid layer, once the water inside the membrane has been released.

This relationship can be obtained by imposing that the amount of solute inside the solution remains constant and a linear distribution of concentration occurs.

The minimum value of concentration at which we could observe organized flows was of the order of 0.3 g/dl for a layer 1.5 mm thick. We shall suppose that the linear concentration profile along the z direction has an upper boundary value of 0.3 g/dl. If the mem-

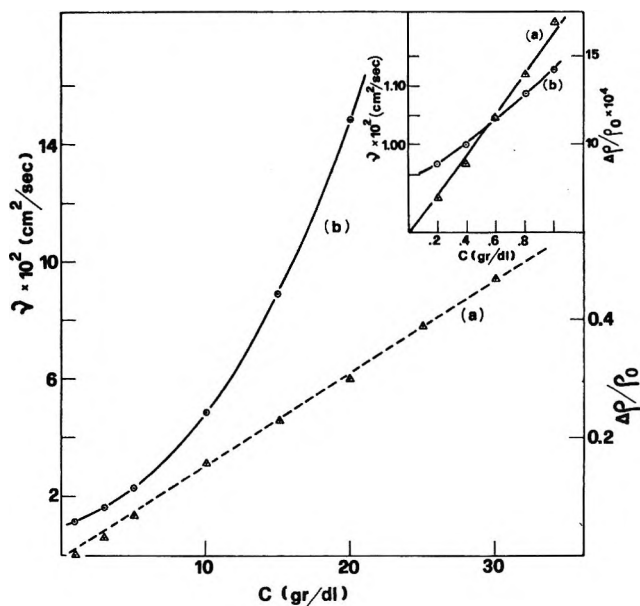


Figure 6. (a) The relative density variation, $\Delta\rho/\rho_0$, of the POEG solution as a function of concentration c of solute, (b) the kinematic viscosity, ν , as a function of concentration; $T = 22^\circ$.

brane releases all its water content (measured to be 5.7 mm³/cm²) the consequent concentration difference calculated with the above relationship is 0.022 g/dl, sufficient to give rise to the instability. The behavior of our system when a more dilute solution is employed can be explained by observing that, in this case, even all the water content inside the membrane is insufficient to determine a concentration gradient above the critical one and therefore the instability cannot occur.

We shall now analyze the behavior of the dimension of the cells l , with regard to the thickness and the concentration of the fluid layer. The mean area for each figure has been measured with the following procedure. A certain number of contiguous cells (usually 100–200) was counted on a photograph and the total area occupied by these cells was determined with an Ott integrator. The actual value of the mean area per cell was obviously determined dividing the total area by the number of cells and taking into account the proper magnification of the system. The value l was determined as the side of the hexagons of that given area. Figure 7a shows the l vs. d plot obtained with a 30% solution. One can observe a linear dependence between the side of the hexagons and the thickness of the layer.

This procedure could be easily followed using highly concentrated solutions (e.g., 30% by weight), but was difficult to perform with solutions of concentration smaller than 20%. In fact in this case the pattern does not appear simultaneously in all the zones, and

(18) C. Rossi, E. Bianchi, and G. Conio, *Chim. Ind. (Milan)*, **45**, 1498 (1963).

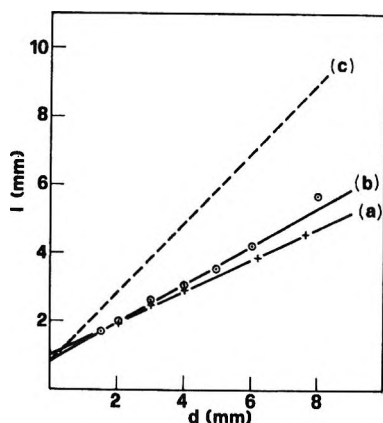


Figure 7. The sides of the hexagons, l , as a function of the thickness of the fluid layer, d (a) for a 30% solution, (b) for a 20% solution. The curve (c) has been theoretically calculated for a 0.3% solution.

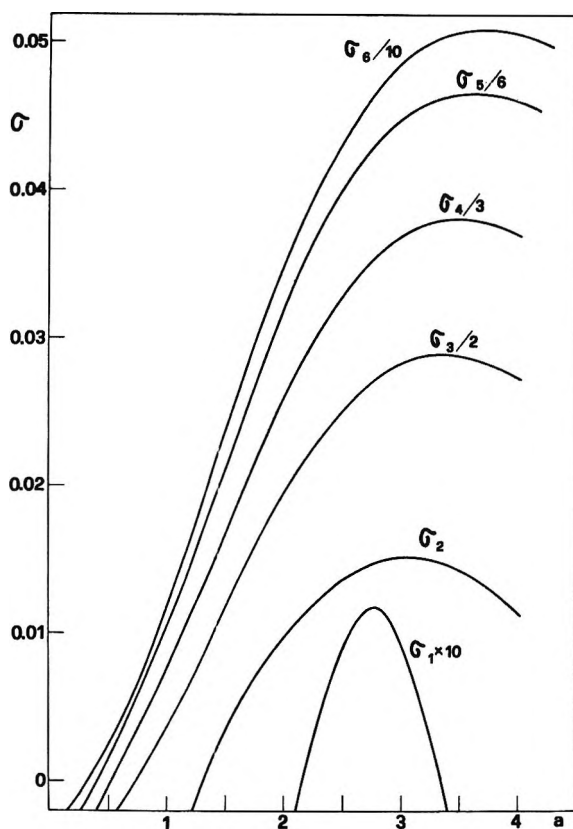


Figure 8. The temporal factor, σ , as function of the wave number, a , for different thickness $d = 1.5, 2, 3, 4, 6, 8$ mm, respectively. $\tau = 1.28 \times 10^{-4}$ l./g., $\nu = 10^{-2}$ cm²/sec, and $D = 10^{-6}$ cm²/sec.

therefore it is difficult to photograph a number of cells sufficient to make reliable statistics.

In order to compare the experimental results with the theoretical expectations, we have performed a numerical analysis of eq 2 for a fixed value of the upper concentration (0.3% by weight) and for different values of the thickness of the fluid layer (and therefore of the concentration difference Δc). τ and ν have been deduced

by the experimental data reported in Figure 6, the diffusion coefficient D by data from the literature,¹⁸ while $\beta = \Delta c/d$ has been calculated using eq 25. Figure 8 shows σ as a function of a for the given values of the parameters. The corresponding value of R is deduced from eq 14. One can observe that the curve has a maximum, σ_{\max} , which defines the wavelength prevailing in the system, and which is shifted towards greater values of a as the value of R increases. Relation 19, in conjunction with the results reported in Figure 8, gives the values of the hexagon sides l , corresponding to σ_{\max} , at the different values of d . The results are summarized in Table I. The value of l is plotted as a function of d in Figure 7c which shows that, on increasing the thickness d of the fluid layer, the pattern dimension increases linearly, in agreement with the experimental results.

Table I

d (mm)	R	$10^2 \sigma_{\max}$	σ_{\max}	l (mm)
1.5	1181	1.18	2.77	2.26
2	2138	15.2	3.08	2.7
3	4900	57.7	3.33	3.76
4	8552	114.3	3.5	4.78
6	19243	279.6	3.65	6.87
8	34210	507	3.73	8.96

Figure 7 shows that the experimental straight line for a 30% concentration has a lower slope than the theoretical curve determined at 0.3% concentration.

This fact suggests that, while the character of the pattern does not undergo substantial changes when the system is far from the marginal state, the cell dimension at the same thickness should be slightly greater. This expectation is confirmed by the experiments performed at a lower concentration (20% by weight) which are reported in Figure 7b. One can observe, in this case, that the slope of the straight line is increasing. Therefore it seems justified to argue that a further decrease in the concentration of the solution would make the slope tend to the theoretical value determined for a much lower concentration.

Conclusions

We have interpreted the observed phenomenon as an instability due to the gravitational field. The analogy with the Bénard problem suggests that even local variations in concentration may originate stresses due to concentration dependent surface tension forces. In principle this fact could be important in determining the behavior of the system. In fact in the case of the Bénard cells it has been demonstrated⁶⁻⁹ that in some conditions (*e.g.*, thickness of the layer lower than 1 mm.) the surface tension forces can be of fundamental importance. In the present case, at least for layers of thickness ranging between 1.5 and 10

mm, we observed that the same kind of pattern formation occurs also when the fluid layer is interposed between two rigid surfaces. Moreover we observed depressions on the free surface in correspondence with the descending flows and elevations in correspondence with the ascending ones. Figure 3 shows such behavior. All these observations support the hypothesis that, at least in the presently studied conditions, the dominant forces are the gravitational ones.⁹ The agreement between the theoretical expectations (where we consider only gravitational forces) and the experimental values in determining Δc_r supports this hypothesis.

It could be of some interest to mention at this point a final test that we have performed in order to be sure of our interpretation. We have inverted the system, *i.e.*, we have placed the wet membrane over the solution. Surprisingly also in this case a kind of organized

pattern appeared, however in a time much greater than in the previously analyzed system. Moreover we observed that this pattern was strongly related to the evaporation process through the membrane. In fact preventing evaporation we did not observe any kind of pattern. The mechanism for the instability in this case is therefore ascribed to the formation of a denser solution on the upper layer of fluid as a result of water leaving the solution through the membrane (evaporative cooling is quickly dissipated). However a more detailed description of this phenomenon requires a further investigation which will be object of a further study.

Acknowledgments. The authors wish to express their thanks to Professor A. Borsellino, for his interest in this work, and to Professor E. Bianchi, for providing us the diffusion data of POEG.

X-Ray Study of the Conformation of the Molecule of

1,2-*trans*-Cyclopentanedicarboxylic Acid

by E. Benedetti,* P. Corradini, and C. Pedone

Istituto Chimico, Laboratorio di Chimica Generale e Inorganica della Università, Naples, Italy (Received August 6, 1971)

Publication costs borne completely by The Journal of Physical Chemistry

The crystal structures of the racemic (+, -) and the optically active (+) forms of the 1,2-*trans*-cyclopentanedicarboxylic acid have been solved by three-dimensional X-ray analysis using data collected by counter techniques (Cu K α). The crystal data for the two compounds are the following: racemic: monoclinic, space group $C2/c$, $a = 9.252$, $b = 6.659$, $c = 12.185$ Å, $\beta = 100^\circ 38'$, $Z = 4$; optically active: monoclinic, space group $P2_1$, $a = 5.957$, $b = 6.645$, $c = 12.041$ Å, $\gamma = 129^\circ 13'$ (c unique axis), $Z = 2$. The determination of the structure for the racemic compound has been achieved by means of the close-packing criteria. The crystal structure of the optically active form was derived from the structure of the racemic, once the occurrence of certain structural relations was recognized. Both the structures were refined to an R value of 6.3% utilizing 625 and 602 independent measured reflections for the (\pm) and the (+) forms, respectively. The more relevant results are those concerning the conformations of the molecule in the two structures. The two different experimental conformations for the cyclopentane ring are in excellent agreement with those of minimum energy calculated by Lifson and Warshel for the cyclopentane molecule. The internal rotation angle φ_1 in the ring takes the highest possible value in order to bring the carboxylic groups as more equatorial as possible; on the other hand this value leaves the highest residual flexibility to the remaining internal rotation angles of the ring. In the two structures rows of hydrogen bonded molecules along a crystallographic direction are found and planes of isomorphous molecules are recognized. The twinning, always present in the racemic crystals, is associated with a "fault" in the piling up of such planes in the crystal structure.

Introduction

Many systems appear to be conformationally rigid, because of constraints which are imposed by the chemical nature or by the physical state of the system itself; however, very often, their flexibility may be larger than usually thought.

A system of this kind is provided by the cyclopentane

ring, whose geometry is dependent on nine internal coordinates. Once the five carbon-carbon bond lengths are fixed, since the bond angles of carbon compounds usually fall into fairly small angular ranges near the tetrahedral value, apparently no variation should be allowed for the internal rotation angles.

It has been shown, however, that in many cases large

variations of the internal rotation angles are possible if we only take into account the possibility of the coupling of small bond angle deformations or the simultaneous variation of bond angles and other internal rotation angles.¹ It is well known, for instance, that the conformation of the cyclopentane ring can vary continuously on an equipotential energy surface.² In the absence of substituents, the molecule possesses a normal mode of motion, called pseudorotation. As calculated by Lifson and Warshel,³ the energy remains constant (to less than 0.005 kcal/mol) while bond angles and internal rotation angles vary in a concerted way.

In order to contribute accurate experimental information on the geometry of the cyclopentane ring, we have undertaken the study of the crystal structure of the (+) and the (±) 1,2-cyclopentanedicarboxylic acid.

Experimental Section

A. X-Ray Data Collection. Crystals of (+)-1,2-cyclopentanedicarboxylic acid were obtained by slow evaporation of aqueous solutions, mp 181–183° (uncorrected), $[\alpha]^{25D} + 91.5^\circ$ (water). From preliminary Weissenberg and rotating photographs taken with Cu K α radiation along the *a* and *b* axes, the crystals were found to belong to the monoclinic system. The systematic extinctions of the 00*l* reflections with *l* odd indicate the acentric space group *P*2₁, with two molecules per unit cell (*c* unique axis).

Crystals of (±)-1,2-*trans*-cyclopentanedicarboxylic acid were obtained from aqueous as well as acetone solutions, mp 160–161° (corrected). Weissenberg and rotating photographs taken with Cu K α radiation indicate that the crystals belong to the monoclinic system. The extinctions of *hkl* reflections for $h + k = 2n + 1$ and $h0l$ for $l = 2n + 1$ indicate two possible space groups: the centrosymmetric *C*2/*c* or the acentric *C**c*.

We prepared crystals from different solvents and we always observed the occurrence of twinning. While the Weissenberg photograph along the *a* axis (0*kl* reflections) does not show any evidence of twinning, the photographs taken in the other two directions (*h*0*l* and *hk*0 reflections) clearly demonstrate the presence of two individuals in twin orientation. In reciprocal space the *c** axes for the two individuals have the same orientation, the *b** axes have opposite directions, and the *a** axes are at an angle of β^* from the *c** axes in the appropriate direction to obtain a right-handed coordinated system. (A rather similar kind of twinning was earlier reported by us⁴.)

Hence the 0*kl* reflections of the two individuals overlap perfectly as indicated by the Weissenberg photographs along the *a* axis. Moreover, the geometry of the unit cell is such that the *hkl* reflections of one individual of the twin are found to overlap the $\bar{h}, \bar{k}, l + h/2$ reflections of the other individual when *h* was even (0, 2, 4, 6, ...). For *h* odd no overlapping occurs.

From the knowledge of the relative intensities of corresponding reflections for the two individuals of the twin (obtained by measuring the intensities of non-overlapping reflections), it was possible to establish that the ratio of intensities was 10:1 for the particular crystal under examination.

We were then able to correct each reflection *hkl* (for *h* even) setting up the following equations for pairs of reflections

$$I(hkl)_{\text{obsd}} = I(h\bar{k}l)_1 + I(\bar{h}, \bar{k}, \bar{l} + h/2)_2$$

$$I(\bar{h}, \bar{k}, l + h/2)_{\text{obsd}} = I(\bar{h}, \bar{k}, l + h/2)_1 + I(hkl)_2$$

where the subscripts obsd, 1, and 2 for the intensity of the reflections refer to the observed value of the intensity and to the values of the intensity due to the individuals 1 and 2, respectively. Since

$$\frac{I(hkl)_1}{I(hkl)_2} = \alpha$$

where α is a measurable factor (for each crystal the ratio of the intensities of corresponding reflections is found to vary—though we did not succeed in obtaining untwinned crystals, we were able to find a crystal with a large α value: larger the α value, less are the errors in the correction process; in our case $\alpha = 10$), it was possible then to solve the equations for pairs of reflections and correct each of them.

A single crystal of (+)-1,2-cyclopentanedicarboxylic acid and a twinned crystal of the racemic isomer were used for the X-ray data collection using the Ni-filtered Cu K α radiation ($\lambda = 1.5418 \text{ \AA}$). An automated diffractometer (Picker FACS-1) equipped with a digital computer (PDP-8) was used according to a procedure described before.⁵

The determination of the lattice constants for the two compounds was carried out by a least-squares treatment of the 2θ , χ , and φ setting angles (automatically refined) of twelve reflections with $2\theta \geq 80^\circ$ (Cu K α , $\lambda = 1.5418 \text{ \AA}$) using a program prepared by Busing and Levy.⁶

The unit cell parameters obtained are as follows: (±)-1,2-cyclopentanedicarboxylic acid: $a = 9.252 \pm 0.006 \text{ \AA}$, $b = 6.659 \pm 0.007 \text{ \AA}$, $c = 12.185 \pm 0.10 \text{ \AA}$, $\beta = 100^\circ 38' \pm 10'$. Assuming four molecules (C₇H₁₀O₄) per unit cell the calculated density is $d_{\text{calcd}} = 1.341 \text{ g/cm}^3$ ($d_{\text{exptl}} = 1.34 \text{ g/cm}^3$ by flotation). (+)-

(1) E. Benedetti, P. Corradini, M. Goodman, and C. Pedone, *Proc. Nat. Acad. Sci. U. S. A.*, **62**, 650 (1969).

(2) J. E. Kilpatrick, K. S. Pitzer, and R. Spitzer, *J. Amer. Chem. Soc.*, **69**, 2483 (1947); K. S. Pitzer and W. E. Donath, *J. Amer. Chem. Soc.*, **81**, 3213 (1959).

(3) S. Lifson and A. Warshel, *J. Chem. Phys.*, **49**, 5116 (1968).

(4) E. Benedetti, P. Corradini, and C. Pedone, *J. Amer. Chem. Soc.*, **91**, 4075 (1969).

(5) E. Benedetti, P. Corradini, C. Pedone, and B. Post, *J. Amer. Chem. Soc.*, **91**, 4072 (1969).

(6) W. R. Busing and H. A. Levy, *Acta Crystallogr.*, **22** 457 (1967).

1,2-trans-cyclopentanedicarboxylic acid: $a = 5.957 \pm 0.005 \text{ \AA}$, $b = 6.645 \pm 0.006 \text{ \AA}$, $c = 12.041 \pm 0.009 \text{ \AA}$, $\gamma = 129^\circ 13' \pm 10'$, space group: $P2_1$ from systematic extinctions of the $00l$ reflections with l odd (c unique axis). Assuming two molecules ($C_7H_{10}O_4$) per unit cell the calculated density is $d_{\text{calcd}} = 1.340 \text{ g/cm}^3$ ($d_{\text{exptl}} = 1.34 \text{ g/cm}^3$, by flotation).

For the twinned crystal of the racemic compound the intensity data collection was carried out for both the individuals of the twin. In the range of 2θ examined (2° – 130°) a total of 602 and 625 independent reflections were measured by counter techniques for the optically active and the racemic forms, respectively.

B. Structure Determinations and Refinements. The structure of the racemic compound was determined by a relatively straightforward application of close-packing criteria.⁷ If the space group is $C2/c$ then the C_2 symmetry of the molecule must be retained as a crystallographic element of symmetry. On the other hand the reasonable hypothesis of hydrogen bonded rows of molecules (hydrogen bonds between carboxylic groups across symmetry centers) dictates that the c axis will be the identity period of the row. Under these conditions the choice of the appropriate orientation of the row was made on the basis of packing considerations: one of the two possible orientations was easily discharged because of unfavorable van der Waals contacts between atoms of neighboring molecules. We tested the remaining model by checking the intensities of a few strong reflections.

The starting trial model after four cycles of full matrix least-squares brought the conventional R factor

$$R = \frac{\sum ||F_o| - |F_c||}{\sum |F_o|}$$

from 0.42 to 0.18. After introduction of anisotropic thermal factors the R value dropped to 0.10. Subsequently a difference Fourier clearly revealed the positions of the five hydrogens which were then introduced in the final three cycles of full matrix least-squares. The atomic coordinates and the isotropic thermal factors of the hydrogens were let refine in the last two cycles.

The crystal structure of the optically active form was easily derived from the structure of the racemic form from the occurrence of certain structural relations between racemic and optically active structures.⁸ In fact, upon transformation of the unit cell constants of the optically active compound into those of a centered space group, $C2_1$, c unique axis, we get $a' = 2a + b = 9.27$ (5) \AA , $b' = b = 6.645$ (6) \AA , $c' = c = 12.041$ (9) \AA , and $\gamma' = 95^\circ 32'$ ($30'$).

This transformation evidences a close similarity in unit cell dimensions of the two compounds; an associated similarity in structure is evidenced by the fact that the $0kl$ reflections are almost identical for the two compounds in the C -centered space groups.

The fractional coordinates x and y of the racemic structure were then considered to build a starting model for the optically active structure. In fact, a reasonable structure of the optically active form can be generated from that of the racemic one considering that the model of packing in the ab plane of the racemic structure, which contains molecules of identical chirality, is very similar to the mode of packing of molecules in the $a'b'$ plane of the optically active form.

The slight differences in the geometry of the two ab planes ($\gamma_{\text{rac.}} = 90^\circ$, $\gamma_{\text{opt. act.}} = 95^\circ 32'$) can be ascribed to the differences in the conformation of the cyclopentane rings and to the differences in the packing of these planes with each other.

Four cycles of full matrix least-squares brought the R factor to 0.17. Finally, anisotropic thermal factors were introduced followed by the introduction of the hydrogen atoms in their stereochemically expected positions with isotropic thermal factor equal to the average of the B_{ij} 's of the carrier atom. The atomic parameters of the hydrogens were kept fixed in the refinement process.

The refinements of the two structures were continued until the maximum shift in the atomic parameters of the heavy atoms was less than 5% of their standard deviations (for the hydrogen atoms in the case of the racemic form these changes were about 10%). The weighting scheme suggested by Cruickshank and Philling has been adopted throughout the refinement of these structures.⁹

The final R value for 625 independent measured reflections was 0.063 for the (\pm) form and 0.063 for the 602 independent measured reflections of the (+) form.¹⁰ A list of observed and calculated structure factors will appear following these pages in the microfilm edition of this volume of the journal. Single copies may be obtained from the Business Operations Office, Books and Journals Division, American Chemical Society, 1155 Sixteenth St., N.W., Washington, D. C. 20036, by referring to author, title of article, volume, and page number. Remit check or money order for \$3.00 for photocopy or \$2.00 for microfiche.

The final atomic parameters for both compounds are reported in Tables I and II, together with their standard deviations.

(7) P. Corradini, P. Ganis, C. Pedone, and G. Diana, *Makromol. Chem.*, **61**, 242 (1963).

(8) C. Pedone and E. Benedetti, *Acta Crystallogr.*, in press.

(9) D. W. T. Cruickshank and D. E. Philling, "Computing Methods and the Phase Problem in X-Ray Crystal Analysis," R. Pepinsky, J. M. Robertson, and J. C. Speakman, Ed., Pergamon Press, New York, N. Y., 1967, p 32.

(10) A complete set of crystallographic programs (FORTRAN IV) written by A. Immirzi was used throughout the determination and refinement of the structure: A. Immirzi, *Ric. Sci.*, **37**, 743, 846, 850 (1967). All the computations were carried out at the Centro di Calcolo Elettronico della Facolta di Scienze dell'Universita di Napoli (Italy) (IBM 360/44).

Table I: Final Atomic Parameters of the (+, -)1,2-*trans*-Cyclopentanedicarboxylic Acid^a

Final Positional Parameters			
	<i>x</i>	<i>y</i>	<i>z</i>
C(1)	0.0560 (3)	0.3486 (3)	0.2109 (2)
C(2)	0.0370 (3)	0.5615 (4)	0.1580 (2)
C(3)	0.0000	0.6975 (5)	0.2500
C(4)	0.0311 (3)	0.1895 (3)	0.1218 (2)
O(1)	0.1475 (2)	0.1260 (4)	0.0892 (2)
O(2)	-0.0937 (2)	0.1296 (3)	0.0818 (1)
H(1)C(1)	0.151 (3)	0.337 (4)	0.252 (2)
H(1)C(2)	0.127 (5)	0.593 (6)	0.134 (4)
H(2)C(2)	-0.051 (4)	0.551 (5)	0.092 (3)
H(1)C(3)	0.076 (4)	0.795 (6)	0.279 (3)
H(1)O(1)	0.137 (6)	0.050 (9)	0.030 (5)

Final Thermal Parameters ^b							
<i>B</i>	<i>B</i> ₁₁	<i>B</i> ₂₂	<i>B</i> ₃₃	<i>B</i> ₁₂	<i>B</i> ₁₃	<i>B</i> ₂₃	
C(1)		4.1 (1)	3.9 (1)	2.5 (1)	-0.2 (1)	1.0 (1)	-0.1 (1)
C(2)		6.1 (1)	4.1 (1)	3.2 (1)	-0.4 (1)	1.6 (1)	0.1 (1)
C(3)		5.3 (2)	3.8 (1)	3.9 (2)	0.0	1.5 (1)	0.0
C(4)		4.3 (1)	3.8 (1)	2.5 (1)	0.1 (1)	0.9 (1)	0.3 (1)
O(1)		4.7 (1)	7.8 (1)	4.8 (1)	0.2 (1)	1.3 (1)	-2.6 (1)
O(2)		4.6 (1)	5.8 (1)	4.2 (1)	-0.4 (1)	1.0 (1)	-1.3 (1)
H(1)C(1)	1.6 (5)						
H(1)C(2)	4.9 (9)						
H(2)C(2)	2.7 (6)						
H(1)C(3)	4.7 (9)						
H(1)O(1)	8.2 (14)						

^a Esd's in unit of the last significant figure. ^b Temperature factor in the form: $T = \exp[-1/4(B_{11}h^2a^{*2} + B_{22}k^2b^{*2} + B_{33}l^2c^{*2} + 2B_{12}hka^*b^* + 2B_{13}hla^*c^* + 2B_{23}klb^*c^*)]$.

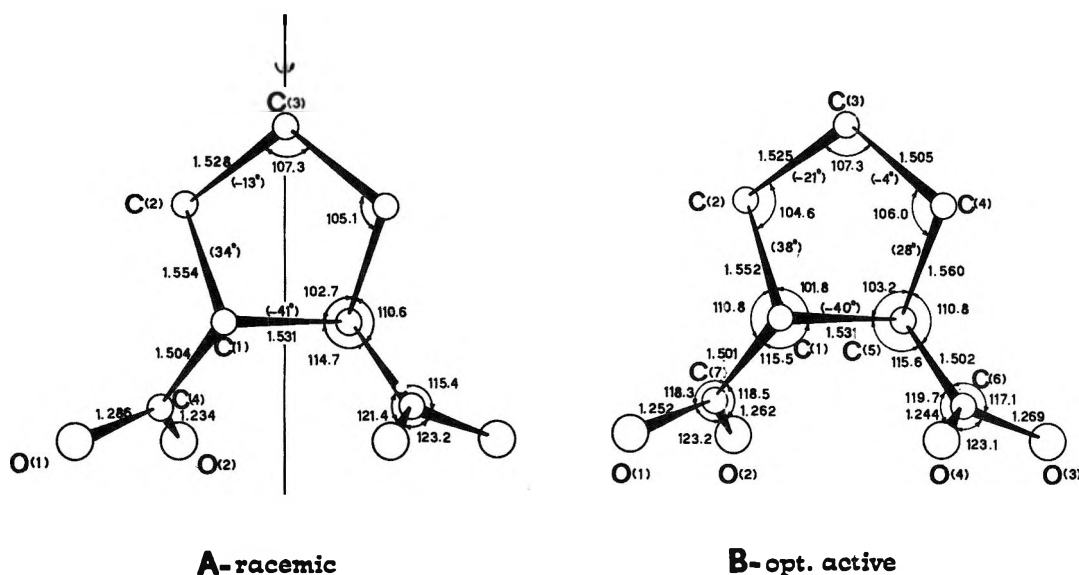


Figure 1. Molecular models for the racemic and the optically active 1,2-*trans*-cyclopentanedicarboxylic acids. Bond lengths, bond angles, and the internal rotation angles in the ring are indicated.

Results and Discussion

The molecular parameters (bond lengths, bond angles, and internal rotation angles) of the molecules of the 1,2-*trans*-cyclopentanedicarboxylic acid in the two

studied forms (+) and (+, -) are given in Figure 1 and reported together with their standard deviations in Table IV. The parameters relating to the hydrogen bond formation in the two compounds are very similar

Table II: Final Atomic Parameters of (+)-1,2-*trans*-Cyclopentanedicarboxylic Acid^a

Final Positional Parameters			
	<i>z</i>	<i>y</i>	<i>z</i>
C(1)	-0.1125 (8)	-0.4124 (7)	0.7100
C(2)	-0.0837 (10)	-0.6085 (8)	0.6576 (4)
C(3)	0.0184 (10)	-0.6845 (8)	0.7257 (5)
C(4)	0.1505 (12)	-0.4746 (10)	0.8393 (4)
C(5)	0.1475 (9)	-0.2602 (7)	0.7889 (3)
C(6)	0.1344 (9)	-0.1116 (7)	0.8791 (3)
C(7)	-0.1145 (9)	-0.2542 (7)	0.6217 (3)
O(1)	-0.3542 (8)	-0.3259 (8)	0.5883 (3)
O(2)	0.1246 (7)	-0.0609 (6)	0.5821 (3)
O(3)	0.3738 (7)	0.0908 (6)	0.9155 (3)
O(4)	-0.1044 (6)	-0.1948 (6)	0.9174 (3)
H(1)C(1)	-0.310	-0.519	0.758
H(1)C(2)	-0.289	-0.776	0.626
H(2)C(2)	0.075	-0.157	0.592
H(1)C(3)	-0.165	-0.870	0.786
H(2)C(3)	0.178	-0.699	0.723
H(1)C(4)	0.013	-0.553	0.915
H(2)C(4)	0.363	-0.402	0.741
H(1)O(2)	0.133	0.048	0.522
H(1)O(3)	0.378	0.197	0.976

Final Thermal Parameters

	<i>B</i> ₁₁	<i>B</i> ₂₂	<i>B</i> ₃₃	<i>B</i> ₁₂	<i>B</i> ₁₃	<i>B</i> ₂₃
C(1)	3.1 (2)	3.2 (1)	1.9 (1)	2.0 (1)	0.2 (1)	0.2 (2)
C(2)	4.8 (2)	3.5 (1)	2.6 (2)	2.8 (2)	-0.3 (2)	-0.3 (1)
C(3)	4.7 (2)	3.7 (2)	3.6 (2)	2.8 (2)	0.0 (2)	0.3 (2)
C(4)	6.0 (3)	5.4 (2)	3.2 (2)	4.4 (2)	-1.0 (2)	-0.5 (2)
C(5)	3.5 (2)	3.6 (2)	2.0 (1)	2.3 (1)	-0.1 (1)	-0.2 (1)
C(6)	3.6 (2)	3.1 (1)	2.0 (1)	2.0 (1)	0.1 (1)	0.2 (1)
C(7)	3.2 (2)	3.2 (1)	1.9 (1)	1.9 (1)	0.2 (1)	0.0 (2)
O(1)	3.8 (2)	7.2 (2)	4.4 (2)	3.3 (1)	0.5 (1)	2.4 (2)
O(2)	3.9 (2)	4.1 (1)	4.0 (2)	2.0 (1)	0.3 (1)	1.5 (1)
O(3)	3.9 (2)	4.9 (1)	4.1 (2)	1.8 (1)	0.1 (1)	-1.7 (1)
O(4)	3.7 (1)	5.2 (1)	3.5 (1)	2.7 (1)	0.2 (1)	-1.0 (1)

^a Esd's in unit of the last significant figure.

and agree with the observations made in analogous compounds; however, the C—O and C=O distances are clearly differentiated only in the racemic structure; in the optically active compound a statistical distribution of the C—O and C=O bonds is probably at hand.

The results obtained for the conformation of the cyclopentane ring in the derivatives studied in this paper are in excellent agreement with those of minimum energy calculated by Lifson and Warshel for the cyclopentane molecule.

In both cases the 1,2-*trans*-cyclopentanedicarboxylic acid molecule takes a conformation, in which the two carboxylic groups are as nearly equatorial as possible.

Since the internal rotation angle φ_1' (that is C(4)–C(1)–C(1)–C(4)' or C(7)–C(1)–C(2)–C(6) for the racemic and the optically active molecules, respectively, with C(1)' and C(4)' being related to C(1) and C(4) by a twofold axis parallel to the *b* direction) is approxi-

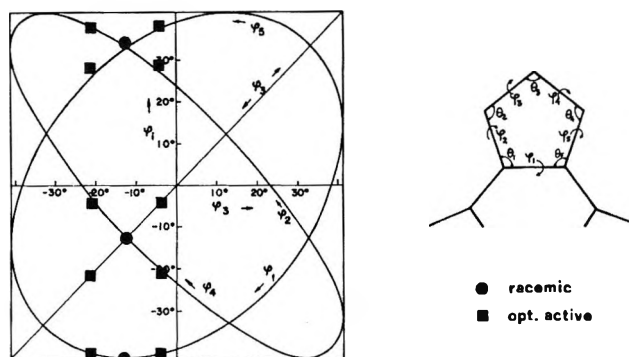


Figure 2. Internal rotation angles (φ_1) along the pseudorotational path of cyclopentane. The experimental values determined for the racemic and the optically active forms of the 1,2-*trans*-cyclopentanedicarboxylic acid are reported. The two sets of values reported for the optically active form correspond to the exchange of φ_3 with φ_4 and φ_2 with φ_5 .

mately equal to $120^\circ - \varphi_1$, φ_1 being the internal rotation angle in the ring (*cf.* Figure 2), this means that the internal rotation angle φ_1 tends to assume the highest possible value within the constraints of the ring. In fact, we observe experimentally $\varphi_1 = 40^\circ$ and 41° for the racemic and optically active structures, respectively. The highest possible value of the internal rotation angles in the ring for the minimum energy conformations of a cyclopentane ring was indicated by Lifson and Warshel as 42° .

However, the other internal rotation angles in the ring differ much more widely between themselves in the two structures. It was evidenced³ that the torsional angles along the pseudorotational path of the cyclopentane ring vary in a concerted way: to a small variation of φ_1 in the neighborhood of its maximum value, much larger variations of the other internal rotation angles are allowed; this is shown in Figure 2, redrawn from Figure 3 of the paper of the quoted authors, with the indications of the experimental values of the φ_1 angles found by us in the two structures.

Thus, the internal rotation angle φ_1 , which determines the geometry of the characteristic hydrogen bonded rows in these two structures, seems to take the value which leaves the highest residual flexibility to the remaining internal rotation angles of the ring.

Table III: Bond Angles θ_i of the Cyclopentane Ring^a

Angle	—Experimental Values—		—Interpolated from Ref 3—	
	Racemic	Opt. Active	Racemic	Opt. Active
θ_1	102.3	103.2	103.2	103.8
θ_2	105.1	106.0	105.3	105.9
θ_3	107.3	107.3	106.3	106.2
θ_4	105.1	104.6	105.3	104.5
θ_5	102.3	101.8	103.2	102.8

^a *Cf.* Figure 2.

Table IV: Final Molecular Parameters of the 1,2-*trans*-Cyclopentanedicarboxylic Acids

Racemic		Optically Active	
Bond Lengths ^a			
C(1)-C(1) ^b	1.531 (3)	C(1)-C(2)	1.552 (8)
C(1)-C(2)	1.554 (3)	C(2)-C(3)	1.525 (8)
C(1)-C(4)	1.504 (3)	C(3)-C(4)	1.505 (10)
C(2)-C(3)	1.528 (3)	C(4)-C(5)	1.560 (9)
C(4)-O(1)	1.286 (3)	C(5)-C(1)	1.531 (7)
C(4)-O(2)	1.234 (3)	C(5)-C(6)	1.502 (7)
C(1)-H(1)C(1)	0.93 (3)	C(1)-C(7)	1.501 (8)
C(2)-H(1)C(2)	0.96 (5)	C(7)-O(1)	1.252 (7)
C(2)-H(2)C(2)	1.04 (3)	C(7)-O(2)	1.262 (7)
C(3)-H(1)C(3)	0.97 (4)	C(6)-O(3)	1.269 (8)
O(1)-H(1)O(1)	0.90 (6)	C(6)-O(4)	1.244 (7)
Bond Angles ^a			
C(1)-C(2)-C(3)	105.1 (1)	C(1)-C(2)-C(3)	104.6 (2)
C(2)-C(3)-C(2)'	107.3 (1)	C(2)-C(3)-C(4)	107.3 (2)
C(2)-C(1)-C(1)'	102.7 (1)	C(3)-C(4)-C(5)	106.0 (2)
C(2)-C(1)-C(4)	110.6 (1)	C(4)-C(5)-C(1)	103.2 (2)
C(4)-C(1)-C(1)'	114.7 (1)	C(5)-C(1)-C(2)	101.8 (2)
C(1)-C(4)-O(1)	115.4 (1)	C(2)-C(1)-C(7)	110.8 (2)
C(1)-C(4)-O(2)	121.4 (1)	C(4)-C(5)-C(6)	110.8 (2)
O(1)-C(4)-O(2)	123.2 (1)	C(5)-C(1)-C(7)	115.5 (2)
		C(1)-C(5)-C(6)	115.6 (2)
		C(1)-C(7)-O(1)	118.3 (2)
		C(1)-C(7)-O(2)	118.5 (2)
		C(5)-C(6)-O(3)	117.1 (3)
		C(5)-C(6)-O(4)	119.7 (3)
		O(1)-C(7)-O(2)	123.2 (3)
		O(3)-C(6)-O(4)	123.1 (2)
Internal Rotation Angles ^c			
C(2)'-C(1)'-C(1)-C(2)	-41	C(1)-C(2)-C(3)-C(4)	-21
C(1)'-C(1)-C(2)-C(3)	34	C(2)-C(3)-C(4)-C(5)	-4
C(1)-C(2)-C(3)-C(2)'	-13	C(3)-C(4)-C(5)-C(1)	28
C(4)'-C(1)'-C(1)-C(4)	78	C(4)-C(5)-C(1)-C(2)	-40
C(4)'-C(1)'-C(1)-C(2)	-162	C(5)-C(1)-C(2)-C(3)	38
C(1)'-C(1)-C(4)-O(1)	-151	C(3)-C(2)-C(1)-C(7)	161
C(1)'-C(1)-C(4)-O(2)	31	C(3)-C(4)-C(5)-C(6)	153
C(2)-C(1)-C(4)-O(1)	94	C(2)-C(1)-C(5)-C(6)	-161
C(2)-C(1)-C(4)-O(2)	-84	C(2)-C(1)-C(7)-O(1)	96
C(3)-C(2)-C(1)-C(4)	157	C(2)-C(1)-C(7)-O(2)	-82
		C(4)-C(5)-C(1)-C(7)	-160
		C(4)-C(5)-C(6)-O(3)	91
		C(4)-C(5)-C(6)-O(4)	-86
		C(6)-C(5)-C(1)-C(7)	79
		C(1)-C(5)-C(6)-O(3)	-152
		C(1)-C(5)-C(6)-O(4)	31
		C(5)-C(1)-C(7)-O(1)	-149
		C(5)-C(1)-C(7)-O(2)	33

^a Esd in unit of the last significant figure. ^b The atoms marked with ' are those generated by twofold axis. ^c Trans conformation = 180°. The esd on the average is $\pm 2^\circ$.

The fact that the puckering of the cyclopentane rings is associated with fluctuations of the bond angles around $\theta = 104.5^\circ$, in a foreseeable way, is shown in Table III, where our experimental data are compared with the results of the calculations of Lifson and Warshel; it is remarkable that the trends are in very good agreement.

The mode of packing of the molecules, Figure 3 and Figure 4, in rows of *tci* and *t2* symmetry¹¹ (along the

c and *b* directions for the racemic and the optically active structure, respectively) is very similar to that observed in the case of the (+, -) and -(+)-1,2-*trans*-cyclohexanedicarboxylic acids.

A further analogy may be found in the side by side

(11) P. Corradini, *Atti Accad. Naz. Lincei, Cl. Sci. Fis. Mat. Nat., Rend.*, **28**, 1 (1950).

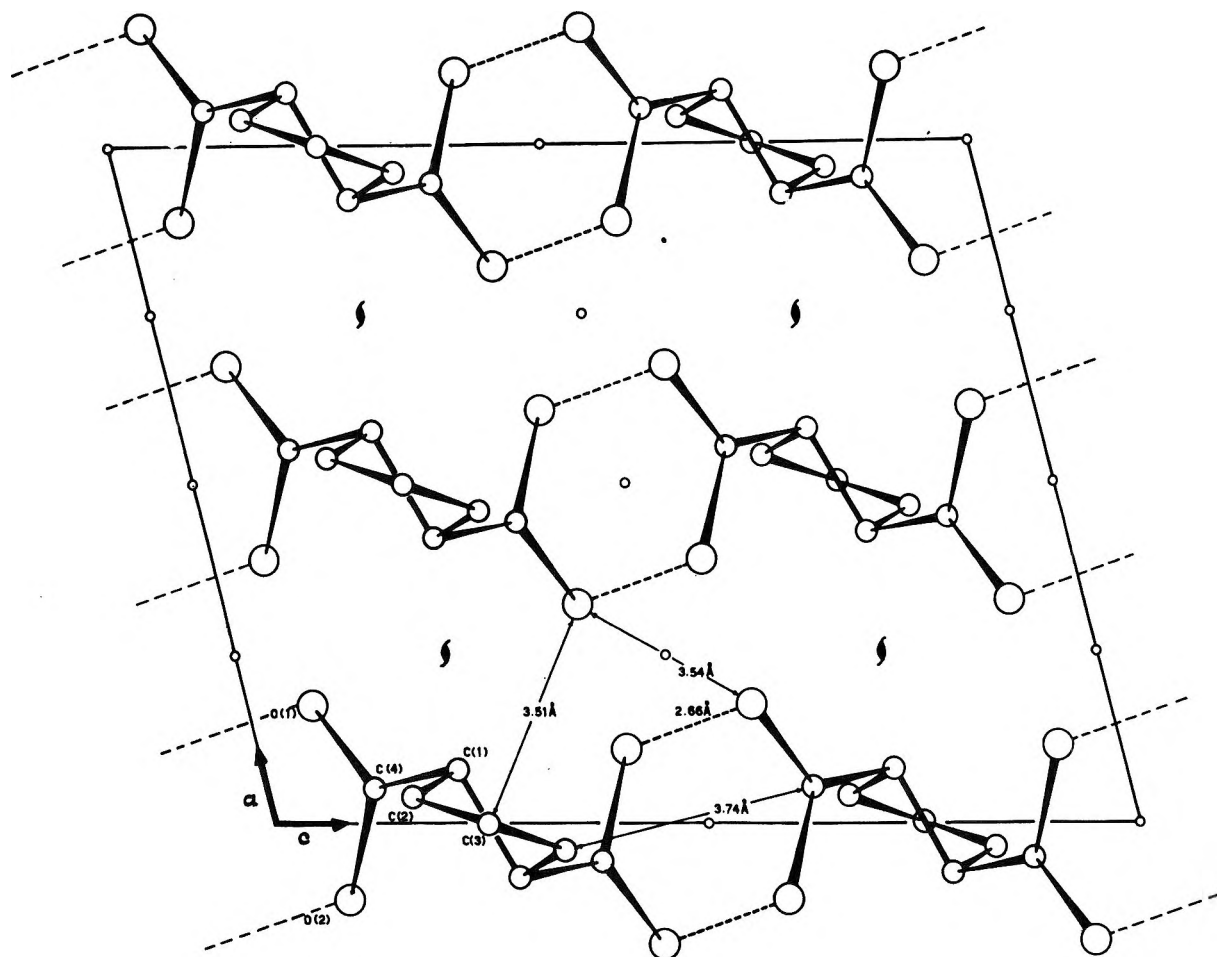


Figure 3. The mode of packing of the (\pm) -1,2-*trans*-cyclopentanedicarboxylic acid along the b direction. The shortest intermolecular contacts are reported.

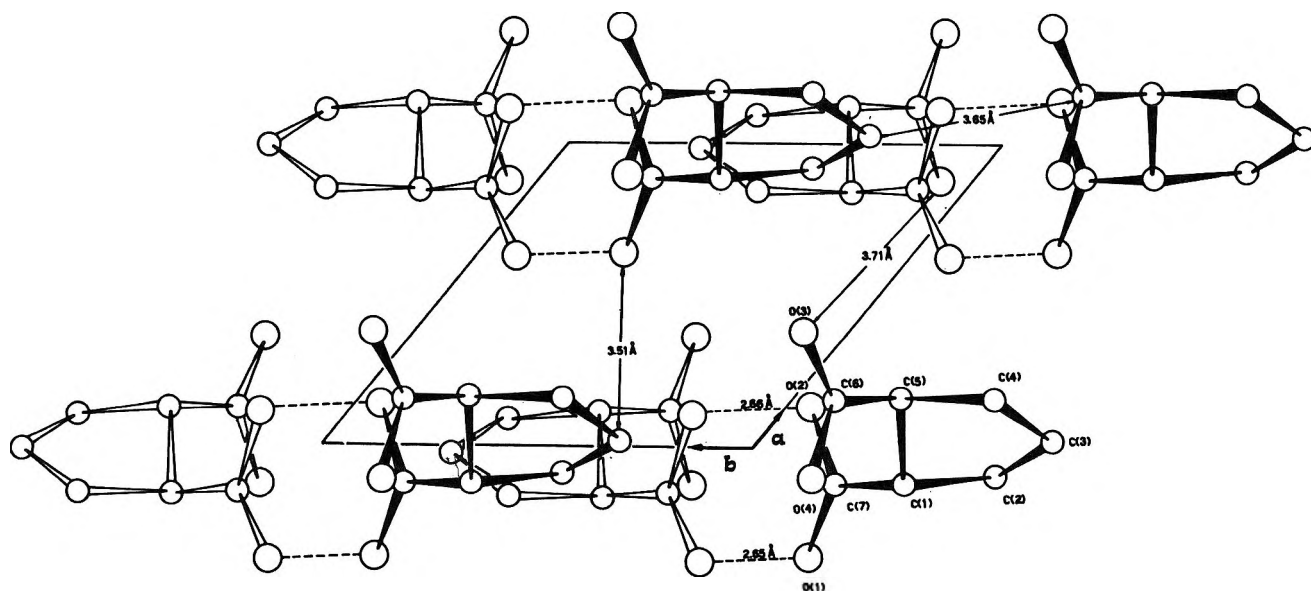


Figure 4. The mode of packing of the $(+)$ -1,2-*trans*-cyclopentanedicarboxylic acid along the c direction. The shortest intermolecular contacts are reported.

packing of the rows. Both in the structures of the $(+)$ - and $(+, -)$ -1,2-*trans*-cyclohexanedicarboxylic acids and in the structure of the $(+)$ - and $(+, -)$ -1,2-*trans*-cyclo-

pentanedicarboxylic acids it is possible to recognize planes of isomorphous molecules, which are packed in an almost identical way.

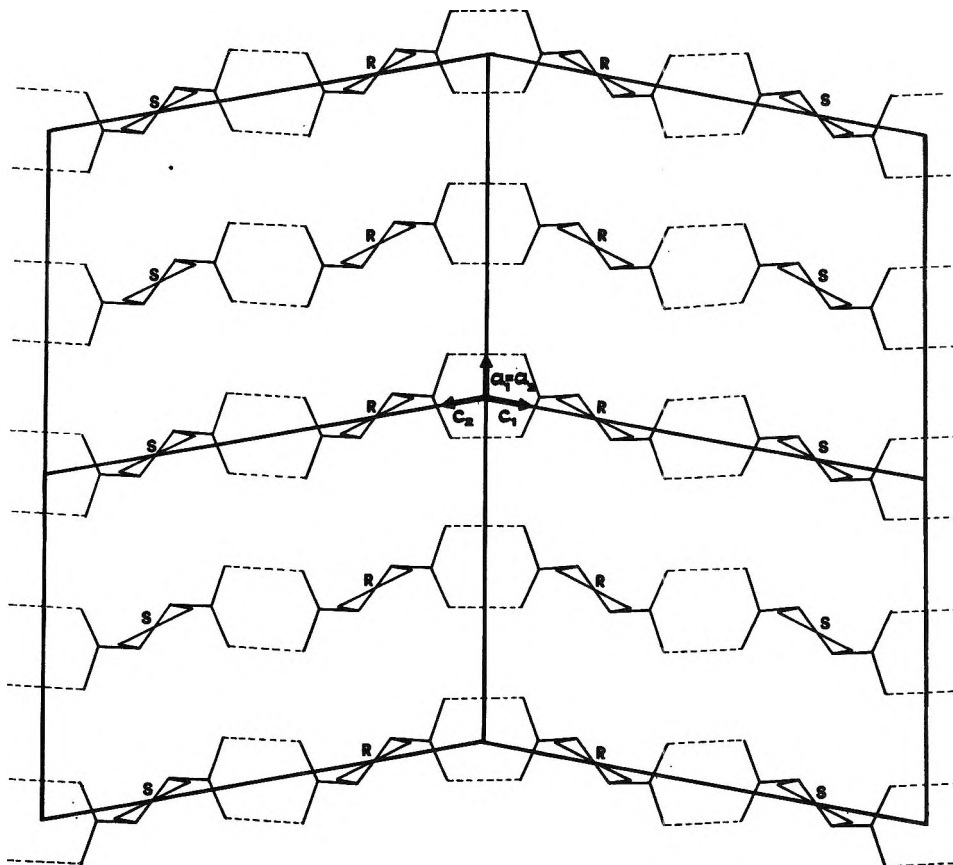


Figure 5. Model of the twinning of the racemic 1,2-*trans*-cyclopentanedicarboxylic acid. The absolute configurations of the molecules are indicated. The *b* axes for the two individuals of the twin have opposite directions.

Thus the *ab* plane of the (\pm)-1,2-*trans*-cyclopentanedicarboxylic acid contains isomorphous molecules packed in the same way as the *a'b'* plane of the (\pm)-1,2-*trans*-cyclopentanedicarboxylic acid.

The observation of twinning in the racemic crystals of the 1,2-cyclopentane is associated with a "fault" in

the piling up of such planes as indicated in Figure 5. The structure at the fault plane is locally similar to that of the optically active compound.

Acknowledgments. We gratefully acknowledge the support of Research Grant (70/01939) from the C.N.R. of Italy.

Thermal Decomposition of 3-Halo-3-phenyldiazirine in Solution

by Michael T. H. Liu* and K. Toriyama

Department of Chemistry, University of Prince Edward Island, Charlottetown, Prince Edward Island, Canada (Received October 1, 1971)

Publication costs assisted by the University of Prince Edward Island

Thermal decomposition of 3-chloro- and 3-bromo-3-phenyldiazirines was investigated in several solvents over the 60–110° temperature range. The primary decomposition appears to be unimolecular and shows very little solvent effects. The Arrhenius parameters for these decompositions have been determined. The possible transition state for diazirine decomposition will be discussed.

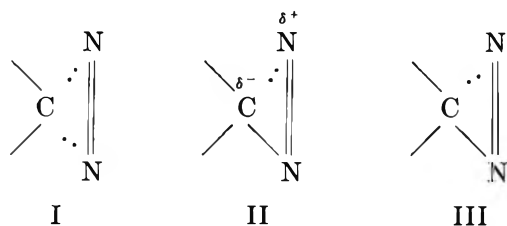
Introduction

In the past decade, the thermal and photolytic decompositions of diazirines have become important tools for the generation of free carbene. Many investiga-

tions on carbene chemistry with the use of diazirines have been reported, but only a few mechanistic studies for the decomposition have been done and the details are still unknown. It is important that the mechanism

be elucidated, not only for the application of these compounds but also for fundamental interests in the nature of such strained ring systems.

In the thermal decomposition of 3-chloro-3-alkyldiazirines Frey, *et al.*,^{1,2} have provided some evidence for the intermediate production of carbenes and proposed transition state I as the simplest representation for a diazirine decomposition. This transition complex shows that the two carbon-nitrogen bonds are broken simultaneously. However, it is also possible to suggest other transition complexes which are consistent with the data available to us in the literature. Schmitz³ suggested an ionic transition state, II, for the decomposition of diazirines. In the thermal decomposition of difluorodiazirine⁴ and the polymerization of difluorodiazirine,⁵ Mitsch and coworkers prefer a mechanism involving the transient existence of difluorodiazomethane or its equivalent prior to the loss of nitrogen. It seems likely that such a mechanism would require transition state III. Bottomly and Nyberg⁶ also suggest a diazomethane intermediate for the formation of free carbene in the gas phase decomposition of 3,3-dimethyldiazirine. In this paper, we will give an account of the kinetic studies of the thermal decomposition of 3-chloro- and 3-bromo-3-phenyldiazirine and discuss the possible transition state in the light of the results.



Experimental Section

Materials. The 3-chloro-3-phenyldiazirine was prepared from amidine hydrochloride by oxidation with sodium hypochlorite in the presence of lithium chloride, with the experiment carried out in a solution of dimethyl sulfoxide. The method is essentially that described by Graham.⁷ 3-Bromo-3-phenyldiazirine was prepared by a similar method using NaOBr. Purification of these compounds was accomplished by column chromatography. The ir spectra of these compounds agreed well with Graham's⁸ and had only one spot on tlc.

Cyclohexene was passed through an alumina column and was distilled. A middle fraction was retained for the experiments reported here. Ethanol, diethylene glycol monoethyl ether (DEGME), and DMSO were stirred in calcium hydride and were distilled under dried conditions. Carbon tetrachloride (spectrograde) was used directly without any treatment. Pyridine was kept over KOH pellets for several days and distilled. Tetrachloroethylene was distilled and collected, bp 120–121°.

Kinetics Procedure. (a) *By Vapor Phase Chromatography.* The rates of reaction were measured by following the disappearance of diazirine. The stock solution consisting of about 0.2 M of the diazirine and 0.08 M of bromobenzene (internal standard) was placed in Pyrex tubes, degassed, sealed under reduced pressure, and suspended in a constant temperature oil bath regulated to $\pm 0.1^\circ$. After a specific time the tubes were removed from the oil bath, and the reaction was quenched in a Dry Ice-acetone mixture. Analysis was conducted with the use of a Perkin-Elmer F11 fitted with a hydrogen flame detector; the peak areas of the diazirine were integrated with a ball and disk integrator. For work with the 3-chloro-3-phenyldiazirine in cyclohexene, carbon tetrachloride, and tetrachloroethylene, a $1/8 \times 6$ ft copper column packed with 20% Carbowax 20M on Chromosorb W was used. The column temperature was 50°. The peaks of the diazirine were symmetrical, and during the analysis no obvious decomposition of the diazirine was detected. The rates of reactions were followed to at least 80% completion, and the first-order rate coefficients were determined graphically from the plot of log (area ratio of the diazirine/standard) vs. time.

(b) *By Nitrogen Evolution Method.* The reaction was carried out by mixing a specific amount of the diazirine with the appropriate thermoequilibrated solvent in the reaction vessel, which was immersed in the oil bath and connected to a gas buret. At appropriate time intervals, the volumes of nitrogen were measured at atmospheric pressure and corrected for changes in room temperature. The infinite volume, V_∞ , was taken at about ten half-lives of the reaction. The first-order rate coefficients were determined graphically from the plot of log ($V_\infty - V_t$) against time, where V_t is the nitrogen volume evolved at time t .

(c) *By Uv Spectrophotometry.* The kinetics were obtained by following the characteristic absorption of diazirine with the use of a Unicam S.P. 800A. uv spectrophotometer. In the case of volatile solvents, such as cyclohexene, ethanol, and aqueous acetic acid, the reactions were conducted in sealed Pyrex tubes containing a solution of 0.18 M of the diazirine, and the reaction mixtures were treated in the same manner as those described in part a. The mixtures were diluted to 10 ml with cyclohexane, and the optical densities were observed.

In the case of nonvolatile solvents, such as DMSO

- (1) M. R. Bridge, H. M. Frey, and M. T. H. Liu, *J. Chem. Soc. A*, 91 (1969).
- (2) H. M. Frey and M. T. H. Liu, *ibid.*, 1916 (1970).
- (3) E. Schmitz, *Angew. Chem., Int. Ed. Engl.*, **3**, 333 (1964).
- (4) E. W. Neuvar and R. A. Mitsch, *J. Phys. Chem.*, **71**, 1229 (1967).
- (5) P. H. Ogden and R. A. Mitsch, *J. Heterocycl. Chem.*, **5**, 41 (1968).
- (6) G. A. Bottomly and G. L. Nyberg, *Aust. J. Chem.*, **17**, 406 (1964).
- (7) W. H. Graham, *J. Amer. Chem. Soc.*, **87**, 4396 (1965).
- (8) W. H. Graham, private communication.

and diethylene glycol monoethyl ether (DEGME), the reactions were carried out by mixing a specific amount of the diazirine with the thermoequilibrated solvent in a reaction vessel immersed in an oil bath. The solutions were then withdrawn from the thermobath at appropriate time intervals. In this case, the optical densities of the reaction mixtures were observed directly without dilution. The wavelengths measured were the following: 3-chloro-3-phenyldiazirine in cyclohexene at 394 nm and in DMSO, ethanol, and 90% aqueous acetic acid at 390 nm; 3-bromo-3-phenyldiazirine in cyclohexene at 396 nm and in DEGME at 395 nm. The first-order rate coefficients were determined graphically from the plot of $(\log D_t - D_\infty)$ against time, where D_t is the optical density at the wavelength mentioned and D_∞ is the wavelength corresponding to that of the complete reaction.

Reaction Products. When 3-chloro-3-phenyldiazirine was left at room temperature for several months, 1,4-diphenyl-1,4-dichloro-3,3-diaza-1,3-butadiene was obtained, mp 124°. In cyclohexene, the main product was 7-chloro-7-phenylnorcarane⁹ as reported by Graham.⁷ In addition, small amounts of C-H insertion isomers were detected. These compounds were characterized by the nmr spectrum, which showed two sharp doublets at $\tau = 5.4$ and 5.25. The nitrogen evolution was quantitative, and the azine formation was not detected under our present experimental condition. In DEGME, a mixture of benzaldehyde ethylene acetal, product of insertion to O-H bond, and benzaldehyde was obtained. In DMSO, benzaldehyde and benzoic acid were isolated, and in the case of ethanol, mixtures of α -ethoxytoluene, α,α -diethoxytoluene, and benzaldehyde were formed.

Results and Discussion

Three representative solvents were chosen for these experiments: cyclohexene for nonpolar, dimethyl sulfoxide (DMSO) for polar aprotic, and diethylene glycol monoethyl ether (DEGME) for polar protic. The decompositions were carried out in the temperature range between 60 and 110° in sealed tubes. The kinetics were followed by the disappearance of the diazirine with vapor phase chromatography, with uv spectrophotometry at the characteristic absorption of diazirine, or with the volume of nitrogen evolution. Sample data for the thermal decomposition of 3-chloro-3-phenyldiazirine in cyclohexene at 90° are given in Table I for which the data were obtained from the uv characteristic absorption of diazirine shown in Figure 1. The same reaction was followed by vpc method and the data are given in Table II. The agreement of the rate constants obtained by different methods is very good ($\pm 3\%$), and excellent first-order plots were obtained even up to 80% completion of the reaction. In the temperature range between 60 and 110°, 3-chloro-3-phenyldiazirine decomposes unimolecularly to yield nitrogen and the

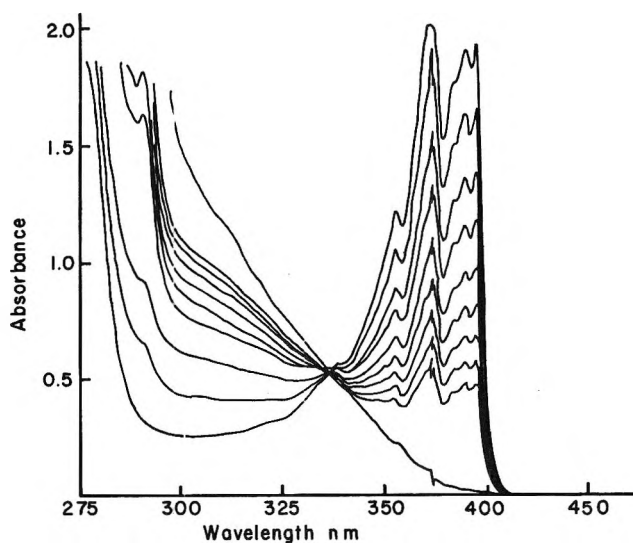
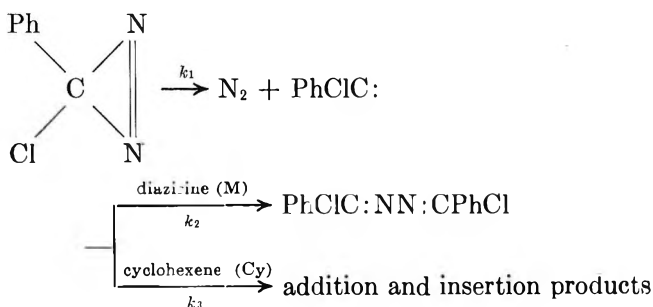


Figure 1. Absorbance vs. wavelength at different reaction time intervals for 3-chloro-3-phenyldiazirine.

corresponding carbene. The resulting carbene can either react with diazirine to give dimeric product, or with the solvent to yield the appropriate compounds. In cyclohexene, the decomposition products consist of 80% of 7-chloro-7-phenylnorcarane and 20% of the insertion products at the 3 and 4 positions of cyclohexene ($\sim 1:1$).¹⁰ This scheme may be represented as



In terms of the rate constants for the individual steps of the reaction, the overall rate may be expressed in the following expression

$$v = k_1[M] \left[1 + \frac{k_2[M]}{k_2[M] + k_3[\text{Cy}]} \right]$$

However, at high concentration of cyclohexene, $k_2[M]$ will be small compared to $k_3[\text{Cy}]$ and can be neglected; the rate equation becomes $v = k_1[M]$; hence, $k_{\text{obsd}} \approx k_1$.

In these experiments the initial concentration of diazirine is always less than 0.2 M, and the formation of azine was suppressed. On the other hand, if the concentration of the diazirine is too high, the reaction will

(9) In the thermal decomposition of 3-chloro-3-anisyldiazirine in cyclohexene and 3-chloro-3-*p*-nitrophenyldiazirine in cyclohexene, the addition products 7-chloro-7-anisylnorcarane and 7-chloro-7-*p*-nitrophenylnorcarane, respectively, have been isolated and analyzed.

(10) J. Hine, "Divalent Carbon," Ronald Press, New York, N. Y., 1964, p 110.

Table I: Sample Data for the Thermal Decomposition of 3-Chloro-3-phenyldiazirine in Cyclohexene at 90° Obtained from an Uv Spectrophotometer^a

Time, min	D_t	$D_t - D_\infty$
0	1.930	1.924
3	1.655	1.649
6	1.383	1.377
9	1.171	1.165
12	0.970	0.964
15	0.819	0.813
18	0.689	0.683
21	0.575	0.559
24	0.478	0.472
∞	0.006	...

$$^a k = 9.9 \times 10^{-4} \text{ sec}^{-1}$$

Table II. Kinetics for the Thermal Decomposition of 3-Chloro-3-phenyldiazirine in Cyclohexene at 90° by Vpc^a

Reaction time, min	Peak area		Area ratio diazirine/bromobenzene
	Diazirine	Bromobenzene	
0.00	3586, 4997, 8225, 5365	1396, 1967, 3296, 2335	2.520 ± 0.033
3.00	5213, 7442, 4180	2431, 3574, 1983	2.098 ± 0.030
6.00	5436, 4263, 4773	2954, 2577, 2759	1.716 ± 0.012
9.00	4867, 5190, 4870	3227, 3447, 3393	1.461 ± 0.032
10.00	4326, 5156, 3137	3378, 4194, 2506	1.245 ± 0.009
15.00	3039, 4040, 3342	3104, 4010, 3300	1.014 ± 0.005
25.00	1073, 2097, 2026	1951, 3746, 3574	0.559 ± 0.006
30.00	1592, 1565, 1333	3797, 3773, 3308	0.421 ± 0.013

$$^a k = 10.1 \times 10^{-4} \text{ sec}^{-1}$$

probably be of mixed order, and a first-order plot would not be linear.

The data in Table III give the rate constants for the thermal decomposition of 3-chloro-3-phenyldiazirine in various solvents; the data of Table IV give the rate constants for the thermal decomposition of 3-bromo-3-phenyldiazirine in cyclohexene. For each rate constant, a number of runs were carried out at different times and first-order rate constants computed from the usual plot. The activation parameters were obtained by a least-squares analysis, and the quoted errors are standard deviations. The Arrhenius plots of these results are shown in Figure 2. Finally, the rate constants for the decomposition of 3-halo-3-phenyldiazirine at 75° in various solvents are tabulated in Table V.

The present study indicates that there is a lowering in the activation energy of 3-chloro-3-phenyldiazirine

Table III: Rate Constants for the Thermal Decomposition of 3-Chloro-3-phenyldiazirine in Various Solvents

(a) In cyclohexene (by vpc)						
Temp, °C	70.0	75.0	80.0	90.0	100.0	110.0
10 ⁴ k, sec ⁻¹	1.06	1.95	3.60	10.1	28.9	79.0

$$k = 10^{13.87 \pm 0.13} \exp(-28,000 \pm 215/RT) \text{ sec}^{-1}$$

(b) In DMSO (by uv)					
Temp, °C	60.0	70.0	75.0	80.0	90.0
10 ⁴ k, sec ⁻¹	0.47	1.60	3.04	5.00	15.8

$$k = 10^{14.11 \pm 0.20} \exp(-28,110 \pm 320/RT) \text{ sec}^{-1}$$

(c) In DEGME (by uv)					
Temp, °C	65.0	70.0	75.0	80.0	85.0
10 ⁴ k, sec ⁻¹	0.70	1.32	2.30	4.00	6.90

$$k = 10^{13.57 \pm 0.17} \exp(-27,420 \pm 260/RT) \text{ sec}^{-1}$$

Table IV: Rate Constants for the Thermal Decomposition of 3-Bromo-3-phenyldiazirine in Cyclohexene. Reaction Followed by Vpc

Temp, °C	60.0	65.0	70.0	75.0	80.0	85.0	90.0
10 ⁴ k, sec ⁻¹	0.61	1.20	2.34	3.80	5.90	11.5	20.0

$$k = 10^{13.75 \pm 0.40} \exp(-27,360 \pm 410/RT) \text{ sec}^{-1}$$

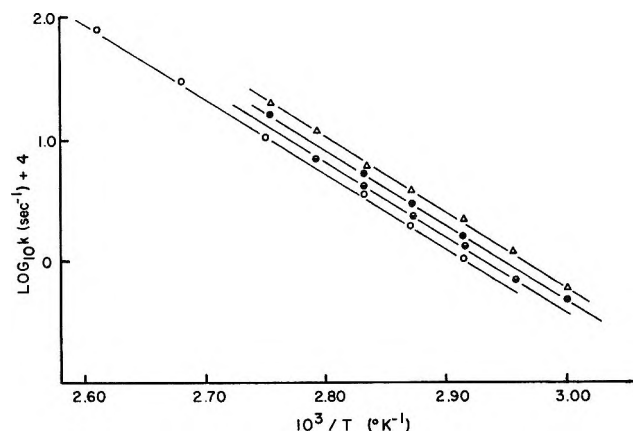


Figure 2. Arrhenius plots of first-order rate constants for 3-halo-3-phenyldiazirine in various solvents: O, 3-chloro-3-phenyldiazirine in cyclohexene; ●, 3-chloro-3-phenyldiazirine in DEGME; ●, 3-chloro-3-phenyldiazirine in DMSO; Δ, 3-bromo-3-phenyldiazirine in cyclohexene.

of about 3 kcal/mol from that of 3-chloro-3-methyldiazirine;¹ this reflects the resonance stabilization effects of the phenyl group on the transition state of diazirine decomposition. It is interesting to note that in the decomposition of azo compounds,¹¹ the stabilization effect per phenyl group is about 4 kcal/mol. The Arrhenius parameters of the present work correspond reasonably well with the values for the decomposition

(11) C. G. Overberger, J-P. Anselme, and J. G. Lombardino, "Organic Compounds with Nitrogen-Nitrogen Bonds," Ronald Press, New York, N. Y., 1966.

Table V: Rate Constants for the Decomposition of 3-Halo-3-phenyldiazirine at 75°

Diazirine	Solvent	10 ⁴ k, sec ⁻¹	Method
3-Chloro-3-phenyl	Cyclohexene	1.95	Vpc
3-Chloro-3-phenyl	DMSO	3.04	Uv
3-Chloro-3-phenyl	DEGME	2.30	Uv
3-Chloro-3-phenyl	AcOH	1.87	Uv
3-Chloro-3-phenyl	Ethanol	1.89	Uv
3-Chloro-3-phenyl	CCl ₄	2.05	Vpc
3-Chloro-3-phenyl	Pyridine	2.08	N ₂ evolution
3-Chloro-3-phenyl	C ₂ Cl ₄	2.04	N ₂ evolution
3-Bromo-3-phenyl	Cyclohexene	3.80	Vpc
3-Bromo-3-phenyl	DEGME	4.70	Uv
3-Bromo-3-phenyl	AcOH	3.80	N ₂ evolution

of 3-chloro-3-alkyldiazirine,^{1,2} diethyldiazirine,¹² and difluorodiazirine,⁴ a feature which suggests that the mechanisms for all the diazirine decompositions are similar. The *A* factor of $\sim 10^{14}$ ($\Delta S^\ddagger = +3$ eu) shows that the reaction is typically unimolecular with a relatively tight transition state. The results also show that the rate of decomposition does not change as the solvent is varied. This regularity indicates that the

transition state of the rate-determining step is likely to be more radical than ionic. The fact that the rate of the 3-bromo compound is faster than the rate of the 3-chloro compound suggests that the α -bromo substituent is more effective in stabilizing the radical, in agreement with the results reported by Haszeldine.¹³ We feel that the substituent effects provide some evidence for a radical intermediate such as III, but at this stage we can only conclude that the transition state in diazirine decomposition is of a nonpolar nature. It is recognized that more experiments will have to be carried out to distinguish transition states I and III. Such work is in progress in our laboratory.

Acknowledgment. The authors wish to thank Dr. W. H. Graham for providing experimental details of phenylchlorodiazirine preparation. Grateful acknowledgment is made by one of us, M. T. H. L., for a grant-in-aid of research from the National Research Council of Canada and the Senate Research Committee of U.P.E.I.

(12) H. M. Frey and A. W. Scaplehorn, *J. Chem. Soc. A*, 968 (1966).

(13) R. N. Haszeldine, *ibid.*, 1764 (1953).

Electron Spin Resonance Study of Transient Radicals in γ -Irradiated Organic

Inclusion Compounds. II. The Palmitic Acid Urea Clathrate

by A. Faucitano, A. Perotti,* G. Allara, and F. Faucitano Martinotti

Istituto di Chimica Generale dell'Universita' di Pavia, 27100 Pavia, Italy (Received June 18, 1971)

Publication costs assisted by E.N.I., Rome

An esr study of the low-temperature γ radiolysis of the hexadecanoic acid urea adduct is reported. The prominent radical species observed after irradiation at -196° are the alkyl radical $\sim\text{CH}_2\dot{\text{C}}\text{HCH}_2\sim$ and the radical anion $\sim\text{CH}_2\dot{\text{C}}(\text{O}^-)\text{OH}$. The latter decomposes above -78° yielding the σ -type radical $\sim\text{CH}_2\dot{\text{C}}=\text{O}$, which decays, at room temperature, with a half-time of 10–15 min, yielding finally the radical $\sim\text{CH}_2\dot{\text{C}}\text{HCOOH}$. Reaction mechanisms are proposed.

The clathrates may afford convenient systems for the esr study of primary radicals and radical ions produced by low-temperature irradiation of organic compounds.

In fact, provided the reactivity of the host compound is low enough, the stability of these transient species is expected to be enhanced because of the inhibition by the walls of the cavities of secondary reactions within parent guest molecules. Another important advantage, from the esr standpoint, arises from the fact that within "the cage" of the host compound free radicals

usually have rather more freedom of movement than within the lattice of the pure compound; as a consequence the esr lines are considerably narrower.¹

In this note we present an esr study of radicals obtained in the urea adduct of palmitic acid γ -irradiated at -196° .

(1) (a) O. H. Griffith, *J. Chem. Phys.*, **41**, 1093 (1964); (b) O. H. Griffith, *ibid.*, **42**, 2644 (1965); (c) O. H. Griffith, *ibid.*, **42**, 2651 (1965); (d) G. A. Helckè and R. Fantechi, *Mol. Phys.*, **18**, 1 (1970).

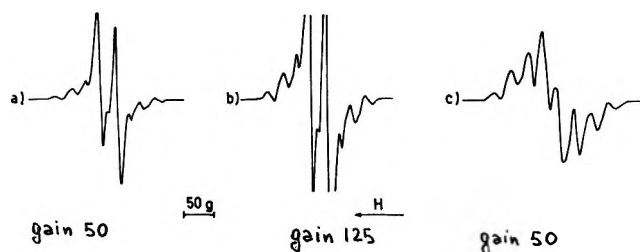


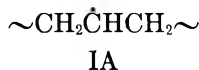
Figure 1. ESR spectra (-196°) of γ -irradiated urea adducts of palmitic acid (a, b) and *n*-hexadecane (c). (b was recorded at higher gain.)

Experimental Section

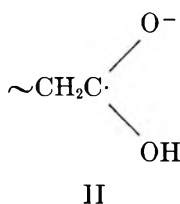
The palmitic acid urea clathrates were precipitated by adding a methanol solution of palmitic acid into a saturated methanol solution of urea.¹ Polycrystalline samples for the esr measurements were sealed under high vacuum in Pyrex tubes and irradiated at -196° in a ^{60}Co source with total γ doses of about 10 Mrads. The esr spectra have been recorded with the spectrometer elsewhere described.²

Results and Discussion

A. Nature of Radicals Trapped at -196° . After irradiation at -196° , the dominant component of the esr spectrum is a doublet of two equally intense lines with a hyperfine splitting of 25–26 G and a line width of 9–10 G. This signal is superimposed on a weak eight-line spectrum with a splitting of about 20 G (Figure 1a and b). The octet is very similar, both in splitting and intensity distribution, to the one obtained under the same conditions from the urea adduct of *n*-hexadecane³ (Figure 1c) and may therefore be attributed to alkyl radicals of the type

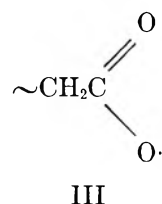


These radicals are known⁴ to assume sometimes a particular conformation or a hybridization state such that one α and two β equivalent protons interact with the unpaired spin with a coupling constant of about 20 G whereas for the other two β protons the coupling constant is nearly twice as much; the result is an octet with a line to line splitting of 20 G and an intensity distribution approximately 1:3:5:7:7:5:3:1. Doublets of 24–25 G of splitting have been often observed in the low-temperature spectra of mono- and dicarboxylic acids and amino acids,⁵ and these have been attributed to the radical anions



formed by electron capture by carboxyl group. With ^{13}C and deuterium substitution experiments it was shown^{5a-d} that the unpaired electron occupies mainly a 2p carbon orbital, with a small 2s mixture; as a consequence the doublet obtained is explained with the interaction of two nonequivalent protons, one of which has a coupling constant less than the line width.

B. Temperature Dependence of the ESR Spectra. At -135° the octet changes irreversibly into a sextet with a hyperfine splitting of 23–24 G; this change is most likely caused by a relaxation of alkyl radicals (IA) into a more stable conformation (IB) (Figure 2a), with five protons nearly equally interacting with the unpaired spin. As the temperature is raised above -135° , the doublet converts into a triplet (Figure 2b) and successively (above -78°) into a singlet, which deviates significantly toward the high-field region (Figure 2c). This conversion is nearly quantitative in fact. The singlet accounts for more than 80% of the doublet total area. The appearance of the triplet may be tentatively explained by assuming that the increase of the temperature causes a change of the rotational state of the methylene group in the radical anion (II) so that two β protons become nearly equivalent; on the other hand, the change into the singlet calls for a chemical transformation of the radical anion into a new radical species. A single line has also been observed at room temperature in γ -irradiated succinic and other dicarboxylic acids⁶ and was originally attributed to carboxy radicals of the type^{6b}



(2) A. Faucitano, P. Locatelli, F. F. Martinotti, and A. Perotti, *Rend. Acc. Naz. Lincei, Ser. VIII*, **48**, 523 (1970).

(3) A. Faucitano, in press.

(4) (a) P. B. Ayscough and H. E. Evans, *Trans. Faraday Soc.*, **60**, 801 (1964); (b) P. B. Ayscough and H. E. Evans, *J. Phys. Chem.*, **68**, 3066 (1964).

(5) (a) I. Miyagawa and W. Gordy, *J. Amer. Chem. Soc.*, **83**, 1036 (1961); (b) J. E. Bennet and L. H. Gale, *Trans. Faraday Soc.*, **64**, 1174 (1968); (c) H. C. Box, H. G. Freund, and K. T. Lilga, *J. Chem. Phys.*, **42**, 1471 (1965); (d) H. C. Box, H. G. Freund, K. T. Lilga, and E. E. Budinski, *J. Phys. Chem.*, **74**, 40 (1970); (e) H. M. Vyas, J. Janecka, and M. Fujimoto, *Can. J. Chem.*, **48**, 2804 (1970); (f) M. Fujimoto and W. A. Seddon, *ibid.*, **48**, 2809 (1970); (g) B. L. Bales, R. N. Schwarz, and M. W. Hanna, *J. Chem. Phys.*, **51**, 1974 (1969); (h) R. N. Schwarz, M. W. Hanna, and B. L. Bales, *ibid.*, **51**, 4336 (1969); (i) J. Sinclair and M. W. Hanna, *ibid.*, **50**, 2125 (1969); (j) M. Iwasaki, B. Eda, and K. Toriyama, *J. Amer. Chem. Soc.*, **92**, 3211 (1970); (k) R. C. McCalley and A. L. Kwiram, *ibid.*, **92**, 1441 (1970); (l) K. Leibler, J. Wozniak, S. Krauze, and K. Checinski, *J. Chim. Phys.*, **743** (1970).

(6) (a) Yu. N. Molin, I. I. Chkeidze, N. Y. Buben, and V. V. Volvodskii, *Zh. Strukt. Khim.*, **2**, 293 (1961); (b) N. Tamura, M. A. Collins, and D. H. Whiffen, *Trans. Faraday Soc.*, **62**, 1037 (1966); (c) N. Tamura, M. A. Collins, and D. H. Whiffen, *ibid.*, **62**, 2434 (1966); (d) S. Minc, Z. Kecki, and S. Kosek, *Nukleonika*, **10**, 371 (1965).

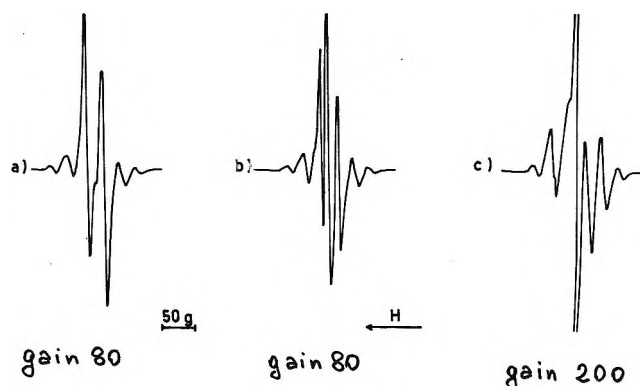


Figure 2. Effect of the temperature on the esr spectrum of the palmitic acid urea adduct: a, ca. -135° ; b, ca. -90° ; c, ca. -50° .

successively, on the basis that the g tensors were found identical with those in the CO_2^- ion, Schwarz, *et al.*,^{5h} suggested that the singlet had to be attributed to CO_2^- radical anions. Recently Leibler, *et al.*,⁵ⁱ observed a singlet in γ -irradiated polycrystalline palmitic and oleic acids, which was attributed by them again to carboxy radicals (III). Radicals of the type III, being π radicals with the unpaired spin density mainly localized on oxygen atoms, show an average g greater than the free spin value.⁷ As the clathrate signal has a g value not greater than the free spin value ($g = 2.002$), we suggest that its attribution to carboxy radicals of the type III must be ruled out.

The CO_2^- radical anion has an ionization potential in the range of 2.3–2.9 eV;^{8a} as a consequence its signal is bleached by ultraviolet radiations. We have made bleaching experiments at -196° by using filtered radiations (wavelength $>3000 \text{ \AA}$) from a 200-W high-pressure mercury lamp; however, no appreciable decay of the singlet was detected after a 2-hr exposure. Another important feature of CO_2^- trapped in a glassy hydrocarbon matrix is that its signal shows a greater tendency to become power saturated than the underlying alkyl radical spectrum.^{8a} On the contrary, in our case the relative intensity of the singlet was enhanced with increasing microwave power. Although the power saturation test should be cautiously considered since the saturation behavior depends on the extent of the coupling of radicals with the environment, which may be quite different in the clathrate as compared to hydrocarbon glasses, these results point to the singlet shown in Figure 2c not being generated by CO_2^- radical ions. As an alternative hypothesis for the decomposition of radical anions of the type II in crystalline succinic acid, Schwarz, *et al.*,^{5h} suggested a reaction giving the succinyl radical $\text{HOOC}-\text{CH}_2-\text{CH}_2-\dot{\text{C}}=\text{O}$ which being of σ type is expected to have an average g lower than the free spin value. This hypothesis however was disregarded on the base that hyperfine coupling with the β hydrogen atoms less than the observed line width of 4–7 G had to be considered unlikely. Recent works^{5,9} indicate that

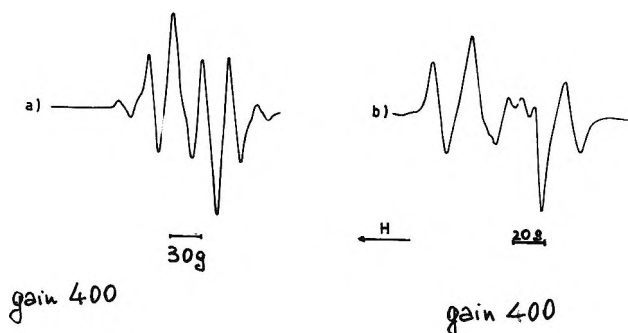
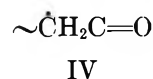
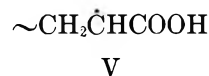


Figure 3. Room temperature esr spectra of the palmitic acid urea adduct, a and b, after 1.5 hr and few days annealing at room temperature, respectively.

in formyl-type radicals the isotropic coupling of β protons may be limited to 5–6 G; as a consequence these radicals would still give a singlet in a polycrystalline system such as that we have used. On this basis and considering especially the negative results of the bleaching experiments, we tentatively suggest that the singlet of the palmitic acid adduct is generated by neutral σ -type radicals



This assumption implies in turn that the radical anions II are the precursors of radicals IV in the palmitic acid radiolysis. Once the singlet has reached its maximum amplitude, it begins to decay at a rate which increases with increasing temperature (the half-time being about 10–15 min at room temperature); as a consequence after about 1.5 hr at room temperature, the esr spectrum consists of a composite sextet (Figure 3a). This esr transformation is accompanied by about 50% decrease of the overall radical concentration. The graphical analysis of this sextet² has shown that it cannot be attributed exclusively to radicals of the type IB, but rather to a nearly equimolecular mixture of radicals IB with radicals of the type



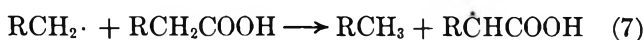
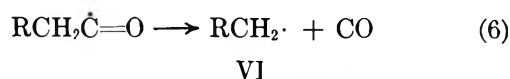
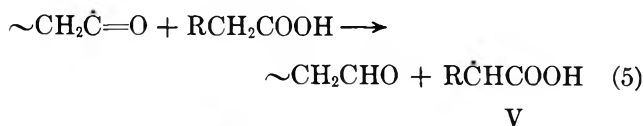
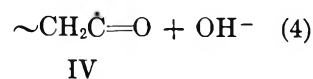
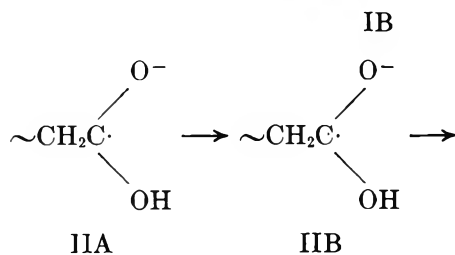
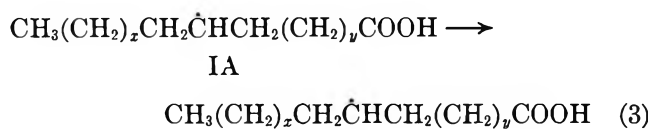
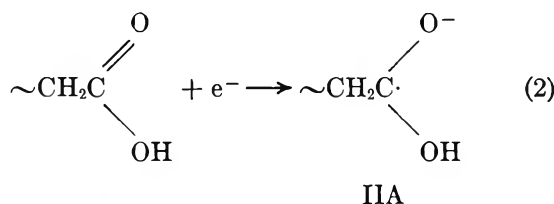
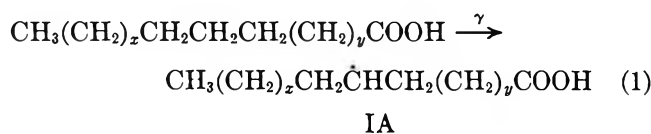
Radicals V are probably already present in the system before the annealing above -196° ; their relative concentration however is likely to be much lower than that of radicals I judging from the relative intensity of the outer lines in the spectrum of Figure 1a. This suggests that the decay of radicals II results, at least in part, in the formation of radicals of the type V. Further, prolonged annealing of the sample at room temperature, leads to complete decay of the sextet so that, finally,

(7) H. C. Heller and T. Cole, *J. Amer. Chem. Soc.*, **84**, 4448 (1962).

(8) (a) P. M. Johnson and A. C. Albrecht, *J. Chem. Phys.*, **44**, 1845 (1966); (b) M. Shiram, R. F. C. Claridge, and J. E. Willard, *ibid.*, **47**, 286 (1967).

only the quartet remains in the spectrum (Figure 3b). This latter change has been already discussed in a previous paper,² where it was considered as evidence of intramolecular hydrogen atom transfer taking place within the urea clathrate, and leading to a migration of the free valence toward carbon atoms adjacent to the carboxylic groups.

C. Reaction Mechanisms. The results can be summarized and rationalized with the following proposed mechanisms.



The intermolecular reactions 5 and 7 implies that the mobility of radicals IV and VI in the urea channels is large enough to make the approach to methylene groups adjacent to nearest-neighbor carboxyls possible. Alternatively a mechanism based on hydrogen atom transfer through the hydrogen bond system can be considered; the latter hypothesis however is conflicting with the fact that very similar esr changes were observed with the clathrate of methyl palmitate. The mechanism of decay of radicals IV *via* the reactions 6 and 7 is expected to be favored by the low energy of the RCO bond (10–20 kcal),⁹ but leads to intermediate RCH₂CH₂· radicals whose esr spectra were not observed in the experimental conditions employed. As a consequence the mechanism based on the reaction 5 must be preferred.

Acknowledgment. This investigation has been carried out with financial support granted by E.N.I., Rome, Italy, through its branch SNAM-Progetti.

(9) J. C. Bennet, B. Mile, and B. Ward, *Chem. Commun.*, 13 (1969).

WILEY-INTERSCIENCE

WATER AND AQUEOUS SOLUTIONS:

Structure, Thermodynamics,
and Transport Processes

Edited by **R. A. HORNE**, *JBF Scientific Corporation,
Burlington, Massachusetts*

Here is a collection of cohesive articles on the structure and properties of liquid water and aqueous solutions, ice and fused salts. Topics range from the surface and transport properties of ice, through the structure, thermodynamics and transport properties of water and aqueous solutions, to the state of water in living cells and tissues.

1972 832 pages 172 illus. \$37.50

PHOTOPHYSICS OF AROMATIC MOLECULES

By **JOHN B. BIRKS**, *Manchester University*

"The author, a physicist of long standing and reputation has attempted successfully the difficult task of collating masses of information and presenting it, whilst remarkably achieving a clear cut type of approach to the various viewpoints of interpretation.

"[*Photophysics of Aromatic Molecules*]...is ideal for the specialist and active research worker in this fascinating field."

—*Laboratory Practice*

1970 704 pages \$29.00

THERMODYNAMICS

Principles and Applications

By **FRANK C. ANDREWS**, *University of California,
Santa Cruz*

Here is a fully understandable account of the principles of thermodynamics which will increase the reader's ability to organize, interpret, and predict an enormous variety of properties of matter. Individual systems are examined in terms of p-V-T data and heat capacities. For simple-component systems coverage ranges over entropy changes, isentropic processes, energy changes, Joule expansions, enthalpy changes, Joule-Thomson expansions, free energy changes and phase equilibria. Multi-component systems are given careful treatments for ideal and real solutions.

1971 288 pages illus. \$9.95

SYSTEMATIC ANALYSIS OF SURFACE-ACTIVE AGENTS

Second Edition

By **MILTON J. ROSEN**, *Brooklyn College and
HENRY A. GOLDSMITH*, *Turco Products, Inc.,
Los Angeles, California*

Volume 12 in Chemical Analysis, a series of Monographs on Analytical Chemistry and Its Applications, edited by P. J. Elving and I. M. Kolthoff

The second edition furnishes new, up-dated methods for the qualitative and quantitative analysis of surface active agents, as well as their isolation and separation. Most of the new material in this edition is devoted to instrumental methods, notably infrared and nuclear magnetic resonance spectrometry for the elucidation of molecular structure, and chromatographic methods of all types for the separation of mixtures and the quantitative determination of their components.

1972 624 pages (approx.) In press

CHEMICAL DYNAMICS:

Papers in Honor of Henry Eyring

Edited by **JOSEPH O. HIRSCHFELDER**, *University of
Wisconsin*, and **DOUGLAS HENDERSON**, *IBM Research
Laboratory, San Jose, California*

Volume 21 in the series, *Advances in Chemical Physics*,
edited by I. Prigogine and S. Rice

"This is a tribute to Eyring on his seventieth birthday. It is a highly specialized monograph containing more than 50 papers in the areas of molecular quantum mechanics, theory of reaction rates, properties of molecules, theory of liquids, biological applications of chemical dynamics, and engineering applications of chemical dynamics. These are all fields in which Eyring has been active; authors are former students and associates of Eyring. Among the authors are found practically all the big names in theoretical chemistry. The book contains excellent articles in the area of theoretical chemical dynamics and structure of liquid. It is highly recommended to student and faculty members with an interest in this area..."

—*Choice*

1971 816 pages 256 illus. \$22.50

PHOTOCHEMISTRY AND SPECTROSCOPY

By **J. P. SIMONS**, *University of Birmingham*

The photo-excited molecule may decay by several alternative paths, not all of which lead to chemical change. Photochemistry is, as a result, a hybrid interdisciplinary subject, and in order to explain the details of the primary photochemical process the language and concepts of both spectroscopy and chemistry have to be understood. This book explores some of the common territory between these two fields.

1971 343 pages \$16.50

ADVANCES IN CHEMICAL PHYSICS

Volumes 20 & 22

Edited by **I. PRIGOGINE**, *University of Brussels*, and
STUART A. RICE, *University of Chicago*

CONTENTS OF VOLUME 20

Multipolar interactions in Molecular Crystals. The Computation of Virial Coefficients. The Origin of Hysteresis in Simple Magnetic Systems. The Linear Gas. Low-Energy Electron Diffraction. High-Resolution Electronic Spectra of Large Polyatomic Molecules. Author Index. Subject Index.

1971 407 pages \$22.50

CONTENTS OF VOLUME 22

Functional Integral Methods and the Statistical Mechanics of Polymer Systems. Equilibrium Denaturation of Natural and of Periodic Synthetic DNA Molecules. The Lattice Vibrations of Molecular Solids. An Introduction to C*-Algebraic Methods in Physics. Radiative and Nonradiative Processes in Benzene. Author Index. Subject Index.

1971 448 pages \$22.50

Available from your bookstore or from Dept. 093-A2608-WI

wiley

WILEY-INTERSCIENCE

a division of JOHN WILEY & SONS, Inc.
605 Third Avenue, New York, N.Y. 10016

In Canada: 22 Worcester Road, Rexdale, Ontario

WILEY-INTERSCIENCE, Dept. 093-A2608-WI
605 Third Avenue, New York, N.Y. 10016

Gentlemen:

Please send me each of the books I have checked below:

- 0 471 40945-6 HORNE: Water and Aqueous Solutions\$37.50
- 0 471 07420-9 BIRKS: Photophysics of Aromatic Molecules\$29.00
- 0 471 40066-1 HIRSCHFELDER/HENDERSON: Chemical Dynamics\$22.50
- 0 471 03183-6 ANDREWS: Thermodynamics\$ 9.95
- 0 471 79202-0 SIMONS: Photochemistry and Spectroscopy\$16.50

- 0 471 69925-X PRIGOGINE/RICE: *Advances in Chemical Physics, Vol. 20*\$22.50
- 0 471 69926-8 PRIGOGINE/RICE: *Advances in Chemical Physics, Vol. 22*\$22.50

- My check (money order) for \$_____ is enclosed.
- Please bill me.

Name _____

Title _____ Firm _____

Address _____

City _____ State _____ Zip _____